

NUREG/CP-0119  
Vol. 1

Proceedings of the U.S. Nuclear Regulatory Commission

---

---

# Nineteenth Water Reactor Safety Information Meeting

Volume 1

- Plenary Session
- Pressure Vessel and Piping Integrity
- Metallurgy and NDE
- Aging and Components
- Probabilistic Risk Assessment Topics

Held at  
Bethesda Marriott Hotel  
Bethesda, Maryland  
October 28-30, 1991

---

---

**U.S. Nuclear Regulatory Commission**

**Office of Nuclear Regulatory Research**

Proceedings prepared by  
Brookhaven National Laboratory



## NOTICE

These proceedings have been authored by a contractor of the United States Government. Neither the United States Government nor any agency thereof, or any of their employees, makes any warranty, expressed or implied, or assumes any legal liability or responsibility for any third party's use, or the results of such use, of any information, apparatus, product or process disclosed in these proceedings, or represents that its use by such third party would not infringe privately owned rights. The views expressed in these proceedings are not necessarily those of the U.S. Nuclear Regulatory Commission.

Available from

Superintendent of Documents  
U.S. Government Printing Office  
P.O. Box 37082  
Washington D.C. 20013-7082

and

National Technical Information Service  
Springfield , VA 22161

NUREG/CP-0119  
Vol. 1  
R1,R2,R3,R4,R5,  
R9,RD,RF,RM,RV

Proceedings of the U.S. Nuclear Regulatory Commission

---

---

# Nineteenth Water Reactor Safety Information Meeting

## Volume 1

- Plenary Session
- Pressure Vessel and Piping Integrity
- Metallurgy and NDE
- Aging and Components
- Probabilistic Risk Assessment Topics

Held at  
Bethesda Marriott Hotel  
Bethesda, Maryland  
October 28-30, 1991

---

---

Manuscript Completed: April 1992

Compiled by: Allen J. Weiss

Office of Nuclear Regulatory Research  
U.S. Nuclear Regulatory Commission  
Washington, DC 20555

Proceedings prepared by  
Brookhaven National Laboratory



## ABSTRACT

This three-volume report contains 83 papers out of the 108 that were presented at the Nineteenth Water Reactor Safety Information Meeting held at the Bethesda Marriott Hotel, Bethesda, Maryland, during the week of October 28-30, 1991. The papers are printed in the order of their presentation in each session and describe progress and results of programs in nuclear safety research conducted in this country and abroad. Foreign participation in the meeting included 14 different papers presented by researchers from Canada, Germany, France, Japan, Sweden, Taiwan, and USSR. The titles of the papers and the names of the authors have been updated and may differ from those that appeared in the final program of the meeting.

**PROCEEDINGS OF THE  
19th WATER REACTOR SAFETY INFORMATION MEETING**

**October 28-30, 1991**

**Published in Three Volumes**

**GENERAL INDEX**

**VOLUME 1**

- **Plenary Session**
- **Pressure Vessel and Piping Integrity**
- **Metallurgy & NDE**
- **Aging and Components**
- **Probabilistic Risk Assessment Topics**

**VOLUME 2**

- **Severe Accident Research**
- **Severe Accident Policy Implementation**
- **Accident Management**

**VOLUME 3**

- **Structural Engineering**
- **Advanced Reactor Research**
- **Advanced Passive Reactors**
- **Human Factors Research**
- **Human Factors Issues Related to Advanced Passive LWRs**
- **Thermal Hydraulics**
- **Earth Sciences**

REGISTERED ATTENDEES(NON NRC)  
19th WATER REACTOR SAFETY INFORMATION MEETING

D. ACKER  
CEA FRENCH ATOMIC ENERGY COMMISSION  
CEB SACLAY DMT/SEMT  
GIF SUR YVEYTE, 91191  
FRANCE

S. ADDITON  
TENERA/ARSAP  
7272 WISCONSIN AVE., SUITE 300  
BETHESDA, MD 20814  
USA

T. AJIMA  
NUPEC-NUCLEAR POWER ENG. TEST CENTER  
3-17,1-CHOME,TORANOMON,MINATO-KU  
TOKYO, 105  
JAPAN

R. ALLEN  
WESTINGHOUSE SAVANNAH RIVER COMPANY  
P.O. BOX 818  
AIKEN, SC 29802  
USA

R. ALLEN  
BATTELLE-PACIFIC NORTHWEST LABS.  
P.O. BOX 999  
RICHLAND, WA 99352  
USA

C. ALLISON  
EG&G IDAHO, INC.  
P.O. BOX 1625  
IDAHO FALLS, ID 83404  
USA

A. ALONSO  
MADRID POLYTECHNICAL UNIVERSITY  
JOSE GUTIERREZ ABASCAL, 2  
MADRID, 28006  
SPAIN

H. AMARASOORIYA  
SCIENTECH, INC  
11821 PARKLAWN DRIVE  
ROCKVILLE, MD 20852  
USA

T. ANDREYCHEK  
WESTINGHOUSE ELECTRIC  
PO BOX 355  
PITTSBURGH, PA 15230  
USA

F. ARAYA  
JAPAN ATOMIC ENERGY RES. INST  
TOKAI-MURA, NAKA-GUN  
IBARAKI-KEN, 319-11  
JAPAN

R. ARCHULETA  
UNIVERSITY OF CALIFORNIA, SANTA BARBARA  
DEPT. OF GEOLOGICAL SCIENCES  
SANTA BARBARA, CA 93106  
USA

W. ARCIERI  
EG&G  
11426 ROCKVILLE PIKE, SUITE 300  
ROCKVILLE, MD 20852  
USA

N. ARNE  
KOREA ELECTRIC POWER CORP., NY OFFICE  
270 SYLVAN AVENUE  
ENGLEWOOD CLIFFS, NJ 07632  
USA

V. ASMOLOV  
I. V. KURCHATOV INST. OF ATOMIC ENERGY  
KURCHATOV SQUARE  
MOSCOW, 123182  
USSR

M. AZARM  
BROOKHAVEN NATIONAL LABORATORY  
BUILDING 130  
UPTON, NY 11973  
USA

S. BALL  
OAK RIDGE NATIONAL LABORATORY  
P.O. BOX 2008  
OAK RIDGE, TN 37831-6010  
USA

A. BARATTA  
PENN STATE UNIVERSITY  
231 SAKETT BLDG.  
UNIVERSITY PARK, PA 16802  
USA

R. BARI  
BROOKHAVEN NATIONAL LABORATORY  
BUILDING 197C  
UPTON, NY 11973  
USA

G. BAROIS  
FRAMATOME  
TOUR FIAT CEDEX 18  
PARIS-LA-DEFENSE, 92084  
FRANCE

J. BASSELIER  
BELGONUCLEAIRE  
AVENUE ARIANE 4,  
BRUSSELS, 1200  
BELGIUM

J. BAST  
STRATEGIC BUSINESS SYSTEMS  
8 MOUNTAINVIEW TERRACE  
BALLSTON LAKE, NY 12019  
USA

J. BASURTO  
CNSNS-MEXICO  
AV. INSURGENTES SUR, 1776  
MEXICO CITY, 01030  
MEXICO

G. BALMGARTNER  
BASLER & HOFMANN  
FORCHSTRASSE 395  
ZURICH, 8029  
SWITZERLAND

R. BEATY  
SCIENCE & ENGINEERING ASSOCIATES, INC.  
1421 PRINCE STREET, SUITE 300  
ALEXANDRIA, VA 22314  
USA

L. BELL  
OAK RIDGE NATIONAL LABORATORY  
P.O. BOX 2009, MS-8083  
OAK RIDGE, TN 37831  
USA

R. BELL  
NUMARC  
1776 EYE STREET NW, SUITE 300  
WASHINGTON, DC 20006  
USA

G. BERNA  
EG&G IDAHO, INC.  
P.O. BOX 1625  
IDAHO FALLS, ID 83404  
USA

R. BEYER  
WESTINGHOUSE  
206 NAVADO ROAD  
W. PGM, PA 15241  
USA

D. BHARGAVA  
VIRGINIA POWER  
5000 DOMINION BLVD.  
GLEN ALLEN, VA 23060  
USA

J. BICKEL  
EG&G IDAHO, INC.  
P.O. BOX 1625, MS 2405  
IDAHO FALLS, ID 83415-2406  
USA

W. BINNER  
RES. CTR. SIEBERSDORF  
KRAMERGASSE 1  
VIENNA, A-1010  
AUSTRIA

D. BLAHNIK  
BATTELLE-PACIFIC NORTHWEST LABS.  
P.O. BOX 999  
RICHLAND, WA 99352  
USA

M. BOHN  
SANDIA NATIONAL LABORATORIES  
P.O. BOX 5800, DIVISION 8419  
ALBUQUERQUE, NM 87185  
USA

R. BOSCH  
FOSTER WHEELER ENERGY GROUP  
8 PEACH TREE HILL ROAD  
LIVINGSTON, NJ 07021  
USA

E. BOUCHERON  
SANDIA NATIONAL LABORATORIES  
P.O. BOX 5800, DIVISION 8418  
ALBUQUERQUE, NM 87185-8800  
USA

M. BOWMAN  
BALTIMORE GAS & ELECTRIC CO.  
P.O. BOX 1535  
LUSBY, MD 20657  
USA

B. BOYACK  
LOS ALAMOS NATIONAL LABORATORY  
P.O. BOX 1663, MS K551  
LOS ALAMOS, NM 87545  
USA

R. BOYD  
WESTINGHOUSE SAVANNAH RIVER COMPANY  
SAVANNAH RIVER SITE  
AIKEN, SC 29808  
USA

U. BREDOLT  
ABB ATOM  
BOX 53  
VASTERAS, 72163  
SWEDEN

C. BUCHHOLZ  
GENUCLEAR ENERGY  
175 CURTNER AVE, M/C 754  
SAN JOSE, CA 95125  
USA

R. BUDNITZ  
FUTURE RESOURCES ASSOCIATES INC  
2000 CENTER STREET, SUITE 418  
BERKELEY, CA 94704  
USA

J. BUTLER  
NUMARC  
1778 EYE STREET NW, SUITE 300  
WASHINGTON, DC 20008  
USA

N. BUTTERY  
NUCLEAR ELECTRIC P/C  
PWR PROJECT GROUP, BOOTH'S HALL,  
KNUTSFORD, CHESHIRE WA188QP  
UK

A. CAMP  
SANDIA NATIONAL LABORATORIES  
P.O. BOX 5800, DIVISION 6418  
ALBUQUERQUE, NM 87185  
USA

J. CAREW  
BROOKHAVEN NATIONAL LABORATORY  
BUILDING 475B  
UPTON, NY 11973  
USA

D. CASADA  
OAK RIDGE NATIONAL LABORATORY  
P.O. BOX 2009  
OAK RIDGE, TN 37831-8063  
USA

R. CHAMBERS  
EG&G IDAHO, INC.  
P.O. BOX 1825  
IDAHO FALLS, ID 83415-1580  
USA

F. CHANG  
ARGONNE NATIONAL LABORATORY  
9700 S. CASS AVENUE  
ARGONNE, IL 60439  
USA

S. CHAVEZ  
EG&G IDAHO, INC.  
P.O. BOX 1825 MS-2508  
IDAHO FALLS, ID 83404  
USA

C. CHEN  
GILBERT/COMMONWEALTH  
P.O. BOX 1498  
READING, PA 19603  
USA

S. CHENG  
INSTITUTE OF ENERGY RESEARCH, AEC  
P.O. BOX 3-3  
LUNG-TAN, 32500  
TAIWAN

R. CHEVERTON  
OAK RIDGE NATIONAL LABORATORY  
P.O. BOX 2009, BLDG 9204-1  
OAK RIDGE, TN 37831-8047  
USA

Q. CHOPRA  
ARGONNE NATIONAL LABORATORY  
9700 S. CASS AVENUE  
ARGONNE, IL 60439  
USA

S. CHOW  
STONE & WEBSTER ENG. CORP.  
#3 EXECUTIVE CAMPUS, ROUTE 70  
CHERRY HILL, NJ 08003  
USA

L. CHU  
BROOKHAVEN NATIONAL LABORATORY  
BUILDING 130  
UPTON, NY 11973  
USA

R. COLE, JR.  
SANDIA NATIONAL LABORATORIES  
P.O. BOX 5800, DIVISION 6418  
ALBUQUERQUE, NM 87185-5800  
USA

M. CONFLANT  
DIRECTORATE SAFETY INSTALLATION NUCLEAR  
CENFAR DRSN BP NO. 8  
FONTENAY-AUX-ROSES, 92265  
FRANCE

C. COOPER  
AEA TECHNOLOGY, WINFRITH  
WINFRITH TECHNOLOGY CENTRE  
DORCHESTER, DORSET DT2 8OH  
UK

J. COOPER  
MPR ASSOCIATES, INC  
1050 CONNECTICUT AVE, NW  
WASHINGTON, DC 20038  
USA

W. COPELAND  
WESTINGHOUSE SAVANNAH RIVER COMPANY  
SAVANNAH RIVER SITE  
AIKEN, SC 29808  
USA

E. CORLUS  
SANDIA NATIONAL LABORATORIES  
41 EAGLE TR  
TIJERAS, NM 87059  
USA

P. CORTICELLI  
ENEA  
VIA MARTIRI DI MONTESOLE  
BOLOGNA, 40100  
ITALY

W. CORWIN  
OAK RIDGE NATIONAL LABORATORY  
P.O. BOX 2008, BLDG 4500S  
OAK RIDGE, TN 37831-8151  
USA

D. COX  
OAK RIDGE NATIONAL LABORATORY  
P.O. BOX 2009  
OAK RIDGE, TN 37831-8038  
USA

K. COZENS  
NUMARC  
1778 EYE STREET NW, SUITE 300  
WASHINGTON, DC 20008  
USA

D. CRAMER  
WESTINGHOUSE SAVANNAH RIVER COMPANY  
SAVANNAH RIVER SITE  
AIKEN, SC 29808  
USA

R. CURTIS  
JUPITER CORPORATION  
15909 WHITE ROCK RD.  
GAITHERSBURG, MD 20878  
USA

D. DAHLGREN  
SANDIA NATIONAL LABORATORIES  
P.O. BOX 5800, DIVISION 6410  
ALBUQUERQUE, NM 87185  
USA

R. DAIL  
APTECH ENGINEERING SERVICES, INC  
9672 PENNSYLVANIA AVE  
UPPER MARLBORO, MD 20772  
USA

R. DALLMAN  
LNC ANALYTICAL SERVICES  
P.O. BOX 5400  
ALBUQUERQUE, NM 87185  
USA

P. DAMERELL  
MPR ASSOCIATES, INC  
1050 CONNECTICUT AVE, NW  
WASHINGTON, DC 20038  
USA

J. DANKO  
UNIV. OF TENNESSEE  
COLLEGE OF ENGINEERING, PERKINS HALL  
KNOXVILLE, TN 37996-2000  
USA

N. DAVIES  
AEA TECHNOLOGY  
RISLEY  
WARRINGTON, CHESHIRE WA3 6AT  
UK

M. DAVISTER  
U.S. DEPARTMENT OF ENERGY, DP-621  
19801 GERMANTOWN ROAD  
GERMANTOWN, MD 20874  
USA

B. DE L'EPINOIS  
DIRECTORATE SAFETY INSTALLATION NUCLEAR  
CENFAR DRSN BP NO. 8  
FONTENAY-AUX-ROSES, 92265  
FRANCE

R. DE WIT  
NATL INST. OF STANDARDS & TECHNOLOGY  
ROOM B144, MATERIALS BLDG.  
GAITHERSBURG, MD 20899  
USA

J. DEBOR  
SCIENCE APPLICATIONS INTL CORP.  
1710 GOODRIDGE DRIVE  
MCLEAN, VA 22102  
USA

R. DENNING  
BATTELLE COLUMBUS  
505 KING AVE.  
COLUMBUS, OHIO 43201  
USA

J. DEVOS  
CEA FRENCH ATOMIC ENERGY COMMISSION  
CEB SACLAY DMT/SEMT  
GIF SUR YVETTE, 91190  
FRANCE

K. DEWALL  
EG&G IDAHO, INC.  
P.O. BOX 1825  
IDAHO FALLS, ID 83404  
USA

H. DIETERSHAGEN  
KNOLLS ATOMIC POWER LAB, GENERAL ELEC.  
P.O. BOX 1072  
SCHENECTADY, NY 12301-1072  
USA

M. DIMARZO  
UNIVERSITY OF MARYLAND  
M.E. DEPT.  
COLLEGE PARK, MD 20742  
USA

C. DIPALO  
SCIENCE APPLICATIONS INTL. CORP.  
1710 GOODRIDGE DRIVE  
MCLEAN, VA 22102  
USA

S. DOCTOR  
BATTELLE-PACIFIC NORTHWEST LABS.  
P.O. BOX 899  
RICHLAND, WA 99352  
USA

M. DROUIN  
SCIENCE APPLICATIONS INTL. CORP.  
2109 AIR PARK RD., S. E.  
ALBUQUERQUE, NM 87106  
USA

R. DUFFEY  
BROOKHAVEN NATIONAL LABORATORY  
BUILDING 187C  
UPTON, NY 11973  
USA

R. DURANTE  
AECL TECHNOLOGIES  
15400 CALHOUN DRIVE, SUITE 100  
ROCKVILLE, MD 20855  
USA

K. DWIVEDI  
VIRGINIA POWER  
5000 DOMINION BLVD.  
GLEN ALLEN, VA 23060  
USA

J. EAST  
WESTINGHOUSE SAVANNAH RIVER COMPANY  
SAVANNAH RIVER SITE  
AIKEN, SC 29808  
USA

K. EBISAWA  
JAPAN ATOMIC ENERGY RES. INST  
TOKAI-MURA, NAKA-GUN  
IBARAKI-KEN, 319-11  
JAPAN

J. EDSON  
EG&G IDAHO, INC.  
P.O. BOX 1625  
IDAHO FALLS, ID 83415-2408  
USA

Z. ELAWAR  
ARIZONA PUBLIC SERVICE  
P.O. BOX 52034  
PHOENIX, AZ 85029  
USA

P. EMAIN  
ÉLECTRICITÉ DE FRANCE  
12-14, AVENUE DUTRIEVOZ  
VILLEURBANNE, 69628  
FRANCE

G. EMBLEY  
GENERAL ELECTRIC  
P.O. BOX 1072  
SCHENECTADY, NY 12301  
USA

B. ETTINGER  
MPR ASSOCIATES, INC  
1050 CONNECTICUT AVE, NW  
WASHINGTON, DC 20036  
USA

B. EVANS  
NUMARC  
1776 EYE STREET NW, SUITE 300  
WASHINGTON, DC 20006  
USA

R. FAKORY  
S3 TECHNOLOGIES  
8930 STANFORD BLVD.  
COLUMBIA, MD 21045  
USA

M. FELTUS  
PENN STATE UNIVERSITY  
231 SAKETT BLDG.  
UNIVERSITY PARK, PA 16802  
USA

R. FERCH  
ATOMIC ENERGY CONTROL BOARD  
P.O. BOX 1048, STATION B  
OTTAWA, ONTARIO KIP 5S9  
CANADA

M. FISCHER  
SIEMENS-KWJ  
LAMPERNBUHL 45  
ERLANGEN, W8520  
GERMANY

S. FLEGER  
SCIENCE APPLICATIONS INTL. CORP.  
1710 GOODRIDGE DRIVE  
MCLEAN, VA 22102  
USA

M. FONTANA  
OAK RIDGE NATIONAL LABORATORY  
P.O. BOX 2009  
OAK RIDGE, TN 37831-8063  
USA

T. FORTUNATO  
BETTIS ATOMIC POWER LABORATORY  
P.O. BOX 79  
WEST MIFLIN, PA 15122  
USA

E. FOX  
OAK RIDGE NATIONAL LABORATORY  
P.O. BOX 2009  
OAK RIDGE, TN 37831-8063  
USA

W. FRID  
SWEDISH NUCLEAR POWER INSPECTORATE  
P.O. BOX 27106  
STOCKHOLM, S-102 52  
SWEDEN

T. FUNAHASHI  
TOS-IEA CORPORATION  
& SHINSUGITA-CHO, ISOGO-KU  
YOKOHAMA, 235  
JAPAN

H. FURUKAWA  
HITACHI WORKS, HITACHI LTD.  
1-1, 3-CHOME, SAIWAI-CHO  
HITACHI-SHI, IBARAKI-KEN 317  
JAPAN

R. GAMBLE  
SARTREX CORP.  
1700 ROCKVILLE PIKE, STE. 400  
ROCKVILLE, MD 20852  
USA

D. GERTMAN  
EG&G IDAHO, INC.  
P.O. BOX 1625 MS-2405  
IDAHO FALLS, ID 83404  
USA

B. GILBERT  
EG&G IDAHO, INC.  
P.O. BOX 1825 MS-2405  
IDAHO FALLS, ID 83404  
USA

J. GLEASON  
WYLE LABORATORIES  
P.O. BOX 07-7777  
HUNTSVILLE, AL 35807-7777  
USA

M. GOMOLINSKI  
CEA FRENCH ATOMIC ENERGY COMMISSION  
321 RUE DE CHAVEVTON  
PARIS, 75012  
FRANCE

W. GRANT  
MPR ASSOCIATES, INC  
1050 CONNECTICUT AVE, NW  
WASHINGTON, DC 20036  
USA

R. GREENE  
OAK RIDGE NATIONAL LABORATORY  
P.O. BOX 2009  
OAK RIDGE, TN 37831-8038  
USA

E. GROUNDWATER  
SCIENCE APPLICATIONS INTL. CORP.  
1710 GOODRIDGE DRIVE  
MCLEAN, VA 22102  
USA

E. GROVE  
BROOKHAVEN NATIONAL LABORATORY  
BUILDING 130  
UPTON, NY 11973  
USA

T. HAKE  
SANDIA NATIONAL LABORATORIES  
P.O. BOX 5800, DIVISION 8412  
ALBUQUERQUE, NM 87185  
USA

R. HALL  
BROOKHAVEN NATIONAL LABORATORY  
BUILDING 130  
UPTON, NY 11973  
USA

R. HAMMERSLEY  
FAUSKE & ASSOCIATES  
16W070 W. 83RD ST  
BURR RIDGE, IL 60521  
USA

S. HAO  
BECHTEL  
9801 WASHINGTON BLVD.  
GAITHERSBURG, MD 20878-5356  
USA

F. HARPER  
SANDIA NATIONAL LABORATORIES  
P.O. BOX 5800, DIVISION 8413  
ALBUQUERQUE, NM 87185-5800  
USA

C. HARRISON  
ATOMIC ENERGY CONTROL BOARD  
270 ALBERT ST.  
OTTAWA, ONTARIO KIP 5S9  
CANADA

L. HARROP  
HM NUCLEAR INSTALLATIONS INSPECTORATE  
ST. PETERS HOUSE, BALLIOL ROAD  
BOOTLE, MERSEYSIDE L20 3LZ  
UK

E HARVEGO  
EG&G IDAHO, INC.  
P.O. BOX 1625  
IDAHO FALLS, ID 83415-2408  
USA

R. HARVEY  
YANKEE ATOMIC ELECTRIC CO.  
580 MAIN ST.  
BOLTON, MA 01740  
USA

H. HASHEMIAN  
AMS CORPORATION  
9111 CROSS PARK DRIVE  
KNOXVILLE, TN 37923  
USA

M. HASSAN  
BROOKHAVEN NATIONAL LABORATORY  
BUILDING 130  
UPTON, NY 11973  
USA

J. HAWTHORNE  
MATERIALS ENGINEERING ASSOCIATES  
9700-B MARTIN L. KING, JR. HWY  
LANHAM, MD 20706  
USA

N. HAYASHI  
NUPEC-NUCLEAR POWER ENGL. TEST CENTER  
3-17, 1-CHOME, TORANOMON, MINATO-KU  
TOKYO, 105  
JAPAN

G. HEDRICK  
DUKE ENGINEERING & SERVICES, INC  
P.O. BOX 1004, M/S ST02A  
CHARLOTTE, NC 28201-1004  
USA

S. HENRY  
BALTIMORE GAS & ELECTRIC CO.  
P.O. BOX 1535  
LUSBY, MD 20657  
USA

H. HEPER  
UNIVERSITY OF MARYLAND  
9314 CHERRY HILL ROAD #217  
COLLEGE PARK, MD 20740  
USA

D. HIDINGER  
GENERAL ELECTRIC  
P.O. BOX 1072  
SCHENECTADY, NY 12301  
USA

J. HIGGINS  
BROOKHAVEN NATIONAL LABORATORY  
BUILDING 130  
UPTON, NY 11973  
USA

P. HILL  
PENNSYLVANIA POWER & LIGHT  
TWO NORTH NINTH STREET  
ALLENTOWN, PA 18101  
USA

R. HOBBS  
EG&G IDAHO, INC.  
P.O. BOX 1625  
IDAHO FALLS, ID 83415-1560  
USA

N. HOBSON  
HM NUCLEAR INSTALLATIONS INSPECTORATE  
ST. PETERS HOUSE, BALLIOL ROAD  
BOOTLE, MERSEYSIDE L20 3LZ  
UK

L. HOCHREITER  
WESTINGHOUSE ELECTRIC  
PO BOX 355  
PITTSBURGH, PA 15230  
USA

S. HODGE  
OAK RIDGE NATIONAL LABORATORY  
P.O. BOX 2009  
OAK RIDGE, TN 37831-8057  
USA

P. HOFMANN  
KERNFORSCHUNGSZENTRUM KARLSRUHE  
P.O. BOX 3640  
KARLSRUHE, W-7500  
GERMANY

C. HOFMAYER  
BROOKHAVEN NATIONAL LABORATORY  
BUILDING 475C  
UPTON, NY 11973  
USA

P. HOLDEN  
AEATECH-NOLOGY  
RISLEY  
WARRINGTON, CHESHIRE WA3 62RQ  
UK

H. HOLMSTRÖM  
OECD NUCLEAR ENERGY AGENCY  
38, BOULEVARD SUCHET  
PARIS, F-75018  
FRANCE

R. HOPPE  
BETTS ATOMIC POWER LABORATORY  
P.O. BOX 79  
WEST MIFFLIN, PA 15122  
USA

Y. HORIKAWA  
THE KANSAI ELECTRIC POWER CO., INC.  
1100 17TH STREET, N.W., SUITE 500  
WASHINGTON, DC 20036  
USA

D. HORSCHEL  
SANDIA NATIONAL LABORATORIES  
P.O. BOX 5800, DIVISION 6473  
ALBUQUERQUE, NM 87185-5800  
USA

T. HSU  
VIRGINIA POWER  
5000 DOMINION BLVD.  
GLEN ALLEN, VA 23060  
USA

F. HSU  
BROOKHAVEN NATIONAL LABORATORY  
BUILDING 130  
UPTON, NY 11973  
USA

Y. HUANG  
INSTITUTE OF ENERGY RESEARCH, AEC  
P.O. BOX 3-3  
LUNG-TAN, 32500  
TAWAN

T. HUNT  
GULF STATES UTILITIES  
P.O. BOX 220  
ST. FRANCISVILLE, LA 70776  
USA

T. HUNT  
EG&G IDAHO, INC.  
P.O. BOX 1625  
IDAHO FALLS, ID 83415-2408  
USA

S. HYTEN  
WYLE LABORATORIES  
P.O. BOX 07-7777  
HUNTSVILLE, AL 35807-7777  
USA

S. INAMDAR  
ONTARIO HYDRO  
700 UNIVERSITY AVE.  
TORONTO, ONTARIO M5G 1X6  
CANADA

L. INNES  
ATOMIC ENERGY CONTROL BOARD  
270 ALBERT ST.  
OTTAWA, ONTARIO KIP 5S9  
CANADA

J. IRELAND  
LOS ALAMOS NATIONAL LABORATORY  
P.O. BOX 1663, MS K551  
LOS ALAMOS, NM 87545  
USA

H. ISBIN  
NRC-NSRRRC  
2815 MONTEREY PKWY  
ST. LOUIS PARK, MN 55418  
USA

J. ISHIGURO  
JAPAN NUS  
910 CLOPPER ROAD  
GAITHERSBURG, MD 20877  
USA

R. JACOBS  
PENN STATE UNIVERSITY  
DEPARTMENT OF PSYCHOLOGY  
UNIVERSITY PARK, PA 16802  
USA

M. JACOBUS  
SANDIA NATIONAL LABORATORIES  
P.O. BOX 5800, DIVISION 6419  
ALBUQUERQUE, NM 87185  
USA

J. JANSKY  
BTB-JANSKY  
GERLINGER STRASSE 151  
LEONBERG, 7250  
GERMANY

D. JARRELL  
BATTELLE-PACIFIC NORTHWEST LABS.  
P.O. BOX 999  
RICHLAND, WA 99352  
USA

J. JARVIS  
BECHTEL  
9801 WASHINGTON BLVD.  
GAITHERSBURG, MD 20878-5356  
USA

A. JIMENEZ  
CSN  
JUSTO DORADO 11  
MADRID, 28040  
SPAIN

G. JOHNSON  
EG&G IDAHO, INC.  
P.O. BOX 1625  
IDAHO FALLS, ID 83404  
USA

B. JOHNSON  
BATTELLE-PACIFIC NORTHWEST LABS.  
P.O. BOX 999  
RICHLAND, WA 99352  
USA

J. JONES  
OAK RIDGE NATIONAL LABORATORY  
P.O. BOX 2009  
OAK RIDGE, TN 37831-8083  
USA

K. JONES  
EG&G IDAHO, INC.  
P.O. BOX 1625 MS-2508  
IDAHO FALLS, ID 83404  
USA

C. JUPITER  
JUPITER CORPORATION  
SUITE 503 WHEATON PLAZA N, 2730 UNIVERSITY BLVD. WEST  
WHEATON, MD 20902  
USA

H. KARWAT  
TECHN. UNIV. MUNICH  
FORSCHUNGAREA  
GARCHING, BAVARIA W8048  
GERMANY

W. KASTENBERG  
UCLA  
48-121 ENGINEER IV  
LOS ANGELES, CA 90024  
USA

S. KATANISHI  
JAPAN ATOMIC ENERGY RES. INST  
TOKAI-MURA, NAKA-GUN  
IBARAKI-KEN, 319-11  
JAPAN

W. KATO  
BROOKHAVEN NATIONAL LABORATORY  
BUILDING 187C  
UPTON, NY 11973  
USA

S. KAWAKAMI  
NUPREC-NUCLEAR POWER ENG. TEST CENTER  
3-13, 4-CHOME, TORANOMON, MINATO-KU  
TOKYO, 105  
JAPAN

K. KAWANISHI  
MITSUBISHI HEAVY INDUSTRIES, LTD.  
2-1-1, SHINHAMA, ARAI-CHO  
TAKASAGO-SHI, HYOGO-KEN 678  
JAPAN

D. KELLY  
EG&G IDAHO, INC.  
P.O. BOX 1625 MS-2405  
IDAHO FALLS, ID 83404  
USA

J. KELLY  
SANDIA NATIONAL LABORATORIES  
P.O. BOX 5800, DIVISION 6401  
ALBUQUERQUE, NM 87185-5800  
USA

M. KHATIB-RAHBAR  
ENERGY RESEARCH, INC.  
PO BOX 2034  
ROCKVILLE, MD 20847  
USA

H-HO KIM  
KOREA INSTITUTE OF NUCLEAR SAFETY  
P.O. BOX 16 DAEDUK-DANJI  
DAEJON, 305353  
KOREA

H. KIM  
KAERI  
P.O. BOX 7 DAEDUK-DANJI  
DAEJON,  
KOREA

I. KIM  
BROOKHAVEN NATIONAL LABORATORY  
BUILDING 130  
UPTON, NY 11973  
USA

S. KINNERSLY  
AEA TECHNOLOGY, WINFRITH  
WINFRITH TECHNOLOGY CENTRE  
DORCHESTER, DORSET DT2 8DH  
UK

E. KINTNER  
NRC/RAC  
P.O. BOX 682  
NORWICH, VT 05055  
USA

P. KLOEG  
KEMA  
UTRECHTSEWEG 310  
ARNHEM, 6812 AR  
THE NETHERLANDS

G. KLOPP  
COMMONWEALTH EDISON  
1400 OPUS PLACE, SUITE 400  
DOWNERS GROVE, IL 60515  
USA

L. KMETKY  
SANDIA NATIONAL LABORATORIES  
P.O. BOX 5800, DIVISION 6418  
ALBUQUERQUE, NM 87185-5800  
USA

S. KOBAYASHI  
ISHIKAWAJIMA-HARIMA HEAVY INDUSTRIES  
1, SHIN-NAKAHARA-CHO, ISOGO-KU  
YOKOHAMA, 235  
JAPAN

T. KODAMA  
MITSUBISHI HEAVY INDUSTRIES, LTD.  
2-1-1, SHINHAMA, ARAI-CHO  
TAKASAGO-SHI, HYOGO-KEN 678  
JAPAN

E. KOHN  
ONTARIO HYDRO  
700 UNIVERSITY AVE.  
TORONTO, ONTARIO M5A  
CANADA

C. KOT  
ARGONNE NATIONAL LABORATORY  
9700 S. CASS AVENUE  
ARGONNE, IL 60439  
USA

P. KRISHNASWAMY  
BATTELLE COLUMBUS  
505 KING AVE.  
COLUMBUS, OHIO 43201  
USA

P. KUJAN  
EG&G IDAHO, INC.  
P.O. BOX 1625 MS-1580  
IDAHO FALLS, ID 83404  
USA

T. KUBOKOYA  
TOSHIBA CORPORATION  
8, SHINSUGITA-CHO, ISOGO-KU  
YOKOHAMA, 235  
JAPAN

Y. KUKITA  
JAPAN ATOMIC ENERGY RES. INST  
TOKAI-MURA, NAKA-GUN  
IBARAKI-KEN, 319-11  
JAPAN

M. KURIHARA  
MITSUBISHI HEAVY INDUSTRIES, LTD.  
4-1, 2-CHOME, SHIBAKOJEN, MINATO-KU  
TOKYO, 105  
JAPAN

Y. KUSAMA  
JAERI, TAKASAKI RAD. CHEM. RES. INST.  
1233 WATANUKI-MACHI  
TAKASAKI, GUNMA, 370-12  
JAPAN

K. KUSSMAUL  
MPA STUTTGART  
P.O. BOX 2009  
STUTTGART 80, D-7000  
GERMANY

J. LAKE  
EG&G IDAHO, INC.  
P.O. BOX 1625 MS-2507  
IDAHO FALLS, ID 83415-1660  
USA

M. LAMBERT  
ÉLECTICITÉ DE FRANCE  
12-14, AVENUE DUTRIEVOZ  
VILLEURBANNE, 69628  
FRANCE

F. LANDY  
PENN STATE UNIVERSITY  
RESEARCH BLDG. D  
UNIVERSITY PARK, PA 16802  
USA

D. LEAVER  
TENERA  
1340 SARATOGA-SUNNYVALE ROAD  
SAN JOSE, CA 95129  
USA

C. LECOMTE  
CEA FRENCH ATOMIC ENERGY COMMISSION  
CENFAR DRSN BP NO. 6  
FONTENAY-AUX-ROSES, 92265  
FRANCE

J. LEE  
KOREA INSTITUTE OF NUCLEAR SAFETY  
P.O. BOX 16 DAEDUK-DANJI  
DAEJON, 305353  
KOREA

S. LEE  
FAUSKE & ASSOCIATES  
18W070 W. 63RD ST  
BURR RIDGE, IL 60521  
USA

J. LEHNER  
BROOKHAVEN NATIONAL LABORATORY  
BUILDING 130  
UPTON, NY 11973  
USA

R. LIN  
LOS ALAMOS NATIONAL LABORATORY  
P.O. BOX 1663, MS K557  
LOS ALAMOS, NM 87545  
USA

M. LINDQUIST  
WESTINGHOUSE HANFORD CO.  
BOX 1970  
RICHLAND, WA 99352  
USA

M. LIVOLANT  
CEA FRENCH ATOMIC ENERGY COMMISSION  
CENFAR DRSN BP NO. 6  
FONTENAY-AUX-ROSES, 92265  
FRANCE

R. LOFARO  
BROOKHAVEN NATIONAL LABORATORY  
BUILDING 130  
UPTON, NY 11973  
USA

J. LOPEZ-MONTERO  
MADRID POLYTECHNICAL UNIVERSITY  
JOSE GUTIERREZ ABASCAL, 2  
MADRID, 28008  
SPAIN

F. LOSS  
MATERIALS ENGINEERING ASSOCIATES  
9700-B MARTIN L. KING, JR. HWY  
LANHAM, MD 20708  
USA

K. LYNCH  
GROVE ENGINEERING  
15215 SHADY GROVE RD., STE. 202  
ROCKVILLE, MD 20850  
USA

P. MacDONALD  
EG&G IDAHO, INC.  
P.O. BOX 1825  
IDAHO FALLS, ID 83415-2408  
USA

A. MacKINNEY  
NUMARC  
1778 EYE STREET NW, SUITE 300  
WASHINGTON, DC 20008  
USA

I. MADNI  
BROOKHAVEN NATIONAL LABORATORY  
BUILDING 130  
UPTON, NY 11973  
USA

D. MAGALLON  
CEC-JRC ISPRA  
JRC EURATOM ISPRA  
ISPRA, VARESE 21020  
ITALY

H. MAGLEBY  
EG&G IDAHO, INC.  
P.O. BOX 1825  
IDAHO FALLS, ID 83415-2408  
USA

M. MANAHAN  
PENN STATE UNIVERSITY  
231 SACKETT  
UNIVERSITY PARK, PA 16802  
USA

P. MANBECK  
BALTIMORE GAS & ELECTRIC CO.  
P.O. BOX 632  
LUSBY, MD 20657  
USA

R. MANDL  
SIEMENS/KWU  
HAMMERBACHENSTR 12  
ERLANGEN,  
GERMANY

J. MARRINUCCI  
GILBERET/COMMONWEALTH  
P.O. BOX 1498  
READING, PA 19603  
USA

P. MARSILI  
ENEA-DISP  
VIA V. BRANCATI, 48  
ROME, 00144  
ITALY

I. MASACKA  
HITACHI RESEARCH LABORATORY  
3-1, SAIWAI-CHO  
HITACHI-SHI, IBARAKI-KEN 317  
JAPAN

H. MASSIE  
DNF SAFETY BOARD  
825 INDIANA AVENUE, SUITE 700  
WASHINGTON, DC 20004  
USA

A. MATSUMOTO  
JAPAN ATOMIC ENERGY RES. INST  
TOKAI-MURA, NAKA-GUN  
IBARAKI-KEN, 319-11  
JAPAN

B. MAVKO  
J. STEFAN INSTITUTE  
JAMOVA 39  
LJUBLJANA, 61000  
SLOVENIA

B. MAVKO  
J. STEFAN INSTITUTE  
JAMOVA 39  
LJUBLJANA, 61000  
SLOVENIA

E. McCRAW  
DUKE ENGINEERING & SERVICES, INC  
P.O. BOX 1004, M/S ST02A  
CHARLOTTE, NC 28201-1004  
USA

W. McCURDY  
MPR ASSOCIATES, INC  
1050 CONNECTICUT AVE, NW  
WASHINGTON, DC 20036  
USA

D. McMULLAN  
KNOLLS ATOMIC POWER LAB, GENERAL ELEC.  
P.O. BOX 1072  
SCHENECTADY, NY 12301-1072  
USA

C. MEDICH  
SIET  
VIA NINO BIXIO N. 27  
PIACENZA, 29100  
ITALY

J. MEINCKE  
CONSUMERS POWER COMPANY  
27780 BLUE STAR HIGHWAY  
COVERT, MI 49043  
USA

B. MENKE  
MATERIALS ENGINEERING ASSOCIATES  
9700-B MARTIN L. KING, JR. HWY  
LANHAM, MD 20708  
USA

J. METCALF  
STONE & WEBSTER ENG. CORP.  
245 SUMMER STREET  
BOSTON, MA 02107  
USA

Y. MEYZAUD  
FRAMATOME  
TOUR FIAT CEDEX 18  
PARIS-LA-DEFENSE, 92084  
FRANCE

L. MILLER  
SCIENCE APPLICATIONS INTL. CORP.  
1710 GOODRIDGE DR  
MCLEAN, VA 22102  
USA

S. MIRSKY  
SCIENCE APPLICATIONS INTL. CORP.  
1710 GOODRIDGE DRIVE  
MCLEAN, VA 22102  
USA

D. MOEEN  
NUMARC  
1778 EYE STREET NW, SUITE 300  
WASHINGTON, DC 20008  
USA

S. MOORO  
EG&G IDAHO, INC.  
4417 S. HOLMES AVE.  
IDAHO FALLS, ID 83404  
USA

K. MCKI-TARIAN  
CBI TECHNICAL SERVICES  
800 JORIE BLVD.  
OAK BROOK, IL 60521  
USA

F. MOODY  
GENUCLEAR ENERGY  
175 CURTNER AVENUE  
SAN JOSE, CA 95125  
USA

N. MORAY  
UNIVERSITY OF ILLINOIS  
DEPT. OF MECH. & IE  
URBANA, IL 61801  
USA

D. MORRISON  
MPRE CORPORATION  
7525 COLSHIRE DRIVE  
MCLEAN, VA 22102  
USA

V. MUBAYI  
BROOKHAVEN NATIONAL LABORATORY  
BUILDING 130  
UPTON, NY 11973  
USA

M. MUHLHEIM  
OAK RIDGE NATIONAL LABORATORY  
P.O. BOX 2009, MS-8065  
OAK RIDGE, TN 37831-8065  
USA

M. MURASE  
HITACHI LTD.  
1188 MORIYAMA-CHO  
HITACHI-SHI, IBARAKI 318  
JAPAN

K. MURATA  
SANDIA NATIONAL LABORATORIES  
P.O. BOX 5800  
ALBUQUERQUE, NM 87185-5800  
USA

S. NAFF  
EG&G IDAHO, INC.  
P.O. BOX 1825  
IDAHO FALLS, ID 83415  
USA

H. NAGASAKI  
NUSPEC-NUCLEAR POWER ENG. TEST CENTER  
3-17-1-CHOME, TORANOMON, MINATO-KU  
TOKYO, 106  
JAPAN

T. NAKAYAMA  
HITACHI WORKS, HITACHI LTD.  
1-1, 3-CHOME, SAIWAI-CHO  
HITACHI-SHI, IBARAKI-KEN 317  
JAPAN

K. NAMATAME  
JAPAN ATOMIC ENERGY RES. INST  
TOKAI-MURA, NAKA-GUN  
IBARAKI-KEN, 319-11  
JAPAN

H. NARIAI  
UNIVERSITY OF TSUKUBA  
1-CHOME, TENNODAI  
TSUKUBA-SHI, IBARAKI-KEN 305  
JAPAN

D. NAUS  
OAK RIDGE NATIONAL LABORATORY  
P.O. BOX 2009  
OAK RIDGE, TN 37831-8063  
USA

C. NEGIN  
GROVE ENGINEERING  
15215 SHADY GROVE RD., STE. 202  
ROCKVILLE, MD 20850  
USA

A. NELSON  
US GEOLOGICAL SURVEY  
P.O. BOX 25046  
DENVER, CO 80225  
USA

W. NELSON  
EG&G IDAHO, INC.  
PO BOX 1625  
IDAHO FALLS, ID 83415  
USA

S. NESBIT  
DUKE ENGINEERING & SERVICES, INC  
600 MARYLAND AVE., SW, SUITE 890  
WASHINGTON, DC 20024  
USA

J. NESTELL  
MPR ASSOCIATES, INC  
1050 CONNECTICUT AVE, NW  
WASHINGTON, DC 20036  
USA

MAW NI  
ATOMIC ENERGY COUNCIL  
87 LANE 144 KEELUNG RD, SECT 4  
TAIPEI, TAIWAN  
ROC

M. NICHOLS  
UNIVERSITY OF MINNESOTA  
271 19TH AVE SOUTH  
MINNEAPOLIS, MN 55455  
USA

T. NISHIMOTO  
JAPAN ELEC. POWER INFORMATION CENTER  
1728 M ST., NW, STE. 403  
WASHINGTON, DC 20036  
USA

H. NIU  
ATOMIC ENERGY COUNCIL  
87 LANE 144 KEELUNG RD, SECT 4  
TAIPEI, TAIWAN 10772  
ROC

A. NONAKA  
NUPEC-NUCLEAR POWER ENG. TEST CENTER  
3-13, 4-CHOME, TORANOMON, MINATO-KU  
TOKYO, 105  
JAPAN

H. NOURBAKHSH  
BROOKHAVEN NATIONAL LABORATORY  
BUILDING 130  
UPTON, NY 11973  
USA

J. O'BRIEN  
EG&G IDAHO, INC.  
301 RANCH DR.  
IDAHO FALLS, ID 83404  
USA

D. O'MALLEY  
TITAN CORP.  
4201 CATHEDRAL AVE, NW APT 1410W  
WASHINGTON, DC 20016  
USA

S. OBERMEYER  
US GEOLOGICAL SURVEY  
922 NATIONAL CENTER  
RESTON, VA 22092  
USA

Y. OCHI  
COMPUTER SOFTWARE DEVELOPMENT  
2-4-1, SHIBA KOEN  
TOKYO, MINATO-KU 105  
JAPAN

R. OLETTE  
UNIVERSITY OF CALIFORNIA, SANTA BARBARA  
DEPT. OF CHEM. & NUCLEAR ENGINEER  
SANTA BARBARA, CA 93106  
USA

B. OLAND  
OAK RIDGE NATIONAL LABORATORY  
P.O. BOX 2009  
OAK RIDGE, TN 37831-8063  
USA

R. OLMSTEAD  
AEOL RESEARCH  
CHALK RIVER LABORATORY  
CHALK RIVER, ONTARIO K0J1J0  
CANADA

R. OLSON  
BALTIMORE GAS & ELECTRIC CO.  
P.O. BOX 1535  
LUSBY, MD 20657  
USA

A. ONYEMAECHI  
S3 TECHNOLOGIES  
8930 STANFORD BLVD.  
COLUMBIA, MD 21045  
USA

M. ORTIZ  
EG&G IDAHO, INC.  
P.O. BOX 1625 M/S 2404  
IDAHO FALLS, ID 83415-2402  
USA

L. OTT  
OAK RIDGE NATIONAL LABORATORY  
P.O. BOX 2009  
OAK RIDGE, TN 37831-8057  
USA

N. PAL  
PAL CONSULTANTS, INC.  
1885 THE ALAMEDA STREET 100H  
SAN JOSE, CA 95128  
USA

D. PALMROSE  
EG&G IDAHO, INC.  
P.O. BOX 1625 M/S 2404  
IDAHO FALLS, ID 83415-2412  
USA

F. PANISKO  
BATTELLE-PACIFIC NORTHWEST LABS.  
P.O. BOX 999  
RICHLAND, WA 99352  
USA

M. PARADIES  
SYSTEM IMPROVEMENTS, INC.  
236 PETERS ROAD, SUITE 301  
KNOXVILLE, TN 37923  
USA

S. PARISH  
COUNCIL FOR NUCLEAR SAFETY  
P.O. BOX 7106  
HENNOPSMEER, 0046  
SOUTH AFRICA

M. PARKS  
SANDIA NATIONAL LABORATORIES  
P.O. BOX 5800, DIVISION 6473  
ALBUQUERQUE, NM 87185-5800  
USA

W. PASEDAG  
U. S. DEPARTMENT OF ENERGY  
NE-42  
WASHINGTON, DC 20585  
USA

M. PATTERSON  
SCIENITECH, INC  
11821 PARKLAWN DRIVE  
ROCKVILLE, MD 20852  
USA

P. PAUL  
DUKE POWER CO.  
P.O. BOX 1006  
CHARLOTTE, NC 28201  
USA

A. PAYNE, JR.  
SANDIA NATIONAL LABORATORIES  
P.O. BOX 5800, DIVISION 8412  
ALBUQUERQUE, NM 87185-5800  
USA

W. PENNELL  
OAK RIDGE NATIONAL LABORATORY  
P.O. BOX 2009  
OAK RIDGE, TN 37831-8056  
USA

K. PEREIRA  
ATOMIC ENERGY CONTROL BOARD  
P.O. BOX 1046, STATION B  
OTTAWA, ONTARIO KIP 5S9  
CANADA

G. PEREZ  
CNSNS-MEXICO  
AV. INSURGENTES SUR. 1776  
MEXICO CITY, 01030  
MEXICO

G. PETRANGELO  
ENEA-DISP  
VIA V. BRANCATI, 48  
ROME, 00144  
ITALY

J. PHILLIPS  
EG&G IDAHO, INC.  
P.O. BOX 1625 MS-2406  
IDAHO FALLS, ID 83415-1660  
USA

L. PHILPOT  
GILBERT/COMMONWEALTH  
P.O. BOX 1498  
READING, PA 19603  
USA

B. PIKUL  
MITRE CORPORATION  
7525 COLSHIRE DRIVE  
MCLEAN, VA 22102  
USA

G. PNO  
ENEA-DISP  
VIA V. BRANCATI, 48  
ROME, 00144  
ITALY

M. PODOWSKI  
RPI, TROY NEW YORK  
DEPT. OF NUCLEAR ENGINEERING  
TROY, NY 12180-3592  
USA

S. POPE  
HALLIBURTON NUS  
18804 LINDENHOUSE RD.  
GAITHERSBURG, MD 20879  
USA

L. PRICE  
EG&G IDAHO, INC.  
P.O. BOX 1625  
IDAHO FALLS, ID 83415-2408  
USA

J. PUGA  
UNESA  
FLO. GERVAS 3  
MADRID, 28020  
SPAIN

C. PUGH  
OAK RIDGE NATIONAL LABORATORY  
P.O. BOX 2009, MS 8063  
OAK RIDGE, TN 37822  
USA

D. RAKOVICH  
ONTARIO HYDRO  
700 UNIVERSITY AVE.  
TORONTO, ONTARIO M5G 1X8  
CANADA

J. RANTAKIVI  
FINNISH CENTRE FOR RAD. & NUCL. SAFETY  
P.O. BOX 268  
HELSINKI, SF-00101  
FINLAND

W. REECE  
EG&G IDAHO, INC.  
P.O. BOX 1625 MS-2405  
IDAHO FALLS, ID 83404  
USA

J. REMPE  
EG&G IDAHO, INC.  
P.O. BOX 1625 MS-2508  
IDAHO FALLS, ID 83404  
USA

M. REDCREUX  
CEA FRENCH ATOMIC ENERGY COMMISSION  
CEN CADARACHE DRASSEMAR  
ST PAUL LEZ DURANCE, 13108  
FRANCE

W. RETTIG  
U. S. DEPARTMENT OF ENERGY  
785 DOE PLACE  
IDAHO FALLS, ID 83402  
USA

L. RIB  
AECL TECHNOLOGIES  
15400 CALHOUN DRIVE, SUITE 100  
ROCKVILLE, MD 20855  
USA

M. RIGHTLEY  
SANDIA NATIONAL LABORATORIES  
P.O. BOX 5800, DIVISION 8463  
ALBUQUERQUE, NM 87185-5800  
USA

G. ROBINSON  
PENN STATE UNIVERSITY  
231 SAKETT BLDG.  
UNIVERSITY PARK, PA 16802  
USA

U. ROHATGI  
BROOKHAVEN NATIONAL LABORATORY  
BUILDING 475B  
UPTON, NY 11973  
USA

G. ROMBOLD  
NUMARC  
1778 EYE STREET NW, SUITE 300  
WASHINGTON, DC 20006  
USA

A. ROOSEBOOM  
SZW/NUCLEAR SAFETY DEPARTMENT  
KERSENGAARDE 215  
VOORBURG, 2272ND  
THE NETHERLANDS

E. ROTH  
WESTINGHOUSE  
1310 BEULAH ROAD  
PITTSBURGH, PA 15217  
USA

H. RYALS  
BETTIS ATOMIC POWER LABORATORY  
P.O. BOX 79  
WEST MIFLIN, PA 15122  
USA

B. SAFFELL  
BATTELLE COLUMBUS  
505 KINE AVE.  
COLUMBUS, OH 43201  
USA

R. SALIZZONI  
WESTINGHOUSE SAVANNAH RIVER COMPANY  
SAVANNAH RIVER SITE  
AIKEN, SC 29802  
USA

P. SAMANTA  
BROOKHAVEN NATIONAL LABORATORY  
BUILDING 130  
UPTON, NY 11973  
USA

R. SAMMATARO  
GENERAL DYNAMICS  
75 EASTERN POINT ROAD  
GROTON, CT 06340  
USA

J. SANCHEZ  
CSN  
JUSTO DORADO 11  
MADRID, 28040  
SPAIN

O. SANDERVAG  
SWEDISH NUCLEAR POWER INSPECTORATE  
P.O. BOX 27108  
STOCKHOLM, S-102 52  
SWEDEN

L. SANTOMA  
CSN  
JUSTO DORADO 11  
MADRID, 28040  
SPAIN

M. SARRAM  
UNITED ENGINEERS  
30 S. 17TH ST.  
PHILADELPHIA, PA 19101  
USA

K. SATO  
HITACHI LTD  
3-1-1 SAIWAI-CHO  
HITACHI-SHI, IBARAKI-KEN 317  
JAPAN

R. SCHMIDT  
BATTELLE COLUMBUS  
505 KING AVE.  
COLUMBUS, OHIO 43201  
USA

R. SCHNEIDER  
ABB/C-E  
1000 PROSPECT HILL ROAD  
WINDSOR, CT 06095  
USA

G. SCHLUECKTANZ  
UNIVERSAL TESTING LABORATORIES  
5959 SHALLOWFORD RD., SUITE 531  
CHATANOOGA, TN 37421  
USA

E. SCHULTZ  
INDUSTRIAL POWER CO. LTD -TVO  
27180 OLKILUOTO  
SUOMI, SF-27180  
FINLAND

G. SCHWARZ  
ATOMIC ENERGY CONTROL BOARD  
270 ALBERT ST.  
OTTAWA, ONTARIO K1P 5S9  
CANADA

W. SEDDON  
HM NUCLEAR INSTALLATIONS INSPECTORATE  
ST. PETERS HOUSE, BALLIOL ROAD  
BOOTLE, MERSEYSIDE L20 3LZ  
UK

B. SEHGAL  
ELECTRIC POWER RESEARCH INSTITUTE  
3412 HILLVIEW AVE, P.O. BOX 10412  
PALO ALTO, CA 94303  
USA

S. SERHAN  
GILBERT/COMMONWEALTH  
P.O. BOX 1498  
READING, PA 19603  
USA

S. SETH  
MITRE CORPORATION  
7525 COLSHIRE DRIVE  
MCLEAN, VA 22102  
USA

W. SHA  
ARGONNE NATIONAL LABORATORY  
9700 S. CASS AVENUE  
ARGONNE, IL 60439  
USA

W. SHACK  
ARGONNE NATIONAL LABORATORY  
9700 S. CASS AVENUE, BLDG 212  
ARGONNE, IL 60439  
USA

R. SHARMA  
AMERICAN ELECTRIC POWER  
ONE RIVERSIDE PLAZA  
COLUMBUS, OHIO 43215  
USA

A. SHARON  
QUANTUM TECHNOLOGIES  
2825 BUTTERFIELD RD.  
CAK BROOK, IL 60521  
USA

K. SHIBA  
JAPAN ATOMIC ENERGY RES. INST  
TOKAI-MURA, NAKA-GUN  
IBARAKI-KEN, 319-11  
JAPAN

J. SHIN  
EBASCO SERVICES, INC.  
TWO WORLD TRADE CENTER  
NEW YORK, NY 10048  
USA

J. SIENICKI  
ARGONNE NATIONAL LABORATORY  
9700 S. CASS AVENUE, BLDG 208  
ARGONNE, IL 60439  
USA

F. SIMONM  
BATTELLE-PACIFIC NORTHWEST LABS.  
P.O. BOX 999  
RICHLAND, WA 99352  
USA

A. SIMPKINS  
WESTINGHOUSE SAVANNAH RIVER COMPANY  
SAVANNAH RIVER SITE  
AIKEN, SC 29808  
USA

C. SLATER  
EG&G IDAHO, INC.  
P.O. BOX 1625  
IDAHO FALLS, ID 83404  
USA

G. SLAUGHTER  
OAK RIDGE NATIONAL LABORATORY  
P.O. BOX 2008, BLDG 4500S  
OAK RIDGE, TN 37831-6152  
USA

S. SLOAN  
EG&G IDAHO, INC.  
PO BOX 1625  
IDAHO FALLS, ID 83415  
USA

G. SLOVAK  
BROOKHAVEN NATIONAL LABORATORY  
BUILDING 475B  
UPTON, NY 11973  
USA

L. SMITH  
LOS ALAMOS NATIONAL LABORATORY  
P.O. BOX 1663, MS E561  
LOS ALAMOS, NM 87544  
USA

K. SODA  
JAPAN ATOMIC ENERGY RES. INST  
TOKAI-MURA, NAKA-GUN  
IBARAKI-KEN, 319-11  
JAPAN

M. SOEJIMA  
MITSUBISHI HEAVY INDUSTRIES, LTD.  
1-1,1-CHOME,WADASAKI-CHO,HYOGO-KU  
KOBE-SHI, 652  
JAPAN

C. SORRELL  
VIRGINIA POWER  
5000 DOMINION BLVD.  
GLEN ALLEN, VA 23060  
USA

W. SPEZIALETTI  
WESTINGHOUSE SAVANNAH RIVER COMPANY  
37 VARDEN DRIVE  
AIKEN, SC 29803  
USA

K. STAHLKOPF  
ELECTRIC POWER RESEARCH INSTITUTE  
3412 HILLVIEW AVE, P.O. BOX 10412  
PALO ALTO, CA 94303  
USA

R. STARCK  
MPR ASSOCIATES, INC  
1050 CONNECTICUT AVE, NW  
WASHINGTON, DC 20036  
USA

M. STRAND  
JUPITER CORPORATION  
2730 UNIVERSITY BLVD. WEST, #403  
WHEATON, MD 22092  
USA

D. STRAWSON  
MPR ASSOCIATES, INC  
1050 CONNECTICUT AVE, NW  
WASHINGTON, DC 20036  
USA

E. STUBBE  
TRACTEBEL  
AV. ARIANE 7  
BRUSSELS, B-1200  
BELGIUM

M. SUBUDHI  
BROOKHAVEN NATIONAL LABORATORY  
BUILDING 130  
UPTON, NY 11973  
USA

K. SUH  
FALUSKE & ASSOCIATES  
18W070 W. 83RD ST  
MURR RIDGE, IL 60521  
USA

R. SUMMERS  
SANDIA NATIONAL LABORATORIES  
P.O. BOX 5800, DIVISION 6418  
ALBUQUERQUE, NM 87185-5800  
USA

J. SUN  
ARGONNE NATIONAL LABORATORY  
9700 S. CASS AVENUE  
ARGONNE, IL 60439  
USA

M. TAEBI  
S3 TECHNOLOGIES  
8930 STANFORD BLVD.  
COLUMBIA, MD 21045  
USA

H. TAKEDA  
NUPEC-NUCLEAR POWER ENG. TEST CENTER  
3-13,4-CHOME,TORANOMON,MINATO-KU  
TOKYO, 105  
JAPAN

K. TAKUMI  
NUPEC-NUCLEAR POWER ENG. TEST CENTER  
3-13,4-CHOME,TORANOMON,MINATO-KU  
TOKYO, 105  
JAPAN

J. TAYLOR  
BROOKHAVEN NATIONAL LABORATORY  
BUILDING 130  
UPTON, NY 11973  
USA

T. THEOFANOUS  
UNIVERSITY OF CALIFORNIA, SANTA BARBARA  
6740 CORTONE DR.  
SAN GOLETA, CA 93117  
USA

W. THOMAS  
QUANTUM TECHNOLOGY, INC.  
2625 BUTTERFIELD RD.  
OAK BROOK, IL 60521  
USA

S. THOMPSON  
SANDIA NATIONAL LABORATORIES  
P.O. BOX 5800, DIVISION 6418  
ALBUQUERQUE, NM 87185-5800  
USA

H. THORNBERG  
ABB ATOM, INC.  
901 S. WARFIELD DRIVE  
MT. AIRY, MD 21771  
USA

J. TILLS  
JACK TILLS & ASSOCIATES, INC.  
PO BOX 549  
SANDIA PARK, NM 87047  
USA

D. TONG  
AEA TECHNOLOGY, SPD  
WIGSHAW LANE  
CULCHETH, CHESHIRE WA3 4NE  
UK

T. TRAN  
WESTINGHOUSE SAVANNAH RIVER COMPANY  
SAVANNAH RIVER SITE  
AIKEN, SC 29808  
USA

P. TROY  
NEWMAN & HOLTZINGER  
1615 L STREET, N.W.  
WASHINGTON, DC 20036  
USA

J. TUCCIARONE  
WESTINGHOUSE SAVANNAH RIVER COMPANY  
SAVANNAH RIVER SITE  
AIKEN, SC 29808  
USA

M. TUTTLE  
LAMONT-DOHERTY GEOLOGICAL OBS.  
COLUMBIA UNIVERSITY  
PALISADES, NY 10964  
USA

K. UMEKI  
NUPEC-NUCLEAR POWER ENG. TEST CENTER  
3-13,4-CHOME,TORANOMON,MINATO-KU  
TOKYO, 105  
JAPAN

L. UNGER  
SYSTEM IMPROVEMENTS  
238 PETERS BLVD., SUITE 301  
KNOXVILLE, TN 37923  
USA

R. VALENTIN  
ARGONNE NATIONAL LABORATORY  
9700 S. CASS AVENUE, BLDG 308  
ARGONNE, IL 60439  
USA

S. VAN HEMEL  
STAR MOUNTAIN, INC.  
113 CLERMONT AVENUE  
ALEXANDRIA, VA 22304  
USA

J. VEEDER  
AECL RESEARCH  
CHALK RIVER LABORATORY  
CHALK RIVER, ONTARIO K0J1J0  
CANADA

R. VOGEL  
CONSULTANT  
2081 ROBIN HOOD LANE  
LOS ALTOS, CA 94024  
USA

W. VON RIESEMANN  
SANDIA NATIONAL LABORATORIES  
P.O. BOX 5800, DIVISION 6473  
ALBUQUERQUE, NM 87185-5800  
USA

R. VOSS  
WESTINGHOUSE SAVANNAH RIVER COMPANY  
SAVANNAH RIVER SITE  
AIKEN, SC 29808  
USA

B. WALSH  
SCIENCE & ENGINEERING ASSOCIATES, INC.  
8100 UPTOWN BLVD., NE  
ALBUQUERQUE, NM 87110  
USA

D. WALTERS  
NUMARC  
1778 EYE STREET NW, SUITE 300  
WASHINGTON, DC 20006  
USA

S. WANG  
INSTITUTE OF ENERGY RESEARCH, AEC  
P.O. BOX 3-3  
LUNG-TAN, 32500  
TAIWAN

L. WARD  
EG&G  
11426 ROCKVILLE PIKE, SUITE 300  
ROCKVILLE, MD 20852  
USA

K. WASHINGTON  
SANDIA NATIONAL LABORATORIES  
P.O. BOX 5800, DIVISION 6429  
ALBUQUERQUE, NM 87185-5800  
USA

R. WATSON  
SANDIA NATIONAL LABORATORIES  
P.O. BOX 5800, DIVISION 6473  
ALBUQUERQUE, NM 87185-5800  
USA

J. WERNER  
U. S. DEPARTMENT OF ENERGY  
785 DOE PLACE  
IDAHO FALLS, ID 83402  
USA

P. WHEATLEY  
EG&G IDAHO, INC.  
P.O. BOX 1625 M/S 2412  
IDAHO FALLS, ID 83415-2412  
USA

D. WHITEHEAD  
SANDIA NATIONAL LABORATORIES  
P.O. BOX 5800, DIVISION 6412  
ALBUQUERQUE, NM 87185  
USA

B. WHITESEL  
NUMARC  
1778 EYE STREET NW, SUITE 300  
WASHINGTON, DC 20006  
USA

K. WHITT  
SOUTHERN NUCLEAR  
40 INVERNESS CENTER PARKWAY  
BIRMINGHAM, AL 35201  
USA

G. WILKOWSKI  
BATTELLE COLUMBUS  
505 KING AVE.  
COLUMBUS, OHIO 43201  
USA

K. WILLIAMS  
SCIENCE APPLICATIONS INTL. CORP.  
2109 AIR PARK RD., S. E.  
ALBUQUERQUE, NM 87108  
USA

J. WILSON  
AEA TECHNOLOGY  
HARWELL LABORATORY  
DIDLOT, OXFORDSHIRE OX11 0RA  
UK

H. WINGO  
WESTINGHOUSE SAVANNAH RIVER COMPANY  
SAVANNAH RIVER SITE  
AIKEN, SC 29808  
USA

G. WIRE  
WESTINGHOUSE  
5893 KEYSTONE DR.  
BETHEL PARK, PA 15102  
USA

F. WITT  
WESTINGHOUSE  
P.O. BOX 2728  
PITTSBURGH, PA 15230-2728  
USA

M. WITTE  
LAWRENCE LIVERMORE NATIONAL LAB  
P.O. BOX 808, L-198  
LIVERMORE, CA 94550  
USA

L. WOLF  
KIK/PMDR, BATTELLE-EUROPE  
POSTFACH 900180, AM ROMESHOF 35  
FRANKFURT AM MAIN 90, 6000  
GERMANY

L. WOLF  
NATIONAL ACADEMY OF SCIENCE  
2101 CONSTITUTION AVENUE NW  
WASHINGTON, DC 20418  
USA

N. WOODY  
WESTINGHOUSE SAVANNAH RIVER COMPANY  
SAVANNAH RIVER SITE  
AIKEN, SC 29808  
USA

W. WULFF  
BROOKHAVEN NATIONAL LABORATORY  
BUILDING 475B  
UPTON, NY 11973  
USA

M. YOKOTA  
TOKYO ELECTRIC POWER  
1901 1ST N.W. SUITE 720  
WASHINGTON, DC 20036  
USA

K. YOON  
B&W NUCLEAR SERVICE  
PO BOX 10935  
LYNCHBURG, VA 24503  
USA

R. YOUNGBLOOD  
BROOKHAVEN NATIONAL LABORATORY  
BUILDING 130  
UPTON, NY 11973  
USA

G. ZIGLER  
SCIENCE & ENGINEERING ASSOCIATES, INC.  
8100 UPTOWN BLVD., NE  
ALBUQUERQUE, NM 87110  
USA

F. ZIKRIA  
HALLIBURTON NUS CORP  
910 KLOPPER ROAD  
GAITHERSBURG, MD 20878  
USA

P. ZIOLA  
C & P ENGINEERING  
5408 NEWINGTON ROAD  
BETHESDA, MD 20816  
USA

R. ZOGRAN  
MPR ASSOCIATES, INC  
1050 CONNECTICUT AVE, NW  
WASHINGTON, DC 20036  
USA

P. ZWICKY  
BASLER & HOFMANN  
FORCHSTRASSE 396  
ZURICH, 8029  
SWITZERLAND

**PROCEEDINGS OF THE  
NINETEENTH WATER REACTOR SAFETY INFORMATION MEETING  
October 28-30, 1991**

**CONTENTS - VOLUME 1**

	<u>Page</u>
ABSTRACT .....	iii
GENERAL INDEX .....	v
REGISTERED ATTENDEES .....	vii
<u>Plenary Session</u>	
Opening Remarks .....	1
E. Beckjord, Director (RES/NRC)	
Five Priorities for the Future of Nuclear Power in this Country .....	3
I. Selin, Chairman (NRC)	
Accomplishments and Prospects .....	9
E. Beckjord, Director (RES/NRC)	
<u>Pressure Vessel and Piping Integrity</u> Chairman: C.Z. Serpan, Jr.	
Heavy-Section Steel Technology Program: Recent Developments in Crack Initiation and Arrest Research .....	29
W. Pennell (ORNL)	
Pipe Fracture Behavior Under High-Rate (Seismic) Loading -- the IPIRG Program .....	53
R. Schmidt et al. (Battelle)	
Short Cracks in Piping and Piping Welds .....	73
G. Wilkowski et al. (Battelle)	
Heavy-Section Steel Irradiation Program: Embrittlement Issues .....	97
W. Corwin (ORNL)	
<u>Metallurgy &amp; NDE</u> Chairman: C.Z. Serpan, Jr.	
Fatigue and Environmentally Assisted Cracking in Light Water Reactors .....	127
T. Kassner et al. (ANL)	
Estimation of Mechanical Properties of Cast Stainless Steels During Thermal Aging in LWR Systems .....	151
O. Chopra (ANL)	

## CONTENTS - VOLUME 1 (Cont'd)

	<u>Page</u>
Mechanical-Property Degradation of Cast Stainless Steel Components from the Shippingport Reactor . . . . .	179
O. Chopra (ANL)	
Progress in Evaluation and Improvement in Nondestructive Examination Reliability For Inservice Inspection of Light Water Reactors (LWRs) and Characterizing Fabrication Flaws in Reactor Pressure Vessels . . . . .	197
S. Doctor et al. (PNL)	
Validation and Transfer of Advanced NDE Technologies . . . . .	219
S. Doctor (PNL)	
 <u>Aging &amp; Components I</u> Chairman: G. Weidenhamer  	
Aging Studies of 1E Power and Reactor Protection Systems and Transformers . . . . .	235
J. Edson, V. Sharma, E. Roberts (INEL)	
New Method for Detecting Degradation in Installed Cables in Nuclear Power Plants . . . . .	261
Y. Kusama, T. Yagi, Y. Morita (JAERI) S. Kamimura, H. Yagyu (Hatchi Cable)	
Detecting and Mitigating Aging in Component Cooling Water Systems . . . . .	275
R. Lofaro (BNL)	
The Effects of Aging on Friction of MOVs . . . . .	289
T. Hunt, U. Sinha (INEL)	
NRC Test Results and Operations Experience Provide Insights for a New Gate Valve Stem Force Correlation . . . . .	307
J. Watkins, R. Steele, K. DeWall (INEL)	
Applications And Extensions of Degradation Modeling . . . . .	331
F. Hsu, M. Subudhi, P. Samanta (BNL) W. Vesely (SAIC)	

## CONTENTS - VOLUME 1 (Cont'd)

	<u>Page</u>
<u>Aging &amp; Components II</u> Chairman: J. Burns	
Aging Assessment of BWR Control Rod Drive Systems . . . . .	343
R. Greene (ORNL)	
The Effect of Aging Upon CE and B&W Control Rod Drives . . . . .	363
E. Grove, W. Gunther (BNL)	
Aging Related Degradation in Turbine Drives and Governors for Safety Related Pumps . . . . .	375
D. Cox (ORNL)	
Aging, Condition Monitoring, and Loss-of-Coolant Accident (LOCA) Tests of Class 1E Electrical Cables: Summary of Results . . . . .	383
M. Jacobus (SNL)	
Effects of Aging on Calibration and Response Time of Nuclear Plant Pressure Transmitters . . . . .	399
H. Hashemian (AMS)	
Snubber Aging Assessment: Results of NPAR Phase II In-Plant Research . . . . .	419
D. Blahnik, E. Werry (PNL)	
D. Brown (Lake Engineering)	
<u>Probabilistic Risk Assessment Topics</u> Chairman: J. Johnson	
Preliminary Results of the PWR Low Power and Shutdown Accident Frequencies Program - Coarse Screening Analysis for Surry . . . . .	429
T-L Chu et al. (BNL)	
N. Siu (MIT)	
Status of the Low Power and Shutdown Accident Sequence Analysis Project for the Grand Gulf Nuclear Power Station . . . . .	435
D. Whitehead, B. Staple, T. Brown (SNL)	
J. Darby, B. Walsh (SEA)	
Integrated Level III Risk Assessment for the LaSalle Unit 2 Nuclear Power Plant . . . . .	449
A. Payne Jr., T. Brown, L. Miller (SNL)	
Risk-Based Performance Indicators . . . . .	473
M. Azarm (BNL)	
W. Vesely (SAIC)	

**CONTENTS - VOLUME 1 (Cont'd)**

	<u>Page</u>
<b>Intersystem LOCA Risk Assessment: Methodology and Results</b> .....	<b>481</b>
<b>W. Gaylean et al. (INEL)</b>	
1. Introduction	
2. Methodology	
3. Results	
4. Conclusions	
5. References	
6. Appendix A	
7. Appendix B	
8. Appendix C	
9. Appendix D	
10. Appendix E	
11. Appendix F	
12. Appendix G	
13. Appendix H	
14. Appendix I	
15. Appendix J	
16. Appendix K	
17. Appendix L	
18. Appendix M	
19. Appendix N	
20. Appendix O	
21. Appendix P	
22. Appendix Q	
23. Appendix R	
24. Appendix S	
25. Appendix T	
26. Appendix U	
27. Appendix V	
28. Appendix W	
29. Appendix X	
30. Appendix Y	
31. Appendix Z	

**Opening Remarks  
19th Water Reactor Safety Meeting  
Eric S. Beckjord, Director  
Office of Nuclear Regulatory Research  
U.S. Nuclear Regulatory Commission**

**October 28, 1991**

I am very pleased with the large attendance at this meeting, including foreign visitors. I expect before the meeting ends there will be perhaps 500 people who will have been in attendance. I want to welcome all those who are working on and are interested in reactor safety research and I note that this is an excellent opportunity to hear reports of the work underway and also for questions and answers on the work that you hear reported. It's an opportunity for exchange of ideas and to find out what is going on in this field of nuclear reactor safety. You have three days ahead of you of technical sessions that span all of the areas that the Nuclear Regulatory Commission is working on in safety research. I look forward to an interesting and a stimulating meeting, a useful meeting and I hope that it will fulfill your expectations and mine.

This is the opening plenary session and the occasion for the keynote address of the 19th Water Reactor Safety Meeting. And I would like now to introduce the keynote speaker, Ivan Selin, Chairman of the Nuclear Regulatory Commission. Dr. Selin received his PhD in electrical engineering with distinction from Yale University in 1960. He was a Fulbright scholar during the year 1960-1961 and received the Doctor of Science Degree with highest honors in mathematics from the University of Paris. From 1960 to 1965, he was a Research Engineer at the Rand Corporation working on statistical communication theory and national security matters. During 1965 to 1970 he served in the Office of the Assistant Secretary of Defense for Systems Analysis, acting as the Assistant Secretary at the end of that period. In 1970, Dr. Selin founded American Management Systems, Inc. and was Chairman of the Board of his company which engaged in computer systems, services and consulting. His principal responsibilities in the firm were corporate strategy and management. His own area of expertise there was comprehensive financial management and procedures. In May of 1989 Dr. Selin became Under Secretary at the Department of State for Management and held that post until July 1st of this year when, after his nomination by the President and confirmation by the Senate, he became the Chairman of the Nuclear Regulatory Commission.

Dr. Selin is going to speak to us this morning and he has, as I understand it, five priorities for the future of nuclear power in this country and he's going to speak to us about those. May I ask you all to give him a warm welcome.

Remarks of Ivan Selin  
19th Water Reactor Safety Meeting  
October 28, 1991

Good morning, ladies and gentlemen. I am delighted to have this opportunity to share my thoughts with you about some issues I believe are important to the nuclear industry. As I do this, I hope to weave in a few examples of how beneficial your projects have been and how they have been used to great advantage in recent Commission decisions.

Over the last few months, I have been refining a message that I want to send to all the diverse elements of the nuclear community. I began to develop the message during my confirmation hearings and you can see part of it in my remarks prepared for that occasion. I continued the development at a speech for a luncheon meeting of a local section of the American Nuclear Society earlier this month. I intended to repeat at this meeting most of what I said there. Imagine my surprise when The Energy Daily picked it to publish in its October 22 issue. I didn't realize that the message was so -- to use the title of The Energy Daily's column -- "quotable." Nonetheless, I do want you to hear the message, so here is a slightly modified version of the "same old theme."

I want to hit hard at the outset about why I came to the agency believing that it is necessary to change the status quo. The change I have in mind entails much more openness to the public. I view this as an important change to facilitate public understanding of the nuclear industry. Without understanding there will be no acceptance of, or support for, nuclear power. And without nuclear power as an option, I believe our country loses the potential benefits of having a range of energy options from which to choose.

The public has a right to know the facts about the NRC and about NRC-licensed activities. If things go wrong, the public must of course be told promptly and candidly. And by the same token, when things go well, the public has a right to know that too. The NRC should be willing to provide realistic assessments at all times. We need to tell the whole story, warts and all.

A recent example of this is the Yankee Rowe pressure vessel embrittlement issue. The petition to shut down the Yankee Rowe plant was dealt with in full view of the interested parties. There were Commission briefings where all interested parties were heard and public meetings near the plant. There was full disclosure of all assumptions and calculations to all parties. I found two research products to be pertinent and helpful in my consideration of the issue: (1) the fracture mechanics research that has been completed over the last several years, and (2) the

thermal hydraulic analysis capability and its underlying experimental data base. Both weighed heavily in the Yankee Rowe evaluations.

I take comfort from the fact that the NRC bases its decisions on the safety judgments of technical experts -- both in-house and independent experts -- and has seen those decisions upheld by reviewing courts. But in the long run, this does not matter if the American public does not have confidence. Confidence in the competence, the integrity, and the candor of those who are in charge of operating the nation's nuclear power plants and confidence in the regulators who are making the decisions. I believe that the NRC has been a strong regulator in the past, but that the regulated industry has not received the benefit in the court of public opinion from that strong regulation. In that respect, it has been the worst of all possible worlds -- the "pain" of a strong regulator without the "credit." Although it will be painful at times, we need to "tell it like it is", or the public will imagine even worse.

I look at the future of nuclear power as depending on five items, but I like to think of them as "one plus four." The "one" is the absolute priority of the safety of operating reactors. After that is assured, we can move on to the issues for the future -- the "four" I mentioned. I see those four issues as: waste disposal, license renewal, licensing under Part 52, and standard designs. I'll return to those in a minute.

First, however, let me focus on the number one priority -- the safety of operating reactors. I see the agency's principal duty to be to ensure that existing nuclear power plants are operated safely. Along with safety goes proper regard for national security and for environmental values. But safety is not just the obligation of the NRC. First and foremost, it is the duty of the nuclear industry. Without safety, safety that is demonstrable, consistent, and proven -- there will be no nuclear industry. Enlightened self-interest is a powerful motivator to sustain efforts to keep the nuclear house in order.

To a great extent, the NRC's role, as I see it, consists of making sure that the efforts of the nuclear industry are both deep enough and broad enough to solve known problems. Our role is also to ensure that attention is given to important areas before problems arise. Not only do we perform extensive evaluations of individual plants, but also we look broadly at areas such as training, waste management, and maintenance. And to hark back to my point earlier about openness, we will be seeking out opportunities to interact with the public as we do this.

While the agency's first obligation is to the public, we have an obligation to the regulated community as well. By

letting the industry know what is expected of it -- measuring off the "playing field" in advance, so to speak -- I believe everyone's interest is served. Fairness goes without saying. We need to ensure that there is consistency in the way we apply our regulations, from one time to another and from one plant to another. The agency has to ensure that we do not impose expenses inadvertently. One example might be through delay in the performance of regulatory responsibilities. Of course, where safety improvements are needed, we will not hesitate to require them. However, unnecessary costs do not serve industry and do not serve the public. Ultimately they wind up on the electric bills of ratepayers. So there is another area where watchfulness by the NRC benefits everyone.

I want to mention here that I have been impressed by the good safety record in the nuclear industry. And this impression has been heightened by my recent visit to European and Eastern European plants. From the time I began preparing for my confirmation hearings and then took my place as the Chairman of the agency, I have realized -- in a way that is not possible as an outsider -- that this good record is not a matter of luck. This safety record represents a commitment to safety by the industry as a whole. I have seen good plants and bad plants, and I want to tell you that I have been impressed by the high level of safety of the plants in the United States. I also have come to appreciate the competence and dedication of the staff of the NRC. This is exemplified by the fact that regulatory bodies around the world regularly draw upon its expertise. Part of that expertise, of course, derives from the research that NRC sponsors. A notable, recent example is the thorough, systematic effort to put together an up-to-date risk profile of five U.S. nuclear power plants. There is an additional facet of that effort that is perhaps of more importance from the point of view of the research community. That is the effort to establish the uncertainty on those profiles by state-of-the-art methods. But, as we say to licensees who have excellent performance reviews, the greatest challenge is to maintain this level of performance and not to rest on past achievements or to become complacent.

I hope you noticed that in referring to my awareness of the good safety record, I deliberately used the phrase "in a way that is not possible as an outsider." I think you will agree that the public does not share this perception. I believe the only way to change public perception is for everyone to reaffirm the commitment to safety and to reaffirm the commitment to the highest levels of performance. In addition, the NRC must continually demonstrate its vigilance, fairness, and rigorous adherence to a safety-first approach to regulation. The more open our processes to public scrutiny, the more our mutual commitment to safety will become evident.

I turn now to the four issues for the future. About nuclear waste -- the ultimate nimby, or not in my backyard. I believe that we cannot in good conscience go forward with the nuclear option without the expectation that a solution will be found for high level waste disposal. Toward this end, the agency has been working with the Environmental Protection Agency to develop a credible standard for a disposal site. We have also been working with DOE on what will be needed to license a high level waste repository. In addition, I have asked the Advisory Committee on Nuclear Waste to take a broad look at issues that may need to be resolved over the next 50 years. Are there technical issues -- technical flaws in our thinking -- that should be addressed? The Commission has in the past expressed its confidence that disposal of high level waste will be achievable within the first quarter of the 21st century. And I believe we can still do so. Nonetheless we will continue to review those plans to ensure that they remain sound.

For the second item on my list of four -- the agency's final license renewal rule, which should be published shortly as Part 54 of our regulations. This rule, and its supporting guidance documents, will define the "playing field" for operation beyond the present 40-year licenses. The NRC will only renew a license if the public health and safety will be adequately protected. The agency has been preparing for the larger issue of plant aging for many years. There have been extensive programs for materials -- such as the embrittlement issue I discussed before -- programs for electrical and mechanical systems -- such as valves, motors and batteries -- and programs for civil structures -- such as the containment. Indeed, since about 20 percent of our research budget has been spent on these programs in recent years, I'm sure many of you are working on these programs.

Another recent example of the results of applied research being used to great advantage is also related to license renewal. The staff has issued for public comment a generic environmental impact statement and supporting documents. These documents will meet part of the agency's responsibility under the National Environmental Policy Act (or NEPA). This act calls for full disclosure of the environmental impacts of continued operation under renewed licenses. If the agency's findings are sustained during the comment period, the fact that the agency was able to make generic findings will reduce the work load on both licensees and the agency.

The final two issues for the future -- licensing under Part 52 and plant standardization -- are closely related. Everyone agrees that the licensing process ought to be streamlined. That streamlining could come from using Part 52 and ordering only standard plants. But unfortunately, not everyone agrees on where the line should be drawn between safety decisions that would be made early in the process and safety decisions that would come

later. I hasten to add that -- early or late -- the staff will discharge its responsibility to ensure that all final safety decisions will have been made before any plant is allowed to operate. If the proper balance is not struck between decisions that are made early and those that are made late -- and today I don't know where the balance point is -- we may end up only able to repeat the custom plant approach of the past, which would probably doom new plant construction.

To tie the last two of our "four" back to the "one", I believe that safety is not something that goes into a plant after it is designed and built. It needs to be built into the system from square one and carried on from there throughout the lifetime of the plant. But I do not think that the NRC will be doing its job if it does no more than rule up or down on proposed designs that are submitted to it. The agency must act aggressively to seek out not only the problems and flaws in what is proposed -- the errors of commission -- but also to search for the gaps -- the errors of omission -- which are sometimes much harder to find. For the NRC as regulators -- just as for the industry it regulates -- complacency is a luxury we cannot afford.

I believe that standardized design will significantly enhance plant safety. Vendors can achieve major safety and training improvements over several installations. Among the benefits are trained personnel for plants of common design -- leading to a reduction in human errors, improved maintenance, and readily available spare parts. In addition to enhancing safety, standardization should also accelerate licensing and reduce costs. These are two important attributes to evaluate as utilities, ratepayers, and utility commissions consider what type of new generating capacity to develop.

In summary, I would like you to remember openness in communication and "one plus four" as we move into the future. We need to ensure the safe operation of operating plants -- the "one" -- as we continue to work on the four factors for the future -- waste disposal, license renewal, Part 52 licensing and plant standardization. We need to accomplish every bit of this with openness, in spirit and in fact, to the public whom we all serve. And the last thing for you to remember is that the decisions about safety and about future directions will need research input of the highest quality.

I wish you a productive conference and urge you to keep up the good work. Again, I appreciate this opportunity to meet with you and tell you about my views of NRC's priorities.

Second Plenary Session  
19th Water Reactor Safety Meeting  
Eric S. Beckjord, Director  
Office of Nuclear Regulatory Research

October 29, 1991

My name is Eric Beckjord, I'm Director of the Office of Nuclear Regulatory Research. I'm glad to have this opportunity to speak to you this afternoon at the 19th Water Reactor Safety Meeting. It is a forum for the exchange of ideas in reactor safety, it's a great value to the Nuclear Regulatory Commission and I think also to the nuclear safety community in general. I want to thank the Research office staff for organizing the sessions at this meeting. I want to thank the authors for their thoughts and presentations here, I want to thank Al Burda and those on the Research office staff who have made the arrangements and also Allen Weiss and his people from Brookhaven who have done likewise.

My purpose this afternoon is to review with you some of the major accomplishments in NRC research in the past year and I will also speak about the prospects for the coming year. I have more accomplishments and prospects to mention than I have time so I will not speak to every topic that is listed on the viewgraphs. I'm also regretful that I don't have two sets of viewgraphs because the aspect angle is about from here to here. If you're sitting outside of that, it will be difficult to see. If I could have the first please, George.

This should be the structure of the NRC Research program. The first three categories are essentially the lines of defense and the Water Reactor Safety criteria. Advanced Reactors is a new category this year and it signals the growing importance of that subject. You will see this structure is also, and has been for about five years, the organization of our budget. Take a good look at it because from the point of view of the budget structure I expect it will change to move more along the programmatic lines of the NRC budget in the future. If I could have the second slide, please.

International cooperation is very important to the research program. We have activities that are underway with each of the countries listed here. These activities are expanding and I have in mind our cooperation with France on the CEA's Phebus project which is well underway. There are new agreements in 1991 with Japan, through the Ministry of Trade and Industry and NUPEC. They have to do with testing a large pre-stress containment model and also some BWR steel shell containment models. In addition, there is also a high temperature hydrogen combustion research program, combustion and detonation. There is a new agreement that we have all but concluded with the Russians through the Kurchatov Institute on hydrogen research. There is the TMI vessel investigation program through the OECD organization in the Nuclear Energy Agency that is approaching completion now and in early 1993. I think it's going to be a major contribution, in fact, even today it is a major contribution to the understanding of that accident and the capability of a reactor vessel to maintain its integrity under conditions of loading it was never designed for. Also, the completion of the Severe Fuel Damage Partners

Cooperation Program is coming into view. I'll say a bit more about that later. So, I'll turn back to these areas in the structure of the program, first accomplishments and then prospects.

The research people have contributed considerable in the evaluation of the condition of the Yankee Rowe pressure vessel regarding the embrittlement, the thermal hydraulic analysis, and the pressurized thermal shock. The learning from this effort, which has been considerable in the past couple of months, suggests the need for some changes in our reactor vessel fracture mechanics research effort in order to prepare for future cases which are sure to come along in the license renewal program, now getting under way. With regard to annealing, a U.S. team witnessed the annealing of the Novovoronzh 3 vessel early this year through the Soviet/NRC cooperative agreement. This was very interesting to the U.S. team, and U.S. industry is now studying the applicability of the Russian learning and their experience and looking to applying it to U.S. plants. The aging evaluation research program has progressed in the reactor vessel and the other major components, and ten of the systems this year. Development of Regulatory Guides is underway for license renewal. The National Seismographic Center was dedicated at Golden, Colorado this spring and the Research office through the NRC provided funds for the network stations and for the instrumentation and the satellite communications for that facility, a world-class facility for earthquake measurement and recording. I have mentioned already the cooperation with Japan on the containment tests, a final one which I would point out here is the nondestructive testing methodology for primary components and piping, and this method was demonstrated this year. If I could go on the next slide, please.

Now some prospects. Appendices G and H of Part 50 dealing with fracture toughness and reactor vessel surveillance requirements will be updated in the coming year. Seismic siting criteria in Appendix A will be revised and there will be a substitution of what is called the inspection earthquake in place of the OBE or operating basis earthquake, and also the approval of seismic PRAs will be introduced. Regarding the seismic hazard question, many people are well aware of the differences between the Electric Power Research Institute curves of seismic hazard and the Lawrence Livermore set of curves. The work on the resolution of the differences between those two should be essentially complete in 1992; however, we are going through a process of consensus and peer review which will extend that time, with completion around the end of 1993. If I could have the next slide, please.

Core damage prevention - regarding boiling water reactor stability, the LaSalle event study was completed this past year and there are a number of important results; first, the available codes predict the phenomenon, secondly the most important stability parameters are inlet subcooling and axial power profile and I must say I'm personally somewhat amused and delighted that the importance of inlet subcooling has been rediscovered since I published a number of papers on that subject about 30 years ago using rather cruder methods, the punch card computer systems that were then available, and some analogues and integral methods. The other point on the LaSalle stability event is that we have concluded that the industry programs for detection and suppression of instability will turn out to be adequate. Accident management strategies - a lot of work under way there, with good progress on the

pressurized water reactor applications. Workshops were held in both the case of the BWRs and the PWRs. With regard to BWR recriticality after a core damage event, it is concluded that 700 parts per million of boron ten is sufficient for all possible core configurations to maintain subcriticality. A risk-based performance indicator of safety systems, the unavailability of safety systems, was developed, the work was completed, and the validity of that performance indicator demonstrated in the past year. It's an indicator which is based on the fraction of time in each quarter of the year when a separate train of a particular system would not have functioned when it was called upon to function. If there are two systems it's the product of the unavailability of each system and so forth. If I could have the next slide, please.

Core damage prevention - we are completing the ICAP program and will be moving into the international code application and maintenance program in this coming year for the thermal hydraulics codes. Also we expect to complete the accident management analysis for ice condensers and Mark I containments. This is important, as you know, because of the smaller safety margins in these containment systems. If I could have the next slide, please.

Reactor containment performance - the methodology for resolution of the Mark I containment liner melt-through issue has been developed and peer reviewed, and in this past year the work on the remaining four issues is almost complete. We expect to complete that with a final peer review in the coming year. Severe accident scaling methods, SASM, has been developed over the last two years. We delayed the continuation of the direct containment heating tests at SURTSEY until the completion of the SASM development so that it would be applied to give us some assurance on the scale up of SURTSEY results to full scale. As I say, that work has been done now, and it's completed. A report will be coming out very soon. The SURTSEY one-tenth scale model tests, accordingly, have begun again. The results in the early tests are excellent, and I have great hopes for the completion of that program in this coming year. If I could have the next slide, please.

With regard to the prospects for further work in containment performance, we are now in a position to compare the results of DCH testing between the one-tenth scale model and the one-fortieth scale model, the two at Sandia and at Argonne as you know. Sandia is also planning to do DCH tests on the one-sixth scale containment model which was used for testing containment performance capability a few years ago. That work is getting under way now and I hope that we may have a test by the end of next year. Accordingly, with this program in prospect now, I feel that we can see the closure of DCH essentially by the end of 1992. Debris coolability tests - we will be doing some more work, and that is very important and has application to the advanced reactors now beginning the review process. If you attended Brian Sheron's talk this morning you would have heard some more about that. We have made significant progress on resolving severe accident issues, those that were set forth in the Severe Accident Research Program of 1988. The severe accident research of the last ten years, together with a systematic engineering approach to identifying the issues that have high risks, have brought closure of these severe accident issues in sight. It's my own view that severe accidents are a problem of enormous practical importance to the world and they have also been a great scientific difficulty. I don't believe that this point has received

due recognition in the scientific community, and I hope that these accomplishments, as they are published, will gain recognition and credit for the men and women who have worked on them with brilliance and with success, on what a few years ago appeared to be an intractable set of problems. If I could have the next slide, please.

There is a lot of work to do for advanced reactors. That is the collection, the study, the distillation of experience on the more than 1,500 reactor years of operation of light water reactors in the United States, the additional experience available world-wide, the feedback and application of that knowledge to new designs to assure as far as possible that they will not have the faults of the first generation. I am saying that there is a need for some research on new and different features in these reactors and the advanced LWRs particularly. We are seeing some very creative ideas in the passive systems, but there are also unanswered questions; the passive system performance under the range of conditions that might be expected to occur in accidents and transients; systems interactions in the case of the AP-600, which Brian Sheron touched on this morning; the general reliability of passive systems depending on operation of check valves at low differential pressures. In operating reactors the check valve is considered to be a passive system, and I think it's an interesting question as to what the view is going to be on the check valve in these new passive systems. There are also questions about the advanced instrumentation and control, the reliability of the low signal level logic circuits and computer circuitry, and also the very important matter of software verification and validation as these systems move into more sophisticated uses of computer technology and control and advisory functions in new plants. The research in these areas has been planned and is getting underway. I think that Chairman Selin said it very well yesterday, and I think I'm quoting him right when he said that safety does not go into a plant after it is built. Safety needs to be built into the system from square one and to be carried throughout the life of the plant. I completely agree with that thought. If I could have the next slide, please.

There is a list here of accomplishments in the matter of resolving safety issues and developing regulations. If you look down that list, I don't think I need to spell out for you the significance of these rules because I think they are self-evident ranging in application from the new Part 54 license renewal rule to the update of Part 20, the first in many, many years bringing our radiation protection standards up to international standards. And so on down the list. These are things that we do in the Office of Research, in addition to the safety research projects which you are hearing about here and they are extremely important because they become the regulations that govern the activities at licensed power plants. So I just don't want to let this pass without a nod to the people who have carried forward these efforts with great diligence and timeliness. If I could have the next slide, please.

I think the prospects in this area of rules and regulations are also self-evident. I'll just mention a couple of things. A source term revision of Parts 50 and 100 is expected to be completed. This represents a major change in regulatory philosophy that will essentially separate reactor siting requirements from the design and engineering requirements on the reactor safety systems themselves. There is a line there about the Individual Plant Examination. Probably some of you are aware of the recent submittal on the

part of the Surry plant for Virginia Electric Power and the turbine hall flooding issue. Despite the bad press on this issue, I think that we see here proof that the IPE process can do what the Commission intended, which was to uncover severe accident vulnerabilities, so that actions could be taken to remedy whatever needs to be remedied. I'm not sure exactly what actions will be the final ones at Surry, but I think it certainly makes this point very clearly. We will also complete the U.S. reactor studies in 1992 of low-power and shutdown risk. This is a very important issue and it was pointed out to us by our colleagues a few years ago in France.

There are a couple of slides which I included and if anybody is interested, I didn't bring enough copies, but I can get them over here tomorrow. There are three other issues that I want to say something about briefly. The first is the budget prospect for FY 1993. As I've said in the past, I occasionally do have comments on the budget process which a few of you have an interest in. The prospects for FY 1993, as I see it, are as follows. The 100 percent NRC fee tax on licensees is in effect now. The first tax bills were sent out to licensees in September for the last fiscal year, the one that ended in September. This is going to affect the budgeting process for NRC in fundamental ways. There is a very strong industry reaction to the 100 percent fee not only in reactor licensing, but throughout the whole range of licenses that NRC has in the industrial and medical use area. Nobody is happy with it who has to pay the tax. It is interesting that the sharpest attack on this fee issue comes on the research budget of NRC. That is evident now and I thought, to make the point, I would read to you a short paragraph in a part of the Senate report on the NRC budget which came out in August and I'm quoting, "Finally, the Committee notes increases in the Commission's requests year after year in staffing and funding in every mission area. At some point, increased spending on research in areas with direct connections to operational reactor safety and increased numbers of regulations in ever expanding areas of reactor operations will bring diminishing returns and lead to over regulation that may, in fact, impact the level of safety achieved today. Therefore, the Committee questions the need for across-the-board increases in all mission areas and directs the Commission to initiate an external review of the effectiveness and cost efficiency of proposed additional programs." Now, that is talking about research, I'm sure that point came across. I guess what I'm saying is there are some trials ahead for the research budget, I think that is evident and I really can't tell you more about that now except that I know that this independent outside review of the program will be undertaken shortly.

The second matter that I wanted to talk about briefly is what is known as the CFO, or the Chief Financial Officers Act. This is now effective in all government agencies of the United States, and the net effect of it greatly increases the oversight of NRC expenditures as well as all other government expenditures. Commercial procurements are hardly at all affected by this because of the procedures and regulations in the Government Procurement Manual which are already in effect. But there will be an impact on research that is conducted at the national laboratories. I expect more exacting project management of our national laboratory programs. The NRC research managers will be responsible for conducting a more businesslike relationship with their counterparts at the national laboratories. I will shortly be sending out some guidance on how we are going to carry this out. But what it means, I think,

can be summarized as follows: more precise work statements for one thing, better cost estimates including a cost estimate which the research project managers in the Office will prepare, careful expenditure control, and finally a set of project records which will pass audit, because I am reasonably certain that there will be a program audit undertaken throughout our programs at the national laboratories in the coming year. So it is going to have an impact. I hope that it will not alter the fundamental mode of cooperation and contribution on the part of the national laboratories to our safety research, but it's going to put some more focus on the manner in which our cooperation is managed on both sides.

The third thing I wanted to mention concerns the Inspector General's investigation of the Research Office. I think it is no secret in the reactor safety research community that the Inspector General performed an investigation of the Office of Research, beginning in July 1990, as the result of an allegation of preferential treatment of contractors on the part of several research managers. The investigation was underway for nearly a year, and many RES employees and contractor personnel were interviewed in its course.

The Inspector General's report was given to the Commission in June of this year. In essence, the investigation did not substantiate the allegations against the research managers. After careful review of the report, I met with all the Research staff in order to tell them of the findings. I mention this now, because I think it is important for all the safety research community to be aware of this finding. It supports the integrity and rectitude of the research management in carrying out its responsibility for the nuclear safety research program.

**NINETEENTH WATER REACTOR SAFETY  
INFORMATION MEETING**

**ACCOMPLISHMENTS AND PROSPECTS**

**ERIC S. BECKJORD, DIRECTOR  
OFFICE OF NUCLEAR REGULATORY RESEARCH  
U.S. NUCLEAR REGULATORY COMMISSION**

**OCTOBER 29, 1991**

# **SCOPE OF RESEARCH**

**INTEGRITY OF REACTOR COMPONENTS**

**PREVENTING DAMAGE TO REACTOR CORES**

**REACTOR CONTAINMENT PERFORMANCE**

**ADVANCED REACTOR RESEARCH**

**RESOLVING SAFETY ISSUES AND DEVELOPING  
REGULATIONS**

**CONFIRMING THE SAFETY OF WASTE DISPOSAL**

SLIDE 1

## **INTERNATIONAL COOPERATIVE ACTIVITIES**

**AUSTRALIA**

**BELGIUM**

**CANADA**

**FINLAND**

**FRANCE**

**GERMANY**

**ITALY**

**JAPAN**

**KOREA**

**MEXICO**

**NETHERLANDS**

**NORWAY**

**PHILIPPINES**

**SOVIET UNION**

**SPAIN**

**SWEDEN**

**SWITZERLAND**

**AM. INST. IN  
TAIWAN**

**UNITED KINGDOM**

**YUGOSLAVIA**

**CEC**

**NEA (OECD)**

SLIDE 2

# **INTEGRITY OF REACTOR COMPONENTS**

## **ACCOMPLISHMENTS**

**YANKEE ROWE PRESSURE VESSEL EMBRITTLEMENT**

**ANNEALING OF SOVIET REACTORS**

**AGING EVALUATION OF COMPONENTS AND SYSTEMS**

**NATIONAL SEISMOGRAPHIC NETWORK DEDICATED**

**CONTAINMENT STRUCTURAL TEST AGREEMENT  
WITH JAPAN (MITI)**

**RISK-BASED INSPECTION METHODOLOGY DEVELOPED  
AND DEMONSTRATED**

SLIDE 3

# **INTEGRITY OF REACTOR COMPONENTS**

## **PROSPECTS**

**REACTOR VESSEL FRACTURE TOUGHNESS  
REQUIREMENTS AND MATERIAL SURVEILLANCE  
PROGRAM REQUIREMENTS TO BE CLARIFIED  
(10 CFR PART 50 APPENDICES G & H)**

**SEISMIC/GEOLOGIC SITING CRITERIA  
TO BE REVISED**

**SEISMIC HAZARD RESOLUTION  
TO BE ACHIEVED**

**SLIDE 4**

# PREVENTING DAMAGE TO REACTOR CORES

## ACCOMPLISHMENTS

**CONFIRMED LOW FREQUENCY FOR LOSS OF SHUTDOWN MARGIN DURING PWR REFUELING**

**COMPLETED REEVALUATION OF BWR STABILITY**

**KEY ACCIDENT MANAGEMENT STRATEGIES IDENTIFIED AND ASSESSED**

**DEMONSTRATED  $^{10}\text{B}$  CONCENTRATION FOR BWR SUBCRITICALITY FOR ALL CORE CONFIGURATIONS**

**QUALIFICATIONS AND TRAINING REGULATORY GUIDE (1.8) PREPARED**

**GUIDANCE FOR ANALYSIS OF HUMAN RELIABILITY IN IPES COMPLETED**

**RISK-BASED PERFORMANCE INDICATOR OF SYSTEMS UNAVAILABILITY COMPLETED**

# **PREVENTING DAMAGE TO REACTOR CORES**

## **PROSPECTS**

**COMPLETE ICAP PROGRAM AND INITIATE  
I CAMP (INTERNATIONAL CODE APPLICATION &  
MAINTENANCE PROGRAM)**

**ISSUE REPORT ON ANALYSIS OF NATURAL  
CIRCULATION DURING TMI ACCIDENT**

**COMPLETE ANALYSIS OF BWR TRANSIENTS USED TO  
BENCHMARK NRC'S BLACK FOX SIMULATOR  
(CHATTANOOGA)**

**COMPLETE ANALYSIS OF ACCIDENT MANAGEMENT  
STRATEGIES FOR ICE CONDENSER AND MK I  
CONTAINMENT PLANTS**

## **REACTOR CONTAINMENT PERFORMANCE**

### **ACCOMPLISHMENTS**

**SCALING METHODOLOGY DEVELOPED AND APPLIED TO  
DCH TEST FACILITY**

**FIRST DCH INTEGRAL-EFFECTS TEST COMPLETED IN  
1/10 SCALED FACILITY**

**COMPLETED COMPREHENSIVE PLAN TO PRIORITIZE  
RESEARCH NEEDS ON MELT PROGRESSION;  
EXPERIMENTS AND ANALYSES IN PROGRESS**

SLIDE 7

## **REACTOR CONTAINMENT PERFORMANCE**

### **PROSPECTS**

**DCH RESULTS FROM 1/10 SCALED FACILITY AND  
1/40 SCALED FACILITY TO BE COMPARED**

**DCH CLOSURE**

**DEBRIS COOLABILITY TESTS TO EXAMINE CRUST  
BEHAVIOR AND COMPLEMENT EPRI-CONSORTIUM  
TESTS**

**HIGH-SPEED HYDROGEN COMBUSTION TO BE STUDIED  
AT HIGH TEMPERATURE IN PROGRAM WITH JAPAN  
(NUPEC)**

**MELT PROGRESSION EXPERIMENTS AND ANALYSES**

SLIDE 8

# **ADVANCED REACTOR RESEARCH**

## **ACCOMPLISHMENTS**

**AP600 RESEARCH NEEDS IDENTIFIED; SBWR NEEDS  
BEING STUDIED**

**SCALING STUDY COMPLETED FOR AP600 INTEGRAL  
TEST FACILITY**

**ADVANCED I&C CONSIDERATIONS BEING STUDIED**

**ALMR AND MHTGR REVIEWS TRANSFERRED TO NRR  
FOR SER PREPARATION**

# **ADVANCED REACTOR RESEARCH**

## **PROSPECTS**

**AP600 INTEGRAL SYSTEMS TEST FACILITY**

**ALWR DESIGN CERTIFICATION CODES & ANALYSES**

# **RESOLVING SAFETY ISSUES AND DEVELOPING REGULATIONS**

## **ACCOMPLISHMENTS**

**LICENSE RENEWAL (PART 54) FINAL RULE  
SUBMITTED TO COMMISSION (10/18/91)**

**ENVIRONMENTAL IMPACT FOR LICENSE RENEWAL  
PROPOSED RULE (PART 51 REVISION) AND DRAFT  
GEIS ISSUED (9/17/91)**

**MAINTENANCE RULE (§50.65) ISSUED**

**RADIATION PROTECTION (PART 20) FINAL RULE  
ISSUED**

**EMERGENCY RESPONSE DATA SYSTEMS (PART 50)  
FINAL RULE ISSUED**

**URANIUM ENRICHMENT:**

**MATERIAL CONTROL FINAL RULE (§74.33)  
APPROVED BY COMMISSION (10/17/91)**

**IPEEE (EXTERNAL EVENTS) STAFF GUIDANCE  
ISSUED**

# **RESOLVING SAFETY ISSUES AND DEVELOPING REGULATIONS**

## **PROSPECTS**

**LICENSE RENEWAL FINAL RULE (PART 54) TO BE  
ISSUED**

**FINAL RULE ON ENVIRONMENTAL IMPACT FOR  
LICENSE RENEWAL (PART 51 REVISION) AND FINAL  
GEIS TO BE ISSUED**

**REVISED SOURCE TERM TO BE ISSUED, AND  
LICENSING (PART 50) AND SITING (PART 100)  
TO BE REVISED**

**IPE (INTERNAL EVENTS) REVIEWS**

**LOW POWER AND SHUTDOWN RISK STUDY**

**INDUSTRY CODES AND STANDARDS UPDATING  
(50.55A)**

SLIDE 12

# Heavy-Section Steel Technology Program: Recent Developments in Crack Initiation and Arrest Research\*

W. E. Pennell  
Engineering Technology Division  
Oak Ridge National Laboratory  
Oak Ridge, Tennessee

## Abstract

Technology for the analysis of crack initiation and arrest is central to the reactor pressure vessel fracture-margin-assessment process. Regulatory procedures for nuclear plants utilize this technology to assure the retention of adequate fracture-prevention margins throughout the plant operating license period. As nuclear plants age and regulatory procedures dictate that fracture-margin assessments be performed, interest in the fracture-mechanics technology incorporated into those procedures has heightened. This has led to proposals from a number of sources for development and refinement of the underlying crack-initiation and arrest-analysis technology. This paper presents an overview of ongoing Heavy-Section Steel Technology (HSST) Program research aimed at refining the fracture toughness data used in the analysis of fracture margins under pressurized-thermal-shock loading conditions.

## Introduction

Pressurized-thermal-shock (PTS) has emerged as a loading condition of dominant concern in the structural-integrity evaluation of pressurized-water-reactor (PWR) pressure vessels. This loading condition can result from activation of the plant safety injection system (SIS) in response to detection of a loss-of-coolant accident (LOCA) condition. The resulting injection of cool SIS water into the reactor vessel downcomer annulus generates the thermal-shock portion of the loading condition. Thermal stresses resulting from this thermal shock can be high. They constitute the major element of a transient stress field which has been shown capable of initiating cracks from pre-existing flaws, should the vessel material fracture toughness be sufficiently low.

---

\*Research sponsored by the Office of Nuclear Regulatory Research, U.S. Nuclear Regulatory Commission under Interagency Agreement 1886-8011-9B with the U.S. Department of Energy under Contract DE-AC05-84OR21400 with Martin Marietta Energy Systems, Inc.

The submitted manuscript has been authored by a contractor of the U. S. Government under Contract DE-AC05-84OR21400. Accordingly, the U. S. Government retains a nonexclusive, royalty-free license to publish or reproduce the published form of this contribution, or allow others to do so, for U. S. Government purposes.

Pressure loading, while contributing in a minor way to crack initiation, is the dominant influence on the behavior of the crack once it has penetrated deep within the reactor vessel wall. Activation of the SIS in response to a small break LOCA can produce pressure recovery in the reactor vessel sufficient to drive the crack through the vessel wall. The major contribution to reactor vessel failure rates predicted in a PTS analysis comes from a small number of dominant transients, many of which are characterized by recovery of high vessel internal pressures.

It will be evident from the above discussion of the PTS scenario that an accurate definition of the vessel material crack initiation and arrest toughness is essential to the PTS analysis process. A major segment of the Heavy-Section Steel Technology (HSST) Program is devoted to refining the definition of vessel material crack initiation and arrest toughness for the unique combination of conditions existing during a PTS event. This paper provides a status report on this ongoing research. Specific areas of research reviewed are (a) the effect of crack-tip constraint on crack-initiation toughness as influenced by both crack depth and biaxial loading and (b) the influence of vessel dynamic response following crack initiation on the subsequent crack-arrest behavior.

### **Shallow Flaw Fracture Toughness**

Research conducted at the University of Kansas has demonstrated enhanced fracture toughness for shallow flaws in both A36 and A517 structural steels.<sup>1,2</sup> This result is attributed to the loss of crack-tip constraint associated with the proximity of the free surface of the material to the crack tip. Enhanced fracture toughness for shallow flaws has a special significance in the analysis of PTS events since prior studies<sup>3</sup> have shown that the majority of crack initiations originate from shallow flaws. Major elements of the HSST shallow-flaw task are devoted to (a) the generation of a shallow-flaw data base for the A 533, Grade B Class 1 material used in the construction of many U.S. PWR vessels, and (b) the development of technology for application of this data base to the analysis of reactor vessel response to PTS transients.

The HSST shallow-flaw tests are generating fracture-toughness data for A 533 Grade B Class 1 material for a range of crack depths of interest to the PTS analysis. Specimens used in the development phase of the testing are shown in Fig. 1. They are nominally 102 mm (4 in.) deep with widths ranging from 51 mm (2 in.) to 152 mm (6 in.). Analysis, preparation and testing of these specimens has been described by Theiss et al. in Refs. 4 and 5.

Use of such a large test specimen is expensive in terms of consumption of valuable, fully characterized test material. Selection of the test specimen size reflects a concern that the test results must be capable of interpretation in terms of both the absolute crack depth "a" and the relative crack depth a/w. Finite-element analysis of shallow-flaw specimens recently reported by Kirk et al.<sup>6</sup> reinforces the need for this approach. They found that neither a nor a/w, when considered alone, provided an adequate basis for transfer of data from test specimen to differing application geometries. Their results show that interaction of the plastic field generated by stress concentrations at the crack tip with that generated by overall response of the structural section to the applied loading controls the magnitude of stresses ahead of the crack tip and, thereby, the fracture toughness.

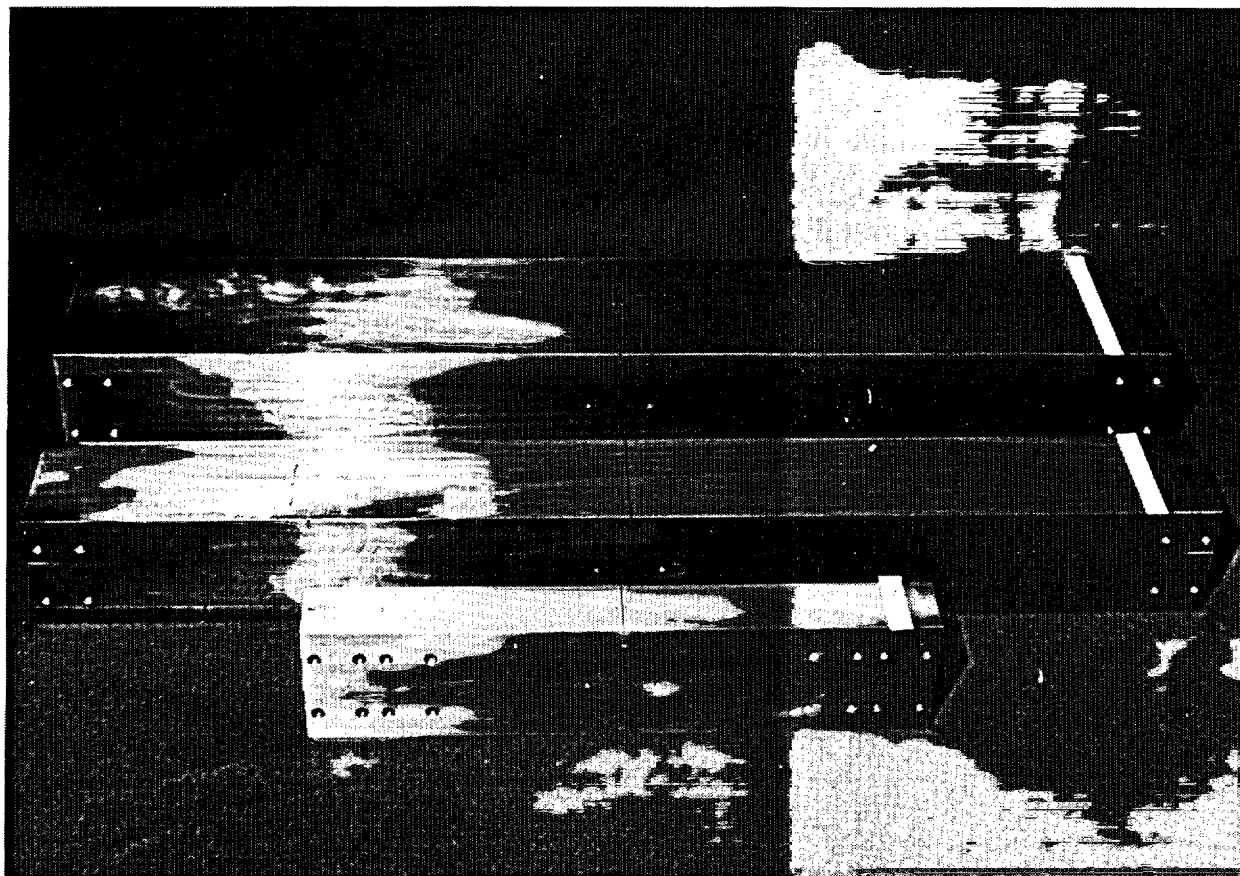


Fig. 1 102 mm (4 in.) deep test beams with B/W ratios of 0.5, 1.0, and 1.5 used in the development phase of the A 533 B shallow flaw fracture toughness testing program.

Results obtained to date from the HSST shallow-flaw fracture-toughness testing task are shown in Fig. 2. The trend of increasing fracture toughness for shallow flaws in the lower-transition region is clearly evident. Lower-bound fracture toughness for cracks in the range 10 to 15 mm (0.4 in. to 0.6 in.) deep is seen to be more than double that for the deep cracks. The difference is seen to disappear at lower-shelf temperatures. This is consistent with trends observed in Refs. 1 and 2 for low- and high-yield strength material respectively.

Professor Rolfe of the University of Kansas has recently completed a comprehensive review<sup>7</sup> of the HSST shallow-flaw task. The review identified actions required to validate the shallow-flaw fracture-toughness data for use in reactor vessel structural margin assessments. A key recommendation was for the analysis of both test specimens and cracked reactor vessels to confirm that the recently developed dual-parameter fracture-toughness correlations provide a basis for transfer of the test data. This analysis is currently in progress at the University of Maryland under the direction of Prof. C. W. Schwartz. Preliminary results from the analysis gave Q factors in a dual-parameter, J-Q fracture correlation of  $-0.135$  and  $-0.95$  for test specimens with  $a/w$  ratios of 0.5 and 0.1, respectively.

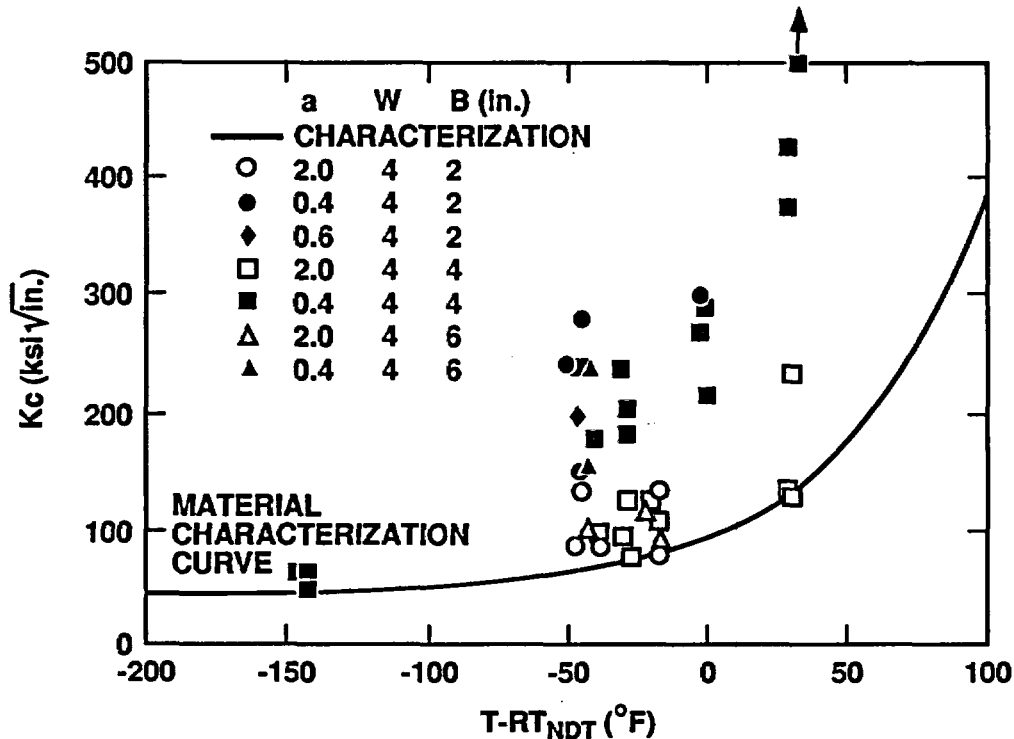


Fig. 2 Preliminary results from the shallow flaw testing program confirm the existence of enhanced fracture toughness for shallow flaws in A 533 B Class 1 material at temperatures in the lower transition range.

### Constraint Effects in Ductile Tearing

PTS transient loading produces biaxial stress fields in the reactor vessel wall (Figs. 3 and 4). In the case of transient thermal stresses, which dominate the crack-initiation process for shallow flaws, the resulting ratio of principal stresses at the inside surface of the vessel is 1:1. These stresses are in a plane oriented parallel to the inner surface of the vessel. One of the principal stresses in this field is, therefore, aligned parallel to the crack tip for both axial and circumferential flaws. This was identified in Ref. 8 as a condition with the potential to degrade the material ductile-tearing toughness.

A number of researchers have addressed the issue of crack-tip constraint on fracture toughness, including the effect of biaxial stress fields. Their focus has been on the effects of in-plane biaxial stresses. Their research has produced the dual-parameter elastic K-T<sup>9</sup> and elastic-plastic J-Q<sup>10</sup> fracture-toughness correlations, which predict a significant influence of in-plane biaxial stresses on fracture toughness. The K-T and J-Q correlations, however, incorporate an assumption of plane-strain boundary conditions. Out-of-plane (OP) stresses considered in these dual-parameter fracture correlations are limited to those generated by the restraint of Poisson's ratio contractions. In their current state of development, therefore, the K-T and J-Q dual-parameter fracture correlations can not address the effect on ductile tearing toughness of large far-field OP stresses which are characteristic of the PTS loading condition.

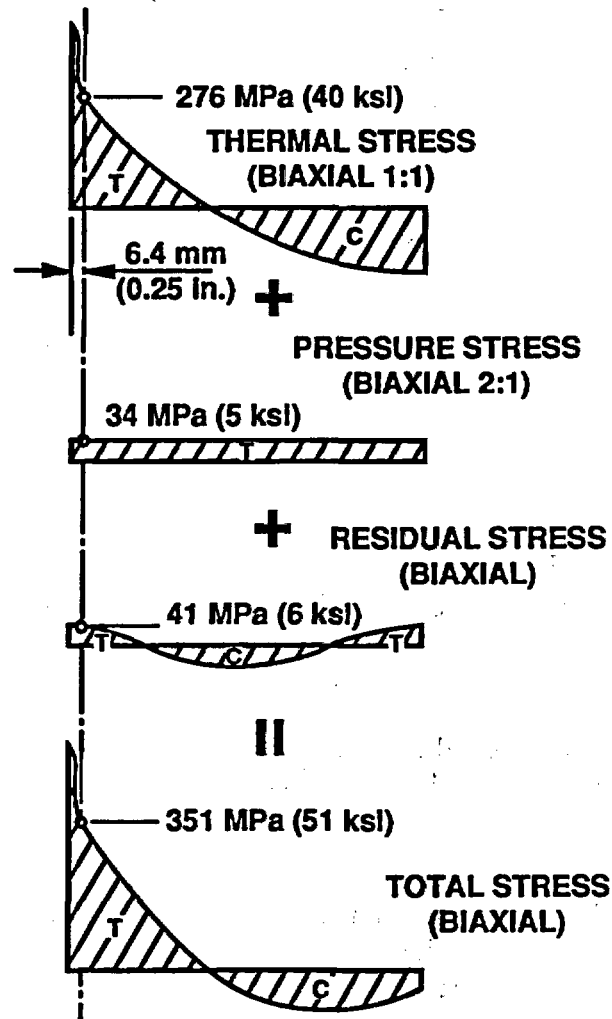


Fig. 3 The three contributing stress distributions which together define the overall stress distribution in a pressure vessel wall during a PTS transient are all biaxial.

The HSST Program is investigating potential effects of prototypical PTS OP far-field stresses on fracture toughness using a variety of analytical models. Results obtained to date have been paradoxical in that the magnitude of the predicted effects of OP far-field stresses (and strains) appears to be dictated by the approach adopted in formulating the fracture models.

Models based on a detailed definition of the stress and strain fields in the region immediately adjacent to the crack tip predict a minimal impact of OP stresses and strains on fracture toughness. This is a reflection of the fact that the far-field strains represent a very small addition to the large strains already existing at the crack tip.

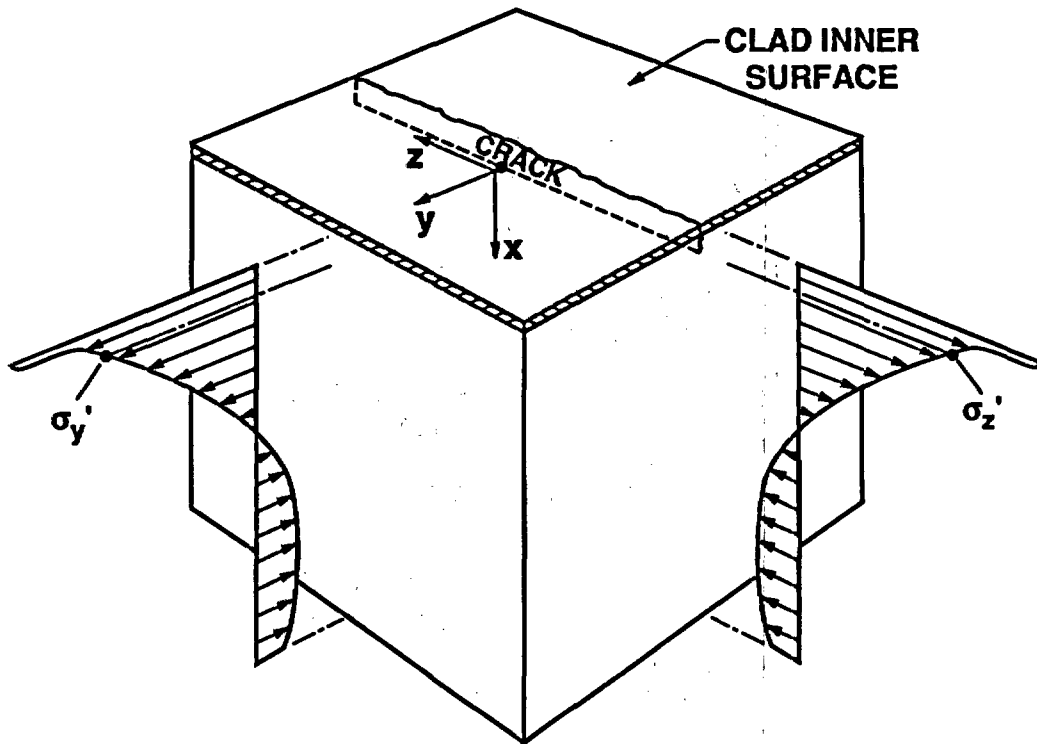


Fig. 4 One of the far-field principal stresses existing in a pressure vessel wall during a PTS transient is aligned parallel to the crack front of any axial or circumferential crack.

In contrast, a model that focuses on the effect of far-field OP stresses on the stress state at the boundary of the plastic zone, indicates there may be a significant effect on fracture toughness. This is due to the increase in the hydrostatic to Von Mises' equivalent stress ratio ( $\sigma_H/\sigma_e$ ) generated by the additional OP stress increment and the pronounced effect of that increase on fracture ductility.

The following brief review of the analysis results will illustrate the nature of the paradox. A detailed description of the near-tip models used to investigate the effect of OP stresses and strains on fracture toughness has been given by Shum et al.<sup>11</sup> Both stress and strain-based fracture criteria were investigated.

A micromechanical model based on a generalized plane-strain adaptation of the Rice-Johnson analysis<sup>12</sup> of a blunted notch was used to evaluate the effect of far-field OP stresses on crack-tip stress triaxiality and fracture ductility. The model was used to predict strains and  $\sigma_H/\sigma_e$  in the near crack-tip region in the presence of an OP strain. Failure was assumed to occur when the strains reached a stress-state-dependent limiting value. An estimate for the fracture ductility under conditions of multiaxial stress was derived from data generated by MacKenzie et al.<sup>13</sup> for a range of materials.

Results produced using this model are illustrated in Fig. 5. The model predicted that for the case of a zero-strain hardening material the applied strain would reach critical values in a

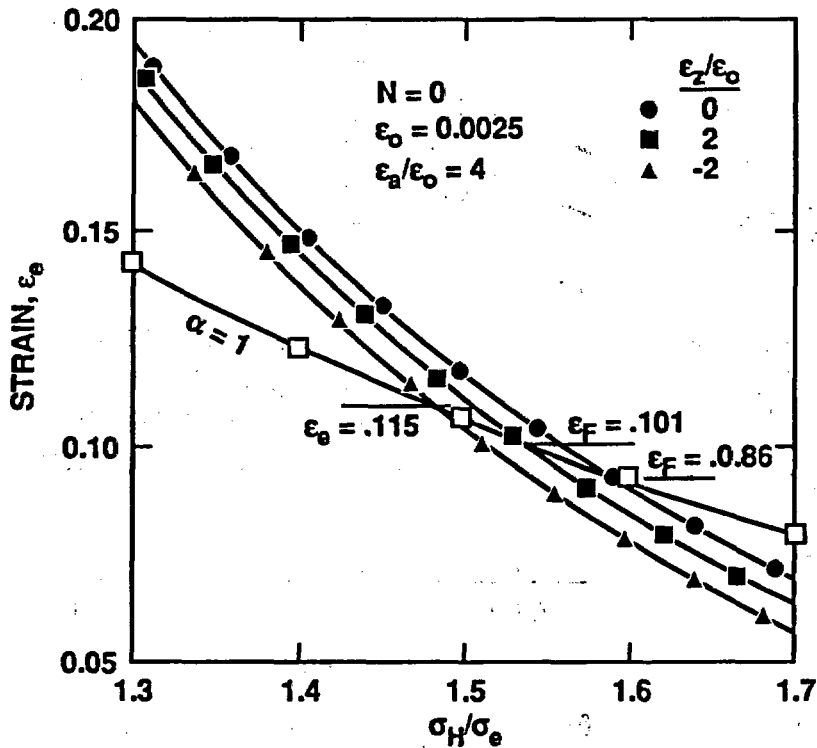


Fig. 5 A crack-tip micromechanical model predicts intersection of the material critical strain curve with the applied strain curves for a range of generalized plane strain boundary conditions in a region of the crack-tip plastic zone where the  $\sigma_H/\sigma_e$  value is less than 1.6. (From Ref. 11)

region of the plastic zone where  $\sigma_H/\sigma_e$  was in the range 1.5 to 1.6. Out-of-plane far-field strains in the range  $\pm 2\%$  were predicted to have a  $\mp 14\%$  influence on the critical strains. This variation in the critical strains was predicted to influence the fracture toughness by only  $\mp 2\%$ .

A second model, based upon a hollow-cylinder analogy, confirmed the stress-strain field results predicted by the micromechanical model. Any questions relating to results from these models would, therefore, appear to be confined to the fracture ductility estimates and/or the location within the plastic zone of the critical combination of applied strain and fracture ductility.

A third model was based on a dual-parameter cleavage fracture-toughness correlation previously demonstrated by Keeney-Walker.<sup>14</sup> This model uses the area ( $A_{CR}$ ) within a critical stress contour centered at the crack tip as a second correlation parameter. The effectiveness of this model in the plane-stress to plane-strain domain had been previously demonstrated in an analysis of the Oak Ridge National Laboratory (ORNL) Wide-Plate fracture test results, where unanticipated elevations in the  $K_I$  required to initiate fracture had been encountered.

Results produced by the J- $A_{CR}$  model are shown in Fig. 6. An out-of-plane strain of +0.114% is predicted to result in a reduction of 22% in  $J_{IC}$ , which translates to a reduction of less than 12% in  $K_{IC}$  from the reference plane strain value.

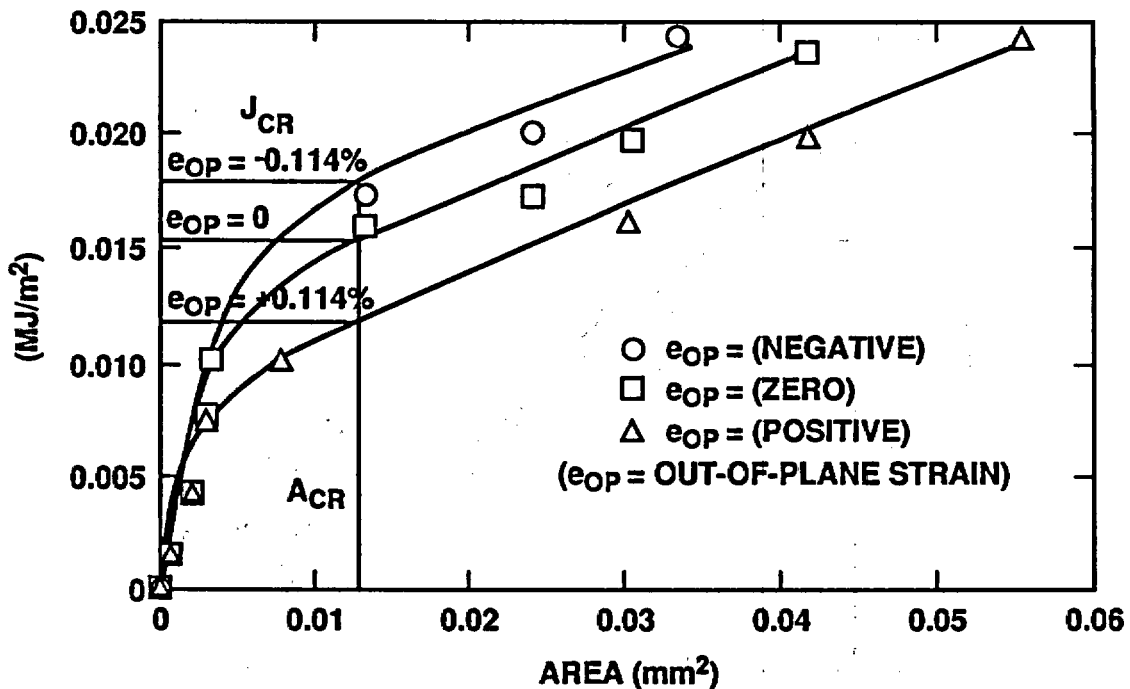


Fig. 6 The dual parameter J-ACR fracture toughness correlation predicts a 22% reduction in  $J_{IC}$  (12% in  $K_{IC}$ ) relative to the plane-strain fracture toughness when a positive far-field strain of .114% is applied parallel to the crack front. (From Ref. 11)

A common result produced using diverse models gives reason for confidence in that result. Prior to acceptance of the result, however, it is prudent to verify that the models do not share any common features which could detract from their value as independent cross checks. The models discussed above are truly independent in the failure-criteria area in that one uses a critical stress and the other uses a critical strain to predict fracture. They do, however, share a common element in that they are all based on a detailed definition of the near-tip stress-strain field where strains are very high. A fourth model has been generated to investigate the possible significance of this common element of the prior models. The fourth model utilizes elastic analysis of the stresses in the region immediately adjacent to the crack-tip plastic zone to infer the influence of far-field OP stresses on fracture toughness. The model does not, therefore, share the common element described previously for the other models.

Elastic stresses on the plane of propagation of the crack are defined using the equations of Inglis,<sup>15</sup> as interpreted by J. G. Merkle.\* For the case of a center-cracked panel with zero crack-tip radius the equations are as follows.

\*J. G. Merkle, "Special Technical Assistance, Chapter 4," in "Heavy-Section Steel Technology Program Semiannual Progress Report for April-September 1991," USNRC Report NUREG/CR-4219, Vol 8, No. 2 (ORNL/TM-9593/V8&N2) (to be published early in 1992).

$$\begin{aligned}\sigma_y &= \sigma_y' \frac{\left(\frac{r+a}{a}\right)}{\sqrt{\left(\frac{r+a}{a}\right)^2 - 1}} \\ \sigma_x &= \sigma_y - \sigma_y' \\ \sigma_z &= \nu(\sigma_x + \sigma_y)\end{aligned}\tag{1}$$

where: directions x, y, and z are as defined in Fig. 4.

a = the half length of a through-thickness crack in a plate

r = is the distance along the x axis ahead of the crack tip

$\nu$  = Poisson's ratio

$\sigma_y'$  = the far field opening mode stress

$\sigma_x$ ,  $\sigma_y$  and  $\sigma_z$  are the three principal stresses along the x axis

Adaptation of the above equations for the present study can be made simply by adding the far field stress  $\sigma_z'$  directly to the constraint induced  $\sigma_z$  stresses. This is possible because the closed crack does not cause any perturbation of the far-field  $\sigma_z'$  stresses. The body is free to contract in both the x and y directions in response to a uniform  $\sigma_z'$  stress, and the  $\sigma_z'$  stress does not therefore generate any contribution to either the  $\sigma_x$  or  $\sigma_y$  stresses.

Equations 1 are for a panel of infinite dimensions with a center through crack of finite length 2a. For the purpose of a study relating to PTS crack initiation, a more appropriate geometry is that of a single-edged notch in a finite-thickness plate. Equations 1 were converted to this form by incorporating the appropriate factors. The final form of the equations as used in the model was then as follows.

$$\begin{aligned}\sigma_y &= 1.12 \times f(a/W) \times \sigma_y' \frac{\left(\frac{r+a}{a}\right)}{\sqrt{\left(\frac{r+a}{a}\right)^2 - 1}} \\ \sigma_x &= \sigma_y - \sigma_y' \\ \sigma_z &= \nu(\sigma_x + \sigma_y) + \sigma_z'\end{aligned}\tag{2}$$

where

$\sigma_z'$  is the far-field stress parallel to the crack front and  
 $f(a/w)$  is a coefficient accounting for the effect of the finite-plate geometry on the stress-intensity factor.<sup>16</sup>

Equations (2) were used to calculate the Von Mises' equivalent stress ( $\sigma_e$ ) and the hydrostatic stress ( $\sigma_H$ ) for a potential part-through surface cracked biaxial test specimen for plane-stress, plane-strain and biaxial-loading constraint conditions. The far-field stress was set at 345 MPa (50 ksi) to match typical stress levels predicted at a depth of 6 mm (0.25 in.) beneath the inner surface of a vessel at the time of crack initiation during a PTS transient (Figs 3 and 4). A plate thickness of 76.2 mm (3 in.) was selected based on the loading capacity of potential test machines. The crack depth was selected as 23 mm (0.9 in.) to produce a crack tip  $K_I$  value of  $154 \text{ MPa}\sqrt{\text{m}}$  ( $140 \text{ ksi}\sqrt{\text{in.}}$ ). This value was selected to match the plane-strain fracture toughness reported by Landes and McCabe<sup>17</sup> in a series of plane-stress and plane-strain fracture toughness tests on A 533 Grade B Class 2 material. Plane stress and plane strain fracture-toughness data produced under otherwise identical conditions were required as input to this scoping analysis model.

Fig. 7 shows the test specimens used in the study of Ref. 17. Out-of-plane stresses in the analysis of the plane-stress case were set at 20% of the plane-strain value rather than zero in recognition of the finite transverse dimension of the plane-stress specimen shown in Fig. 7.

Results generated using the modified Inglis equations are shown in Fig. 8. The elastically estimated crack-tip plastic-zone boundary is defined by the intersection of the equivalent-stress curve with the yield-stress line for each of the three boundary-condition cases considered. Corresponding  $\sigma_H/\sigma_e$  values at the elastic-plastic boundary are obtained as 0.68, 1.82, and 3.38 for the plane-stress, plane-strain, and biaxial-loading cases, respectively. The  $\sigma_H/\sigma_e$  value for the plane-strain case is similar to that obtained from the micromechanical model, as illustrated in Fig. 5. The biaxial-loading case, in contrast, gives a  $\sigma_H/\sigma_e$  value approximately double that given in Fig. 5.

The  $\sigma_H/\sigma_e$  ratio is of interest because of its influence on fracture ductility. Weiss<sup>18</sup> has investigated the effect of stress state on fracture strain and proposed the following relationships:

$$\frac{\bar{\epsilon}_{F,\alpha,\beta}}{\bar{\epsilon}_{TF}} = (\omega m)^{1/n} \quad (3)$$

where

$\bar{\epsilon}_{F,\alpha,\beta}$  is the effective fracture strain (plastic strain) predicted in a triaxial stress field characterized by stress ratios  $\alpha$  and  $\beta$ .

$\bar{\epsilon}_{TF}$  is the effective fracture strain in uniaxial tension

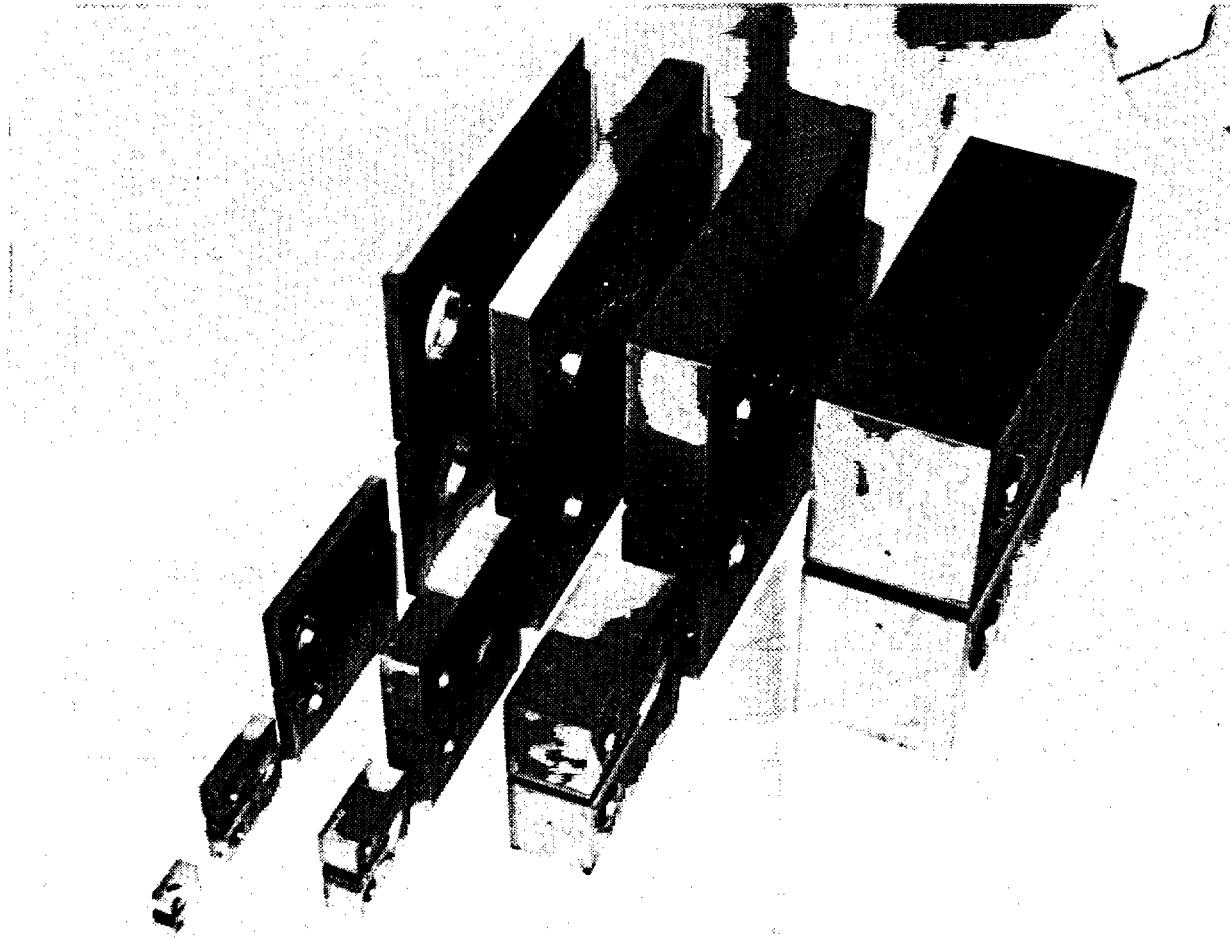


Fig. 7 Fracture toughness specimens from which the plane-stress and plane-strain fracture toughness data used in this study were generated. (From Ref. 17)

$$\omega = \frac{1}{1 + \alpha + \beta} \quad (4)$$

$$m = [(1 + \alpha + \beta)^2 - 3(\alpha + \beta + \alpha\beta)]^{1/2} \quad (5)$$

$$\alpha = \frac{\sigma_x}{\sigma_y} \quad \text{and} \quad \beta = \frac{\sigma_z}{\sigma_y} \quad (6)$$

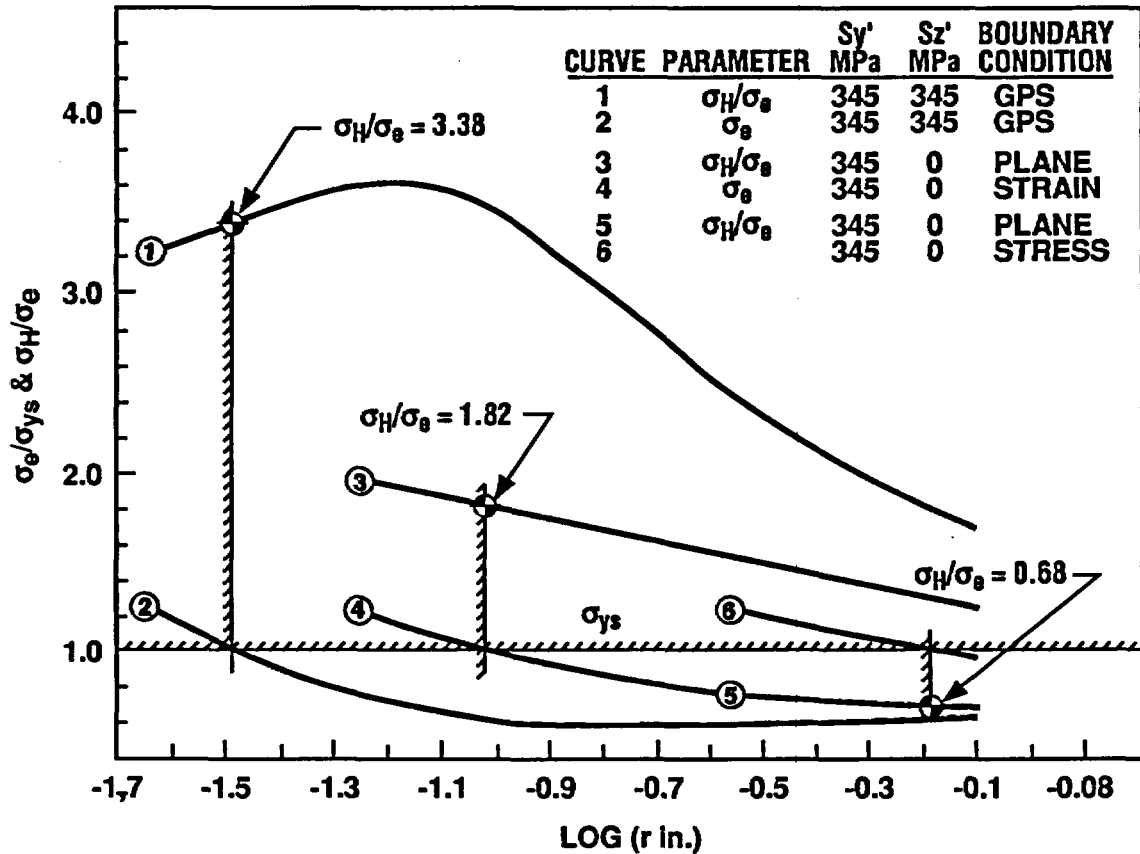


Fig. 8  $\sigma_H/\sigma_e$  stress ratios predicted at the crack-tip plastic zone boundary by the modified Inglis equations for plane-stress, plane-strain and 1:1 biaxial-loading boundary conditions.

$n$  is the material strain hardening exponent in an equation for the effective stress-effective strain curve of the form:

$$\bar{\sigma} = k\bar{\epsilon}^n \quad (7)$$

Equations (3) through (6) require the input of principle-stress data from an elastic-plastic analysis for the crack tip plastic zone in order to provide estimates of the material fracture strain in the fracture zone within the plastic zone. Clearly, this input is not available from the elastic analysis results obtained using Eq. 2. Those results can, however, be used to predict the material fracture strain for the  $\sigma_H/\sigma_e$  value existing on the elastic-plastic boundary. Plastic strains at this location are, by definition, zero. The fracture strain at the boundary is of interest, therefore, only because it fixes one end of the fracture-strain curve within the plastic zone. This information is useful, however, in that it serves to indicate if potential tearing initiation sites may exist in regions of the plastic zone beyond the boundaries of the previously discussed crack-tip models.

Principal-stress data at the plastic-zone radius were input to Eqs. (3) through (6) to calculate the failure strain for each of the three constraint conditions considered. A value of 0.31

was selected for the strain-hardening coefficient (n). Results from this analysis are shown in Table 1. Note that the predicted fracture strain for the case of biaxial loading is approximately 14% (0.06/0.43) of that for the plane-strain case.

Table 1 Constraint-Dependant Fracture Ductility Estimates n = 0.31

Constrain condition	$\sigma_x/\sigma_{ys}$	$\sigma_y/\sigma_{ys}$	$\sigma_z/\sigma_{ys}$	$\alpha$	$\beta$	$\frac{\bar{\epsilon}_{F,\alpha,\beta}}{\bar{\epsilon}_{TF}}$ %
Plane stress	0.64	1.27	0.11	0.51	0.09	10.41
Plane strain	1.79	2.41	1.26	0.74	0.52	0.43
Biaxial	3.35	3.98	2.82	0.84	0.71	0.06

Equation (2) can not provide any information on either effective strains or  $\sigma_H/\sigma_e$  ratios within the plastic zone. Large displacement elastic-plastic, finite-element analyses by Bass et al.\* have, however, shown that  $\sigma_H/\sigma_e$  ratios remain at or above the plastic-zone boundary levels over a large portion of the plastic-zone radius. Relative fracture strains in the process zone for varying constraint conditions can, therefore, be inferred from the ratio of fracture strains established at the plastic-zone boundary.

Weiss<sup>18</sup> has derived the following expression for fracture toughness in terms of the fracture strain under conditions of triaxial loading.

$$K_{Ic}^2 = \pi \sigma_y^2 \rho^* \left[ \left( \frac{\bar{\epsilon}_{F,\alpha\beta}}{\bar{\epsilon}_y} \right)^{n+1} - 1 \right] \quad (8)$$

where  $\sigma_y$  is the opening mode stress at the plastic-zone boundary,

$\rho^*$  is Neubers micro-support effect constant,

$\bar{\epsilon}_y$  is the effective plastic strain at the plastic-zone radius.

For the purpose of estimating the effect of departures from plane-strain constraint on fracture toughness, Eq. (8) can be simplified by eliminating all terms that remain constant for each of the constraint conditions. The resulting equation for the relative fracture toughness at a given constraint condition is as follows.

\*B. R. Bass et al, "Constraint Effects on Fracture Toughness for Circumferentially Oriented Cracks in Reactor Pressure Vessels," USNRC Report NUREG/CR-5792 (ORNL/TM-11968) (to be published February 1992).

$$\frac{(K_c)_{NPS}}{(K_{Ic})_{PS}} = \frac{\left[ \sigma_y \sqrt{\left( \frac{\bar{\epsilon}_{F,\alpha\beta}}{\bar{\epsilon}_y} \right)^{n+1} - 1} \right]_{NPS}}{\left[ \sigma_y \sqrt{\left( \frac{\bar{\epsilon}_{F,\alpha\beta}}{\bar{\epsilon}_y} \right)^{n+1} - 1} \right]_{PS}} \quad (9)$$

where suffixes PS and NPS denote plane-strain and nonplane-strain constraint conditions, respectively.

Fracture-toughness results for A 533 B Class 2 material at a test temperature of 0°C (32°F) were obtained from the tests of Ref. 17 as 150 MPa·√m (137 ksi·√in.) and 629 MPa·√m (572 ksi·√in.) for the plane-strain and plane-stress "4 T profile" test specimens, respectively. Inserting these values, together with the corresponding parameters from Table 1 and a value of 0.001% for  $\bar{\epsilon}_y$  into Eq. 9, gave the previously quoted value of 0.31 for n. This value of n was then used in Eq. 9 together with the plane-strain and biaxial-loading parameters from Table 1 to produce an estimate of 0.47 for the ratio of fracture toughness under biaxial loading and plane-strain constraint conditions.

The estimate of the effect of out-of-plane biaxial stresses given by the above scoping analysis differs significantly from that given by the crack-tip fracture models. At this time it would be inappropriate to attach any significance to the scoping-analysis results beyond recognition of the fact that uncertainty exists relative to the effect of out-of-plane biaxial loading. Biaxial test data will be required to calibrate and validate models for prediction of the effects of out-of-plane biaxial loading on fracture toughness.

Biaxial fracture toughness tests have been performed by S. J. Garwood<sup>19</sup> at The Welding Institute in the United Kingdom. The specimen size used in those tests was such, however, that a condition of general yielding was generated in the specimen ligament. It will be evident from the above analysis that prototypical elastic conditions in the test-specimen ligament are necessary for the test data to be used to resolve the paradox outlined above.

Geometric irregularity of the crack front is a further factor which can temper the buildup of out-of-plane  $\sigma_z$  stresses and thereby influence the location within the plastic zone of the maximum  $\sigma_H/\sigma_E$  stress ratio. Crack front geometry data obtained from a post-test microscopic examination of one of the deep flaw ( $a/w = 0.5$ ) specimens used in the shallow flaw task are shown in Fig. 9. The data cover a 12.7 mm (0.5 in.) length of the fatigue crack front at the center of the 102 mm wide specimen. Within that length the fatigue crack front exhibits considerable irregularity, with several projections in the range .08 to .11 mm (.003 to .0045 in.). These projections break the transverse load path at the crack tip and thereby inhibit the buildup of transverse stresses. The crack tip in effect is seen to be a zone rather than a point with a finite width in the direction of crack propagation. The diffuse nature of the crack tip will have the effect of reducing the rate of buildup of transverse stresses in the plane of crack propagation and displacing the maximum constraint condition further into the plastic zone.

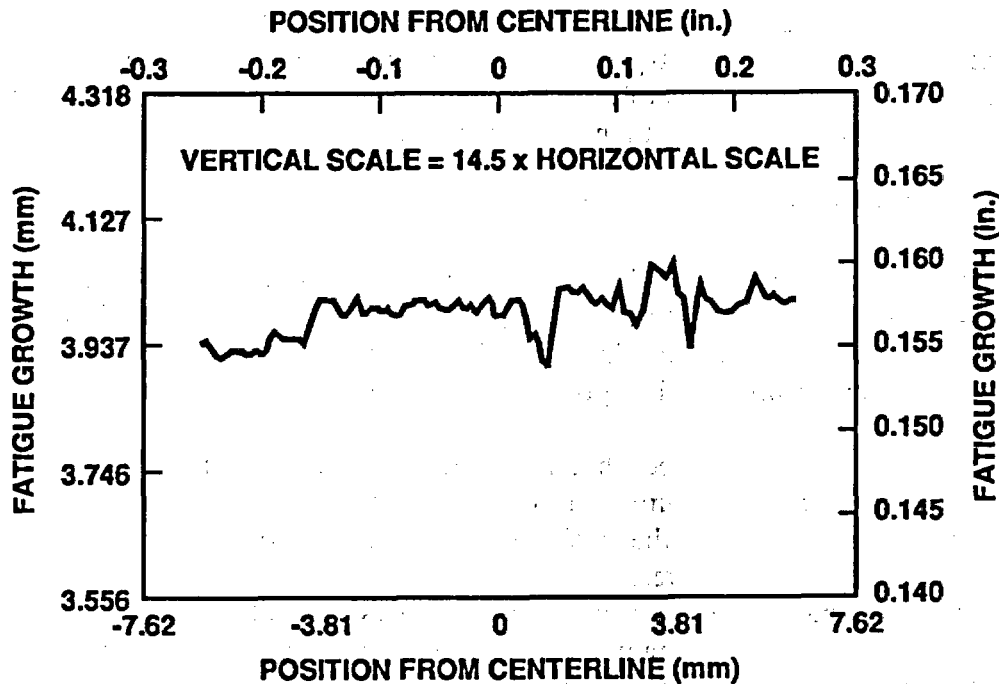


Fig. 9 Data from the microscopic examination of the fracture surface from one of the deep cracked beam specimens show that the fatigue crack front is a zone rather than a point with a finite width in the direction of crack propagation.

The potential significance of geometric irregularity of the crack front can be gauged by comparing the crack front indentation data of Fig. 9 with the elastically calculated plastic zone radii from Fig. 8. The crack front indentation to plastic zone radius ratio is 4.5% (0.11/2.4) for the plane strain case but increases to 14% (0.11/0.8) for the biaxial loading case. This suggests that the location of the process zone within the plastic zone becomes increasingly sensitive to crack front geometric irregularity as the out-of-plane far field stress  $\sigma'_z$  increases.

The principal result to date from the HSST Program investigation of out-of-plane biaxial stress effects on fracture toughness has been the decision to perform a pilot series of biaxial, fracture-toughness tests. The specimen size will be such as to satisfy the ligament elastic condition requirement outlined above. This requirement will necessitate the use of a large biaxial test specimen and a test machine with matching capabilities.

Before leaving this topic, it is appropriate to place the concern for the potential effect of biaxial loading on fracture toughness into the correct perspective. It appears there is some potential for out-of-plane biaxial loading to reduce fracture toughness below what it would be under otherwise identical uniaxial loading. This should not be taken to infer that the resulting fracture toughness will be less than that obtained from compact test specimens meeting the size requirements of Ref. 20 for plane strain constraint. The compact-test specimen geometry provides a degree of crack-tip constraint higher than that associated with most cracked structures. It is unlikely, therefore, that the biaxial stress effects discussed above will reduce the fracture toughness under prototypical reactor vessel loading conditions below that obtained from

compact-test specimens conforming with the requirements of Ref. 20. An improved understanding of the effects of out-of-plane loading on fracture toughness is of value, however, in refining the probabilistic analysis of PTS transients where best estimate fracture-toughness properties for the actual crack tip constraint conditions can be used.

### Dynamic Crack Arrest

Analysis of crack-arrest behavior in the present generation of PTS-analysis computer programs<sup>21,22</sup> is based a vessel-wall stress distribution derived using static equilibrium loading of the cracked structure. Implicit in this approach is the assumption that dynamic conditions existing during the crack-propagation process will have no significant effect on the final configuration of the arrested crack.

It has long been recognized that intermediate arrest and reinitiation of a crack propagating in a large-scale structure will occur prior to its final arrest.<sup>23</sup> This arrest and reinitiation behavior occurs because the crack propagation time is so much less than the dynamic response time for large-scale structures.

Recent papers have presented crack-arrest analysis results obtained using a model reflecting some aspects of the dynamic crack-propagation process.<sup>24-26</sup> This prompted a renewed HSST Program study of the propagation of cracks in a reactor vessel during a PTS event. This ongoing study is being conducted by Keeney-Walker and Bass\* using the 180° thermoelastic-dynamic ADINA/VPF finite-element model of the reactor vessel wall shown in Fig. 10. The model incorporates an application-mode crack propagation capability which permits the crack to advance when the crack-tip stress-intensity factor exceeds the material dynamic fracture toughness  $K_{ID}$ . Estimates of  $K_{ID}$  as a function of crack-tip velocity and the local material temperature were taken from Refs. 27 and 28.

The model of Fig. 10 was used to analyze the dynamic response of a vessel with a 2.39 cm (0.94 in.) deep surface crack to a PTS transient. The transient and initial crack depth selected for this analysis were taken from a previously completed OCA-P analysis. The OCA-P analysis predicted crack initiation with a subsequent arrest when the crack had propagated to the mid point of the vessel wall.

Transient stress intensity-factor results from the initial dynamic analysis of the cracked vessel are shown as the lower curve in Fig. 11. The crack initiated when the crack-tip stress-intensity factor reached a value of  $110 \text{ MPa}\sqrt{\text{m}}$  ( $100 \text{ ksi}\sqrt{\text{in.}}$ ) and arrested after it had penetrated to a depth of 8.51 cm (3.35 in.). The vessel wall T-RT<sub>NDT</sub> temperature and crack tip stress intensity factor at the initial crack arrest were  $87.9^\circ\text{C}$  ( $158^\circ\text{F}$ ) and  $172 \text{ MPa}\sqrt{\text{m}}$  ( $157 \text{ ksi}\sqrt{\text{in.}}$ ), respectively. The crack-tip stress-intensity factor continues to increase, following arrest of the crack, due to the dynamic overshoot effect. In addition, higher order vibration response of the reactor vessel generates an oscillation of the crack-tip stress-intensity factor time history about the mean value. These oscillations generate high-straining rates at the crack tip and by so doing reduce the stress-intensity factor required for crack reinitiation. The basic question relative to

---

\*J. Keeney-Walker and B. R. Bass, "Issues in Dynamic Fracture Analysis of Reactor Pressure Vessels," USNRC NUREG/CR-5793 (ORNL/TM-11969), (to be published January, 1992).

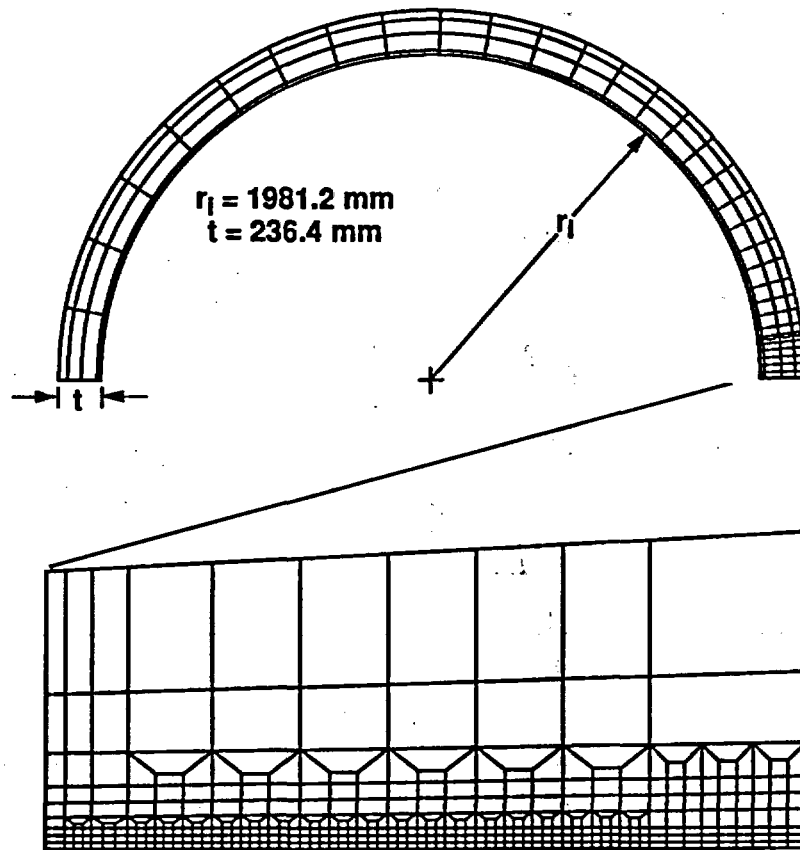


Fig.10 The ADINA elastic-dynamic finite element model used in the study of reactor vessel dynamic response effects on crack arrest during a PTS transient.

the utility of dynamic crack arrest relates to the stability of the arrested crack when exposed to the combined effects of dynamic overshoot loading and dynamic degradation of the material fracture toughness ( $K_{I,d}$ ).

Lower bound ( $-2\sigma$ ) estimates of  $K_{I,d}$  for the straining rates shown in Fig. 11 were obtained using the data of Ref. 29 to interpolate between the lower-bound  $K_{I,c}$  and  $K_{I,a}$  curves of Ref. 30. At the  $T-RT_{NDT}$  value appropriate to the arrested crack depth, the estimated dynamic crack-initiation toughness  $K_{I,d}$  was obtained as  $263 \text{ MPa}\cdot\sqrt{\text{m}}$  ( $240 \text{ ksi}\cdot\sqrt{\text{in.}}$ ). The post-arrest  $K_{I,d}$  curve in Fig. 11 is seen to reach the critical  $K_{I,d}$  value at approximately 20 ms following the first arrest, thereby triggering reinitiation of the crack. The reinitiated crack finally arrests at a depth of 10.9 cm (4.3 in.).

Crack arrest depths predicted by the static and dynamic-crack-arrest analysis models evaluated are shown in Fig. 12. The static equilibrium model<sup>21</sup> of OCA-P is seen to give a slightly conservative crack arrest depth prediction when compared with the dynamic-analysis prediction with crack reinitiation included.

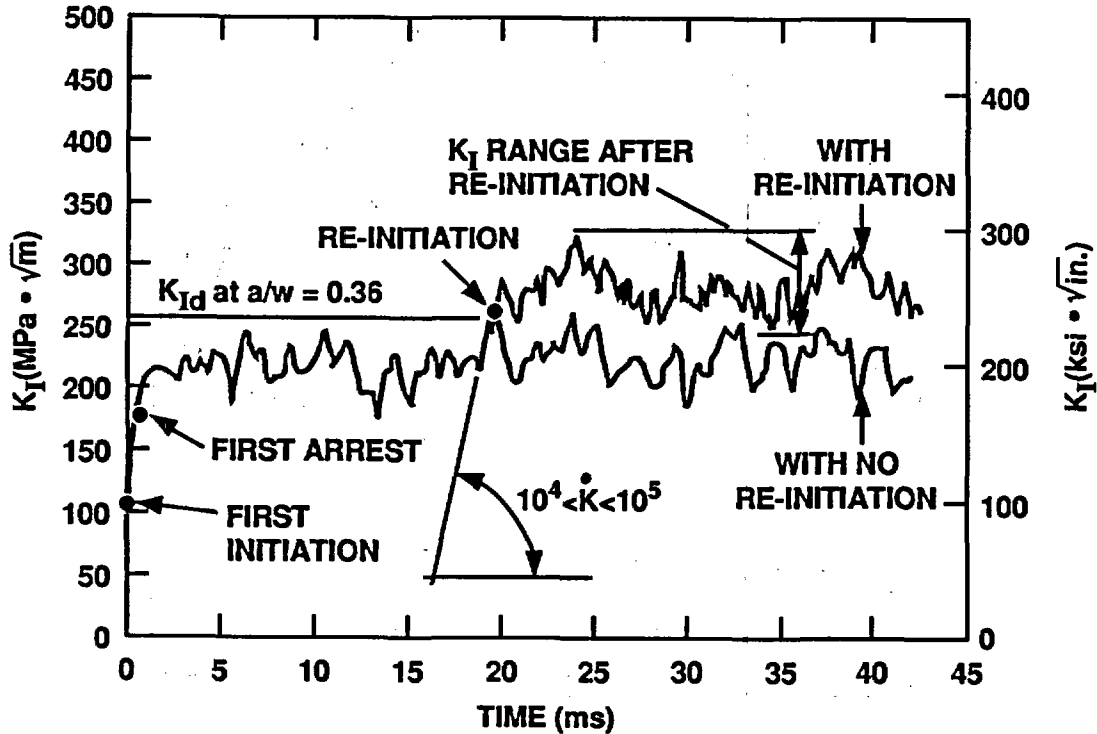


Fig.11 Time history of the crack-tip stress intensity factor following crack initiation showing the effect of reinitiation of the the crack after an initial arrest.

It will be evident from the above discussion that the current analyses provide what is probably a lower bound estimate of the influence of vessel dynamic response effects on crack arrest. The plane strain analysis model of Fig. 10 incorporates the assumption of an infinite flaw length. Prior analyses<sup>31,32</sup> have shown that the stress intensity factor at the deepest point of a semielliptical surface crack remains less than that for an infinite flaw even when the flaw surface dimension becomes very long. The stress-intensity-factor time history given in Fig. 11 for the period following the initial crack arrest will therefore be conservative for flaws of finite length. Incorporation of finite-length-flaw stress intensity factors into the analysis together with a statistical rather than a lower bound representation of  $K_{I_d}$  would preclude crack reinitiation in many cases. The initial crack arrest would then become the final arrest.

The analysis results of Fig. 12 shows that without reinitiation, the crack depth to vessel-wall-thickness ratio ( $a/w$ ) at arrest would be 0.36 rather than the value of 0.5 predicted by the OCA-P static equilibrium model. This difference could be very important in a probabilistic fracture mechanics analysis since, beyond a critical depth, the arrested cleavage crack becomes unstable due to the onset of ductile tearing. This effect is illustrated in the critical-crack-depth curves and tearing-instability curves of Fig. 13, which are reproduced from Ref. 33. The OCA-P static-equilibrium analysis (point 5) and the dynamic analysis with crack reinitiation (point 4) both predict crack arrest at depths where ductile tearing would cause an infinitely long arrested cleavage crack to propagate to failure. In the event cleavage crack reinitiation does not occur however, the crack would arrest at a depth where it would remain stable, provided that the vessel does not contain low-upper-shelf material.

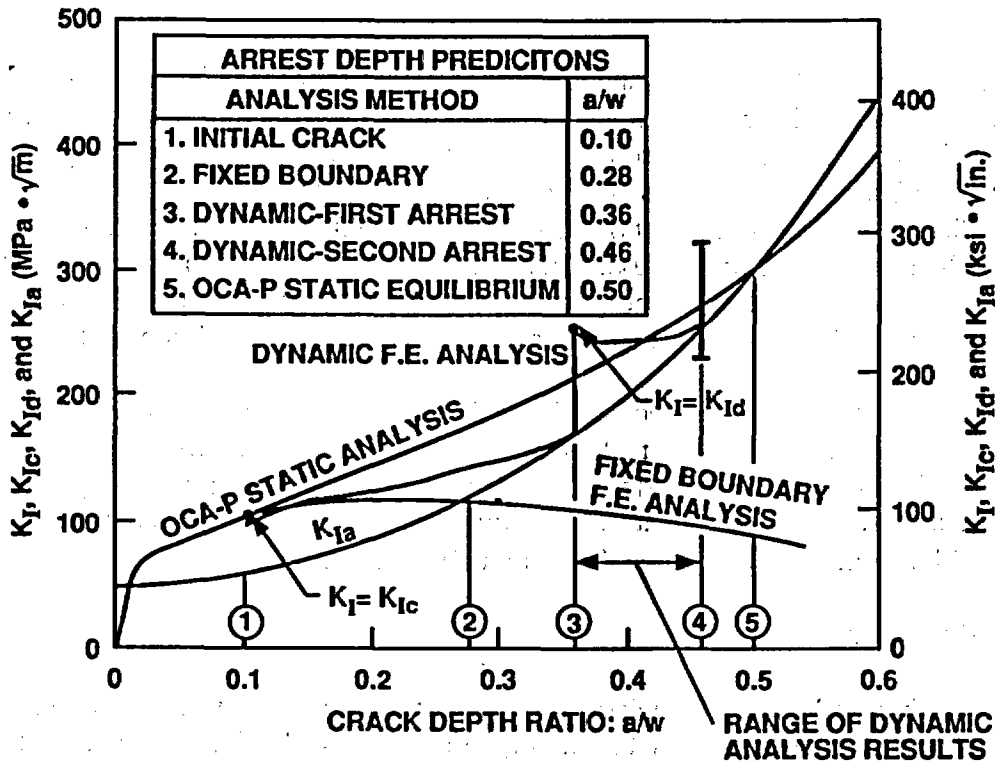


Fig.12 Crack arrest depths predicted by the static and dynamic analysis models.

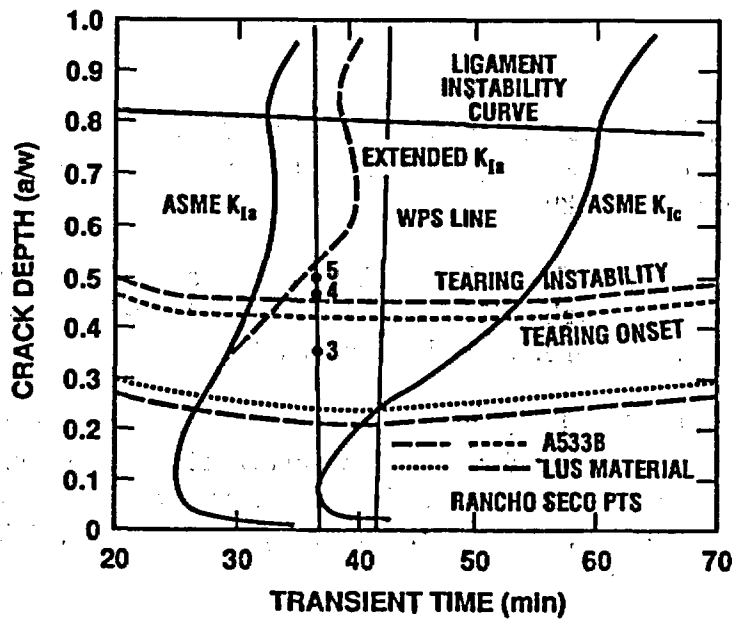


Fig.13 Results from the dynamic analysis indicate that, if reinitiation occurs following the initial arrest, then the second arrest will occur at a depth where the crack will subsequently become unstable due to ductile tearing.

## Conclusions

Preliminary results from the shallow-flaw fracture-toughness testing of A533 B Class 1 material confirm the existence of an enhanced shallow flaw fracture toughness effect for this material. This property may decrease the significance to pressure vessel integrity of the shallow flaws which are both most numerous and most difficult to detect.

Studies of the potential effect of out-of-plane biaxial stresses on fracture toughness have been inconclusive to this point. Biaxial fracture toughness tests, with specimens of sufficient size to permit retention of elastic conditions in the unbroken ligament up to the point of fracture, are required to provide a basis for the further development and validation of out-of-plane biaxial fracture models.

Reactor vessel dynamic response effects during crack propagation may have a significant influence on the number of stable crack arrests predicted in a probabilistic PTS analysis. Finite flaw length effects are also important with regard to the arrest and subsequent stability of propagating cracks. Additional dynamic crack initiation toughness ( $K_{I,d}$ ) data for A533 B Class 1 material will be required to determine the magnitude of this effect.

## Acknowledgements

The author wishes to acknowledge the support, assistance and consultation received from the staff of the Heavy Section Steel Technology program at Oak Ridge National Laboratory and the program consultants at Brown University, The University of Maryland and the University of Kansas. The support and encouragement provided by M. E. Mayfield (HSST Program Monitor) and C. Z. Serpan (Chief, Materials Engineering Branch) of the NRC is also gratefully acknowledged.

## References

1. William A. Sorem, The Effect of Specimen Size and Crack Depth on the Elastic-Plastic Fracture Toughness of a Low-Strength High-Strain-Hardening Steel, Ph.D. dissertation, University of Kansas, May 1989.
2. J. A. Smith and S. T. Rolfe, "The Effect of Crack Depth to Specimen Width Ratio on the Elastic-Plastic Fracture Toughness of a High-Strength Low-Strain Hardening Steel," *Welding Research Council Bulletin 358*, November 1990.
3. R. D. Cheverton and D. G. Ball, "Chapter 5, Probabilistic Fracture Mechanics Analysis of Potential Overcooling Sequences for H. B. Robinson Unit 2," pp. 263-306 in *Pressurized-Thermal-Shock-Evaluation of the H. B. Robinson Nuclear Power Plant*, NUREG/CR-4183, Vol. 1 (ORNL/TM- 9567/VI), Martin Marietta Energy Systems Inc., Oak Ridge National Laboratory (September 1985).

4. T. J. Theiss, G. C. Robinson, and S. T. Rolfe, "Preliminary Test Results from the Heavy-Section Steel Technology Shallow-Crack Fracture Toughness Program," *PVP-Vol.-13/MPC-Vol.32, Pressure Vessel Integrity*, American Society of Mechanical Engineers, June 1991.
5. Timothy J. Theiss and John W. Bryson, "Influence of Crack Depth on the Fracture Toughness of Reactor Pressure Vessel Steel," presented at the ASTM Symposium in Indianapolis on Constraint Effects in Fracture, May 8-9, 1991, ASTM STP-xxx, American Society of Testing and Materials (to be published).
6. M. T. Kirk, K. C. Koppenhoefer, and C. F. Shih, "Effect of Constraint on Specimen Dimensions Needed to Obtain Structurally Relevant Toughness Measures," presented at the ASTM Symposium in Indianapolis on Constraint Effects in Fracture, May 8-9, 1991, ASTM STP-xxx, American Society of Testing and Materials (to be published).
7. S. T. Rolfe, University of Kansas, "Interpretive Report on the Application of Shallow-Flaw CTOD Test Data to the Structural Margin Assessment of Reactor Pressure Vessels with Flaws," Prepared for Marietta Energy Systems Inc., USNRC Report NUREG/CR-5767, ORNL/Sub/90-SH640/1, November 1991.
8. W. E. Pennell, Martin Marietta Energy Systems, Inc., Oak Ridge Natl. Lab., "Heavy-Section Steel Technology Program : Fracture Issues," pp. 1-16 in *Proceedings of the U.S. Nuclear Regulatory Commission Seventeenth Water Reactor Safety Meeting*, October 23-25, 1989, USNRC Report NUREG/CP-0105, March 1990.
9. C. Betegón and J. W. Hancock, "Two-Parameter Characterization of Elastic-Plastic Crack Tip Fields," *Journal of Applied Mechanics* (58) (1991), pp. 311-325.
10. C. F. Shih, N. P. Dowd, and M. T. Kirk, "A Framework for Quantifying Crack Tip Constraint," presented at the ASTM Symposium in Indianapolis on Constraint Effects in Fracture, May 8-9, 1991, ASTM STP-xxx, American Society of Testing and Materials (to be published).
11. D. K. M. Shum et al., Martin Marietta Energy Systems, Inc., Oak Ridge Natl. Lab., "Analytical Studies of Transverse Strain Effects on Fracture Toughness for Circumferentially Oriented Cracks," NUREG/CR-5592, (ORNL/TM-11581), Martin Marietta Energy Systems, Inc., Oak Ridge National Laboratory, April 1991.
12. J. R. Rice and M. A. Johnson, Brown University, Providence, R.I., "The Role of Large Crack Tip Geometry Changes in Plane Strain Fracture," Report NYO-2394-38, September 1969.

13. A. C. MacKenzie, J. W. Hancock, and D. K. Brown, "On the Influence of the State of Stress on Ductile Failure Initiation in High Strength Steels," Department of Mechanical Engineering, University of Glasgow, Scotland, *Engineering Fracture Mechanics* (9) 1977, Pergamon Press, pp. 167-188.
14. J. Keeney-Walker, "A Numerical Study of Local Crack-Tip Fields for Modeling Cleavage Fracture Initiation," Masters Thesis, The University of Tennessee, Knoxville, May 1990.
15. C. E. Inglis, "Stresses in a Plate Due to the Presence of Cracks and Sharp Corners," *Transactions of the Institution of Naval Architects*, London, England (55) 1913, pp. 219-230.
16. John M. Barsom and Stanley T. Rolfe, *Fracture & Fatigue Control in Structures—Applications of Fracture Mechanics*, second edition, 1987, Prentice-Hall Inc., pp. 41, Table 2.2.
17. J. D. Landes and D. E. McCabe, Westinghouse R&D Center, Pittsburgh, PA, "Effect of Section Size on Transition Temperature Behavior of Structural Steels," *Fracture Mechanics: Fifteenth Symposium*, ASTM STP 833, 1984, pp. 378-39.
18. V. Weiss, Syracuse University, *Material Ductility and Fracture Toughness of Metals, Proceedings of the International Conference on Mechanical Behavior of Materials*, Kyoto, Japan, August 15-20, 1971, The Society of Materials Science, Japan 1972.
19. S. J. Garwood, The Welding Institute of the United Kingdom, "The Significance of Biaxial Loading on the Fracture Performance of a Pressure Vessel Steel," *PVP-Vol. 213/MPC-Vol 32, Pressure Vessel Integrity*, American Society of Mechanical Engineers, June 1991.
20. ASTM E399-83, "Standard Method for Plane-Strain Fracture Toughness of Metallic Materials," *Metals-Mechanical Testing; Elevated and Low-Temperature Tests; Metallography*, Annual Book of ASTM Standards, Vol. 03.01, 1990.
21. R. D. Cheverton and D. G. Ball, Martin Marietta Energy Systems, Inc., Oak Ridge Natl. Lab., "A Deterministic and Probabilistic Fracture-Mechanics Code for Application to Pressure Vessels," USNRC Report NUREG/CR-3618 (ORNL-5991), May 1984.
22. F. A. Simonen et al., Pacific Northwest Laboratory, "VISA-II - A Computer Code for Predicting the Probability of Reactor Pressure Vessel Failure," USNRC Report NUREG/CR-4486 (PNL-5775), March 1986.
23. D. J. Naus et al., Martin Marietta Energy Systems, Inc., Oak Ridge Natl. Lab., "SEN Wide-Plate Crack-Arrest Tests Using A 533 Grade B Class 1 Material: WP-CE Test Series," USNRC Report NUREG/CR-5408 (ORNL/TM-11269), November 1989.

24. David J. Ayres, et al., "Comparison of Analysis and Experimental Data for a Unique Crack Arrest Specimen," ASTM Special Technical Publication 969, American Society for Testing and Materials, 1988, pp. 724–751.
25. E. Smith and T. J. Griesbach, "Simulating the Effect of Pressure Plus Thermal Loadings on Crack Arrest During a Hypothetical Pressurized Thermal Shock Event," pp. 41–46 in *PVP-Vol. 213/MPC-Vol 32, Pressure Vessel Integrity*, American Society of Mechanical Engineers, June 1991.
26. D. S. Moelling et al., "Probabilistic Fracture Mechanics Application of Dynamic Crack Arrest by Static Analogy," pp. 261–268 in *PVP-Vol. 213/MPC-Vol 32, Pressure Vessel Integrity*, American Society of Mechanical Engineers, June 1991.
27. B. R. Bass et al., "Fracture Analyses of Heavy-Section Steel Technology Wide-Plate Crack-Arrest Experiments," *Fracture Mechanics: Nineteenth Symposium*, ASTM STP 969, T. A. Cruse, ed., American Society for Testing and Materials, pp. 691–723, 1988.
28. M. F. Kanninen, J. Ahmad, and V. Papaspyropoulos, pp. 119–121 in "Heavy-Section Steel Technology Program Semiannual Progress Report for April–September 1984," USNRC Report NUREG/CR-3744, Vol. 2 (ORNL/TM-9154/V2), December 1984.
29. W. O. Shabbits, W. H. Pryle, and E. T. Wessel, Westinghouse Electric Corporation, PWR Systems Division, Pittsburgh, Pa., *Heavy-Section Fracture Toughness Properties of A 533 Grade B Class 1 Steel Plate and Submerged Arc Weldment*, WCAP-7414, December 1969.
30. Section XI, Appendix A of the American Society of Mechanical Engineers Boiler and Pressure Vessel Code, Rules for Inservice Inspection of Nuclear Power Plant Components, 1989.
31. J. G. Merkle et al., *Comparisons of 3-D and 2-D Computed K Values for Long, Inside Surface Flaws in a PWR for Combined Pressure-Thermal Loading*, pp. 3–4 in "Heavy-Section Steel Technology Program Quarterly Progress Report for July–September 1982," USNRC/CR-2571, Vol. 3 (ORNL/TM-8369/V3), January 1983.
32. R. D. Cheverton and D. G. Ball, "A Reassessment of PWR Pressure Vessel Integrity During Overcooling Accidents, Considering 3-D Flaws," in *Journal of Pressure Vessel Technology* (6) 1984, pp. 375–382.
33. T. L. Dickson and T. J. Theiss, "Potential Impact of Enhanced Fracture-Toughness Data on Fracture Mechanics Assessment of PWR Vessel Integrity for Pressurized-Thermal-Shock," pp. 101–108 in *PVP-Vol. 208, Power Plant Systems/Components Aging Management and Life Extension*, American Society of Mechanical Engineers, June 1991.

## **Pipe Fracture Behavior Under High-Rate (Seismic) Loading -- the IPIRG Program**

by

**R.A. Schmidt, G.M. Wilkowski,  
P.M. Scott, and R.J. Olson**

**BATTELLE  
Columbus, Ohio**

### **ABSTRACT**

Results are summarized from numerous experiments and supporting analyses conducted to investigate the behavior of circumferentially flawed piping and piping systems subjected to high-rate loading typical of seismic events. The investigation included both "separate effects" experiments on simple pipe specimens with either pure inertial or displacement-controlled loading, and full-scale experiments on a representative piping system with combined loading tested at pressurized water reactor (PWR) conditions.

### **INTRODUCTION**

The International Piping Integrity Research Group (IPIRG) program was an international group program managed by the U.S. Nuclear Regulatory Commission (USNRC) and funded by a consortium of organizations from nine nations: Canada, France, Italy, Japan, Sweden, Switzerland, Taiwan, the United Kingdom, and the United States. The organizations and cognizant individuals in the IPIRG program are listed in Table 1. A Technical Advisory Group (TAG), consisting of experts from all member countries, met formally twice a year to exchange ideas, data, and analysis and to provide technical guidance to the program. Figure 1 is a photo of the participants at one of these meetings. The active participation of the members provided a forum for discussing significant technological issues and for working towards achieving an international consensus on LBB and flaw evaluation criteria. The five-year program, conducted at Battelle in Columbus, Ohio, was completed in June 1991.

The objective of the program was to develop data needed to verify engineering methods for assessing the integrity of nuclear power plant piping that contains circumferential defects. These data are considered essential to verify the validity and degree of conservatism of current LBB analyses and in-service flaw assessment methods. Many flawed-piping research programs have been conducted in the U.S. (e.g. Wilkowski et al. 1989; Vassilaros et al. 1984; Tang et al. 1985) and in other countries (e.g. Takumi 1989; Darlaston and Harrison 1977; Maricchiolo and

**Table 1. IPIRG Technical Advisory Group Members.**

United Kingdom		Japan <sup>(a)</sup>	
Nuclear Elec.	Dr. J. Darlaston	CRIEPI	Dr. K. Kashima
Switzerland		Canada	
HSK	Mr. H. Njo	AECB	Dr. A. Omar
KKL	Dr. D. Burns	Ontario Hydro	Mr. M. Kozluk
Taiwan		France	
AIT	Mr. Y. Cheng <sup>(b)</sup>	CEA	Mr. Ph. Jamet
ROC-AEC	Mr. R. Wu	EDF	Mr. C. Faigy
INER	Dr. K. Ting	Framatome	Dr. S. Bhandariu
Sweden		Italy	
SKi	Dr. B. Brickstad <sup>(c)</sup>	ENEA	Dr. P. Milella
United States			
	USNRC-RES	Mr. M. Mayfield	
	USNRC-NRR	Mr. K. Wichman	
	EPRI	Mr. J. Gilman	

(a) Other Japanese members include, Mitsubishi, Toshiba, Hitachi, IHI, and 13 electric utilities.

(b) Taiwan Power Company.

(c) AB Statens Anläggningsprovning.

Milella 1989; Faigy et al. 1988). However, most of these programs involved quasi-static loading of cracked pipe, rather than the high-rate loading typical of seismic events.

The IPIRG Program encompassed numerous tasks, but the primary focus was an experimental task designed to investigate the behavior of circumferentially flawed piping and piping systems subjected to high-rate loading typical of seismic events. The task consisted of both "separate effects" experiments on simple small-diameter pipe specimens and experiments on a large-diameter piping system tested at nominal pressurized water reactor (PWR) conditions. The separate effects experiments provided an evaluation of the effects of loading rate and cyclic loading on the fracture behavior of flawed pipe subjected to displacement-controlled loads and inertial loads. The pipe system experiments were conducted to investigate the complex interaction of loading conditions and system dynamics. Results from these experiments provide an important data base that can be used for the critical assessment of analytical procedures. Other program efforts that supported the pipe fracture work included material characterization studies, updates of a pipe fracture data base, a leak-rate investigation, finite element analyses of

circumferential through-wall-cracked pipe fracture experiments, two 30-inch diameter quasi-static pipe fracture experiments, seminars, and workshops.

## **PIPE FRACTURE EXPERIMENTS**

The design of piping systems in nuclear power plants recognizes the existence of both inertial and displacement-controlled loads. Uncertainties in the ability to characterize inertial loads has, in part, led to a prevailing industry design practice that results in inherently stiff piping systems. However, stiff systems are less tolerant of displacement-controlled loads caused by thermal expansion and differential anchor motion. Furthermore, the hardware used to restrict pipe motion in nuclear plants, such as pipe hangers, snubbers, and pipe whip restraints, makes pipe system inspection difficult. As a result operators and designers are considering more flexible piping systems. A concern with flexible piping systems is the stability of cracks in piping which may be subjected to loads with a high inertial component. The IPIRG program was formulated to investigate the separate effects of both inertial and displacement-controlled stresses on flawed piping as well as the combined effects on representative piping systems.

### **Displacement-Controlled Experiments**

Eleven experiments were conducted on 6-inch diameter Schedule 120 pipe samples containing circumferential through-wall cracks and loaded in four-point bending under displacement control. Pipe specimens were either wrought TP304 stainless steel or A106 Grade B carbon steel. The through-wall crack lengths were 37 percent of the circumference. All experiments were conducted at 288 C, but unlike the other pipe experiments conducted in this program, these pipe specimens did not contain pressurized water.

One objective of these experiments was to isolate the effects of high loading rates typical of seismic events, and the effects of cyclic loading during ductile tearing. Displacement-controlled loading was used for this investigation since it is generally the easiest to conduct and analyze, and since existing data from the USNRC's Degraded Piping Program (Wilkowski et al. 1989) on displacement-controlled experiments could be efficiently utilized for a direct comparison of results. In addition, tensile and C(T) fracture toughness tests were conducted at both quasi-static rates and at high rates of loading for direct comparison to the pipe experiments.

Figures 2 and 3 summarize the tensile test results. At high loading rates, the strength, as well as the toughness, of the wrought TP304 stainless steel improved slightly. For the A106 Grade B, both strength and toughness decreased significantly at the higher loading rates. These trends are reflected in the moment-rotation behavior from the pipe fracture experiments. A slight increase is observed in the load-carrying capacity of the stainless steel at the high loading rate (Fig. 4), while a significant decrease in load-carrying capacity is observed for the carbon steel (Fig. 5). J-R curves calculated for the pipe fracture experiments also show little effect of high-rate loading on stainless steel toughness, while the toughness of the carbon steel decreased significantly at the high loading rate. The lowering of strength and toughness of the carbon steel at high loading rates is believed to be due to dynamic strain aging of this particular A106 Grade B pipe.

The effects of cyclic loading on ductile tearing in pipe fracture experiments showed that there are two important parameters to consider. One is the ratio of minimum to maximum load or load ratio, R, and the other is the incremental plastic displacement or incremental crack growth. The effects of load ratio on the moment-rotation behavior of stainless and carbon steel pipe fracture

experiments are summarized in Figures 6 and 7. (The curves for the cyclic experiments represent the envelope of successive maximum points achieved during cycling.) Little cyclic effect is observed for  $R = 0$ , but for  $R = -1$  (fully reversed cycling) a significant drop in load-carrying capacity is observed. J-R curves calculated for these experiments reflect similar trends.

The effect of incremental plastic displacement on fracture behavior was investigated for the stainless steel pipe. Generally, the amount of incremental plastic displacement allowed between cycles was held constant throughout a given experiment. In several of the stainless steel pipe fracture experiments the amount of incremental plastic displacement for each cycle was held constant for a block of cycles and then changed to a new value for the next block (Fig. 8). Figure 9 shows the effect of the incremental plastic displacement on the normalized crack-tip-opening angle (CTOA) for the stainless steel at  $R = 0$  and  $R = -1$ . These results suggest that as the incremental plastic displacement gets smaller (smaller crack growth per cycle), the apparent fracture resistance can drop significantly.

Estimates of load ratios for typical seismic loading on nuclear plant piping indicate that  $R$  may be as low as  $-0.6$ . However, typical seismic load histories would be expected to have relatively few cycles that produce crack growth. Results displayed in Figure 9 suggest that a cyclic loading history with few, large amplitude cycles may be of little consequence to maximum load predictions in these applications.

### Inertially Loaded Experiments

Several pipe fracture experiments with inertial loading were conducted on the same 6-inch diameter carbon and stainless steel pipe used for the displacement-controlled experiments. The primary objective of these experiments was to investigate the effect of inertial loading on the stability of pressurized cracked pipe. Five cracked-pipe specimens with either through-wall cracks or surface cracks were loaded to failure at 288 C. The length of the through-wall cracks was 37 percent of the circumference. The surface cracks had a length that was 50 percent of the circumference and a depth that was approximately 70 percent of the pipe thickness. The pipes were pressurized with water at 15.2 MPa.

A unique computer-controlled test system was designed and fabricated to conduct these dynamic experiments (Fig. 10). The test system is a servo-hydraulic design with the test pipe mounted horizontally and with a large mass attached to each end. The computer controls force a rapid, vertical motion at 3.5 Hz, which is 83 percent of the system's first natural frequency, 4.2 Hz. The pipe test frame and specimen configuration were analyzed using a finite element model and the ANSYS code to aid in design of the test system.

The pipe specimens were loaded by applying a sinusoidal displacement function of increasing amplitude. This produced a bending moment that varied in time, such as seen in Figure 11. The resulting moment-rotation behavior is seen in Figure 12. One of the more important observations that can be made from these experiments is that once maximum load was achieved, there were very few additional cycles until the pipe essentially broke into two pieces. For four of the five cracked pipe experiments there were only 2 to 4 cycles that the pipe specimens survived past maximum load. The implication from a fracture viewpoint is that, in seismic applications, inertial stresses should be considered as load-controlled (primary) stresses, not displacement-controlled (secondary) stresses.

## **Pipe System Experiments**

The objective of the pipe system experiments was to provide the data necessary to assess the analysis methodologies for characterizing the fracture behavior of circumferentially cracked pipe in a representative piping configuration under combined inertial and displacement-controlled stresses. Results from the separate effects experiments conducted with purely displacement-controlled and inertially controlled loading were used to evaluate results of these complex experiments. By developing data on a full-scale representative piping system, the complex interaction of loading conditions and system dynamics provided important test cases for the assessment of current analytical procedures. The piping system was designed to have flexibility that is representative of typical nuclear piping systems.

While this task was primarily experimental, extensive supporting analyses were conducted to design the facility and the piping system as well as to design the individual experiments and analyze the results. The pipe system experiments involved one uncracked pipe experiment designed to investigate system dynamics and boundary conditions, and five cracked pipe experiments, each on a different material. All experiments, except the uncracked pipe experiment, were taken to failure, as evidenced by the occurrence of a double-ended break or, at least, a very long through-wall crack.

A unique experimental facility was designed and constructed to conduct these experiments (Fig. 13 and 14). The piping system was fabricated as an expansion loop with over 30 m of 16-inch diameter Schedule 100 pipe and five long radius elbows. The pipe loop configuration, its supporting framework, and the foundation were designed by means of dynamic finite element calculations using the ANSYS code. One of the key design criteria included the requirement that the pipe loop be reusable for all six experiments in the original test matrix. The cracked test specimens were welded into the pipe loop at a location of high bending stress as identified from the calculations. Each experiment was conducted by simply replacing the failed test section with a new one. In order to minimize plastic deformation in the pipe loop and to concentrate the deformation in the cracked specimen, the pipe loop was fabricated using high strength steel pipe (ASTM A710, Grade A, Class 3).

The pipe loop is supported and constrained at several locations using various specialized pieces of hardware. These supports and hardware were designed to produce specific well-defined boundary conditions that could be easily modeled in numerical calculations. There was no intent to simulate supports used in actual nuclear plants. The emphasis was to gather data that can be used to test analytical capabilities without the complication of large unknowns in test conditions. The pipe loop is rigidly constrained at two fixed ends, it is vertically supported on hydrostatic bearings at two locations, and it is constrained from motion perpendicular to the pipe by spherical bearings at three locations (Fig. 13).

System loads are applied by a computer-controlled hydraulic actuator with a 1560-kN load capacity and a 460-mm stroke. The actuator is driven by an 8000 liter per minute three-stage servovalve. The servovalve is supplied with oil at 21 MPa by piston accumulators of 380 liter capacity. Nitrogen gas used to drive the accumulators is stored in a separate pressure vessel. Heat for bringing the pipe loop and water to test temperature is supplied by heater tapes wrapped continuously around the exterior of the pipe loop. The pipe loop is covered with fiberglass insulation. Water in the pipe loop is circulated by a pump connected to the two fixed ends to provide an even temperature distribution. The entire pipe loop contains approximately 3000 liters of water. The pipe system was extensively instrumented. A computerized data

acquisition system recorded the various parameters during the experiments including displacements, accelerations, strains, loads, bending moments, pressures, crack opening, crack rotation, and crack growth.

The uncracked pipe experiment was conducted to investigate system response characteristics. The first four natural frequencies of the pipe were measured and compared to those determined in the finite element analysis (Table 2). The damping characteristics of the system were measured and found to be primarily viscous in nature with a value of approximately 0.5 percent. (This low value is consistent with the low friction pipe supports and the high strength pipe used in the system.) A prescribed displacement-time forcing function was applied to the hydraulic actuator and the system response was measured by the extensive instrumentation. Figure 15 shows the measured bending moment, and that predicted by finite element calculations, as a function of time at the specimen location. The close agreement between measured and predicted results indicates that the boundary conditions and loads are well characterized.

**Table 2. Comparison of measured and predicted natural frequencies for pipe loop test facility.**

	Measured	Analysis	
$F_1$	4.5	4.4	} P=15.5 MPa T=20C
$F_2$	12.0	14.5	
$F_3$	13.9	14.5	
$F_4$	18.0	18.7	
$F_1$	4.4	4.2	P=15.6 MPa T=297C

Five cracked-pipe experiments were conducted to evaluate the fracture behavior of five different materials. These materials were: (1) A106 Grade B carbon steel, (2) SA-358 Type 304 stainless steel, (3) submerged-arc weld in A106 Grade B carbon steel, (4) submerged-arc weld in SA-358 Type 304 stainless steel, and (5) artificially-aged Type CF8M centrifugally cast stainless steel. A relatively long and deep internal surface crack was introduced into each of these test specimens (Table 3). All cracked pipe experiments contained subcooled water at 288 C at a pressure of 15.5 MPa.

A displacement-time forcing function was designed using the ANSYS code for each experiment with the intent of obtaining surface crack penetration in 5 to 15 cycles while achieving a reasonably equal mix of inertial and displacement-controlled loads. Key results from the five cracked pipe experiments are shown in Table 3. The forcing function for the cast stainless steel experiment is shown in Figure 16 and the resulting bending moment at the cracked section is shown in Figure 17. Pretest predictions were made using the ANSYS code with a special nonlinear spring element that was developed to represent the response of the cracked section. A schematic of the nonlinear spring model is shown in Figure 18. Fracture behavior input to the nonlinear spring model was obtained from companion quasi-static experiments that had been

performed on these materials in previous programs and from J-estimation scheme analyses. A comparison of analytical prediction with experimental results is shown in Figure 19 for the stainless steel base metal experiment.

In all five experiments the surface crack penetrated the pipe wall and grew unstably until it arrested at the ends of the surface crack. Subsequent cyclic loading caused additional through-wall crack growth. Two of the five experiments included a sufficient number of extra cycles after penetration to produce a double-ended break. The forcing function for the aged cast stainless steel experiment is shown in Figure 16 which indicates that thirteen additional cycles of increasing amplitude were required after surface crack penetration to produce the final double-ended break. Results showed that each additional cycle advanced the through-wall crack until the double-ended break occurred when the crack was 94 percent of the circumference and only 75 mm of ligament remained. Figure 20 is a photograph of the fracture surface showing the remaining ligament.

The results of a Net-Section Collapse analysis with fixed and free boundary conditions are shown in Figure 21. The fixed-end assumption gives an instability prediction that coincides well with the results for the aged cast stainless steel experiment. This suggests that either the piping system itself restricts the bending of the cracked section, or some other factor such as the thrust loads of the steam jet help to restrict pipe rotations, and thus delay the final instability until membrane stress alone can produce the failure.

Results from the five cracked pipe experiments were analyzed on the basis of elastic stress analyses and elastic-plastic fracture analyses. In the elastic stress analyses, finite element calculations were used to predict the total stress (bending plus membrane) that would occur at the crack location using the known actuator displacement at the time of maximum measured stress. The calculated stress varied from 0.93 to 1.43 of the measured stress in these five experiments. These results support the finding that this pipe system primarily behaves elastically and that most of the nonlinear behavior is concentrated within the cracked section.

Various fracture analyses were conducted to evaluate the margins inherent in these methods. Analyses evaluated were: (1) Net-Section-Collapse (NSC), (2) Dimensionless plastic-zone parameter (DPZP), (3) ASME Section XI flaw evaluation criteria, (4) R6 Revision 3 Option 1, and (5) J-estimation schemes. Margins are determined by dividing the measured stress by the predicted stress at the time of maximum measured bending moment. Figure 22 shows the range of margins calculated for both the IPIRG pipe system experiments as well as the companion quasi-static experiments conducted previously.

## **FINDINGS AND CONCLUSIONS**

### **Loading Rate Effects**

For the two carbon steels examined at 288 C there was a modest degradation of fracture resistance at loading rates typical of seismic events. The reduced toughness in this carbon steel is attributed to dynamic strain aging (DSA). In contrast, for the stainless steels and welds tested there appeared to be little effect of high-rate loading on fracture properties and strength.

### **Cyclic Loading Effects**

For both carbon steel and stainless steel, cyclic loading was found to reduce the load-carrying capacity of through-wall-cracked pipe by as much as 26 percent depending on load-ratio and the size of the incremental plastic displacement. Effects of cyclic loading on surface-cracked pipe are less clear, but results from the pipe system experiments suggest that cyclic effects may be more significant for the surface crack geometry.

### **Inertial Versus Displacement-Controlled Loading**

The inertial load experiments showed markedly less fracture stability than those conducted under displacement-controlled loads. While the maximum load results for the two types of loading compare closely, inertial loading was shown to produce complete fracture instability in only a few cycles past maximum load. The inertial stresses produced in these experiments were similar to load-controlled stresses for fracture stability analyses and should probably be considered as primary loads.

### **Use of Laboratory Data to Predict Fracture Behavior of a Piping System**

Data from C(T) tests, in some cases, were shown to overestimate the effective fracture resistance observed in a surface-cracked piping system under dynamic loads. Results of pipe system experiments were compared with companion quasi-static experiments. While results of these pipe system experiments cannot, as yet, be completely rationalized and modeled on the basis of standard laboratory specimen data, the IPIRG Program has increased the understanding of controlling parameters and is pointing the way to defining the specific laboratory data that are needed. Once the effects of these controlling parameters are understood better, analytical models coupled with laboratory specimen data should be able to predict the behavior of large-diameter piping systems to a variety of loading conditions.

### **Stress Analysis of Pipe System Experiments**

Straightforward linear-elastic dynamic finite element analyses with 0.5 percent damping were shown to give an excellent description of the response of the uncracked piping system. The dynamic behavior of the piping system containing a section of surface-cracked pipe was accurately modeled with a nonlinear, time-dependent finite element analysis that included a nonlinear spring model to simulate the cracked section. Results of linear elastic stress analysis support the finding that this piping system primarily behaves elastically and that most of the nonlinear behavior is concentrated within the cracked section.

### **Fracture Analysis**

All quasi-static and dynamic pipe fracture experiments, as well as pipe system experiments, were analyzed using state-of-the-art predictive fracture methods (Net Section Collapse, Dimensionless Plastic Zone Parameter, and J-estimation) and failure avoidance methods (R6 and ASME Section XI). The predictive methods gave relatively accurate predictions of maximum bending moments. R6 and ASME analyses generally underestimated the maximum bending moments.

## **The Double-Ended Guillotine Break**

In the past, a nearly instantaneous double-ended guillotine break (DEGB) that occurs in a time of one millisecond has been postulated as the worst case failure mode. The results from the five pipe system experiments suggest that a DEGB is not likely to occur on a single loading cycle during a seismic event unless a very long surface crack exists. A double-ended break was achieved in two of the five pipe system experiments, but only after extensive through-wall crack growth occurred as a result of numerous loading cycles. This degree of stability was unexpected and may be due to the reduction in bending moment caused by the thrust forces produced by the steam jetting from the crack. Other factors, such as inertial mass, may also contribute to this stabilizing effect. Fracture speed results also suggest that the time required to create a DEGB is orders of magnitude longer than one millisecond.

## **ACKNOWLEDGEMENTS**

The authors wish to extend their appreciation to the many organizations who funded this effort and especially to all the members of the IPIRG Technical Advisory Group and their representatives who worked so hard to make this international group program a success. Their active participation throughout the program was a critical factor in that success. We also wish to thank the many engineers, technicians, and secretaries at Battelle who worked many diligent hours to produce a quality research product.

## **REFERENCES**

- Darlaston, B. J., and Harrison, R. P. (1977). Ductile Failure of Thin-Walled Pipes with Defects Under Combinations of Internal Pressure and Bending, 3rd International Conference on Pressure Vessel Technology, Part II, Materials and Fabrication, pp 669-676.
- Faidy, C., Jamet, P., and Bhandari, S. (1988). Developments in Leak Before Break Approach in France, NUREG/CP-0092, pp 69-82.
- Maricchiolo, C., and Milella, P. P. (1989). Fracture Behavior of Carbon Steel Pipes Containing Circumferential Cracks at Room Temperature and 300 C, Nuclear Engineering and Design, 111, pp. 35-46.
- Takumi, K. (1989). Results of the Japanese Carbon Steel Pipe Fracture Program, presented at IPIRG Leak-Before-Break Seminar, Taipei, Taiwan.
- Tang, H. T., Duffey, R. B., Sing, A., and Bausch, P. (1985). Experimental Investigation of High Energy Pipe Leak and Rupture Phenomena, ASME Special Publication PVP Volume 98-8, Fracture, Fatigue and Advanced Mechanics.
- Vassilaros, M. G., Hays, R. A., Gudas, J. P., and Joyce, J. A. (1984). J-Integral Testing Instability Analysis for 8-Inch Diameter ASTM A106 Steel Pipe, NUREG/CR-2347.
- Wilkowski, G. M., et al. (1989). Degraded Piping Program - Phase II, NUREG/CR-4082, Vol. 8.

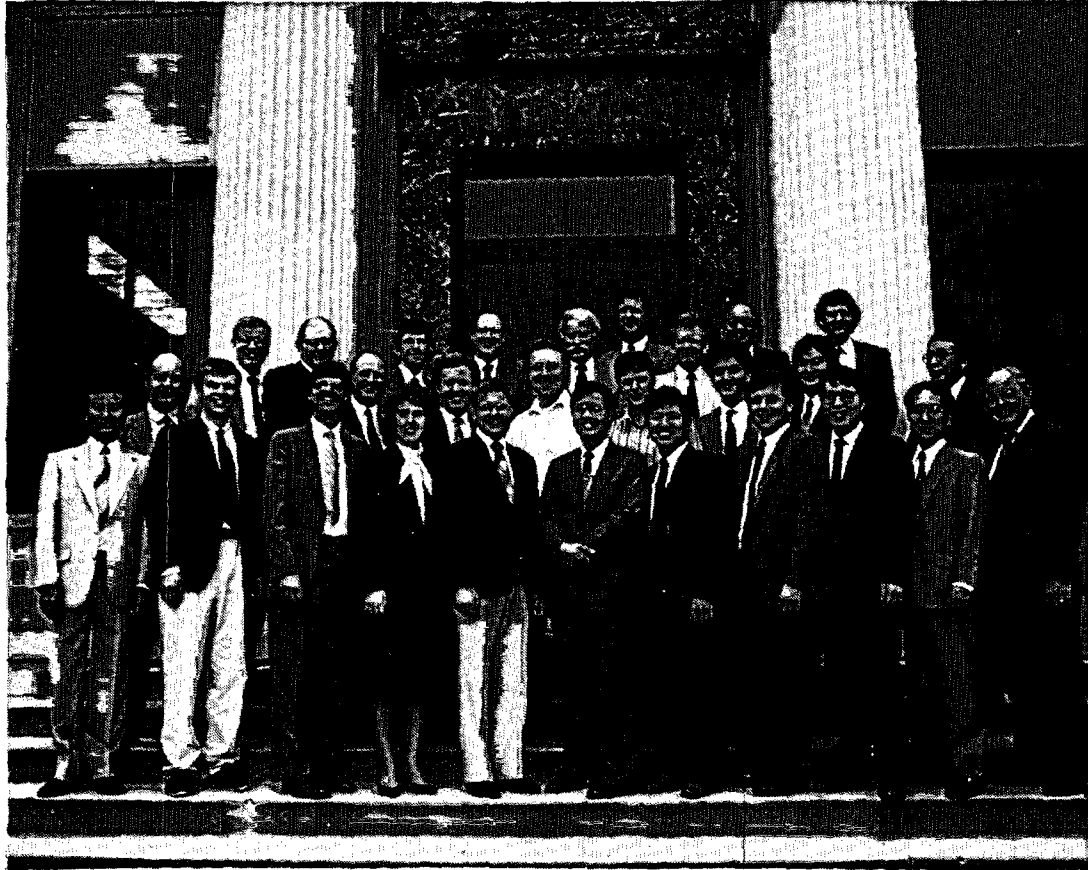


Fig. 1. Participants at a Technical Advisory Group meeting.

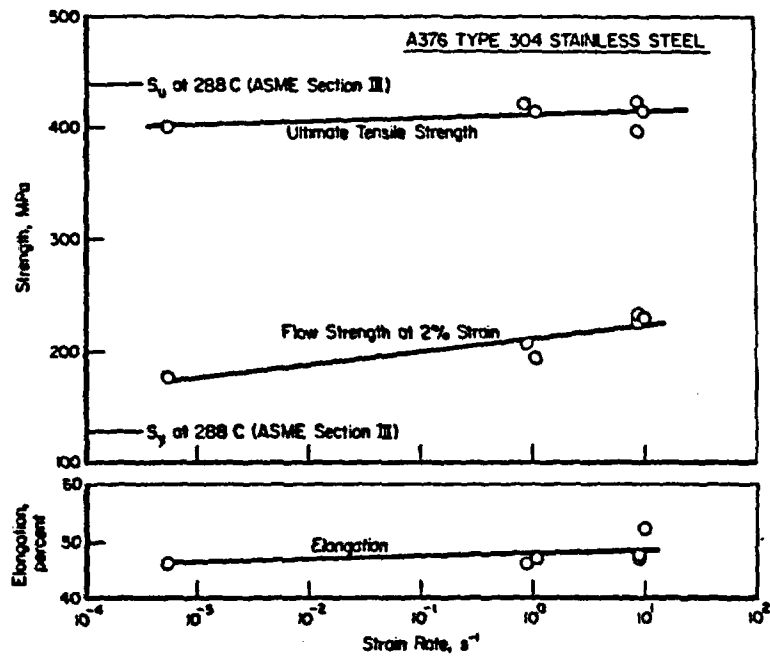


Fig. 2. Effect of strain rate on tensile properties of A376 Type 304 Stainless Steel at 288 C.

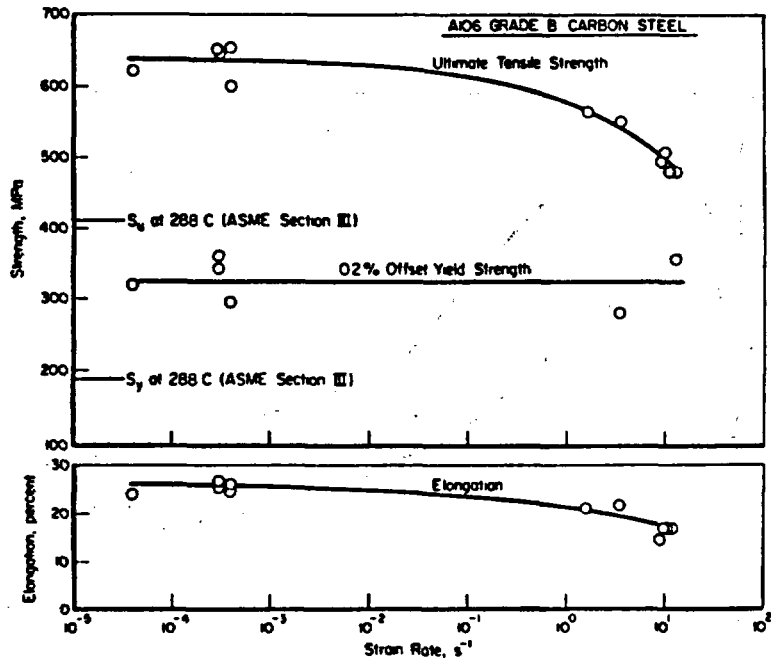


Fig. 3. Effect of strain rate on tensile properties of A106 Grade B carbon steel at 288 C.

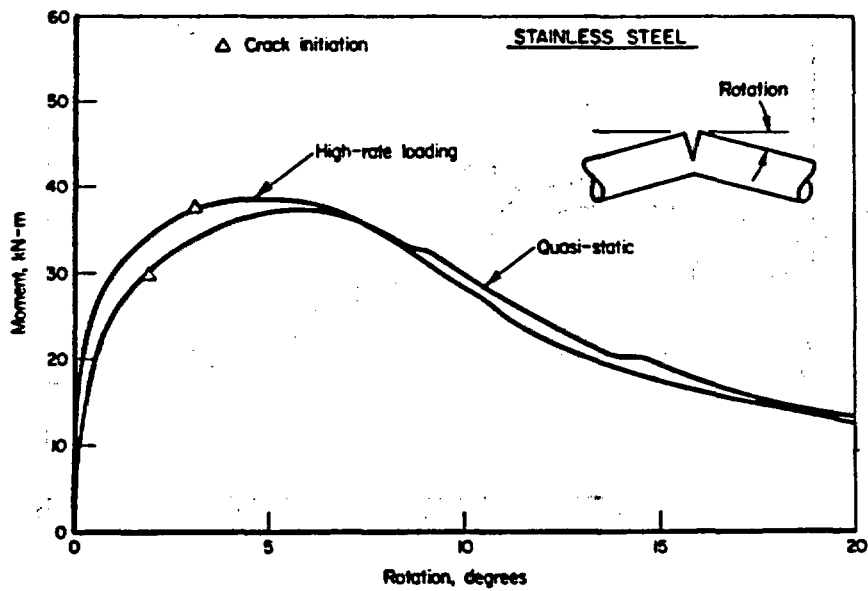


Fig. 4. Effect of high-rate loading on the moment-rotation behavior of stainless steel cracked pipe.

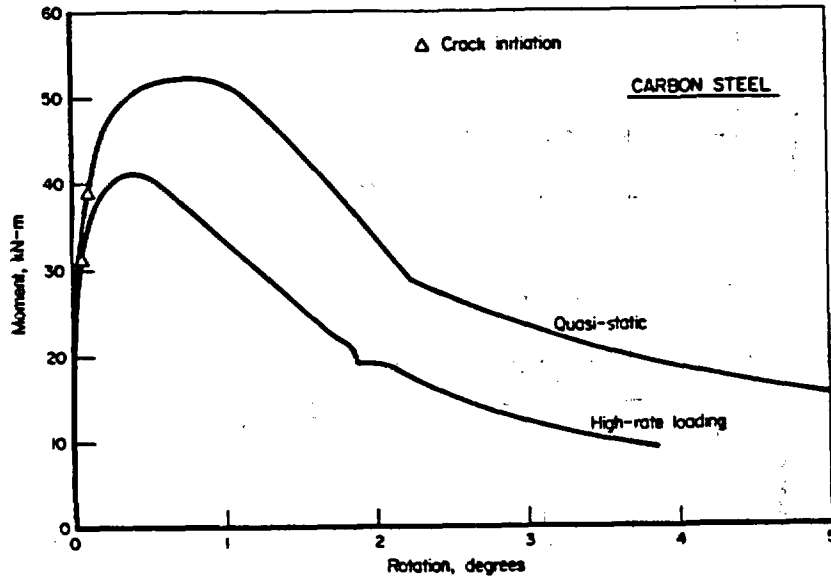


Fig. 5. Effect of high-rate loading on the moment-rotation behavior of carbon steel cracked pipe.

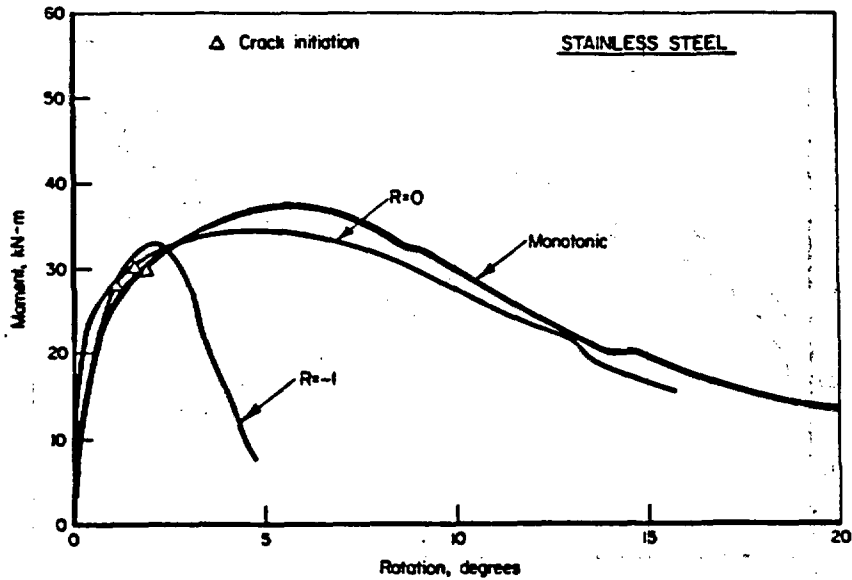


Fig. 6. Moment-rotation envelopes of stainless steel cracked pipe under cyclic loading as a function of load ratio.

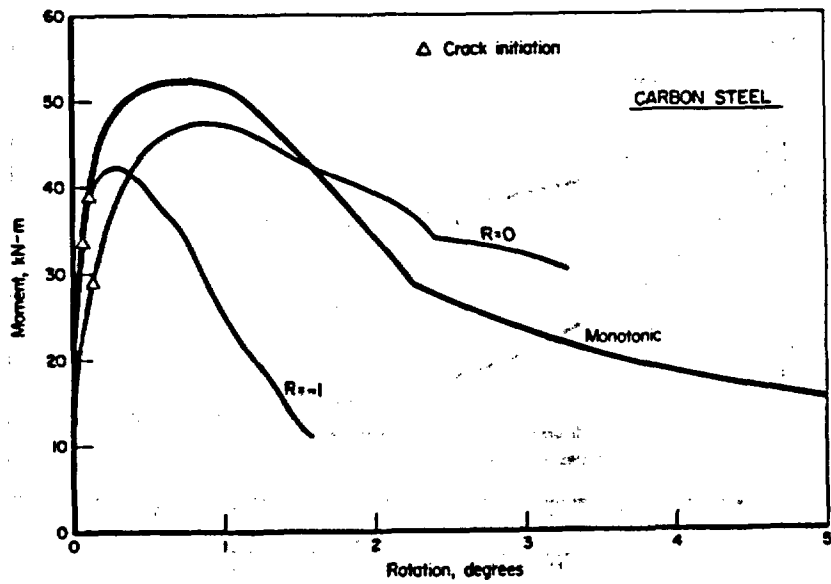


Fig. 7. Moment-rotation envelopes of carbon steel cracked pipe under cyclic loading as a function of load ratio.

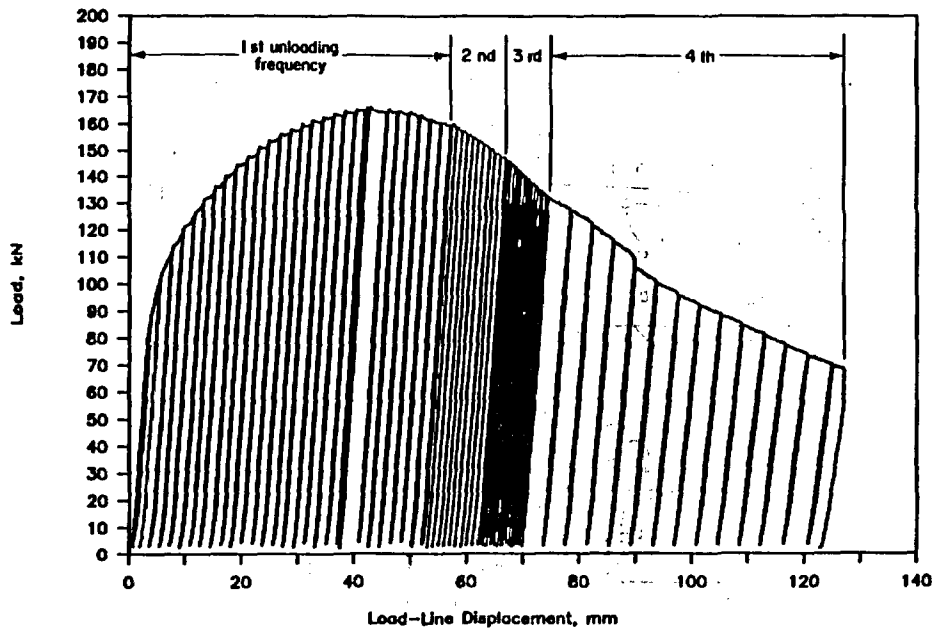


Fig. 8. Cyclic loading blocks at  $R=0$  with various values of incremental plastic displacement.

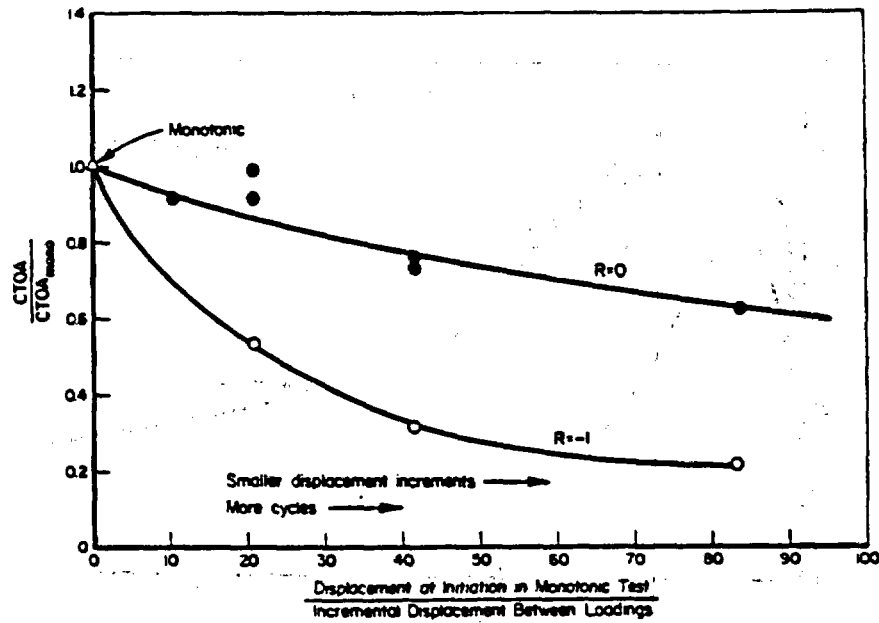


Fig. 9. Effects of incremental plastic displacement and load ratio on cyclic behavior of stainless steel.

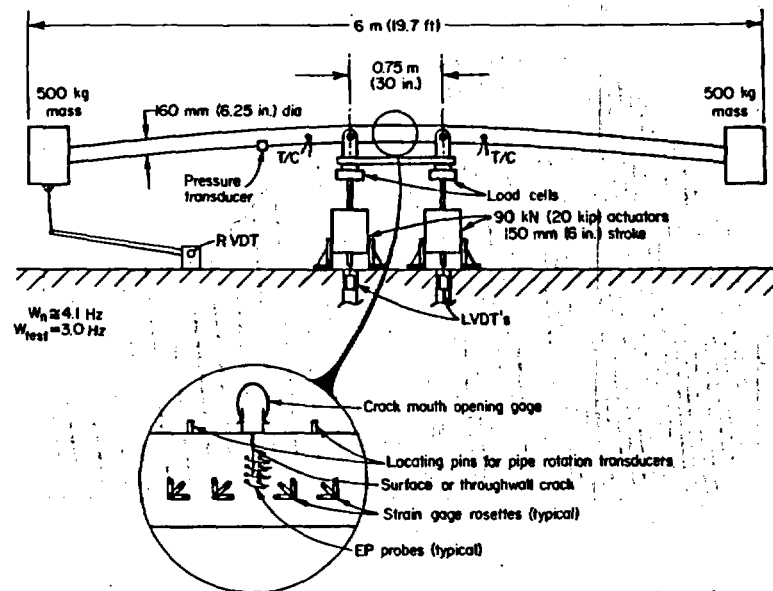


Fig. 10. Inertial test system.

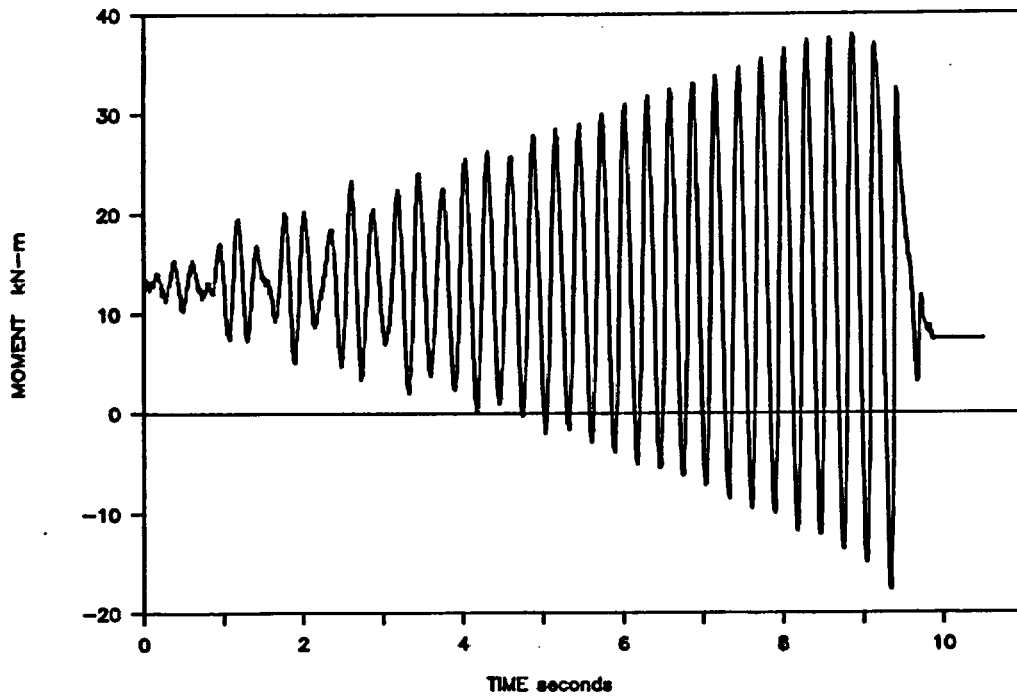


Fig. 11. Moment-time of inertially loaded carbon steel pipe specimen with through-wall crack.

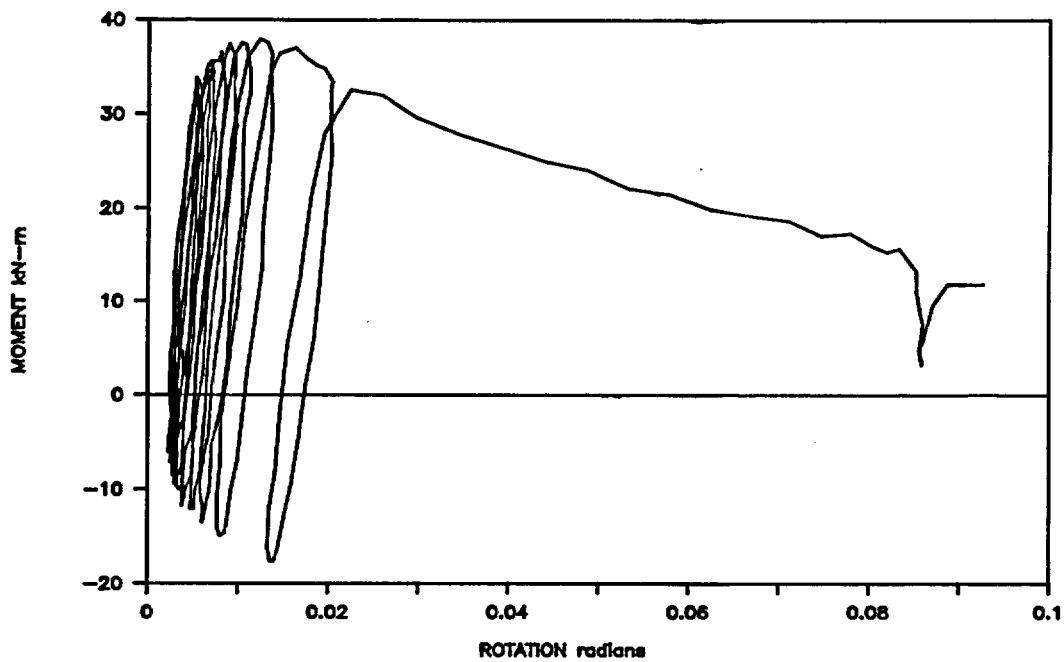
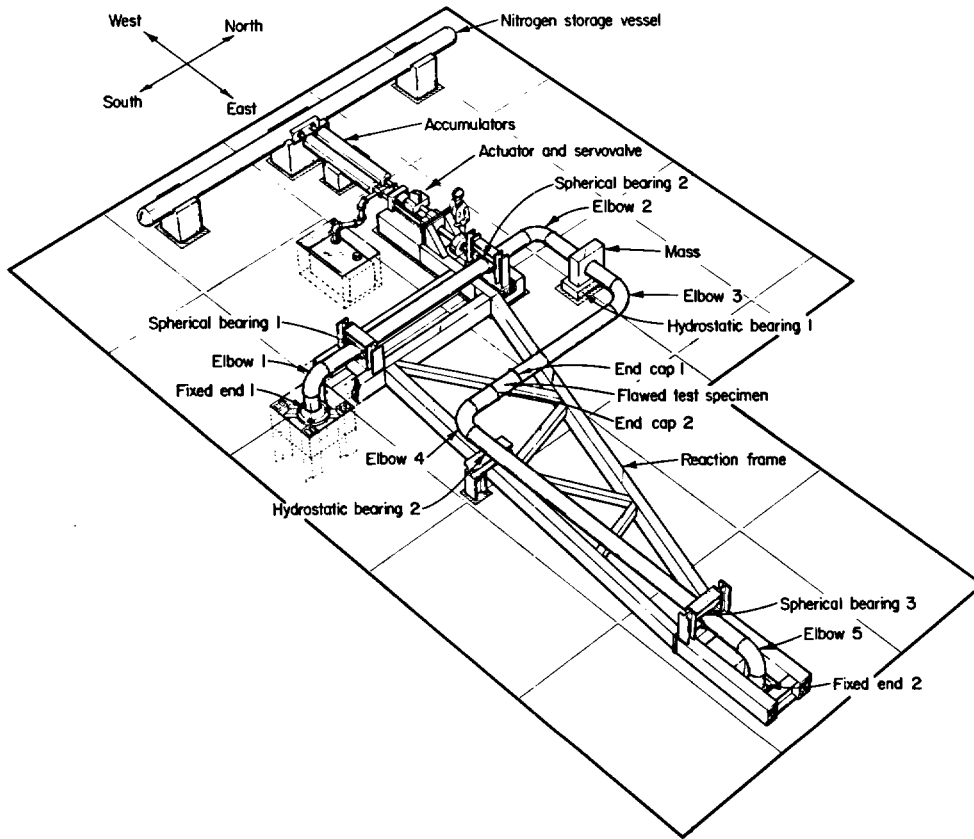
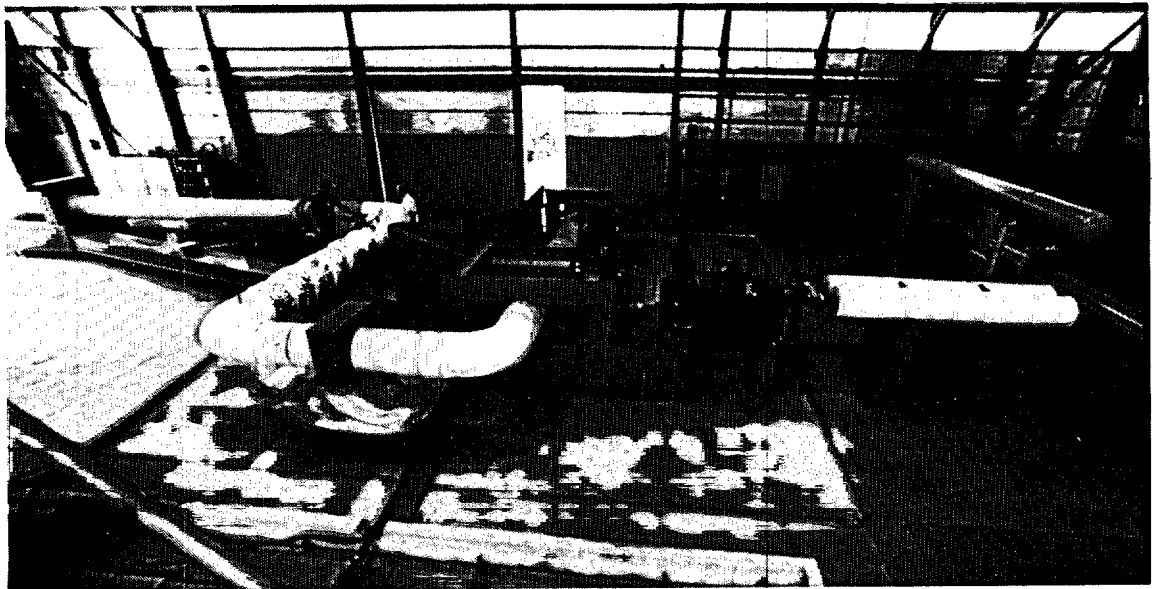


Fig. 12. Moment-rotation of inertially loaded carbon steel pipe specimen with through-wall crack.



**Fig. 13. IPIRG Pipe Loop Test Facility.**



**Fig. 14. IPIRG Pipe Loop Test Facility.**

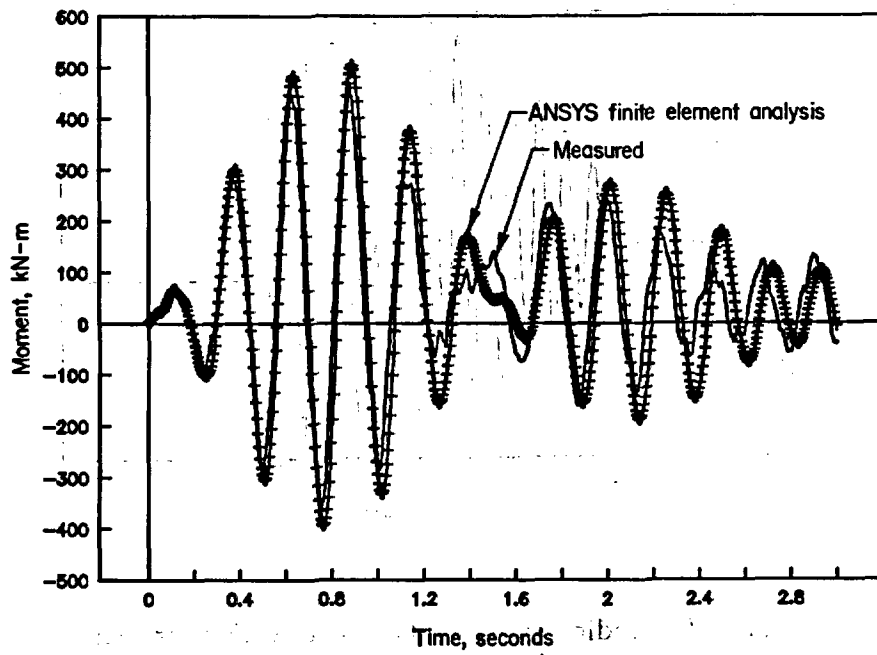


Fig. 15. Comparison of elastic analysis and experimental results for uncracked pipe system experiment.

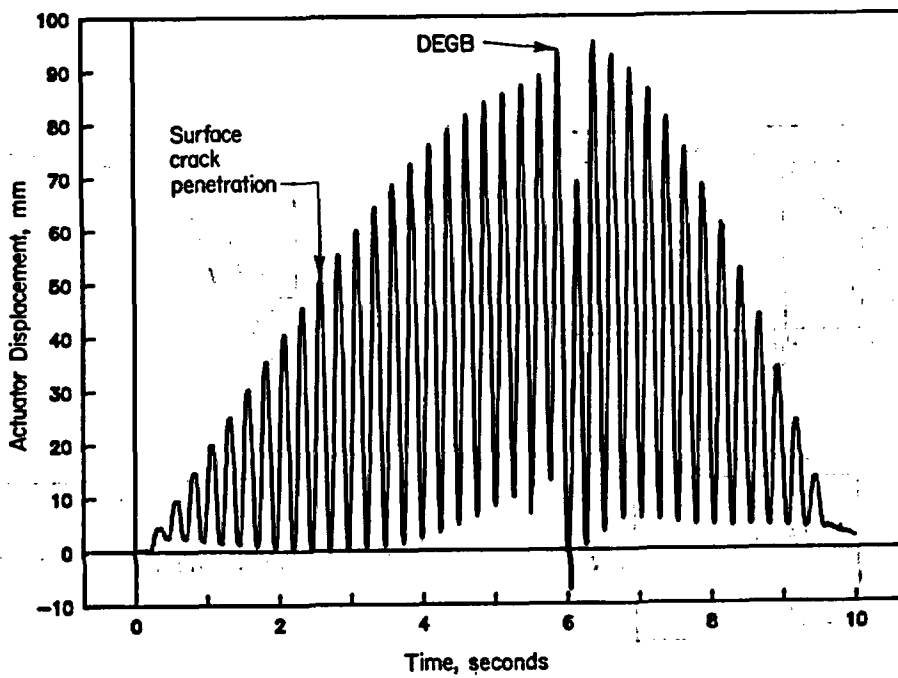


Fig. 16. Forcing function used in aged cast stainless steel pipe system experiment.

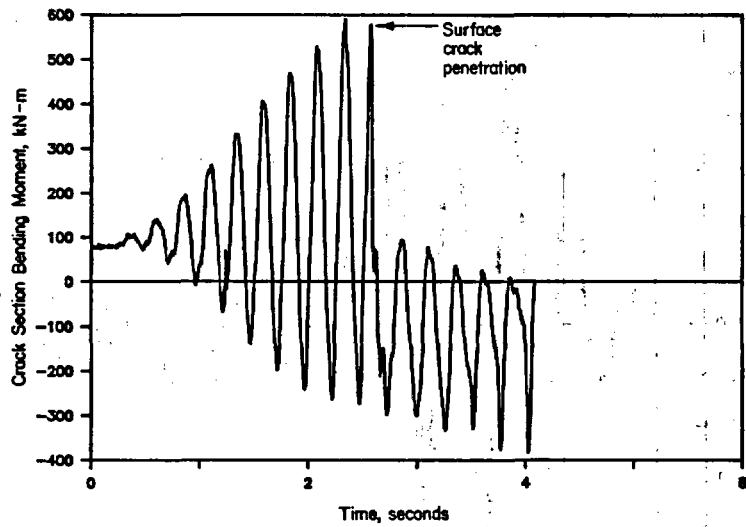


Fig. 17. Bending moment at cracked section for aged cast stainless steel pipe system experiment.

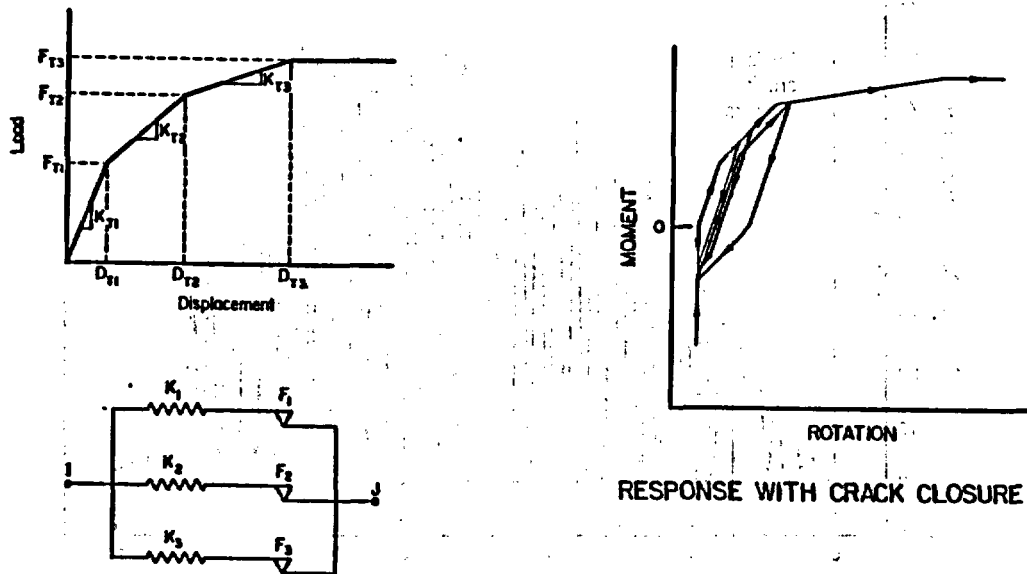


Fig. 18. Nonlinear spring model of crack.

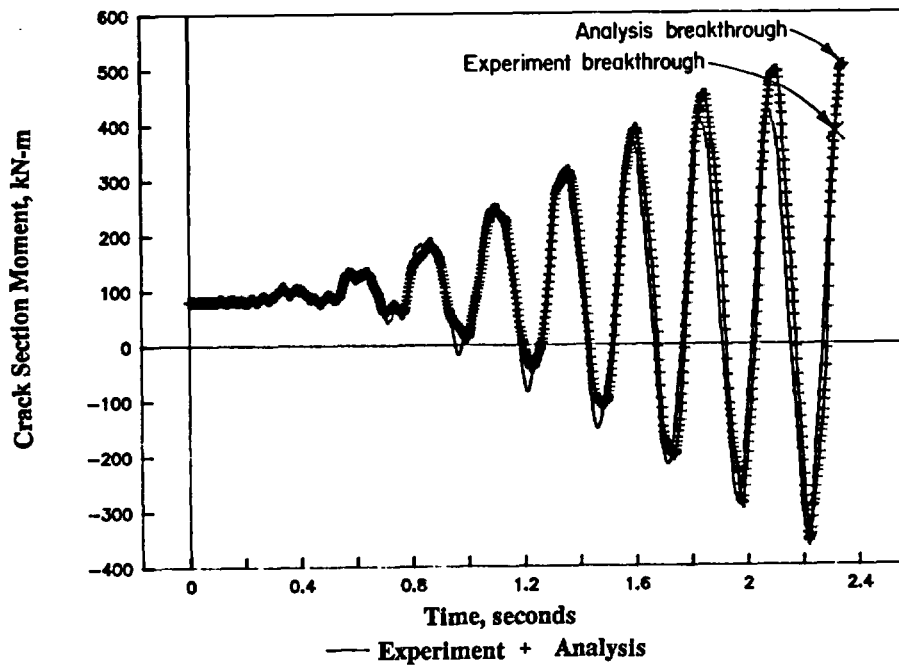


Fig. 19. Dynamic nonlinear finite element results compared with measured values.

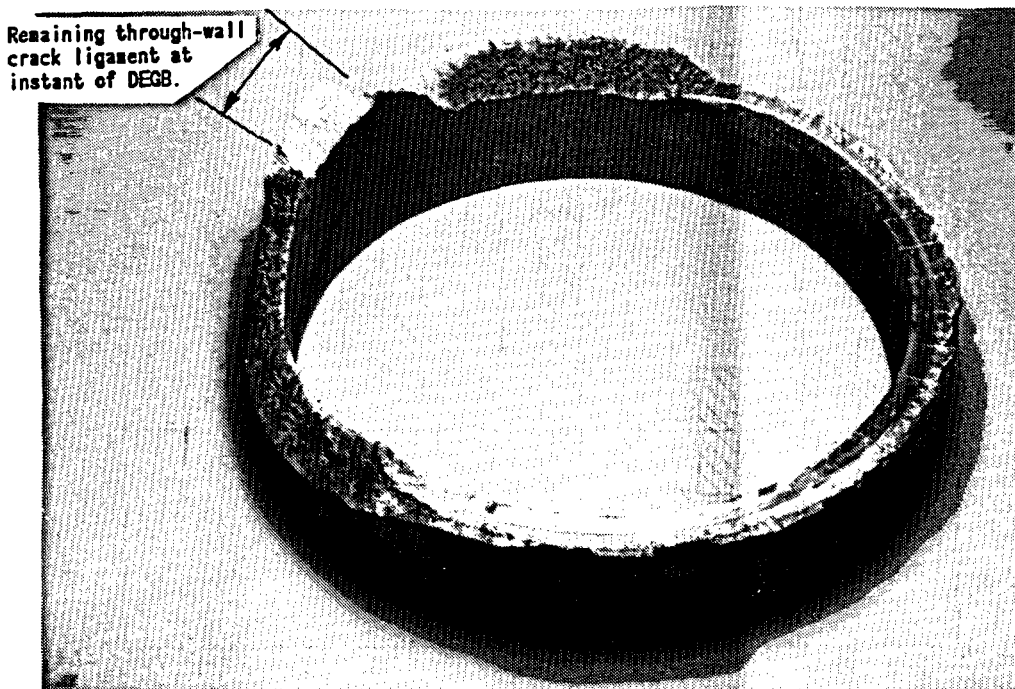


Fig. 20. Fracture surface of aged cast stainless steel experiment showing small remaining ligament at time of double-ended break.

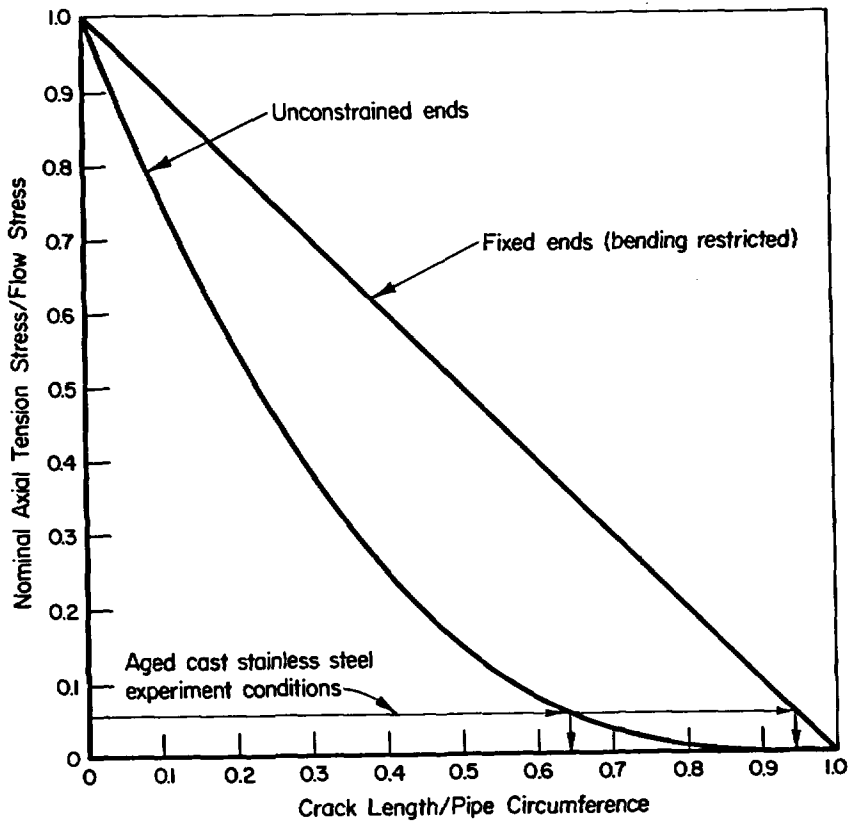


Fig. 21. Effect of constraint on crack stability by Net-Section-Collapse analysis.

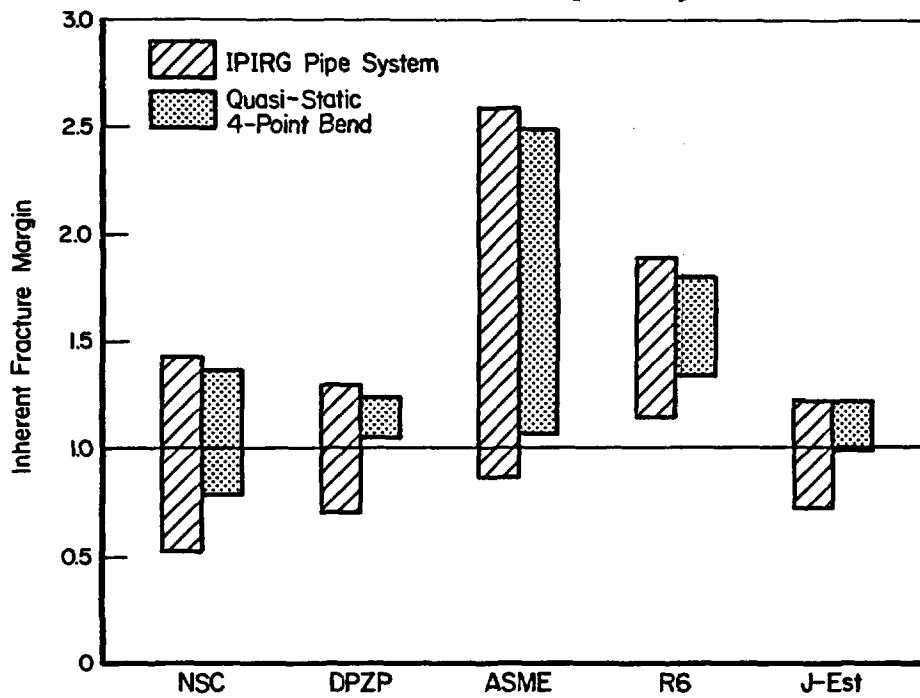


Fig. 22. Range of inherent fracture margins for pipe system and quasi-static experiments.

## **SHORT CRACKS IN PIPING AND PIPING WELDS**

by

**G. Wilkowski, F. Brust, R. Francini, T. Kilinski  
P. Krishnaswamy, M. Landow, C. Marschall,  
S. Rahman, and P. Scott**

### **BATTELLE COLUMBUS DIVISION**

#### **1.0 INTRODUCTION**

The overall objective of the Short Cracks in Piping and Piping Welds Program is to verify and improve engineering analyses to predict the fracture behavior of circumferentially cracked pipe under quasi-static loading with particular attention to crack lengths typically used in LBB or flaw evaluation criteria. Specific efforts focus on clarification of technical issues that evolved during the Degraded Piping Program - Phase II.

The program consists of 7 technical tasks. The tasks and whether they were active to date or not are listed below.

Task 1	Short through-wall-cracked (TWC) pipe evaluations	(Active)
Task 2	Short surface-cracked (SC) pipe evaluations	(Active)
Task 3	Bi-metallic weld crack evaluations	(Inactive)
Task 4	Dynamic strain aging and crack instabilities	(Active)
Task 5	Fracture evaluations of anisotropic pipe	(Active)
Task 6	Crack-opening-area evaluations	(Active)
Task 7	NRCPIPE Code improvements	(Active)

#### **2.0 SUMMARY OF RESEARCH PROGRESS**

Technical efforts in the NRC's Short Cracks in Piping and Piping Welds research program started in May of 1990. Because of the number of activities in the program, not all of them can be summarized in this paper. Further details of the program efforts are given in Refs. 1 and 2. The full-scale pipe experimental efforts involve conducting large-diameter-pipe fracture experiments at LWR conditions. These data will then be used to validate and/or develop improved analysis procedures for leak-before-break or in-service flaw inspection criteria such as the ASME Section XI Article IWB-3640 and 3650 criteria. Table 1 gives a list of the pipe experiments to be conducted.

### Task 1 - Short Through-Wall-Cracked (TWC) Pipe Evaluations

There are five subtasks in this task. These are:

- |             |  |
|-------------|--|
| Subtask 1.1 | Material characterization of pipes to be tested            |
| Subtask 1.2 | Facility modifications for large diameter pipe experiments |
| Subtask 1.3 | Conduct large diameter pipe experiments                    |
| Subtask 1.4 | Analysis modification and verifications                    |
| Subtask 1.5 | Topical report.  |

Of these subtasks, the major progress was in Subtask 1.3 and 1.4. In Subtask 1.3, three pipe fracture experiments have been completed. These results are summarized below.

#### Progress from Subtask 1.3 - Conduct Large Diameter Pipe Experiments

Two 28-inch diameter TWC pipe experiments were conducted with the specific objective to evaluate the effects of a short TWC on the analytical predictions. A third experiment was conducted on a French stainless steel pipe, with the specific objective to replicate an Electricité de France (EDF) pipe test to evaluate reproducibility of the Battelle and EDF systems.

**28-inch Diameter Pipe Experiments.** The first pipe fracture experiment was on a 28-inch diameter Schedule 60 A516 Grade 70 steam-line pipe. The second test (Experiment 1.1.1.23), was on a 28-inch diameter Schedule 80 TP304 stainless steel pipe with a crack in the center of a submerged-arc weld (SAW). Similar experiments were conducted in the Degraded Piping Program with 37-percent circumferential cracks, Ref. 3.

The initial through-wall-crack length in these experiments were 6.25 percent of the circumference, typical of an LBB size through-wall crack in large diameter pipe. Figures 1 and 2 show the experimental record of the total load versus average load-line displacement for the two experiments.

For Experiment 1.1.1.21, the A516 Grade 70 pipe, there were approximately 22 relatively small crack instabilities which are evident by the load drops in the load-displacement curve, see Figure 1. The lengths of the crack jumps in this experiment are similar to those evident in the past Degraded Piping Program experiment on the same pipe.

For Experiment 1.1.1.23, the TP304 stainless steel pipe with a TWC in the center of an SAW, the crack initiated earlier on one side than on the other, and grew in the center of the weld on that side. On the other side, the crack initiated later and the crack quickly turned into the base metal. The crack growth on the base metal side was approximately half of that evident on the weld metal side.

**4-inch Diameter French Pipe Experiment.** This experiment was conducted out of concerns from the IPIRG Program, Ref. 4. In that program, finite element analyses were conducted on two TWC stainless steel pipe experiments. One experiment was conducted at Battelle with a circumferential through-wall crack in a TP304 stainless steel pipe at 288 C without internal pressure. The other experiment was conducted at Electricité de France (EDF), also with a

circumferential through-wall crack in a TP316 stainless steel pipe at 20 C without internal pressure.

The FEM analysis of the Battelle test by two round-robin participants underpredicted the experimental maximum load by 27 percent, see Figure 3. Conversely, the FEM analysis of the EDF test by four round-robin participants agreed well with the experimental data, see Figure 4. Differences of up to 30 percent in past FEM analyses of through-wall-cracked stainless steel pipe experimental loads has been observed in the past, Refs. 5 and 6. Conversely Ref. 7 showed excellent agreement between FEM results and experimental loads for an entirely different stainless steel TWC test. Clearly either the experimental data or the analyses needed to be checked further. The first step was to conduct this experiment to check the Battelle and EDF experimental systems.

EDF sent a piece of pipe that was part of the moment arm from their Experiment Number 24. The pipe for Experiment 24 had a 90 degree through-wall crack. At Battelle, the EDF pipe was machined with the same initial flaw size and then welded to other pipe of similar size for the moment arms. The test pipe was then tested in four-point bending. The results showed that the maximum loads were only 3.6 percent different, which is within the  $\pm 5$  percent variation typically seen in replicate experiments at Battelle. Hence, the experimental test systems at EDF and Battelle give good agreement.

Since the two test systems agreed with each other, there appears to be no significant experimental error that would account for the FEM discrepancies. The discrepancy in the FEM results must be due to differences in the behavior of the different stainless steels. One observed difference was that the EDF stainless steel had a significant amount of anisotropy in that the fracture surface of the round-bar tensile specimen had an elliptical shape with a 2 to 1 ratio of the major to minor axis. Further work on constitutive modeling of stainless steels appears to be needed.

#### **Progress from Subtask 1.4 - Analysis Modification and Verifications**

Analyses efforts are underway in several activities. One is to assess current analyses methods using the newly developed short TWC data. Another is to pursue improvements in TWC analyses.

**Assessment of Current TWC Analyses Methods.** The maximum load predictions using current calculational methods were made for the short crack experiments, as well as the companion long crack experiments in the Degraded Piping Program. The calculations were made for various crack lengths for all the analyses. Figures 5 and 6 show the various predicted maximum moments from the various TWC analyses to the data from the experiments in this program and the companion experiments from the Degraded Piping Program.

**Improvements to TWC Analyses.** Two main efforts that have been undertaken to improve TWC pipe J-estimation scheme analyses involve improvements in the GE/EPRI functions for short crack lengths, and modifications to the LBB.ENG analyses to include the effect of weld metal strength along with the base metal strength in the J-estimation scheme analysis.

**Improvements in the GE/EPRI functions for short TWCs.** A matrix of FEM analyses was conducted with the purpose of refining the GE/EPRI functions for elastic and fully plastic loading. These calculations were made using ABAQUS 20 noded isoparametric brick

elements. In the GE/EPRI analysis for through-wall-cracked pipe in bending, the displacement functions for short crack lengths were negative, Ref. 8. This is impossible, which indicates some errors existed in the development of the functions from the finite element analyses.

The elastic functions  $F$ ,  $V_1$ , and  $V_3$  were calculated as well as the fully plastic functions  $h_1$ ,  $h_2$ , and  $h_4$ . The largest disagreements were for the elastic and plastic rotation functions  $V_3$  and  $h_4$ , respectively. The Battelle/ABAQUS elastic rotation function ( $V_3$ ) was a positive value whereas the GE/EPRI value was negative, see Tables 2 and 3, and the Battelle/ABAQUS plastic rotation function ( $h_4$ ) was typically 5 to 10 times larger than the GE/EPRI value. These rotation relations are used in the LBB.GE J-estimation scheme, Ref. 9.

Interestingly, the  $h_1$  function which relates load to the applied  $J$  was 8 to 20 percent lower in the Battelle/ABAQUS calculations than the GE/EPRI solutions for both the tension and bending solutions. This is consistent with the comparisons with the experimental results in Ref. 3 where the GE/EPRI handbook solutions typically overestimated the crack driving force and gave the most conservative load predictions which were approximately 15 percent on the average below the experimental loads.

Improvements to LBB.ENG analysis to account for weld metal strength. Typically flaws in welds are assessed by using the weld metal J-R curve and the base metal stress-strain curve. Several FEM analyses have shown this to be reasonable. However, data from the Degraded Piping Program on two sets of as-welded and solution-annealed pipe experiments with identical cracks suggest that the weld metal strength can affect the predictions by more than 15 percent, see Ref. 6. Consequently, an effort was undertaken to modify an estimation scheme to account for weld metal strength differences.

The LBB.ENG analysis lends itself to inclusion of the weld metal strength properties. However, a series of finite element analyses were needed to calibrate the model. This was done since there was a disposable parameter called  $\hat{\alpha}$  which required FEM calibration, see further details in Ref. 2. The FEM analyses were conducted for different pipe  $R/t$  ratios and different ratios of the base and weld metal strain-hardening exponent. Figure 7 shows a typical result for base and stainless steel submerged-arc weld metal properties. These results show that the  $\hat{\alpha}$  value of 4 is a good selection. Further calculations are needed to assess the effect of varying the reference stress (or yield strength) as well as the strain-hardening exponent.

### Task 2 - Short Surface-Cracked (SC) Pipe Evaluations

This task has been divided into five subtasks. These are:

- |             |   |
|-------------|---|
| Subtask 2.1 | Material characterization of pipes to be tested |
| Subtask 2.2 | Conduct small diameter pipe experiments         |
| Subtask 2.3 | Conduct large diameter pipe experiments         |
| Subtask 2.4 | Analysis modification and verifications         |
| Subtask 2.5 | Topical report.                                 |

Of these subtasks, the material characterization efforts have started. The stainless steel weld data has been determined. However, the weld procedure for a low toughness carbon-

manganese-molybdenum SAW used in a PWR is still being pursued. The two small-diameter pipe experiments have been conducted, and the two large diameter pipe experiments will be conducted by the end of FY91.

For the analysis subtask, there are five activities. These are:

- |                |   |
|----------------|---|
| Activity 2.4.1 | Uncracked pipe analysis   |
| Activity 2.4.2 | Improve SC.TNP and SC.TKP analyses  |
| Activity 2.4.3 | Compare limit-load analyses to short-surface-cracked small-diameter pipe data |
| Activity 2.4.4 | Analyze large diameter SC pipe test data                                      |
| Activity 2.4.5 | Evaluate procedures in J-estimation schemes for surface cracks in welds.      |

Efforts are underway in several of these activities. The first being to conduct uncracked pipe analyses. These efforts are needed for several different reasons. The first is to determine the smallest size surface crack that can be tested without buckling the pipe. Details of these efforts are given in Ref. 2. The second is to assess simple closed-form buckling solutions that could be of potential value to improve limit-load and J-estimation scheme solutions for short surface-cracked pipe.

#### Progress from Subtask 2.2 - Conduct Small Diameter Pipe Experiments

Two 6-inch diameter stainless steel experiments were conducted with short circumferential surface cracks in four-point bending at 288 C. The objective of these experiments was to develop data where the toughness of the material is sufficiently high enough that limit-load analyses should be appropriate. One of the 6-inch diameter TP304 pipes was a thin wall, Schedule 40, and the other was a heavy-wall pipe, Schedule XXS. The objective of including the different thickness pipes was to assess the effect of R/t ratio on the NSC analysis. The crack size was 50 percent of the circumference in length and 66 percent of the wall thickness in depth. The effect of different crack sizes needs to be evaluated by the data in this program and other data in the literature.

The first problem encountered in conducting these experiments was to determine what was the smallest flaw size that could be tested without having the pipe fail by buckling. Uncracked pipe buckling analyses were compared to experimental data, see Ref. 2. The accuracy of those analyses were not as good as desired and empirical corrections were needed for more accurate predictions. The flaw size selected was the one that would be the most marginal for the worst case experiment. The worst case experiment was the 6-inch diameter Schedule 40 pipe experiment. The flaw size selected to be used in all the short surface-crack experiments was 25 percent of the circumference and 50 percent of the thickness.

Figure 8 shows the load-displacement record of the thin-wall pipe experiment (1.2.1.22). In this experiment, buckling started prior to crack initiation and breakthrough of the surface crack. This behavior of buckling followed by fracture was not thought to be possible, since it was believed that if a buckle started, the deformation energy would be going towards forming the buckle and not driving the crack. However, during the buckling while the load was dropping, the crack was still locally being loaded. The buckle formed at a girth weld about

one pipe diameter from the crack. The girth weld was necessary for installing the internal instrumentation.

The heavy-wall pipe experiment (1.2.1.21) load-displacement data are shown in Figure 9. Here the pipe did not buckle and crack initiation occurred at maximum load.

#### Progress from Subtask 2.4 - Compare Limit-Load Analyses to Short Surface-Cracked Small-Diameter Pipe Data

The initial analysis of these experiments involved comparison of the experimental results to the Net-Section-Collapse predicted loads, with the objective of assessing the accuracy of this analysis for pipe with short circumferential surface cracks. In addition to the two experiments from this program, there were two experiments from an older EPRI/Battelle Program, Ref. 10, considered.

The experimental moment was normalized by the predicted Net-Section-Collapse moments in Figure 10. For the thin-walled pipe experiment (1.2.1.22), the maximum load used was the buckling load, not the load at crack initiation or breakthrough. The upper bound line comes from the Degraded Piping Program data with larger cracks, i.e.,  $d/t = 0.66$  and  $2c/\pi D = 0.5$ . All the short crack experiments had lower normalized failure stresses than the Degraded Piping Program empirical fit for larger surface cracks. This may be a reflection of the fact that the pipe samples for the short crack experiments flattened (i.e., ovalized) more due to the higher applied loads. The trend of the data with R/t ratio does not appear to be as clear. An additional experiment on 16-inch diameter TP304 pipe with a larger R/t ratio is to be conducted. That experiment should shed some light on the trend with R/t ratio for short cracks.

#### Task 3 - Bi-Metallic Weld Crack Evaluations

The objective of this task is to conduct experiments and develop the necessary analytical engineering estimation schemes to assess the behavior of through-wall and surface cracks in bi-metallic welded pipe under combined bending and tension.

In nuclear piping systems, there are several bi-metallic welds. Some examples are: welds from Westinghouse cast stainless steel hot and cold legs to the reactor pressure vessel and steam generators, CE and B&W ferritic piping to cast stainless steel pump housings, as well as at many nozzle locations. For BWR's, the stainless steel piping welds to the reactor pressure vessels are also bi-metallic. Such welds are difficult to fabricate and inspect. Consequently, a more thorough evaluation of the fracture behavior of such welds is warranted. These efforts will be initiated in FY92.

#### Task 4 - Dynamic Strain Aging and Crack Instabilities

The objective of this task is to predict the effects of crack instabilities, believed to be due to dynamic strain aging, on the fracture behavior of ferritic pipe. Specific objectives are to establish a simple screening criterion to predict which ferritic steels may be susceptible to unstable crack jumps, and to evaluate the ability of current J-based analysis methodologies to assess the effect of unstable crack jumps on the fracture behavior of ferritic steel pipe. If

necessary, alternative procedures for predicting pipe behavior in the presence of crack jumps will be derived.

The methodology developed here will be applicable to both LBB and in-service flaw evaluations. It will also be valuable for selection of materials for future inherently safe reactor designs.

There are four subtasks and two optional subtasks in this task. These are:

- Subtask 4.1      Establish a screening criterion to predict unstable crack jumps in ferritic steels
- Subtask 4.2      Evaluate procedures for characterizing fracture resistance during crack jumps in laboratory specimens
- Subtask 4.3      Assess current procedures for predicting crack jump magnitude in pipes
- Subtask 4.4      Prepare interim and topical report on dynamic strain aging induced crack instabilities in ferritic nuclear piping steels at LWR temperatures
- Subtask 4.5      Refine procedures for characterizing fracture resistance during crack jumps in laboratory specimens (Optional)
- Subtask 4.6      Refine procedures for predicting crack jump magnitude in pipes (Optional)

The approach in Task 4 is based on experimental data obtained in the Degraded Piping Program, Ref. 3. In several pipe steels tested at 288 C, crack instabilities were observed both in laboratory and pipe specimens, interspersed between periods of stable, ductile tearing. These instabilities have been assumed to be related to a steel's susceptibility to DSA, Ref. 11. However, no firm proof of that tie-in presently exists.

The significance of crack instabilities in flawed-pipe safety analyses has already been demonstrated in at least one 288 C pipe test conducted at David Taylor Research Center. During that experiment a crack jump of approximately one-fourth of the pipe circumference was observed for a through-wall circumferential crack. Therefore, it is important to determine how to predict the occurrence and magnitude of crack instabilities.

**Progress from Subtask 4.1 - Establish a Screening Criterion to Predict Unstable Crack Jumps in Ferritic Steels**

The first step was to assess if a simple screening criterion can be developed to assess if a steel is susceptible to dynamic strain aging. Five different ferritic pipes from the Degraded Piping Program were selected for this study. These pipes were known to have relatively different amounts of dynamic strain aging susceptibility, i.e., they exhibited either large, small, or no unstable crack jumps in laboratory or pipe tests at 288 C.

Dynamic strain aging occurs when the strength at elevated temperatures is higher than the strength at room temperature. It follows that since hardness can be related to the material strength, that the dynamic strain aging sensitivity can be related to the hardness at room and elevated temperatures.

Figure 11 shows the yield, ultimate, and hardness data as a function of temperature for the five different steels. There is a peak in the ultimate strength curve in all but Pipe F11, which was thought to be a ferritic steel pipe with little to no dynamic strain aging sensitivity. For the steels with peaks in the ultimate strength curves, there is also peak in the hardness curve, but at a temperature approximately 100 C higher than the quasi-static ultimate strength peak. This difference in the peak temperatures may be due to the fact that dynamic strain aging is also strain rate sensitive, and the hardness tests are faster than the tensile tests. Typically, a Brinell hardness test loads the material for 6 seconds.

Some other interesting features from the graphs in Figure 11 are:

- The peak temperature is the highest for the 16-inch diameter submerged arc weld. In the IPIRG Program, this weld actually showed an increase in toughness at seismic rates compared to quasi-static rates, Ref. 4, whereas all the ferritic base metals showed a decrease in strength and toughness at seismic rates.
- Pipe F30 showed two distinctly different hardness versus temperature curves from samples taken relatively close to each other. In the IPIRG Program, this pipe showed considerable variability in dynamic monotonic pipe fracture experiments at 288 C, Ref. 12.

In summary, the ratio of high temperature hardness data to room temperature hardness data appears to be a reasonable relation to determine if a material is susceptible to dynamic strain aging. In the future, the magnitude of the hardness ratios will be related to the propensity for unstable crack jumps.

#### **Task 5 - Fracture Evaluations of Anisotropic Pipe**

The objective of this subtask is to assess if anisotropic fracture properties (where the toughness is typically lower in the helical or axial direction than in the circumferential direction for ferritic seamless pipe) together with having high principal stresses in a helical direction can cause a lower failure stress than calculated using the toughness in the circumferential (L-C) orientation and using only the longitudinal stresses.

The rationale for this task is to assess if current LBB and ASME flaw evaluation procedures may have lower margins for out-of-plane crack growth under certain service loading conditions. If current procedures are found to have significantly lower margins, modifications to existing fracture analysis method will be made. Five subtasks will be conducted in this task, two of which are optional.

- |             |  |
|-------------|--|
| Subtask 5.1 | Assess effect of toughness anisotropy on pipe fracture under combined loads  |
| Subtask 5.2 | Determine magnitude of toughness anisotropy and establish a screening criterion to predict out-of-plane crack growth |
| Subtask 5.3 | Prepare interim and topical reports on anisotropy and mixed-mode studies   |
| Subtask 5.4 | Establish ductile crack growth resistance under mixed-mode loading (Optional)  |
| Subtask 5.5 | Refine J-estimation scheme analyses for pipes (Optional)   |

Of these subtasks, work has started in Subtask 5.1 only. The general objective of this subtask is to conduct a parametric analysis to determine if there is significant nonconservatism in current LBB fracture analyses for service loading conditions of circumferentially through-wall cracked pipe with anisotropic fracture toughness. Subtask 5.1 involves six activities.

Activity 5.1.1	Determine driving force for angled stationary crack
Activity 5.1.2	Conduct tensile tests at different orientations, and additional skewed orientation C(T) specimens on a 4-inch diameter pipe to assess strength and toughness variations
Activity 5.1.3	Determine driving force for angled growing crack
Activity 5.1.4	Determine angled crack principal stresses
Activity 5.1.5	Formulate approximate corrections
Activity 5.1.6	Assess if optional efforts are necessary

Of these activities, significant progress has been made in Activity 5.1.2.

**Progress from Activity 5.1.2 on Effect of Orientation on Strength and Toughness**

In Activity 5.1.2, efforts to date involved testing tensile and C(T) specimens in various orientations. Initial work on the effect of specimen orientation in carbon steel pipes came from efforts in Ref. 13 where C(T) specimens were taken at different angles to the pipe axis. This was done on a 4-inch diameter pipe (Battelle Pipe number F11). The toughness was found to be lower in a helical direction, which corresponded to the alignment direction of the inclusions in the pipe.

In this effort we examined five different pipes used in the Degraded Piping Program pipe experiments where the crack grew in a helical direction. Four of these were seamless and the other was seam welded. The seam welded pipe obviously should have the low toughness direction and inclusions aligned in the axial direction of the pipe. However, in the experiment the crack grew at a 30 degree angle with respect to the circumferential plane. Furthermore, the results of the metallurgical analysis showed that all but one of the pipes had the inclusions oriented in the axial direction of the pipe. Only the 4 inch seamless pipe from the prior Degraded Piping Program investigation had helical orientations.

Charpy V-notch tests were also conducted at various orientations to the pipe axis. The upper shelf energy versus orientation is shown in Figure 12. The smallest ratio of the transverse to longitudinal upper shelf Charpy energy was 0.29. Further tests and analyses will be conducted next year.

**Task 6 - Crack-Opening-Area Evaluations**

The objective of this subtask is to make improvements in the crack-opening area predictions for circumferentially cracked pipe, with particular attention to cracks in welds. The crack-opening-area analyses will be incorporated into the NRCPIPE code, and then into the SQUIRT code.

From past efforts in the Degraded Piping Program, and ASME Section XI round-robin efforts, it has been found that the leakage area predictions are reasonably good for

circumferential through-wall-cracked pipe in bending (with the cracks in the base metal). For the case of a crack in the center of the weld, the predictions showed more scatter in the intermediate to higher bending load levels. For the case of a crack in the base metal, but with the pipe in combined bending and tension, the scatter in the results was significantly worse. If the crack had been in a weld under combined loading, the scatter probably would have increased further. The accuracy of the solutions for a crack in a weld needs verification and improvement for LBB analyses.

There are five specific subtasks in this task. These are:

Subtask 6.1	Combined loading improvements
Subtask 6.2	Implement short TWC crack opening improvements
Subtask 6.3	Improve weld crack evaluations
Subtask 6.4	Modify SQUIRT Code
Subtask 6.5	Prepare topical report on crack-opening-area improvements.
Subtask 6.6	Quantifying leak-rates for updating Reg. Guide 1.45

Of these, progress was made in Subtasks 6.1 and 6.6.

#### *Progress from Subtask 6.1 - Combined Load Improvements*

As part of the IPIRG Program, Ref. 4, a leak-rate code called SQUIRT was created. This code used the GE/EPRI estimation scheme to calculate the crack-opening area. Another crack-opening analysis approach is used in the LBB.NRC and the NUREG/CR-3464 approaches, Refs. 14 and 15. The crack-opening analyses have generally been checked using experiments with pipe in pure bending. The effect of combined loading is first being checked by making crack-opening analysis improvements in the NRCPIPE Code, prior to incorporating these improvements into the SQUIRT code.

The first effort involved incorporating a crack-opening analysis in the LBB.ENG2 J-estimation scheme analysis. The LBB.ENG2 J-estimation scheme was found to give slightly conservative, but reasonably accurate maximum load predictions, whereas the GE/EPRI estimation scheme gave the most conservative predictions of all the analyses, Ref. 3. Efforts in this program show that for up to crack initiation, both the GE/EPRI and LBB.ENG2 analyses gave similar predictions for pipes in pure bending, see Figure 13.

For pure pressure loading of a through-wall circumferentially cracked pipe with end caps, the LBB.ENG2 and GE/EPRI analyses gave good predictions. These comparisons are shown for a 6-inch diameter TP304 stainless steel pipe experiment in Figure 14.

For combined pressure and bending loading, the predictions were not as good. Figure 15 shows experimental and predicted load versus center-crack-opening displacements from a 6-inch diameter TP304 stainless steel pressure and bend pipe experiment from the Degraded Piping Program. Figure 16 is a similar comparison for a 10-inch diameter A333 Grade 6 carbon steel pipe experiment under pressure and bending. Note that: (1) the various methods are not in agreement with each other nor with the experimental data, (2) the LBB.NRC method consistently underpredicts the crack opening, whereas, the LBB.ENG2 and LBB.GE analyses underpredict the crack opening in one experiment and overpredict the crack opening in the other experiment, and (3) the GE/EPRI solution is not given since there is only very limited combined load GE/EPRI solutions. (Under pure linear elastic

conditions, the GE/EPRI tension and bending displacements could be added to get combined load center-crack-opening displacements.)

Further efforts are also underway to evaluate the effect of weld metal strength on the crack-opening displacement using the LBB.ENG2 analysis method.

Progress from Subtask 6.6 - Quantifying Leak-Rates for Updating Reg. Guide 1.45

The objective of this effort is to perform analyses to support changes to the NRC's current Regulatory Guide 1.45, "Reactor Coolant Pressure Boundary Leakage Detection Systems". Regulatory Guide 1.45 was published in May, 1973, and is considered outdated. The NRC currently wants to update this procedure taking into account the current leak-detection instrumentation capabilities, experience from the accuracy of leak detection systems in the past, and current analysis methods to assess the significance of the detectable leakage relative to the structural integrity of the plant. Leak-detection capabilities at normal operating conditions are used in current leak-before-break (LBB) analyses. The consistency of the LBB procedures needs to be considered in any changes to Regulatory Guide 1.45. Additionally, the impact of such changes on structural integrity of piping not approved for LBB needs to be considered.

The analyses to be performed shall build on other work being done in Task 6. The specific work to be performed shall include the following activities.

- Activity 6.6.1      Develop the technical background information for verification of analyses to be used
- Activity 6.6.2      Evaluate the proposed changes in leak detection requirements in terms of the potential impact on LBB analyses
- Activity 6.6.3      Evaluation of the proposed changes on leak rate for "non-LBB" piping systems
- Activity 6.6.4      Coordination with NRC-RES and NRC-NRR staff
- Activity 6.6.5      NUREG report

The progress in this subtask to date involves evaluation of the effect of induced bending restraint for axial tension loads for circumferentially cracked pipe, as part of Activity 6.6.1. Current analyses assume that for axial stresses (generally pressure induced), the pipe is free to rotate. The restraint of the rotation increases the failure stresses (Ref. 17), but can decrease the crack opening at a given load. If the pipe system restrains the bending (i.e., from cracks being close to a nozzle or restraint from the rest of the piping system) then the leak rate will be less than calculated by using analyses that assume that the pipe is free to rotate. This will cause the actual crack to be larger than calculated by the current analyses methods for the same leak rate. Since normal operating stresses have a large component of the total stress being the pressure stress, this can have an effect on LBB analyses.

As a numerical example, consider a TWC pipe with mean radius  $R_m = 355.6$  mm, thickness  $t = 35.56$  mm,  $R_m/t = 10$ , and two distinct cases of initial crack angle ( $2\theta$ ), i.e.,  $\theta/\pi = 1/8$  and  $\theta/\pi = 1/4$ . For material properties, it is assumed that the modulus of elasticity  $E = 200$  GPa and the Poisson's ratio  $\nu = 0.3$ . The pipe is subjected to remote pressure with the resultant force applied at the centroid of uncracked pipe cross-section. Linear elastic

analyses by finite element method (FEM) are performed to examine the effects of restraint due to induced bending in a piping system when the pressure load is applied.

Figure 17 presents the results of crack opening displacements (COD) as a function of "restraint length" normalized with respect to the mean pipe diameter  $D_m$  ( $D_m = 2R_m$ ). The restraint length defined here simply represents the location of restrained pipe cross-section from the cracked plane. The COD values are also normalized with reference to the crack-opening displacement when there are no external constraints present in the pipe (i.e., when the restraint length becomes infinity) allowing free rotation and ovalization.

The results suggest that when the crack angle is "small" ( $\theta/\pi = 1/8$ ), the restraint effects may be neglected. However, for larger crack angles ( $\theta/\pi = 1/4$ ), the restrained COD can be significantly different than the unrestrained COD, and hence, will affect the margins in the crack opening area analysis for leak rate quantification. It is interesting to note that a significant input parameter like the "restraint length" is not considered in either the current versions of the thermohydraulic codes SQUIRT, PICEP (Ref. 18), or in any other leak-rate analyses.

#### Task 7 - NRCPIPE Code Improvements

The main objective of this task is to incorporate the analysis improvements from Tasks 1, 2, and 6 into the NRCPIPE code. A secondary objective is to make the NRCPIPE code more efficient and also to restructure the code to allow for ease of implementation of the activities described below.

In the Degraded Piping Program, the computer code NRCPIPE was developed for circumferential through-wall-cracked pipe fracture analyses. Numerous J-estimation schemes were developed or modified. The improvements made in this program need to be incorporated into this code to take advantage of the technology developments, as well as to facilitate the comparisons with the experimental results. To accomplish the objectives of this task, there are four subtasks to be undertaken.

- |             |   |
|-------------|---|
| Subtask 7.1 | Improve efficiency of current version   |
| Subtask 7.2 | Incorporate TWC improvements in NRCPIPE |
| Subtask 7.3 | Make SC version of NRCPIPE              |
| Subtask 7.4 | Provide new user's manual               |

The crack-opening-area analysis improvements will also be incorporated into the SQUIRT code in Subtask 6.4.

### 3.0 CONCLUSIONS

From the work conducted to date, several conclusions can be drawn.

- (1) The replicate TWC pipe test showed good agreement between the Battelle and EDF facilities. This eliminated experimental error as a reason for FEM analysis significantly underpredicting the experimental loads from several TWC stainless steel pipe experiments. Further efforts are perhaps needed in examining constitutive modeling of the different stainless steels tested in the past pipe fracture experiments.
- (2) The Battelle/ABAQUS reassessment of the GE/EPRI elastic and fully plastic F, V, and h functions showed: (a) good agreement with the F-function, (b) developed improved rotation functions ( $V_3$  and  $h_4$ ) that were not negative values for short crack lengths, and (c) the  $h_1$  function most frequently used to relate J to moment or load was found to be 8 to 20 percent lower than the GE/EPRI values. The lower  $h_1$  values are consistent with past experimental comparisons that showed that on the average the GE/EPRI predicted loads were 15 percent below the experimental loads.
- (3) Short circumferential surface-cracked pipe in bending has lower failure stress than predicted by the Net-Section-Collapse analysis, but the data to date does not show a clear trend with R/t ratio.
- (4) A comparison of high temperature and room temperature hardness testing appears to be a useful method for determining the dynamic strain aging sensitivity of ferritic steels.
- (5) Most ferritic seamless pipe had inclusions oriented in the axial direction, which is the low toughness direction. Hence, helical crack growth is due to the ratio of the crack growth resistance to crack driving force being a minimum at a particular angle, even if the lowest toughness is not at that angle.
- (6) Crack-opening area analyses were found to be accurate for pure bending or pure tension. Comparison of combined tension and bending experimental results and analyses showed significantly lower accuracy in the analyses.
- (7) For the effect of tension (pressure) loading on circumferential through-wall-cracked pipe, currently all leak-rate analyses assume the pipe is free to rotate as if the pipe was an endcapped piece of straight pipe. Linear elastic analyses conducted showed that if the crack is in a piping system, a fixed end (i.e., a nozzle) can restrain the crack opening. This effect was found to be more significant as the crack length increased, and as it was closer to the fixed end.

### 4.0 REFERENCES

- (1) Wilkowski, G. M. and others, "Short Cracks in Piping and Piping Welds - First Program Report, March-September 1990", NUREG/CR-4599, Vol. 1, No. 1, May 1991.
- (2) Wilkowski, G. M. and others, "Short Cracks in Piping and Piping Welds - Second Program Report, October 1990 to March 1991", NUREG/CR-4599 Vol 1, No. 2, October 1991.

- (3) Wilkowski, G. M. and others, "Degraded Piping Program -Phase II", Summary of Technical Results and Their Significance to Leak-Before-Break and In-Service Flaw Acceptance Criteria, March 1984-January 1989, by Battelle Columbus Division, NUREG/CR-4082, Vol. 8, March 1989.
- (4) Schmidt, R. A., Wilkowski, G. M., and Mayfield, M. E., "The International Piping Integrity Research Group (IPIRG) Program -- An Overview", SMiRT-11, Division G, Paper G23/1, August 1991.
- (5) Ahmad, J., Nakagaki, M., Papaspyropoulos, V., and Wilkowski, G., "Elastic-Plastic Finite Element Analysis of Crack Growth in Large Compact Tension and Circumferentially Through-Wall-Cracked Pipe Specimen", NRC Topical Report by Battelle Columbus Division, NUREG/CR-4573, October 1986.
- (6) Wilkowski, G. M. and others, "Analysis of Experiments on Stainless Steel Flux Welds", NUREG/CR-4878, April 1987.
- (7) Nakagaki, M., Marschall, C., and Brust, F., "Analysis of Cracks in Stainless Steel TIG Welds", Battelle Topical Report from NRC Degraded Piping Program, NUREG/CR-4806, December 1986.
- (8) Kumar, V. and others, "Advances in Elastic-Plastic Fracture Analysis", EPRI Final Report NP-3607, August 1984.
- (9) Brust, F. W., "Approximate Methods for Fracture Analyses of Through-Wall Cracked Pipes", NRC Topical Report by Battelle Columbus Division, NUREG/CR-4853, February 1987.
- (10) Kanninen, M. F. and others, "Instability Predictions for Circumferentially Cracked Type 304 Stainless Steel Pipes Under Dynamic Loadings", Final Report on EPRI Project T118-2, by Battelle Columbus Laboratories, EPRI Report Number NP-2347, April 1982.
- (11) Marschall, C. W., Landow, M. P., and Wilkowski, G. M., "Effect of Dynamic Strain Aging on Fracture Resistance of Carbon Steels Operating at Light-Water-Reactor Temperatures", in ASTM STP 1074, 1990, pp. 339-360.
- (12) Wilkowski, G. M., Vieth, P., Kramer, G., Marschall, C., and Landow, M., "Results of Separate Effects Pipe Fracture Experiments", Post SMiRT-11 Conference Seminar No. 2, Taiwan, Taipei, August 1991.
- (13) Scott, P. and Brust, F., "An Experimental and Analytical Assessment of Circumferential Through-Wall Cracked Pipes Under Pure Bending", Battelle Topical Report from NRC Degraded Piping Program, NUREG/CR-4574 September 1986.
- (14) Klecker, R. and others, "NRC Leak-Before-Break (LBB.NRC) Analysis Method for Circumferentially Through-Wall-Cracked Pipes Under Axial Plus Bending Loads", NUREG/CR-4572, May 1986.

- (15) Paris, P. C. and Tada, H., "The Application of Fracture Proof Design Methods Using Tearing Instability Theory to Nuclear Piping Postulating Circumferential Through-Wall Cracks", NUREG/CR-3464, September 1983.
- (16) Hiser, A. L. and Callahan, G. M., "A User's Guide to the NRC's Piping Fracture Mechanics Database (PIFRAC)", NUREG/CR-4894, May 1987.
- (17) Wilkowski, G. M. and others, "Degraded Piping Program - Phase II", Semiannual Report, October 1984-March 1985, by Battelle Columbus Laboratories, NUREG/CR-4082, Vol. 2, July 1985, see Section 2.5.
- (18) Norris, D., Okamoto, A., Chexal, B., and Griesbach, T., "PICEP: Pipe Crack Evaluation Program", EPRI report NP-3596-SR, August 1984.

**Table 1 Summary of pipe experiments**

<b>Expt. No. <sup>(a)</sup></b>	<b>Diameter</b>	<b>Schedule</b>	<b>Material</b>	<b>Temperature</b>
<b><u>Unpressurized through-wall-cracked pipe experiments</u></b>				
1.1.1.21 <sup>(b)</sup>	28 inch	60	A516 Gr70	288C (550F)
1.1.1.22	36 inch	160	A516 Gr70	288C (550F)
1.1.1.23 <sup>(b)</sup>	28 inch	80	TP316 SAW	288C (550F)
1.1.1.24	24 inch	100	A333 Gr6 SAW	288C (550F)
1.1.1.26 <sup>(b)</sup>	4 inch	80	TP316 LN	288C (550F)
<b><u>Unpressurized uncracked pipe experiment</u></b>				
1.1.1.25	28 inch	80	A516 Gr70	288C (550F)
<b><u>Bi-metallic weld fusion line experiments - TWC</u></b>				
1.1.3.8	36 inch	160	A516/SS-SAW	288C (550F)
<b><u>Unpressurized surface-cracked pipe experiments</u></b>				
1.2.1.20	16 inch	40S	TP316	288C (550F)
1.2.1.21 <sup>(b)</sup>	6 inch	XXS	TP304	288C (550F)
1.2.1.22 <sup>(b)</sup>	6 inch	40	TP304	288C (550F)
<b><u>Pressurized surface-cracked pipe experiments</u></b>				
1.2.3.15	28 inch	60	A516	288C (550F)
1.2.3.16	28 inch	80	TP316 SAW	288C (550F)
1.2.3.17	36 inch	160	A516 SAW	288C (550F)
<b><u>Bi-metallic weld fusion line experiments - SC</u></b>				
1.2.3.21	36 inch	160	A516/SS-SAW	288C (550F)

(a) Experiment numbers are consecutive with Degraded Piping Program Data Record Book entries.

(b) Completed.

**Table 2 Comparison of Battelle/ABAQUS to GE/EPRI elastic and fully plastic functions for a through-wall-cracked pipe in tension ( $R/t = 10$ ,  $\theta/\pi = 0.0625$ )**

<b>Functions</b>	<b>3D Solid ABAQUS</b>	<b>GE/EPRI</b>
<b>Elastic</b>		
F	1.0487	1.0770
V <sub>1</sub>	1.1786	1.0820
V <sub>2</sub>	0.0540	0.0520
V <sub>3</sub>	0.0198	0.0210
<b>Fully Plastic<sup>(a)</sup></b>		
h <sub>1</sub>	3.9240	4.6550
h <sub>2</sub>	5.0080	5.1960
h <sub>3</sub>	1.1800	0.5100
h <sub>4</sub>	0.2950	0.3090

(a)  $n = 3$

**Table 3 Comparison of Battelle/ABACUS to GE/EPRI functions for circumferentially TWC pipe in bending ( $R/t = 10$ ,  $\theta/\pi = 0.0625$ )**

<b>Functions<sup>(a)</sup></b>	<b>3D Solid ABAQUS</b>	<b>GE/EPRI</b>
<b>Elastic</b>		
F	1.0490	1.0700
V <sub>1</sub>	1.2060	1.0810
V <sub>3</sub>	0.0351	-0.0430
<b><u>n = 3</u></b>		
h <sub>1</sub>	6.207	6.7430
h <sub>2</sub>	7.385	6.9060
h <sub>4</sub>	1.140	0.1440
<b><u>n = 5</u></b>		
h <sub>1</sub>	6.558	7.620
h <sub>2</sub>	7.521	7.867
h <sub>4</sub>	1.720	0.288
<b><u>n = 7</u></b>		
h <sub>1</sub>	6.617	7.969
h <sub>2</sub>	7.478	8.260
h <sub>4</sub>	2.130	0.429

(a) There are no V<sub>2</sub> (tension) displacement or h<sub>3</sub> (tension) functions for pure bending.

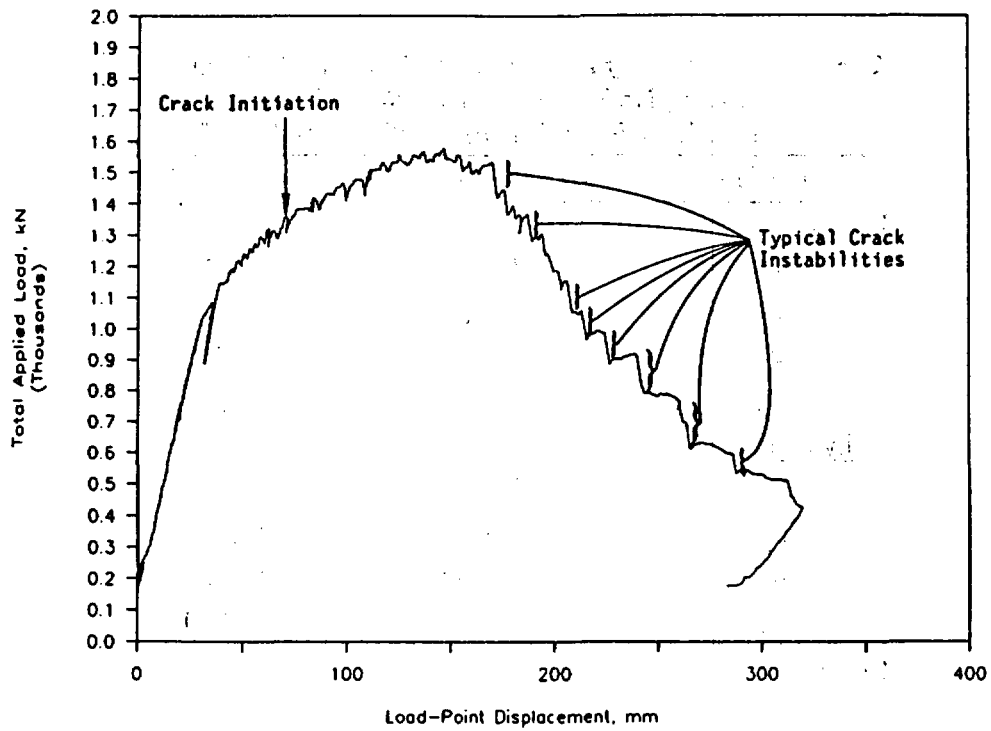


**Figure 1 Total load versus load-line displacement for Experiment 1.1.1.21. (Corrected for dead-weight loads, and machine compliance displacements eliminated.)**

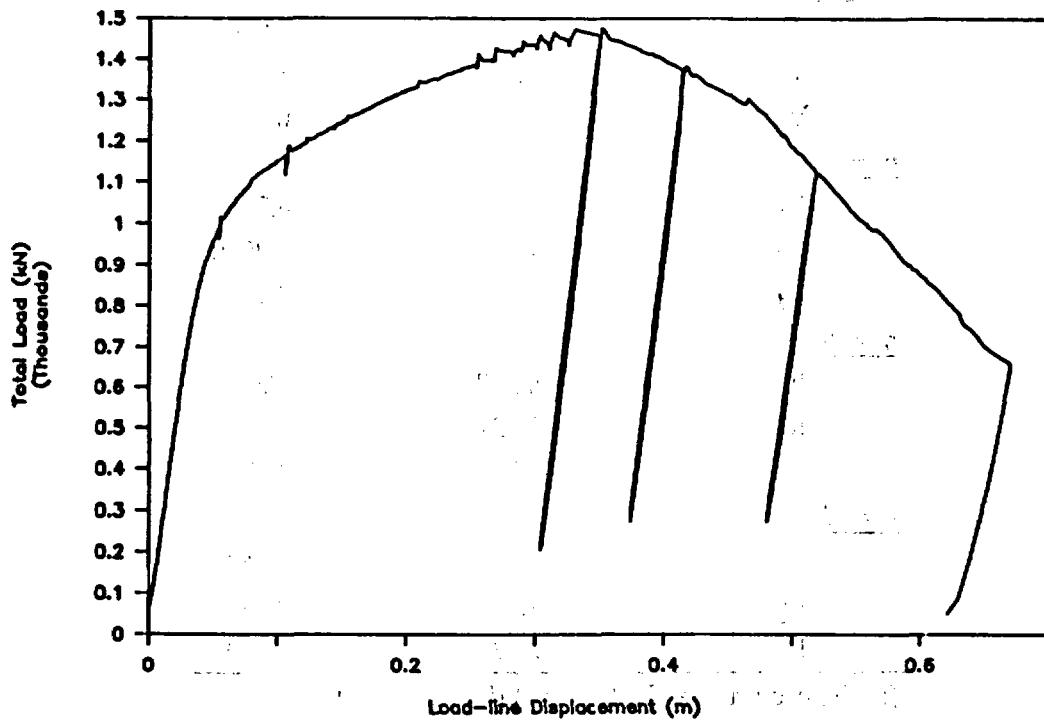


**Figure 2 Total load versus load-line displacement data from Experiment 1.1.1.23 (stainless steel SAW with short crack)**

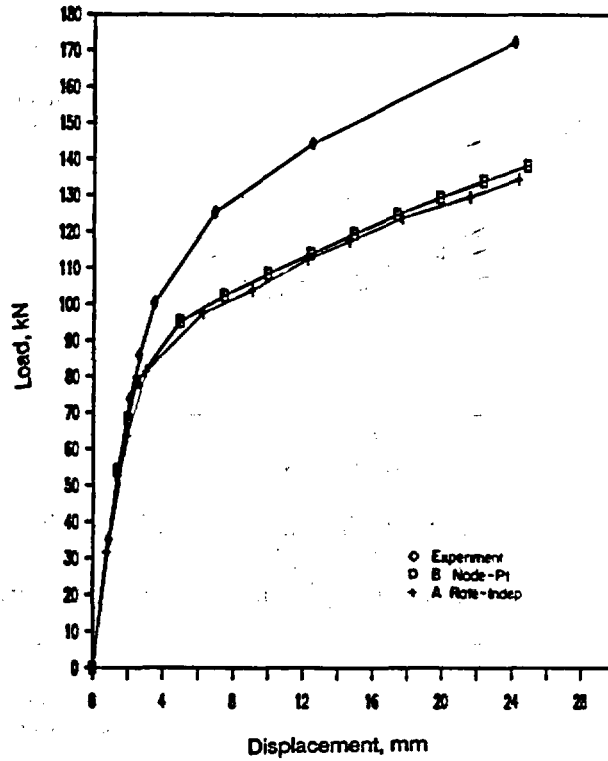
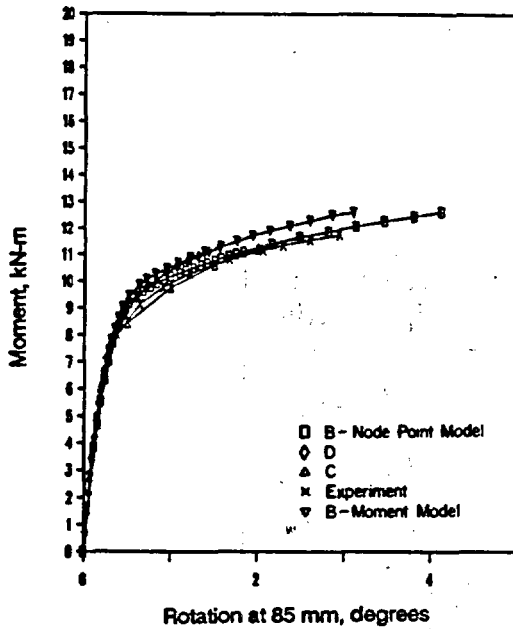
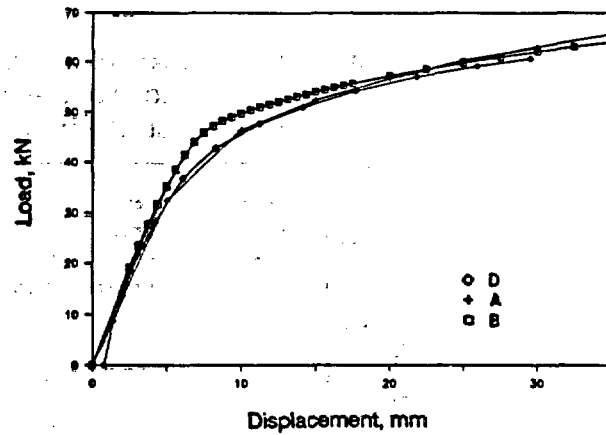


Figure 3 Comparison of FEM and experimental load versus load-line displacement curves for IPIRG Experiment 1.2-1 (IPIRG Round-Robin Problem 3-1b)



(a) Comparison of all FEM predictions to experimental data



(b) Comparison of finite element load-displacement results

Figure 4 Solutions to IPIRG FEM analyses of French Pipe Test EDF-5 (IPIRG Round-Robin Problem 3.1a)

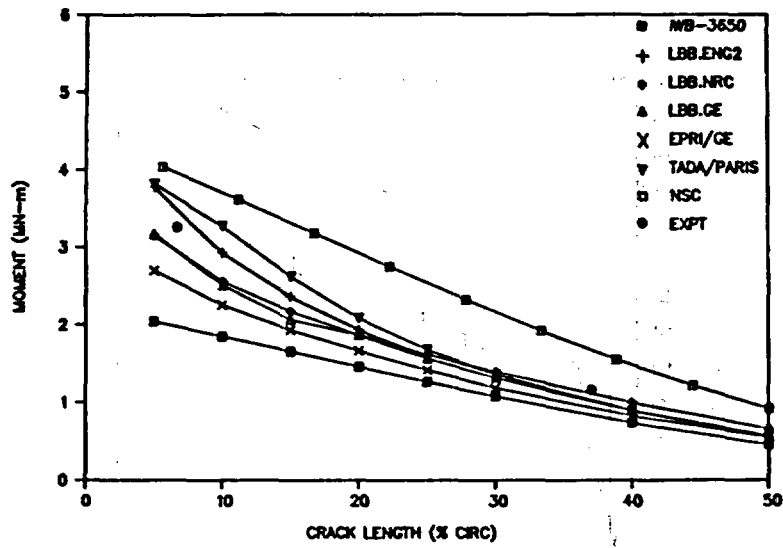


Figure 5 Comparison of maximum load predictions by various analyses of two, 28-inch diameter, Schedule 60, A516 Grade 70, through-wall-cracked, pipe experiments

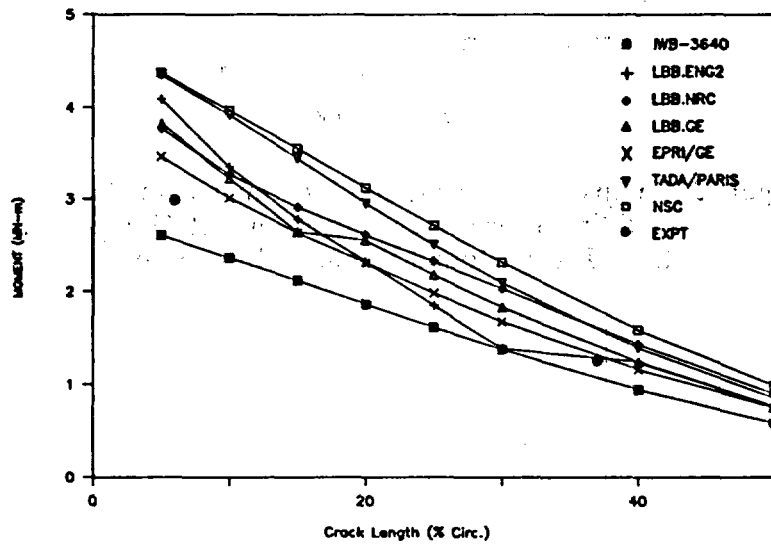


Figure 6 Comparison of maximum load predictions by various analyses to two, 28-inch diameter, Schedule 80, TP316 stainless steel, through-wall-cracked, pipe experiments

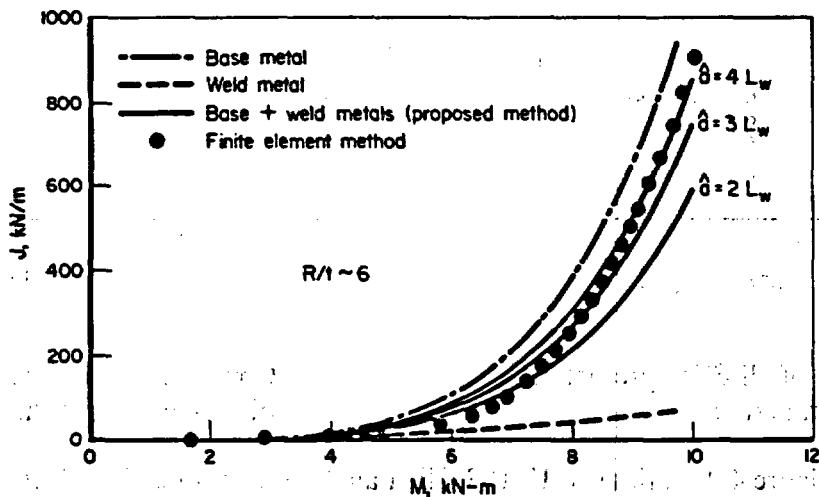


Figure 7 Comparisons of computed J versus M ( $R/t \sim 6$ )

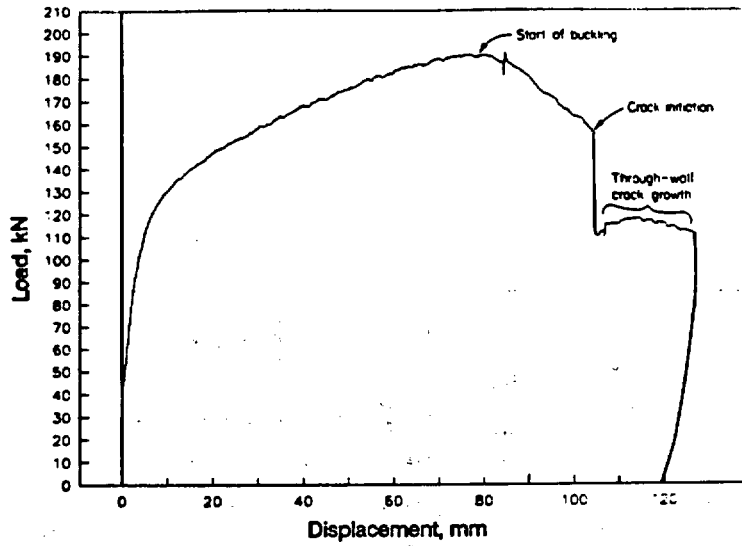


Figure 8 Total load versus load-line displacement of Experiment 1.2.1.22, 6-inch diameter Schedule 40 TP304 pipe with short surface crack ( $d/t = 0.5$ ,  $\theta/\pi = 0.25$ )

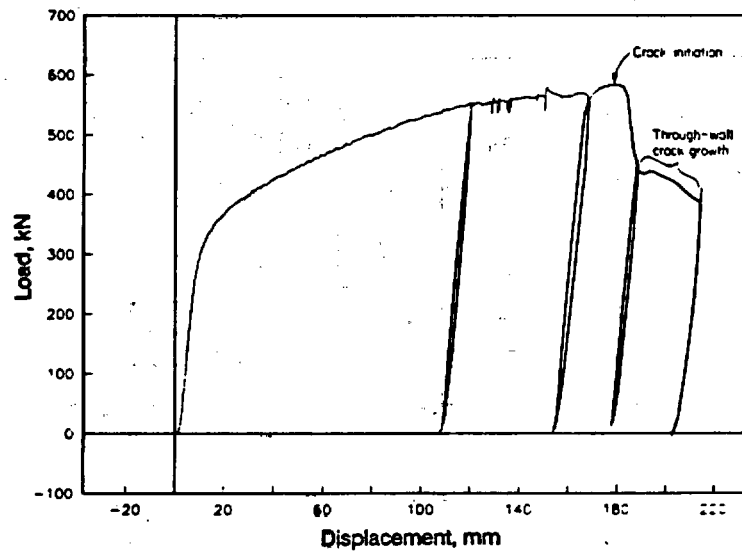


Figure 9 Total load versus load-line displacement of Experiment 1.2.1.21, 6-inch diameter Schedule XXS TP304 pipe with short surface crack ( $d/t = 0.5$ ,  $\theta/\pi = 0.25$ )

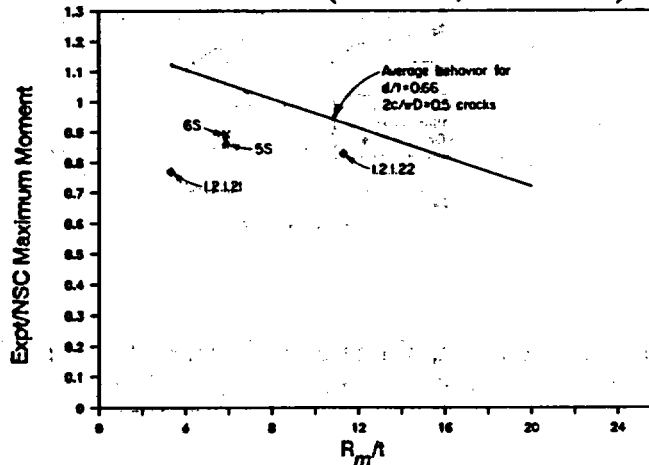


Figure 10 Comparison of experiment maximum moment/Net-Section-Collapse moment versus  $R_m/t$  for short and long surface-cracked pipe experiments

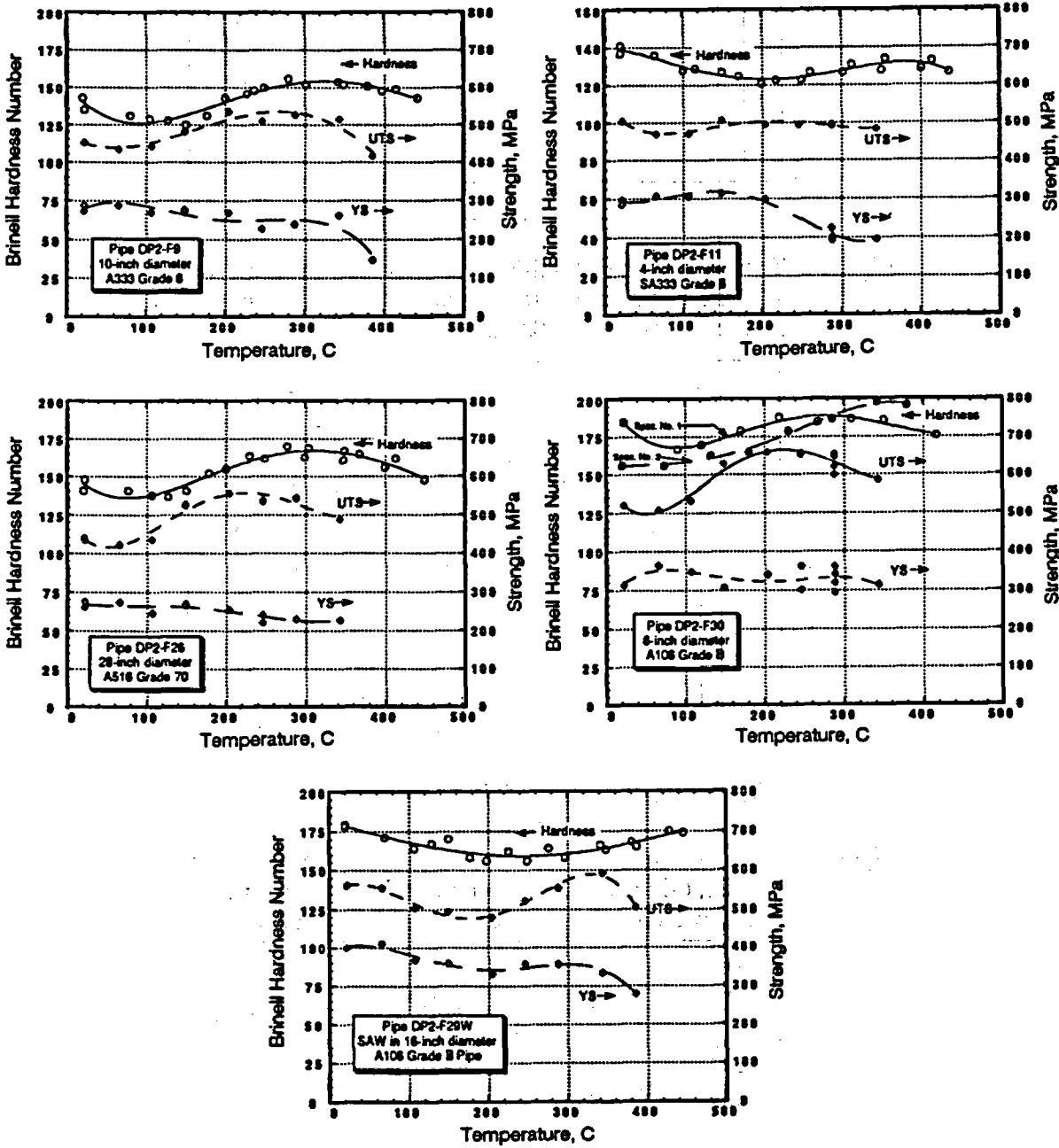


Figure 11 Yield strength, ultimate tensile strength, and Brinell hardness as functions of test temperature for five carbon steels

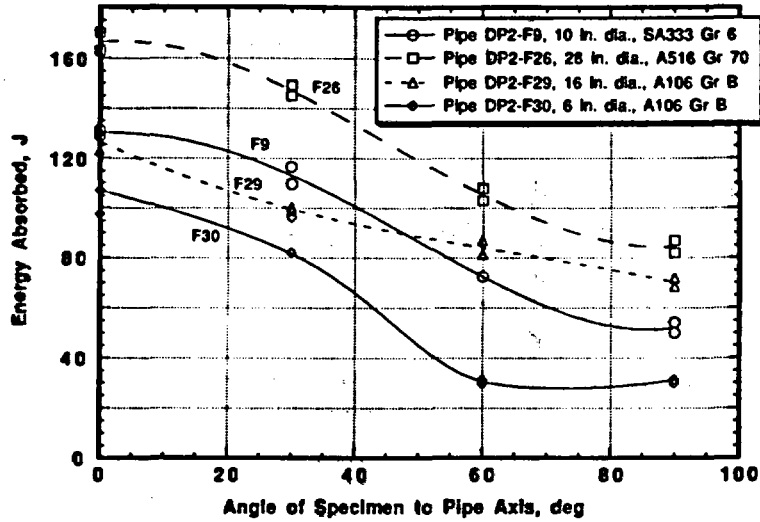


Figure 12 Energy absorbed by Charpy V-notch impact specimens as a function of specimen orientation.  
 Note: All fractures were 100 percent ductile

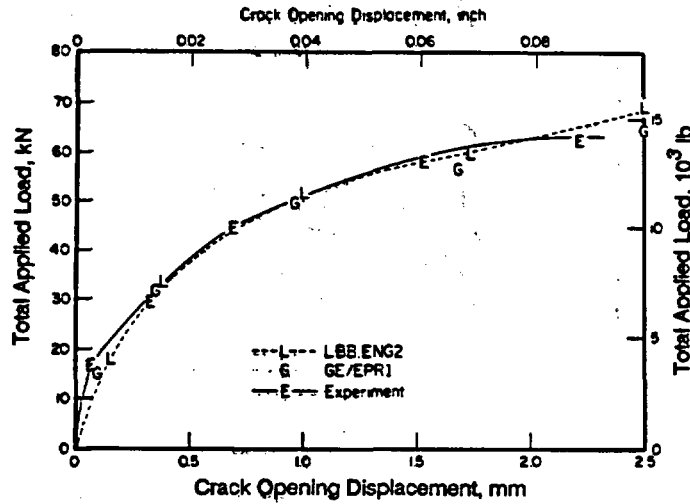


Figure 13 Crack-opening displacement up to load at crack initiation for a 4-inch diameter A333 Gr 6 carbon steel pipe under pure bending (Experiment 4111-1)

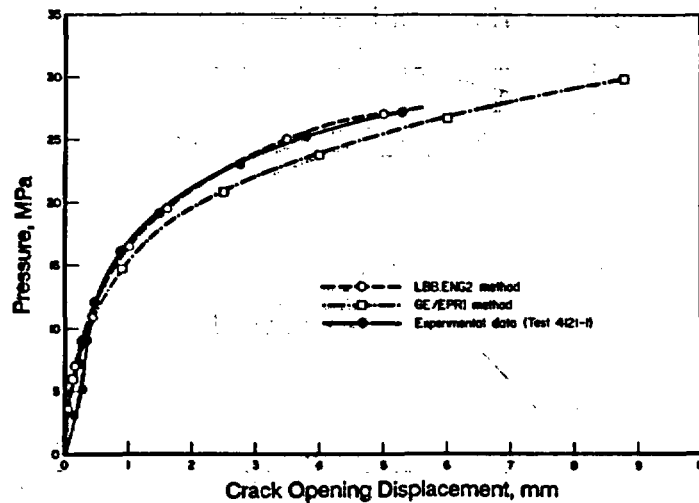


Figure 14 Comparison of various analyses to center-crack-opening displacement for pressurized pipe Experiment 4121-1 on 6-inch diameter TP304 stainless steel pipe

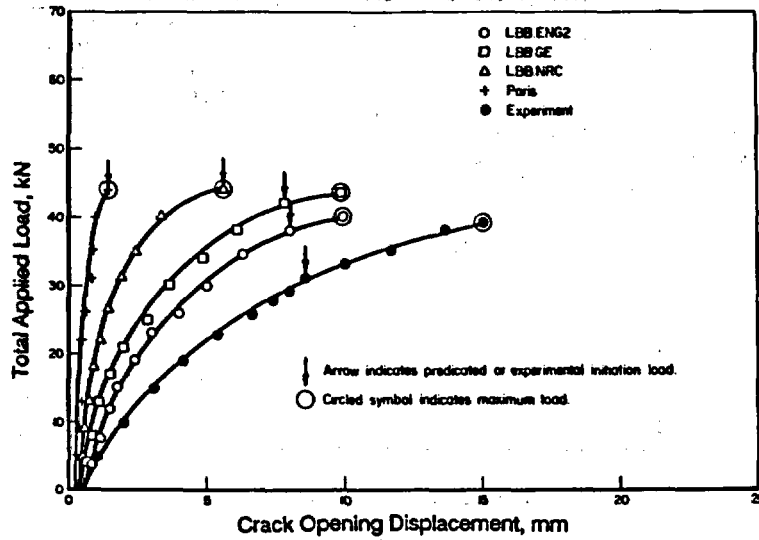


Figure 15 Comparison of predictions of various analyses to experimental center-crack-opening displacement for pressure and bend Experiment 4131-1 on 6-inch diameter TP304 stainless steel pipe

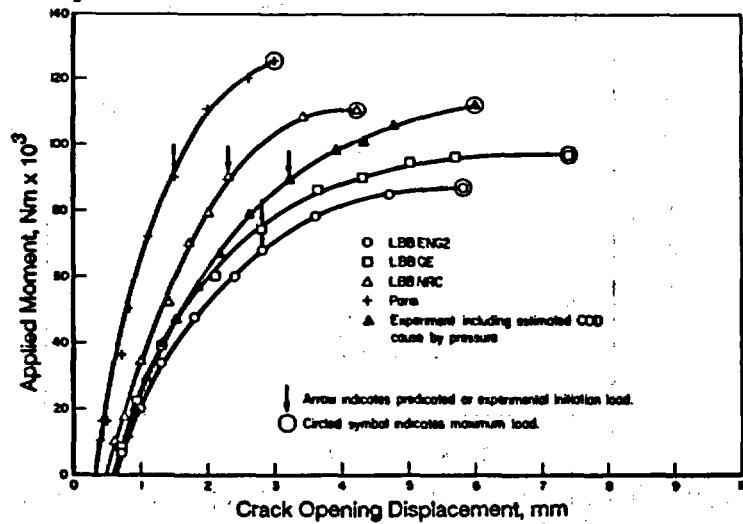


Figure 16 Comparison of predictions of various analyses to experimental center-crack-opening displacement for pressure and bend Experiment 4131-3 on 10-inch nominal diameter A333 Grade 6 pipe

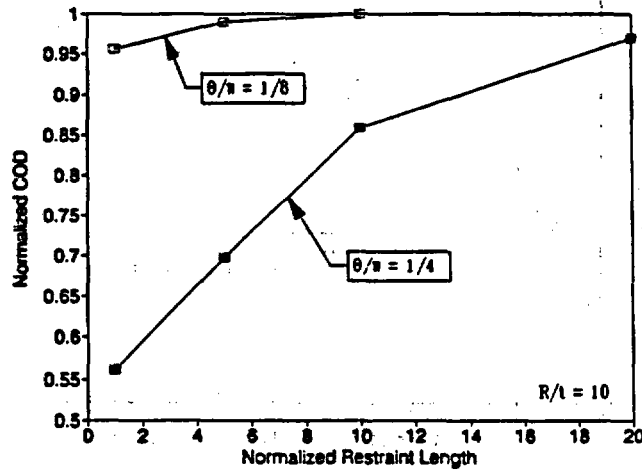


Figure 17 Effect of fully restrained bending conditions from crack location on COD normalized by unrestrained COD

## Heavy-Section Steel Irradiation Program: Embrittlement Issues\*

W. R. Corwin

Oak Ridge National Laboratory  
Oak Ridge, Tennessee 37831

### ABSTRACT

Maintaining the integrity of the reactor pressure vessel (RPV) in a light-water-cooled nuclear power plant is crucial in preventing and controlling severe accidents and the potential for major contamination releases. The RPV is one of only two major safety-related components of the plant for which a duplicate or redundant backup system does not exist. It is imperative to understand and predict the capabilities and limitations of its integrity. In particular, it is vital to fully understand the degree of irradiation-induced degradation of the RPV's fracture resistance which occurs during service, since without that radiation damage it is virtually impossible to postulate a realistic scenario which would result in RPV failure. For this reason, the Heavy-Section Steel Irradiation (HSSI) Program has been established by the U.S. Nuclear Regulatory Commission (USNRC) to provide a thorough, quantitative assessment of the effects of neutron irradiation on the material behavior, and in particular the fracture toughness properties, of typical pressure vessel steels as they relate to light-water reactor pressure-vessel integrity. Effects of specimen size, material chemistry, product form and microstructure, irradiation fluence, flux, temperature and spectrum, and postirradiation annealing are being examined on a wide range of fracture properties including fracture toughness ( $K_{Ic}$  and  $J_{Ic}$ ), crack arrest toughness ( $K_{Ia}$ ), ductile tearing resistance ( $dJ/da$ ), Charpy V-notch (CVN) impact energy, dropweight nil-ductility temperature (NDT), and tensile properties. Models based on observations of radiation-induced microstructural changes using the field ion microprobe and the high resolution transmission electron microscope provide improved bases for extrapolating the measured changes in fracture properties to wider ranges of irradiation conditions. The principal materials examined within the HSSI program are high-copper welds since their postirradiation properties are most frequently limiting in the continued safe operation of commercial RPVs. In addition, a limited effort focuses on stainless steel weld-overlay cladding, typical of that used on the inner surface

---

\*Research sponsored by the Office of Nuclear Regulatory Research, U.S. Nuclear Regulatory Commission under Interagency Agreement DOE 1886-8109-8L with the U.S. Department of Energy under Contract DE-AC05-84OR21400 with Martin Marietta Energy Systems, Inc.

The submitted manuscript has been authored by a contractor of the U.S. Government under Contract DE-AC05-84OR21400. Accordingly, the U.S. Government retains a nonexclusive, royalty-free license to publish or reproduce the published form of this contribution, or allow others to do so, for U.S. Government purposes.

of RPVs, since its postirradiation fracture properties have the potential for strongly affecting the extension of small surface flaws during overcooling transients.

Recent results are described concerning the shifts in fracture toughness and crack arrest toughness in high-copper welds, the effects of irradiation on stainless-steel weld-overlay cladding, the unirradiated examination of a low upper-shelf (LUS) weld from the Midland reactor, irradiation temperature effects on Charpy and tensile properties of several LUS welds, initial theoretical studies related to irradiation-rate effects, and the continued investigation into the causes of accelerated low-temperature embrittlement recently observed in RPV support steels.

## PROGRAM SCOPE AND GOALS

It is vital to fully understand the degree of irradiation-induced degradation of the RPV's fracture resistance which occurs during service, since without that radiation damage it is virtually impossible to postulate a realistic scenario which would result in RPV fracture. For this reason, the HSSI program has been established with its primary goal to provide a thorough, quantitative assessment of the effects of neutron irradiation on the material behavior, and in particular the fracture toughness properties, of typical pressure vessel steels as they relate to light-water reactor pressure-vessel integrity. Results from the HSSI studies will be integrated to aid in resolving major regulatory issues facing the USNRC which involve RPV irradiation embrittlement such as pressurized-thermal shock, operating pressure-temperature limits, low-temperature overpressurization, and the specialized problems associated with LUS welds. Taken together the results of these studies also provide guidance and bases for evaluating both the aging behavior and the potential for plant life extension of light-water reactor pressure vessels.

The HSSI program includes the direct continuation of irradiation studies previously conducted within the Heavy-Section Steel Technology (HSST) program augmented by enhanced examinations of the accompanying microstructural changes. Effects of specimen size, material chemistry, product form and microstructure, irradiation fluence, flux, temperature and spectrum, and postirradiation annealing are being examined on a wide range of fracture properties. The HSSI Program is arranged into 9 tasks: (1) program management, (2)  $K_{Ic}$  curve shift in high-copper welds, (3)  $K_{Ia}$  curve shift in high-copper welds, (4) irradiation effects on cladding, (5)  $K_{Ic}$  and  $K_{Ia}$  curve shifts in LUS welds, (6) irradiation effects in a commercial LUS weld, (7) microstructural analysis of irradiation effects, (8) in-service aged material evaluations, and (9) correlation monitor materials. Recent results and plans for each technical task are described in the following sections.

## $K_{Ic}$ CURVE SHIFTS IN HIGH-COPPER WELDS

In the fracture mechanics integrity analysis of RPVs, the initiation and arrest fracture toughness curves as described in Sect. XI of the *ASME Boiler and Pressure Vessel Code* are often used. These curves are also used for the normal operation of RPVs. The effects of neutron irradiation on toughness are accounted for by shifting the curves upward in temperature without change in shape by an amount equal to the shift (plus a margin term) of the CVN impact energy curve at the 41-J level. Such a procedure implies that the shifts in the fracture toughness curves

are the same as those of the CVN 41-J energy level, and that irradiation does not change the shapes of the fracture toughness curves.

The objectives of the HSSI Fifth Irradiation Series are to determine the  $K_{Ic}$  curve shifts and shapes for two irradiated high-copper, 0.23 and 0.31 wt %, submerged-arc welds (72W and 73W, respectively). All planned unirradiated and irradiated testing for the Fifth Irradiation Series has been completed. The irradiations were performed by the Oak Ridge National Laboratory (ORNL) at the Oak Ridge Research Reactor (ORR) at a nominal temperature of 288°C to average fluences of about  $1.5 \times 10^{19}$  neutrons/cm<sup>2</sup> (>1 MeV). Tests were performed by both ORNL and Materials Engineering Associates, Inc., and included tensile, CVN impact, drop-weight, and fracture toughness. Unirradiated compact specimens of 25-, 51-, 102-, 152-, and 203-mm thickness (1T, 2T, 4T, 6T, and 8TC(T), respectively) were tested, whereas irradiated testing was limited to 1T, 2T, and 4TC(T) specimens.

The results of testing have been presented previously.<sup>1</sup> For the CVN results, the 41-J transition temperature shifts using Weibull-based analyses were very similar to those obtained from hyperbolic or exponential curve-fitting techniques for the 72W and 73W welds. The 41-J shifts were 72 and 82°C, while the 68-J shifts were 82 and 105°C for welds 72W and 73W, respectively. The analyses also indicated that variations in neutron fluence did not influence the shifts or the shapes of the irradiated curves and, therefore, will allow for conclusions concerning effects of irradiation on curve shape.

The first step in the analysis was to evaluate the fracture toughness data to establish the data base appropriate for statistical analyses. For those specimens which met the E 399 criteria for a valid  $K_{Ic}$ , the  $K_{Ic}$  value is used. For those specimens which exhibited curvature in the load-displacement record, indicative of plastic deformation and, perhaps, stable ductile tearing, the  $K_{Jc}$  value was used. Because the data base includes results from both linear-elastic and elastic-plastic fracture mechanics calculations, the fracture toughness data have been designated  $K_{cI}$  for cleavage fracture toughness.

An unexpectedly large number of cleavage pop-ins in the irradiated specimens required examination of those results. Out of 156 unirradiated compact specimens, only two exhibited pop-ins. For the 110 irradiated specimens, however, 28 specimens exhibited a total of 36 pop-ins. For a number of previously stated reasons,<sup>2</sup> only the initial pop-in was used herein to determine cleavage fracture toughness for those specimens exhibiting pop-ins. Pop-ins of any size representing a cleavage event in the specimen were considered significant. Figure 1 shows a plot of cleavage fracture toughness for weld 72W in the irradiated condition. Each datum plotted represents one test specimen (the abscissa is not scaled). As shown, the pop-in results fit generally within the scatter bands of the fracture results and the lowest values are mixed between pop-ins and fracture results. These results suggest that cleavage pop-ins are significant relative to indicating propensity for cleavage fracture in the test specimen.

The  $K_{Ic}$  curve in Sect. XI of the ASME Code is a lower boundary to the data used for its development.<sup>3</sup> Three-parameter nonlinear regression analyses were performed for 72W and 73W in both the unirradiated and irradiated conditions using the simple exponential form of the ASME  $K_{Ic}$  curve. Various intercept values were obtained but statistical analyses revealed that they did not differ significantly from the ASME value of 36.48; thus, the intercept value was fixed at 36.48 MPa√m. Mean curve fits from the subsequent two-parameter nonlinear regression analyses gave fracture toughness temperature shifts, measured at the 100 MPa√m-level, of about 94 and 100°C for 72W and 73W, respectively, the same results obtained from the three-parameter

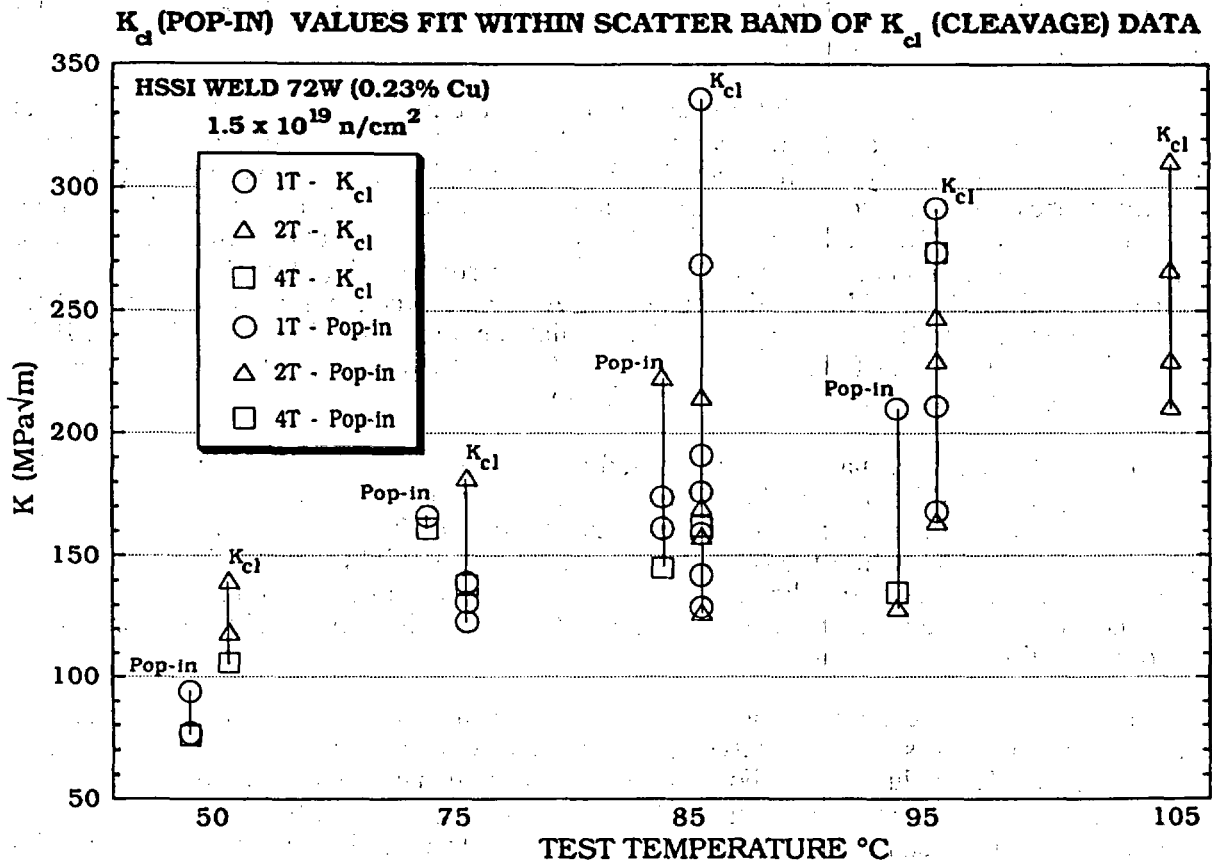


Fig. 1. Cleavage fracture toughness for irradiated HSSI weld 72W comparing first pop-in events with fracture toughness results from fracture events at the same test temperature. Each datum represents one specimen.

nonlinear regression analyses. Additionally, two-parameter analyses with the intercept equal to zero were performed and the results were similar to those discussed above.

In order to better examine changes in shape of the curve, the model was linearized. The fracture toughness 100-MPa√m temperature shifts are about 83 and 99°C for 72W and 73W, respectively. The analyses show some decreases in slopes for the irradiated data for both welds. These decreases, however, are only about 4.1 and 6.9% for 72W and 73W, respectively. The standard errors associated with the coefficients representing the slopes are similar in magnitude implying low significance of the slope changes. The resulting temperature shifts using averaged slope values are about 84 and 100°C for 72W and 73W, respectively. Using only the temperature intervals between the means and lower curves (representing one standard deviation on fracture toughness) results in associated standard deviations of 37 and 30°C for 72W and 73W, respectively, compared to 20°C and 22°C, respectively, for the CVN results.

Considering the combined data sets, with temperature normalized to ASME reference temperature, RT<sub>NDT</sub>, the curve for the irradiated data is displaced upward in temperature because the fracture toughness shifts are greater than the CVN 41-J shifts. At  $K_{cl}$  values of 50, 100, and

200 MPa $\sqrt{m}$ , the differences are about 10, 15, and 17°C. The standard deviation associated with the difference at 100 MPa $\sqrt{m}$  is 13.7°C, a large value relative to the difference observed. The increasing temperature offset between the two curves with increasing  $K_{IC}$  reflects the average change in curve shape. The difference between the normalized unirradiated and irradiated curves for the combined data increases about 7°C over the  $K_{IC}$  range from 50 to 200 MPa $\sqrt{m}$ , while the corresponding changes for 72W and 73W are 5.3 and 8.6°C, respectively, indicating a greater change in slope for the higher copper weld. Similarly, the corresponding change between the ASME  $K_{Ia}$  and  $K_{IC}$  curves is 12.1°C. It is interesting that simple manual construction of bounding curves to the data result in measured temperature shifts within a few degrees of those determined by the various mean fits. Also, manually constructed curves, especially for 73W, suggest a shape change for the lower-bound curves.

Figure 2 shows a plot of the irradiated fracture toughness data and various curves for 73W. The ASME  $K_{IC}$  curve is shown for the unirradiated condition and for the irradiated

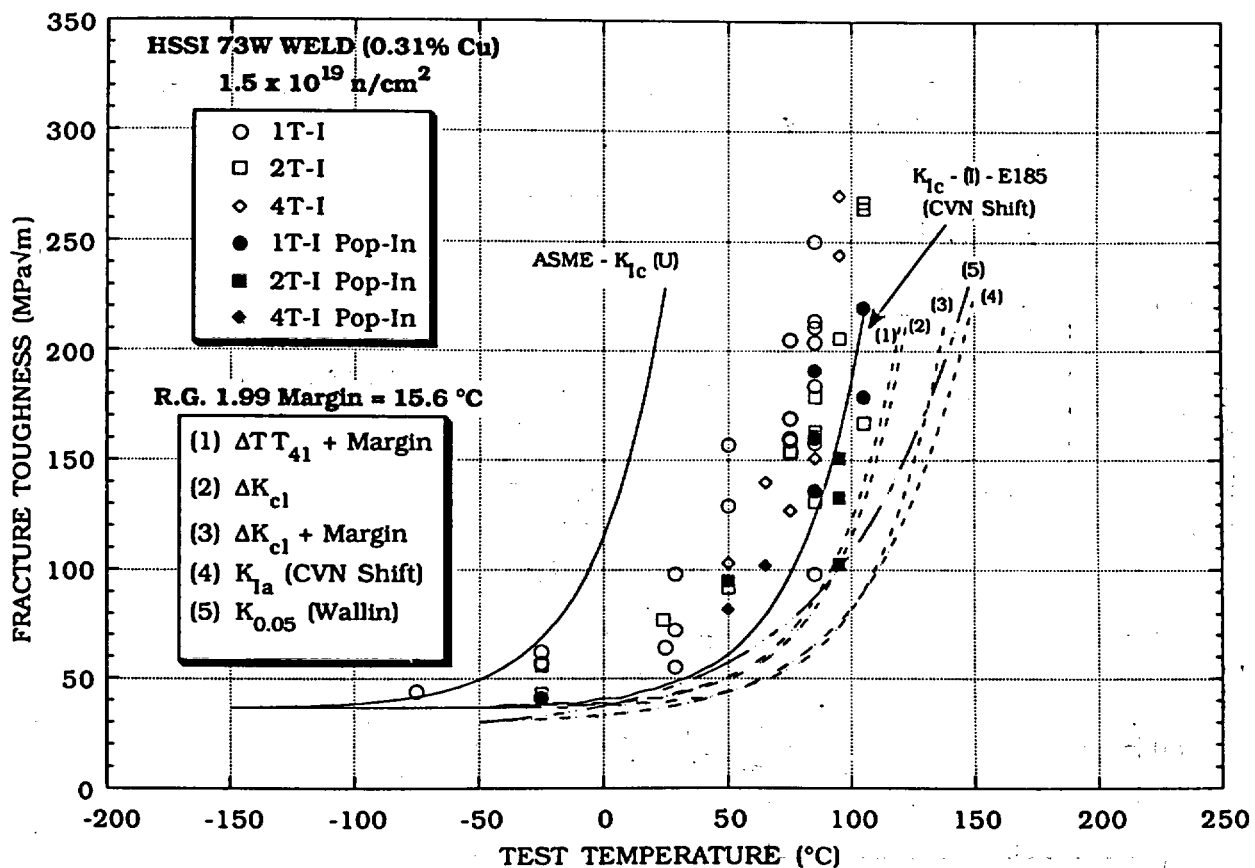


Fig. 2. Fracture toughness,  $K_{IC}$ , vs test temperature for irradiated HSSI weld 73W. The ASME  $K_{IC}$  curve for the unirradiated data is shown as is the same curve after shifting it upward in temperature equal to the Charpy 41-J shift. The curves labeled 1, 2, and 3 represent the ASME curve shifted by the indicated criterion, where Margin is 15.6°C. The  $K_{Ia}$  curve represents the ASME  $K_{Ia}$  curve shifted by the Charpy 41-J shift. The  $K_{0.05}$  curve is the five-percentile curve for all the HSSI 72W and 73W combined data using the Wallin procedure.

condition after shifting the curve upward. The dashed curves labeled 1 through 3 represent different methods for shifting the  $K_{Ic}$  curve. The curve labeled 4 represents the ASME  $K_{Ia}$  curve shifted upward in temperature equal to the Charpy 41-J shift ( $\Delta T_{T41}$ ). The curve labeled 5 is the five-percentile curve produced using the method of Wallin.<sup>4</sup> For 72W, the data are bounded by the  $\Delta T_{T41}$  + Margin curve and the  $\Delta K_{C1}$  curve, but neither of those curves quite bound all the data for 73W. The margin is 15.6°C as defined in *Regulatory Guide 1.99* (Rev. 2) assuming credible surveillance data. The  $K_{Ia}$  curve is shown to allow for comparison of that curve with the shifted  $K_{Ic}$  curves, especially regarding curve shape in view of the observation that the irradiated  $K_{Ic}$  curves for these two welds appear to have exhibited some shape change after irradiation.

Figure 3 shows a plot of all the irradiated fracture toughness data for 72W and 73W plotted vs temperature normalized to the RTNDT. The RTNDT for each weld is defined as the unirradiated RTNDT plus  $\Delta T_{T41}$ . As shown in the figure, a total of eight data points fall below the ASME  $K_{Ic}$  curve. The dashed curve is the  $K_{Ic}$  curve shifted upward in temperature to bound the data; a shift of 18°C is required.

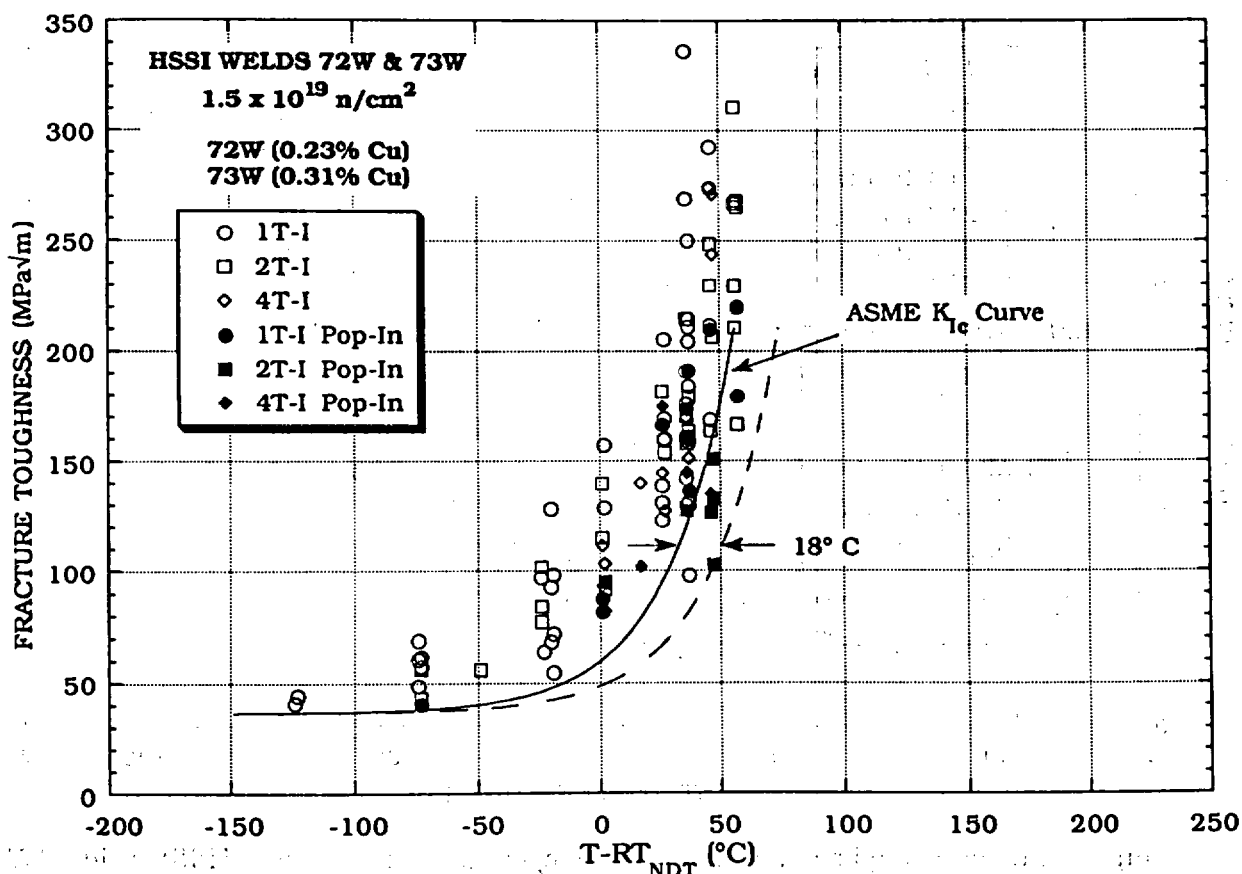


Fig. 3. Fracture toughness,  $K_{Ic}$ , vs normalized temperature,  $T - RT_{NDT}$ , for the irradiated welds 72W and 73W. The dashed curve is simply the ASME curve shifted upward in temperature to just bound the irradiated data. As shown, an additional shift of 18°C beyond that of the Charpy 41-J shift is required.

Principal observations from the HSSI Fifth Irradiation Series are as follows. The fracture toughness values from small cleavage pop-ins suggest that the pop-ins observed in this study are significant relative to indicating propensity for cleavage fracture in the test specimen. Regarding the irradiation-induced temperature shift, statistical analyses and curve fitting showed that the temperature shifts at a fracture toughness of  $100 \text{ MPa}\sqrt{\text{m}}$  were greater than those at a Charpy energy of 41 J, but are in good agreement with the Charpy 68-J transition shifts. The fact that the 68-J temperature shifts are greater than the 41-J shifts reflects the change in the slope of the CVN curves following irradiation.

Regarding the shape of the fracture toughness curve, the results from curve-fitting data are somewhat mixed. The linearized two-parameter fits, however, do indicate some decrease in the slopes, with the higher copper 73W weld exhibiting a somewhat greater change than for 72W. Using a 95% confidence criterion, however, those decreases in slopes are not statistically significant. On the other hand, curves constructed to bound all the data do indicate a substantial slope decrease, especially for weld 73W. Because the ASME  $K_{IC}$  curve is a lower-bound curve for the data used for its construction, this latter observation is important. The five-percentile curve from the Wallin procedure bounds all the data, but the curve has a substantially lower slope than the ASME  $K_{IC}$  curve and appears to be overly conservative at fracture toughness levels above about  $100 \text{ MPa}\sqrt{\text{m}}$ . Of course, concerns about curve shape changes can be accounted for by applying large enough shifts to the  $K_{IC}$  curve, but such a practice begs the issue of the degree of accuracy that can be developed when the trend line (curve shape) does not fit the real fracture toughness trend for the irradiated condition. The data in the present case indicate that the  $K_{IC}$  curve shifted by the 41-J Charpy V-notch plus margin would not have bounded a larger data base, and more margin adjustment is needed. The difficulty is that added margin to cover high toughness  $K_{C1}$  values will result in over-conservatism in the lower transition region. Therefore, shallower curves such as the five-percentile curve of Wallin or the  $K_{Ia}$  curve deserve consideration.

Preliminary observations from the HSSI Sixth Irradiation Series on crack-arrest toughness, described in the following section, indicate no irradiation-induced curve shape changes in the  $K_{Ia}$  curve.<sup>5</sup> One consideration, then, would be to use the  $K_{Ia}$  curve shape to describe the irradiated  $K_{IC}$  curve for materials which exhibit irradiation-induced toughness shifts above some prescribed amount. The procedure used to construct the  $K_a$  curves was simply to translate the ASME  $K_{Ia}$  curve until it just provided a bound to the irradiated data. That procedure showed that, given the available crack-arrest data, the curves needed to bound the unirradiated and irradiated data are shifted from the ASME curve by less than  $\Delta T T_{41}$ . For the combined irradiated data, the bounding curve is about  $28^\circ\text{C}$  lower than the shifted ASME  $K_{Ia}$  curve. Figure 4 shows a comparison of the ASME  $K_{IC}$  and  $K_{Ia}$  curves as well as the bounding curves for the combined irradiated data for 72W and 73W normalized to the  $RT_{NDT}$  as discussed for Fig. 3. The most notable observation is that the  $K_{C1}$  curve has been shifted to higher temperatures than the  $K_a$  curve. An argument can be made that, because irradiation hardening increases yield strength, the strain-rate sensitivity is reduced such that the quasistatic  $K_{IC}$  values tend toward agreement with the dynamic  $K_{Ic}$  and  $K_{Ia}$  values. This does not, of course, account for the transposition of the  $K_{C1}$  and  $K_a$  results shown in Fig. 4. One important factor is the number of tests performed; 110 irradiated fracture toughness results and only 34 irradiated crack-arrest results are available. Further, the fracture toughness and crack-arrest toughness data for the unirradiated welds are not nearly as far apart as the ASME curves. By not considering the pop-ins in the irradiated fracture toughness data, the  $K_{C1}$  and  $K_a$  bounding curves would be very close. On the other hand, because the propensity for crack arrest increases with decreasing

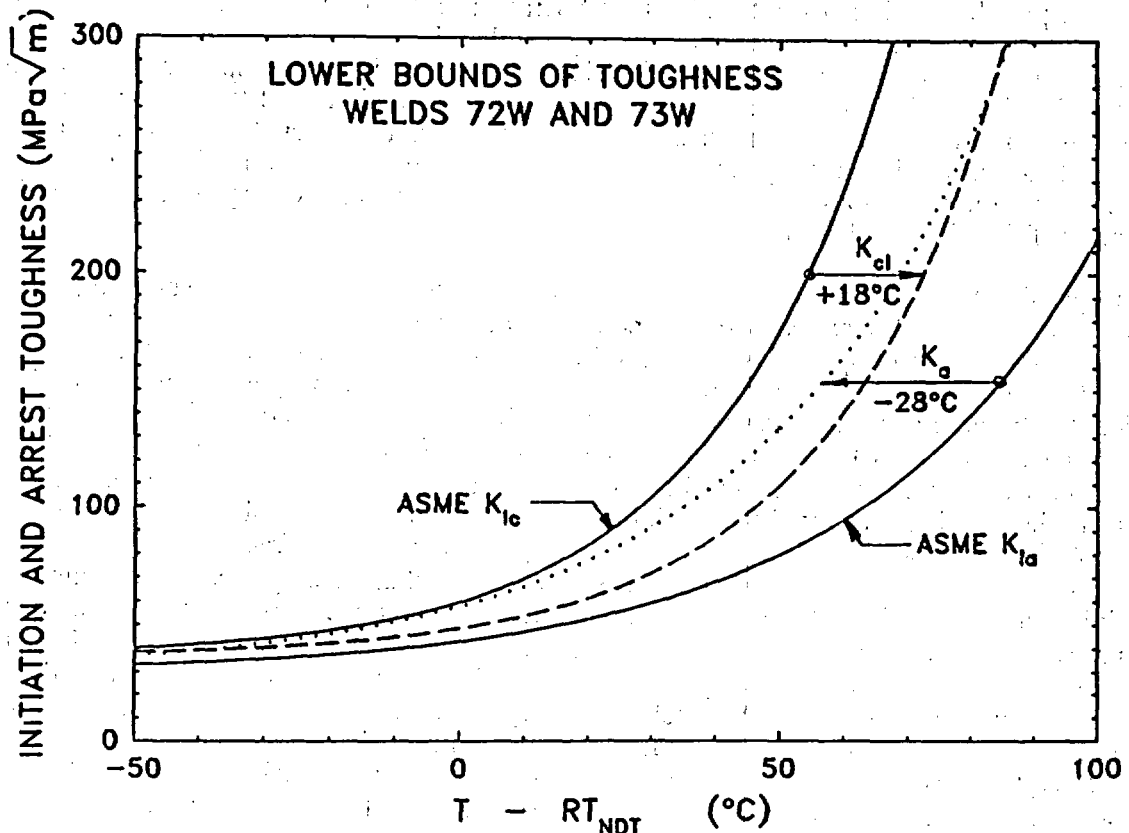


Fig. 4. Comparison of bounding curves for fracture toughness,  $K_{cl}$ , and crack-arrest toughness,  $K_a$ , vs normalized temperature,  $T - RT_{NDT}$ , for the irradiated welds 72W and 73W. The ASME  $K_{Ic}$  and  $K_{Ia}$  curves are included and show that the bounding curve to the  $K_{cl}$  data (110 test results) falls at higher temperatures than that for the  $K_a$  data (34 test results).

temperature interval between the  $K_{Ic}$  and  $K_{Ia}$  curves, many of the pop-ins may otherwise have resulted in fully broken specimens. Resolution of the observations in Fig. 4 most likely resides in consideration of statistical variations.

#### $K_{Ia}$ CURVE SHIFT IN HIGH-COPPER WELDS

The primary objective of the HSSI Sixth Irradiation Series (or, for brevity, the  $K_{Ia}$  program) is to determine the effect of irradiation on the shift and shape of the  $K_{Ia}$  vs  $(T - RT_{NDT})$  curve. The irradiations were performed by ORNL at the ORR at a nominal temperature of 288°C to average fluences of about  $1.9 \times 10^{19}$  neutrons/cm<sup>2</sup> (>1 MeV). Portions of the identical welds examined in the Fifth Series, 72W and 73W, were also used for the crack-arrest program. All crack arrest tests were performed by ORNL. All the dropweight, tensile, and Charpy impact results from the Fifth Series are applicable except for small adjustments required due to the higher fluence experienced by the crack-arrest specimens.

A total of 60 crack arrest specimens ranging in thickness from 25 to 33 mm were irradiated. Unirradiated specimens up to 51 mm in thickness were examined. The irradiated specimens included 36 weld-embrittled and 24 duplex-type specimens. The 36 weld-embrittled specimens have been tested in Phase I of the  $K_{Ia}$  program, and a detailed report has been published.<sup>5</sup>

Principal observations from Phase I are as follows. The shifts of the lower bound curves for the 72W and 73W welds are approximately the same as the corresponding  $\Delta TT_{41}$ . Figures 5 and 6 show the results for welds 72W and 73W, respectively. Moreover, the shape of the lower bound curves compared to those of the ASME  $K_{Ia}$  curve did not seem to have been altered by irradiation for the test temperature range covered by the tests.

The crack-arrest toughness ( $K_a$ ) data for welds 72W and 73W, both unirradiated and irradiated, have been plotted as a function of  $T - RT_{NDT}$  in Fig. 7. The number of results plotted for each type of material tested is given beside each symbol in the legend. This figure includes a total of 77 unirradiated and 34 irradiated data points, many of which overlap. This figure shows that the four sets of  $K_a$  data when indexed to their respective  $RT_{NDT}$ s form a reasonable trend. The  $RT_{NDT}$ s for the four materials are given in Table 1. As shown in Fig. 7, the ASME curve is a conservative estimate of all the crack-arrest toughness data from

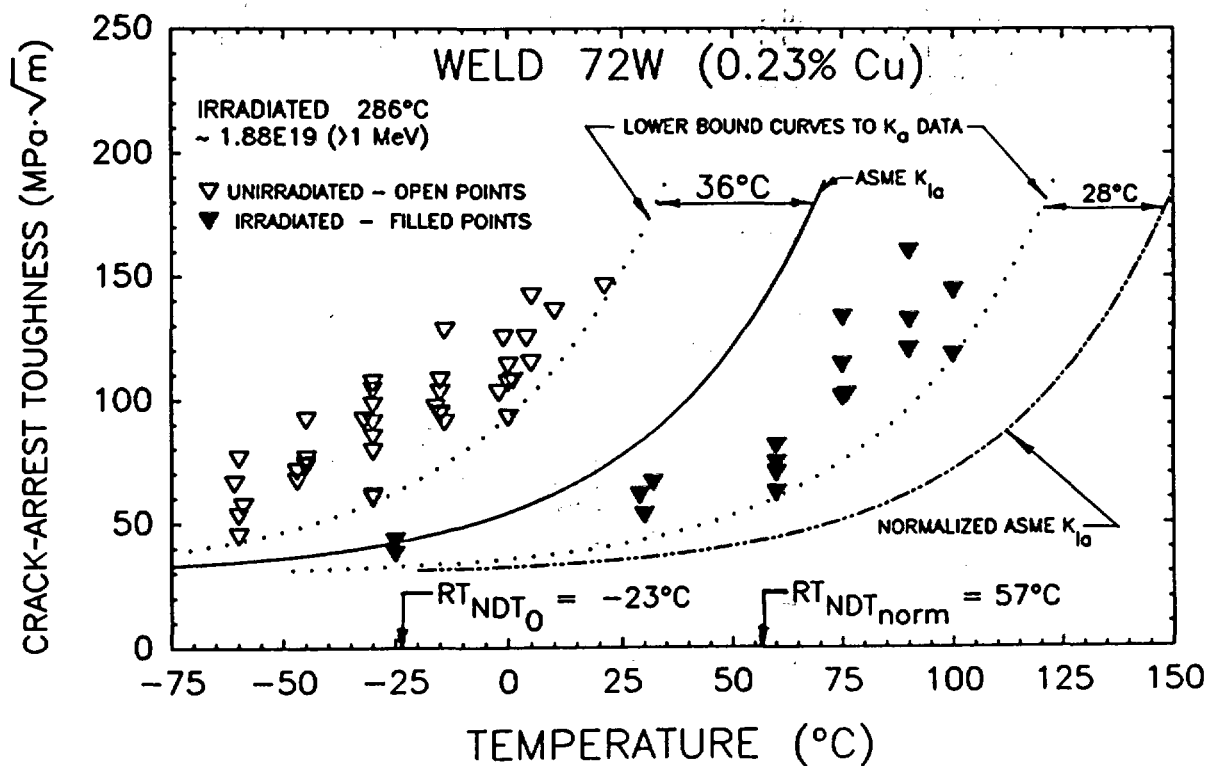


Fig. 5. Unirradiated and irradiated crack-arrest toughness,  $K_a$ , vs test temperature for weldment 72W. The dotted curves are lower bounds to the data obtained by shifting the ASME curves to a lower temperature by the amounts shown.

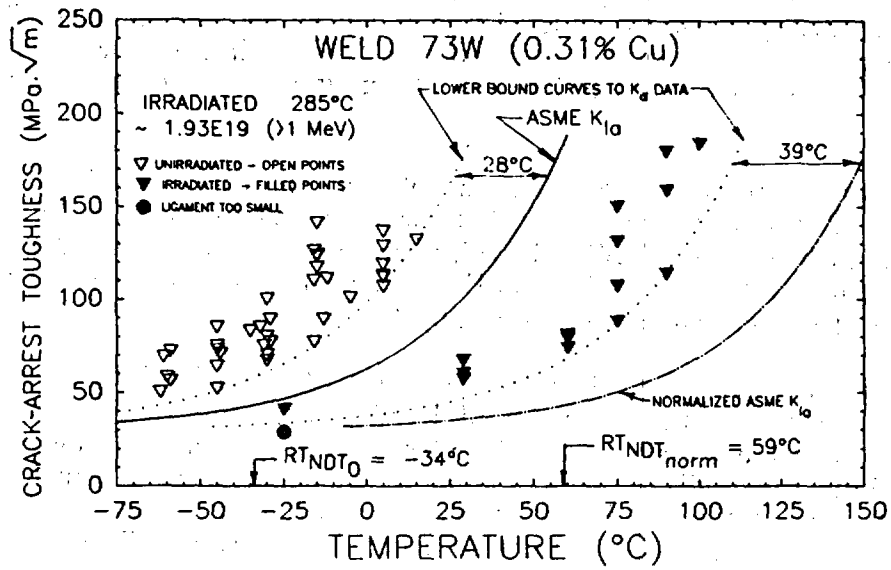


Fig. 6. Unirradiated and irradiated crack-arrest toughness,  $K_a$ , vs test temperature for weldment 73W. The dotted curves are lower bounds to the data obtained by shifting the ASME curves to a lower temperature by the amounts shown.

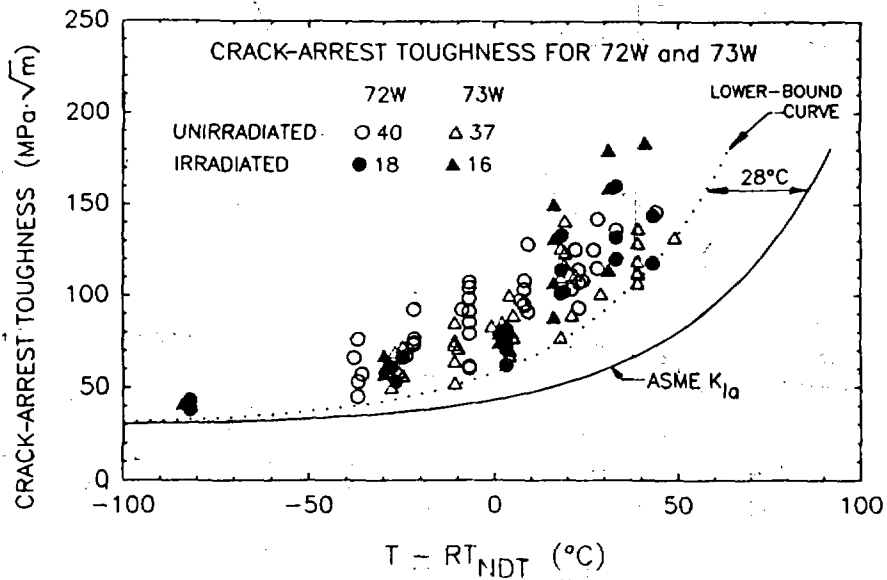


Fig. 7. All crack-arrest toughness  $K_a$  data for welds 72W and 73W plotted as a function of  $(T - RT_{NDT})$ . The number of results plotted are given beside each plot symbol in the legend.

Table 1. Initial, adjusted, and normalized reference temperatures (RT<sub>NDT</sub>) for welds 72W and 73W

Weld	Initial RT <sub>NDT</sub> (°C)	Charpy impact <sup>a</sup> observed results		Adjusted <sup>b</sup> RT <sub>NDT</sub> (°C)	Charpy impact normalized <sup>c</sup> to crack-arrest fluences		Normalized RT <sub>NDT</sub> (°C)
		Fluence, $\Phi$ ( $10^{19}$ n/cm <sup>2</sup> ) (>1 MeV)	$\Delta T_{41}$ (°C)		Fluence, $\Phi'$ ( $10^{19}$ n/cm <sup>2</sup> ) (>1 MeV)	$\Delta T_{41}$ (°C)	
72W	-23	1.51	72	49	1.88	80	57
73W	-34	1.51	82	48	1.93	93	59

<sup>a</sup>Source: R. K. Nanstad et al., "Effects of Radiation of  $K_{Ic}$  Curves for High-Copper Welds," pp. 214-33 in *Effects of Radiation on Materials: 14th International Symposium, Vol. II, ASTM STP 1046*, N. H. Packan, R. E. Stoller, and A. S. Kumar, Eds., American Society for Testing and Materials, Philadelphia, 1990.

<sup>b</sup>Adjusted RT<sub>NDT</sub> = initial RT<sub>NDT</sub> +  $\Delta T_{41}$  (according to ASTM 185-82).

<sup>c</sup>Normalization:  $(\Delta T_{41})(\Phi'/\Phi)^{0.5}$ . Source: G. R. Odette and G. E. Lucas, "Irradiation Embrittlement of Reactor Pressure Vessel Steels: Mechanisms, Models, and Data Correlations," pp. 206-41 in *Radiation Embrittlement of Nuclear Pressure Vessel Steels: An International Review (Second Volume), ASTM STP 909*, L. E. Steele, Ed., American Society for Testing and Materials, Philadelphia, 1986.

NOTE:

- $\Phi$  - fluence for Charpy V-notch impact specimens.
- $\Phi'$  - fluence for crack-arrest specimens.
- n - neutrons.
- $\Delta T_{41}$  - shift in 41-J Charpy V-notch impact energy level.

72W and 73W weldments in the transition region to approximately 50°C above RT<sub>NDT</sub>. At temperatures below RT<sub>NDT</sub>, there seems to be a smaller toughness margin between the lower-bound curves and the ASME  $K_{Ia}$  curves. For example, the lower-bound values are approximately 70, 35, and 10% higher than the ASME  $K_{Ia}$  values at temperatures with respect to RT<sub>NDT</sub> of 50, 0, and -50°C.

The lower-bound curve, shown as a dotted curve in Fig. 7, is the ASME  $K_{Ia}$  curve shifted downward by 28°C in temperature until the first data point is encountered. The 28°C shift shown is the minimum shift from all four sets of data (unirradiated and irradiated welds 72W and 73W). The 28°C shift was obtained for the irradiated 72W weld and the unirradiated 73W weld and, thus, no trend can be established. However, it is quite possible that more experimental data may alter this lower bound significantly. The evaluation of the 72W and 73W crack-arrest toughness data obtained from the weld-embrittled specimens is ongoing. Statistical analyses, similar to those described in the previous section on the  $K_{Ic}$  program, will also be performed on the data.

The remaining 24 irradiated crack-arrest specimens, which are all duplex-type specimens, are being tested during Phase II of Series 6. Four of the 24 duplex-type specimens, two each from the 72W and 73W welds, have already been tested. In all four specimens the flaw arrested

in the fusion zone between the hardened crack-starter material and the weld metal test section. Porosity and lack of fusion were the major reasons for the crack arresting in that region. That is likely to preclude successful testing of the remaining duplex specimens in their present form. In order to utilize these specimens, various modifications to the duplex specimens are being considered. The initial modification being pursued is to increase the crack-driving force by increasing the diameter of the crack-starter hole. At present, the diameter of the hole in the 24 irradiated duplex specimens is approximately 4 mm. The idea behind this modification is that a sufficiently large increase in crack-driving force may cause the propagating flaw to jump across the unfused, porous zone, but still allow arrest within the test section of the specimen.

## IRRADIATION EFFECTS ON STAINLESS STEEL CLADDING

The objective of the HSSI Seventh Irradiation Series is to obtain toughness properties for two types of stainless steel cladding in the unirradiated and irradiated conditions. The properties obtained include tensile, CVN impact, and J-integral toughness. The goal is to evaluate the fracture resistance of irradiated weld metal cladding representative of that used in early pressurized-water reactors. Irradiation effects on the single-wire, submerged-arc cladding have been published previously,<sup>6</sup> as have the irradiation effects on the tensile and Charpy impact behavior of three-wire cladding.<sup>7</sup> This section will summarize recently completed testing of irradiation effects on the fracture toughness of three-wire series-arc cladding.

The commercially produced three-wire series-arc stainless steel cladding was evaluated under similar irradiation and testing conditions as had been used previously for the single-wire cladding. To summarize results of CVN testing of the three-wire cladding specimens, irradiated at 288°C to fluence levels of 2 and  $5 \times 10^{19}$  neutrons/cm<sup>2</sup> (>1 MeV), it was observed that the CVN upper-shelf energy decreased by 15 and 20% and the 41-J transition temperature increased by 13 and 28°C, respectively. Irradiation also degraded the CVN lateral expansion significantly; expansion on the upper shelf was reduced by approximately 40% for both fluence levels. These results generally agree with those for the single-wire cladding produced with good welding practice.

Figure 8 shows that irradiation at 288°C to an average fluence of  $2.41 \times 10^{19}$  neutrons/cm<sup>2</sup> (>1 MeV) resulted in decreases in initiation ductile fracture toughness,  $J_{Ic}$ . Decreases in the tearing modulus were observed as well but the tearing modulus values did not change significantly with test temperature from about room temperature to 288°C. The  $J_{Ic}$  decreases generally agree with the reductions in both the CVN upper-shelf energy and lateral expansion except that the CVN data do not show a significant change with increasing test temperature.

Figure 9 provides a graphical comparison of the  $J_{Ic}$  values vs test temperature for the three-wire cladding with a typical A533 grade B class 1 plate (HSST Plate 02, 0.14 wt % copper) and a low upper-shelf weld (HSSI Weld 61W, 0.28 wt % copper), all in the unirradiated condition. Figure 10 shows a similar comparison of the same materials following irradiation at 288°C to similar fluence levels. Weld 61W gave the lowest  $J_{Ic}$  value (43.1 kJ/m<sup>2</sup>) observed for the LUS welds tested in the HSSI Second and Third Irradiation Series.<sup>9</sup> The  $J_{Ic}$  of the irradiated cladding at 288°C is only about half that of 61W. It is also substantially lower than the lowest  $J_{Ic}$  value (83.3 kJ/m<sup>2</sup>) obtained for HSST Plate 02 in the HSSI Fourth Irradiation Series.<sup>10</sup> The low fracture toughness of the three-wire stainless steel cladding has the potential for strongly affecting the extension of small surface flaws during overcooling transients.

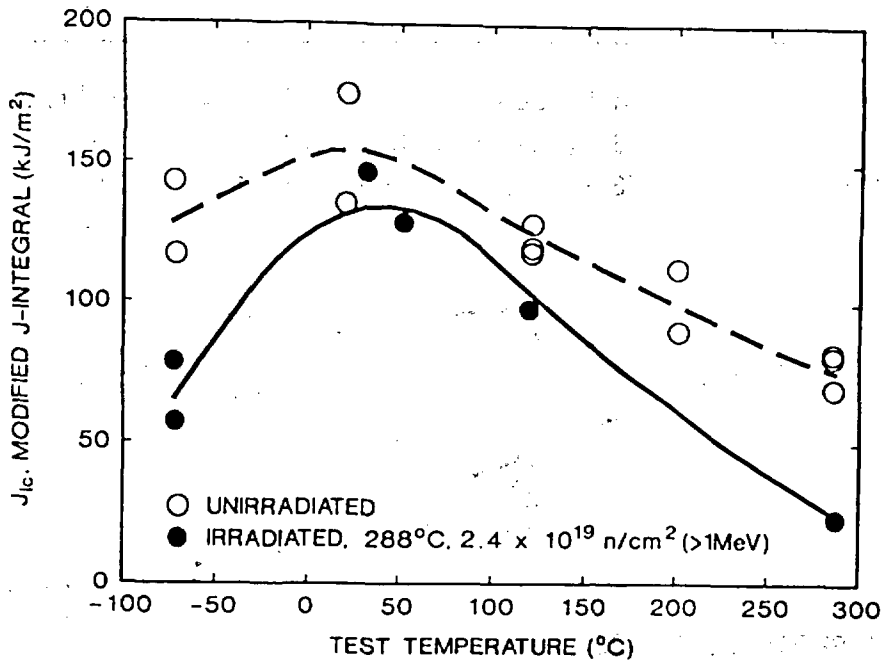


Fig. 8. Effect of irradiation on  $J_{IC}$  initiation fracture toughness (modified J-integral) for type 308 stainless steel weld overlay cladding.

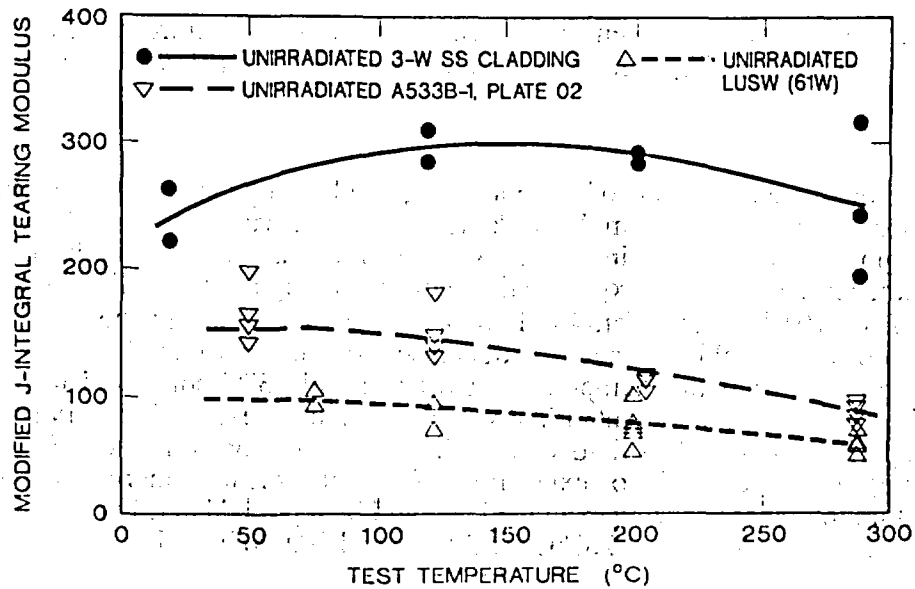


Fig. 9. Comparison between unirradiated  $J_{IC}$  initiation fracture toughness (modified J-integral) for three materials, three-wire stainless steel cladding, low-upper shelf weld, and A533 grade B class 1 plate.

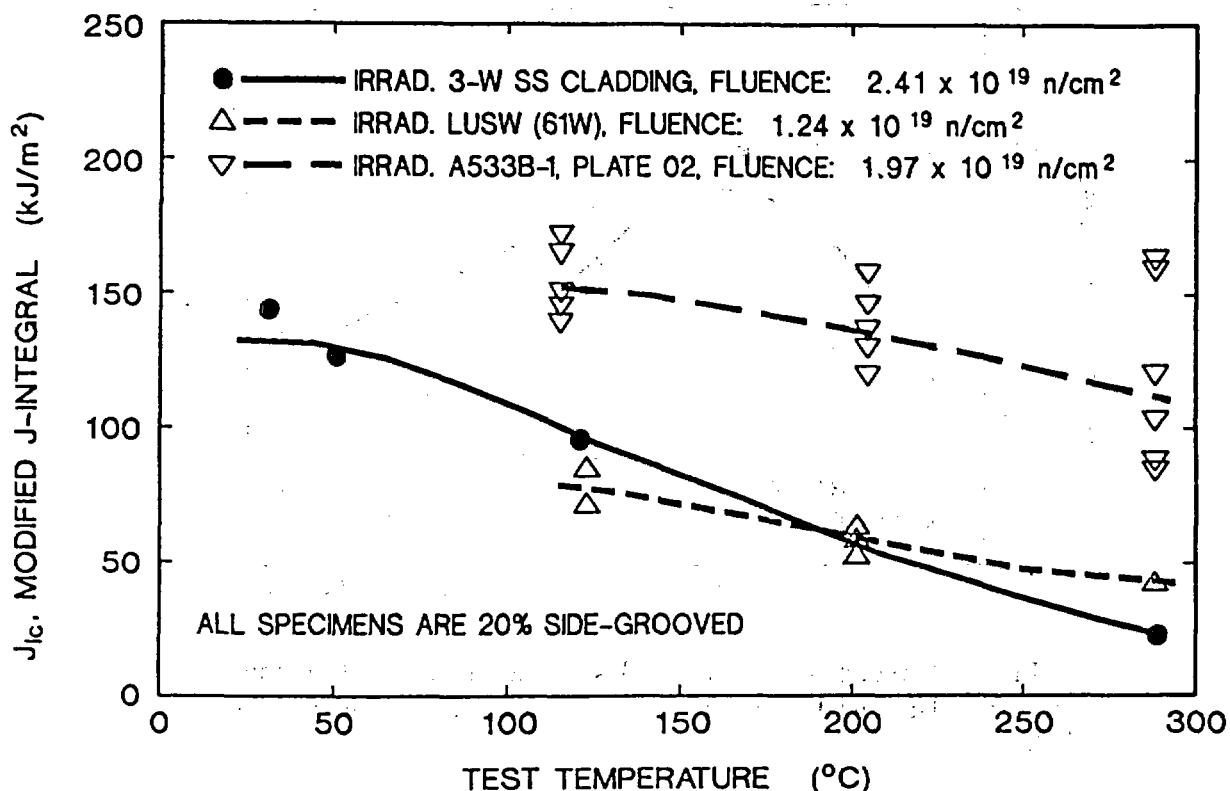


Fig. 10. Comparison between irradiated J<sub>Ic</sub> initiation fracture toughness (modified J-integral) for three materials, three-wire stainless steel cladding, low-upper shelf weld, and A533 grade B class 1 plate.

A task to evaluate the effects of thermal aging on cladding is under way within the HSST program and some of the results from that task are directly germane to the HSSI Program. Short-term thermal aging of three-wire stainless steel weld-overlay cladding was conducted at 288°C for 1605 h, the same temperature and exposure time corresponding to the irradiation of this material to a fluence of  $5 \times 10^{19}$  neutrons/cm<sup>2</sup> (>1 MeV). The Charpy upper-shelf energy showed a decrease of 16%, comparable to the 22% decrease from the combined effects of aging and irradiation. The 41-J transition temperature shift was only 3°C compared to the 29°C shift observed in the irradiation experiment. Finally, thermal aging caused only a very small change in the tensile properties compared to yield strength increases varying from 6 to 34% (dependent on test temperature) due to the irradiation exposure. Effects of short-term thermal aging on dynamic and static fracture toughness is being examined and will be reported later. Furthermore, long-term aging experiments are under way at 288°C for 20,000 and 50,000 h, and at 343°C for 20,000 h.

#### K<sub>Ic</sub> AND K<sub>Ia</sub> CURVE SHIFTS AND ANNEALING IN LOW UPPER-SHELF WELDS

This task focuses on examining the fracture behavior of irradiated and post-irradiated and annealed welds with low resistance to ductile tearing. It will provide, if needed, a basis for

modification of the current method for shifting the various ASME fracture toughness curves ( $K_{Ic}$ ,  $K_{Ia}$ ,  $K_{IR}$ ) to account for irradiation embrittlement, specifically in LUS welds. The information developed under this task will augment that obtained in experiments performed on two high upper-shelf weldments under the Fifth and Sixth Irradiation Series and provide an expanded basis for accounting for irradiation-induced embrittlement in reactor vessel materials. Additionally, it will examine the effects of thermal annealing and reirradiation on  $K_{Ic}$ ,  $K_{Ia}$ , and ductile tearing resistance (J-R) in large specimens representative of reactor vessels. The planning for these irradiation experiments, designated Series 8 ( $K_{Ic}$  and  $K_{Ia}$  curve shifts) and Series 9 (annealing effects) has begun but procurement of material and irradiations will not start before 1992.

## IRRADIATION EFFECTS IN COMMERCIAL LOW UPPER-SHELF WELDS

The focus in this task is the investigation of commercially produced submerged-arc welds with low Charpy upper-shelf energy. It will substantially augment the information obtained in the HSSI Second and Third Irradiation Series which examined the effects of irradiation on the ductile fracture toughness of commercially fabricated LUS welds. All of these welds have been fabricated with Linde 80 flux and copper-coated weld wire. The task currently includes two subtasks, the investigation of welds from the Midland Reactor Vessel, and the final analyses of irradiation temperature and fluence variations on the tensile and Charpy impact data from the Second and Third Series.

### Irradiation Effects in the Midland Reactor Vessel Weld

The primary objective of the HSSI Tenth Irradiation Series is to investigate the postirradiation fracture toughness of the WF-70 submerged-arc weld from the Midland Unit 1 reactor vessel. The weld metal is known to be low upper-shelf energy material, and this same weld material (WF-70) is known to be the controlling material in five commercial operating reactors. The test program will provide vital information on the significance of test methods that are applied in surveillance programs.

Consumers Power Company canceled and legally abandoned the facilities at Unit 1 of the Midland Power Station. The reactor vessel of Unit 1 was fabricated with a complete circumferential seam weld of WF-70 material at the core beltline. The WF-70 designation by Babcock and Wilcox, Co. (B&W) is the identification of a particular heat of weld wire (72105) and particular lot of Linde 80 welding flux (8669). The circumferential double-butt nozzle weld seam, interrupted by the nozzles, was fabricated using WF-70 on the outer half and WF-67 on the inner half of the weldment. Procedure WF-67 used the same Linde 80 welding flux as for WF-70, but used a different heat of weld wire (72442). Consumers Power Company provided the material free of charge as an act of goodwill for the benefit of the nuclear industry. A joint effort was initiated, at the instigation of the USNRC and the Electric Power Research Institute (EPRI), to obtain the WF-70 welds from the Unit 1 reactor vessel. Participants in the effort included Commonwealth Edison, B&W Owners Group, Westinghouse Electric Owners Group, and ORNL (representing the USNRC). Blocks of material, about 1.2 m long and 0.7 m wide, were removed from the 216-mm-thick vessel beltline region and the 305-mm-thick nozzle region by air-arc gouging the stainless steel cladding and flame cutting the base material using a vacuum-mounted fixture. Five beltline and two nozzle course sections were obtained by ORNL.

A plan for evaluating the WF-70 welds has been completed and includes both unirradiated and irradiated testing. In addition to a detailed characterization of the bulk chemical composition

of the welds, the field-ion microscope-atom probe will be used to determine the matrix composition of certain elements, e.g., copper, thought to better represent the amount of those elements available to the radiation damage process. Charpy and drop-weight tests have been performed at various locations through the weld thickness as well as at various locations along the weld to examine the variability in the unirradiated RTNDT. Charpy, tensile, drop-weight, and compact specimens of various sizes will be tested in the irradiated and unirradiated conditions. In the transition region, 0.5T, 1T, 2T, and 4TC(T) specimens will be tested in the unirradiated condition, while 0.5T, and 1TC(T) will be tested in the irradiated condition. On the ductile shelf, J-integral resistance curves will be obtained using compact specimens from 0.5T to 4T unirradiated and up to 2T irradiated, with the possibility that 4TC(T) specimens would be irradiated if the unirradiated J-R tests show significant size effects. The J-R behavior of the WF-70 weld metal is of great interest, especially regarding potential size effects on the tearing modulus. In addition a limited number of crack-arrest specimens will be irradiated and tested.

The first of two levels of testing is the preliminary evaluation of the material for uniformity of properties. Four beltline weld sections that cover the full 360° have been sampled and the testing is complete except for chemical analyses on two of the sections. The nozzle course weld sections have been sampled but the testing is not yet completed. Table 2 summarizes the transition temperature indices for the four beltline sections. Only the 1/4 thickness (1/4t) position of section 15 appeared to show significantly different 41- and 68-J temperatures as a function of depth in the weld. Nil-ductility temperatures appear to be consistent also. The variation in 41-J transition temperature throughout the weld, however, is from -19 to +15°C. In all cases, the RTNDTs are determined by the CVN data. The upper-shelf energies vary from 66 to 107 J; the 3/4t location in section 15 is the only sampled location which resulted in an upper-shelf below the 68-J (50 ft-lb) limit permitted by the USNRC.

Table 2. Transition temperatures for Midland beltline welds, codes 13, 9, 11, and 15

Through-thickness position	Charpy V-notch tests												NDT temperature (°C) at code number			
	41-J temperature (°C) at code number				68-J temperature (°C) at code number				Upper-shelf energy (J) at code number				13	9	11	15
	13		9		11		15		13		9					
	13	9	11	15	13	9	11	15	13	9	11	15	13	9	11	15
1/4t	-13	-6	-7	4.1	22	34	26	53	102	76	90	84	-60	-60	-60	-45
1/2t	-17	-11	-2	-13	29	25	21	23	105	83	90	90				
5/8t	-19	-15			10	14			107	87	90	90				
3/4t	0	3	15	12	36	53	53	a	89	81	83	66	-45	-45	-50	-55
7/8t		-3	-14	-10		44	31	27		78	79	84				

<sup>a</sup>Material did not attain 68-J energy level.

Test results of  $K_{Jc}$  fracture toughness with compact specimens are shown in Fig. 11. The beltline specimens came from 1/4t and 3/4t positions, while nozzle course specimens came only from the 3/4t position. Variable conditions of side-grooved vs not side-grooved and through-thickness position did not show significant trends.

Chemical analyses have been performed on two beltline and two nozzle course sections with a full analysis at five locations through the thickness in each case. The chemical

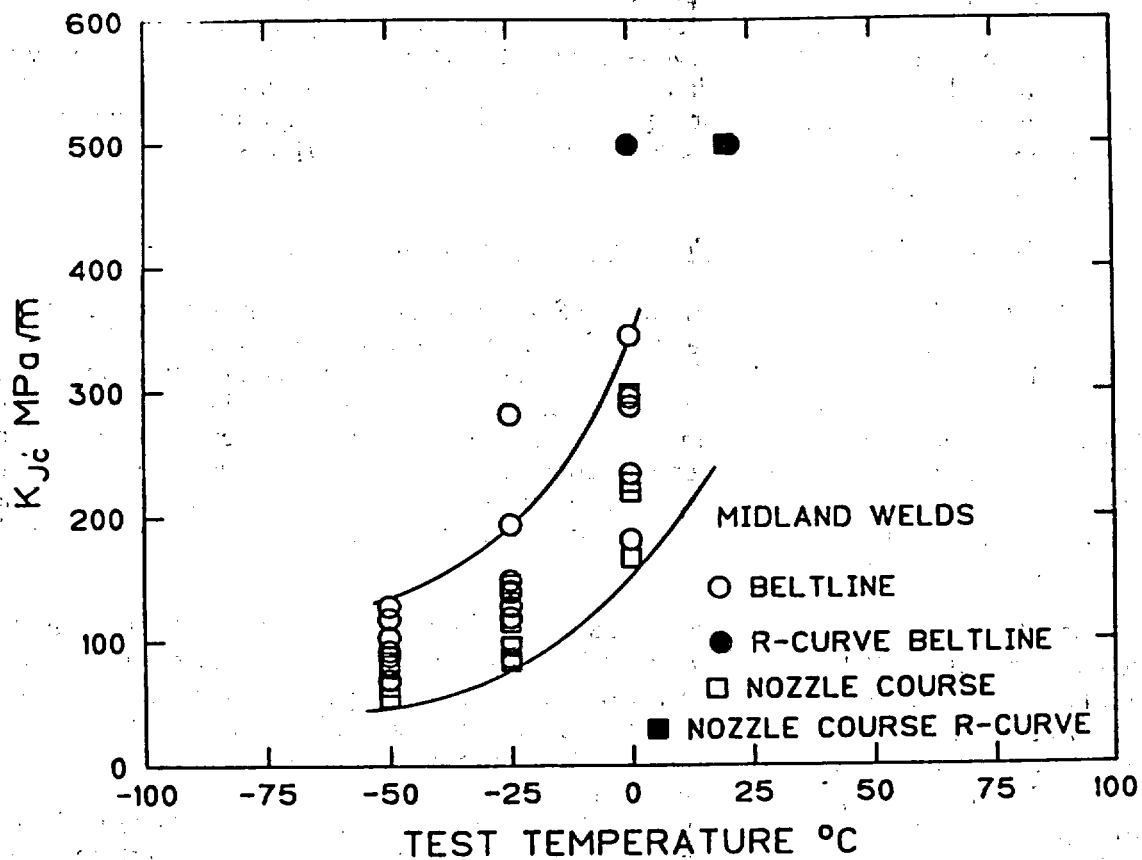


Fig. 11.  $K_{Jc}$  data from the Midland WF-70 welds at four locations around the beltline and two locations around the nozzle course.

compositions are generally as expected except that the copper content in the beltline sections is significantly lower than that in the nozzle course sections. The copper content ranges from about 0.21 to 0.32% with an average value of about 0.26% in the beltline, while the nozzle sections show a range of 0.36 to 0.46 with an average value of about 0.41% for the WF-70 portion of the weld. The most likely cause of the large variation derives from the variability of the coating processes used to apply the copper coating to the weld wire. This observation required revision of the preliminary irradiation plan which was predicated on a Linde 80 weld with typical copper variation. Thus, the current irradiation plan has been modified to incorporate the investigation of two weld metals, one obtained from the high-copper WF-70 of the nozzle weld and the other from the lower copper beltline weld.

Evaluation of the degradation of properties due to irradiation damage will begin following the completion of the initial study of chemistry and fracture property distributions. Both high and low copper-content weldmetals will be examined at three levels of irradiation,  $5 \times 10^{18}$ ,  $1 \times 10^{19}$ , and  $5 \times 10^{19}$  neutrons/cm<sup>2</sup> (>1 MeV). The lowest and highest fluences would be investigated only with CVN, tensile, and 0.5TC(T) specimens. The bulk of the irradiations would be conducted at  $1 \times 10^{19}$  and would include at least two large capsules with the specimen complement stated earlier. Sufficient specimens will be irradiated and tested to investigate

material variability. One area of emphasis will be a comparison of transition temperature shifts from surveillance capsule size specimens vs those from the larger specimens. The latter are more likely to agree with ASME Code curve behavior. R-curve trends for upper-shelf behavior will also be evaluated in terms of surveillance specimens vs the larger specimens that will yield more J values (as per ASTM E 1152) for JR curve development. Design of the large capsules is presently underway with irradiations scheduled to begin during 1991 at the Ford Nuclear Reactor at the University of Michigan.

### Analyses of Charpy and Tensile Data From Irradiation Series 2 and 3

The HSSI Second and Third Irradiation Series had the primary objective to investigate the effects of irradiation on the ductile fracture of seven commercially fabricated LUS submerged-arc welds. All the welds were fabricated with copper-coated wire and Linde 80 flux which produced welds with relatively low Charpy upper-shelf energy in the unirradiated condition and of relatively high sensitivity to neutron radiation. The development of experimental elastic-plastic fracture mechanics methods was pursued concurrently with the conduct of these irradiation series. The irradiation of compact specimens up to 4TC(T) and testing of those specimens to obtain J-integral resistance curves represented a major undertaking which was shared by a number of organizations.

Irradiation of the compact specimens at a nominal temperature of 288°C to an average fluence of about  $8 \times 10^{18}$  neutrons/cm<sup>2</sup> (>1 MeV) was relatively successful and their results have been published previously.<sup>9</sup> However, the Charpy impact and tensile specimens were located at positions in the capsule where temperature control was less and the irradiation temperatures spanned the range 235 to 345°C for those specimens. Additionally, the neutron fluences for the small specimens varied from about 4 to  $13 \times 10^{18}$  neutrons/cm<sup>2</sup> (>1 MeV). Although not desirable within the intended context of the experiments, those variations did provide the opportunity to investigate the effects of irradiation temperature and fluence (over the ranges observed) on the tensile and Charpy impact properties of these LUS welds. The data available for such analyses was limited from a statistical viewpoint, yet allowed for some reasonable observations which could be compared with results from other studies. For most of those comparisons, the Charpy and tensile results were normalized for fluence variations to the average fluence of  $8 \times 10^{18}$ . The results of the irradiations and their analyses have been recently published.<sup>11</sup> The important observations and conclusions which can be stated based on the results of those analyses are summarized here.

Analyses of irradiated tensile data showed a dependence on irradiation temperature of -1.15 MPa/°C for yield strength, -0.79 MPa/°C for ultimate strength, and -0.014%/°C for total elongation. Analyses of irradiated Charpy data showed a dependence on irradiation temperature of about -0.5°C/°C for transition temperature shift and -0.05 J/°C for upper-shelf energy drop.

The results indicated that the radiation-induced changes in yield strengths (in megapascals) and Charpy transition temperature shifts (in degrees Celsius) for the seven welds can be expressed as  $\Delta TT_{41} = 0.70 \cdot \Delta s_y$ . The Charpy results indicated a dependence on copper concentration which can be expressed as  $\Delta TT_{41} = 234 \cdot (\text{Cu} - 0.1)^{0.57}$ , where  $\Delta TT_{41}$  is degrees Celsius and copper (Cu) is weight percent.

Comparison of the Charpy results with data for the same materials irradiated in power reactor surveillance programs showed mixed results with the power reactor changes being greater in some cases and the test reactor changes greater in others.

## MICROSTRUCTURAL ANALYSIS AND MODELING

Over the past thirty years, a large amount of experimental data has been accumulated on the irradiation embrittlement of pressure vessel steels. Specimens irradiated in materials test reactors and surveillance locations of operating power reactors have been used to flesh out the irradiation property change response of these materials. However, in the broader context of research on radiation effects phenomena in materials, embrittlement historically has been treated in a qualitatively different manner. Other phenomena such as irradiation-induced swelling, creep, solute segregation, precipitation and helium-affected ductility loss have been subject to more mechanistically oriented work covering two areas. The first is extensive microstructural and microcompositional analysis using analytical electron microscopy (AEM) and other techniques. Irradiation response on the atomic and microstructural scales has been characterized with respect to both materials parameters and irradiation variables. The second is the development of fundamental understanding of the observed phenomena. The most detailed and quantitative expression of this understanding is in the formulation of physically-based theoretical models describing macroscopic property changes and their relation to the atomic and defect level structure.

The situation has changed recently concerning pressure vessel steels. Greatly increased capabilities are now available for atomic- and defect-scale characterization. It is now possible to reliably identify the irradiation-induced clusters responsible for hardening and to characterize them with respect to size, density, and elemental composition, for example. Modern capabilities can now be used to develop an understanding of embrittlement on a physical basis commensurate with the current knowledge in the other areas of radiation effects.

A physical theory based on defect reactions and microstructural evolution can now be formulated. It needs to be tethered soundly on the microstructural level by results from the microstructural characterization techniques, and constrained at the macroscopic level to produce predictions consistent with the large array of macroscopic embrittlement measurements. Models of this type formulated to describe swelling, irradiation creep, solute segregation and high temperature ductility loss have proven remarkably successful. A viable theoretical model will result in predictions of embrittlement for conditions where experimental data are unavailable (temperature, dose rate, dose) but where behavior must be known. It is expected to also provide guidance for the design of embrittlement-resistant alloys tailored for specific irradiation conditions. Results of the initial work within the HSSI program in this task are described below, focussing on two principal areas of effort. One is an analytical evaluation of embrittlement effects focusing on rate effects in general and the initial hardening transient in particular. The other is an experimental effort to obtain definitive information on spectrum and rate effects at low temperatures, similar to those at which vessel supports operate.

### Transient and Rate Effect on Embrittlement

The reaction rate theory description of radiation damage has been widely used to model phenomena such as void swelling and irradiation creep. That work has generally been concerned with irradiation conditions of relatively high doses (>1 dpa) and high temperatures ( $T > 300^{\circ}\text{C}$ ). In that regime, the vacancies and interstitials rapidly come into equilibrium with the microstructure and it is safe to assume that the point defect concentrations are at their steady state values. Point defect behavior in the steady state has been thoroughly explored.<sup>11-15</sup> Analytical solutions to the rate equations have been obtained for certain limiting cases that describe the dependence of the point defect concentrations on the total dose or the displacement rate.<sup>11-16</sup>

In contrast, the time required for the point defect concentrations to reach steady state at the lower temperatures typical of reactor pressure vessels and reactor support structures can be quite long, at the lowest temperatures even exceeding the in-service component lifetime.<sup>16</sup> Therefore, the use of the steady-state point defect concentrations in models for the behavior of materials in this regime can give irrelevant and misleading results. A simple model has been developed and used to conduct a detailed numerical analysis of the influence of the point defect transient. This initial work has focused on the influence of the displacement rate because of the importance of accelerated testing to research on pressure vessel embrittlement. The number or fraction of point defects that are lost to bulk recombination have been used as a measure of radiation sensitivity, since it is only defects that escape recombination that are available to contribute to radiation-induced embrittlement.

The number of point defects that have recombined up to some time,  $t$ , can be calculated as

$$NR = \int_0^t RC_i C_v dt, \quad (1)$$

where  $R$  is the bulk recombination coefficient and  $C_i$  and  $C_v$  are the interstitial and vacancy concentrations, respectively. Using the limiting values of  $C_i$  and  $C_v$  that are obtained during the linear portion of the point defect transient and at steady state for sink-dominated point defect absorption,<sup>12,16</sup> analytical expressions for the number and fraction of point defects lost to recombination were derived. These expressions are listed in Table 3, where the dose,  $\Delta$ , is the product of the modified displacement rate ( $G'_{dpa}$ ) and the time, and the  $D_{i,v}$  and  $S_{i,v}$  are the diffusivities and total sink strengths for interstitials and vacancies.

Table 3. Number ( $NR$ ) and fraction ( $fR$ ) of point defects lost to recombination for limiting cases

	$NR$	$fR$
Linear transient	$\frac{R}{3} \frac{\Delta^3}{G'_{dpa}}$	$\frac{R}{3} \frac{\Delta^2}{G'_{dpa}}$
Steady state, recombination dominant	$\frac{RG'_{dpa}}{D_i D_v S_i^T S_v^T} \Delta$	$\frac{RG'_{dpa}}{D_i D_v S_i^T S_v^T}$

The symbol  $G'_{dpa}$  represents the generation rate of defects that avoid in-cascade recombination, i.e., the actual displacement rate times the fraction that avoids in-cascade recombination. The expressions listed in Table 3 provide an estimate for how the recombination fraction changes with the displacement rate. Alternately, the change in the irradiation time required to give equivalent recombination fractions at different displacement rates can be

calculated. The recombination fraction exhibits a quadratic dependence on the dose during the transient (low doses) and is independent of the dose at steady state (high doses). At a given dose, the recombination fraction is inversely proportional to the displacement rate during the transient and linearly dependent on the displacement rate at steady state.

The number of vacancies lost to recombination at doses between the limits discussed above was obtained by explicitly integrating the rate equations describing the time dependence of the point defect concentrations and using Eq. (1). The results obtained at 275°C for a range of displacement rates that include test reactor and LWR surveillance specimen conditions are shown in Fig. 12. For the value of the dislocation sink strength used here,  $10^{11} \text{ cm}^{-2}$ , point defect loss is sink-dominated for most of the curves shown in Fig. 12. This can be seen in Fig. 13 where the fraction of the radiation-produced vacancies lost to recombination is plotted in the same way for these same conditions. For displacement rates less than  $\approx 10^{-8} \text{ dpa/s}$ , the bulk recombination fraction is less than 10%. The recombination fraction increases with displacement rate because the interstitial and vacancy concentrations increase. While the number of point defects lost to sinks increases linearly with  $C_i$  or  $C_v$ , the number recombining in the bulk increases quadratically. 12,16

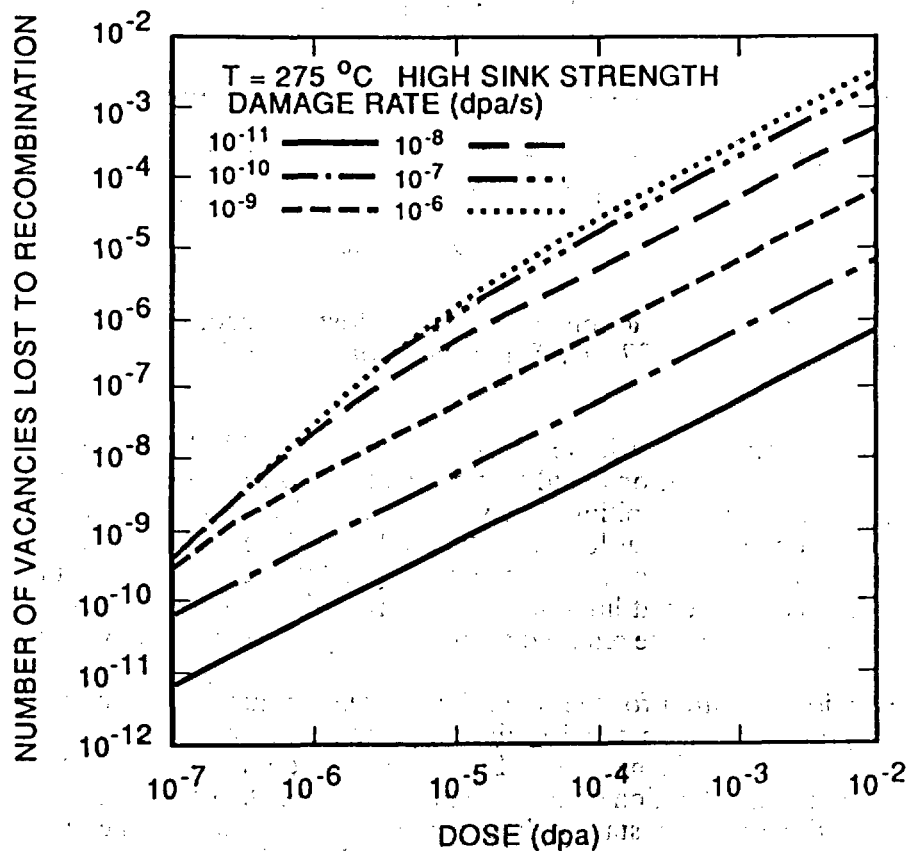


Fig. 12: Displacement rate dependence of the number of vacancies lost to recombination as a function of dose at 275°C. Dislocation sink strength is  $10^{11} \text{ cm}^{-2}$ .

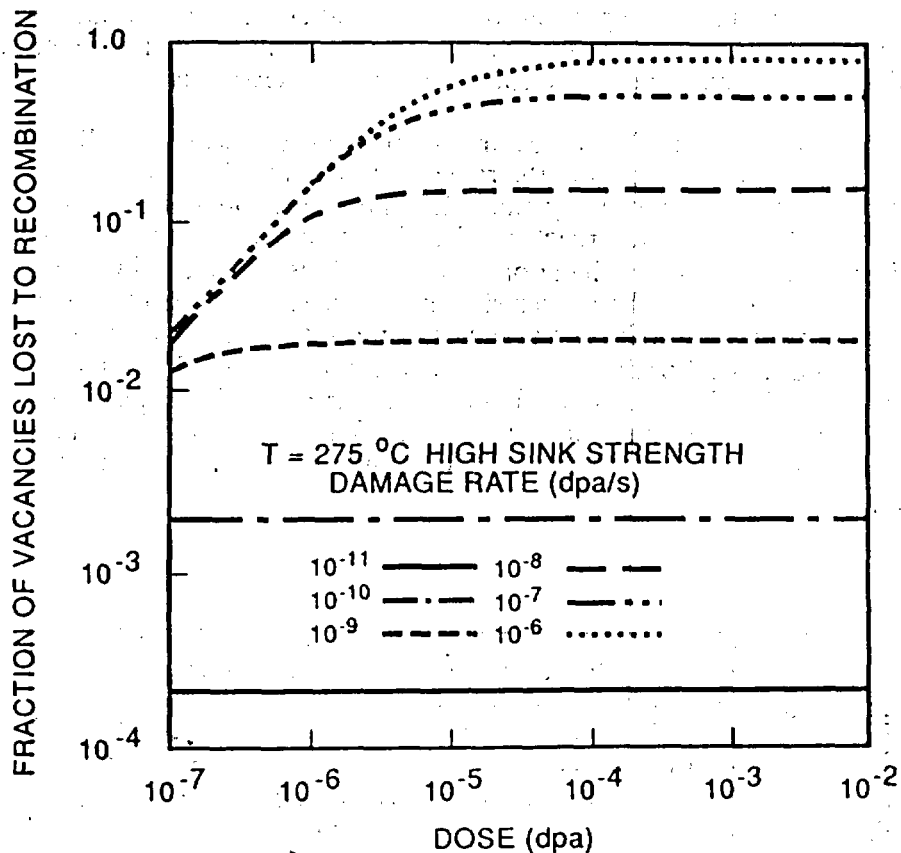


Fig. 13. Fraction of vacancies lost to recombination as a function of dose at 275°C. Same conditions as Fig. 12.

To illustrate the range of observed behavior, and to highlight the difference between transient and steady-state conditions, additional results at lower doses are shown in Fig. 14. Consistent with the calculated limiting behavior listed in Table 3, the number recombining exhibits a cubic dose dependence at low doses and a linear dependence at high doses. At low doses, the number recombining decreases as the displacement rate increases, but the dependence on displacement rate is reversed at high doses. The transition between "low-dose" and "high-dose" behavior occurs near the dose required for the vacancy concentration to reach steady state.

The time or dose required for the point defect concentrations to reach their steady state values is strongly dependent on the irradiation temperature and the sink structure. For temperatures below about 200°C, the extent of the point defect transient can be comparable to the component lifetime or to the duration of an irradiation experiment. Thus, theoretical analysis that relies on the assumption of steady state at these conditions is not valid. The results of the time-dependent analysis presented here show how the dose dependence of point defect absorption (measured as the complement of the recombination fraction) changes continuously between limiting values characteristic of the initial transient and the steady state. The displacement rate dependence of point defect absorption also varies between these limits and is a function of the sink structure.

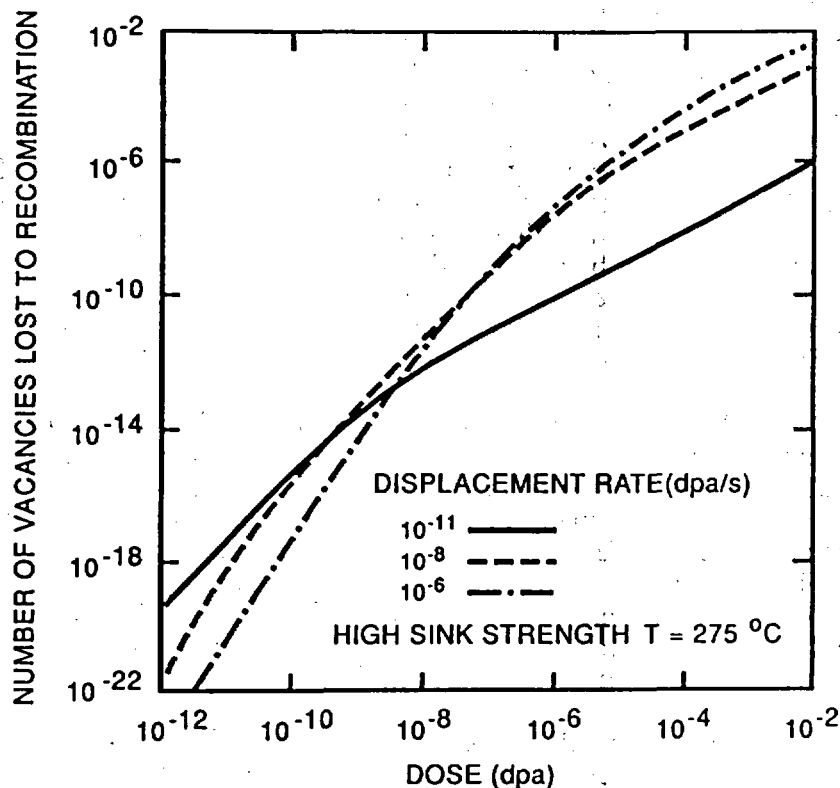


Fig. 14. Displacement rate dependence of the number of vacancies lost to recombination as a function of dose at 275°C for sink-dominant conditions. Similar to Fig. 12, but over a large dose range.

The use of test reactor irradiations to predict behavior at lower displacement rates must then consider these two confounding factors. First, the duty cycle of the test reactor can influence the analysis. For power reactor pressure vessels and other out-of-core components, where operating temperatures may be above 200°C, the point defect transient may be exceeded at a relatively small fraction of the component lifetime. But, in a test reactor at the same temperature, frequent start-ups and shut-downs may lead to the experiment being conducted entirely within the point defect transient. Secondly, since the effect of displacement rate is different in the transient and steady state regimes, data extrapolation from test reactor irradiations may cross mechanism boundaries and lead to poor estimates of material response at low displacement rates.

#### Neutron Spectrum and Flux Effects Experiments

The assessment of the premature embrittlement of the pressure vessel of the High Flux Isotope Reactor (HFIR) at ORNL<sup>17</sup> prompted an analysis of the effects of neutron spectrum on embrittlement of ferritic steels,<sup>18,19</sup> that indicated thermal neutrons as the likely cause of the early embrittlement. It was pointed out that embrittlement arises from self- and solute-clusters of irradiation-produced point defects. Only a small fraction of the total point defects produced by

atomic displacements are involved in the clusters. The bulk of the point defects are lost by recombination within the displacement cascades where they are created, so only the surviving point defects are relevant to embrittlement. Thermal neutrons make small cascades via (n,g) recoils, and the point defects made in such cascades have a much greater probability of survival than those born in the large dense cascades associated with fast neutrons. Therefore, thermal neutrons should create more surviving point defects per unit displaced atom than fast neutrons, perhaps a factor of ten more. Determining the magnitude of the weighting factor for the thermal neutrons is crucial. It means that for irradiations in a neutron spectrum where more than 10% of the atomic displacements are caused by thermal neutrons, the resulting damage to microstructure and mechanical properties should be dominated by thermal neutrons, not by fast neutrons as is traditionally supposed. If damage is assessed solely in terms of fast neutrons, which is the conventional way, the contribution from thermal neutrons will be considered negligible or minor, and embrittlement in a highly thermalized neutron spectrum will appear to be accelerated.

At the HFIR vessel, preliminary calculations indicate that the spectrum contains upwards of 96% thermal neutrons, which implies that more than 30% of the atomic displacements are created by thermal neutrons. But the neutron fluxes there are too low to permit confirmatory embrittlement experiments to be made in reasonable times. Therefore, to substantiate the hypothesis regarding spectrum effects experiments were initiated in the heavy-water High Flux Beam Reactor (HFBR) at Brookhaven National Laboratory. One scoping run was made before the reactor was shutdown in response to a safety question. When it became apparent that the HFBR would be down for a protracted period, it also became apparent another reactor with a high flux, highly-thermalized spectrum would be required.

The hydraulic facility of the NRU reactor at Chalk River, Canada was selected with Chalk River to provide neutron exposures and mechanical testing and ORNL to provide specimens, encapsulation and neutron dosimetry. Irradiation capsule designs have been approved and a thorough dosimetry survey of two sites in the hydraulic facility has been completed. The neutron conditions in the facility are ideal for the experiments. The neutron fluxes ( $>10^{12}$  fast neutrons/cm<sup>2</sup>-s and  $>10^{14}$  thermal neutrons/cm<sup>2</sup>-s) are high enough to induce embrittlement in exposure times of a few weeks, and the spectrum is more than 95% thermal neutrons.

The experiments have two goals. One is to obtain embrittlement data in a soft spectrum to compare with existing data for a harder spectrum. The other is to measure the contribution of thermal neutrons to embrittlement by using cadmium wrappers around the specimens to absorb the thermal neutrons. Specimens will be irradiated over a range of fluences, with and without cadmium wrappers, and the changes in tensile yield stress will be measured as an index of embrittlement. The test materials consist of four different ferritic steels. Two of these, A212B and A350, are HFIR pressure vessel archive materials for which there is reference tensile embrittlement data obtained after irradiations in the HFIR and the ORR. A third steel is A36, which is of interest for external reactor support structures. The fourth is A533B, pertinent to commercial light water reactor vessels. Irradiation of the specimens is scheduled for late in 1991.

To fully explore the possibilities which may influence irradiation effects on pressure vessel support materials, which experience a temperature and neutron exposure rate in some ways similar to that of the HFIR vessel,<sup>17</sup> experiments were begun to examine potential neutron flux effects under realistic exposure conditions for vessels supports. To compliment the experiments in the Chalk River reactor designed to explore the potential for a spectrum-induced acceleration during low temperature irradiation embrittlement, specimens are being exposed in the cavity surrounding the RPV in the Trojan pressurized water reactor. It is anticipated that these specimens will be exposed to a neutron fluence of roughly  $2 \times 10^{17}$  neutrons/cm<sup>2</sup> ( $E > 1\text{MeV}$ )

over a period of about two years. This will produce a fast neutron exposure of a level comparable to that seen in the HFIR vessel, at a flux of only one order of magnitude higher. In addition the spectrum, which is being extensively characterized for the HSST program, will be typical of at least one possible set of conditions which exist in a reactor cavity and could be experienced by vessel support materials. By comparing the results from this effort with the those from the HFIR surveillance program and those from the Chalk River reactor exposure, it should be possible to gain a substantially enhanced knowledge of the causes of the accelerated embrittlement observed in the HFIR vessel and its application to reactor pressure supports.

Specimens being irradiated in the Trojan Reactor cavity were machined from A212 grade B, A350 LF3, and A36 steels. The A212 grade B and A350 LF3 specimens were taken from HFIR archival materials to allow direct comparisons with existing data. The A36 specimens were included since it is a material which has been frequently used in pressure vessel supports. Five and six Charpy V-notch impact specimens from A36 and A212 grade B, respectively, in the L-T orientation were included. A holder, whose external dimensions are equal to that of a standard Charpy V-notch specimen, was designed, manufactured and assembled with 44 mini-tensile specimens. It contained an approximately equal number of mini-tensile specimens machined in the L orientation from each of the three materials mentioned above.

### IN-SERVICE AGED MATERIAL EVALUATIONS

The primary objective of this task is to evaluate nuclear reactor components as a consequence of aging. The task focuses on directly examining structural components to allow for the assessment of actual material condition caused by exposure to normal or off-normal conditions.

The initial efforts under this task have addressed the assessment of existing facilities at ORNL and the establishment of supplementary facilities needed for conducting investigations of components removed from service. The examination of irradiated materials requires, of course, not only the usual mechanical property testing equipment, but facilities for determining physical properties and for detailed metallurgical studies, such as optical metallography, scanning electron fractography, and transmission electron microscopy. Also, machining of irradiated materials requires a remote machining operation in a hot cell or hot shop.

The efforts to date have focused on a detailed assessment of the extensive existing capabilities at ORNL for such examinations as well as individual deficiencies and courses of proposed action. The two items have been identified as most urgently needed. A remotely operated electrodischarge machining facility is required for efficient sectioning of activated materials and their fabrication into test specimens. An automated hardness tester is needed for screening of embrittlement on received components. Plans have been made and funding tentatively secured to obtain and install these items over the next two years.

### CORRELATION MONITOR MATERIALS

Correlation monitor materials have been widely used to provide added confidence of the results of commercial power reactor surveillance capsule results. The recently approved revision the ASTM Standard Practice E 185 for Conducting Surveillance tests for Light-Water Cooled Nuclear Power Reactor Vessels now makes their use mandatory for the results to be considered credible. This increased need for and the recognition of decreasing supplies of suitable

correlation monitor materials were the bases for the establishment of a task with the specific goal of assuring an adequate supply of these materials for the foreseeable future.

Since two of the heavy-section plates procured in the early years of the HSST program, HSST plates 02 and 03, have been used for this purpose,<sup>20</sup> and moreover represent virtually all of the originally qualified correlation monitor material still available, the initial activity within this task is to prepare a detailed inventory of all remaining material from these plates and to establish an archival-quality storage facility in which to keep it. This effort was begun within the past year and is expected to be completed in 1993. In conjunction with archiving and maintaining custody of the material, the HSSI program has been authorized by the USNRC to release appropriately pedigreed correlation monitor material at no cost to qualified users who require it. In the past year, material has been supplied to General Electric for use in the BWR Owners Group Supplemental Surveillance Program and to Korean Heavy Industries for use in the surveillance program for Units 3 and 4 of the Yong Gwang pressurized water reactors.

## SUMMARY

The HSSI program is actively involved in providing information in several technical areas regarding the irradiation embrittlement behavior of RPVs which is vital to their continued safe operation. In the HSSI Fifth and Sixth Irradiation Series, designed to examine the shifts and possible changes in shape in the ASME  $K_{Ic}$  and  $K_{Ia}$  curves for two irradiated high-copper welds, it was seen that both the lower bound and mean fracture toughness shifts were greater than those of the associated Charpy-impact energies, whereas the shifts in crack arrest toughness were comparable. The irradiation-shifted fracture toughness data fell slightly below the appropriately indexed ASME  $K_{Ic}$  curve even when it was shifted according to Revision 2 of Regulatory Guide 1.99 including its margins.

The beltline weld which was removed from the Midland reactor, fabricated by B&W using Linde 80 flux, is being examined in the Tenth Irradiation Series to establish the effects of irradiation on a commercial LUS weld. A wide variation in the unirradiated fracture properties of the Midland weld were measured with values of  $RT_{NDT}$  ranging from  $-22$  to  $54^{\circ}F$  through its thickness. In addition, a wide range of copper content from 0.21 to 0.45 wt % was found, compared to the 0.42 wt % previously reported. The remainder of the unirradiated fracture testing and preparations for the irradiations of this material are under way.

Results from the Seventh Irradiation Series on stainless steel cladding have shown that the ductile fracture toughness initiation and tearing modulus of the cladding were significantly reduced by irradiation. The degree of reduction was such that post-irradiation ductile fracture resistance is as low or lower than comparably irradiated low upper-shelf weld metal.

Initial studies have shown that the time or dose required for the point defect concentrations, which ultimately contribute to irradiation embrittlement, to reach their steady state values can be comparable to the component lifetime or to the duration of an irradiation experiment. Thus, embrittlement models which rely on the assumption of steady state at these conditions are not valid. Consequently, simple direct comparisons of embrittlement generated under different rates of exposure (eg. test reactors vs power reactors) may be misleading because the relative state within the initial defect production transient will likely be different. Since the effect of displacement rate is different in the transient and steady state regimes, data extrapolation from test reactor irradiations may cross mechanism boundaries and lead to poor estimates of material response at low displacement rates.

A theoretical examination of the detailed irradiation mechanics which exist in low-temperature irradiations such as those which produced the accelerated embrittlement of the HFIR pressure vessel has led to the tentative conclusion that the cause of the acceleration is the high fraction of very low-energy thermal neutrons which existed rather than the low rate at which the fluence was accumulated. This conclusion is being investigated in two experiments. Specimens are being irradiated at low temperatures and high-fluence rates in spectra with and without large components of thermal neutrons. Other specimens are being exposed in the cavity of a pressurized water reactor at low temperatures and low fluence rates. As a result of the two experiments it should be possible to establish the mechanism primarily responsible for the accelerated low-temperature embrittlement.

Additional activities have been initiated which will provide for more detailed examination of the irradiation, annealing, and reirradiation response of LUS weldmetal, establish an improved facility for the examination of materials irradiated in service, and to assure a continuing source of supply for correlation monitor materials for use in light-water reactor surveillance programs.

### ACKNOWLEDGMENTS

The author would like to acknowledge the numerous members of the Heavy-Section Steel Irradiation Program who contributed to the technical content of this work including C. A. Baldwin, K. Farrell, F. M. Haggag, S. K. Iskander, F. B. K. Kam, L. K. Mansur, D. E. McCabe, M. K. Miller, R. K. Nanstad, R. E. Stoller, K. R. Thoms, and J. A. Wang. In addition the author would like to thank A. Taboada, technical monitor of the program, and the rest of the U.S. Nuclear Regulatory Commission for the financial and technical support of this research effort.

### REFERENCES

1. R. K. Nanstad et al, "Effects of Radiation on  $K_{Ic}$  Curves for High Copper Welds," pp. 214-233 in *Effects of Radiation on Materials: 14th International Symposium (Volume II)*, ASTM STP 1046, N. H. Packan, R. E. Stoller, and A. S. Kumar, Eds., American Society of Testing and Materials, Philadelphia, Pa., 1990.
2. W. R. Corwin, Martin Marietta Energy Systems, Inc., Oak Ridge Natl. Lab., Oak Ridge, Tenn., *Heavy-Section Steel Irradiation Program Semiannual Progress Report for October 1989-March 1990*, USNRC Report NUREG/CR-5591, Vol.1, No.1 (ORNL/TM-11568/V1&N1), August 1990.
3. *ASME Boiler and Pressure Vessel Code, An American National Standard*, Sect. XI, Appendix A, American Society of Mechanical Engineers, New York, 1986.
4. K. Wallin, "The Scatter in  $K_{Ic}$ -Results," *Engineering Fracture Mechanics*, 19(6), 1085-93 (1984).
5. S. K. Iskander, W. R. Corwin, and R. K. Nanstad, Martin Marietta Energy Systems, Inc., Oak Ridge Natl. Lab., Oak Ridge, Tenn., *Results of Crack-Arrest Tests on Two Irradiated High-Copper Welds*, USNRC Report NUREG/CR-5584 (ORNL/TM-11575), December 1990.

6. W. R. Corwin, R. G. Berggren, and R. K. Nanstad, Martin Marietta Energy Systems, Inc., Oak Ridge Natl. Lab., Oak Ridge, Tenn., *Charpy Toughness and Tensile Properties of a Neutron Irradiated Stainless Steel Submerged-Arc Weld Cladding Overlay*, USNRC Report NUREG/CR-3927 (ORNL/TM-9709), September 1984.
7. F. M. Haggag, W. R. Corwin, D. J. Alexander, and R. K. Nanstad, "Tensile and Charpy Impact Behavior of an Irradiated Three-Wire Series-Arc Stainless Steel Cladding," pp. 361-372 in *Effects of Radiation on Materials: 14th International Symposium (Volume II)*, ASTM STP 1046, N. H. Packan, R. E. Stoller, and A. S. Kumar, Eds., American Society of Testing and Materials, Philadelphia, Pa., 1990.
8. F. M. Haggag, W. R. Corwin, and R. K. Nanstad, Martin Marietta Energy Systems, Inc., Oak Ridge Natl. Lab., Oak Ridge, Tenn., *Irradiation Effects on Strength and Toughness of Three-Wire Series-Arc Stainless-Steel Weld Overlay Cladding*, USNRC Report NUREG/CR-5511 (ORNL/TM-11439), February 1990.
9. A. L. Hiser, F. J. Loss, and B. H. Menke, Material Engineering Assoc., Lantham, Md., *J-R Curve Characterization of Irradiated Low Upper Shelf Welds*, USNRC Report NUREG/CR-3506, MEA-2028, April 1984.
10. J. J. McGowan, R. K. Nanstad, and K. R. Thoms, Martin Marietta Energy Systems, Inc., Oak Ridge Natl. Lab., Oak Ridge, Tenn., *Characterization of Irradiated Current-Practice Welds and A533 Grade B Class 1 Plate for Nuclear Pressure Vessel Service*, USNRC Report NUREG/CR-4880 Vols. 1 and 2 (ORNL/TM-6484/V1 and V2), July 1988.
11. R. K. Nanstad and R. G. Berggren, Martin Marietta Energy Systems, Inc., Oak Ridge Natl. Lab., Oak Ridge, Tenn., *Irradiation Effects on Charpy Impact and Tensile Properties of Low Upper-Shelf Welds, Heavy-Section Steel Irradiation Program, Irradiation Series 2 and 3*, USNRC Report NUREG/CR-5696 (ORNL/TM-11804), June 1991.
12. L. K. Mansur, American Nuclear Society Critical Reviews, *Nucl. Technol.* **40**, 5-34 (1978).
13. R. E. Stoller and G. R. Odette, "A Composite Model of Microstructural Evolution in Austenitic Stainless Steel Under Fast Neutron Irradiation," pp. 371-392 in *Radiation-Induced Changes in Microstructure: 13th International Symposium*, ASTM STP 955, F. A. Garner, N. H. Packan and A. S. Kumar, Eds., American Society of Testing and Materials, Philadelphia, Pa., 1987.
14. L. K. Mansur, "Irradiation Creep by Climb-Enabled Glide of Dislocations Resulting From Preferred Absorption of Point Defects" in *Phil. Mag. A* **39**, 497-506 (1979).
15. A. D. Brailsford and R. Bullough, AERE Harwell, UK, *The Theory of Sink Strengths*, AERE Harwell Report TP 854, 1980.
16. R. E. Stoller and L. K. Mansur, "The Influence of Displacement Rate on Damage Accumulation during the Point Defect Transient in Irradiated Materials," pp. 52-67 in *Proceedings of PM-90: International Conference on Radiation Materials Science, Vol. 1*, May 22-25, 1990, Alushta, The Crimea, USSR.

17. R. K. Nanstad, K. Farrell, D. N. Braski and W. R. Corwin, "Accelerated Neutron Embrittlement of Ferritic Steels at Very Low Damage Rate," *J. Nucl. Mater.* **158**, 1-6 (1988).
18. L. K. Mansur and K. Farrell, "On Mechanisms by Which a Soft Neutron Spectrum May Induce Accelerated Embrittlement," *J. Nucl. Mater.* **170**, 236—245 (1990).
19. L. K. Mansur and K. Farrell, "New Insights on Reactor Vessel Embrittlement," *Oak Ridge National Laboratory Review*, **22—4**, 30—35 (1989).
20. F. W. Stallman, Martin Marietta Energy Systems, Inc., Oak Ridge Natl. Lab., Oak Ridge, Tenn., *Analysis of A302B and A533B Standard Reference Materials in Surveillance Capsules of Commercial Power Reactors*, USNRC Report NUREG/CR-4947 (ORNL/TM-10459), January 1988.

## FATIGUE AND ENVIRONMENTALLY ASSISTED CRACKING IN LIGHT WATER REACTORS\*

T. F. Kassner, W. E. Ruther, H. M. Chung, P. D. Hicks, A. G. Hins, J. Y. Park, and W. J. Shack

Materials and Components Technology Division  
Argonne National Laboratory  
Argonne, Illinois 60439 USA

### Abstract

Fatigue and environmentally assisted cracking of piping, pressure vessels, and core components in light water reactors are important concerns as extended reactor lifetimes are envisaged. Topics that have been investigated during this year include (1) fatigue and stress corrosion cracking (SCC) of low-alloy steel used in piping and in steam generator and reactor pressure vessels, (2) role of chromate and sulfate in simulated boiling water reactor (BWR) water on SCC of sensitized Type 304 SS, and (3) radiation-induced segregation (RIS) and irradiation-assisted SCC of Type 304 SS after accumulation of relatively high fluence. Fatigue data obtained on medium-sulfur-content A533-Gr B and A106-Gr B pressure-vessel and piping steels in high-purity (HP) deoxygenated water, in simulated pressurized water reactor (PWR) water, and in air all lie above the ASME design curve. Crack-growth-rate (CGR) measurements on composite specimens of A533-Gr B/Inconel-182/Inconel-600 (plated with nickel) and on homogeneous specimens of A533-Gr B material (plated with gold or nickel) indicate that CGRs increased markedly during small-amplitude cyclic loading ( $R = 0.95$ ) in HP water with  $\approx 300$  ppb dissolved oxygen. Under cyclic loading, crack growth was observed at  $K_{max}$  values that produced no crack growth under constant ( $R = 1$ ) loading. The CGR dependence on dissolved-oxygen concentration (0.3 to 30 ppm) was also investigated under different loading conditions. Possible synergistic reactions involving chromate and sulfate in SCC of sensitized Type 304 SS have been investigated by fracture-mechanics CGR tests. Low chromate concentrations in BWR water (25-35 ppb) may actually have a beneficial effect on SCC if the sulfate concentration is below a critical level. Failures of reactor-core internal components in BWRs and PWRs after accumulation of relatively high fluence have been attributed to RIS of Si, P, S, Ni, and Cr; however, the degree to which RIS produces susceptibility to irradiation-assisted SCC is unclear. Microchemical and microstructural changes in HP and commercial-purity (CP) Type 304 SS specimens from control-blade absorber tubes used in two operating BWRs were studied by Auger electron spectroscopy and scanning electron microscopy, and slow-strain-rate-tensile tests were conducted on tubular specimens in air and in simulated BWR water at 289°C. Intergranular stress corrosion cracking (IGSCC) susceptibility of the CP absorber tubes was similar to that of other CP heats of Types 304 and 316 SS reported in the literature. However, the HP absorber tubes exhibited greater IGSCC susceptibility than did the CP materials. High SCC susceptibility seems to be consistent with irradiation-induced Cr depletion at grain boundaries, which was more significant in the HP heat than in the CP heat.

\*Work supported by the Office of Nuclear Regulatory Research, U.S. Nuclear Regulatory Commission, FIN Nos. A22122 and A22562; Program Managers: Drs. J. Muscara and E. Woolridge.

The submitted manuscript has been authored by a contractor of the U.S. Government under contract No. W-31-109-ENG-38. Accordingly, the U.S. Government retains a nonexclusive, royalty-free license to publish or reproduce the published form of this contribution, or allow others to do so, for U.S. Government purposes.

## 1 Introduction

---

Fatigue and environmentally assisted cracking of piping, pressure vessels, and core components in light water reactors (LWRs) are important concerns as extended reactor lifetimes are envisaged. The degradation processes include intergranular stress corrosion cracking (IGSCC) of austenitic stainless steel (SS) piping in boiling water reactors (BWRs), and propagation of fatigue or SCC cracks (which initiate in sensitized SS cladding) into low-alloy ferritic steels in BWR pressure vessels. Similar cracking has also occurred in upper shell-to-transition cone girth welds in pressurized water reactor (PWR) steam generator vessels. Another concern is failure of reactor-core internal components after accumulation of relatively high fluence, which has occurred in both BWRs and PWRs. Research during the past year focused on (1) fatigue and SCC of ferritic steels used in piping and in steam generator and reactor pressure vessels, (2) role of chromate and sulfate in simulated BWR water in SCC of sensitized Type 304 SS, and (3) irradiation-assisted SCC in high- and commercial-purity Type 304 SS specimens from control-blade absorber tubes used in two operating BWRs. Failure after accumulation of relatively high fluence has been attributed to radiation-induced segregation (RIS) of elements such as Si, P, S, Ni, and Cr.

## 2 Summary of Research Progress

---

### 2.1 Fatigue of Ferritic Steels

Plain carbon and low-alloy steels are used extensively in PWR and BWR nuclear steam supply systems as piping and pressure-vessel materials. The steels of interest for these applications include A106-Gr B and A333-Gr 6 for seamless pipe and A302-Gr B, A508-2, and A533-Gr B plate for pressure vessels. The current Section III fatigue curves for carbon and low-alloy steels are based on tests in air at room temperature.<sup>1</sup> Tests in air at reactor operating temperatures show some deviation from the ASME mean data curve, but all data lie above the ASME design curve.<sup>2</sup> However, in tests at high strain amplitudes in oxygenated water, the fatigue life of carbon steels is significantly decreased, and in some cases failures were observed below the ASME Section Design Curve.<sup>3,4</sup> Iida et al.<sup>5</sup> studied the fatigue of alloys equivalent to A508-C13 and A333-C16 in deionized water at temperatures up to 290°C. They showed that in oxygenated water at large strain amplitudes, fatigue lives were reduced in tests at lower strain rates. The magnitude of the decrease depended strongly on alloy composition, temperature, and concentration of dissolved oxygen in the water. At dissolved-oxygen concentrations of <100 ppb, the aqueous environment had little effect on the fatigue life of either alloy.

Nagata et al.<sup>6</sup> performed fatigue tests on forged ASTM A508 C1-3 and on the rolled-equivalent ASTM A533-Gr B C1-1 under strain control (at various strain rates) in pure water at several dissolved-oxygen levels. Compared to tests in air, water containing 100 ppb dissolved oxygen had very little effect on the fatigue behavior of both alloys at a strain rate of  $1 \times 10^{-3} \text{ s}^{-1}$ . Alloy A508 also showed little effect of strain rate, whereas a decrease in strain rate by up to two orders of magnitude decreased the fatigue life of A533-Gr B steel. Nagata

et al.<sup>6</sup> attributed this to initiation effects due to the higher sulfide content of the A533-Gr B steel compared to the A508 material. They argue that A533-Gr B is more susceptible to surface pitting near manganese sulfide (MnS) inclusions, and the surface pitting near these inclusions decreases the initiation time for cracking. The lower strain rates simply provide more time for the pitting to occur. All tests were at a strain range of 0.7–0.8% and a strain rate of 0.1% with a triangular wave form. For dissolved-oxygen levels >1 ppm, the fatigue lives of both alloys decreased by up to 66%. However, it should be noted that Iida et al.<sup>5</sup> saw very little environmental effect in the high-cycle regime where initiation would be expected to dominate even in high-sulfur materials.

Terrell<sup>7</sup> tested A106-Gr B in PWR environments. For cyclic frequency in the range of 1.0–0.017 Hz, the fatigue life of smooth test specimens was virtually unaffected by the environment, whereas a small decrease in life occurred for notched specimens in tests at the lowest frequency. However, all data lie above the ASME design curve.

### 2.1.1 Experimental Methods

Uniaxial fatigue properties of A533-Gr B pressure vessel and A106-Gr B piping steels in water and in air were investigated. The A533-Gr B material for the test specimens was obtained from the lower head of the Midland Reactor, which was scrapped before the plant was completed. The medium-sulfur-content (0.016% S) steel had a tempered bainitic microstructure in the as-fabricated condition. Chemical analyses of these two materials and of the ferritic and austenitic steels used in CGR tests are given in Table 1.

Fatigue tests were performed on smooth (1.0- $\mu$ m surface-polished gage length, 19 mm) cylindrical hourglass-type specimens. During polishing of the specimen gage length, pullout of MnS inclusions occasionally occurred, tending to scuff the surface of the specimen. These inclusions were visible under a low-power microscope and appeared as slight surface roughness. The final polish of the specimen gage length was in a lengthwise direction to prevent circumferential scratches that might act as stress raisers during fatigue. The specimens were loaded uniaxially with a triangular wave form at a strain rate of  $4 \times 10^{-3} \text{ s}^{-1}$ .

Tests were first performed in air at 288°C, under strain control at zero mean strain measured with an axial extensometer. Strain ranges of 1.0, 0.75, 0.50, and 0.35% were selected. The stroke response was recorded so that subsequent fatigue tests in water could be run in stroke control. This experimental procedure avoids difficulties associated with using a strain extensometer in a pressurized-water environment. After obtaining the strain control data in air, a repeat test was performed under stroke control in air at 288°C. The mean stroke and stroke amplitude settings for these tests were the same as the stroke values obtained at the half-lives of the strain control tests. During the stroke-control tests, the strain was accurately monitored to give a better indication of the true strain experienced by the specimens when they are tested in water under stroke control. The strain amplitude in amplitude-versus-fatigue-life plots corresponds to that at the specimen half-life, as determined in high-temperature tests in air under stroke control.

Table 1. Chemical Composition (wt.%) of Ferritic and Austenitic Steels in Fatigue<sup>a,b</sup> and Compact-Tension Specimens<sup>c,d</sup>

Material	C	P	S	Si	Fe	Cr	Ni	Mn	Mo	Ta/Nb	Ti
A533-Gr B <sup>a</sup>	0.20	0.014	0.016	0.17	Bal	0.19	0.50	1.28	0.47	-	-
A106-Gr B <sup>b</sup>	0.29	0.014	0.014	0.28	Bal	0.19	0.11	0.92	0.04	-	-
A533-Gr B <sup>c</sup>	0.22	0.011	0.019	0.22	Bal	0.12	0.69	1.45	0.53	-	-
IN-182 <sup>f</sup>	0.10	0.03	0.01	1.0	10.0	14.0	65.0	7.0	-	1.75	1.0
IN-600	0.07	-	0.001	0.19	9.41	15.23	73.84	0.30	-	0.12	0.31
Type 304 SS <sup>d</sup>	0.06	0.019	0.007	0.48	Bal	18.70	8.00	1.63	0.20	-	-

<sup>a</sup>Medium-S-content steel for fatigue specimens was obtained from the lower head of the Midland Reactor.

<sup>b</sup>Heat No. J-7201 (20-in.-diameter schedule 140 pipe) fabricated by the Cameron Iron Works, Houston, TX.

<sup>c</sup>Composite Alloy-600/In-182/A533-Gr B compact-tension (1T) specimen was fabricated such that the low-alloy steel was in the T-L orientation according to the ASTM nomenclature. Other 1TCT specimens of low-alloy steel were also in the T-L orientation.

<sup>d</sup>Heat No. 30956 for crack-growth-rate tests on 1T specimens in simulated BWR water.

<sup>e</sup>A533-Gr B Class 1 plate (Heat No. A-1195-1) was obtained from the Oak Ridge National Laboratory HSST Program.

<sup>f</sup>Nominal composition of undiluted Inconel-182 weld metal (AWS Type ENiCrFe-3 per AWS Specification A5.11). A layer, ~6 mm thick, was buttered to the A533-Gr B plate with a 3/32-in.-diameter weld rod and the material was heat treated at 621°C for 24 h and air-cooled. Inconel-600 (Heat No. NX5922-G11) was electron-beam-welded to the Inconel-182 to form the 1TCT specimen. Entire specimen was nickel-plated.

Tests were conducted in high-purity (HP) deoxygenated water and in simulated PWR water at a flow rate of 8 mL·min<sup>-1</sup> in a small autoclave (annular volume of 12 mL) at 288°C and a system pressure of 9 MPa. The nominal water chemistries are given in Table 2. Simulated PWR water was formulated by dissolving HP boric acid and lithium hydroxide in 20 L of deionized water before adding the solution to 132-L SS feedwater tanks. For tests in deionized water, the dissolved-oxygen concentration was reduced to <10 ppb by bubbling nitrogen through the water. A vacuum was drawn on the tank gas outlet to speed deoxygenation. After the dissolved oxygen was reduced to the desired level, a 20-kPa overpressure of nitrogen was maintained on the feedwater tank. Preparation of the simulated PWR water was similar, except that a 20-kPa overpressure of hydrogen was sustained to maintain ~2 ppm dissolved hydrogen in the deoxygenated feedwater. Water from the once-through system was discarded in the drain.

### 2.1.2. Results

The fatigue test results are summarized in Tables 3 and 4 and Fig. 1. The number of cycles to failure (fatigue life  $N_{25}$  in Fig. 1) is determined when the tensile stress amplitude decreases to 75% of the value observed at one-half the fatigue life. The life is plotted in terms of the pseudostress  $S_a = E(\Delta\epsilon_t/2)$ , where  $\Delta\epsilon_t$  is the strain range, and  $E$  is Young's modulus (namely, 200 GPa for A533-Gr B steel). The data can be compared with curves in

**Table 2. Nominal Water Chemistries for Fatigue Tests**

Water Chemistry	Deionized Water	PWR Water
Conductivity ( $\mu\text{S}\cdot\text{cm}^{-1}$ )	0.17	25
pH (room temperature)	5.8	6.6
Dissolved O <sub>2</sub> (ppb)	<10	<10
Boron (ppm)	-	1000
Lithium (ppm)	-	2
Chloride (ppm)	<0.03	<0.03
Fluoride (ppm)	<0.01	<0.01
Dissolved H <sub>2</sub> (cm <sup>3</sup> /kg)	-	18

the ASME Boiler and Pressure Vessel Code (Section III) "Design Fatigue Curves for Carbon, Low Alloy and High Tensile Steels for Metal Temperatures not Exceeding 700°F."<sup>1</sup> The ASME Section III mean-data curve is also included in the figure.

Our fatigue data for A106-Gr B steel are consistent with data obtained by Terrell<sup>7</sup> in simulated PWR water (<10 ppb dissolved oxygen) where no noticeable effect of frequency or environment on fatigue life of this alloy was found (Fig. 1). The results are also consistent with the data of Prater and Coffin<sup>8,9</sup> and Iida et al.,<sup>5</sup> in which the effects of environment were minimal at dissolved oxygen levels of <100-200 ppb. All data at higher stress amplitudes tend to fall further below the the ASME mean-data curve than do data at longer lives.

## 2.2 Stress Corrosion Cracking of Ferritic Steels

Over the past 15 years, the corrosion fatigue properties of low-alloy steels in LWR primary-system water chemistries have been studied extensively.<sup>10-13</sup> Much less information is available on SCC of these materials.<sup>14-18</sup> Because it is clear that very high crack-growth rates (CGRs) can occur in some materials under some combinations of loading and environment, the objective of the current work is to better define the circumstances that can produce SCC in these steels.

### 2.2.1 Experimental Methods

Fracture-mechanics CGR tests have been carried out on a heat of medium-sulfur-content (0.019 wt.%) A533-Gr B pressure vessel steel (chemical composition is given in Table 1). In addition to conventional I-T compact-tension specimens, specimens plated with either nickel or gold, together with a composite specimen of A533-Gr B/Inconel-182/Inconel-600 plated with nickel, were tested. The nickel-plated specimens were used to better simulate a clad ferritic steel vessel, where only the low-alloy steel at the crack surface is exposed to the environment. Surface films on the nickel- and gold-plated

**Table 3. Test Conditions and Fatigue Lives for A533-Gr B Steel**

Test No.	Total Strain Range, $\Delta\epsilon_t$ (Test Control)	Environment (at 288°C)	Cycles = N <sub>25</sub>
1505	0.50% (strain)	Air	31,200
1508	1.00% (strain)	Air	3,305
1515	0.75% (strain)	Air	6,792
1517	0.35% (strain)	Air	2,053,295
1522	-0.89% (stroke)	Air	3,419
1523	-0.90% (stroke)	Air	2,200
1524	-0.94% (stroke)	Air	3,714
1525	-0.45% (stroke)	Air	65,758
1526	-0.90% (stroke)	Delontized water	3,330
1527	-0.45% (stroke)	Delontized water	10,334
1528	-0.45% (stroke)	Delontized water	25,890
1529	-0.45% (stroke)	PWR water	31,751
1530	-0.90% (stroke)	PWR water	1,355
1533 <sup>a</sup>	-0.90% (stroke)	PWR water	3,416
1538	-0.39% (stroke)	Air	>1,000,000
1539	-0.39% (stroke)	PWR water	136,969
1542	-0.39% (stroke)	PWR water	>1,154,892
1545	-0.91% (stroke)	PWR water	3,264

<sup>a</sup>Positive sawtooth test: tensile-going strain rate of  $4 \times 10^{-5} \text{ s}^{-1}$  (slower by 100X than the other tests) and a compression-going rate of  $4 \times 10^{-3} \text{ s}^{-1}$ .

**Table 4. Test Conditions<sup>a</sup> and Fatigue Lives for A106-Gr B Steel**

Test No.	Total Strain Range, $\Delta\epsilon_t$ (Test Control)	Environment (at 288°C)	Cycles = N <sub>25</sub>
1498	1.00% (strain)	Air	1,051
1543	0.50% (strain)	Air	14,525
1546	-1.03% (stroke)	Air	1,365
1547	-1.03% (stroke)	PWR water	692
1548	0.50 % (stroke)	Air	10,632
1549	0.50% (stroke)	PWR water	9,396
1552	0.35 % (strain)	Air	93,322
1553	0.75% (strain)	Air	3,253

<sup>a</sup>Positive sawtooth tests with a tensile-going strain rate of  $4 \times 10^{-3} \text{ s}^{-1}$ .

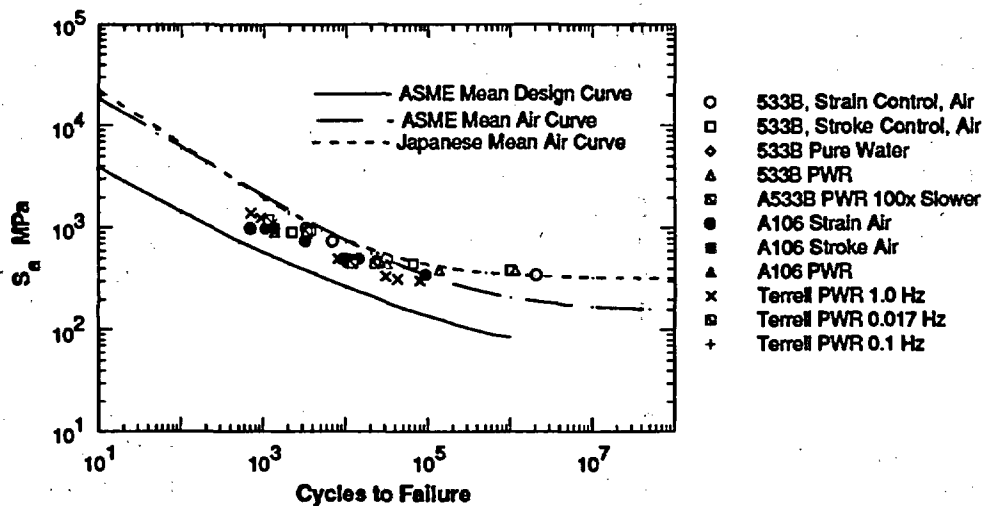


Figure 1. Elastic pseudostress versus fatigue-life data for A533-Gr B Cl 1 and A106-Gr B steels at 288°C

specimens are different from those on the nonplated ferritic specimens. Because virtually all of the existing data have been obtained on specimens without cladding, it is important to verify that those results were not unduly affected by the character of the surface film.

The composite specimen was tested in simulated BWR water with ~200 ppb dissolved oxygen at 289°C under cyclic loading with a positive sawtooth wave form (12-s loading and 1-s unloading time) at 0.08 Hz, load ratios ( $R = K_{\min}/K_{\max}$ ) of 0.9 to 1.0, and maximum stress intensities,  $K_{\max}$ , of ~28 to 62  $\text{MPa}\cdot\text{m}^{1/2}$ . Crack-length measurements in conventional and plated specimens were made by a DC-potential-drop technique. Because no potential-drop calibration was available for the composite specimen, crack length was measured by the compliance method.

## 2.2.2 Results

Results from SCC tests on the composite specimen are given in Table 5. The fatigue precrack in the specimen traversed the Inconel-182 weld metal so that the initial 7.2 mm of crack growth over a time interval of 1000 h (Test 1) occurred in the underlying A533-Gr B material at an average rate of  $2.0 \times 10^{-9} \text{ m}\cdot\text{s}^{-1}$ . The  $K_{\max}$  increased from 28 to 35  $\text{MPa}\cdot\text{m}^{1/2}$ . No periods of crack arrest or transient crack growth occurred during this phase of the test. This CGR is virtually identical to the "average" value for a previous composite specimen ( $2.3 \times 10^{-9} \text{ m}\cdot\text{s}^{-1}$ ), which included several crack extensions of 1-2 mm within ~170-h time intervals followed by ~800-h periods of very slow steady-state growth.<sup>19</sup> For no apparent reason, the CGR of the composite specimen in the current test decreased abruptly at ~1050 h to a very low value that continued over an ~1000-h time period. This behavior is similar to that observed in the previous experiment.<sup>19</sup>

In Test 2, the  $K_{\max}$  of the composite specimen was increased to  $40 \text{ MPa}\cdot\text{m}^{1/2}$  at an R of 0.95. Whereas an increase of  $K_{\max}$  in the previous experiment,<sup>19</sup> in general, resulted in a brief increase in the CGR, no such increase was noted during the next 300-h period in this test. After that period, the dissolved-oxygen concentration in the feedwater was increased to  $\approx 30$  ppm (Test 3). This action initiated a return to the high-CGR regime, which we allowed to persist for two weeks. The feedwater was then returned to the normal dissolved-oxygen concentration of  $\approx 0.4$  ppm in Test 4, and shortly thereafter the CGR returned to a low level ( $7.6 \times 10^{-11} \text{ m}\cdot\text{s}^{-1}$ ) for 800 h. The dissolved-oxygen level was then increased to 6 ppm in Test 5, and two days later rapid crack growth resumed. These experiments indicate that dissolved-oxygen concentration is an important variable at a load ratio of 0.95.

In the next series of tests, the effect of load ratio was investigated. In Test 6, the load ratio was increased from 0.95 to 1.0 (i.e., constant load); shortly thereafter, the CGR returned to the low level even though the dissolved-oxygen level remained at 6 ppm. The low CGR persisted for an additional 1200 h, after which the dissolved-oxygen level was increased to  $\approx 30$  ppm in Test 7. This caused a modest increase in the CGR over an additional exposure period of 800 h. The load ratio was then decreased to 0.98 in Test 8 and the CGR decreased slightly during an additional 310-h period. The load ratio was decreased further to 0.95 in Test 9 and the CGR remained at the same low value ( $3.8 \times 10^{-11} \text{ m}\cdot\text{s}^{-1}$ ) over a 200-h interval. In Test 10, the load ratio was decreased to 0.9, and within 24 h, crack growth resumed a high rate ( $7.8 \times 10^{-9} \text{ m}\cdot\text{s}^{-1}$ ). The test was terminated after  $\approx 20$  h because the crack length exceeded the maximum allowable value. Even at a high K level ( $62 \text{ MPa}\cdot\text{m}^{1/2}$ ), a load ratio of  $<1$  is required to initiate a high CGR. No crack growth occurred in a conventional (nonplated) A533-Gr B specimen at a stress intensity factor of  $28.7 \text{ MPa}\cdot\text{m}^{1/2}$  over the entire  $\approx 6600$ -h experiment under the different environmental and loading conditions.

The CGR results in Table 5 at different dissolved-oxygen levels and load ratios fall into two ranges, i.e.,  $\approx 2$  to  $8 \times 10^{-11}$  and  $\approx 2$  to  $8 \times 10^{-9} \text{ m}\cdot\text{s}^{-1}$ . High CGRs occurred at an R of 0.95 in water containing 0.3, 6, and 30 ppm dissolved oxygen (Tests 1, 5, and 3, respectively). Low CGRs were also measured at this R value in water containing  $\approx 0.3$ –0.4 and 28 ppm dissolved oxygen (Tests 2, 4, and 9). As mentioned previously, under constant load (R = 1.0), an increase in dissolved-oxygen concentration from 6 to 30 ppm produced a relatively small increase in the CGRs (Tests 6 and 7). A significant decrease in load ratio from 1.0 to 0.9 (sequentially in Tests 7–10) caused an abrupt transition to the high-CGR regime at an R of 0.9 in water containing  $\approx 30$  ppm dissolved oxygen.

These results, along with those from a previous composite specimen in which unusually large jumps in crack length ( $\approx 1$ –2 mm) occurred whenever  $K_{\max}$  was increased (followed by periods of relatively slow crack growth),<sup>19</sup> indicate that triggering events in the environment and/or in the loading conditions can produce abrupt changes in the CGRs by two orders of magnitude. For example, increases in dissolved-oxygen concentration and  $K_{\max}$  and decreases in load ratio can lead to high CGRs. Conversely, a transition from the high- to low-CGR regime can occur by decreasing the dissolved-oxygen concentration or by

**Table 5. Crack Growth of Inconel-182/A533-Gr B Composite Specimen<sup>a</sup> at Constant Load and Low-Frequency, High-R Loading<sup>b</sup> in High-Purity Water Containing ~0.3 to 30 ppm Dissolved Oxygen at 289°C**

Test No.	Time, h	Water Chemistry			Electrode Potential		Load Ratio	CGR Parameters		
		Cond., $\mu\text{S cm}^{-1}$	pH at 25°C	Oxygen, <sup>c</sup> ppm	304 SS, mV(SHE)	Pt, mV(SHE)		$K_{\text{max}}$ , <sup>d</sup> MPa·m <sup>1/2</sup>	$\Delta K$ , <sup>e</sup> MPa·m <sup>1/2</sup>	Growth Rate, m· $\sigma^{-1}$
1	0-1058	0.16	6.25	0.3	112	126	0.95	35.0	1.75	$2.0 \times 10^{-9}$
	1058-2156							37.0	1.85	$3.0 \times 10^{-11}$
2	2156-2492	0.13	6.20	0.3	49	82	0.95	40.0	2.00	$3.0 \times 10^{-11}$
3	2492-2827	0.15	6.24	30	260	323	0.95	49.1	2.46	$3.1 \times 10^{-9}$
4	2827-3666	0.12	6.27	0.4	96	137	0.95	50.5	2.53	$7.6 \times 10^{-11}$
5	3666-3834	0.15	6.19	5.9	198	231	0.95	58.6	2.93	$6.9 \times 10^{-9}$
6	3834-5005	0.13	6.36	6	183	204	1.0	59.0	0	$2.5 \times 10^{-11}$
7	5009-6069	0.17	6.27	30	220	222	1.0	60.0	0	$8.1 \times 10^{-11}$
8	6069-6379	0.14	6.33	31	205	204	0.98	60.1	1.20	$3.8 \times 10^{-11}$
9	6379-6573	0.14	6.34	28	223	219	0.95	60.2	3.01	$3.8 \times 10^{-11}$
10	6573-6592	0.14	6.34	28	220	215	0.90	62.4	6.24	$7.8 \times 10^{-9}$

<sup>a</sup>Composite compact tension specimen (1TCT) (No. 02C-11) was fabricated from Inconel-600/Inconel-182/A533-Gr B Steel (Heat No. A-1195-1). Specimen was electroplated with nickel.

<sup>b</sup>Frequency of the positive sawtooth wave form was  $8 \times 10^{-2}$  Hz; rise time of 12 s and fall time of 1 s.

<sup>c</sup>Effluent dissolved-oxygen concentrations below 20 ppm were determined with an Orbisphere dissolved-oxygen meter; higher values were measured with CHEMetrics™ ampules.

<sup>d</sup>Stress intensity,  $K_{\text{max}}$ , value at the end of each time period.

<sup>e</sup> $\Delta K = K_{\text{max}}(1 - R)$ , where the load ratio  $R = K_{\text{min}}/K_{\text{max}}$ .

increasing the load ratio. However, steady-state CGRs can lie in either the high- or low-CGR regime for any given set of loading or environmental conditions. This is illustrated in Fig. 2, which summarizes the results in Table 5 at an R of 0.95 for composite specimen 02C-11, the composite specimen (02C-1) from a previous experiment,<sup>19</sup> and data from gold-plated and nonplated specimens of the same heat of ferritic steel.<sup>19</sup>

The heavy lines in Fig. 2 represent the predicted dependence of CGR on  $K_{\text{max}}$  for ferritic steels in 289°C water at an R of 0.95 and a rise-time  $T_R$  of 10 s, according to the

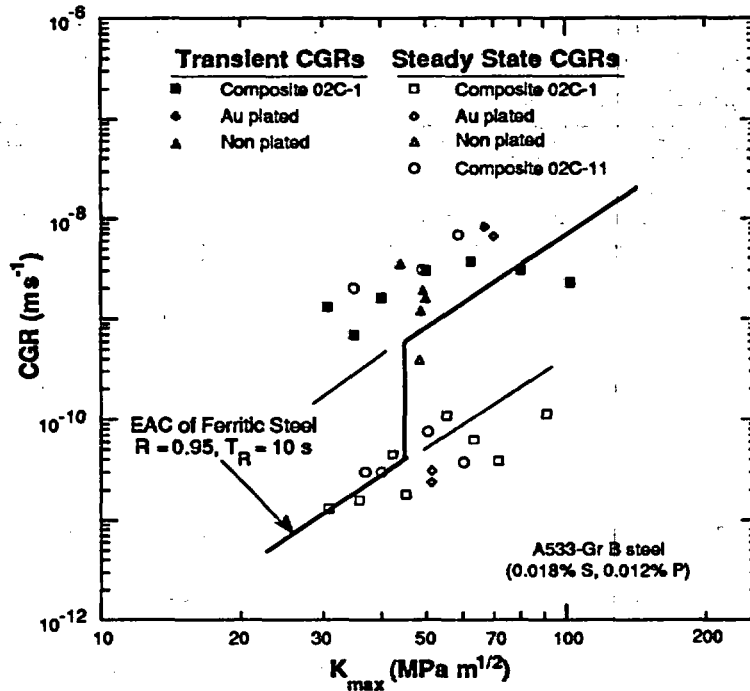


Figure 2. CGRs of A533-Gr B steel under  $R = 0.95$  loading in HP oxygenated water at  $289^{\circ}\text{C}$  versus  $K_{\max}$ . Heavy line represents predicted behavior from a modified version of Section XI of the ASME code.

fatigue CGR curves for ferritic steels in LWR environments proposed recently by Eason.\* The model predicts a threshold for a transition from a low, nonenvironmentally assisted CGR to a much higher rate. The threshold  $K_{\max}$  predicted by the model (which includes high-oxygen environments that may be more aggressive than those used in tests on which the model is based) is somewhat higher than the present data would indicate. The persistence of low CGRs above the "threshold" is consistent with a hysteresis observed in similar tests at lower  $R$  values in other investigations. One can "move up" the lower curve above the threshold without triggering high CGRs, but once high rates are achieved they persist at lower  $K_{\max}$  levels. The interpretation of the present tests in terms of the threshold model is complicated because we have not run "classical" threshold tests with a fixed environment and a fixed  $R$ . The threshold is a function of  $R$  and probably of oxygen level. Instead of the single illustrative curve shown in Fig. 2, there should be a family of curves corresponding to the different conditions. The single curve is representative but not necessarily predictive.

\*Personal Communication, David Jones, Chairman MPC Task Force on Crack Propagation Technology, to W. J. Shack, Argonne National Laboratory, August 15, 1991.

The upper-bound values for the experimental data in the high- and low-CGR regimes are  $\approx 2 \times 10^{-9}$  and  $2 \times 10^{-11} \text{ m}\cdot\text{s}^{-1}$  ( $\approx 2.5$  and  $0.025 \text{ in}\cdot\text{yr}^{-1}$ ), respectively, at a  $K_{\text{max}}$  value of  $35 \text{ MPa}\cdot\text{m}^{1/2}$ . Crack-growth rates in the upper regime are clearly unacceptable. The nature of the transitions between the two regimes and the observation that the initial fatigue crack in companion nonplated specimens did not propagate will be investigated further in future experiments.

### 2.3 Role of Chromate and Sulfate in SCC of Type 304 SS

Soluble corrosion products from system materials are the major species present in BWR water when ingress of ionic impurities into the coolant system from leaks in condenser tubes and from ion-exchange resins in the reactor water cleanup system (RWCS), including resin fines, is maintained at very low levels. Examples include  $\text{Cu}^+$  and  $\text{Cu}^{2+}$  in plants with either copper alloy condenser tubes and/or feedwater heaters and  $\text{HCrO}_4^-$  from corrosion of SS piping, weld cladding on the interior of the reactor vessel, and internal components fabricated from this material. Although chromate ( $\text{K}_2\text{CrO}_4$ ) is used as a corrosion inhibitor in component cooling water systems (CCWS) in BWRs and PWRs, these systems operate at relatively low temperatures ( $\approx 170^\circ\text{C}$ ) and pressures ( $\approx 150 \text{ psig}$ ); thus, direct ingress of chromate from the CCWS into the reactor coolant water is unlikely under normal operating conditions. Nevertheless, because only a small fraction of the recirculation water in BWRs passes through the RWCS, the concentration of corrosion-product ions in the reactor water can be considerably greater than in the feedwater (e.g.,  $\approx 25\text{--}35 \text{ ppb}$  versus  $<1 \text{ ppb}$ , respectively). Consequently,  $\text{HCrO}_4^-$  and the counterbalancing hydronium cation ( $\text{H}_3\text{O}^+$ ) are major contributors to water conductivity. To further mitigate IGSCC of sensitized Type 304 SS in these systems through water chemistry control, utilities have considered (1) neutralizing the residual chromic acid by NaOH additions to the feedwater (to take advantage of the lower specific conductivity of  $\text{Na}^+$  relative to that of  $\text{H}_3\text{O}^+$ ), and (2) devising methods to remove chromate from the water by ion exchange.<sup>20</sup>

#### 2.3.1 Experimental Methods

A fracture-mechanics CGR experiment was performed to determine the effect of chromate additions to simulated BWR water (without and with low levels of sulfate) on SCC of our reference heat (No. 30956) of Type 304 SS (composition is given in Table 1). Crack length was measured by the DC potential-drop technique over time intervals of  $\approx 800\text{--}1500 \text{ h}$  at each test condition. Three specimens were heat treated to produce a solution-annealed condition, and moderate and high levels of sensitization corresponding to electrochemical potentiokinetic reactivation (EPR) values of 0, 8, and  $30 \text{ C}\cdot\text{cm}^{-2}$ , respectively. The specimens were fatigue-precracked in HP water containing 200–300 ppb dissolved oxygen at  $289^\circ\text{C}$ . CGR tests were conducted in oxygenated water with different chromate and sulfate additions under several loading conditions.

## 2.3.2 Results

The water chemistry, loading conditions, and results of the CGR tests are given in Table 6. Steady-state CGRs were measured over time periods of ~800–1200 h under each test condition.

**Table 6. Crack Growth Results for Sensitized<sup>a</sup> Type 304 SS Specimens under High-R Loading<sup>b</sup> in High-Purity Oxygenated Water and in Oxygenated Water Containing Chromate and Sulfate at 289°C**

Test No.	Test Time, h	Water Chemistry <sup>c</sup>				Electrode Potential		Material (Sensitization)					
		CrO <sub>4</sub> <sup>2-</sup> Conc., <sup>d</sup> ppb	SO <sub>4</sub> <sup>2-</sup> Conc., ppb	Cond. at 25°C, $\mu\text{S cm}^{-1}$	pH at 25°C	304 SS mV(SHE)	Pt mV(SHE)	304 SS (EPR = 0 C·cm <sup>-2</sup> )		304 SS (EPR = 8 C·cm <sup>-2</sup> )		304 SS (EPR = 30 C·cm <sup>-2</sup> )	
								K <sub>max</sub> <sup>e</sup> , MPa·m <sup>1/2</sup>	Growth Rate, m·s <sup>-1</sup>	K <sub>max</sub> <sup>e</sup> , MPa·m <sup>1/2</sup>	Growth Rate, m·s <sup>-1</sup>	K <sub>max</sub> <sup>e</sup> , MPa·m <sup>1/2</sup>	Growth Rate, m·s <sup>-1</sup>
1	0–300 <sup>f</sup>	–	–	0.12	6.22	308	213	27.6	5 x 10 <sup>-12</sup>	29.2	9.2 x 10 <sup>-10</sup>	28.2	1.0 x 10 <sup>-10</sup>
2	300–1204	–	–	0.17	6.20	119	119	27.7	5 x 10 <sup>-12</sup>	30.9	3.3 x 10 <sup>-10</sup>	28.5	8.3 x 10 <sup>-11</sup>
3	1204–2350	50	–	0.30	6.21	67	58	27.7	5 x 10 <sup>-12</sup>	31.2	4.3 x 10 <sup>-11</sup>	28.5	8.7 x 10 <sup>-12</sup>
4	2350–3400	–	–	0.12	6.33	91	88	27.7	5 x 10 <sup>-12</sup>	31.5	4.3 x 10 <sup>-11</sup>	28.6	8.7 x 10 <sup>-12</sup>
5	3400–4400	200	–	0.82	5.81	80	80	27.7	5 x 10 <sup>-12</sup>	31.8	4.3 x 10 <sup>-11</sup>	28.7	8.7 x 10 <sup>-12</sup>
6	4400–5200	50	–	0.31	6.09	58	51	27.8	5 x 10 <sup>-12</sup>	31.8	4.3 x 10 <sup>-11</sup>	28.7	8.7 x 10 <sup>-12</sup>
7	5200–5900	50	25	0.46	6.01	91	96	27.8	5 x 10 <sup>-12</sup>	32.7	3.4 x 10 <sup>-10</sup>	28.7	8.7 x 10 <sup>-12</sup>
8	5900–7300	50	100	1.06	5.71	104	107	27.8	5 x 10 <sup>-12</sup>	35.3	4.1 x 10 <sup>-10</sup>	29.9	2.5 x 10 <sup>-10</sup>
9	7300–8800	50	–	0.27	6.15	88	71	27.8	9 x 10 <sup>-12</sup>	35.6	7.0 x 10 <sup>-11</sup>	30.0	3.6 x 10 <sup>-11</sup>
10	8800–10000	50	6	0.37	6.23	38	101	27.8	4 x 10 <sup>-12</sup>	35.7	2.3 x 10 <sup>-11</sup>	30.0	1.2 x 10 <sup>-11</sup>
11	10000–11200	50	15	0.44	6.09	37	107	27.9	6 x 10 <sup>-12</sup>	36.2	2.8 x 10 <sup>-11</sup>	30.1	1.1 x 10 <sup>-11</sup>
12	11200–11800	200	100	1.70	5.59	108	142	27.9	<5 x 10 <sup>-12</sup>	37.9	3.0 x 10 <sup>-10</sup>	30.7	1.7 x 10 <sup>-10</sup>
13	11800–12400 <sup>f</sup>	200	50	1.32	5.66	14	39	27.9	<5 x 10 <sup>-12</sup>	38.2	1.0 x 10 <sup>-10</sup>	30.9	8.1 x 10 <sup>-11</sup>

<sup>a</sup>Compact-tension specimens (1TCT) of Type 304 SS (Heat No. 30956) received a solution-anneal heat treatment at 1050°C for 0.5 h. Specimen No. 32 was tested in the solution-annealed condition (EPR = 0 C·cm<sup>-2</sup>). Specimen No. 34 was sensitized at 700°C for 0.67 h (EPR = 8 C·cm<sup>-2</sup>) and Specimen No. 33 at 700°C for 24 h (EPR = 30 C·cm<sup>-2</sup>).

<sup>b</sup>Frequency and load ratio, R, for the positive sawtooth wave form were 8 x 10<sup>-2</sup> Hz and 0.95, respectively.

<sup>c</sup>Effluent dissolved-oxygen concentration was ~200–300 ppb, except in Test 1 at 5.5 ppm; feedwater oxygen concentration was higher by a factor of 3 in Tests 2–13 to compensate for oxygen depletion by corrosion of the autoclave system.

<sup>d</sup>Chromate and sulfate were added to the feedwater as acids; effluent chromate concentrations were ~9 and 13 ppb for feedwater levels of 50 and 200 ppb on the basis of colorimetric analyses of grab samples.

<sup>e</sup>Stress intensity, K<sub>max</sub>, values at the end of the time period.

<sup>f</sup>Test in progress; values based on initial results.

Baseline CGRs were determined under low-frequency (0.08 Hz), high-R (0.95) loading conditions in Tests 1 and 2 in Table 6. In Tests 3–6 and 9, either 0, 50, or 200 ppb chromate was added to the oxygenated feedwater and the CGRs were measured. In Tests 7, 8, 10, and 11, different concentrations of sulfate (between 6 and 100 ppb) were added to feedwater containing 50 ppb chromate to determine their combined effect on the CGRs of

the steel. In Tests 12 and 13, the chromate concentration in the feedwater was increased to 200 ppb and the sulfate concentrations were 100 and 50 ppb, respectively.

The results in Table 6 reveal that the solution-annealed specimen ( $EPR = 0 \text{ C}\cdot\text{cm}^{-2}$ ) exhibited very low CGRs ( $<5 \times 10^{-12} \text{ m}\cdot\text{s}^{-1}$ ) under all water chemistry conditions. Of the two sensitized specimens ( $EPR = 8$  and  $30 \text{ C}\cdot\text{cm}^{-2}$ ), the specimen with the lower EPR value exhibited the highest CGRs under each test condition. This level of sensitization produced maximum SCC susceptibility in slow-strain-rate-tensile (SSRT) tests at  $289^\circ\text{C}$  in oxygenated water without and with 100 ppb sulfate.<sup>21</sup> The results for the sensitized specimens can be summarized as follows. In oxygenated feedwater, 50–200 ppb chromate has a beneficial effect, as indicated by the low CGRs ( $<7 \times 10^{-11} \text{ m}\cdot\text{s}^{-1}$ ) in Tests 3, 5, 6, and 9. In water containing 50 ppb chromate, low levels of sulfate (6 or 15 ppb) did not lead to high CGRs in Tests 10 and 11. In water containing 50 ppb chromate and 25 or 100 ppb sulfate (Tests 7 and 8), CGRs of the moderately sensitized specimen ( $EPR = 8 \text{ C}\cdot\text{cm}^{-2}$ ) increased significantly (to  $>3 \times 10^{-10} \text{ m}\cdot\text{s}^{-1}$ ), whereas the heavily sensitized specimen exhibited this rate in water containing 100 ppb sulfate. At a higher chromate concentration (e.g., 200 ppb) in oxygenated feedwater containing 100 ppb sulfate (Test 12), the CGRs of the sensitized specimens were high ( $>1 \times 10^{-10} \text{ m}\cdot\text{s}^{-1}$ ). However, chromate appears to have a small beneficial effect at a somewhat lower sulfate concentration of 50 ppb in Test 13.

The present results indicate that the CGRs of the sensitized specimens may exhibit a unique dependence on sulfate and chromate concentrations in oxygenated feedwater. Figure 3 shows the CGRs of the moderately sensitized specimen ( $EPR = 8 \text{ C}\cdot\text{cm}^{-2}$ ) as a function of the ratio of the concentrations of chromate and sulfate in the feedwater. When these species were not added to the feedwater (Table 6), their concentrations were assumed to be  $\sim 1$  ppb for the purpose of obtaining the ratios in Fig. 3. The limited data suggest that the CGRs are in the low regime if the  $(\text{CrO}_4^{2-})/(\text{SO}_4^{2-})$  ratio in the feedwater is  $\geq 3$ . Chromate concentrations in feedwater and effluent water were determined by colorimetric analyses ( $\text{Cr}^{+6}$ ) on grab samples. The measured feedwater concentrations were in excellent agreement with the amounts added to the water; however, the effluent values were lower by a factor of  $>5$  owing to the low flow velocity and reaction with the large surface area of stainless steel in the autoclave system at  $289^\circ\text{C}$ . The feedwater and effluent sulfate concentrations were virtually the same in all experiments.

Although SSRT tests indicated that chromate at concentrations  $>100$  ppb in oxygenated water contributes to IGSCC in a manner similar to that of other oxyanions,<sup>20,22</sup> the present CGR results suggest that this species has a mitigating effect on IGSCC at lower concentrations, provided that the sulfate concentration is lower by a factor of  $\sim 3$ . Because chromate concentrations in BWR recirculation water are  $\sim 25$ – $35$  ppb, the sulfate concentration should be maintained at  $<10$  ppb to mitigate IGSCC. Achievable values for sulfate are  $<15$  ppb and typically can be maintained at the  $\sim 5$  ppb level. Consequently, these water chemistry conditions would place sensitized Type 304 SS in the low-CGR regime. Efforts to remove chromate from recirculation loop water without decreasing the critical sulfate level could be counterproductive. Furthermore, maintaining sulfate concentrations at levels of  $<5$  ppb may be impractical.

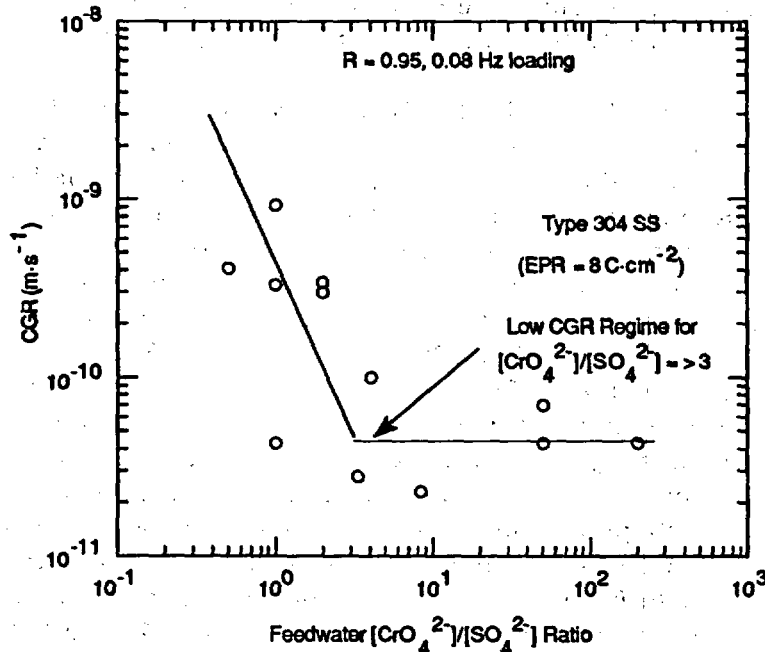


Figure 3. Regime of high and low CGRs for moderately sensitized ( $\text{EPR} = 8 \text{ C}\cdot\text{cm}^{-2}$ ) Type 304 SS specimen at  $289^\circ\text{C}$  as a function of ratio of the chromate and sulfate concentrations in feedwater water containing  $\sim 300$  ppb dissolved oxygen

#### 2.4 RIS and IASCC of HP and CP Type 304 SS from BWR Control-Blade Absorber Tubes

In recent years, failures of reactor-core internal components in both BWRs and PWRs have increased after accumulation of relatively high fluence ( $>5 \times 10^{20} \text{ n}\cdot\text{cm}^{-2}$ ,  $E > 1 \text{ MeV}$ ). The general pattern of the observed failures indicates that as nuclear plants age and neutron fluence increases, various apparently nonsensitized austenitic materials become susceptible to intergranular failure. Some components are known to have cracked under minimal applied stress. Although most failed components can be replaced, some safety-significant structural components, such as the BWR top guide, shroud, and core plate, would be very difficult or impractical to replace. Therefore, structural integrity of these components after accumulation of high fluence has been a subject of concern, and extensive research has been conducted to provide an understanding of this type of degradation, commonly termed irradiation-assisted stress corrosion cracking (IASCC).<sup>23-40</sup>

Most of the safety-significant structural components are fabricated from solution-annealed austenitic SSs, primarily commercial-purity Type 304 SS. Component fabrication procedures and reactor operational parameters, such as neutron flux, fluence, temperature,

water chemistry, residual stress, and mechanical loads, have been reported to influence susceptibility to IASCC.<sup>23-34</sup> However, results from research at several laboratories on materials irradiated under a wide variety of simulated conditions are often inconsistent and conflicting as to the influence of these parameters.<sup>26,33</sup>

Failures of austenitic SS after accumulation of high fluence have been attributed to irradiation-induced segregation (RIS) or depletion of elements such as Si, P, S, Ni, and Cr at grain boundaries. It is generally believed that the nonequilibrium process of RIS of impurity or alloying elements is strongly influenced by irradiation temperature and fast-neutron dose rate. However, the exact identity of the elements that segregate and the extent to which RIS contributes to the enhanced susceptibility of the core-internal components of LWRs to IASCC are not clear. Unfortunately, this is particularly true for Type 304 SS, from which the majority of the safety-significant in-core components have been fabricated, although analyses of RIS of impurity elements and grain-boundary depletion of Cr have been reported for Type 304 SS specimens irradiated under simulated conditions, i.e., either in test reactors,<sup>27,28,30</sup> by electrons,<sup>27</sup> or ions.<sup>32,34</sup>

In view of the strong influence of irradiation temperature and dose rate, results obtained from specimens irradiated in test reactors and accelerators must be considered as tentative, and benchmark analyses on actual reactor components must be obtained. For this purpose, high- and commercial-purity (HP and CP) Type 304 SS specimens obtained from neutron absorber tubes of two operating BWRs were analyzed by Auger electron spectroscopy (AES) previously.<sup>38,39</sup> HP Type 304 SS has been suggested as an alternative to CP Type 304 SS. In-reactor and laboratory experience<sup>24,25,31</sup> indicate better IASCC performance of an HP heat of Type 348 SS compared to a CP heat of Type 304 SS. Auger analyses of specimens from a CP Type 304 SS neutron absorber rod revealed significant segregation of Si, P, Ni, and an unidentified element or compound that gives rise to an Auger energy peak at 59 eV.<sup>38,39</sup> Such segregation was negligible in HP material, except for Ni. No evidence of S segregation was observed in either material. However, Cr depletion was more pronounced in the HP material than in the CP material.

The results of the AES analyses of irradiation-induced grain-boundary segregation of impurity and alloying elements have been correlated with SCC susceptibility information from SSRT tests on specimens from neutron absorber rod tubes to provide insight into mechanism(s) of IASCC.

#### 2.4.1 Experimental Methods

Slow-strain-rate-tensile (SSRT) tests have been conducted on a 12 specimens of CP and HP neutron-absorber-rod tubes in air and in simulated BWR water at 289°C to determine tensile properties and IASCC susceptibility as a function of neutron fluence. The chemical compositions of the HP and CP heats are given in Table 7. The dissolved-oxygen concentration and conductivity of the simulated BWR water were ~280 ppb and 0.13  $\mu\text{S}\cdot\text{cm}^{-1}$ , respectively. SEM fracture surface maps of the SSRT specimens were also obtained. SEM fractography was conducted at a magnification of 125X, and an entire fracture-surface composite was constructed for each specimen to determine the fraction of intergranular, transgranular, and ductile failure.

**Table 7. Chemical Composition and Fast-Neutron Fluence of Irradiated Type 304 SS BWR Absorber-Rod Cladding**

Material	Component Code	Chemical Composition (wt.%)										Specimen Code	Fluence, n·cm <sup>-2</sup>
		Cr	Ni	Mn	C	N	Si	P	S	O	B		
304 SS	BAR <sup>a</sup>	16.80 <sup>b</sup>	8.77	1.65	-	0.052	1.55	-	-	0.024	-	BL-H	2.0 x 10 <sup>21</sup>
304 SS	BAR <sup>c</sup>	18.58	9.44	1.22	0.017	0.037	0.02	0.002	0.003	-	0.0002	VH	1.4 x 10 <sup>21</sup>

<sup>a</sup>Commercial-purity grade BWR absorber-rod tube containing B<sub>4</sub>C.

<sup>b</sup>Composition measured after service.

<sup>c</sup>High-purity grade BWR absorber-rod tube containing B<sub>4</sub>C.

## 2.4.2 Results

Test conditions, SSRT data, and SEM analyses of the 12 specimens are summarized in Table 8. Stress versus elongation curves from HP and CP specimens tested in the simulated BWR water are shown in Fig. 4. From the figure, relative characteristics of stress corrosion of the HP and CP specimens can be deduced. For all the three fluence levels, total elongations of specimens from the HP heat were smaller than those from the CP heat, indicating that susceptibility to stress corrosion was higher in the HP than in the CP heat. For example, for fluence level of 0.6 to 0.7 x 10<sup>21</sup> n·cm<sup>-2</sup> (Fig. 4B), total elongation of the HP specimen was ~1.8% compared to ~8.3% of the CP specimen. Figure 5 shows the ultimate tensile strength (UTS) versus fast-neutron fluence (E > 1 MeV) of the CP and HP specimens strained to failure in air (from Table 8). The figure contains similar data for CP-grade BWR plate<sup>23</sup> and CP-grade tensile specimens of Types 304 and 304L SS irradiated in the Advanced Test Reactor (ATR) at 300°C.<sup>28</sup> Data obtained from the present CP material (Vermont Yankee BWR neutron absorber rod) seem to be consistent with those of other CP materials shown in the figure. However, the UTS and yield strength of the HP material (Peach Bottom BWR neutron absorber rod) were higher than those of the CP materials. Figure 6 shows the total elongation versus fast-neutron fluence for the HP and CP materials in Fig. 5. Ductility decreases monotonically as fluence increases, apparently leveling out at a fluence level > 1.5 x 10<sup>21</sup> n·cm<sup>-2</sup>. All specimens tested in air failed in a ductile manner, and no evidence of intergranular or transgranular fracture was observed. Morphologies of ductile fracture surfaces of the CP and HP materials were somewhat different; however, it is not understood why the HP material is stronger than the CP material.

For SSRT specimens tested in simulated BWR water, the percent IGSCC determined from SEM fractography was, in general, consistent with the decrease in total elongation. This is shown in Fig. 7. Literature data from SSRT tests on Types 304 and 316 SS from CP-grade BWR components are also plotted. The figure indicates that total elongation is also a good measure of IGSCC susceptibility.

The percent IGSCC versus fast-neutron fluence (E > 1 MeV) of the present CP and HP heats is shown in Fig. 8, along with similar results from SSRT tests on BWR dry tubes in water containing ~200 ppb dissolved oxygen reported by Kodama et al.<sup>40</sup> The figure indicates that IGSCC susceptibility of CP material from our neutron absorber tube and the

**Table 8. Slow-Strain-Rate-Tensile<sup>a</sup> Test Results on Irradiated CP and HP Type 304 SS in Air and in HP Water Containing ~280 ppb Dissolved Oxygen at 289°C**

Absorber Rod Specimen No.	Hot-Cell Identification No.	Fast-Neutron Fluence, n-cm <sup>-2</sup>	SSRT No.	Feedwater Chemistry			SSRT Parameters				
				Oxygen Conc., ppb	Cond. at 25°C, μS-cm <sup>-1</sup>	pH at 25°C	Failure Time, h	Maximum Stress, MPa	Total Elong., %	TGSOC, %	IGSOC, %
BL-BWR-2H	389E3A	2.0 x 10 <sup>21</sup>	IR-9	b	b	b	228	631	13.5	0	0
BL-BWR-2H	389E3D	2.0 x 10 <sup>21</sup>	IR-12	300	0.13	6.27	21	415	1.2	8	28
BL-BWR-2M	389E2D	0.6 x 10 <sup>21</sup>	IR-3	b	b	b	580	485	34.8	0	0
BL-BWR-2M	389E2A	0.6 x 10 <sup>21</sup>	IR-8	290	0.15	6.32	140	359	8.3	55	0
BL-BWR-2L	389E1A	0.2x 10 <sup>21</sup>	IR-2	b	b	b	260	390	15.6	0	0
BL-BWR-2L	389E1D	0.2x 10 <sup>21</sup>	IR-1	280	0.13	6.23	107	337	6.7	43	0
VH-A7A-L2	406A1F	1.4 x 10 <sup>21</sup>	IR-5	b	b	b	93	786	5.6	0	0
VH-A7A-L1	406A1E	1.4 x 10 <sup>21</sup>	IR-4	280	0.10	6.28	11	417	0.6	2	58
VM-D5B-L2	406C3	0.7x 10 <sup>21</sup>	IR-6	b	b	b	405	684	24.2	-	-
VM-D5B-L1	406C2	0.7x 10 <sup>21</sup>	IR-7	280	0.12	6.26	31	552	1.8	8	34
VL-A4C-L2	406B3	0.2x 10 <sup>21</sup>	IR-10	b	b	b	231	607	13.7	-	-
VL-A4C-L1	406B2	0.2x 10 <sup>21</sup>	IR-11	330	0.14	6.33	77	520	4.6	47	14

<sup>a</sup>Strain rate of 1.65 x 10<sup>-7</sup> s<sup>-1</sup>.

<sup>b</sup>Test in air at 289°C and strain rate of 1.65 x 10<sup>-7</sup> s<sup>-1</sup>.

dry tube is similar at a comparable fluence level, and that the HP material exhibits greater SCC susceptibility. Duplicate tests will be performed on specimens from the HP-grade absorber tube and the CP-grade control-blade-sheath to further confirm the results.

### 3 Conclusions

#### Fatigue of Ferritic Piping and Pressure Vessel Steels

- The fatigue life of a medium-sulfur-content A533-Gr B pressure vessel and A106-Gr B piping steels was studied in high-purity deoxygenated water, in simulated PWR water, and in air. All fatigue data lie above the ASME design curve.

#### Stress Corrosion Cracking of Ferritic Steels

- Fracture-mechanics CGR tests have been performed on composite specimens of A533-Gr B/Inconel-182/Inconel-600 plated with nickel, and on homogeneous specimens of A533-Gr B material plated with gold and nickel. The effects of load history and dissolved-oxygen content were examined. The CGRs increased markedly during small-amplitude cyclic loading (R = 0.95). Under the cyclic loading, crack growth was observed at K<sub>max</sub> values that produced no crack growth under constant R = 1 loading. Under R = 0.95 loading, relatively high CGRs (2 x 10<sup>-9</sup> m-s<sup>-1</sup>) were observed in HP water containing ~300 ppb dissolved oxygen. When the specimen is in the low-CGR regime (2 x 10<sup>-11</sup> m-s<sup>-1</sup>), increasing the dissolved-oxygen concentration to 6 ppm or higher initiated a return to the high CGR regime, at least at an R value of 0.95.

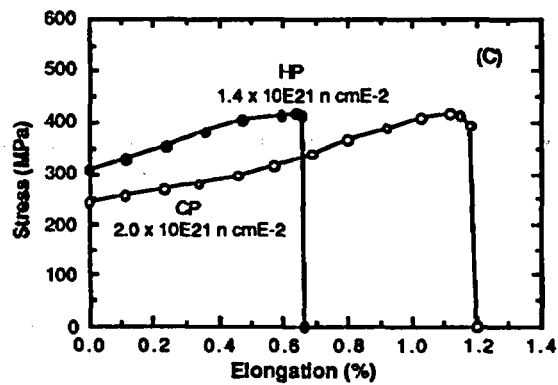
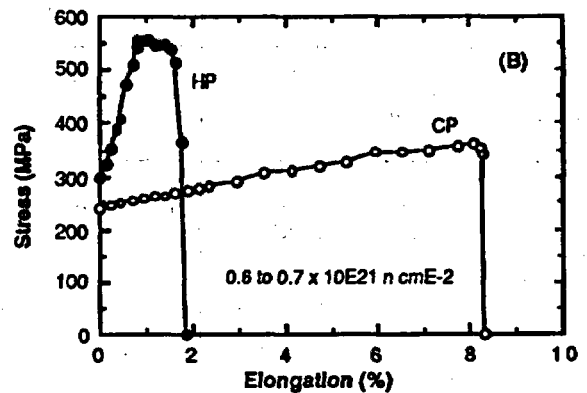
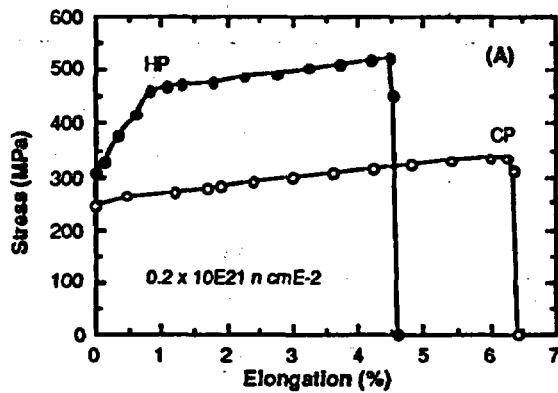


Figure 4. Stress vs. elongation from SSRT tests in simulated BWR water at 289°C on HP and CP Type 304 SS BWR neutron absorber tubes; irradiated to a fluence of (A)  $0.2 \times 10^{21}$ ; (B)  $0.6$  to  $0.7 \times 10^{21}$ ; and (C)  $1.4$  to  $2.0 \times 10^{21} \text{ n}\cdot\text{cm}^{-2}$

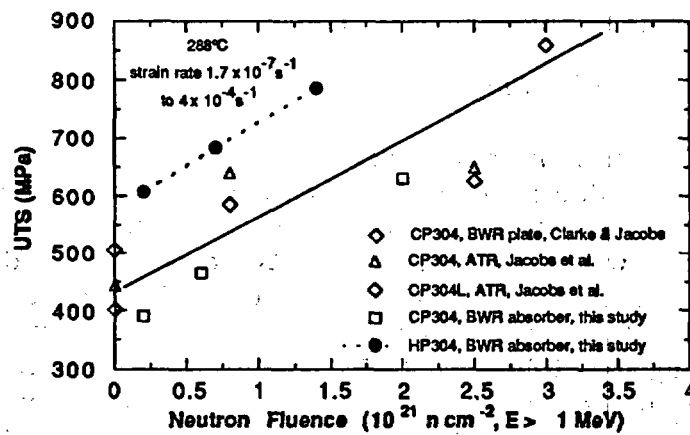


Figure 5. Ultimate tensile stress (UTS) vs. fast-neutron fluence ( $E > 1 \text{ MeV}$ ) for solution-annealed CP and HP Type 304 SS from tensile tests in air at 288°C

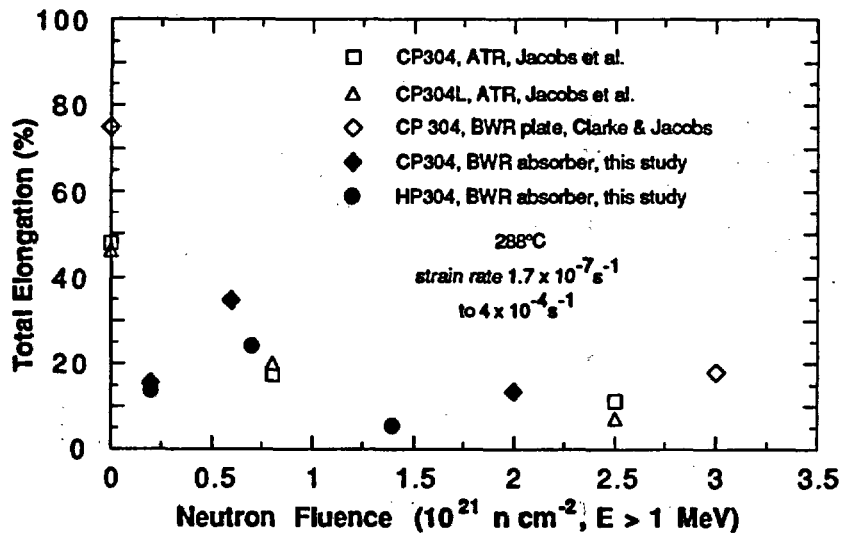


Figure 6. Comparison of total elongation vs. fast-neutron fluence ( $E > 1 \text{ MeV}$ ) of solution-annealed CP and HP Type 304 SS from tensile tests in air at 288°C

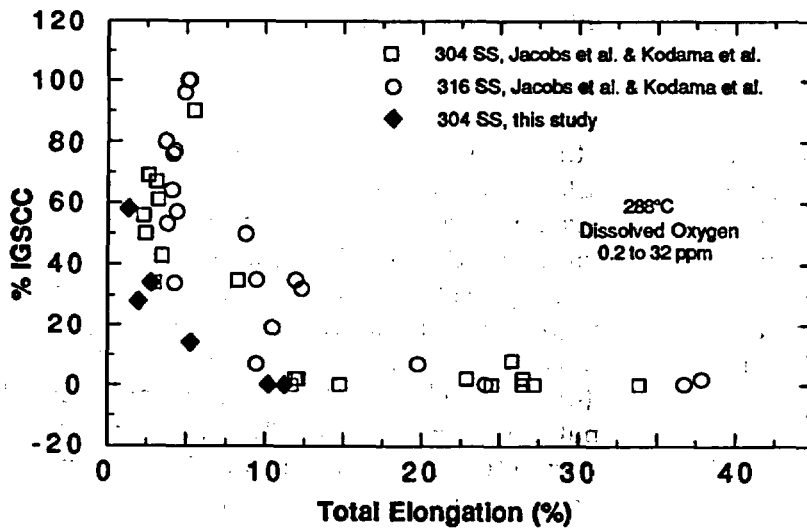


Figure 7. Percent IGSCC vs. total elongation of CP and HP Type 304 SS in the present study and similar data from the literature<sup>28,30,31,40</sup> from SSRT tests at 288°C in simulated BWR water containing 0.2 to 32 ppm dissolved oxygen

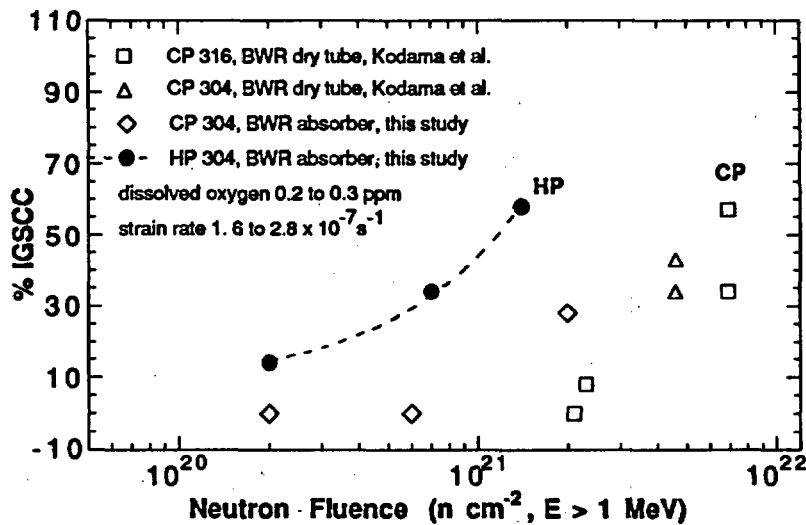


Figure 8. Percent IGSCC vs. fast-neutron fluence ( $E > 1$  MeV) for HP Type 304 SS and CP Type 304 and 316 SS<sup>40</sup> from SSRT tests at 288°C in simulated BWR water containing 200–300 ppb dissolved oxygen. HP material exhibits higher susceptibility than CP heats.

#### Effects of Chromate and Sulfate on SCC of Type 304 SS

- Current BWR operating practices have reduced to very low levels the ingress of ionic impurities (e.g., sulfate, chloride) into the coolant system. Soluble corrosion products viz., chromate and the counterbalancing hydronium ion, are now the major ionic species present. Because only a small fraction of the recirculation water in BWRs passes through the reactor water cleanup system, the concentration of chromate ions in the reactor water can be much greater than in the feedwater (e.g., ~25–35 ppb versus <1 ppb, respectively). The CGRs of sensitized Type 304 SS under high-R, low-frequency loading are low ( $< 4 \times 10^{-11} \text{ m}\cdot\text{s}^{-1}$ ) provided that the chromate/sulfate concentration ratio in oxygenated feedwater is  $> 3$ . Thus, a low chromate concentration in BWR water (25–35 ppb) may actually have a beneficial effect on SCC, provided that the sulfate concentration is below a critical level (i.e., ~10 ppb).

#### Irradiation-Assisted Stress Corrosion Cracking of Type 304 SS

- Failures of austenitic SS after accumulation of high fluence have been attributed to radiation-induced segregation (RIS) of elements such as Si, P, S, Ni, and Cr. Microchemical and microstructural changes in high- and commercial-purity (HP and CP) Type 304 SS specimens from control-blade absorber tubes in two operating BWRs were studied by Auger electron spectroscopy and SEM. SSRT tests were conducted on

tubular specimens in air and in simulated BWR water at 289°C. Results in air showed that the yield and ultimate tensile strengths of the HP material were higher than those of the CP material for a comparable fluence.

- Stress versus elongation characteristics of the SSRT specimens were consistent with results of SEM analyses of the percent IGSCC on fracture surfaces. IGSCC susceptibility of the present CP absorber tubes was similar to those of other CP heats of Types 304 and 316 SS reported in literature. However, the HP absorber tubes exhibited greater IGSCC susceptibility than did the CP materials.
- It is difficult to explain the relatively high susceptibility of the HP material on the basis of Si or P segregation, because impurity segregation in the HP absorber tubes was negligible for all fluence levels. Rather, the high susceptibility seems to be consistent with the observation that irradiation-induced Cr depletion was more significant in the HP heat than in the CP heat, indicating that irradiation-induced grain-boundary depletion of Cr is the primary process in IASCC, at least in simulated BWR water.

## References

---

1. *Criteria of Section III of the ASME Boiler and Pressure Vessel Code for Nuclear Vessels*, The American Society of Mechanical Engineers, United Engineering Center, New York, Library of Congress Catalog No. 56-3934, (1989).
2. J. B. Terrell, *Fatigue Life Characterization of Smooth and Notched Piping Steel Specimens in 288°C Air Environments*, NUREG/CR-5013, MEA-2232 (May 1988).
3. D. Weinstein, *BWR Environment Cracking Margins for Carbon Steel Piping-Final Report*, EPRI Report NP-2046, Electric Power Research Institute, Palo Alto, CA (1982).
4. D. Hale, S. A. Wilson, J. W. Kass, and E. Kiss, *Low Cycle Fatigue of Commercial Piping Steels in a BWR Primary Water Environment*, *J. Eng. Mater. and Technol.* **103**, 15-25 (1981).
5. K. Iida, H. Kobayashi, and M. Higuchi, *Predictive Method of Low Cycle Fatigue Life of Carbon and Low Alloy Steels in High Temperature Water Environments*, NUREG/CP-0067, MEA-2090, Vol. 2 (April 1986).
6. N. Nagata, S. Sato, and Y. Katada, *Low Cycle Fatigue Behavior of Low Alloy Steels in High Temperature Pressurized Water*, *Structural Mechanics in Reactor Technol.* **10**, 209-214 (1989-8).
7. J. B. Terrell, *Effect of Cyclic Frequency on the Fatigue Life of ASME SA-106-B Piping Steel in PWR Environments*, *J. Mater. Eng.* **10**, 193-203 (1988).
8. T. A. Prater and L. F. Coffin, *The Use of Notched Compact-Type Specimens for Crack Initiation Design Rules in High-Temperature Water Environments*, *Corrosion Fatigue: Mechanics Metallurgy, Electrochemistry, and Engineering*, ASTM STP 801, T. W. Crooker and B. N. Leis, eds., American Society for Testing and Materials, Philadelphia, pp. 423-444 (1983).

9. T. A. Prater and L. F. Coffin, *Notch Fatigue Crack Initiation in High Temperature Water Environments: Experiments and Life Prediction*, J. of Pressure Vessel Technol., Trans. ASME, **109**, 124-134 (1987).
10. P. D. Hicks and F. P. A. Robinson, *Fatigue Crack Growth Rates in a Pressure Vessel Steel under Various Conditions of Loading and the Environment*, Met. Trans. **17A**, 1837-1849 (1986).
11. *Proc. of the Int. Atomic Energy Agency Specialists' Meeting on Subcritical Crack Growth*, NUREG/CP-0044, MEA-2014, Vols. 1 & 2 (May 1983).
12. *Proc. of the 2nd Int. Atomic Energy Agency Specialists' Meeting on Subcritical Crack Growth*, NUREG/CP-0067, MEA-2090, Vols. 1 & 2 (April 1986).
13. *Proc. of the 3rd Int. Atomic Energy Agency Specialists' Meeting on Subcritical Crack Growth*, NUREG/CP-0112, Vols. 1 & 2 (August 1990).
14. T. A. Prater, W. R. Catlin, and L. F. Coffin, *Surface Crack Growth Behavior of Structural Metals in High Temperature Water Environments*, J. Eng. Mater. Technol. **108**, 2-9 (1986).
15. M. O. Speidel and R. M. Magdowski, *Stress Corrosion Cracking of Nuclear Reactor Pressure Vessel Steel in Water: Crack Initiation versus Crack Growth*, Corrosion **88**, Paper No. 283, St. Louis, MO (March 1988).
16. D. A. Hale, *The Effect of BWR Startup Environments on Crack Growth in Structural Alloys*, J. Eng. Mater. Technol. **108**, 44-49 (1986).
17. F. P. Ford and P. L. Andresen, *Stress Corrosion Cracking of Low-Alloy Pressure Vessel Steels in 288°C Water*, in Proc. 3rd Int. Atomic Energy Agency Specialists' Meeting on Subcritical Crack Growth, NUREG/CP-0112, Vol. 1, pp. 37-56 (August 1990).
18. P. M. Scott and D. R. Tice, *Stress Corrosion in Low-Alloy Steels*, Nucl. Eng. Des. **119**, 399-413 (1990).
19. T. F. Kassner, W. J. Shack, W. E. Ruther, and J. Y. Park, in *Environmentally Assisted Cracking in Light Water Reactors: Semiannual Report April-September 1990*, NUREG/CR-4667 Vol. 11, ANL-91/9, pp. 3-8 (May 1991).
20. Proceedings of EPRI Workshop on Significance and Control of Chromate in BWRs, Chicago (November 13-14, 1990).
21. W. E. Ruther, W. K. Soppet, and T. F. Kassner, in *Environmentally Assisted Cracking in Light Water Reactors: Semiannual Report April-September 1988*, NUREG/CR-4667 Vol. 7, ANL-89/40, pp. 18-29 (March 1990).
22. W. E. Ruther, W. K. Soppet, and T. F. Kassner, in *Environmentally Assisted Cracking in Light Water Reactors: Annual Report October 1983-September 1984*, NUREG/CR-4287, ANL-85-33, pp. 93-101 (June 1985).
23. W. L. Clark and A. J. Jacobs, *Effect of Radiation Environment on SCC of Austenitic Materials*, in Proc. 1st Int. Symp. Environmental Degradation of Materials in Nuclear Power Systems - Water Reactors, National Association of Corrosion Engineers, Houston, pp. 451-461 (1984).

24. F. Garzarolli, D. Alter, and P. Dewes, *Deformability of Austenitic Stainless Steels and Ni-Base Alloys in the Core of a Boiling and Pressurized Water Reactor*, in Proc. 2nd Int. Symp. Environmental Degradation of Materials in Nuclear Power Systems - Water Reactors, National Association of Corrosion Engineers, Houston, pp. 131-138 (1986).
25. F. Garzarolli, D. Alter, P. Dewes, and J. L. Nelson, *Deformability of Austenitic Stainless Steels and Ni-Base Alloys in the Core of a Boiling and Pressurized Water Reactor*, in Proc. 3rd Int. Symp. Environmental Degradation of Materials in Nuclear Power Systems - Water Reactors, G. J. Theus and J. R. Weeks, eds., The Metallurgical Society, Warrendale, PA, pp. 657-664 (1988).
26. H. Hanninen and I. Aho-Mantila, *Environment-Sensitive Cracking of Reactor Internals*, *ibid.*, pp. 77-92.
27. K. Fukuya, S. Nakahigashi, S. Ozaki, M. Teresawa, and S. Shima, *Grain Boundary Segregation of Impurity Atoms in Irradiated Austenitic Stainless Steels*, *ibid.*, pp. 665-671.
28. A. J. Jacobs, G. P. Wozaldo, K. Nakata, T. Yoshida, and I. Masaoka, *Radiation Effects on the Stress Corrosion and Other Selected Properties of Type-304 and Type-316 Stainless Steels*, *ibid.*, pp. 673-681.
29. E. P. Simonen and R. H. Jones, *Calculated Solute Segregation Kinetics Related to Irradiation Assisted Stress Corrosion Cracking*, *ibid.*, pp. 683-690.
30. A. J. Jacobs, R. E. Clausen, L. Heatherly, and R. M. Kruger, *Irradiation-Assisted Stress Corrosion Cracking and Grain Boundary Segregation in Heat-Treated Type 304 SS*, in Effects of Radiation on Materials: 14th Int. Symp., Vol. I, ASTM STP 1046, N. H. Packan, R. E. Stoller, and A. S. Kumar, eds., American Society for Testing and Materials, Philadelphia, pp. 424-436 (1989).
31. A. J. Jacobs, R. E. Clausen, M. K. Miller, and C. Shepherd, *Influence of Grain Boundary Composition on the IASCC Susceptibility of Type 304 Stainless Steel*, in Proc. 4th Int. Symp. Environmental Degradation of Materials in Nuclear Power Systems - Water Reactors, National Association of Corrosion Engineers, Houston, pp. 14-21 to 14-45 (1990).
32. C. M. Shepherd and T. M. Williams, *Simulation of Microstructural Aspects of IASCC in Water Reactor Core Components*, *ibid.*, pp. 14-11 to 14-20.
33. P. L. Andresen, F. P. Ford, S. M. Murphy, and J. M. Perks, *State of Knowledge of Radiation Effects on Environmental Cracking in Light Water Reactor Core Materials*, *ibid.*, pp. 1-83 to 1-121.
34. S. Bruemmer, L. A. Charlot, and E. P. Simonen, *Grain Boundary Chemistry Effects on Irradiation-Assisted Stress Corrosion Cracking*, Corrosion 90, Paper No. 506, Las Vegas, NV (April 1990).
35. W. J. S. Yang, *Precipitation Evolution in Type 316 Stainless Steels Irradiated in EBR-II*, in Radiation-Induced Changes in Microstructure: 13th Int. Symp., ASTM STP 955, F. A. Garner, N. H. Packan, and A. S. Kumar, eds., American Society for Testing and Materials, Philadelphia, pp. 628-646 (1987).

36. A. Strasser, J. Santucci, K. Lindquist, W. Yario, G. Stern, L. Goldstein, and L. Joseph, *Evaluation of Stainless Steel Cladding in LWRs*, EPRI NP-2642, Electric Power Research Institute, Palo Alto, CA (December 1982).
37. H. M. Chung and W. E. Ruther, in *Environmentally Assisted Cracking in Light Water Reactors: Semiannual Report, October 1989-March 1990*, NUREG/CR-4667 Vol. 10, ANL-91/5, pp. 14-17 (March 1991).
38. H. M. Chung and W. E. Ruther, in *Environmentally Assisted Cracking in Light Water Reactors: Semiannual Report, April-September 1990*, NUREG/CR-4667 Vol. 11, ANL-91/9, pp. 16-22 (April 1991).
39. H. M. Chung and W. E. Ruther, in *Environmentally Assisted Cracking in Light Water Reactors: Semiannual Report, October 1990-March 1991*, NUREG/CR-4667 Vol. 12, ANL-91/24, pp. 37-54 (August 1991).
40. M. Kodama, S. Nishimura, J. Morisawa, S. Shima, S. Suzuki, and M. Yamamoto, *Effects of Fluence and Dissolved Oxygen on IASCC in Austenitic Stainless Steels*, 5th Int. Symp. Environmental Degradation of Materials in Nuclear Power Systems - Water Reactors, National Association of Corrosion Engineers (August 1992).

### **Acknowledgments**

---

W. F. Burke, D. R. Perkins, W. K. Soppet, J. E. Sanecki, G. J. Talaber, and J. C. Tezak contributed to the experimental effort in this program. This work was conducted in programs titled "Environmentally Assisted Cracking in LWR Systems" and "Materials Studies on Service Aged Components" and sponsored by the Office of Nuclear Regulatory Research, U.S. Nuclear Regulatory Commission, under FIN Numbers A22122 and A22562; Program Managers: Drs. J. Muscara and E. Woolridge.

# Estimation of Mechanical Properties of Cast Stainless Steels during Thermal Aging in LWR Systems

O. K. Chopra

Materials and Components Technology Division  
Argonne National Laboratory  
9700 South Cass Avenue  
Argonne, Illinois 60439

The submitted manuscript has been authored by a contractor of the U.S. Government under contract No. W-31-109-ENG-38. Accordingly, the U.S. Government retains a nonexclusive, royalty-free license to publish or reproduce the published form of this contribution, or allow others to do so, for U.S. Government purposes.

## Abstract

A procedure and correlations are presented for predicting Charpy-impact energy, tensile flow stress, fracture toughness J-R curve, and  $J_{IC}$  of aged cast stainless steels from known material information. The "saturation" impact strength and fracture toughness of a specific cast stainless steel, i.e., the minimum value that would be achieved for the material after long-term service, is estimated from the chemical composition of the steel. Mechanical properties as a function of time and temperature of reactor service are estimated from impact energy and flow stress of the unaged material and the kinetics of embrittlement, which are also determined from chemical composition. The  $J_{IC}$  values are determined from the estimated J-R curve and flow stress. Examples of estimating mechanical properties of cast stainless steel components during reactor service are presented. A common "predicted lower-bound" J-R curve for cast stainless steels of unknown chemical composition is also defined for a given grade of steel, ferrite content, and temperature.

## 1 Introduction

Investigations at Argonne National Laboratory (ANL)<sup>1-4</sup> and elsewhere<sup>5-12</sup> have shown that thermal embrittlement of cast stainless steels used for components of light water reactors (LWRs), e.g., valve bodies, pump casings, and primary coolant piping, can occur during the reactor design lifetime of 40 y. Thermal aging of cast stainless steels at reactor operating temperatures, i.e., 280-320°C (536-608°F) increases hardness and tensile strength and decreases ductility, impact strength, and fracture toughness of the material. The Charpy transition curve shifts to higher temperatures. Most studies on thermal embrittlement of cast stainless steels involve simulation of end-of-life reactor conditions by accelerated aging at higher temperatures, viz., 400°C (752°F), because the time period for operation of power plants (~40 y) is far longer than can generally be considered for laboratory studies. Thus, estimates of the loss of fracture toughness of cast stainless steel components are based on an Arrhenius extrapolation of high-temperature data to reactor operating conditions.

A procedure and correlations are presented for predicting mechanical properties of cast stainless steel components during thermal aging in LWRs at 280-330°C (536-626°F). These correlations are updates of those presented earlier.<sup>13,14</sup> The present analysis focused on developing correlations for fracture properties in terms of material information in certified material test records (CMTRs) and on ensuring that the correlations are adequately

conservative for cast stainless steels defined by ASTM Specification A 351. These correlations do not consider the effect of microstructural differences that may arise from differences in production heat treatment or casting process and, therefore, may be conservative for some steels.

Mechanical properties of a specific cast stainless steel are estimated from the extent and kinetics of thermal embrittlement. The extent of thermal embrittlement is characterized by room-temperature (RT) "normalized" Charpy-impact energy (Charpy-impact energy per unit fracture area). A correlation for the extent of embrittlement at "saturation," i.e., the minimum impact energy that can be achieved for the material after long-term aging, is given in terms of chemical composition. The results indicate that Charpy-impact energy can be  $<85 \text{ J/cm}^2$  ( $<50 \text{ ft}\cdot\text{lb}$ ) for cast stainless steels with ferrite contents as low as 10%.

Extent of thermal embrittlement as a function of time and temperature of reactor service is estimated from the extent of embrittlement at saturation and from the correlations describing the kinetics of embrittlement, which are also given in terms of the chemical composition of the steel. The fracture toughness J-R curve for the material is then obtained from the correlation between fracture toughness parameters and the RT Charpy-impact energy used to characterize the extent of thermal embrittlement. A common lower-bound J-R curve for cast stainless steels of unknown chemical composition is also defined for a given material grade and temperature. In addition, correlations are presented for estimating the increase in tensile flow stress from data on the kinetics of thermal embrittlement; initial tensile flow stress of the unaged material is needed to determine the flow stress of the aged material. Fracture toughness parameters, e.g.,  $J_{IC}$  and tearing modulus, are determined from the estimated J-R curve and tensile flow stress. Examples of estimating mechanical properties of cast stainless steel components during reactor service are included.

## 2 Mechanism of Thermal Embrittlement

Thermal embrittlement of cast duplex stainless steels results in brittle fracture associated with either cleavage of the ferrite or separation of the ferrite/austenite phase boundary. The degree of thermal embrittlement is controlled by the amount of brittle fracture. Cast stainless steels with poor impact strength exhibit  $>80\%$  brittle fracture. In some cast steels, a fraction of the material may fail in brittle fashion but the surrounding austenite provides ductility and toughness. Such steels have adequate impact strength even after long-term aging. A predominantly brittle failure occurs when either the ferrite phase is continuous, e.g., in cast material with a large ferrite content, or the ferrite/austenite phase boundary provides an easy path for crack propagation, e.g., in high-C grades of cast steels that contain phase-boundary carbides. Consequently, the amount, size, and distribution of ferrite in the duplex structure and phase-boundary carbides are important parameters that control the extent of thermal embrittlement. The extent of thermal embrittlement increases with increased ferrite content. The low-C CF-3 steels are the most resistant, and the Mo-bearing, high-C CF-8M steels are the least resistant to thermal embrittlement.

Thermal aging of cast stainless steels at  $<500^\circ\text{C}$  ( $<932^\circ\text{F}$ ) leads to precipitation of additional phases in the ferrite, e.g., formation of a Cr-rich  $\alpha'$  phase by spinodal decomposition; nucleation and growth of  $\alpha'$ ; precipitation of a Ni- and Si-rich G phase,  $\text{M}_{23}\text{C}_6$ , and  $\gamma_2$  (austenite); and additional precipitation and/or growth of existing carbides at the fer-

rite/austenite phase boundaries.<sup>15-21</sup> Formation of  $\alpha'$  phase is the primary strengthening mechanism for ferrite, which increases strain-hardening and local tensile stress. Consequently, the critical stress level for brittle fracture is achieved at higher temperatures. Other precipitate phases in ferrite have little or no effect on the extent of thermal embrittlement.

Phase-boundary separation generally occurs in the high-C steels because of the presence of large  $M_{23}C_6$  carbides at the phase boundaries. For CF-8 steels, the phase-boundary carbides form during production heat treatment of the casting. Consequently, unaged CF-8 steels exhibit low lower-shelf energy and high mid-shelf Charpy transition temperature (CTT) relative to the CF-3 steels. The fracture mode for CF-8 steels in the lower-shelf or transition-temperature regime is predominantly phase-boundary separation.<sup>2-4</sup> In contrast, CF-3 steels show dimpled ductile failure. Fracture by phase-boundary separation is observed in only a few heats of unaged CF-8M steels and is dependent on whether the material contains phase-boundary carbides. Materials aged at 450°C (842°F) show significant precipitation of phase-boundary carbides (also nitrides in high-N steels) and a large decrease in ferrite content of the material.<sup>3,4</sup> At reactor temperatures, such processes either do not occur or their kinetics are extremely slow. Consequently, data obtained at 450°C aging do not reflect the mechanisms active under reactor operating conditions, and extrapolation of the 450°C data to predict the extent of thermal embrittlement at reactor temperatures is not valid.

The kinetics of thermal embrittlement of cast stainless steels are controlled primarily by the kinetics of ferrite strengthening, i.e., the size and spacing of Cr fluctuations produced by spinodal decomposition of ferrite. Small changes in the constituent elements of the material can cause the kinetics of thermal embrittlement to vary significantly. Activation energies of thermal embrittlement can range from 65 to 230 kJ/mole (15 to 55 kcal/mole). Also, the aging behavior at 400°C (752°F) shows significant heat-to-heat variation. The decrease in Charpy-impact energy during thermal aging at 400°C for various heats of cast stainless steels used in studies at ANL,<sup>3,4</sup> Georg Fischer Co. (GF),<sup>5</sup> Framatome (FRA),<sup>10</sup> and Electric Power Research Institute (EPRI)<sup>12</sup> is shown in Fig. 1. The results indicate that all materials reach a saturation impact energy, i.e., minimum value that would be achieved by the material after long-term aging. Saturation impact energy, in general, decreases with an increase in ferrite content or the concentration of C and N in the steel. As discussed above, both of these factors promote brittle fracture.

Figure 1 also indicates that the time for aging at 400°C (752°F) for a given decrease in impact energy varies more than 2 orders of magnitude for the various heats. Production heat treatment, and possibly the casting process, influence aging behavior at 400°C and, therefore, the kinetics of thermal embrittlement. The log of the aging time at 400°C for a 50% reduction in Charpy-impact energy has been shown to be a useful parameter for characterizing the kinetics of thermal embrittlement.<sup>13</sup> Activation energy for thermal embrittlement is high for steels that show fast embrittlement at 400°C, and low for those that show slow embrittlement at 400°C. Also, cast materials with high activation energy of embrittlement do not contain G phase and those with low activation energy contain G phase. It is likely that material parameters, e.g., production heat treatment, that influence the kinetics of thermal embrittlement also affect G-phase precipitation; the physical presence of G phase has little or no effect on either the extent or kinetics of embrittlement.

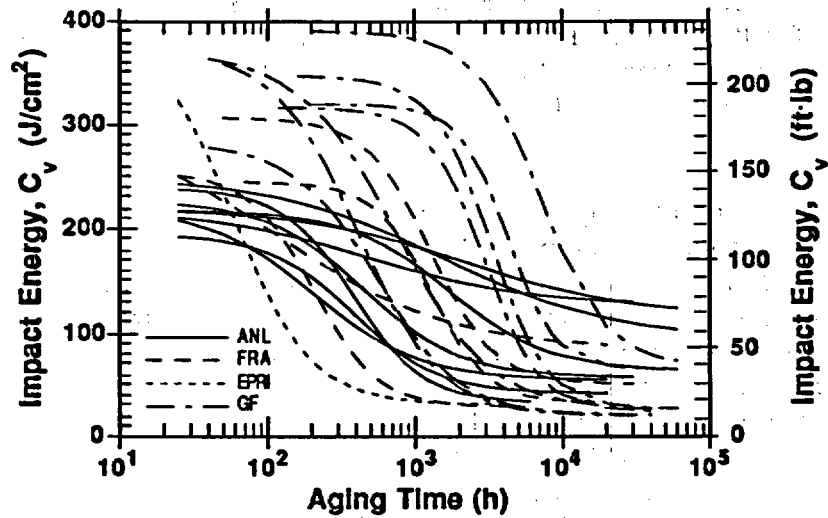


Figure 1. Decrease in Charpy-impact energy for various heats of cast stainless steels aged at 400°C

### 3 Extent of Embrittlement

Charpy-impact data obtained at RT indicate that, for a specific heat of cast stainless steel, a saturation value of minimum impact energy is reached after long-term aging. The saturation impact energy decreases with an increase in the amount of brittle fracture, i.e., in materials with large ferrite content, which provides a path for brittle fracture. An increase in the concentration of C or N in the steel also increases the extent of thermal embrittlement because of the contribution to phase-boundary carbides or nitrides and the subsequent fracture by phase-boundary separation. Furthermore, Charpy-impact data for several heats of cast stainless steel indicate that impact energy decreases with an increase in Cr content, irrespective of the ferrite content of the steel.<sup>20</sup> The concentration of Ni and Si in the steel, i.e., the elements that promote G-phase formation, also appear to increase the extent of thermal embrittlement of Mo-bearing CF-8M steels.

The variation of this saturation impact energy  $C_{Vsat}$  for different materials can be expressed in terms of a material parameter  $\Phi$  that is determined from the chemical composition and ferrite content of the materials. The ferrite content is calculated in terms of the Hull's equivalent factors<sup>22</sup>

$$Cr_{eq} = Cr + 1.21(Mo) + 0.48(Si) - 4.99 \quad (1)$$

and

$$Ni_{eq} = (Ni) + 0.11(Mn) - 0.0086(Mn)^2 + 18.4(N) + 24.5(C) + 2.77, \quad (2)$$

where chemical composition is in wt.%. The concentration of N is often not available in the CMTR; if not known, it is assumed to be 0.04 wt.%. The ferrite content  $\delta_c$  is given by

$$\delta_c = 100.3(Cr_{eq}/Ni_{eq})^2 - 170.72(Cr_{eq}/Ni_{eq}) + 74.22. \quad (3)$$

Different correlations are used to estimate the saturation impact energy of the various grades of cast stainless steel. For CF-3 and CF-8 steels, the material parameter  $\Phi$  is expressed as

$$\Phi = \delta_c(\text{Cr} + \text{Si})(\text{C} + 0.4\text{N}), \quad (4)$$

and the saturation value of RT impact energy  $\text{CV}_{\text{sat}}$  is given by

$$\log_{10}\text{CV}_{\text{sat}} = 1.15 + 1.36\exp(-0.035\Phi). \quad (5)$$

For the Mo-bearing CF-8M steels, the material parameter  $\Phi$  is expressed as

$$\Phi = \delta_c(\text{Ni} + \text{Si} + \text{Mn})^2(\text{C} + 0.4\text{N})/5. \quad (6)$$

The saturation value of RT impact energy  $\text{CV}_{\text{sat}}$  for steels with < 10% Ni is given by

$$\log_{10}\text{CV}_{\text{sat}} = 1.10 + 2.12\exp(-0.041\Phi), \quad (7)$$

and for steels with >10% Ni by

$$\log_{10}\text{CV}_{\text{sat}} = 1.10 + 2.64\exp(-0.064\Phi). \quad (8)$$

The N content in Eqs. 4 and 6 can be assumed to be 0.04 wt.% if the value is not known. The RT saturation impact energy can also be estimated directly from the chemical composition of the steel without the introduction of the  $\phi$  parameter. For CF-3 and CF-8 steels,  $\text{CV}_{\text{sat}}$  (J/cm<sup>2</sup>) is given by

$$\log_{10}\text{CV}_{\text{sat}} = 5.64 - 0.006\delta_c - 0.185\text{Cr} + 0.273\text{Mo} - 0.204\text{Si} + 0.044\text{Ni} - 2.12(\text{C} + 0.4\text{N}), \quad (9)$$

and for CF-8M steels by

$$\log_{10}\text{CV}_{\text{sat}} = 7.28 - 0.011\delta_c - 0.185\text{Cr} - 0.369\text{Mo} - 0.451\text{Si} - 0.007\text{Ni} - 4.71(\text{C} + 0.4\text{N}). \quad (10)$$

The saturation impact energy for a specific cast stainless steel should be determined using both the methods given in Eqs. 4-10, and the lower value used for estimating mechanical properties.

The saturation values of RT impact energy for CF-3 and CF-8 steels predicted by Eqs. 4 and 5 and those observed experimentally at ANL,<sup>3,4</sup> GF,<sup>5</sup> FRA,<sup>10</sup> EPRI,<sup>12</sup> Electricité de France (EdF),<sup>7</sup> and Central Electricity Generation Board (CEGB)<sup>8,9</sup> are shown in Fig. 2a. The chemical composition, ferrite content, and saturation RT Charpy-impact energy of the materials from ANL, GF, FRA, Westinghouse (WH), and EPRI are given in Table 1. The difference between the predicted and observed values is  $\pm 15\%$  for most of the materials. The observed RT impact energy at saturation and the values predicted by Eqs. 6-8 for CF-8M steels are shown in Figs. 2b and 2c for the data from ANL,<sup>3,4</sup> GF,<sup>5</sup> WH,<sup>6</sup> EdF,<sup>7</sup> and FRA<sup>10</sup> studies. The difference between observed and predicted values for the CF-8M steel is larger than that for the CF-3 or CF-8 steels. The correlations expressed in Eqs. 4-10 do not include Nb, and may not be conservative for Nb-bearing steels.

Table 1. Chemical composition, ferrite content, and kinetics of thermal embrittlement for various heats of cast stainless steels

Heat	Chemical Composition (wt.%)							Ferrite (%)		C <sub>Vsat</sub> (J/cm <sup>2</sup> )	Constants			Q (kJ/mole)
	Cr	Mo	Si	Ni	Mn	C	N	Calc.	Meas.		β	θ	α	
<b>Argonne</b>														
52	19.49	0.35	0.92	9.40	0.57	0.009	0.052	10.3	13.5	161.8	-	-	-	-
51	20.13	0.32	0.86	9.06	0.63	0.010	0.058	14.3	18.0	115.9	0.139	3.53	1.15	204.7
47	19.81	0.59	1.06	10.63	0.60	0.018	0.028	8.4	16.3	163.7	0.069	2.29	1.20	195.7
P2	20.20	0.16	0.94	9.38	0.74	0.019	0.040	12.5	15.6	141.3	0.258	2.83	1.09	218.6
I	20.20	0.45	0.83	8.70	0.47	0.019	0.032	20.4	17.1	134.3	0.094	2.10	1.00	250.0
69	20.18	0.34	1.13	8.59	0.63	0.023	0.028	21.0	23.6	76.7	0.214	3.21	1.07	175.9
P1	20.49	0.04	1.12	8.10	0.59	0.036	0.057	17.6	24.1	53.7	0.305	2.57	0.75	252.7
61	20.65	0.32	1.01	8.86	0.65	0.054	0.080	10.0	13.1	93.3	0.214	3.48	1.20	197.8
59	20.33	0.32	1.08	9.34	0.60	0.062	0.045	8.8	13.5	89.1	0.197	3.14	1.20	249.4
68	20.64	0.31	1.07	8.08	0.64	0.063	0.062	14.9	23.4	47.1	0.301	2.88	0.68	161.1
60	21.05	0.31	0.95	8.34	0.67	0.064	0.058	15.4	21.1	44.8	0.291	2.89	0.88	210.9
56	19.65	0.34	1.05	9.28	0.57	0.066	0.030	7.3	10.1	117.6	-	-	-	-
74	19.11	2.51	0.73	9.03	0.54	0.064	0.048	15.5	18.4	63.1	0.269	3.44	0.70	95.0
75	20.86	2.58	0.67	9.12	0.53	0.065	0.052	24.8	27.8	32.1	0.436	2.82	0.51	139.0
66	19.45	2.39	0.49	9.28	0.60	0.047	0.029	19.6	19.8	87.9	0.208	3.16	1.57	163.9
64	20.76	2.46	0.63	9.40	0.60	0.038	0.038	29.0	28.4	41.1	0.338	2.81	0.60	147.3
65	20.78	2.57	0.48	9.63	0.50	0.049	0.064	20.9	23.4	59.7	0.260	2.99	0.59	153.8
P4	19.64	2.05	1.02	10.00	1.07	0.040	0.151	5.9	10.0	62.7	0.289	2.70	0.62	158.7
63	19.37	2.57	0.58	11.85	0.61	0.055	0.031	6.4	10.4	126.5	0.119	2.83	1.11	155.5
<b>Georg Fischer Co.</b>														
284	23.00	0.17	0.52	8.23	0.28	0.025	0.037	43.6	42.0	23.8	0.560	3.71	0.41	87.4
280	21.60	0.25	1.37	8.00	0.50	0.028	0.038	36.3	38.0	24.4	0.591	3.30	0.73	86.7
282	22.50	0.15	0.35	8.53	0.43	0.035	0.040	29.7	38.0	30.2	0.525	3.73	0.43	97.8
281	23.10	0.17	0.45	8.60	0.41	0.036	0.053	31.4	30.0	28.6	0.560	3.76	0.42	92.6
283	22.60	0.23	0.53	7.88	0.48	0.036	0.032	42.6	42.0	23.8	0.580	3.65	0.43	82.9
278	20.20	0.13	1.00	8.27	0.28	0.038	0.030	18.5	15.0	67.6	0.381	4.05	0.47	62.7
279	22.00	0.22	1.36	7.85	0.37	0.040	0.032	39.5	40.0	23.8	0.586	3.21	0.69	91.8
277	20.50	0.06	1.81	8.13	0.54	0.052	0.019	22.5	28.0	33.9	0.488	3.65	0.55	87.7
291	19.60	0.66	1.59	10.60	0.28	0.065	0.054	4.2	6.0	123.0	0.235	3.89	0.79	77.5
292	21.60	0.13	1.57	7.52	0.34	0.090	0.039	23.9	28.0	22.4	0.392	3.08	0.46	99.3
290	20.00	2.40	1.51	8.30	0.41	0.054	0.050	31.3	32.0	21.1	0.602	3.49	0.11	81.0
288	19.60	2.53	1.70	8.40	0.47	0.052	0.022	35.6	28.0	19.4	0.643	3.02	0.64	106.1
287	20.50	2.58	0.51	8.46	0.50	0.047	0.033	37.2	38.0	23.8	0.563	3.52	0.42	91.6
286	20.20	2.44	1.33	9.13	0.40	0.072	0.062	18.9	22.0	20.5	0.571	3.11	0.62	105.5
289	19.70	2.30	1.44	8.25	0.48	0.091	0.032	22.6	30.0	20.9	0.571	3.32	0.39	90.4
285	18.80	2.35	0.86	9.49	0.48	0.047	0.039	14.0	10.0	64.3	0.347	3.76	0.34	82.0
<b>Framatome</b>														
A	18.90	0.10	0.99	8.90	1.14	0.021	0.074	6.0	6.3	166.0	0.090	3.44	0.20	111.7
E	21.04	0.08	0.54	8.47	0.80	0.035	0.051	17.6	16.5	45.7	0.334	2.63	0.65	132.9
F	19.72	0.34	1.16	8.33	0.26	0.038	0.026	17.7	12.0	83.2	0.282	2.45	1.23	176.2
C	20.73	0.13	1.09	8.19	0.91	0.042	0.035	20.9	20.1	51.1	0.393	3.30	0.45	83.1
G	20.65	0.02	1.03	8.08	0.74	0.040	0.073	15.3	17.0	62.5	-	-	-	-
H	20.70	0.05	1.18	8.07	0.71	0.050	0.045	18.3	21.5	50.6	-	-	-	-
D	19.15	2.50	0.94	10.32	1.12	0.026	0.063	12.2	13.9	33.0	0.439	3.30	0.40	99.7
I	19.36	2.40	0.98	10.69	0.70	0.020	0.039	14.1	15.5	150.7	-	-	-	-
K	20.80	2.62	0.75	10.45	1.09	0.060	0.056	15.4	14.0	48.5	-	-	-	-
L	20.76	2.48	0.81	10.56	0.79	0.040	0.042	18.6	19.0	30.4	-	3.00	-	-
B	20.12	2.52	0.93	10.56	0.83	0.053	0.042	14.0	17.3	28.2	0.478	2.55	0.47	128.6
<b>Westinghouse</b>														
C1488	20.95	2.63	0.53	9.48	1.02	0.061	0.056	22.1	14.0	53.1	-	2.80	-	-
<b>Electric Power Research Institute</b>														
EPRI	22.04	0.23	0.84	7.93	0.74	0.030	0.045	36.0	32.0	30.0	0.564	2.10	0.60	-

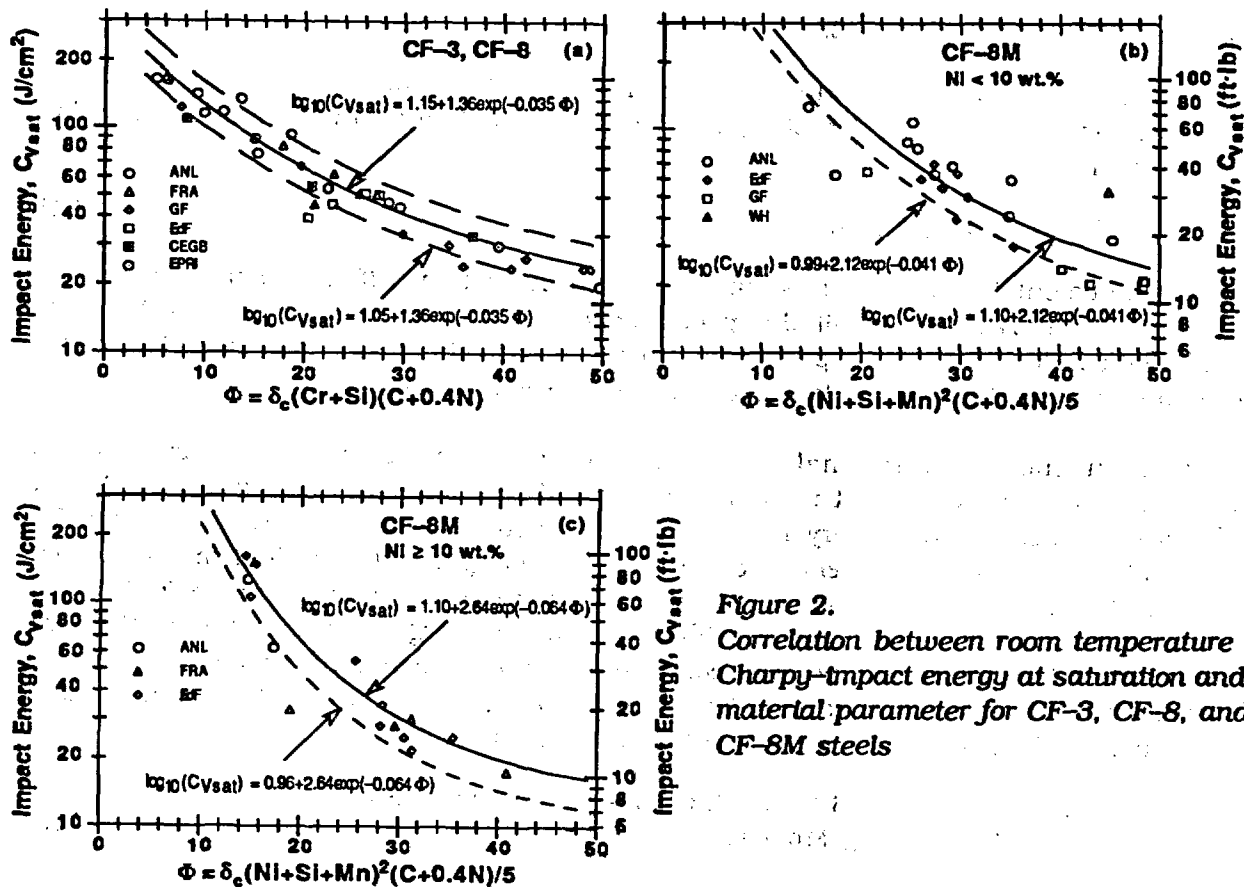


Figure 2. Correlation between room temperature Charpy-impact energy at saturation and material parameter for CF-3, CF-8, and CF-8M steels

#### 4 Kinetics of Embrittlement

Room-temperature impact energy as a function of time and temperature of aging is estimated from the RT saturation impact energy  $C_{v_{sat}}$  ( $J/cm^2$ ) and the kinetics of embrittlement. The decrease in RT Charpy-impact energy  $C_v$  ( $J/cm^2$ ) with time is expressed as

$$\log_{10} C_v = \log_{10} C_{v_{sat}} + \beta [1 - \tanh [(P - \theta)/\alpha]], \quad (11)$$

where  $\beta$  is half the maximum change in  $\log C_v$ ,  $\theta$  is the log of the time at 400°C (752°F) to achieve 50% reduction in impact energy, and  $\alpha$  is a shape factor. The aging parameter  $P$  is the log of the aging time for a specific degree of embrittlement and is defined by

$$P = \log_{10}[t] - \frac{1000Q}{19.143} \left[ \frac{1}{T_s + 273} - \frac{1}{673} \right], \quad (12)$$

where  $Q$  is the activation energy (kJ/mole) and  $t$  and  $T_s$  are the time (h) and temperature (°C) of aging. Equation 12 assumes aging at 400°C as the baseline aging behavior for the material and parameter  $P$  is the log of the aging time at 400°C. The data obtained at 450°C (842°F) aging are not representative of reactor operating conditions; therefore, they were excluded from the analysis. The values of the constants in Eqs. 10 and 11 for the various materials are given in Table 1. The constant  $\beta$  is defined in terms of the initial impact energy of the unaged material  $C_{v_{int}}$  and the saturation impact energy  $C_{v_{sat}}$ , thus

$$\beta = (\log_{10}C_{Vint} - \log_{10}C_{Vsat})/2. \quad (13)$$

Examination of the data for the kinetics of thermal embrittlement suggests that the shape factor  $\alpha$  increases linearly with  $\log_{10}C_{Vsat}$ . A best fit of the data for the various heats yields the expression

$$\alpha = -0.585 + 0.795\log_{10}C_{Vsat}. \quad (14)$$

$C_{Vsat}$  can be calculated from correlations presented in Section 3 if the chemical composition is known. In practice, the initial impact energy is unlikely to be available. Mechanical-property data indicate that Charpy-impact energy of cast stainless steels is typically  $200 \pm 20$  J/cm<sup>2</sup>, however, it can be as low as 60 J/cm<sup>2</sup> for some steels.<sup>4,14</sup>

Activation energy for thermal embrittlement has been expressed in terms of the chemical composition of the cast material. The initial correlations proposed by FRA<sup>10</sup> and ANL<sup>3,4</sup> were either based on very limited data or failed to accurately predict the results from various investigations. A general correlation that is applicable for all chemical compositions within ASTM Specification A 351 and valid for the temperature range 280–400°C (536–752°F) has recently been proposed.<sup>13,14</sup> Activation energy for thermal embrittlement is expressed in terms of both chemical composition and the constant  $\theta$ , which appears to account for the effects of heat treatment and the casting process on the kinetics of thermal embrittlement. The activation energy  $Q$  (kJ/mole) is given by

$$Q = 10 [74.06 - (7.66 - 0.46 I_1) \theta - 4.35 \text{ Si} + 1.38 I_2 \text{ Mo} - 1.67 \text{ Cr} - (2.22 + 3.56 I_1) \text{ Mn} + (108.8 - 75.3 I_1) \text{ N}], \quad (15)$$

where the indicators  $I_1 = 0$  and  $I_2 = 1$  for CF-3 or CF-8 steels and assume the values of 1 and 0, respectively, for CF-8M steels. The ANL data, included in the analysis for obtaining Eq. 15, were based on heats that were aged up to 30,000 h at 290–400°C (554–752°F). Also, the data at 290°C were excluded from the analysis for some of the heats. Equation 15 has been optimized using recent ANL data on materials that were aged up to 58,000 h at 290–400°C. The activation energies and values of the constants in Eq. 11 are given in Table 1. The best fit of the data from ANL, FRA, GF, EdF, and CEGB studies (47 heats) yields the expression

$$Q = 10 [74.52 - 7.20 \theta - 3.46 \text{ Si} - 1.78 \text{ Cr} - 4.35 I_1 \text{ Mn} + (148 - 125 I_1) \text{ N} - 61 I_2 \text{ C}], \quad (16)$$

where the indicators have the same meaning as in Eq. 15. The contribution of Mo and Mn to the kinetics of CF-3 and CF-8 steel is very small; therefore, it is excluded from Eq. 16. For CF-3 and CF-8 steels, the effect of C is included in the new expression.

The estimated and observed values of  $Q$  for the ANL, FRA, CEGB, and GF heats are plotted in Fig. 3. The predicted values are within the 95% confidence limits for all the heats. Equation 16 is applicable for compositions within ASTM Specification A 351, with an upper limit of 1.2 wt.% for Mn content. Actual Mn content is used up to 1.2 wt.% and is assumed to be 1.2 wt.% for steels containing >1.2 wt.% Mn. Furthermore, the values of  $Q$  predicted from Eq. 16 should be between 65 kJ/mole minimum and 250 kJ/mole maximum;  $Q$  is assumed to be 65 kJ/mole if the predicted values are lower and 250 kJ/mole if the predicted values are higher.

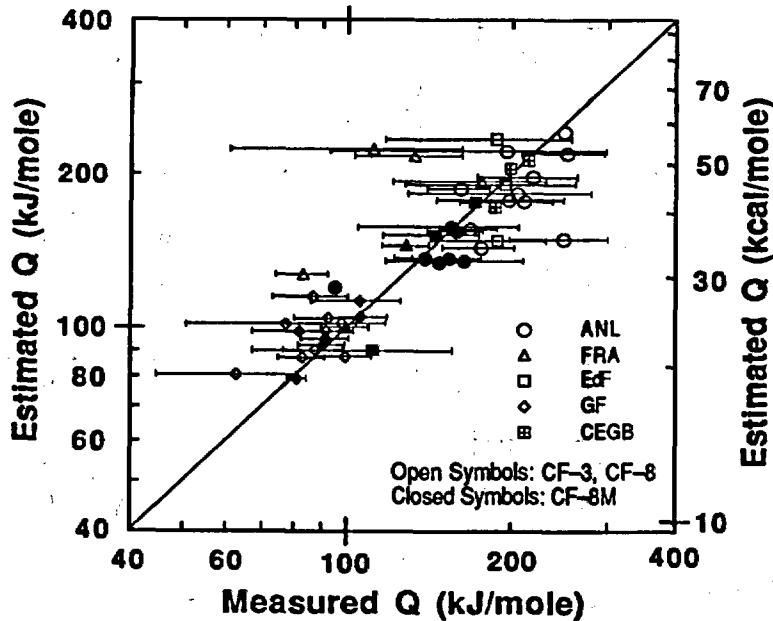


Figure 3. Observed and estimated activation energy for thermal embrittlement of cast stainless steels

## 5 Estimation of Impact Energy

The RT Charpy impact energy of a specific cast stainless steel can be estimated from the correlations in Sections 3 and 4. Impact energy at saturation  $Cv_{sat}$  is determined from the chemical composition of the cast material. Estimation of the decrease in impact energy as a function of time and temperature of service requires additional information, namely, the initial impact energy of the unaged material and the aging behavior at 400°C (752°F), i.e., the value of the constant  $\theta$ . However, parametric studies indicate that at 280–330°C (536–626°F) the aging response is relatively insensitive to the value of  $\theta$ . Varying  $\theta$  between 2.1 and 3.6 results in almost identical aging behavior at 300°C (572°F) and differences in aging behavior at 280–330°C are minimal. A median value of 2.9 for  $\theta$  can be used in Eqs. 7 and 9 to estimate impact energy of cast stainless steel components in service at 280–330°C.

The RT Charpy-impact energy observed experimentally and that estimated from the chemical composition and initial impact energy of some of the ANL, FRA, and GF heats aged at temperatures between 290–350°C (554–662°F), are shown in Figs. 4 and 5. Estimated values for each heat were calculated as follows. The impact energy at saturation was determined from Eqs. 1–10. The activation energy for embrittlement was obtained from Eq. 16; a  $\theta$  value of 2.9 was used for all the heats. Then the change in impact energy with time and temperature of service was estimated from Eqs. 11–14. The estimated change in impact energy at temperatures  $\leq 330^\circ\text{C}$  (626°F) is either accurate or slightly conservative for most of the heats. As discussed above, a value of 2.9 for  $\theta$  can be used to estimate thermal embrittlement at service temperatures of 280–330°C (536–626°F). With an assumed value of 2.9 for  $\theta$ , estimations of impact energies before saturation will be non-conservative at service temperatures  $>330^\circ\text{C}$  for heats with  $\theta < 2.9$  and at temperatures  $<280^\circ\text{C}$  for heats

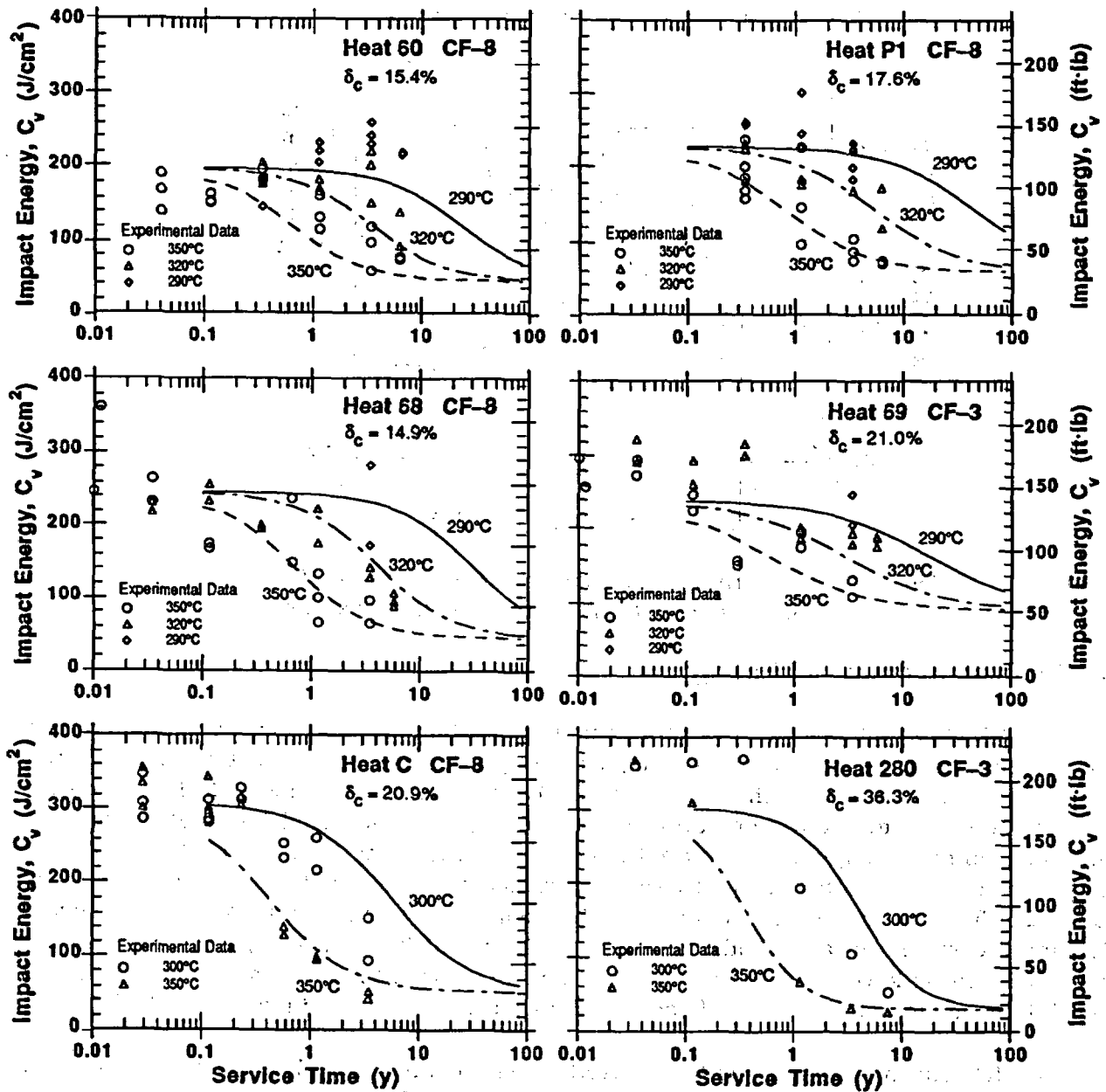


Figure 4. Room temperature Charpy-impact energy for aged CF-3 and CF-8 steels observed experimentally and that estimated from the composition and initial impact energy of the materials from ANL (Heats 60, 68, 69, and P1), FRA (Heat C), and GF (Heat 280) studies.  $\delta_c$  is the calculated ferrite content.

with  $\theta > 2.9$ . A value of 2.5 should be used for estimations at temperatures between 330 and 360°C (626 and 680°F) and a value of 3.3 should be used for estimations at temperatures <280°C (<536°F). Even at 350°C, the estimated impact energies (Figs. 4 and 5) show good agreement with the experimental results because the  $\theta$  values for the heats shown in the figures are either greater or only slightly lower than 2.9.

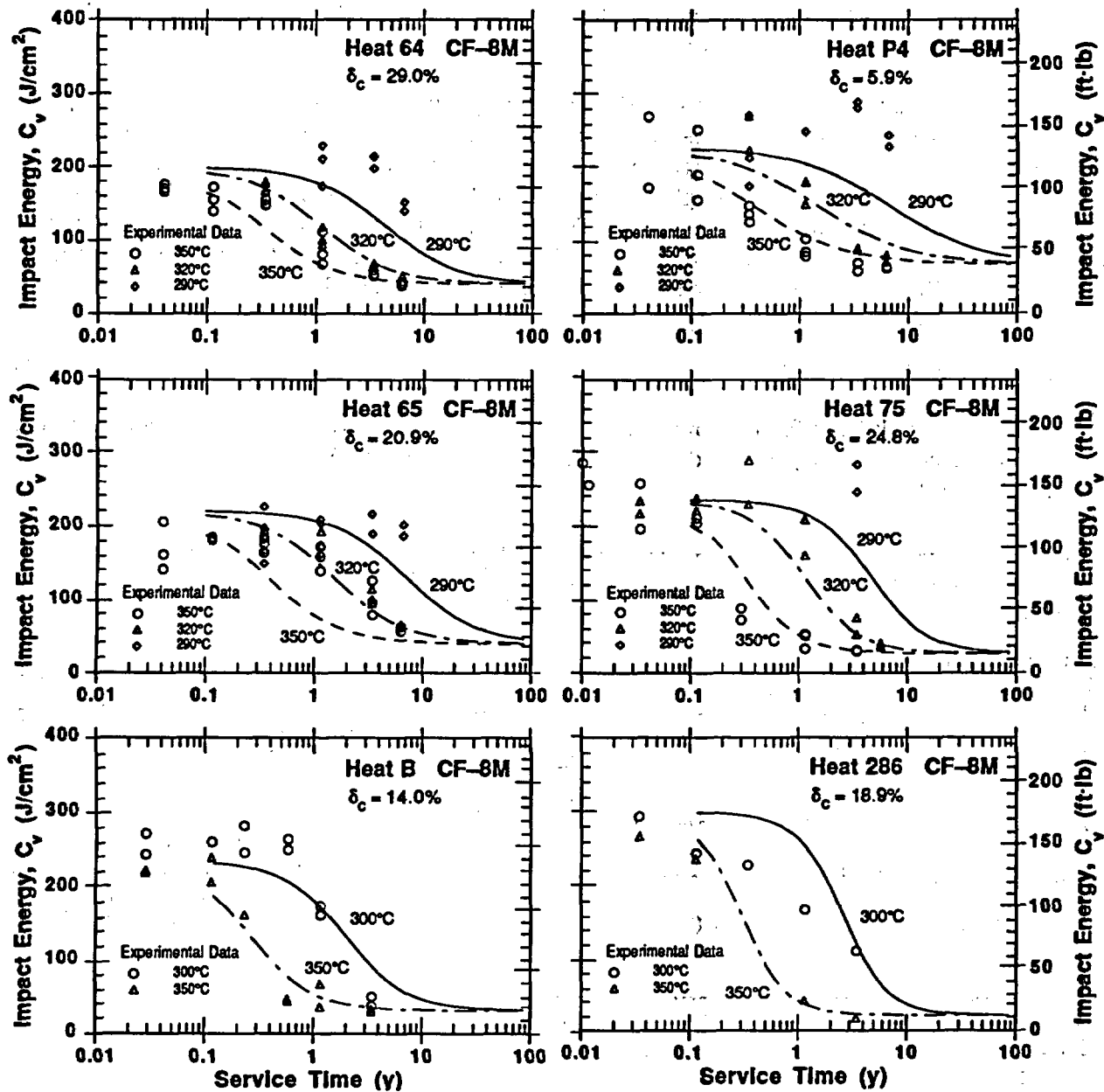


Figure 5. Room temperature Charpy-impact energy for aged CF-8M steels observed experimentally and that estimated from the composition and initial impact energy of the material from ANL (Heats 64, 65, 75, and P4), FRA (Heat B), and GF (Heat 286) studies.  $\delta_c$  is the calculated ferrite content.

## 6 Tensile Properties

Thermal aging leads to an increase in yield and ultimate stress and a slight decrease in ductility. For all heats, the increase in ultimate stress is substantially greater than the increase in yield stress. Some heats show no change in yield stress. Furthermore, specimens

aged for short times at high temperatures, e.g., ~3,000 h at 400 or 450°C (752 or 842°F), often show a decrease in yield and ultimate stresses.

The tensile data generally agree with the Charpy-impact data, i.e., for a specific heat, the increase in tensile stress corresponds to a decrease in impact energy. The ratio of the tensile flow stress of aged and unaged cast stainless steels at RT and 290°C (554°F) is plotted as a function of a normalized aging parameter in Figs. 6 and 7, respectively. Flow stress is characterized as the mean of the 0.2% yield and ultimate stresses, and the aging parameter is normalized with respect to a  $\theta$  value of 2.9. At both temperatures, the increase in flow stress of CF-3 steels is the lowest and that of CF-8M steels the largest. The flow stress ratio  $R = (\sigma_{\text{aged}}/\sigma_{\text{unaged}})$  is given by

$$R = a_1 + b_1(P - \theta + 2.9). \quad (17)$$

Equation 17 is valid for ferrite contents >7% and R values between 1 and a constant  $c_1$ . Values of the constants  $a_1$ ,  $b_1$ , and  $c_1$  for different grades of steel and test temperatures are given in Table 2.

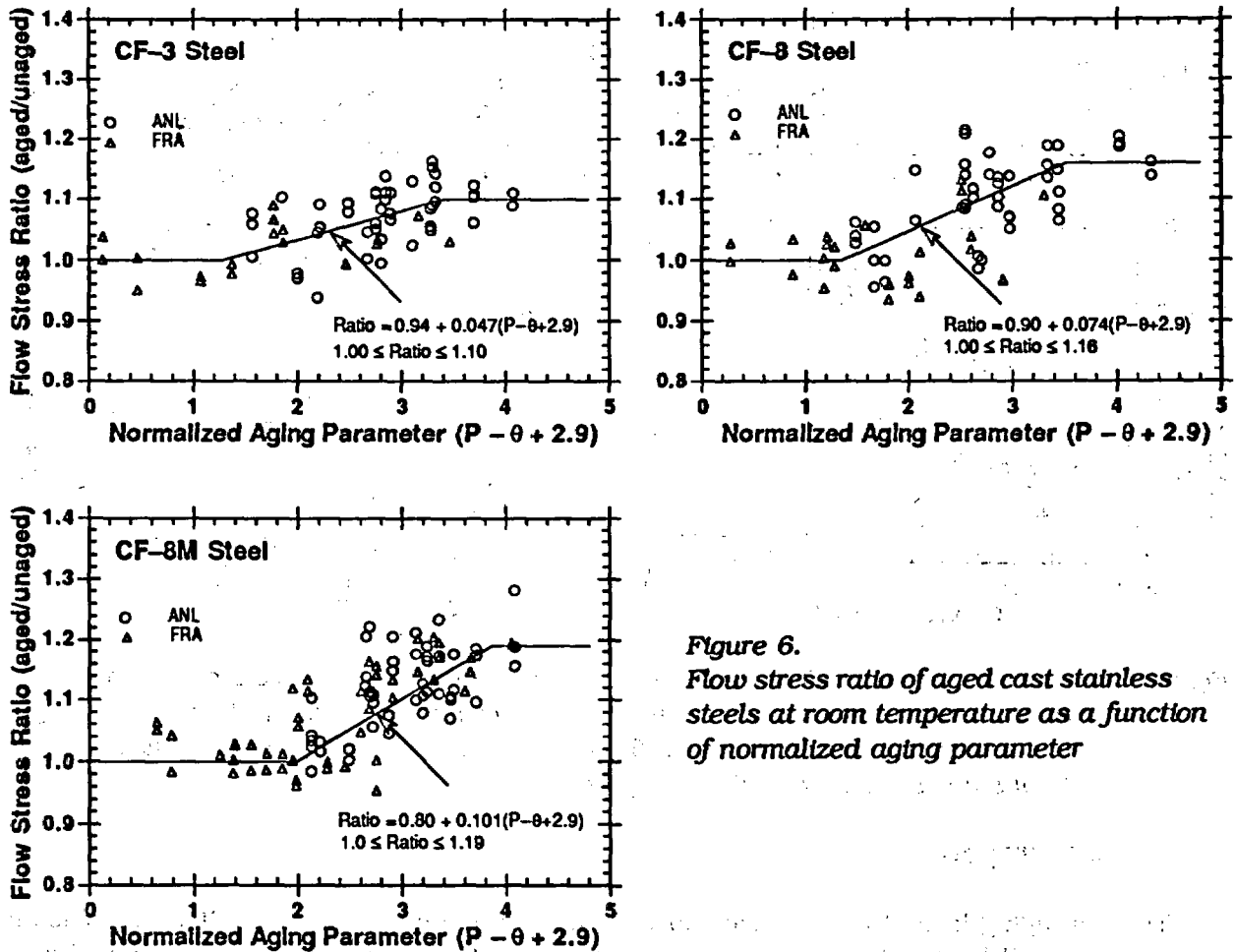


Figure 6. Flow stress ratio of aged cast stainless steels at room temperature as a function of normalized aging parameter

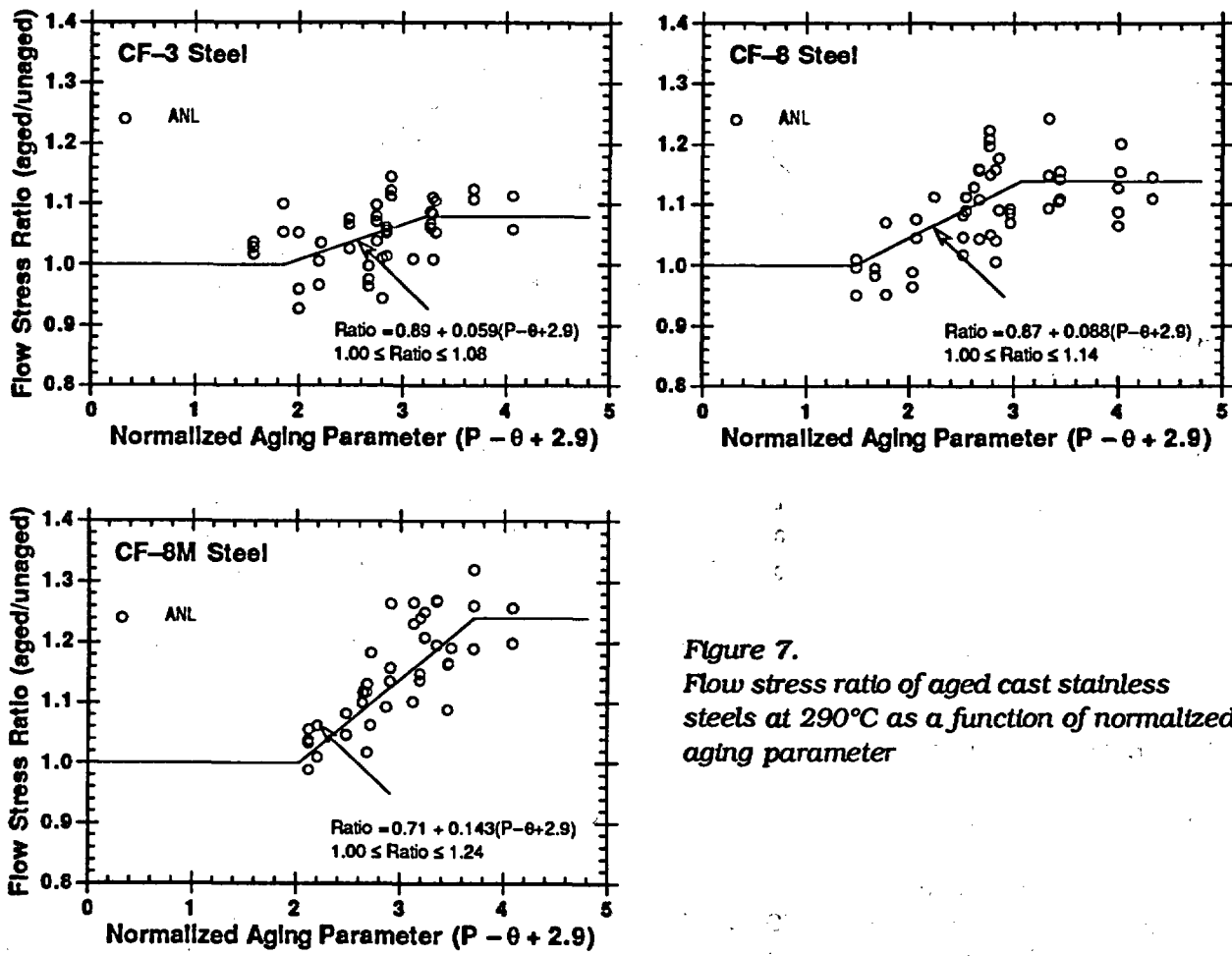


Figure 7. Flow stress ratio of aged cast stainless steels at 290°C as a function of normalized aging parameter

Table 2. Values of the constants in Eq. 17 for estimating tensile flow stress of aged cast stainless steels

Grade	Room Temp.			290-320°C		
	a <sub>1</sub>	b <sub>1</sub>	c <sub>1</sub>	a <sub>1</sub>	b <sub>1</sub>	c <sub>1</sub>
CF-3	0.94	0.047	1.10	0.89	0.059	1.08
CF-8	0.90	0.074	1.16	0.87	0.088	1.14
CF-8M	0.80	0.101	1.19	0.71	0.143	1.24

Experimental and estimated tensile flow stress at 290°C (554°F) and at RT for various heats of aged cast stainless steel are shown in Fig. 8. For each heat, the aging parameter was obtained from Eqs. 12 and 16; because most of the data are for aging temperatures ≥350°C, the actual experimental value of θ was used for all the heats. Tensile flow stress was then estimated from Eq. 17 and the initial flow stress of the materials. The estimated values are within 15% of the observed value for most material and aging conditions.

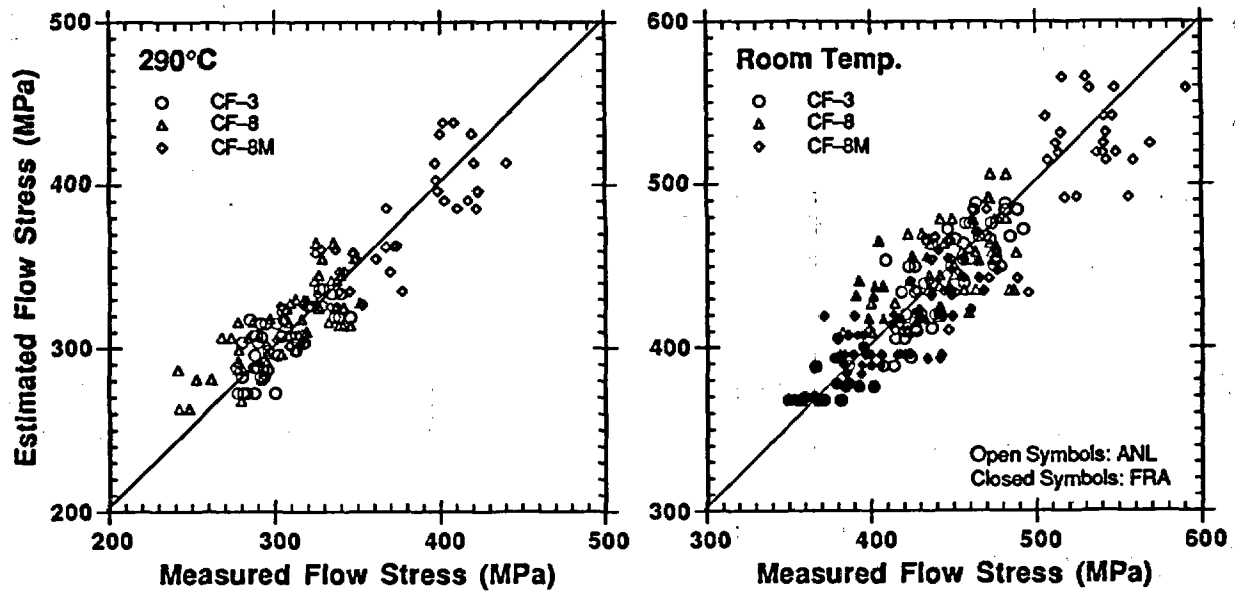


Figure 8. Observed and estimated flow stress of aged cast stainless steel at 290°C and room temperature

## 7 Fracture Toughness

### Estimation of J-R Curves

Thermal aging decreases the fracture toughness of cast stainless steels at RT as well as at reactor temperatures, i.e., 280–320°C (536–608°F). The fracture toughness results are consistent with the Charpy-impact data, i.e., unaged and aged materials that show low impact strength also exhibit lower fracture toughness. The fracture toughness J-R curve for a specific cast stainless steel can be estimated from its RT impact energy.

The J-R curve is expressed by the power-law relation  $J_d = C\Delta a^n$ , where  $J_d$  is deformation J (kJ/m<sup>2</sup>) per ASTM Specifications E 813-85 and E 1152-87,  $\Delta a$  is crack extension (mm), and C and n, respectively, are the coefficient and exponent of the power-law J-R curve. The coefficient C at room and reactor temperatures and the RT Charpy-impact energy for aged and unaged cast stainless steels are plotted in Fig. 9. Fracture toughness data from ANL, FRA,<sup>10,11</sup> EPRI,<sup>12</sup> Materials Engineering Associates, Inc., (MEA),<sup>23</sup> and The Welding Institute (TWI),<sup>24</sup> studies are included in the figure. At both temperatures, the coefficient C decreased with a decrease in impact energy. Separate correlations were obtained for CF-3 or CF-8 steels and for CF-8M steels; the latter showed a larger decrease in fracture toughness for a given impact energy. The correlations used to estimate J-R curves for static-cast materials were obtained by subtracting the value of  $\sigma$  (standard deviation for the fit to the data) from the best-fit curve. They are shown as dash lines in Fig. 9, and help ensure that the estimated J-R curve is conservative for all material and aging conditions. Best-fit correlations were used for centrifugally cast materials. The saturation fracture toughness J-R curve at RT for static-cast CF-3 and CF-8 steels is given by

$$J_d = 49[C_V]^{0.52}[\Delta a]^n, \quad (18)$$

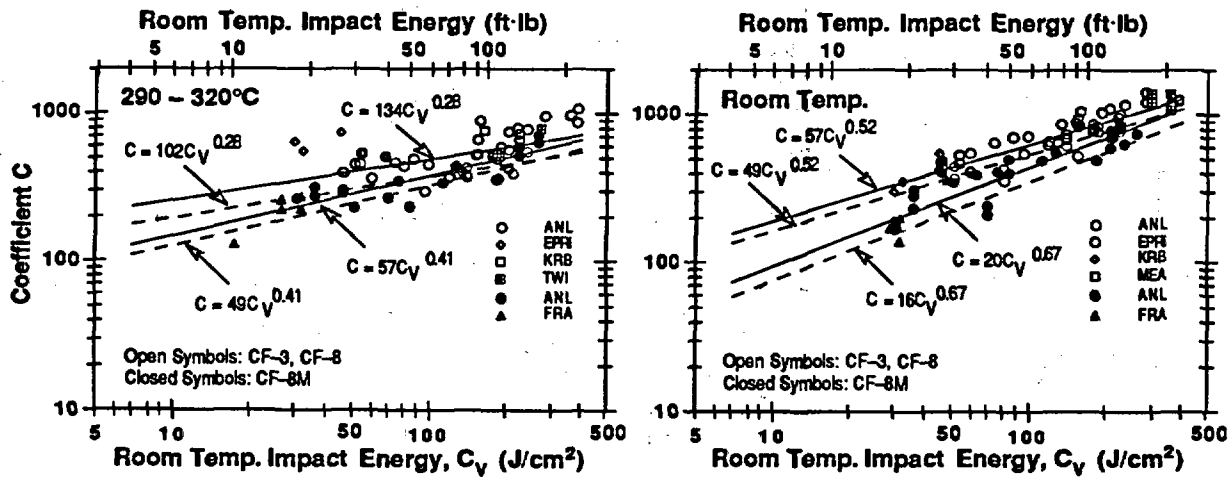


Figure 9. Correlation between RT Charpy-impact energy and coefficient C for cast stainless steel at 290–320°C and at room temperature. The solid and dashed lines represent the correlations used to estimate the J-R curves for centrifugally and static-cast materials, respectively.

and for static-cast CF-8M steels by

$$J_d = 16[C_V]^{0.67}[\Delta a]^n \quad (19)$$

At 290–320°C (554–608°F), the J-R curve for static cast CF-8 steels is given by

$$J_d = 102[C_V]^{0.28}[\Delta a]^n \quad (20)$$

and for static-cast CF-8M steels by

$$J_d = 49[C_V]^{0.41}[\Delta a]^n \quad (21)$$

For centrifugally cast steels, the constants in Eqs. 18–21 are 57, 20, 134, and 57, respectively. At RT, the exponent n for static- or centrifugally cast steels is given by

$$n = a_2 + b_2 \log_{10} C_V \quad (22)$$

where the values of the constants  $a_2$  and  $b_2$  for different grades of steel and test temperature are given in Table 3. J-R curve at any intermediate temperature can be linearly interpolated from the estimated values of C and n at RT and at 290°C (554°F).

The fracture toughness J-R curve at saturation for a specific cast stainless steel can be obtained from its chemical composition by using the correlations for  $C_{V_{sat}}$  given in Eqs. 1–10 and then using the estimated  $C_{V_{sat}}$  in Eqs. 18–22 to obtain the J-R curve. Comparisons of the experimental and estimated J-R curves at saturation, i.e., the minimum fracture toughness that would be achieved for the material by thermal aging, are shown in Figs. 10–12. For most heats, the saturation fracture toughness is achieved after aging for  $\geq 5,000$  h at 400°C (752°F). The experimental and estimated J-R curves for the unaged materials are also shown for comparison; the J-R curves were estimated from Eqs. 18–22 by using the measured initial RT impact energy  $C_{V_{int}}$ . The estimated J-R curves show good agreement

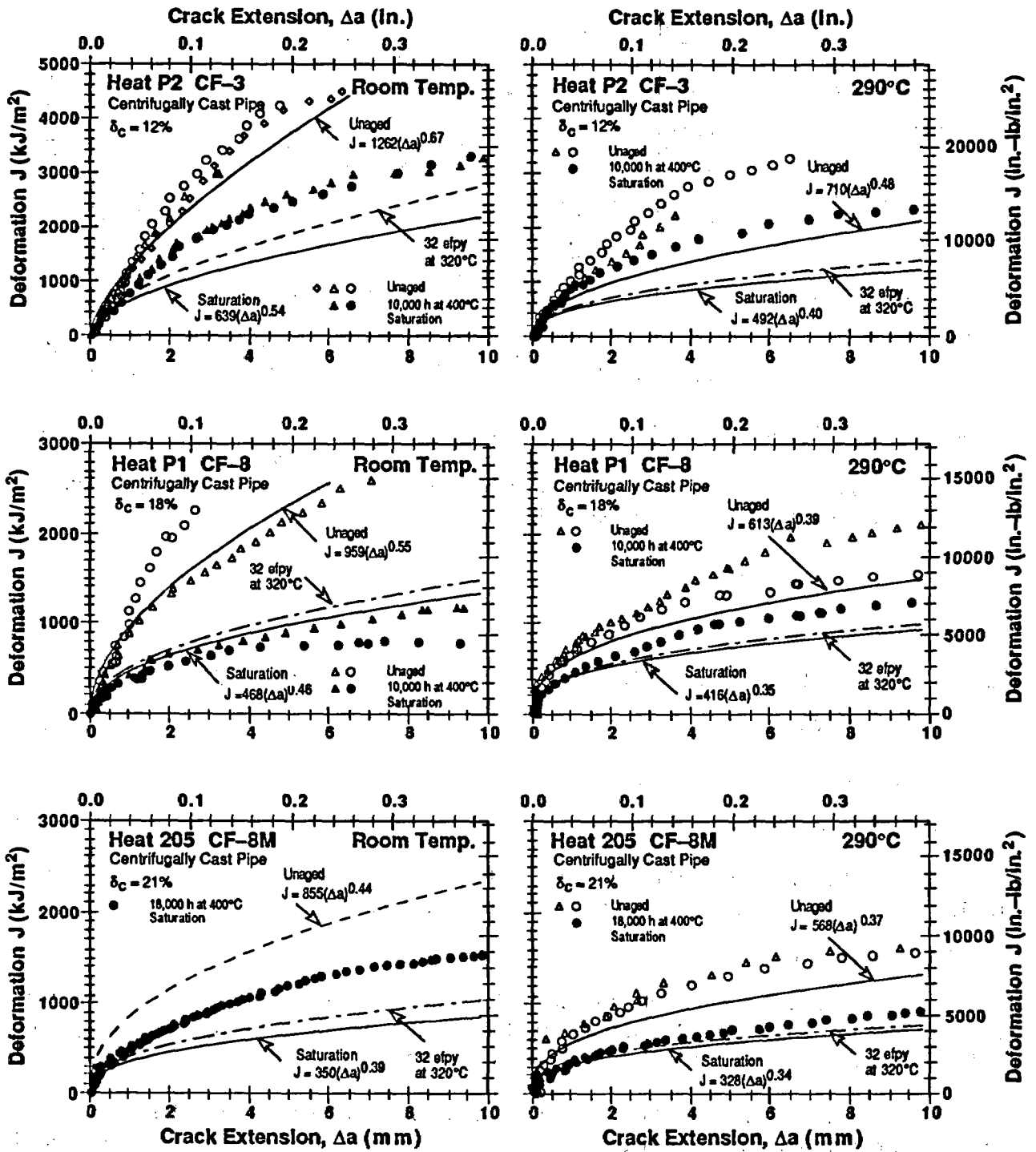


Figure 10. Saturation fracture toughness J-R curves at RT and 290°C estimated from the chemical composition of centrifugally cast CF-3, CF-8, and CF-8M pipes, and determined experimentally.  $\delta_c$  is the calculated ferrite content.

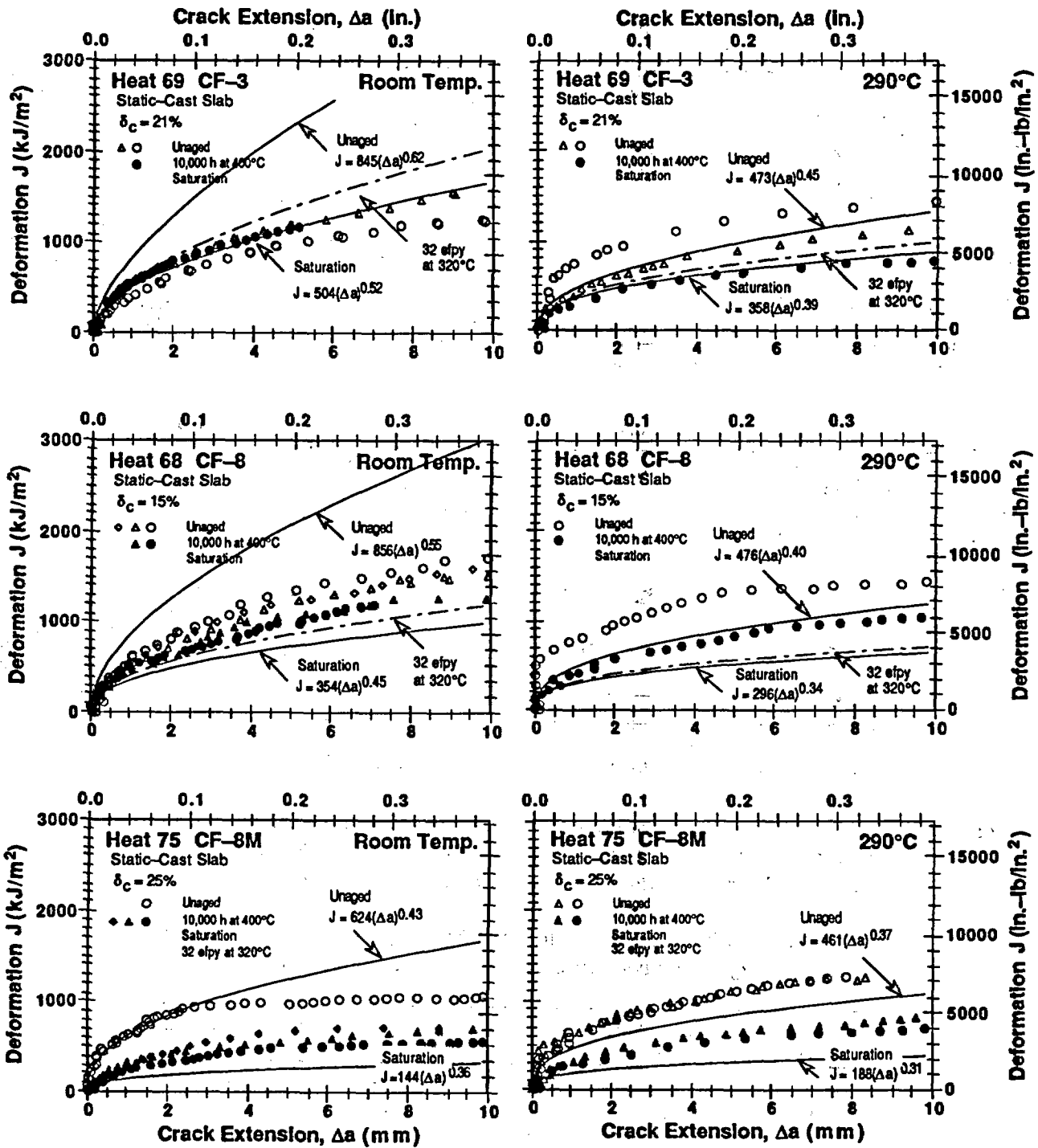


Figure 11. Saturation fracture toughness J-R curves at RT and 290°C estimated from the chemical composition of static-cast CF-3, CF-8, and CF-8M slabs, and determined experimentally.  $\delta_c$  is the calculated ferrite content.

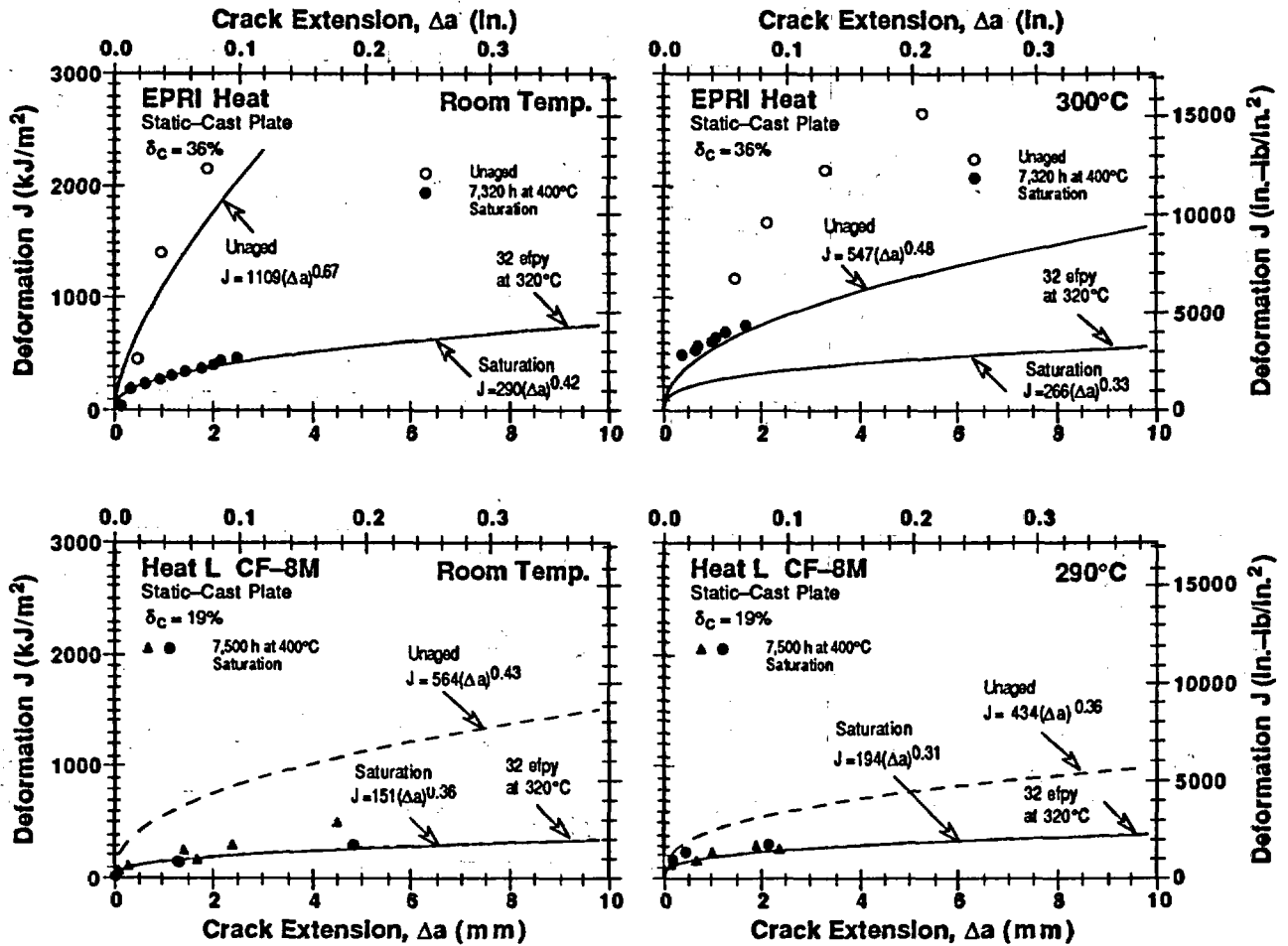


Figure 12. Saturation fracture toughness  $J$ - $R$  curves at RT and 290°C estimated from the chemical composition of static-cast CF-3 and CF-8M plates (Refs. 10, 12), and determined experimentally.  $\delta_c$  is the calculated ferrite content.

Table 3. Values of the constants in Eq. 22 for estimating exponent  $n$  of the power-law  $J$ - $R$  curve for cast stainless steels

Grade	Room Temp.		290–320°C	
	$a_2$	$b_2$	$a_2$	$b_2$
CF-3	0.08	0.228	0.14	0.130
CF-8	0.22	0.139	0.22	0.074
CF-8M	0.25	0.077	0.23	0.057

with the experimental results in most cases and are essentially conservative. The largest difference between the estimated and experimental  $J$ - $R$  curves is for centrifugally cast Heats P2 and 205 at RT and for centrifugally cast Heat P2 and static-cast EPRI heat at 290°C; the estimated curves of these heats are 30–50% lower than those obtained experimentally. The experimental  $J$ - $R$  curves for Heat 75 aged for 30,000 h at 350°C are lower

than those for 10,000-h aging at 400°C (shown in Fig. 11) and are in good agreement with the estimated saturation J-R curve.

Room temperature J-R curves for unaged static-cast Heats 68, 69, and 75 are non-conservative. It is believed that the poor fracture toughness of these unaged static-cast slabs is due to residual stresses introduced in the material during the casting process or production heat treatment. Annealing these heats for a short time at temperatures between 290 and 400°C (554 and 752°F) increased the fracture toughness and decreased the tensile stress without significantly affecting their impact energy.<sup>4</sup> Consequently, the fracture toughness of these heats would initially increase during reactor service before it would decrease due to thermal aging.

The estimated J-R curve after 32 effective full-power years (efpy) of service at 320°C (608°F) is also shown in Figs. 10-12. The results indicate that at 320°C service, fracture toughness of these materials will reach the saturation value or will be close to saturation within the 40-y design life.

The fracture toughness J-R curve for a specific material and aging condition can be obtained by estimating the RT impact energy from the procedure described in Section 5, and then using that value of  $C_v$  in Eqs. 18-22 to estimate the J-R curve. Examples of the experimental and estimated J-R curves for several partially aged (i.e., 30,000 h at 320°C) cast stainless steels are shown in Figs. 13 and 14. The estimated J-R curves show good agreement with experimental results.

The fracture-toughness data for unaged cast stainless steels indicate that the J-R curve for some heats are lower than those for wrought stainless steels. The available J-R curve data at 290-320°C (555-610°F) for unaged cast stainless steels are shown in Fig. 15a. The static-cast pump casing ring (Heat C1 with  $\delta_c = 8\%$ ) shows the lowest and centrifugally cast pipes (Heat P2 with  $\delta_c = 12\%$  and Heat C1488 with  $\delta_c = 21\%$ ) have the highest fracture toughness. Fracture toughness J-R curves for wrought stainless steels are higher than the J-R curve for static-cast pump casing ring; see Fig. 15b. The fracture toughness of unaged cast stainless steels is slightly higher at RT than at 290-320°C (554-608°F). At temperatures up to 320°C, a lower-bound J-R curve for unaged static-cast stainless steels can be expressed as

$$J_d = 400[\Delta a]^{0.40} \quad (23)$$

and for centrifugally cast stainless steels as

$$J_d = 650[\Delta a]^{0.43} \quad (24)$$

The present correlations account for the degradation of toughness due to thermal aging. They do not explicitly consider the initial fracture properties of the original unaged material. To take this into account, when no information is available on the fracture toughness of the unaged material, the lower-bound estimate given by Eq. 23 or 24 is used as upper bound for the predicted fracture toughness of the aged material, i.e., Eq. 23 or 24 is used when fracture toughness predicted by Eqs. 18-22 is higher than that given by Eq. 23 or 24. If the actual fracture toughness of the unaged material or the initial RT Charpy-

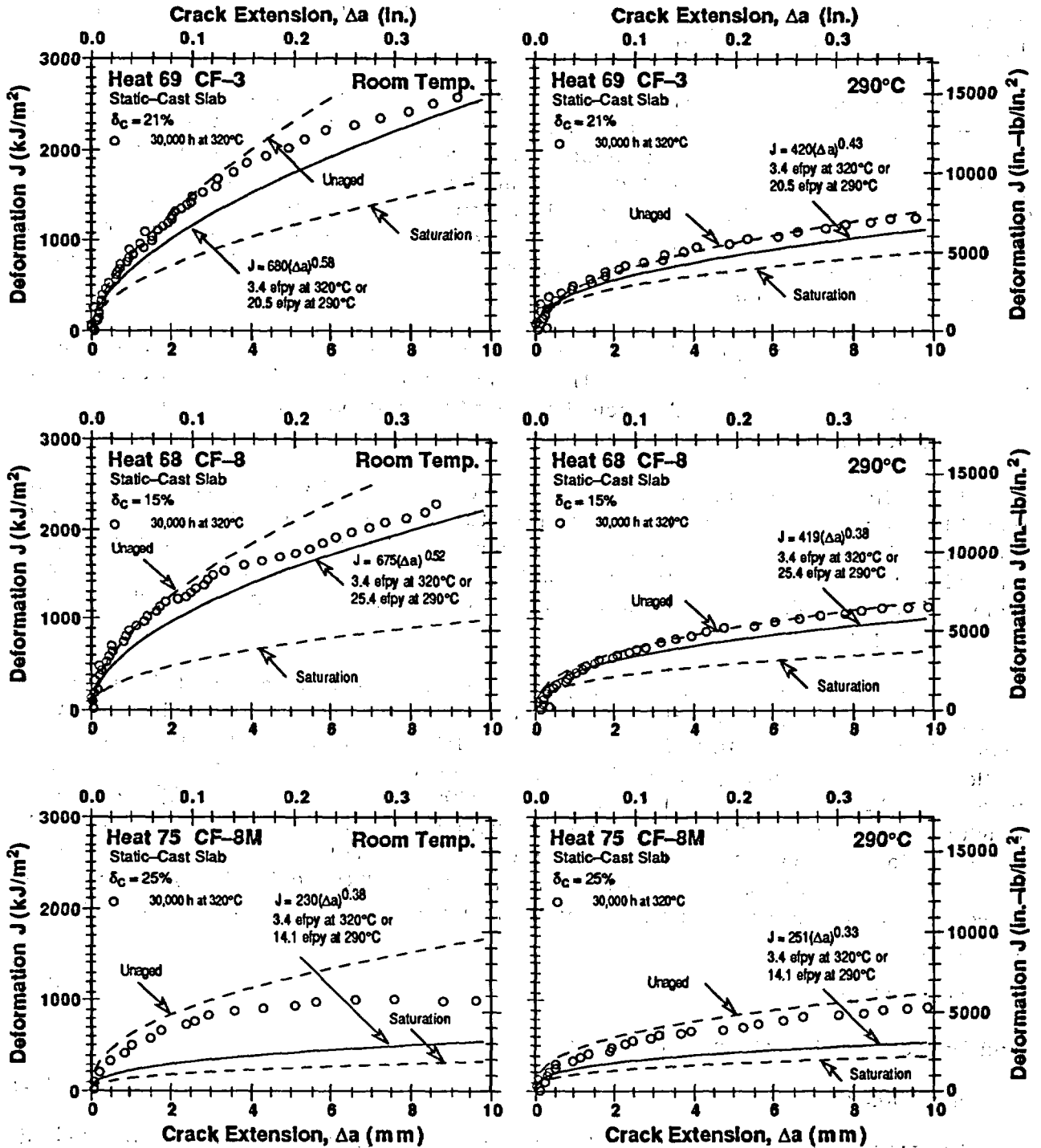


Figure 13. Fracture toughness  $J$ - $R$  curves at room temperature and 290°C, estimated from the chemical composition and initial Charpy-impact energy and determined experimentally for partially aged static-cast CF-3, CF-8, and CF-8M slabs.  $\delta_c$  is the calculated ferrite content.

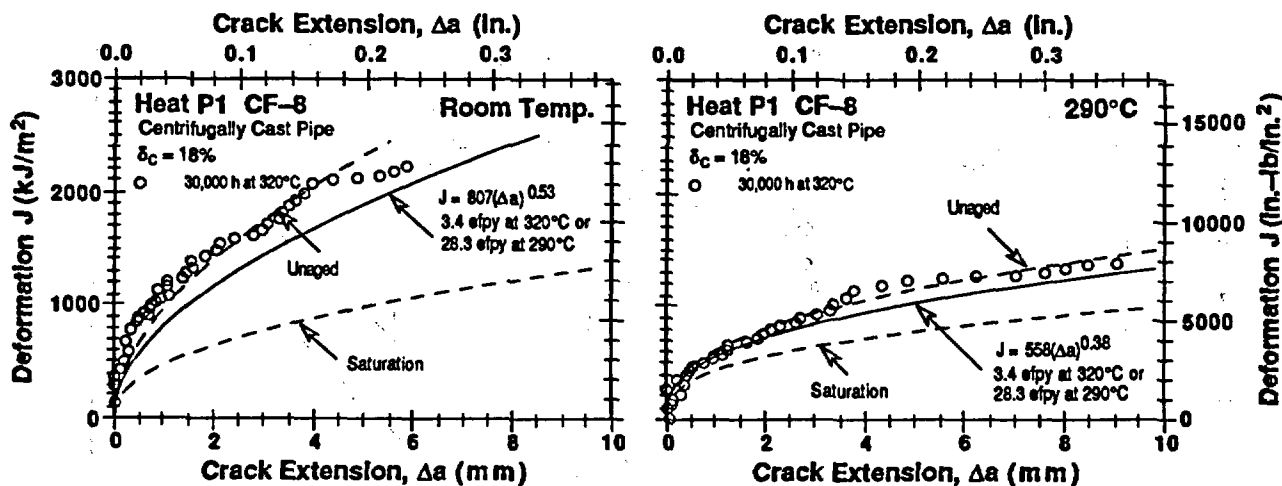


Figure 14. Fracture toughness  $J$ - $R$  curve at room temperature and  $290^{\circ}\text{C}$ , estimated from the chemical composition and initial Charpy-impact energy and determined experimentally for partially aged centrifugally cast CF-8 pipe.  $\delta_c$  is the calculated ferrite content.

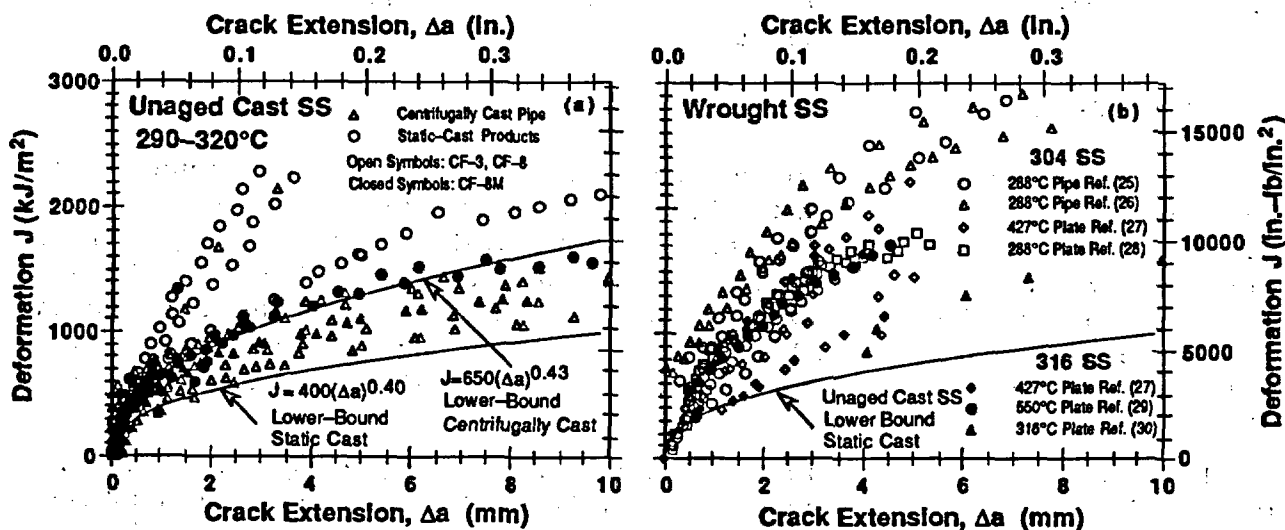


Figure 15. Fracture toughness  $J$ - $R$  curve for (a) unaged cast stainless steels and (b) wrought stainless steels at temperatures  $\geq 290^{\circ}\text{C}$

impact energy for estimating fracture toughness is known, the use of the higher value may be justified.

The fracture toughness  $J_{IC}$  values for aged cast stainless steels can be determined from the estimated  $J$ - $R$  curve and flow stress. The experimental and estimated  $J_{IC}$  for the various heats aged at  $\leq 350^{\circ}\text{C}$  are shown in Fig. 16. The chemical composition and the initial Charpy-impact energy and flow stress of the unaged material were used for the estimations. The estimated  $J_{IC}$  values show good agreement with the experimental results; for most cases the estimated  $J_{IC}$  is lower but within 30% of the observed value.

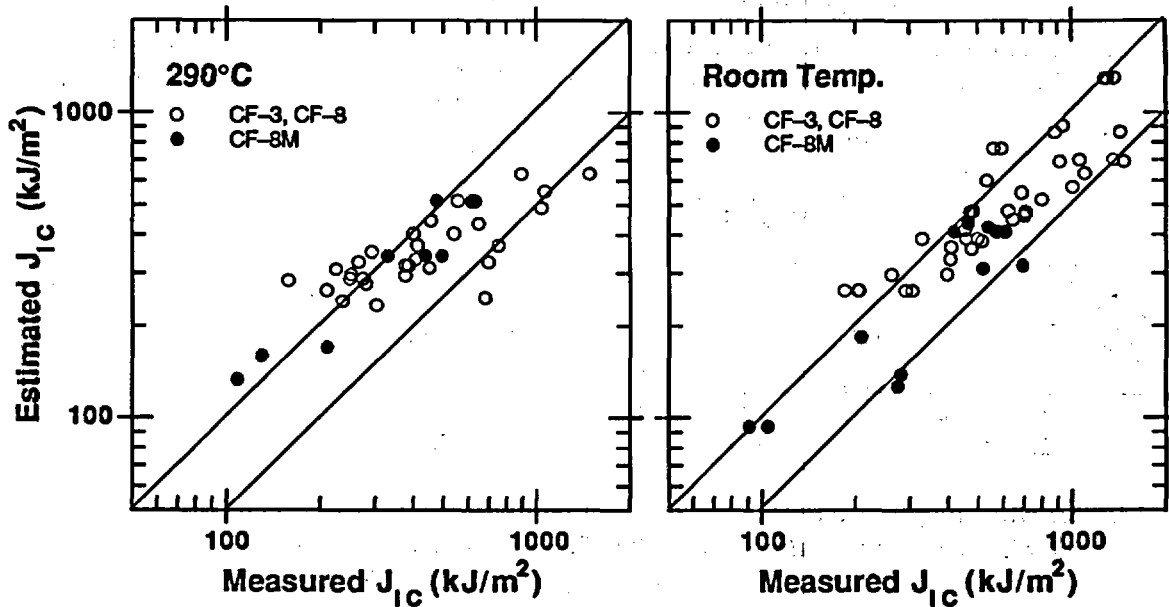


Figure 16. Experimental and estimated values of  $J_{IC}$  for aged cast stainless steels at 290°C and room temperature

#### Lower-bound J-R Curves

For cast stainless steels of unknown chemical composition, lower-bound fracture toughness is defined for a given material grade and temperature. Figure 2 indicates that, for cast stainless steels within ASTM Specification A 351, the saturation RT impact energy can be as low as 30, 25, and 20 J/cm<sup>2</sup> (~12, 15, and 18 ft·lb) for CF-3, CF-8, and CF-8M steels, respectively. The lower-bound J-R curve for different grades of steel and temperature can be determined from Eqs. 18-22. The lower-bound values of C and n for aged cast stainless steels are given in Table 4 and the J-R curves for static- and centrifugally cast CF-3, CF-8, and CF-8M are shown in Figs. 17 and 18.

The cast stainless steels used in the U.S. nuclear industry generally contain <15% ferrite. The lower-bound J-R curves shown in Figs. 17 and 18 are based on the "worst case" chemical composition (>20% ferrite) and are thus very conservative for most steels. Less conservative estimates of lower-bound J-R curves can be obtained if the ferrite content of the steel is known. The ferrite content of a cast stainless steel component can be measured in the field with a ferrite scope and a remote probe. The values of material parameter  $\Phi$  in Eqs. 4 and 6 can be scaled with respect to the measured ferrite content to obtain more realistic estimates of saturation Charpy-impact energy and J-R curves for the material. The values of coefficient C and exponent n representing the lower-bound J-R curve for aged cast stainless steels with 10-15% ferrite and <10% ferrite, respectively, are given in Table 4. This information may be used as a guideline for establishing the upper limit of ferrite content for a specific grade of steel beyond which thermal aging effects are significant. For example, the results indicate that static- or centrifugally cast CF-3 and CF-8 steels with <10% ferrite would have adequate impact strength and fracture toughness even in the fully embrittled condition.

Table 4. Values of the coefficient C and exponent n for the lower bound J-R curve for cast stainless steels

Grade	$\phi$	$C_v$ (J/cm <sup>2</sup> )	Static-Cast				Centrifugally Cast			
			Room Temp.		290°C		Room Temp.		290°C	
			C	n	C	n	C	n	C	n
<b>Ferrite Content &gt;15%</b>										
CF-3	40	30	287	0.42	264	0.33	334	0.42	347	0.33
CF-8	48	25	261	0.41	251	0.32	304	0.41	330	0.32
CF-8M	40	20	119	0.35	167	0.30	149	0.35	195	0.30
<b>Ferrite Content 10-15%</b>										
CF-3	30	42	342	0.45	290	0.35	398	0.45	382	0.35
CF-8	36	34	307	0.42	274	0.33	357	0.43	360	0.33
CF-8M	32	28	149	0.36	192	0.31	186	0.36	223	0.31
<b>Ferrite Content &lt;10%</b>										
CF-3	20	67	400	0.47	331	0.38	507	0.50	435	0.38
CF-8	24	55	394	0.46	313	0.35	458	0.46	412	0.35
CF-8M	24	47	211	0.38	238	0.33	264	0.38	276	0.33

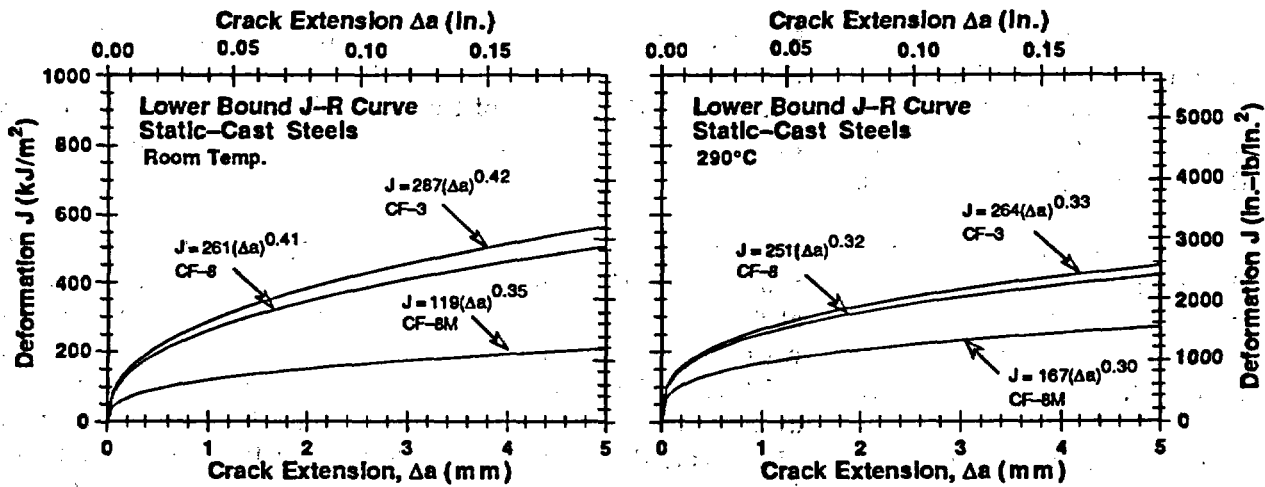


Figure 17. Lower bound J-R curve for static-cast stainless steels at room temperature and 290°C

## 8 Procedure for Estimating Mechanical Properties

A flow diagram of the sequential steps required for estimating fracture toughness J-R curve,  $J_{IC}$ , tensile flow stress, and Charpy-impact energy is shown in Fig. 19. In Section A of the flow diagram, "lower-bound" fracture toughness J-R curves for cast stainless steels of unknown chemical composition are defined. Different lower-bound J-R curves are defined when the ferrite content of the steel is known. Sections B and C of the flow diagram present procedures for estimating mechanical properties when some information is known about the material, e.g., CMTR, is available. Section B describes the estimation of "saturation" impact energy and J-R curve, i.e., the lowest value that would be achieved for the material after long-term service. The only information needed for these estimations is the chemical composition of the material. Nitrogen content is assumed to be 0.04 wt.% if

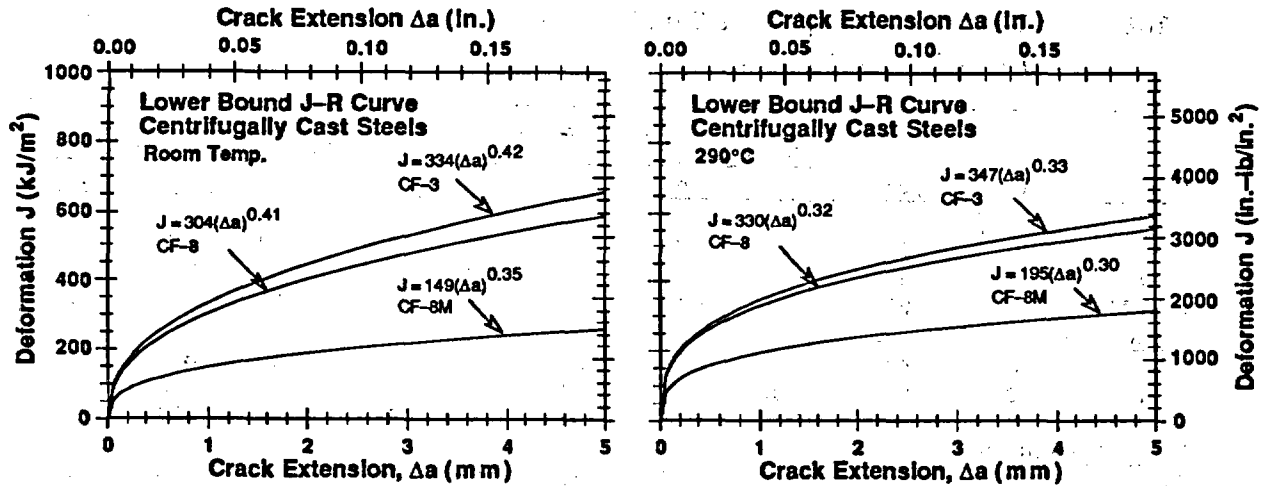


Figure 18. Lower bound J-R curve for centrifugally cast stainless steels at room temperature and 290°C

not known. The lower-bound J-R curve for unaged cast stainless steels is used as the saturation J-R curve of a material when the J-R curve estimated from the chemical composition is higher. Additional information, e.g., J-R curve of the unaged material or RT Charpy impact energy of unaged material for estimating fracture toughness, is required to justify the use of higher J-R curves.

Estimation of mechanical properties at any given time and temperature of service, is described in Section C of the flow diagram. The initial impact energy and flow stress of the unaged material and the constant  $\theta$  are also required for these estimations. The value of  $\theta$  depends on the service temperature; it is assumed to be 3.3 for temperatures <280°C (<536°F), 2.9 for temperatures of 280–330°C (536–626°F), and 2.5 for temperatures of 330–360°C (626–680°F). The initial impact energy of the unaged material can be assumed to be 200 J/cm<sup>2</sup> if not known. However, the lower-bound J-R curve for the unaged cast stainless steels is used when the J-R curve estimated from the chemical composition is higher than the lower bound for the unaged steel. The  $J_{IC}$  value is determined from the estimated J-R curve and flow stress.

## 9 Conclusions

A procedure and correlations are presented for predicting Charpy-impact energy, tensile flow stress, fracture toughness J-R curve, and  $J_{IC}$  value of aged cast stainless steels (ASTM A 351) from known material information. Mechanical properties of a specific cast stainless steel are estimated from the extent and kinetics of thermal embrittlement. Embrittlement of cast stainless steels is characterized in terms of RT Charpy-impact energy. The extent or degree of thermal embrittlement at "saturation," i.e., the minimum impact energy that can be achieved for the material after long-term aging, is determined from the chemical composition of the steel. The results indicate that Charpy-impact energy can be <50 J/cm<sup>2</sup> (<30 ft-lb) for cast stainless steels with ferrite contents as low as 10%.

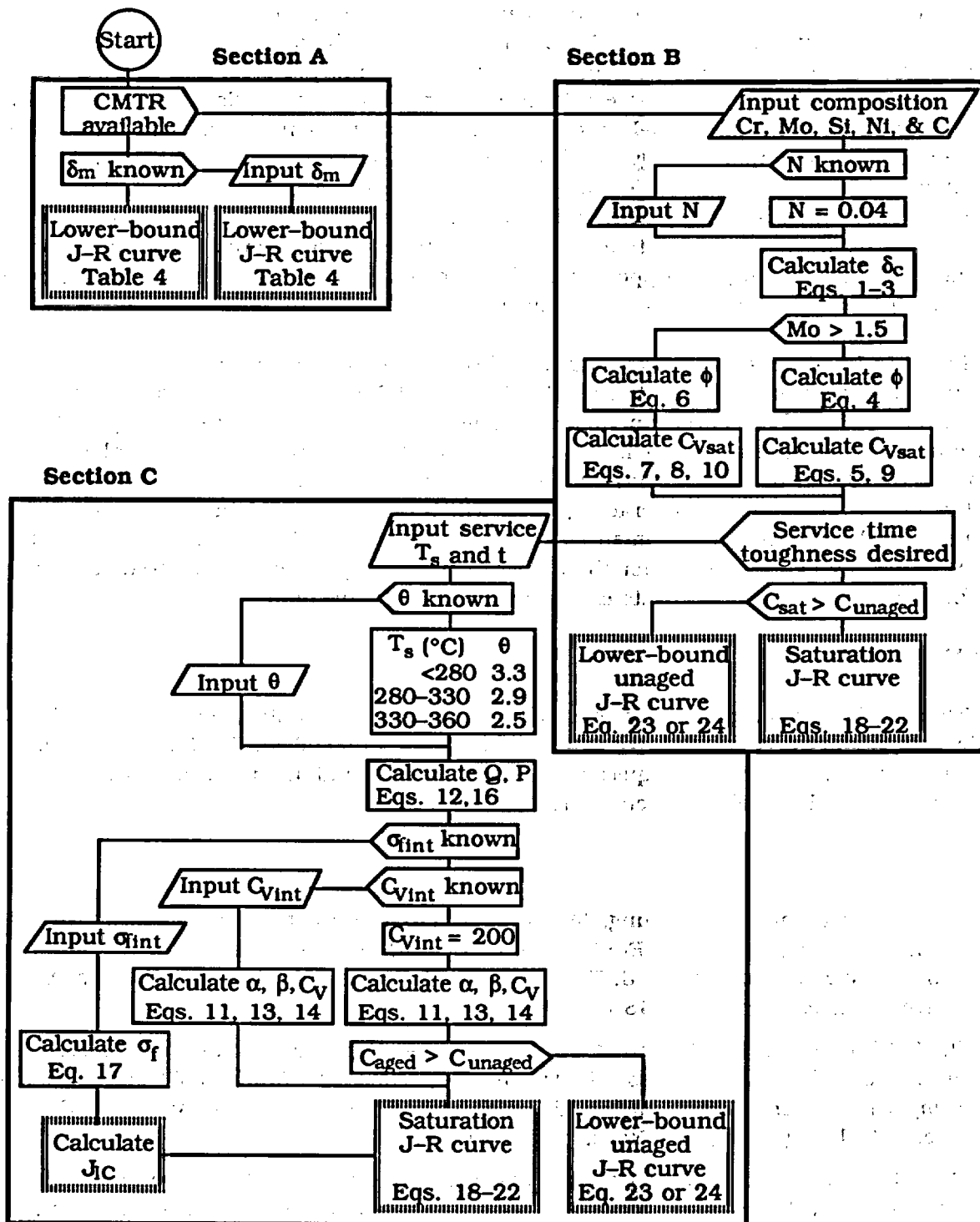


Figure 19. Flow diagram for estimating mechanical properties of aged cast stainless steels in LWR systems

Charpy-impact energy as a function of time and temperature of reactor service is estimated from the kinetics of thermal embrittlement, which is also determined from the chemical composition. The initial impact energy of the unaged steel is required for these estimations. Initial tensile flow stress is needed for estimating the flow stress of aged material. The fracture toughness J-R curve for the material is then obtained from correlations between RT Charpy-impact energy and fracture toughness parameters. The  $J_{IC}$  value is determined from the estimated J-R curve and flow stress. A common "lower-bound" J-R curve for cast stainless steels with unknown chemical composition is also defined for a given grade of steel, ferrite content, and temperature. This information can serve as a guideline for establishing the upper limit of ferrite content for a specific grade of steel beyond which thermal aging effects are significant.

Fracture toughness J-R curve data have been mostly obtained on 1-T compact tension specimens. According to ASTM Specification E 1152-87 they are valid only for crack growth up to 10% of the initial uncracked ligament. However, it is widely accepted that the J-R curve crack growth validity limits fall between 25 and 40% of the initial uncracked ligament, or ~8 mm of crack extension. In future work under this program, these extended validity limits for J-controlled crack growth will be qualified and better defined for cast stainless steels in terms of specimen size, toughness, and crack extension. Representation of J-R curves by expressions other than power law (e.g., by power-exponential relation) will also be evaluated for more accurate extrapolation of J-R curve data.

### Acknowledgments

This work was supported by the Office of Nuclear Regulatory Research of the U.S. Nuclear Regulatory Commission. The author thanks A. Sather, T. M. Galvin, L. Y. Bush, W. F. Michaud, and W. F. Burke for experimental contributions and J. Muscara, W. J. Shack, and T. F. Kassner for their helpful discussions.

### References

1. O. K. Chopra and H. M. Chung, "Aging Degradation of Cast Stainless Steels: Effects on Mechanical Properties," in *Environmental Degradation of Materials in Nuclear Power Systems-Water Reactors*, G. J. Theus and J. R. Weeks, eds. The Metallurgical Society, Warrendale, PA., pp. 737-748 (1988).
2. O. K. Chopra and H. M. Chung, "Effect of Low-Temperature Aging on the Mechanical Properties of Cast Stainless Steels," in *Properties of Stainless Steels in Elevated Temperature Service*, M. Prager, ed., MPC Vol. 26, PVP Vol. 132, American Society of Mechanical Engineers, New York, pp. 79-105 (1988).
3. O. K. Chopra, "Thermal Aging of Cast Stainless Steels: Mechanisms and Predictions," in *Fatigue, Degradation, and Fracture - 1990*, W. H. Bamford, C. Becht, S. Bhandari, J. D. Gilman, L. A. James, and M. Prager, eds., MPC Vol. 30, PVP Vol. 195, American Society of Mechanical Engineers, New York, pp. 193-214 (1990).
4. O. K. Chopra and A. Sather, *Initial Assessment of the Mechanisms and Significance of Low-Temperature Embrittlement of Cast Stainless Steels in LWR Systems*, NUREG/CR-5385, ANL-89/17, Argonne National Laboratory, Argonne, IL (August 1990).

5. A. Trautwein and W. Gysel, "Influence of Long Time Aging of CF-8 and CF-8M Cast Steel at Temperatures Between 300 and 500°C on the Impact Toughness and the Structure Properties," in *Stainless Steel Castings*, V. G. Behal and A. S. Mellilli, eds., ASTM STP 756, pp. 165-189 (1982).
6. E. I. Landerman and W. H. Bamford, "Fracture Toughness and Fatigue Characteristics of Centrifugally Cast Type 316 Stainless Steel Pipe after Simulated Thermal Service Conditions," in *Ductility and Toughness Considerations in Elevated Temperature Service*, MPC-8, American Society of Mechanical Engineers, New York, pp. 99-127 (1978).
7. S. Bonnet, J. Bourgoïn, J. Champredonde, D. Guttman, and M. Guttman, "Relationship between Evolution of Mechanical Properties of Various Cast Duplex Stainless Steels and Metallurgical and Aging Parameters: An Outline of Current EDF Programmes," *Mater. Sci. and Technol.*, **6**, 221-229 (1990).
8. K. N. Akhurst and P. H. Pumphrey, *The Aging Kinetics of CF3 Cast Stainless Steel in the Temperature Range 300°C to 400°C*, RD/L/3354/R88, Central Electricity Generating Board, Leatherhead, UK (November 1988).
9. P. H. Pumphrey and K. N. Akhurst, "Aging Kinetics of CF3 Cast Stainless Steel in Temperature Range 300 - 400°C," *Mater. Sci. and Technol.*, **6**, 211-219 (1990).
10. G. Slama, P. Petrequin, and T. Mager, "Effect of Aging on Mechanical Properties of Austenitic Stainless Steel Castings and Welds," presented at *SMIRT Post-Conference Seminar 6, Assuring Structural Integrity of Steel Reactor Pressure Boundary Components*, August 29-30, 1983, Monterey, CA.
11. Y. Meyzaud, P. Ould, P. Balladon, M. Bethmont, and P. Soulat, "Tearing Resistance of Aged Cast Austenitic Stainless Steel," presented at *Intl. Conf. on Thermal Reactor Safety (NUCSAFE 88)*, October 1988, Avignon, France.
12. P. McConnell and J. W. Sheckherd, *Fracture Toughness Characterization of Thermally Embrittled Cast Duplex Stainless Steel*, Report NP-5439, Electric Power Research Institute, Palo Alto, CA (September 1987).
13. O. K. Chopra, "Estimation of Fracture Toughness of Cast Stainless Steels in LWR Systems," in *Proc. 18th Water Reactor Safety Information Meeting*, U.S. Nuclear Regulatory Commission, NUREG/CP-0114 Vol. 3, p. 195 (April 1991).
14. O. K. Chopra, *Estimation of Fracture Toughness of Cast Stainless Steels during Thermal Aging in LWR Systems*, NUREG/CR-4513, ANL-90/42, Argonne National Laboratory, Argonne, IL (June 1991).
15. M. Vrinat, R. Cozar, and Y. Meyzaud, "Precipitated Phases in the Ferrite of Aged Cast Duplex Stainless Steels," *Scripta Metal.*, **20**, 1101-1106 (1986).
16. H. M. Chung and O. K. Chopra, "Long-Term-Aging Embrittlement of Cast Austenitic Stainless Steels - Mechanism and Kinetics," in *Properties of Stainless Steels in Elevated Temperature Service*, M. Prager, ed., MPC Vol. 26, PVP Vol. 132, American Society of Mechanical Engineers, New York, pp. 17-34 (1988).
17. H. M. Chung and T. R. Leax, "Embrittlement of Laboratory and Reactor Aged CF3, CF8, and CF8M Duplex Stainless Steels," *Mater. Sci. and Tech.* **6**, 249-262 (1990).

18. J. Sassen, M. G. Hetherington, T. J. Godfrey, G. D. W. Smith, P. H. Pumphrey, and K. N. Akhurst, "Kinetics of Spinodal Reaction in the Ferrite Phase of a Duplex Stainless Steel," in *Properties of Stainless Steels in Elevated Temperature Service*, M. Prager, ed., MPC Vol. 26, PVP Vol. 132, ASME, New York, pp. 65-78 (1988).
19. M. K. Miller and J. Bentley, "Characterization of Fine-Scale Microstructures in Aged Primary Coolant Pipe Steels," in *Environmental Degradation of Materials in Nuclear Power Systems-Water Reactors*, Proc. 3rd Intl. Symp., G. J. Theus and J. R. Weeks, eds., The Metallurgical Society, Warrendale, PA., pp. 341-349 (1988).
20. P. Auger, F. Danoix, A. Menand, S. Bonnet, J. Bourgoin, and M. Guttman, "Atom Probe and Transmission Electron Microscopy Study of Aging of Cast Duplex Stainless Steels," *Mater. Sci. and Technol.*, **6**, 301-313 (1990).
21. J. E. Brown, A. Cerezo, T. J. Godfrey, M. G. Hetherington, and G. D. W. Smith, "Quantitative Atom Probe Analysis of Spinodal Reaction in Ferrite Phase of Duplex Stainless Steel," *Mater. Sci. and Technol.*, **6**, 293-300 (1990).
22. L. S. Aubrey, P. F. Wieser, W. J. Pollard, and E. A. Schoefer, "Ferrite Measurement and Control in Cast Duplex Stainless Steel," in *Stainless Steel Castings*, V. G. Behal and A. S. Melilli, eds., ASTM STP 756, pp. 126-164 (1982).
23. A. L. Hiser, *Tensile and J-R Curve Characterization of Thermally Aged Cast Stainless Steels*, NUREG/CR-5024, MEA-2229, Materials Engineering Associates, Inc., Lanham, MD, (September 1988).
24. G. E. Hale and S. J. Garwood, "The Effect of Aging on the Fracture Behaviour of Cast Stainless Steel and Weldments," *Mater. Sci. and Technol.*, **6**, pp. 230-235 (1990).
25. A. L. Hiser, *Fracture Toughness Characterization of Nuclear Piping Steels*, NUREG/CR-5118, MEA-2325, Materials Engineering Associates, Inc., Lanham, MD, (November 1989).
26. G. M. Wilkowski, et. al., *Degraded Piping Program - Phase II*, Semiannual Report, NUREG/CR-4082, Vol. 2 (June 1985).
27. W. J. Mills, "Heat-to-Heat Variations in the Fracture Toughness of Austenitic Stainless Steels," *Eng. Fracture Mech.*, **30**, 469-492 (1988).
28. M. G. Vassilaros, R. A. Hays, and J. P. Gudas, "Investigation of the Ductile Fracture Properties of Type 304 Stainless Steel Plate, Welds, and 4-Inch Pipe," in *Proc. 12th Water Reactor Safety Information Meeting*, U.S. Nuclear Regulatory Commission, NUREG/CP-0058 Vol. 4, p. 176 (January 1985).
29. P. Balladon, J. Heritier, and P. Rabbe, "Influence of Microstructure on the Ductile Rupture Mechanisms of a 316L Steel at Room and Elevated Temperatures," *Fracture Mechanics: Fourteenth Symposium*, ASTM STP 791, pp. II496-II513 (1983).
30. W. H. Bamford and A. J. Bush, "Fracture Behavior of Stainless Steel," *Elastic-Plastic Fracture*, ASTM STP 668, pp. 553-577 (1979).

# Mechanical-Property Degradation of Cast Stainless Steel Components from the Shippingport Reactor

O. K. Chopra

Materials and Components Technology Division  
Argonne National Laboratory  
9700 South Cass Avenue  
Argonne, Illinois 60439

## Abstract

The mechanical properties of cast stainless steels from the Shippingport reactor have been characterized. Baseline properties for unaged materials were obtained from tests on either recovery-annealed material or material from a cooler region of the component. The materials exhibited modest decrease in impact energy and fracture toughness and a small increase in tensile strength. The fracture toughness J-R curve,  $J_{IC}$  value, tensile flow stress, and Charpy-impact energy of the materials showed very good agreement with estimations based on accelerated laboratory aging studies. The kinetics of thermal embrittlement and degree of embrittlement at saturation, i.e., the minimum impact energy that would be achieved after long-term aging, were established from materials that were aged further in the laboratory at temperatures between 320 and 400°C. The results showed very good agreement with estimates; the activation energies ranged from 125 to 250 kJ/mole and the minimum room-temperature impact energy was  $>75$  J/cm<sup>2</sup>. The estimated impact energy and fracture toughness J-R curve for materials from the Ringhals reactor hot and crossover-leg elbows are also presented.

## 1 Introduction

Cast duplex stainless steels used in LWR systems for primary pressure-boundary components such as valve bodies, pump casings, and primary coolant piping are susceptible to thermal embrittlement after extended service at reactor operating temperatures, i.e., 280–320°C (536–608°F). Aging of cast stainless steels at these temperatures leads to increased hardness and tensile strength and decreased ductility, impact strength, and fracture toughness. Most studies of thermal embrittlement of cast stainless steels involve simulation of end-of-life reactor conditions by accelerated aging at higher temperatures, viz., 400°C (752°F), because the time period for operation of power plants ( $\approx 40$  y) is far longer than can generally be considered in laboratory studies. Thus, estimates of mechanical-property degradation suffered by cast stainless steel components during service are based on an Arrhenius extrapolation of high-temperature data to reactor operating conditions.

Several laboratory studies have investigated thermal embrittlement of cast stainless steels under LWR operating conditions.<sup>1-12</sup> A procedure and correlations have been developed for estimating fracture toughness, tensile, and Charpy-impact properties of cast stainless steel components during thermal aging.<sup>13,14</sup> Because the embrittlement mechanisms and kinetics are complex, microstructural studies and mechanical testing of actual component materials that have completed long in-reactor service are necessary, to ensure that the

The submitted manuscript has been authored by a contractor of the U.S. Government under contract No. W-31-109-ENG-38. Accordingly, the U.S. Government retains a nonexclusive, royalty-free license to publish or reproduce the published form of this contribution, or allow others to do so, for U.S. Government purposes.

mechanisms observed in accelerated aging experiments are the same as those occurring in reactors. Cast stainless steels from the decommissioned Shippingport reactor offer a unique opportunity to validate and benchmark the laboratory studies.

The objectives of this paper are to characterize the mechanical-property degradation of cast stainless steel components from the Shippingport reactor and compare the results with estimates from accelerated laboratory aging studies. Cast stainless steel materials were obtained from four cold-leg check valves, two hot-leg main shutoff valves, and two pump volutes of the Shippingport reactor. One of the volutes is a "spare" that had seen service only during the first core loading, whereas the other was in service for the entire life of the plant. The actual time-at-temperature for the materials was ~13 y at ~281°C (538°F) for the hot-leg components and ~264°C (507°F) for the cold-leg components. The components were in a hot stand-by condition of ~204°C (400°F) for an additional ~2 y. Service-aged material was also obtained from the recirculating-pump cover assembly of the KRB reactor, which was in service in Gundremmingen, Germany, for ~8 y at 284°C (543°F).

The chemical composition, hardness, and ferrite content and distribution for the cast materials are given in Table 1. All materials are CF-8 grade cast stainless steel with ferrite contents in the range of 2-16% for the Shippingport components and 34% for the KRB pump cover plate. Results from metallurgical characterization of the various Shippingport materials have been presented earlier.<sup>15</sup> The materials show a lacy ferrite morphology with an average ferrite spacing in the range of 150-300 µm. The check valve materials contain phase-boundary carbides, which most likely formed during production heat treatment of

Table 1. Chemical composition, ferrite morphology, and hardness of cast stainless steel components from the Shippingport, KRB, and Ringhals reactors.

Mater. ID <sup>a</sup>	Composition (wt.%)										Ferrite		Ferrite Spacing (µm)	Hardness (Rp)
	C	N	Si	Mn	P	S	Ni	Cr	Mo	Cu	Calc. (%)	Meas. (%)		
<b>Cold Leg Check Valve<sup>b</sup></b>														
CA4	0.056	0.041	1.45	1.10	0.018	0.009	8.84	20.26	0.01	0.07	10.8	10.9	157	79.8
CA7	0.058	0.041	1.43	1.09	0.018	0.009	8.72	20.22	0.01	0.07	10.9	10.0	148	78.6
CB7	0.052	0.053	1.36	1.07	0.018	0.011	8.85	19.12	0.02	0.06	5.9	3.2	296	75.0
<b>Hot Leg Main Shutoff Valve<sup>b</sup></b>														
MA1	0.052	0.049	0.22	0.72	0.039	0.013	10.50	20.74	0.24	0.13	5.2	9.5	217	76.9
MA9	0.052	0.051	0.24	0.72	0.041	0.011	10.54	20.78	0.24	0.13	5.1	10.0	245	77.6
MB2	0.042	0.073	0.51	0.72	0.043	0.017	10.77	19.74	0.19	0.12	2.6	1.9	-	74.2
<b>Pump Volute<sup>c</sup></b>														
VR	0.046	0.049	1.14	0.50	0.027	0.017	9.56	20.79	0.04	0.07	9.8	16.2	181	82.9
PV	0.108	0.027	0.89	1.11	0.032	0.008	9.30	19.83	0.38	0.25	4.1	13.0	-	-
<b>KRB Pump Cover Plate<sup>d</sup></b>														
KRB	0.062	0.038	1.17	0.31	-	-	8.03	21.99	0.17	-	27.7	34.0	-	-
<b>Ringhals Reactor Elbows<sup>e</sup></b>														
H	0.037	0.044	1.03	0.77	0.022	0.008	10.60	20.00	2.09	0.17	13.0	20.1	-	-
C	0.039	0.037	1.11	0.82	0.020	0.012	10.50	19.60	2.08	0.08	12.3	19.8	-	-

<sup>a</sup> For the valves, the second digit indicates the loop where the valve was located and the number designates the segment of the component from which the material was removed (segments 1, 2, and 7 are from the top of the valve, segment 4 is from the bottom, and segment 9 is from a cooler region).

<sup>b</sup> In service for ~13 y at 264°C for cold leg and at 281°C for hot leg.

<sup>c</sup> Spare pump volute VR in service only during initial core loading and PV in service for ~13 y at 264°C.

<sup>d</sup> In service for ~8 y at 284°C.

<sup>e</sup> In service for ~8 y at 325°C for hot leg and at 291°C for crossover leg, and a hot stand-by for 2.3 y at 303°C for hot leg and at 274°C for crossover leg.

the casting. Also, the check-valve material showed phase boundary migration, and the original phase boundaries were decorated with carbides.

Microstructural examination indicates that the mechanism of low-temperature embrittlement of the cast materials is the same as that of the laboratory-aged materials.<sup>16,17</sup> All materials showed spinodal decomposition of the ferrite to form a chromium-rich  $\alpha'$  phase. In addition, the check-valve materials contained a nickel- and silicon-rich G phase in the ferrite and  $M_{23}C_6$  carbides at the austenite/ferrite phase boundary. An unexpected microstructural feature, i.e.,  $\sigma$  phase precipitates on slip bands and stacking faults, was also observed in the austenite of the check-valve material. Precipitation of  $\sigma$  phase generally occurs at temperatures  $>550^\circ\text{C}$  ( $>1022^\circ\text{F}$ ). The presence of  $\sigma$  phase and phase-boundary migration indicate significant differences between the production heat treatment of the check valves and that of the other materials.

The mechanical-property degradation of cast stainless steel (CF-8M) elbows from the Ringhals reactor hot leg and crossover leg was also assessed and compared with experimental data.<sup>18</sup> The chemical composition, ferrite content, and service conditions for the materials are given in Table 1.

## 2 Mechanical Properties

Specimens for Charpy-impact, tensile, and fracture toughness J-R curve tests were obtained from different locations across the thickness of the various components. All specimens were in the LC orientation.\* Impact tests were conducted on standard Charpy V-notch specimens machined according to ASTM Specification E 23. A Dynatup Model 8000A drop-weight impact machine with an instrumented tup and data readout system was used for the tests. Tensile tests were performed on cylindrical specimens 5 mm in diameter, with a gauge length of 20 mm. The tests were conducted at an initial strain rate of  $4 \times 10^{-4} \text{ s}^{-1}$ . The J-R curve tests were conducted according to ASTM Specifications E 813-85 and E 1152-87. Compact-tension specimens, 25.4-mm thick, were used for the tests.

The baseline mechanical properties for the as-cast materials must be known to establish the thermal-aging effects during reactor service. Microstructural and annealing studies<sup>2,15-17,19</sup> on laboratory- and reactor-aged materials indicate that mechanical properties of unaged material can be determined from recovery-annealed material, i.e., embrittled material that has been annealed for 1 h at  $550^\circ\text{C}$  and then water-quenched. To obtain baseline properties, Charpy-impact tests were also conducted on material from a cooler region of the main shutoff valve. Charpy transition curves for MA9 material and recovery-annealed MA9 and MA1 material are shown in Fig. 1. These materials are from the Loop A main shutoff valve, although MA9 is from a cooler region of the valve. The results indicate that MA9 material suffered little or no thermal-aging embrittlement, i.e., annealing had no effect on the transition curves. The results for annealed MA1 material also show good agreement on the transition curves. The results for annealed MA1 also show good agreement with the transition curve for MA9. The upper-shelf energy (USE) for both materials is not constant but decreases as temperature increases. The average impact energies at room temperature

---

\* The first digit represents the direction normal to the plane of a crack and the second digit indicates the direction of crack propagation: L = longitudinal and C = circumferential.

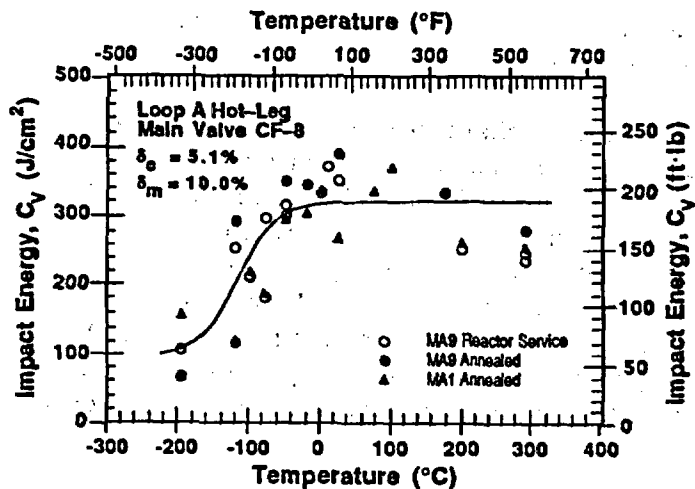


Figure 1. Effect of annealing on Charpy transition curve for cast material from the hot-leg main shutoff valve. Material MA9 is from a cooler region of the valve.  $\delta_c$  and  $\delta_m$  are calculated and measured ferrite contents, respectively.

and at 290°C, respectively, are 356 and 253 J/cm<sup>2</sup> for MA9, and 320 and 254 J/cm<sup>2</sup> for annealed MA1. The Charpy data were fitted with a hyperbolic tangent function of the form

$$C_v = K_0 + B[1 + \tanh \{(T - C)/D\}], \quad (1)$$

where  $K_0$  is the lower-shelf energy,  $T$  is the test temperature in °C,  $B$  is half the distance between upper- and lower-shelf energy,  $C$  is the mid-shelf Charpy transition temperature (CTT) in °C, and  $D$  is the half-width of the transition region. The best-fit curves for MA9, with or without annealing, and for annealed MA1 indicate that the latter is marginally weaker; the CTT of MA1 is ~10°C higher and the average USE ~30 J/cm<sup>2</sup> lower. Such differences in impact energy are most likely due to minor variations in composition and structure of the materials from different locations of the casting. The Charpy data for MA9 and annealed MA1 may be represented by a single best-fit transition curve, as shown in Fig. 1.

#### Charpy Impact Energy

Charpy transition curves for the various cast materials from the Shippingport reactor are shown in Figs. 2-4. The Charpy data were fitted with the hyperbolic-tangent expression given in Eq. 1; the values of the constants for the various materials are given in Table 2. The results indicate that the room-temperature impact energy of the materials is relatively high and the mid-shelf CTT, i.e., constant  $C$  in Eq. 1, is very low. The check valve materials CA4 and CB7 are weaker than MA1 and PV, e.g., the mid-shelf CTT is ~100°C higher for CA4 and CB7. The higher CTTs are due to the presence of phase-boundary carbides in the check-valve materials. The carbides weaken the phase boundaries and thus provide an easy path for fracture.

The decrease in impact strength from ~13 y of service at reactor temperatures is minimal for the materials. The room-temperature impact energy of PV, MA1, and CA4 materials is decreased by ~90, 70, and 40 J/cm<sup>2</sup>, respectively. The large difference in USE for the unaged and service-aged materials from Row 1 of MA1 (Fig. 2), is not due to thermal aging. The inner 15-mm region of the MA1 valve body contains a high density of inclusions/flaws and is inherently weak. The inner surface of all the valves contained repair welds. No significant difference was observed in the chemical composition or ferrite content of the material across the thickness of the valve body.

Table 2. Values of constants in Eq. 1 for Charpy transition curve of CF-8 cast stainless steels from the Shippingport reactor and KRB pump cover plate

Material ID	Service Condition		Constants			
	Temp. (°C)	Time (y)	$K_0$ (J/cm <sup>2</sup> )	B (J/cm <sup>2</sup> )	C (°C)	D (°C)
<b>Cold-Leg Check Valves</b>						
CA4	Annealed	-	25	98.6	-37.0	97.9
CA4	264	13	25	79.2	-20.1	81.8
CB7	264	13	76	108.8	6.0	65.2
<b>Hot-Leg Main Shutoff Valve</b>						
MA9 <sup>a</sup>	Annealed	-	96	112.0	-116.3	54.1
MA9	<200	13	83	110.1	-110.7	48.3
MA1/23 <sup>a</sup>	Annealed	-	96	112.0	-116.3	54.1
MA1/23 <sup>b</sup>	281	13	73	87.6	-114.2	29.8
MA1/1 <sup>c</sup>	281	13	69	63.7	-137.0	38.6
<b>Pump Volutes</b>						
PV	Annealed	-	150	116.2	-151.9	109.7
PV	264	13	75	109.4	-141.9	49.5
VR	Unaged	-	61	88.1	-112.4	38.5
<b>Pump Cover Plate<sup>d</sup></b>						
KRB	Annealed	-	8	161.9	-16.5	87.2
KRB	284	8	8	119.7	36.8	83.2

<sup>a</sup> Determined from combined data for MA9 and annealed MA9 and MA1.

<sup>b</sup> Material from Rows 2 & 3, which corresponds to 15- to 45-mm region of the wall.

<sup>c</sup> Material from Row 1, which corresponds to inner 15-mm region of the wall.

<sup>d</sup> Obtained from the KRB reactor in Gundremmingen, Germany.

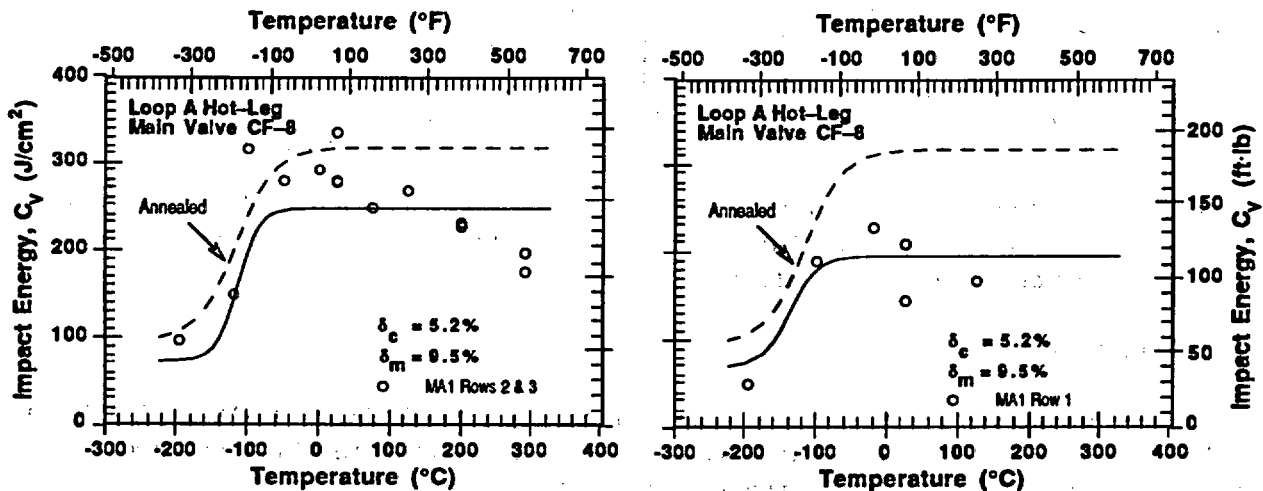


Figure 2. Charpy transition curves for hot-leg main shutoff valve after 13 y service at 281°C. Row 1 represents inner 15-mm region and rows 2 and 3 represent 15- to 50-mm region of the valve body. Results from recovery-annealed MA1 are shown as the baseline Charpy transition curve.

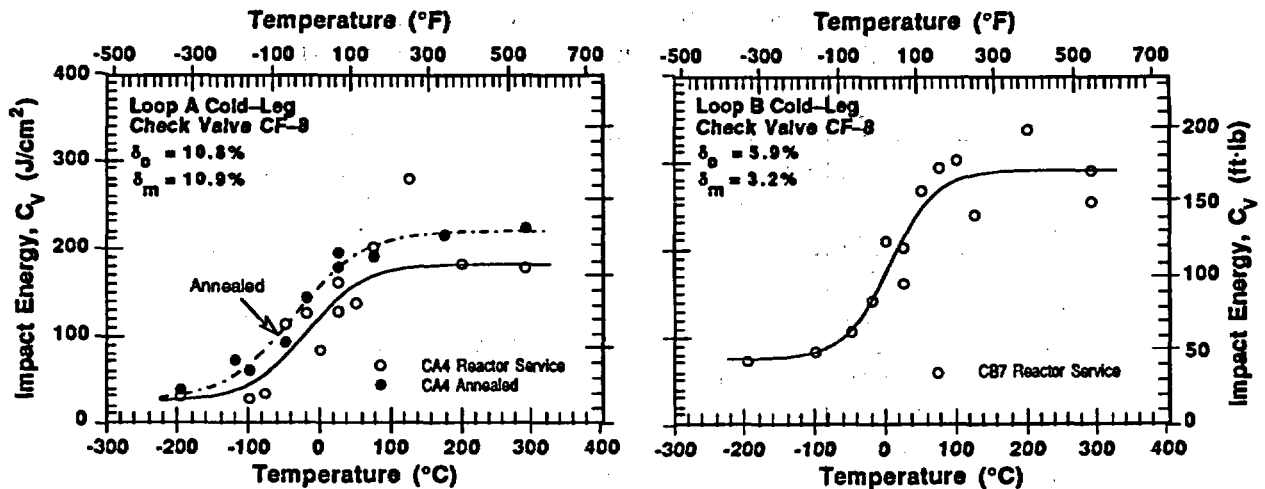


Figure 3. Charpy transition curves for cold-leg check valves from Loops A and B after 13 y of service at 264°C. Baseline transition curve for CA4 is represented by results for recovery-annealed material.

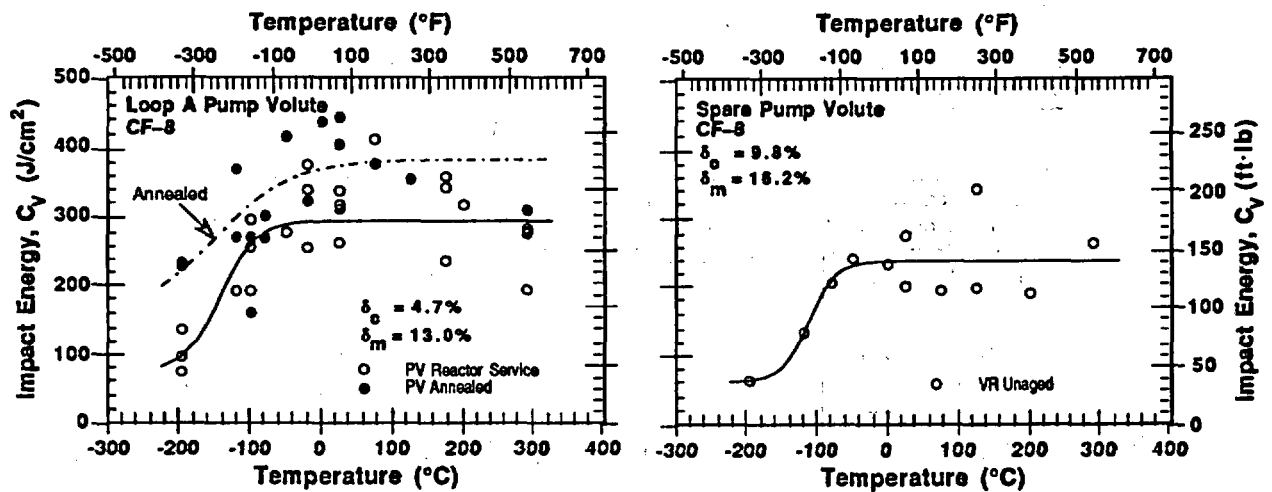


Figure 4. Charpy transition curves for service-aged (13 y of service at 264°C) and spare pump volutes. Baseline transition curve for PV is represented by results for recovery-annealed material.

#### Tensile Properties

Tensile tests were conducted at room temperature and at 290°C on CA4, PV, MA1, and MA9 materials. Tensile properties were also estimated from the instrumented Charpy-impact test data. For a Charpy specimen, yield stress is given by

$$\sigma_y = 1.50P_y B/Wb^2, \quad (2)$$

and ultimate stress by

$$\sigma_u = 2.28P_m B/Wb^2, \quad (3)$$

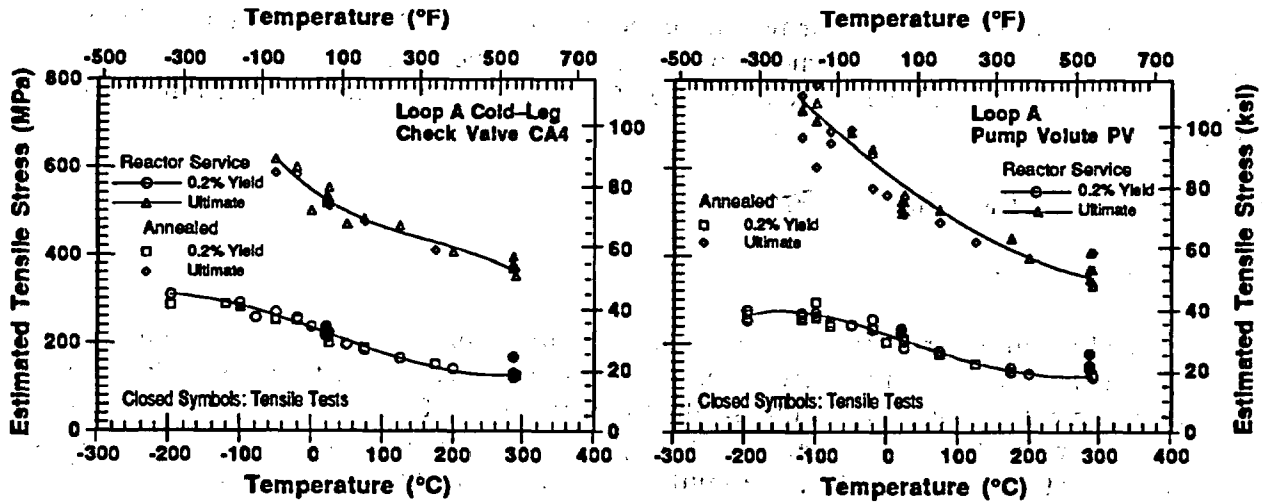


Figure 5. Yield and ultimate stress values (estimated from Charpy-impact data and obtained from tensile tests) for cold-leg check valve and pump volute, and estimated tensile stresses of recovery-annealed materials

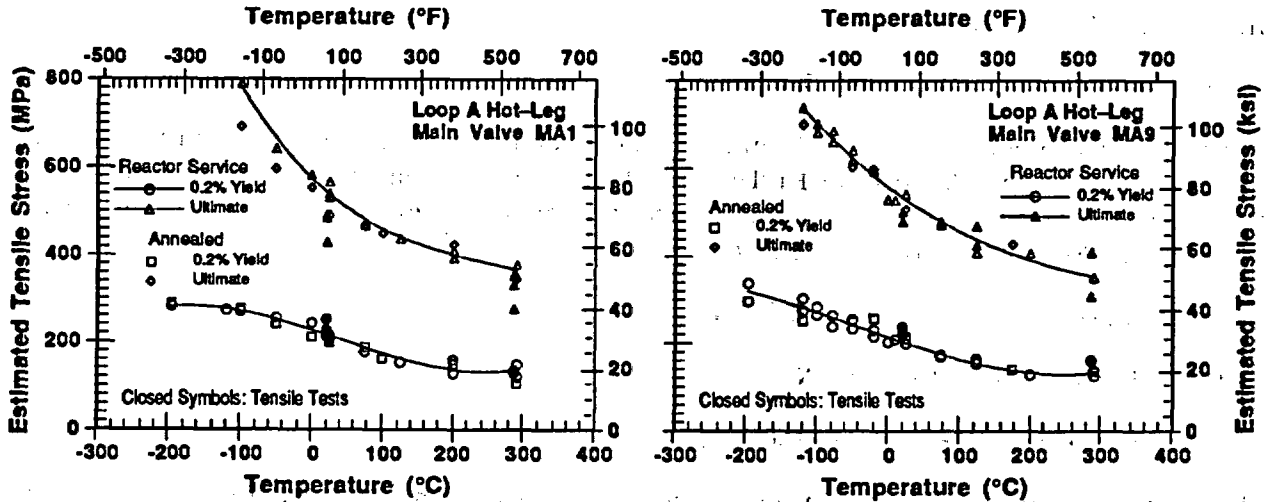


Figure 6. Yield and ultimate stress values (estimated from Charpy-impact data and obtained from tensile tests) for hot-leg main valve, and estimated tensile stresses for recovery-annealed materials. Material MA9 is from a cooler region of the valve.

where  $P_y$  and  $P_m$  are the yield and maximum loads obtained from the load-time traces of the Charpy test,  $W$  is the specimen width,  $B$  is the specimen thickness, and  $b$  is the uncracked ligament.<sup>20</sup> The estimated values of yield and ultimate stress, the values obtained from tensile tests, and estimated tensile stresses for recovery-annealed materials are shown in Figs. 5 and 6.

The estimated tensile properties are in good agreement with the measured values. The tensile strength of CA4, PV, and MA1 materials is comparable. The results show that thermal aging during reactor service had no effect on yield stress and that the increase in ultimate stress is minimal for all materials. Two specimens of MA1 (Fig. 6) show low ultimate strength (and also poor ductility). These specimens were obtained from the inner-15-mm

region of the valve body. The poor tensile properties are caused by inclusions in the material. As discussed above, the room-temperature impact energy of Row 1 specimens is also low, e.g.,  $\approx 177 \pm 33 \text{ J/cm}^2$ , compared to  $\approx 299 \pm 33 \text{ J/cm}^2$  for specimens from other regions of the valve body.

### 3 Estimation of Mechanical Properties

#### Charpy-Impact Energy

A procedure and correlations have been presented\* for predicting Charpy-impact energy, tensile flow stress, and fracture toughness J-R curves of aged cast stainless steels from the chemical composition of the steel. Embrittlement of cast stainless steels is characterized in terms of room-temperature Charpy-impact energy. The extent or degree of embrittlement at "saturation," i.e., the minimum impact energy that would be achieved for the material after long-term aging, is described in terms of a material parameter  $\Phi$ , which, for CF-3 and CF-8 steels, is expressed as

$$\Phi = \delta_c(\text{Cr} + \text{Si})(\text{C} + 0.4\text{N}) \quad (4a)$$

and for CF-8M steels as

$$\Phi = \delta_c(\text{Ni} + \text{Si} + \text{Mn})^2(\text{C} + 0.4\text{N})/5, \quad (4b)$$

where the ferrite content  $\delta_c$  is in % and chemical composition of the steel is in wt.%. The ferrite content is calculated from Hull's equivalent factors;<sup>21</sup> the values for the various cast materials are given in Table 1. The saturation room-temperature impact energy  $Cv_{\text{sat}}$  ( $\text{J/cm}^2$ ) for CF-3 and CF-8 steels is given by

$$\log_{10}Cv_{\text{sat}} = 1.15 + 1.36\exp(-0.035\Phi), \quad (5a)$$

and for CF-8M steels with >10% Ni by

$$\log_{10}Cv_{\text{sat}} = 1.10 + 2.64\exp(-0.064\Phi). \quad (5b)$$

The room-temperature saturation impact energy is also estimated from the chemical composition of the steel. For CF-3 and CF-8 steels,  $Cv_{\text{sat}}$  ( $\text{J/cm}^2$ ) is given by

$$\log_{10}Cv_{\text{sat}} = 5.64 - 0.006\delta_c - 0.185\text{Cr} + 0.273\text{Mo} - 0.204\text{Si} + 0.044\text{Ni} - 2.12(\text{C} + 0.4\text{N}), \quad (6a)$$

and for CF-8M steels by

$$\log_{10}Cv_{\text{sat}} = 7.28 - 0.011\delta_c - 0.185\text{Cr} - 0.369\text{Mo} - 0.451\text{Si} - 0.007\text{Ni} - 4.71(\text{C} + 0.4\text{N}). \quad (6b)$$

The saturation impact energy for a specific cast stainless steel is determined by both the methods given in Eqs. 4-6; and the lower value is then used for estimating mechanical properties.

\* "Estimation of Mechanical Properties of Cast Stainless Steels during Thermal Aging in LWR Systems," this conference.

Room-temperature impact energy as a function of time and temperature of aging is estimated from the room-temperature saturation impact energy  $C_{Vsat}$  and kinetics of embrittlement. The decrease in room-temperature impact energy  $C_V$  ( $J/cm^2$ ) with time is expressed as

$$\log_{10}C_V = \log_{10}C_{Vsat} + \beta(1 - \tanh [(P - \theta)/\alpha]), \quad (7)$$

where  $\beta$  is half the maximum change in  $\log C_V$ ,  $\theta$  is the log of the time at 400°C to achieve  $\beta$  reduction in impact energy at 400°C, and  $\alpha$  is a shape factor. The aging parameter  $P$  is the log of the aging time for a specific degree of embrittlement and is defined by

$$P = \log_{10}t - \frac{1000Q}{19.143} \left[ \frac{1}{T_s + 273} - \frac{1}{673} \right], \quad (8)$$

where  $Q$  is the activation energy (kJ/mole) for thermal embrittlement and  $t$  and  $T_s$  are the time (h) and temperature (°C) of aging, respectively. The activation energy  $Q$  (kJ/mole) is also determined from the chemical composition of the steel. For CF-3 and CF-8 steels

$$Q = 10 [74.52 - 7.20\theta - 3.46Si - 1.78Cr + 148N - 61C], \quad (9a)$$

and for CF-8M steels

$$Q = 10 [74.52 - 7.20\theta - 3.46Si - 1.78Cr - 4.35Mn + 23N], \quad (9b)$$

where the constant  $\theta$  is defined in Eq. (7). The constants  $\beta$  and  $\alpha$  in Eq. (7) can be determined from the initial room-temperature impact energy of the material  $C_{Vint}$  and the saturation room-temperature impact energy  $C_{Vsat}$ . Thus,

$$\beta = (\log_{10}C_{Vint} - \log_{10}C_{Vsat})/2, \quad (10)$$

and

$$\alpha = -0.585 + 0.795\log_{10}C_{Vsat}. \quad (11)$$

For a specific cast stainless steel, the values of room-temperature impact energy as a function of time and temperature of reactor service and the minimum impact energy that would be achieved for the material after long-term aging (i.e., saturation value) can be estimated from Eqs. 4-11. The information required for the estimations includes the chemical composition, initial impact energy of the unaged material, and the constant  $\theta$ . However, parametric studies indicate that the aging response at 280-330°C, is relatively insensitive to the value of  $\theta$ . Varying  $\theta$  between 2.1 and 3.6 results in almost identical aging behavior at 300°C and differences in aging behavior at 280-330°C are minimal. A value of 2.9 is assumed for the constant  $\theta$  in Eqs. 7 and 9 when estimating impact energy of cast stainless steel components in service at 280-330°C.

Room-temperature impact energy of the various service-aged materials was estimated from Eqs. 4-11. The initial impact energy of the unaged materials was determined from the data for recovery-annealed material or material from a cooler region of the casting. Some materials were aged further in the laboratory at 320, 350, and 400°C (608, 662, and 752°F) to obtain an accurate value of  $\theta$  and to validate the estimates of the saturation impact energy  $C_{Vsat}$  and activation energy for embrittlement of the materials.

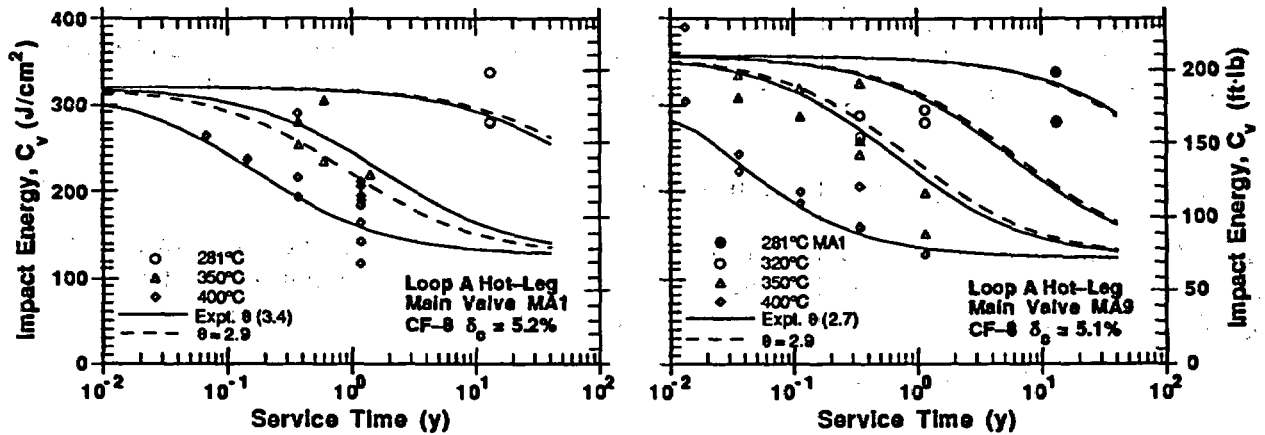


Figure 7. Variation of estimated room-temperature Charpy-impact energy with service time for Loop A hot-leg main valve materials MA1 and MA9. Material MA9 is from a cooler region of the valve.  $\delta_c$  is calculated ferrite content.

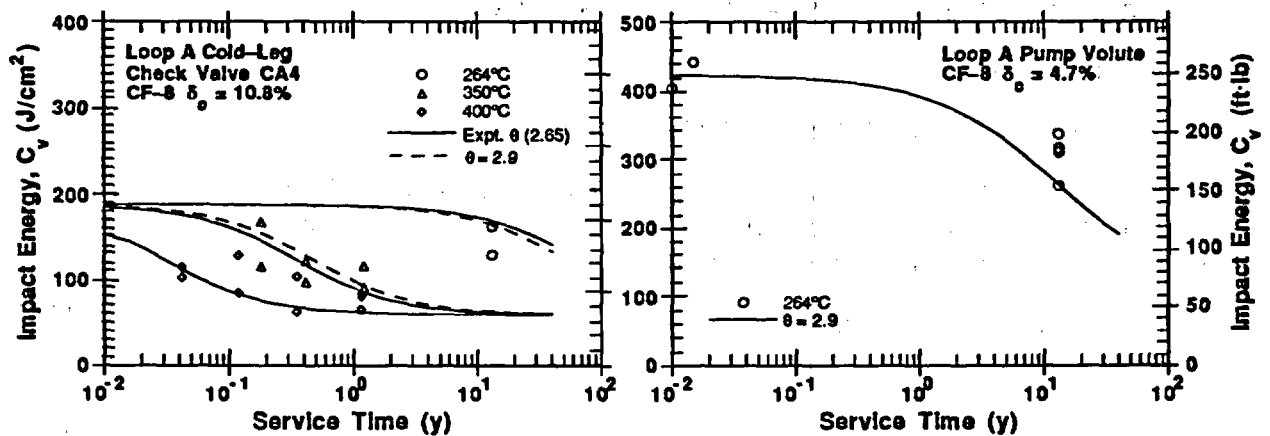


Figure 8. Variations of estimated room-temperature Charpy-impact energy with service time for Loop A cold-leg check valve CA4 and pump volute PV.  $\delta_c$  is calculated ferrite content.

The change in estimated Charpy-impact energy with aging time at temperatures between reactor service temperature for the Shippingport and KRB materials and 400°C is shown in Figs. 7-9. The high-temperature aging data for CA4 and MA1 materials represent service-aged material that was aged further in the laboratory at 350 and 400°C. Aging times were adjusted to include the effect of aging at reactor temperature. The high-temperature aging data for the KRB pump cover plate were obtained on recovery-annealed material.

The impact energies estimated with experimental  $\theta$  show good agreement with the measured impact energies at all temperatures; those estimated with  $\theta = 2.9$  show good agreement at temperatures  $\leq 320^\circ\text{C}$ . As mentioned above, estimations based on  $\theta = 2.9$  are valid only for service temperatures between 280 and 330°C. For higher temperatures, the estimated values would be nonconservative for materials that have a  $\theta$  value  $< 2.9$ , e.g., KRB pump cover plate and VR material (Fig. 9). A  $\theta$  value of 2.5 would give a conservative estimate of impact energy for all materials at 330-360°C service temperature.

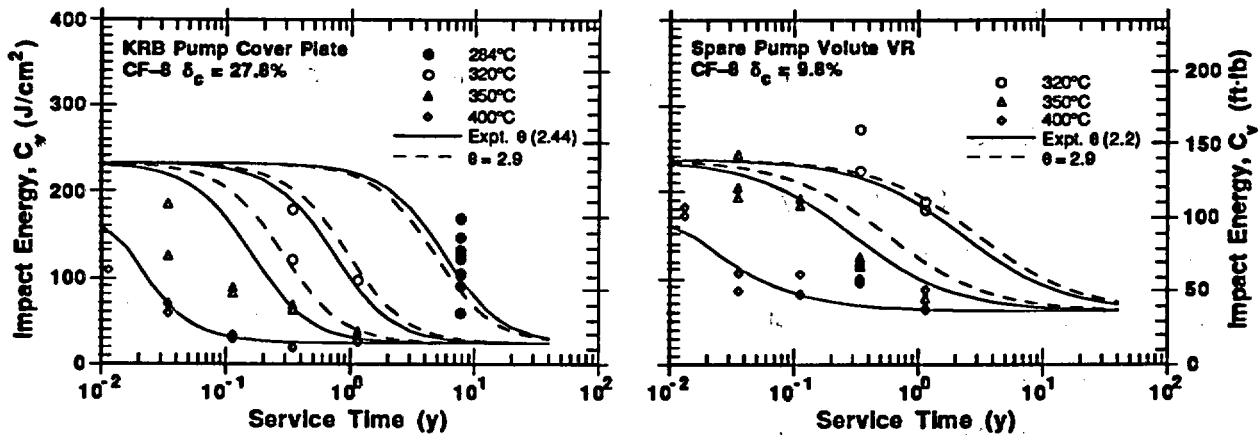


Figure 9. Variations of estimated room-temperature Charpy-impact energy with service time for the KRB pump cover plate and Shippingport spare pump volute VR.  $\delta_c$  is calculated ferrite content.

The impact energy for main valve MA1 was estimated from the compositions of MA1 and MA9 materials; the differences in the compositions of the two materials are minor. Figure 7 shows that, although the aging behavior at 400°C and the kinetics of embrittlement for MA1 and MA9 are significantly different, the estimates based on MA1 and MA9 agree well with the observed values for ~13 y of service at 281°C. The aging behavior estimated from MA9 is slightly slower than that estimated from MA1.

The predicted minimum saturation room-temperature impact energies also are in very good agreement with the experimental data. The measured impact energies for VR, MA9, and KRB materials aged at 400°C achieve saturation at the predicted values.

#### Fracture Toughness

Thermal aging decreases the fracture toughness of cast stainless steels at both room temperature and reactor temperature. The fracture toughness J-R curve for a specific cast stainless steel can be estimated from its room-temperature impact energy  $C_v$  ( $J/cm^2$ ). The J-R curve is expressed by the power-law relation  $J_d = C\Delta a^n$ , where  $J_d$  is deformation J ( $kJ/m^2$ ) per ASTM Specifications E 813-85 and E 1152-87,  $\Delta a$  is crack extension (mm), and C and n are constants. At room temperature, the J-R curve for static-cast CF-8 steels is given by

$$J_d = 49[C_v]^{0.52}[\Delta a]^n, \quad (12a)$$

and for static-cast CF-8M steels by

$$J_d = 16[C_v]^{0.67}[\Delta a]^n. \quad (12b)$$

At 290-320°C, the J-R curve for static cast CF-8 steels is given by

$$J_d = 102[C_v]^{0.28}[\Delta a]^n, \quad (13a)$$

and for static-cast CF-8M steels by

$$J_d = 49[Cv]^{0.41}[\Delta a]^n \quad (13b)$$

At room temperature, the exponent  $n$  for static- or centrifugally cast CF-8 steels is given by

$$n = 0.22 + 0.139\log_{10}Cv. \quad (14a)$$

and for static-cast CF-8M steels by

$$n = 0.25 + 0.077\log_{10}Cv. \quad (14b)$$

At 290-320°C, the exponent  $n$  for static- or centrifugally cast steels is given by

$$n = 0.22 + 0.074\log_{10}Cv. \quad (15a)$$

and for static-cast CF-8M steels by

$$n = 0.23 + 0.057\log_{10}Cv. \quad (15b)$$

The estimated and experimental fracture toughness  $J$ - $R$  curves at room temperature and at 290°C for the CA4, MA1, and PV materials and KRB pump cover plate are shown in Figs. 10 and 11. All materials exhibit relatively high fracture toughness. The estimated  $J$ - $R$  curves for CA4 and MA1 show good agreement with the experimental results and those for PV and KRB materials are 30-50% lower. The lower values for the PV and KRB materials are due to a conservative estimate of the kinetics of embrittlement, i.e., the correlations predict a faster decrease in impact energy than that observed during service, i.e., the estimated room-temperature impact energy is  $\approx 40\%$  lower than the average experimental value.

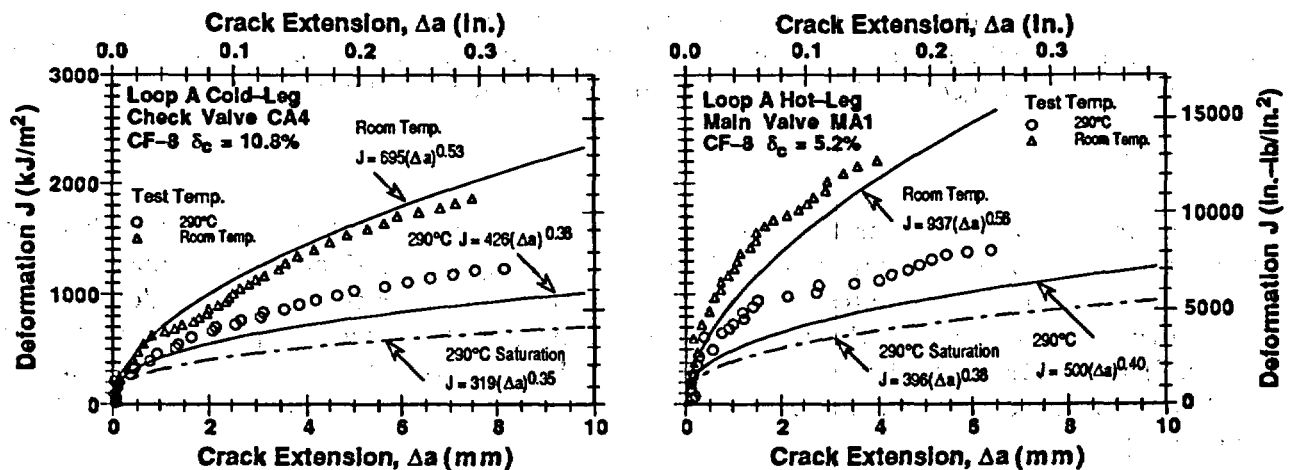


Figure 10. Estimated and measured fracture toughness  $J$ - $R$  curve at room temperature and 290°C for the Shippingport cold-leg check valve and hot-leg main valve

### Tensile Properties

Thermal aging of cast stainless steels increases their tensile strength, particularly their ultimate stress. The tensile strength of the unaged materials from the Shippingport and KRB reactors were determined from tensile tests or estimated from instrumented Charpy-impact tests on recovery-annealed materials. The materials show little or no increase in tensile stress. The increase in flow stress of aged cast stainless steels is estimated from a

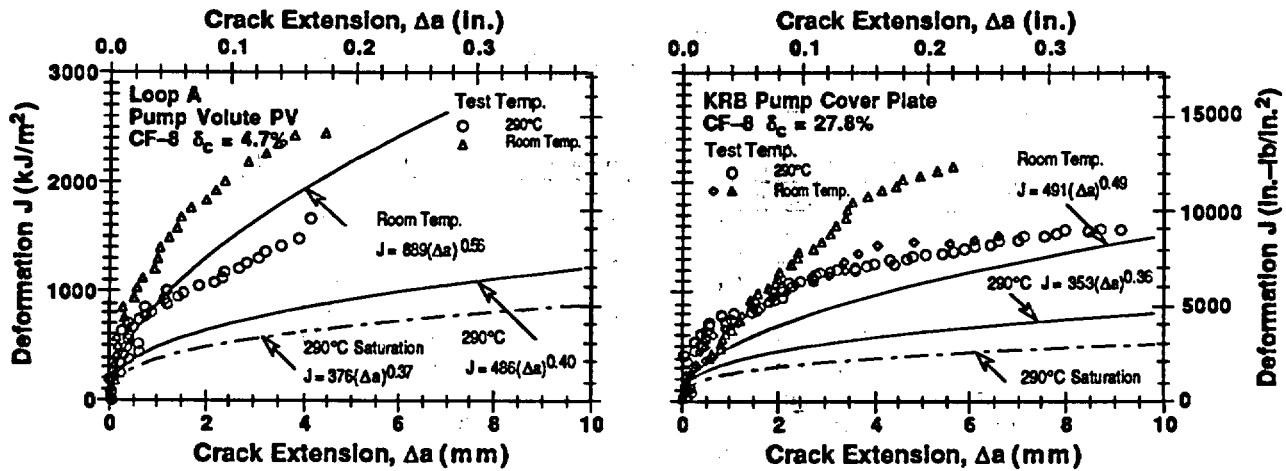


Figure 11. Estimated and measured fracture toughness  $J$ - $R$  curve at room temperature and 290°C for the Shippingport cold-leg pump volute and the KRB pump cover plate

correlation between the ratio of tensile flow stress of aged and unaged material and a normalized aging parameter. Flow stress is characterized as the mean of the 0.2% yield and ultimate stresses, and the aging parameter  $P$  (defined in Eq. 8) is normalized with respect to a  $\theta$  value of 2.9. The flow stress ratio  $R = (\sigma_{\text{aged}}/\sigma_{\text{unaged}})$  is given by

$$R = a + b(P - \theta + 2.9). \quad (16)$$

Equation 16 is valid for ferrite contents  $>7\%$  and  $R$  values between 1 and a constant  $c$ . Values of the constants  $a$ ,  $b$ , and  $c$  for different grades of steel and test temperatures are given in Table 3. The tensile flow stresses for the Shippingport and KRB materials were estimated from Eq. 16 with a value of 2.9 for  $\theta$ . The results, given in Table 4, show good agreement with the measured values.

Fracture toughness  $J_{IC}$  values for service-aged materials can be determined from the estimated  $J$ - $R$  curve and flow stress, and are also given in Table 4. The estimated  $J_{IC}$  shows very good agreement with the measured value for CA4 and is conservative for MA1 and PV.

Table 3. Values of the constants in Eq. 16 for estimating tensile flow stress of aged cast stainless steels

Grade	Room Temp.			290-320°C		
	a	b	c	a	b	c
CF-3	0.94	0.047	1.10	0.89	0.059	1.08
CF-8	0.90	0.074	1.16	0.87	0.088	1.14
CF-8M	0.80	0.101	1.19	0.71	0.143	1.24

#### 4 Ringhals Reactor Elbows

Investigation of the hot- and crossover-leg elbows from the Ringhals reactor indicated significant degradation of impact strength and fracture toughness of the hot-leg elbow after 15 y of service at 325°C, whereas the crossover-leg elbow, in service at 291°C, showed only

Table 4. Measured and estimated tensile flow stress and  $J_{IC}$  values for service-aged cast stainless steels

Material ID	Temp. (°C)	Flow Stress (MPa)		$J_{IC}$ (kJ/m <sup>2</sup> )	
		Observed <sup>a</sup>	Estimated	Observed	Estimated
<b>Shippingport Components</b>					
CA4	25	377 (377)	397	476	485
	290	251 (246)	259	361	331
PV	25	370 (362)	395	1509	692
	290	268 (269)	295	858	373
MA1	25	345 (345)	354	1407	809
	290	237 (233)	238	739	417
<b>KRB Pump Cover Plate</b>					
KRB	25	428 (428)	475	263, 396	297
	290	329 (294)	342	681	249
<b>Ringhals Elbows</b>					
Hot	25	424 (399)	469	250, 330 195, 150	165
	350	315 (292)	362		190
Cross-over	25	392 (369)	409	960, 525 960, 600	247
	350	277 (290)	333		243

<sup>a</sup> The values within parentheses represent unaged material.

moderate degradation.<sup>18</sup> The mechanical properties of the Ringhals elbows were estimated from Eqs. 4-16 with the correlations for CF-8M steel containing >10% Ni. Information on the chemical composition and impact energy of the unaged materials was used in the estimations;  $\theta$  was assumed to be 2.9.

The experimental data and estimated decrease in impact energy for hot- and crossover-leg elbows during service at 325 and 291°C, respectively, are shown in Fig. 12. The estimated value of 67 J/cm<sup>2</sup> for the hot-leg elbow is marginally higher than the measured average values of 45 J/cm<sup>2</sup> (equivalent Charpy V-notch impact energy converted from U-notch value) and 50 J/cm<sup>2</sup> (from Charpy V-notch specimens). The estimated 112 J/cm<sup>2</sup> impact energy for the crossover-leg agrees well with 107 J/cm<sup>2</sup> measured from U-notch specimens and is significantly lower than the 177 J/cm<sup>2</sup> obtained from V-notch specimens. The difference between the V- and U-notch impact energy for the crossover-leg elbow is most likely due to a significant variation in the ferrite content of the material. The saturation impact energies for hot- and crossover-leg elbows are estimated to be 56 and 67 J/cm<sup>2</sup>, respectively.

Fracture toughness J-R curves can be estimated from the impact energy. Room temperature J-R curve for hot- and crossover-leg elbows after ~15 y of service are shown in Fig. 13. Only the experimental  $J_{IC}$  values (not the complete J-R curve) have been reported for these materials.<sup>18</sup> The estimated tensile flow stress and  $J_{IC}$  at room temperature and at 290°C for the Ringhals elbows are given in Table 4. The estimated flow stresses are in good agreement with the measured values. The  $J_{IC}$  for the hot-leg elbow also is comparable to the measured value whereas that for the crossover-leg elbow is 50-70% lower. As mentioned above, the ferrite content of the crossover-leg elbow varies significantly. Furthermore, the correlations do not consider the effect of microstructural differences, and may be conservative for some materials.

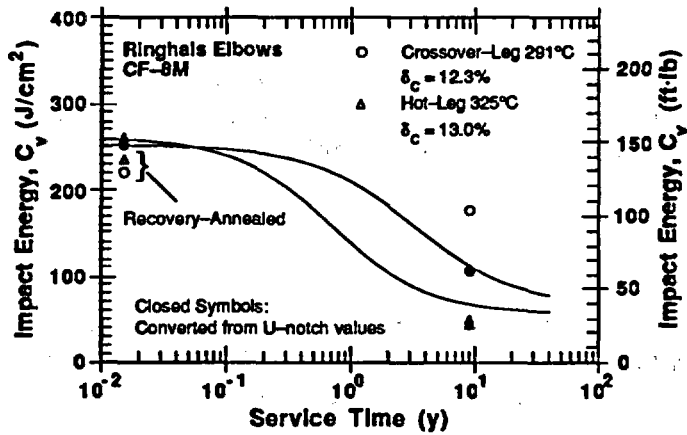


Figure 12. Estimated and experimentally observed room-temperature Charpy-impact energy for the Ringhals hot- and crossover-leg elbow

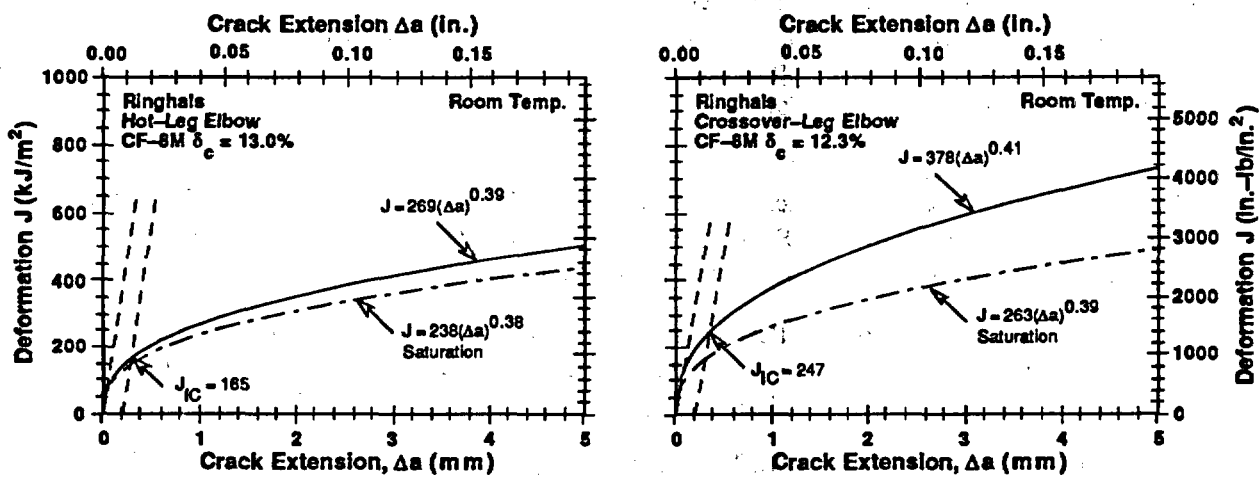


Figure 13. Estimated fracture toughness  $J$ - $R$  curve at room temperature for the Ringhals hot- and crossover-leg elbows after  $\approx 13$  y of service

## 5 Conclusions

Charpy-impact, tensile, and fracture toughness properties of several cast stainless steel materials from the Shippingport, KRB, and Ringhals reactors have been characterized. Baseline mechanical properties for as-cast material were determined from tests on either recovery-annealed material, i.e., material that had been annealed for 1 h at 550°C and then water quenched, or on material from a cooler region of the component. The Shippingport materials exhibited modest degradation of mechanical properties. The room-temperature impact energy was relatively high,  $>120$  J/cm<sup>2</sup> ( $>70$  ft.-lb). Check-valve materials were weaker than main valve materials because of the presence of phase-boundary carbides. The CTT for the check valves was  $\approx 100^\circ\text{C}$  higher than that for the main shutoff valves or pump volute. The results show good agreement with estimations based on accelerated laboratory aging studies. The procedure and correlations developed at ANL for estimating thermal aging degradation of cast stainless steels, predict accurate or slightly conservative values for Charpy-impact energy, tensile flow stress, fracture toughness  $J$ - $R$  curve, and  $J_{IC}$  of the Shippingport and KRB materials. The correlations successfully predict the mechanical properties of the Ringhals reactor hot- and crossover-leg elbows after service of  $\approx 15$  y.

## Acknowledgments

This work was supported by the Office of Nuclear Regulatory Research of the U.S. Nuclear Regulatory Commission. The author is grateful to A. Sather, T. M. Galvin, L. Y. Bush, G. M. Dragel, and W. F. Burke for experimental contributions and thanks W. J. Shack and T. F. Kassner for their helpful discussions.

## References

1. O. K. Chopra and H. M. Chung, "Aging Degradation of Cast Stainless Steels: Effects on Mechanical Properties," in *Environmental Degradation of Materials in Nuclear Power Systems—Water Reactors*, G. J. Theus and J. R. Weeks, eds. The Metallurgical Society, Warrendale, PA., pp. 737-748 (1988).
2. O. K. Chopra and H. M. Chung, "Effect of Low-Temperature Aging on the Mechanical Properties of Cast Stainless Steels," in *Properties of Stainless Steels in Elevated Temperature Service*, M. Prager, ed., MPC Vol. 26, PVP Vol. 132, American Society of Mechanical Engineers, New York, pp. 79-105 (1988).
3. O. K. Chopra, "Thermal Aging of Cast Stainless Steels: Mechanisms and Predictions," in *Fatigue, Degradation, and Fracture - 1990*, W. H. Bamford, C. Becht, S. Bhandari, J. D. Gilman, L. A. James, and M. Prager, eds., MPC Vol. 30, PVP Vol. 195, American Society of Mechanical Engineers, New York, pp. 193-214 (1990).
4. O. K. Chopra and A. Sather, *Initial Assessment of the Mechanisms and Significance of Low-Temperature Embrittlement of Cast Stainless Steels in LWR Systems*, NUREG/CR-5385, ANL-89/17, Argonne National Laboratory, Argonne, IL (August 1990.)
5. A. Trautwein and W. Gysel, "Influence of Long Time Aging of CF-8 and CF-8M Cast Steel at Temperatures Between 300 and 500°C on the Impact Toughness and the Structure Properties," in *Stainless Steel Castings*, V. G. Behal and A. S. Melilli, eds., ASTM STP 756, pp. 165-189 (1982).
6. E. I. Landerman and W. H. Bamford, "Fracture Toughness and Fatigue Characteristics of Centrifugally Cast Type 316 Stainless Steel Pipe after Simulated Thermal Service Conditions," in *Ductility and Toughness Considerations in Elevated Temperature Service*, MPC-8, American Society of Mechanical Engineers, New York, pp. 99-127 (1978).
7. S. Bonnet, J. Bourgoin, J. Champredonde, D. Guttman, and M. Guttman, "Relationship between Evolution of Mechanical Properties of Various Cast Duplex Stainless Steels and Metallurgical and Aging Parameters: An Outline of Current EDF Programmes," *Mater. Sci. and Technol.*, **6**, 221-229 (1990).
8. K. N. Akhurst and P. H. Pumphrey, *The Aging Kinetics of CF3 Cast Stainless Steel in the Temperature Range 300°C to 400°C*, RD/L/3354/R88, Central Electricity Generating Board, Leatherhead, UK (November 1988).
9. P. H. Pumphrey and K. N. Akhurst, "Aging Kinetics of CF3 Cast Stainless Steel in Temperature Range 300 - 400°C," *Mater. Sci. and Technol.*, **6**, 211-219 (1990).

10. G. Slama, P. Petrequin, and T. Mager, "Effect of Aging on Mechanical Properties of Austenitic Stainless Steel Castings and Welds," presented at *SMIRT Post-Conference Seminar 6, Assuring Structural Integrity of Steel Reactor Pressure Boundary Components*, August 29-30, 1983, Monterey, CA.
11. Y. Meyzaud, P. Ould, P. Balladon, M. Bethmont, and P. Soulat, "Tearing Resistance of Aged Cast Austenitic Stainless Steel," presented at *Intl. Conf. on Thermal Reactor Safety (NUCSAFE 88)*, October 1988, Avignon, France.
12. P. McConnell and J. W. Sheckherd, *Fracture Toughness Characterization of Thermally Embrittled Cast Duplex Stainless Steel*, Report NP-5439, Electric Power Research Institute, Palo Alto, CA (September 1987).
13. O. K. Chopra, "Estimation of Fracture Toughness of Cast Stainless Steels in LWR Systems," in *Proc. 18th Water Reactor Safety Information Meeting*, U.S. Nuclear Regulatory Commission, NUREG/CP-0114 Vol. 3, p. 195 (April 1991).
14. O. K. Chopra, *Estimation of Fracture Toughness of Cast Stainless Steels during Thermal Aging in LWR Systems*, NUREG/CR-4513, ANL-90/42, Argonne National Laboratory, Argonne, IL (June 1991).
15. O. K. Chopra, "Studies of Aged Cast Stainless Steel from the Shippingport Reactor," in *Proc. 18th Water Reactor Safety Information Meeting*, U.S. Nuclear Regulatory Commission, NUREG/CP-0114 Vol. 3, 369 (April 1991).
16. H. M. Chung, "Thermal Aging of Decommissioned Reactor Cast Stainless Steel Components and Methodology for Life Prediction," in *Life Assessment and Life Extension of Power Plant Components*, T. V. Narayanan, C. B. Bond, J. Sinnappan, A. E. Meligi, M. Prager, T. R. Mager, J. D. Parker, and K. Means, eds., PVP Vol. 171, American Society of Mechanical Engineers, New York, pp. 111-125 (1989).
17. H. M. Chung and T. R. Leax, "Embrittlement of Laboratory and Reactor Aged CF3, CF8, and CF8M Duplex Stainless Steels," *Mater. Sci. and Tech.* 6, 249-262 (1990).
18. C. Jansson, "Degradation of Cast Stainless Steel Elbows after 15 Years in Service," presented at *Fontevraud II Intl. Symp.*, Sept. 10-14, 1990, Royal Abbey of Fontevraud, France.
19. H. M. Chung and O. K. Chopra, "Long-Term-Aging Embrittlement of Cast Austenitic Stainless Steels - Mechanism and Kinetics," in *Properties of Stainless Steels in Elevated Temperature Service*, M. Prager, ed., MPC Vol. 26, PVP Vol. 132, American Society of Mechanical Engineers, New York, pp. 17-34 (1988).
20. W. L. Server, "Impact Three-Point Bend Testing for Notched and Pre-cracked Specimens," *J. Testing and Eval.* 6, 29 (1978).
21. L. S. Aubrey, P. F. Wieser, W. J. Pollard, and E. A. Schoefer, "Ferrite Measurement and Control in Cast Duplex Stainless Steel," in *Stainless Steel Castings*, V. G. Behal and A. S. Melilli, eds., ASTM STP 756, pp. 126-164 (1982).

PROGRESS IN EVALUATION AND IMPROVEMENT IN NONDESTRUCTIVE EXAMINATION  
RELIABILITY FOR INSERVICE INSPECTION OF LIGHT WATER REACTORS (LWRs) AND  
CHARACTERIZING FABRICATION FLAWS IN REACTOR PRESSURE VESSELS<sup>1</sup>

S. R. Doctor, E. S. Andersen, R. E. Bowey, A. A. Diaz, J. R. Friley,  
M. S. Good, M. S. Greenwood, P. G. Heasler, R. L. Hockey, R. J. Kurtz,  
G. J. Schuster, F. A. Simonen, J. C. Spanner, T. T. Taylor, T. V. Vo  
Pacific Northwest Laboratory  
Operated by Battelle Memorial Institute  
Richland, Washington 99352

ABSTRACT

This paper is a review of the work conducted under two programs. One (NDE Reliability Program) is a multi-year program addressing the reliability of nondestructive evaluation (NDE) for the inservice inspection (ISI) of light water reactor components. This program examines the reliability of current NDE, the effectiveness of evolving technologies, and provides assessments and recommendations to ensure that the NDE is applied at the right time, in the right place with sufficient effectiveness that defects of importance to structural integrity will be reliably detected and accurately characterized. The second program (Characterizing Fabrication Flaws in Reactor Pressure Vessels) is assembling a data base to quantify the distribution of fabrication flaws that exist in U.S. nuclear reactor pressure vessels with respect to density, size, type, and location. These programs will be discussed as two separate sections in this report.

NDE RELIABILITY PROGRAM

INTRODUCTION

This section reports on progress achieved under the NRC program entitled "Evaluation and Improvement in Nondestructive Examination Reliability for Inservice Inspection of Light Water Reactors (LWR)" (NDE Reliability Program). This program consists of eight major tasks as follows: 1) Code Activities, 2) BWR Pressure Vessel Research, 3) Plant Life Extension, 4) UT Equipment Interaction Matrix, 5) New Inspection Criteria, 6) PISC-III, 7) Cast Stainless Steel, and 8) Surface Roughness Conditions. Activities conducted under these tasks are summarized below.

The NDE Reliability Program objectives are to quantify the effectiveness of inservice inspection (ISI) techniques for LWR primary system components through independent research and to establish means for improving the overall

---

<sup>1</sup>Work supported by the U.S. Nuclear Regulatory Commission under Contract DE-AC06-76RLO 1830; FIN B2289 and L1099; Dr. J. Muscara, NRC Program Manager.

reliability of ISI systems and processes. Significant progress was achieved during the past year in several of these areas.

## 1.0 CODE ACTIVITIES

Proactive participation in ASME Section XI activities continued toward achieving ASME Code acceptance of NRC-funded PNL research results to improve the reliability of nondestructive examination/in-service inspection (NDE/ISI). The objective of this task is to develop upgraded criteria and requirements for qualifying ultrasonic testing/in-service inspection (UT/ISI) systems.

During the past year, PNL representatives attended four different series of meetings held in conjunction with the ASME Section XI Subcommittee on In-service Inspection of Nuclear Power Plant Components (SC-XI). PNL staff hold voting memberships on the SC-XI Working Group on Volumetric Examination and Procedure Qualification, SC-XI Working Group on Surface Examination and Personnel Qualification, chair a SC-XI Task Group on Acoustic Emission, and serve as Secretary and voting member of the SC-XI Subgroup on Nondestructive Examination (SGNDE). Following each SGNDE meeting, minutes are prepared and distributed to a mailing list of about 65 addressees, and agenda materials and other information are also assembled and distributed to provide each SGNDE member with a complete package prior to each meeting.

Assistance was also provided in support of related efforts to achieve Code acceptance of new personnel qualification (PQ) and performance demonstration (PD) requirements for eddy current equipment operators and data analysts, and a new SC-V activity to develop requirements and criteria for computerized UT imaging techniques. During a joint meeting of the SC-V Subgroup on Acoustic Emission (SGAE) and the SC-XI Task Group on AE, a proposed scope of a new Section V article on AE monitoring of in-service pressure boundary components was developed and approved.

The development of performance demonstration requirements for the eddy current method continues to encounter obstacles within the Special Working Group on Eddy Current Testing (SWGET). To date, the SWGET has reached a non-unanimous consensus on the scope of this Mandatory Appendix and on a sampling plan approach. During the SGNDE meeting in August 1991, active discussion focused on the sampling plan, specimen set criteria, and other open issues. Concern was expressed regarding the possible consequences of different pass/fail criteria for the eddy current and ultrasonic methods (i.e., Appendix VIII).

Revised visual acuity requirements for NDE personnel were developed and approved for publication in the 1991 Addenda to Section XI. A new requirement for generic practical examinations for Level III NDE personnel was also approved by the BNCS for publication in the 1991 Addenda. A Special Task Group was appointed to study a proposal for Code adoption of the 1988 Edition of SNT-TC-1A, as well as to evaluate the new ASNT Standard on Personnel Qualification. This task group recommended that the ASME Code retain its

current reference to the 1984 Edition of SNT-TC-1A, in lieu of adopting either of the newer documents.

## 2.0 BWR PRESSURE VESSEL RESEARCH

The objective of this task is to assess the development of new technology for the inspection of Boiling Water Reactors (BWRs) reactor pressure vessels (RPVs) and provide guidance to the NRC on the status and potential effectiveness of this development for reliably detecting and characterizing flaws. The work accomplished for the year involved participating in meetings held by industry to demonstrate their equipment and witnessing operation of a system at one operating reactor.

Industry has devoted significant efforts to the development of the technology that will provide access to the RPV. Most of the efforts have focused on performing the examinations from the inside of the RPV. General Electric and the EPRI NDE Center have performed evaluations of the access from the inside to the regions where the jet pumps are located. It appears that most of these areas should be accessible with the hardest region being the welds located in the lower head. The designs of the scanner assemblies are based on the successful designs that have been developed for other examinations. Therefore, the new scanners are only new in that a portion of the scanner has been modified to accommodate the limited inspection access encountered in the vicinity of the jet pumps. This work looks quite good and should provide the necessary scanning equipment.

The more significant problem areas remaining include whether there are many things attached to the RPV walls that are not on drawings but which will limit access for inspecting the vessel. The surface roughness of the cladding is an unknown for most of the RPV, and this condition will have a significant influence on the effectiveness of the ISI that can be performed.

Future work will involve continuing to follow the evolution of the equipment and assessing industry activities that are directed toward resolving the problem areas of access and cladding surface conditions.

## 3.0 PLANT LIFE EXTENSION

The License Renewal Task was initiated in April of this year. The objective of this task is to determine inservice inspection (ISI) requirements for license renewal. Initial efforts have focussed on reviewing the technical bases for existing reactor pressure vessel (RPV) flaw acceptance criteria. The RPV was selected for initial study since it was judged to be the most important component unlikely to be replaced and is the one component most susceptible to radiation damage.

Work during this fiscal year examined the rules and procedures for flaw evaluation presented in ASME Section XI, Division I for the welds in RPVs. The most relevant portions of the Code are presented below.

Subsection IWA describes methods for determining if flaws of various sizes and shapes are linear, laminar, or planar. Furthermore, equivalent sizes (length for linear flaws, and ellipse dimensions for planar and laminar flaws) are determined in accordance with this subsection. The pass/fail evaluation of these flaws is then conducted, starting with Subsection IWB 3500. If a flaw fails to pass under IWB 3500 a more detailed fracture mechanics evaluation (Appendix A of Section XI) can be utilized to see if the flaw is acceptable. Thus, IWB 3500 might be considered to be an initial screening process to accept those flaws with relatively large safety margins, thus avoiding the effort of a more detailed evaluation.

Planar flaws are evaluated with the use of the flaw acceptance standards of Table IWB 3510-1. This table gives allowable equivalent flaw sizes as a function of ellipse aspect ratio and vessel wall thickness. The surface 'reference flaw' size was selected to be one tenth as large as the so called maximum postulated defect ( $a/l=1/6$ ,  $a=t/4$  when  $a$  = through-wall extent,  $l$  = length, and  $t$  = wall thickness) of Appendix G, Section III. This gives a suitable safety factor on stress. Sizes of other elliptical surface flaws (of different aspect ratios) were then computed so that they would have the same safety factor as the surface reference flaw.

The tables in IWB 3500 for flaw evaluation do not directly involve the use of the stress level at the flaw location. It is assumed that the stress state meets the design requirements of Section III. In addition, it is stated that the tables may be used only if minimum fracture toughness can be assured. This is mandated in several places in IWB 3500. The first is Subarticle IWB 3410-1 which states that the material must conform to the requirements of Section III, Division I Appendices in regard to selection of a maximum postulated defect. In addition, the flaw size tables of IWB 3500 state that the material must meet the fracture toughness requirements of NB 2331 and G 2110(b), Section III. Subarticle NB 2331 contains procedures for determining the reference nil ductility temperature ( $RT_{NDT}$ ). This involves performing Charpy V-notch testing and obtaining results of at least 50 ft-lbs and at least 35 mils of lateral expansion.

If a detected flaw does not pass the acceptance standards tables of IWB 3500, then acceptability can still be achieved by performing detailed fracture mechanics analyses as described in Appendix A of Section XI. Appendix A utilizes stress field data at the flaw location, measured flaw size, and estimated material properties (including irradiation effects) and computes the stress intensity factor of the flaw in question, the critical flaw size, and the material fracture toughness. The  $RT_{NDT}$  of Section III, NB-2231 is used for the fracture toughness evaluation. Consideration is given to both normal and faulted loading conditions. For normal loading conditions, the safety factor is 3 for stress and 10 for flaw size -- approximately the same values used for the IWB 3500 tables if the stress level is at the maximum allowable for Section III.

The objective of the work for next fiscal year will be to determine if the flaw acceptance criteria, summarized above, adequately consider the impact of degraded material properties. The goal is to determine if adequate NDE

reliability exists for flaw detection and sizing after considering the effect of material property degradation on the locations, types, and sizes of flaws that may be of concern from a license renewal perspective.

#### 4.0 UT EQUIPMENT INTERACTION MATRIX

The objective of this task is to evaluate the effects of frequency domain, UT/ISI equipment interactions, and determine equipment tolerance values for improving inspection reliability. The equipment interaction matrix study was confined to six months due to budgetary restraints. Recent studies have shown that computer code modifications required to model the effects of component curvature are extensive. This code was transported to a Sun workstation for improved speed and efficiency.

#### 5.0 NEW INSPECTION CRITERIA

The objective of this task is to assess the adequacy of existing ASME Code requirements for inservice inspection of nuclear power plant components, and to develop technical bases for improving these requirements. Work continued to focus on risk-based approaches to inspection planning, which are being applied to establish criteria for improved ISI (type, extent, effectiveness, and frequency).

##### 5.1 Development of Risk-Based Approaches

During the past year PNL has continued to develop approaches for risk-based inspections through participation on the ASME Research Task Force on Risk-Based Inspection Guidelines. This group was organized by ASME as a society supported research activity with a membership representing several industries in addition to nuclear power generation. The ASME group has been identified by PNL as an effective route to achieve long-range goals for improved inspections at nuclear power plants.

The ASME Research Task Force has met quarterly during the past year, and has issued an initial "white paper" (ASME 1991) that reviews the current status of risk-based methods and gives general recommendations for risk-based inspection requirements. This general document is applicable to any industrial facility or structural system where structural integrity failures have the potential to lead to severe safety and/or economic consequences.

The recent focus of the ASME Research Task Force has been on nuclear power applications, and on the development of practical risk-based methods that can be recommended for consideration by ASME Section XI. Completion of a second draft document on the special topic of nuclear power applications was accomplished during the past year (Volume 2 - Part 1). This document recommends and describes specific methods that apply to nuclear power facilities. A draft was distributed for comment and peer review during March of 1991. Publication by ASME is scheduled no later than December of 1991.

Current and future efforts of the ASME Research Task Force are now applying the recommended risk-based methodologies, and will develop improved inspection programs for nuclear power plant components. This work will result in a future document (Volume 2 - Part 2), which is scheduled for publication in the later part of 1993. The document will make recommendations for consideration by ASME Code, Section XI. PNL is performing probabilistic calculations as part of the NDE Reliability Program, which are providing important support to the ASME Research Task Force.

## 5.2 Risk-Based Calculations of ISI Priorities

A major part on this task has been a pilot application of PRA methods to the Surry-1 nuclear plant. The Surry-1 work has applied results of PRA's in combination with the techniques of failure modes and effects analysis (FMEA) to identify and prioritize the most risk-important systems and components at nuclear power plants. The specific Surry-1 systems initially selected for analysis were the reactor pressure vessel, the reactor coolant, the low pressure injection (including the accumulators) and the auxiliary feedwater. Studies of these four systems are now complete and example results are reported below. Ongoing efforts are addressing other systems including the high pressure injection, main feedwater, service water, component cooling water, main steam, condensate, and residual heat removal systems.

Core damage frequency (Level-I PRA) has been used as the bottom line risk measure. FMEA results are applied to calculate the relative importance of each component within the systems being addressed. The calculated importance measures reflect the expected consequences of failure of the component (from the Surry-1 PRA) and the expected probability of failure (rupture) of the component. Estimates of rupture probabilities for the Surry-1 components have been obtained from expert judgement elicitation.

Staff from the Virginia Electric Power Company (VEPCO) have been actively participating in the Surry-1 pilot study. This participation is important to assure that the plant models are as realistic as possible and reflect plant operational practices. Several visits to the Surry-1 plant site have been made for system walkdowns, and for discussions with plant operational technical staff.

Figure 1 shows numerical rankings of the relative risk-importance of components within the initial four selected Surry-1 systems (stated in terms of core damage frequency). On the basis of core damage frequency, the most risk-important components are those located within the beltline region of the reactor pressure vessel. Relatively high rankings were estimated for certain pipe segments of the low pressure injection (LPI) system, and also certain pipe segments within the auxiliary feedwater system. Potential ruptures of most other components had much smaller contributions to core damage frequency. The calculated risk importances covered a range of over eight orders of magnitude in numerical values.

**Cumulative Risk  
(Core Damage Frequency)**

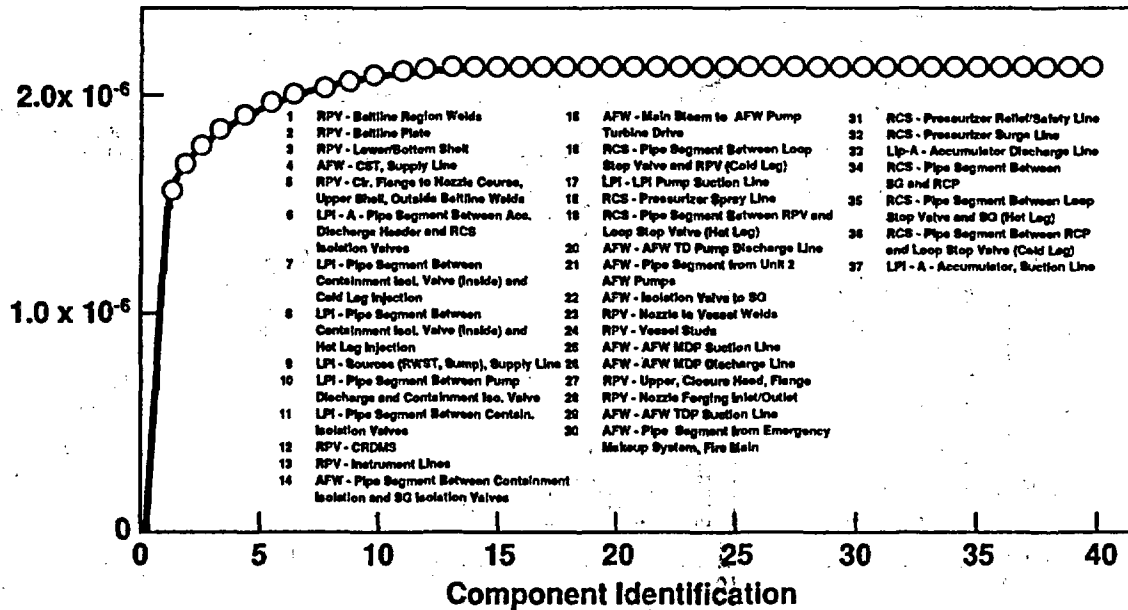


**FIGURE 1. Cumulative Risk Contributions of Surry-1 Components (showing decreasing contributions of lower ranked components)**

R9108092.4

Figure 2 is a plot of risk rankings using a logarithmic scale, which more clearly shows the very large differences (from component to component) in estimated contributions to risk. Also illustrated in Figure 2 is a risk-based approach being considered for determining how much inspection of a given component is enough. In this approach, values of target risk are used to establish acceptable levels for component failure probabilities. The suggested values of target risk as indicated on Figure 2 are intended to assure that structural failures remain an insignificant contribution to the estimated core damage frequency from all causes as estimated by plant specific PRAs.

By focusing the most intensive inspection efforts on only the highest risk important components (as identified by Figures 1 and 2), a relatively small inspection sample can readily address 90 percent or more of the potential for core damage from the rupture of all pressure boundary components. Inspections of additional lower ranked components are unlikely to achieve significant reductions in risk. Nevertheless, some level of inspection for these lower ranked components may be justified to assure that unexpected structural degradation (e.g., aging effects) does not increase these failure probabilities to unacceptable levels. For the very lowest ranked components, risk considerations suggest that little (e.g., visual) or no inspection is required.

**Residual Risk - If Component I and Lower Ranked Components are not Inspected**

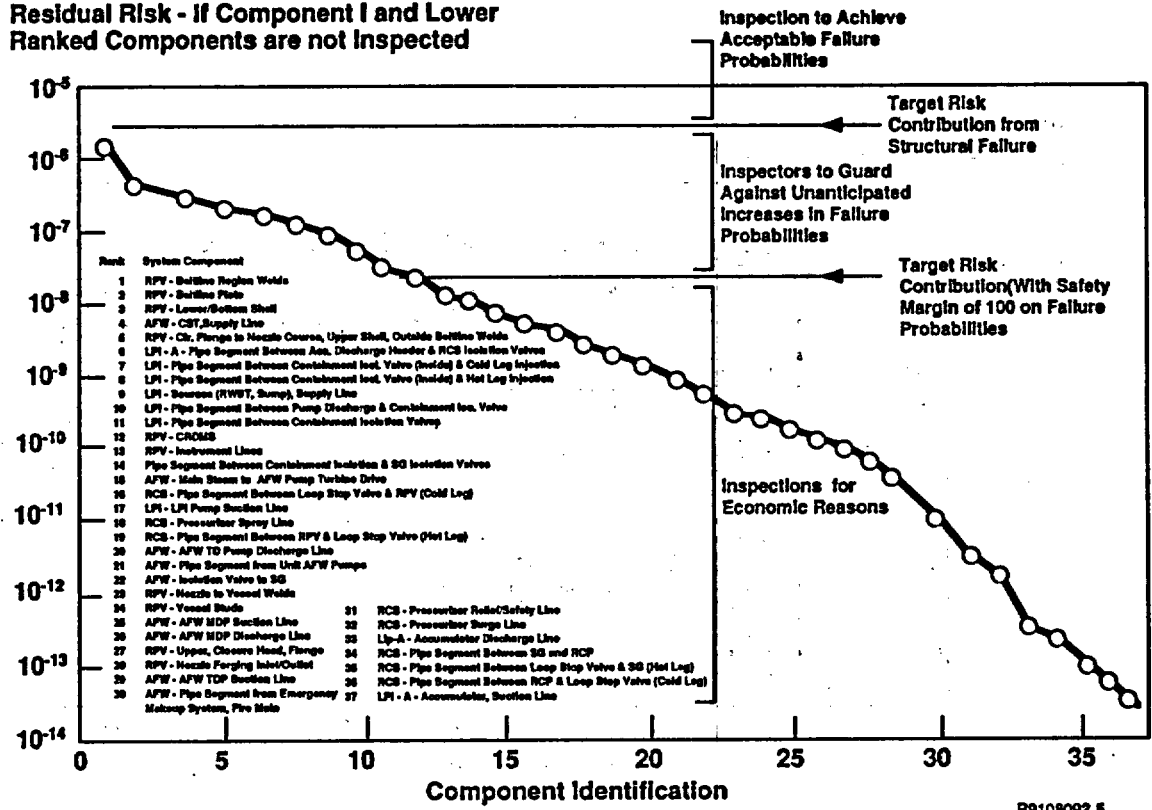


**FIGURE 2. Comparison of Residual Risk with Target Risk from Structural Failures**

Future work in coordination with the ASME Task Force will apply probabilistic fracture mechanics and decision analysis methods to identify optimum inspection strategies (NDE method, NDE effectiveness, inspection frequency, inspection location, and sample size) for high priority components. Output from the New ISI Criteria Task will be made available to the ASME Research Task Force on Risk-Based Inspection Guidelines for their use in preparing the document that will recommend risk-based inspection programs for codes and standards consideration.

**6.0 PISC-III**

The involvement in the Program for the Inspection of Steel Components Phase 3 (PISC III) is to take advantage of a large international program to support the acquisition of data bases for assessing the reliability of NDE. The PISC program has seven actions devoted to the in-depth study of particular aspects of NDE. Tracking and assessment is occurring for all of these actions, but the discussion here will be on Action 4 for studies on Austenitic Stainless Steels (AST). PNL, by virtue of this program, is one of the Action 4 co-leaders and has been actively involved with the design, development, and implementation of this action.

The AST has been initiated with inspections occurring for the capability studies for wrought stainless steel. There have been inspections performed by teams from across Europe and Japan. These specimens will be in the USA at the end of February 1992. Two teams have committed to examine these specimens and efforts are being expended to try to locate additional participants. The cast-to-cast and wrought-to-cast capability specimens are being fabricated with studies on these being planned to start during the second quarter of 1992. PNL has prepared for conducting relative operating characteristic curve (ROC) analysis on the AST data. Data should be received in late fall for conducting this analysis.

The reliability studies on wrought and cast specimens has been slow in starting. There is a shortage of funding that has primarily been responsible for this delay. The reliability study on wrought stainless steel is being rescoped to focus primarily on IGSCC. At this time there is limited interest from most of the European participants in this study. Only two teams have made a commitment to participate in these studies.

The future work will continue to support the studies in progress through both the coordination of teams from the USA and in conducting analysis of data generated in the studies.

## 6.0 CAST STAINLESS STEEL INSPECTION

The objective of the cast-stainless-steel-inspection task is to determine the effectiveness and reliability of ultrasonic inspection on LWR components containing cast stainless steel material. Examples of components containing cast material are clad pipe and pressure vessels, pump and valve bodies, centrifugally cast stainless steel (CCSS) piping, stainless steel and dissimilar metal welds, and weld-overlay-repaired pipe joints.

Work performed this past year entailed a CCSS workshop as part of a training course for NRC staff on computer-based UT systems, a letter report to the NRC on employing critical angle techniques for classifying CCSS microstructure, and publication of two papers for the annual "Review of Progress in Quantitative Nondestructive Evaluation" (QNDE) conference proceedings.

A training course for NRC staff was held at PNL in April 1991. During the course NRC Headquarters and Region personnel were given lecture on studies assessing ultrasonic inservice inspection of cast material and participated in three laboratory exercises for demonstration and hands-on experience. During the lecture, algorithms to classify CCSS microstructures were reviewed which included Rayleigh critical angle imaging by Hildebrand, Good, et al.<sup>2</sup> and

---

<sup>2</sup>Hildebrand, B. P., M. S. Good, A. A. Diaz, and E. R. Green. 1991. "Application of Critical Angle Imaging to the Characterization of Cast Stainless Steels," submitted for publication in Review of Progress in Quantitative Nondestructive Evaluation, Vol. 11, Plenum Publishing, New York, to be published 1992.

techniques developed by Kupperman, Reimann, et al. (1987), which were both developed under NRC sponsorship. These techniques detected microstructural changes as a function of depth and lateral position over piping.

Rayleigh-critical angle is the technique of insonifying a material at an incident angle where the acoustic energy that enters a material is a surface wave instead of a shear or longitudinal wave.<sup>2</sup> The basic principle is that the amplitude of the reflected wave undergoes a substantial decrease and recovery over a one to two degree change in the incident angle. Prior to the second critical angle, the incident wave is partitioned into a reflected wave and transmitted waves. At the Rayleigh critical angle which is just slightly larger than the second critical, a dramatic drop in reflected amplitude occurs due to a highly efficient mode conversion to surface waves. A dramatic recovery is observed one degree past the Rayleigh critical angle due to the wave being totally reflected. This phenomenon, therefore, is a sharp acoustic feature that is extremely sensitive to material properties such as wave velocity and acoustic attenuation. Since wave velocity of different CCSS microstructures vary, the technique should be capable of classifying the CCSS microstructure. Furthermore, since the surface-wave penetration is roughly one wavelength, multi-frequency techniques might be able to detect underlying layers of different microstructures and classify them. The work performed showed that it is feasible to classify microstructures; however, the limitations of the technique have not been determined.

Future work will represent a change in strategy to investigate very low frequency techniques that are expected to be less sensitive to the problems imposed upon ultrasonic ISI by coarse microstructures; e.g., Lamb waves, phase measurements, and large aperture L-wave transducers employing a pitch-catch configuration. The goal is to determine the smallest crack that can be reliably detected and then to assess, using fracture mechanics, the significance of this crack size to structural integrity.

## 8.0 SURFACE ROUGHNESS CONDITIONS

The objective of the surface roughness task is to make Code recommendations which assure that a surface condition does not degrade the effectiveness and reliability of ultrasonic inspection of LWR components.

PNL took an empirical approach to evaluate the effect of surface condition; however, this changed to estimating distortion by means of computer modelling. The empirical work was directed towards weld crowns and piping. The result was a letter report "Significance of Surface Condition Upon Ultrasonic Inspection" submitted to the NRC in 1988. This report stated that the as-built, surface-condition was governed by the subjective judgement of the radiographer during construction and that abrupt surface changes on the order of 1.5 mm are expected. It was also noted that the newer versions of the Code did not circumvent the problem of subjectivity. In other words, the ASME Code does not provide an objective specification to quantify surface condition for inservice inspection.

After the initial study, PNL and the Center for NDE at Iowa State University (CNDE-ISU) discussed possible collaboration using a computer model as a much more efficient means of determining recommendations concerning acceptable/unacceptable surface conditions for ultrasonic ISI. In 1988 a coordination plan between the US NRC and EPRI was approved. Tasks included model refinement by CNDE-ISU under EPRI sponsorship, experimental data acquisition and model validation by PNL under US NRC sponsorship, and submission of ASME Code recommendations by both institutes.

Work performed this past year entailed comparison of longitudinal wave (L-wave) data, transfer of the current model to PNL, and use of a simplistic ray tracing model at PNL.

One objective was to refine the CNDE-ISU model so that it could be validated for the simulation of weld crowns (step discontinuities). Model refinement included an evaluation of normal ( $0^\circ$ ) and oblique ( $45^\circ$ ) L-waves through step discontinuities. Of interest is the field amplitude at the back surface of the plate. The model predicted the response along the back surface while experimental measurements used a through-transmission technique with a microprobe receiver positioned adjacent to the back surface. No comparisons were made for shear waves. This was due to interference from spurious signals when collecting experimental data.

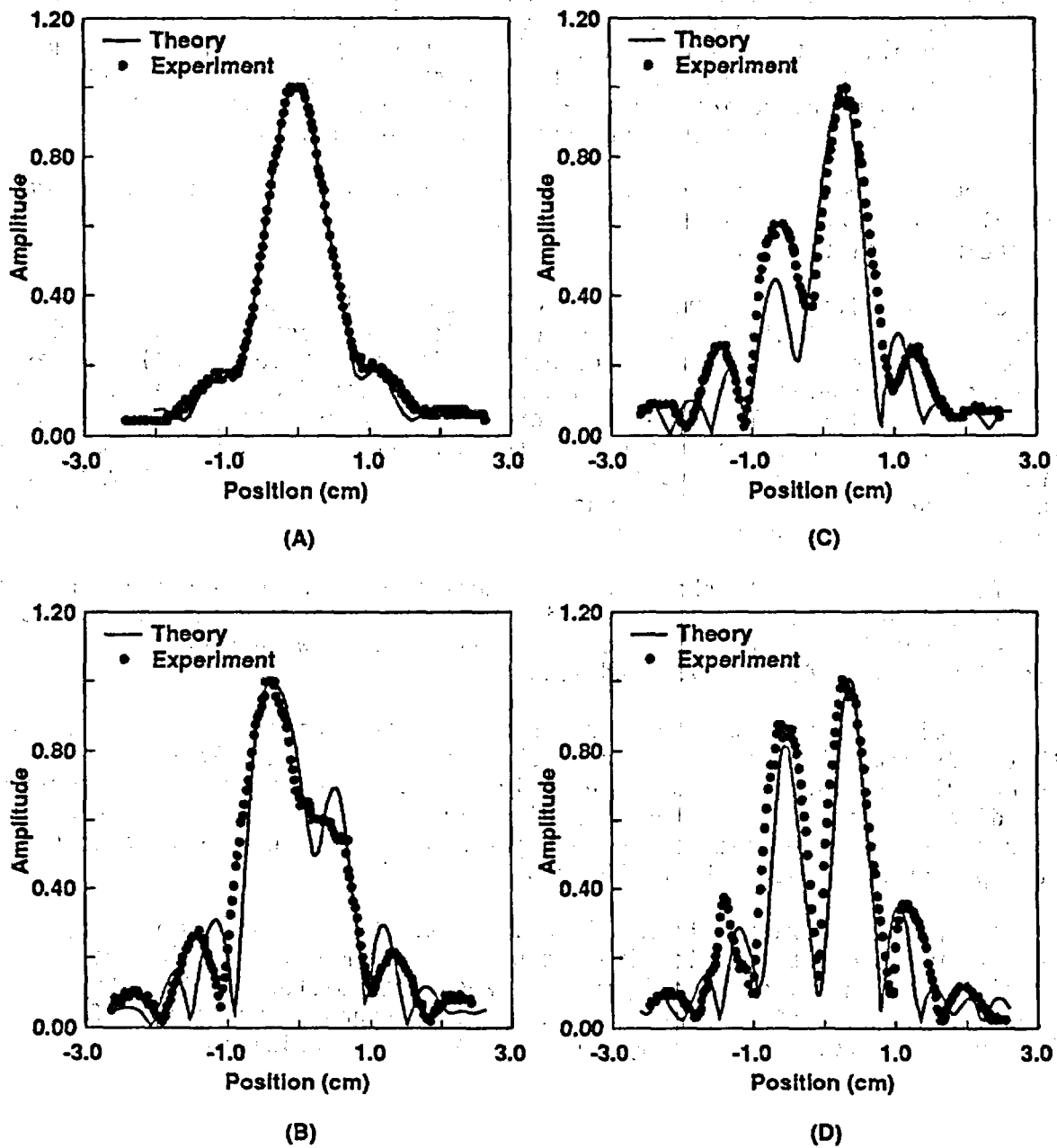
The  $0^\circ$ , L-wave data showed good agreement between model prediction and experimental data (Figure 3). These included the reference case of a flat plate with parallel, planar surfaces as well as cases with step discontinuities of 0.25, 0.75, and 1.50 mm.

The  $45^\circ$ , L-wave data showed discrepancies that were more apparent than with the  $0^\circ$  data (Figure 4). Data matched well for a flat plate with no discontinuity (Figure 4a) and a step height of 0.25 mm (Figure 4b); however, large discrepancies existed for step discontinuities of 0.75 and 1.50 mm. Comparison of model predictions with experimental measurements were documented in a paper by A. Minachi, R. B. Thompson, et al.

Two problems exist with model refinement. One is the discrepancy in L-wave data which may be due to either experiment or model. An obvious possibility is checking the alignment between transmitter and the step discontinuity. The other problem is a spurious signal causing interference with shear wave reception during experimental data acquisition.

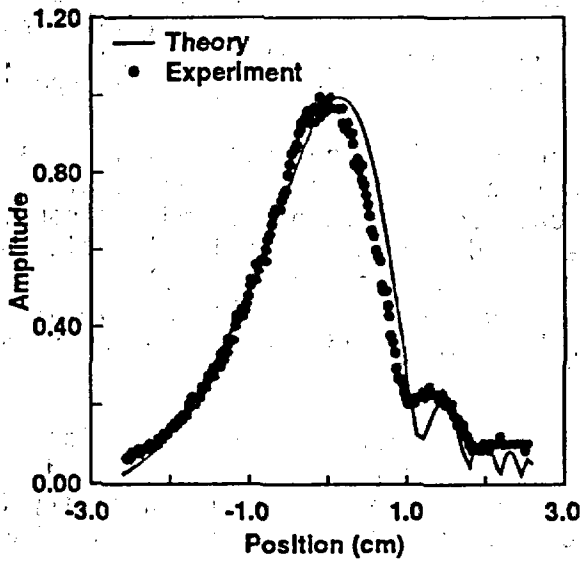
---

<sup>3</sup>Minachi, A., R. B. Thompson, M. S. Good, and A. A. Diaz. 1991. "Ultrasonic Wave Propagation Through an Interface with a Step Discontinuity" submitted for publication in Review of Progress in Nondestructive Evaluation, Vol. 12. Plenum Press, New York, to be published 1992.

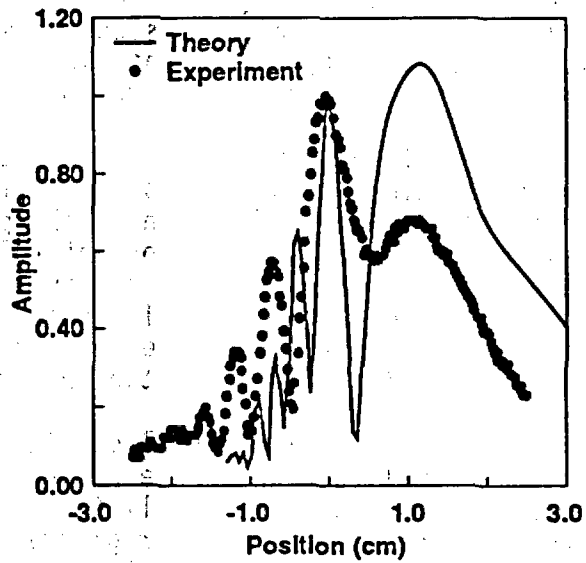


R9110099.1

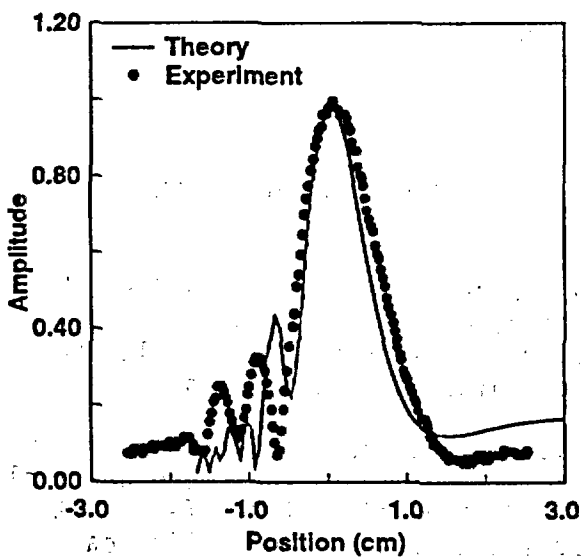
**FIGURE 3.** An Ultrasonic,  $0^\circ$ , Refracted L-Wave Perturbed by a Step Interface: a) reference (no step), b) 0.25-mm step height, c) 0.75-mm step height, and d) 150- $\mu$ m step height



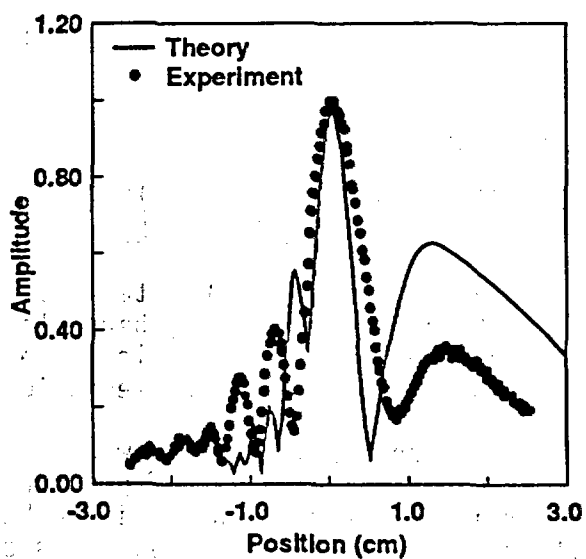
(A)



(C)



(B)



(D)

R9110099.2

**FIGURE 4.** An Ultrasonic, 45°, Refracted L-Wave Perturbed by a Step Interface: a) reference (no step), b) 0.25-mm step height, c) 0.75-mm step height, and d) 150-mm step height

A simplistic central ray model was developed at PNL to gain insight into the use of models and to make better use of the CNDE-ISU model. The technical goal of this activity was to consider how the central beam from a probe travels through a stainless steel pipe as the probe passes over a weld crown (step discontinuity). The data were in good agreement with the model predictions and results were documented in a letter report to the US NRC.<sup>4</sup>

The primary conclusion in the report was that the experimental data from simulated weld crowns matched well with model predictions. Model analysis indicated that the refraction at the probe-wedge-to-couplant and the couplant-to-steel interfaces play important roles in determining spatial location of the beam and arrival time of received responses. As the probe slides over the edge of a weld crown, variables such as probe tilt may result in a volumetric region not being fully scanned, a crack base mispositioned farther away, and crack under-sizing by crack tip analysis.

Future work will entail continued model refinement and validation, including amplitude and phase response from notch reflectors, broadband time response, and expansion to all four geometries; i.e., step discontinuity (weld crown), concave surface (over grind), convex surface (diametrical shrinkage), and elevated point (weld splatter).

## FABRICATION FLAWS

### INTRODUCTION

#### 1.0 SAMPLING PLAN - DETERMINATION OF FABRICATION FLAW DISTRIBUTIONS IN REACTOR PRESSURE VESSELS

The objective of this task is to accurately estimate the distribution of fabrication flaws (i.e., numbers, location, and sizes) that occur in light water reactor pressure vessels. The flaw distribution is generally an important input to fracture mechanics calculations and risk assessments.

Data concerning the flaw distribution is to be acquired by performing NDE examinations of a set of pressure vessel weldments that were never placed in service. The examination is to be conducted using state-of-the-art ultrasonic inspection (SAFT). This section discusses the statistical methodology that will be used to estimate the flaw distribution and the amount of inspection that will be required to accurately estimate the flaw distribution.

---

<sup>4</sup>Greenwood, M. S. 1991. "Modeling of a Step Discontinuity," letter report submitted to US NRC in September Monthly Report, Pacific Northwest Laboratory, Richland, WA.

## 1.1 Estimating the Flaw Distribution

The basic input to a fracture mechanics analysis, for example, PTS calculations is a flaw frequency function<sup>5</sup>. This function describes the average number of flaws of particular size that should be found in a unit of material. To be more specific, the cumulative frequency function,  $\Lambda(s)$  is defined as the average number of flaws less than size  $s$  that will occur in a unit of material. The derivative of this cumulative function is called the frequency function.

Figure 5 illustrates the most famous flaw size frequency function, the Marshall "distribution." To obtain the frequency function plotted in Figure 5, we have made a change of units. The original Marshall "Distribution" was expressed in units of flaws per reactor vessel. Since reactor vessels can be of different sizes, we found this not to be most reasonable and converted the result to "flaws per linear foot" of weldment by using the conversion factor of 180 feet of weldment per reactor vessel. From the frequency function plotted in Figure 5, one can see that two flaws will occur every 100 feet, or an average of 3.6 flaws will occur in every (180 ft.) of reactor vessel weldment. The actual equation for this function is given by

$$\Lambda_{\text{Marshall}}(s) = 0.02 (1 - e^{-4.06s}) \quad (1)$$

where the constant  $-4.06$  is measured in  $\text{in.}^{-1}$  and the constant  $0.02$  is expressed in units of flaws per foot of weldment.<sup>6</sup>

If the inspection procedure could find all flaws and accurately size them, it would be an easy matter to estimate the flaw frequency function; one would only have to assemble the inspection data into a histogram to obtain an unbiased estimate of the true frequency function or, if one wanted to be more sophisticated, fit a parametric form to the data using the method of maximum likelihood. However, biases occur in the data when an imperfect inspection procedure is utilized.

---

<sup>5</sup>There is a good deal of confusion in the nomenclature used for the flaw "distribution." The flaw frequency function is sometimes mis-labeled as a flaw distribution, even though it does not integrate to 1. For example, the original "Marshall Distribution" is a frequency function, not a flaw distribution.

<sup>6</sup>This Marshall "Distribution" was extracted from page 41 of NUREG/CR-4486 (Simonen 1986). Actually there are several variants of the Marshall distribution. The distribution used here represents the incidence of flaws before preservice inspection.

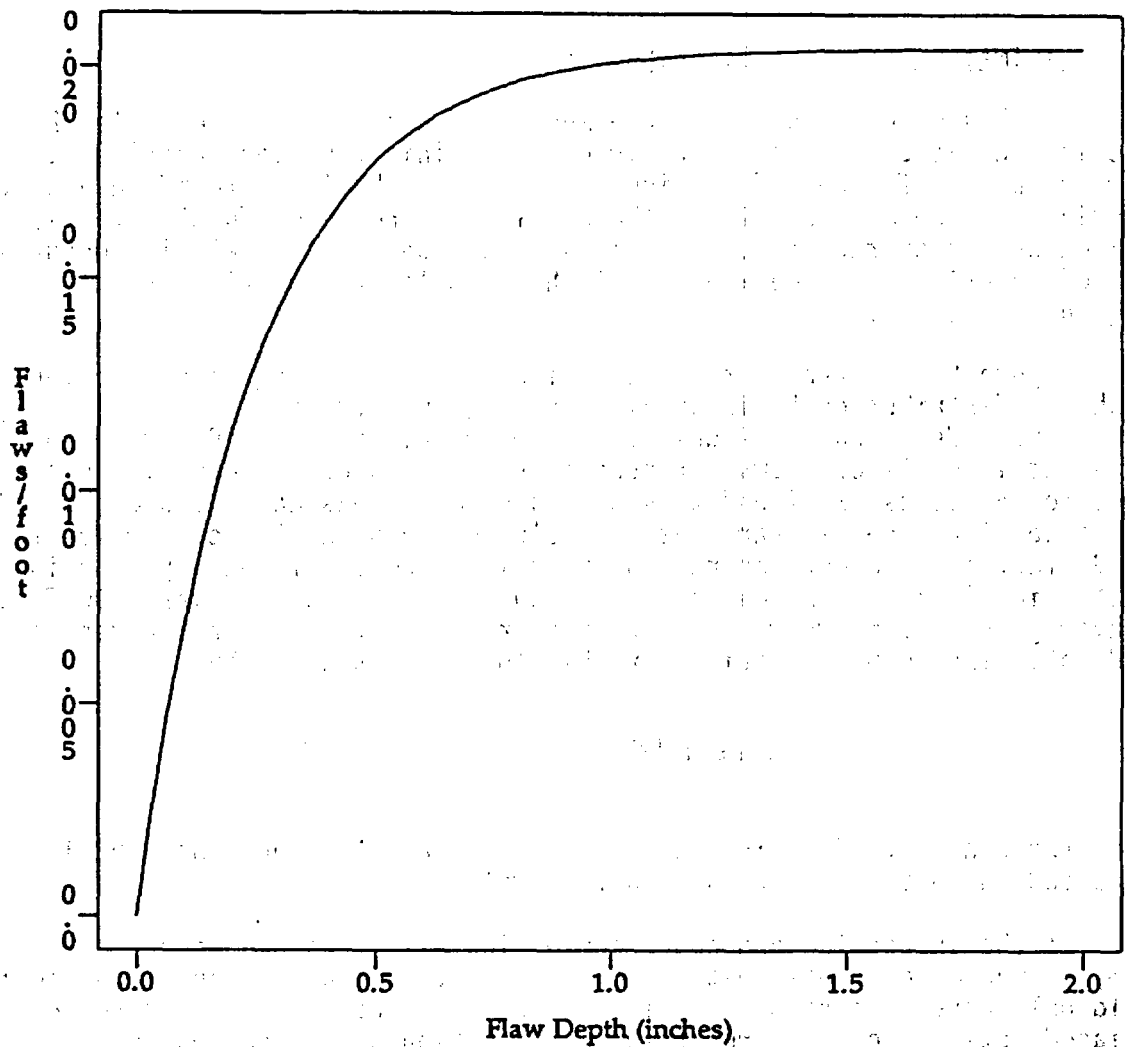


**FIGURE 5. Marshall Flaw Distribution**

The biases are caused by two deficiencies in the inspection procedure; the inspection procedure's inability to detect all flaws, and the procedure's inability to correctly size the flaws. The procedure's detection capability is given by its probability of detection curve  $POD(s)$ , which describes the probability that the procedure will detect a flaw of size  $s$  during inspection. For example, Figure 6 displays the estimated  $POD$  capabilities of the SAFT system. As one can see from the figure, the SAFT system has a high chance of detecting any flaw larger than 0.75 inch. The actual formula for the  $POD$  curve is

$$POD(s) = (1 + \exp(3.01 - 5.61s))^{-1} \quad (2)$$

where the variable  $s$  is measured in inches.

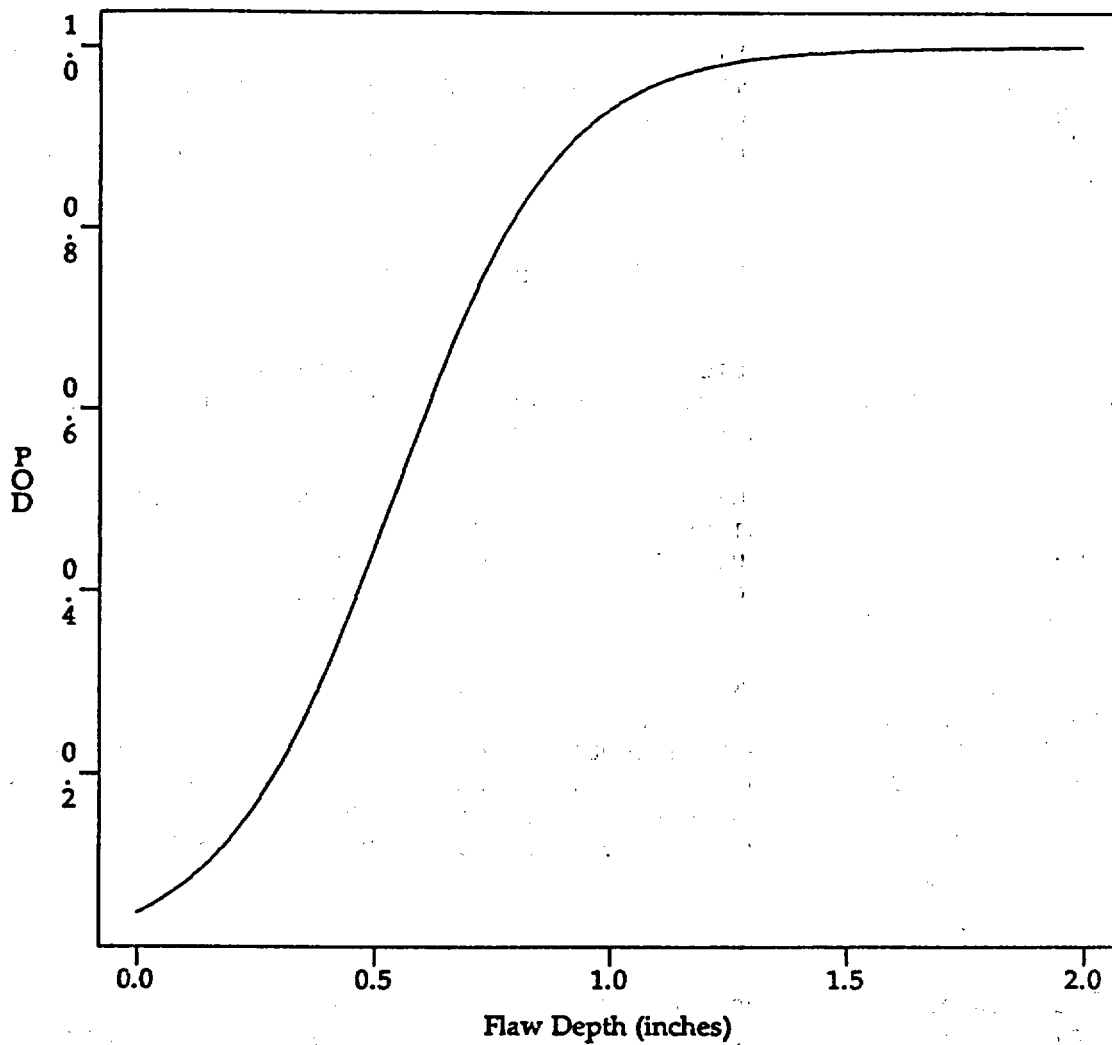


**FIGURE 6. SAFT POD Function**

Given a procedure with detection capabilities described by the POD curve  $POD(s)$ , its observed frequency function will be related to the true function through the formula

$$\Lambda_{obs}(s) = \int_0^s POD(s) \Lambda_{true}(s) ds \quad (3)$$

In other words, the small flaws with low probability of detection are under-represented in the observed data.

A similar formula describes the effects of sizing error on the observed frequency function. For example, if the measurement error (i.e., measured minus true size) is described by the probability density  $\phi(e)$ , then the observed frequency function will be related to the true function through the formula

$$\Lambda_{obs}(S) = \int_0^{\infty} \phi(S-z) \Lambda_{true}(z) dz \quad (4)$$

In other words, measurement error produces a "smeared" version of the true frequency function; the true frequency function is convolved with the error distribution to obtain the observed function.

Equations (3) and (4) describe the basic relationship between the true and observed frequency functions. These formulas can also be used to produce unbiased estimates of the true frequency function. To obtain the simplest estimate, one simply needs to "invert" equations (3) and (4) so that  $\Lambda_{true}(s)$  can be expressed in terms of  $\Lambda_{obs}(s)$ .

This is the method we will use to estimate the flaw size frequency function. It will produce a "non-parametric" estimate for this function; that is the estimate will require no assumptions concerning the shape of the underlying distribution. The method will require that the characteristics of the inspection procedure be accurately known (i.e.,  $POD(s)$  and  $\phi(e)$ ). To obtain this information, the SAFT procedure has been subjected to qualification testing.

## 1.2 Amount of Material to be Inspected

The accuracy (more specifically, standard deviation) with which the frequency function  $\Lambda(s)$  can be estimated is proportional to  $1/\sqrt{N}$ , where  $N$  is the number of flaws found during the inspection; in order for the exercise to be successful, it must examine enough material to be assured of detecting a certain minimal number of flaws. As an initial design criteria, it is reasonable to require the inspection to find at least 10 flaws of size larger than 1/4 inch in order to estimate the flaw distribution with some precision.

Tables for various assumptions for the distribution based on NDE effectiveness and assumed distribution form have been generated. With a limited amount of material being available, the actual sampling plan is based on performing sufficient inspections on the PVRUF RPV that the true flaw distribution can be estimated correctly. The limitation of material necessitates that the distribution will only be as a function of flaw depth. Although, other information will be gathered for each flaw, the limited size of the data base will not allow accurate estimates of the distributional form for these other parameters (location, length size, etc.). At the same time we will perform an analysis based on type of flaw but will most likely lump all of the flaws together. The rationale for performing this last step is that from an NDE standpoint, it will be nearly impossible to prove that non-planar

flaws do not have stress risers that will make them respond in a fracture mechanics sense like a planar flaw.

## 2.0 EQUIPMENT PREPARATION

### 2.1 Upgrades to SAFT-UT Inspection System

This year's improvements to the SAFT-UT system were chosen to facilitate the inspection of the PVRUF RPV that is at ORNL. This includes a series of tasks that need to be performed since the SAFT system will be at ORNL and the plan is to have the data collected there and returned to PNL for analysis. Secondly, because of the complex geometry of the nozzles, a robotic manipulator will be used to scan the inner and outer radius of these nozzles. Thirdly, a Sun SparcStation2 graphics workstation has been set up to analyze the SAFT data.

### 2.2 SAFT-UT Inspection System

A description of the SAFT system can be found in Doctor et al. (1991). The upgraded SAFT-UT system is shown in Figure 7. The existing data acquisition system controls the SAFT pipe scanner and transfers ultrasonic data to the host computer. The host computer receives data from the data acquisition systems, files the data, and prepares the data for processing and display. The real-time processor is a peripheral device to the host computer that performs the computationally intense SAFT algorithm. The existing Ramtek graphics processor provides the image display to the operator for interpretation as does the new Sun graphics workstation. Finally, a new data acquisition system controls a robotic scanner and transfers data to the host computer.

### 2.3 Robotic Data Acquisition System

A robotic data acquisition system has been assembled for scanning the nozzle areas of the reactor pressure vessel. A PUMA 562 industrial robot will be used. This is a six-axis robot with a radial reach of 36 inches and a repeatability of better than 0.004 inches. A preamplifier is located on the robotic arm. This amplifies the received echo signal and provides the input to the main amplifier for data acquisition. The remote preamplifier has a gain of 20 dB and a 3-dB bandwidth of 5 MHz. It significantly increases the signal-to-noise ratio by amplifying the echo signal prior to transmission on the long interconnecting cable; thus, any noise introduced during the transmission will be significantly less with respect to the echo signal.

The data acquisition subsystem uses a 486 computer with SAFT data acquisition software. This subsystem contains the electronics to control the robot, amplify the returned echo, and digitize the full RF signal. Included in the data acquisition subsystem is a Time Variable Gain (TVG) amplifier to compensate for material attenuation and to maximize the system dynamic range. The gain of the TVG amplifier is programmable up to a maximum of 40 dB. The TVG supplies the input signal to the STR8100 digitizer to be sampled, converted, and stored.

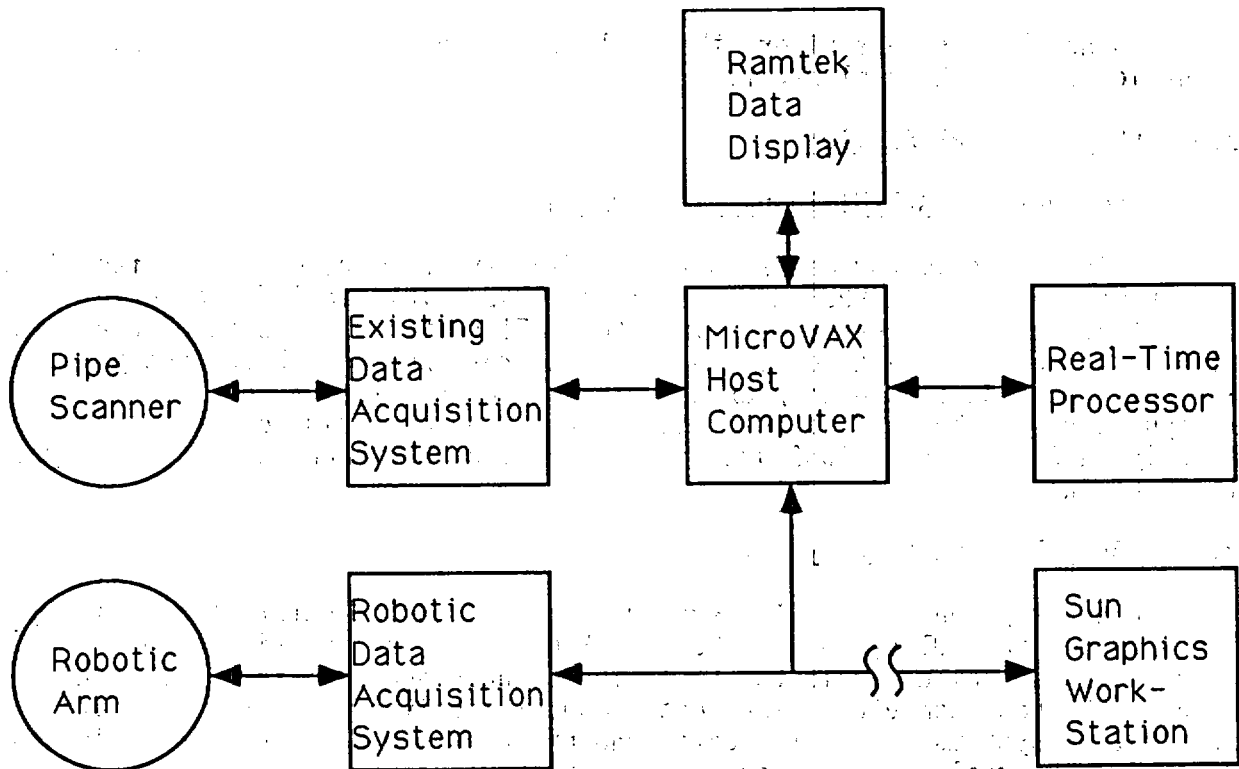


**FIGURE 7. Block Diagram of Upgraded SAFT-UT System**

The 486 computer controls the data acquisition process, provides local data storage, and a data interface to the SAFT processing and analysis subsystem. The 486 computer provides the operator interface for the real-time mode of operation. The software is menu driven to assist in assuring that the SAFT parameters are correctly entered prior to data acquisition. An overview of the menu sequence is given in Doctor, et al. (1991).

If data are to be transferred to the SAFT subsystem concurrent with the scanning operation, then the connection is made to the host computer. A command from the 486 invokes the data transfer utility on the host. The host prompts the user to determine if concurrent SAFT processing and/or display is desired.

#### **2.4 New Graphics Workstation**

A new Sun SparcStation2 graphics workstation has been set up to analyze the SAFT data. Data may be transferred to the workstation for either the robotic data acquisition system or the MicroVAX host computer. All of the SAFT utility software will be available on the graphics workstation. The graphics workstation uses the UNIX operating system with the X-windows utility for window-oriented data presentation and data processing management. The graphics workstation is configured as follows:

- SparcStation2 computer with color monitor
- 48 MB memory
- 400 MB system disk
- 1.5 GB SCSI disk drive for data storage
- 800 MB write once laser disk
- IEEE 488 interface
- color printer

### 3.0 MIDLAND DATA ANALYSIS

The SAFT system was used to perform inspections on four blocks that had been cut from the beltline weldment of the Midland reactor vessel. A total of 164" of circumferential weld length was inspected. This is a weldment that is a double "V" design and the cladding was deposited using a multi-wire process and smoothed with a belt grinder. The SAFT system was operated at maximum sensitivity to try to detect very small flaws and then to characterize them accurately. Table 1 contains a summary of the results from this analysis. It should be noted that these 11 are denoted as indications and follow-up work is planned through some destructive testing to validate the data in this table. It must be remembered that this is a limited data base and the extension to the population of RPVs in a generic sense is difficult to do. The extension of this data to predict the true flaw population of the Midland RPV is not an easy thing to do because the data represents only the conditions of a limited portion of the beltline weldment. Even with these caveats, it should be noted that some useful trends can be seen in the data. The data was analyzed and compared to the "Marshall" distribution and was found to possess the same shape. However, the Midland data is found to be a factor of over 40 times larger than that predicted by the "Marshall" distribution. More work is planned on this data base, and then it will be integrated with the new data to be generated next year on the PVRUF RPV.

### REFERENCES

ASME. 1991. Risk-Based Inspection - Development of Guidelines, Volume 1 General Document, CRTD-Vol. 20-1, prepared by the Research Task Force on Risk-Based Inspection Guidelines, issued by the American Society of Mechanical Engineers Center for Research and Technology Development.

Doctor, S. R., R. E. Bowey, P. H. Hutton, R. J. Kurtz, and G. J. Schuster. 1991. "Advanced NDE Technologies and Characterization of RPV Flaw Distribution," in Proceedings of the U.S. Nuclear Regulatory Commission Eighteenth Water Reactor Safety Information Meeting, NUREG/CP-0114, Vol. 3, pp. 137-155.

Kupperman, D. S., K. J. Reimann, and J. Abrego-Lopez. 1987. "Ultrasonic NDE of Cast Stainless Steel" in NDT International, Vol. 20, No. 3, pp 145-152.

Simonen, F. A. 1986. VISA-II - A Computer Code for Predicting the Probability of Reactor Pressure Vessel Failure, NUREG/CR-4486. Prepared by Pacific Northwest Laboratory for the U.S. Nuclear Regulatory Commission, Washington, D.C.

**TABLE 1. Summary of SAFT-UT Indications from Midland Blocks Exhibiting Measurable Through-Wall Extent**

Indication	Estimated Depth Below Clad Surface, in.	Estimated Through-Wall Extent, in.	Estimated Circumferential Extent, in.	Material
1	7.0	0.7*	1.4	Weld
2	5.7	0.2	0.9	Base
3	7.0	0.4	>0.1**	Base
4	2.5	0.2	0.5	Base
5	4.5	0.2	0.5	Weld
6	4.8	0.3	1.0	Weld
7	4.7	0.1	0.4	Near fusion zone
8	5.2	0.1	0.4	Weld
9	5.9	0.1	0.85	Near fusion zone
10	0.42	0.11***	0.65	Base
11	0.45	0.14***	0.9	Base

\* Three independent flaws bounded by ASME Code Proximity Rules.

\*\* Size uncertain because only part of the flaw was insonified.

\*\*\* Indications conservatively assumed to be crack tips with the through-wall extent calculated as the depth below the clad inner surface minus the clad thickness (0.31 in.).

# VALIDATION AND TRANSFER OF ADVANCED NDE TECHNOLOGIES<sup>1</sup>

S. R. Doctor, P. H. Hutton, R. E. Bowey,  
R. J. Kurtz, L. D. Reid, G. J. Schuster  
Pacific Northwest Laboratory  
Operated by Battelle Memorial Institute  
Richland, Washington 99352

## ABSTRACT

This paper is a review of a program involving the final stages of the development and acceptance of two advanced NDE technologies: acoustic emission (AE) for continuous monitoring of light water reactor components and the synthetic aperture focusing technique for ultrasonic testing (SAFT-UT). This paper covers the activities on this program over the past year.

## INTRODUCTION

This paper is divided into two parts: Acoustic Emission and SAFT-UT. This paper will discuss the highlights of the work performed on these activities in the order listed.

## ACOUSTIC EMISSION

### INTRODUCTION

A major program has been conducted over several years developing technology to support the application of acoustic emission (AE) monitoring to detect the initiation and growth of cracks in nuclear reactor components as it might occur during reactor operation (Hutton et al. 1991). The work has been performed at PNL under support from the U.S. Nuclear Regulatory Commission, Office of Nuclear Regulatory Research (NRC-RES). The ultimate benefits to NRC expected from this program are:

- increased safety through detection and evaluation of crack initiation and growth as it occurs during reactor operation
- provides a means of continuously monitoring flaw indications identified by ultrasonic inspection for indications of growth during reactor operation

---

<sup>1</sup>Work supported by the U.S. Nuclear Regulatory Commission under Contract DE-AC06-76RLO 1830; FIN B2913; Dr. J. Muscara, NRC Program Manager.

- improved capability to detect and locate coolant leaks as they initiate
- reduced exposure of personnel to radiation by reducing the need for manual inspection of reactor components.

The program has produced AE monitoring technology and methodology to detect and evaluate cracking that has been proven in tests performed on piping (IGSCC), on a vessel under simulated reactor operating conditions (fatigue cracking), on vessels during hydrostatic testing (stable and unstable crack growth), and on a reactor system during hot functional testing (reactor background noise interference). The technology has been incorporated into the ASTM Standards (E 1139) and the ASME Code, Section XI (Code Case N-471). The remaining requirement to validate the technology for application to help assure the safety of nuclear system components is to demonstrate detection and evaluation of cracking in an inservice reactor component using AE. This validation is in process at Philadelphia Electric Company's (PECO) Limerick Unit 1 reactor.

### FIELD VALIDATION

AE monitoring of a flaw indication identified by ultrasonic testing in a 12" reactor coolant nozzle-to-safe end weld at Limerick Unit 1 Generating Station was started in May 1989 and continued to the reactor refueling outage in September 1990. AE monitoring of the same location during a second fuel cycle is currently in progress. This discussion focuses on the results obtained during the first AE monitoring period from May 1989 to September 1990. AE system installation was discussed during the 18th Water Reactor Safety Information Meeting and is the subject of a published report (Hutton and Dawson 1989) so it will not be repeated here. A description of the weld being monitored and the flaw indication is given in Figures 1, 2, and 3. The pictorial presentation of the flaw indication in Figure 3 and subsequent illustrations is approximately to scale but is not considered to be exact. Description of the flaw indication is based on ISI results reported by General Electric Company (General Electric Nuclear Energy, 1989).

AE data [AE event count, difference-in-time-of-arrival of each event signal at the various AE sensors (delta-time), sequence of signal arrival at the sensors, peak amplitude of each event signal, time for each event signal to reach peak amplitude, and clock time information] was recorded in digital form on magnetic tape cartridges. The cartridges were replaced on approximately one-month intervals by PECO personnel and the used cartridge was sent to PNL for analysis. The data on the tape cartridge was played back to a computerized analysis program to compile AE event count by source location. Source location format is in terms of signals originating within each of 36 equal segments (source location elements) around a cross-section of the pipe looking into the reactor. Although the AE source location can be very accurate, the accepted accuracy range for field monitoring is  $\pm 1$  wall thickness of the component being monitored. In this case, the location could vary by  $\pm 1.3$  inches which translates to  $\pm 10^\circ$ . The accuracy tolerance is due to variations in the AE signal propagation velocity to the various sensors and

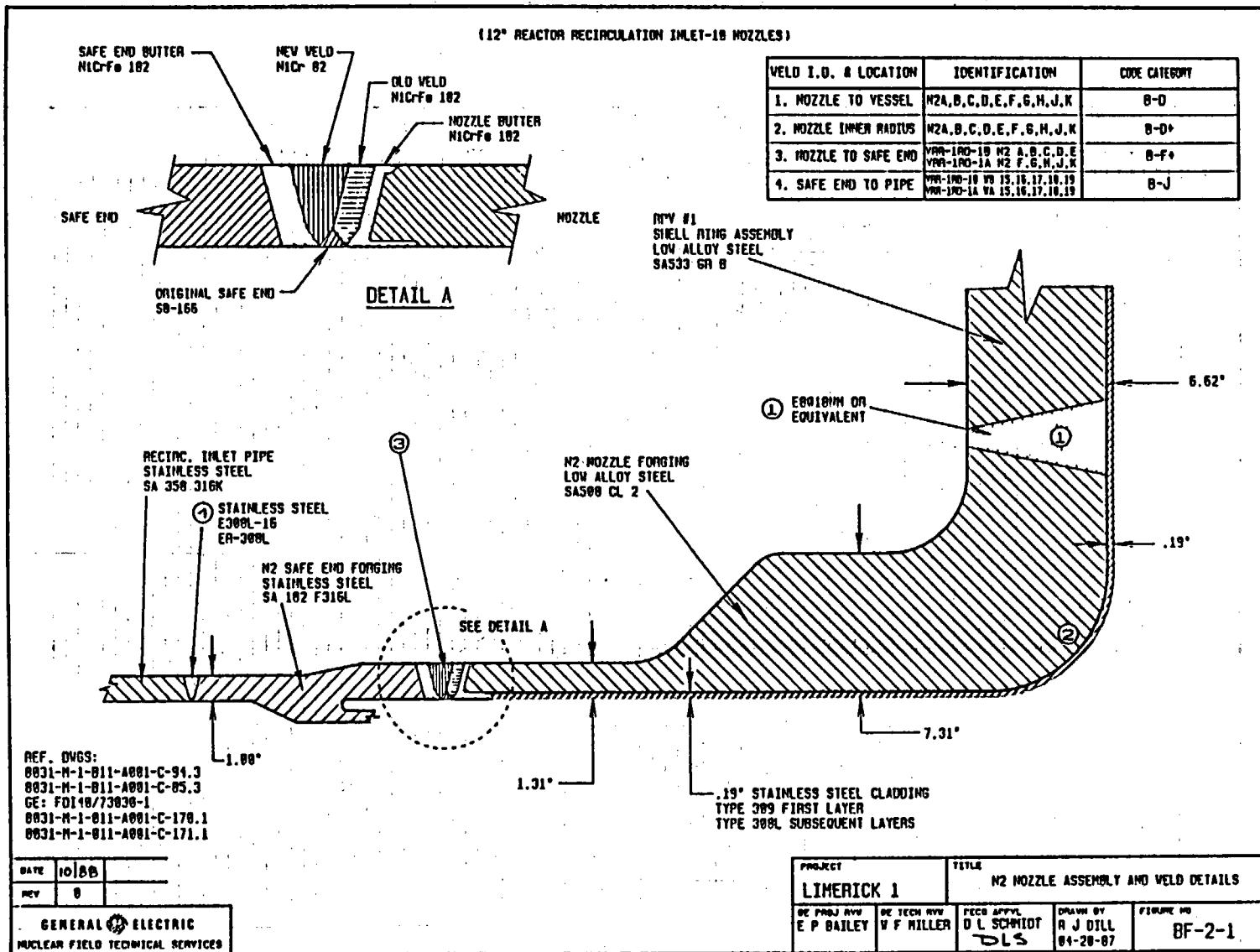


FIGURE 1. N2H Weld Configuration - Limerick Unit 1 Reactor

60° R.L. INDICATION RESOLUTION SHEET

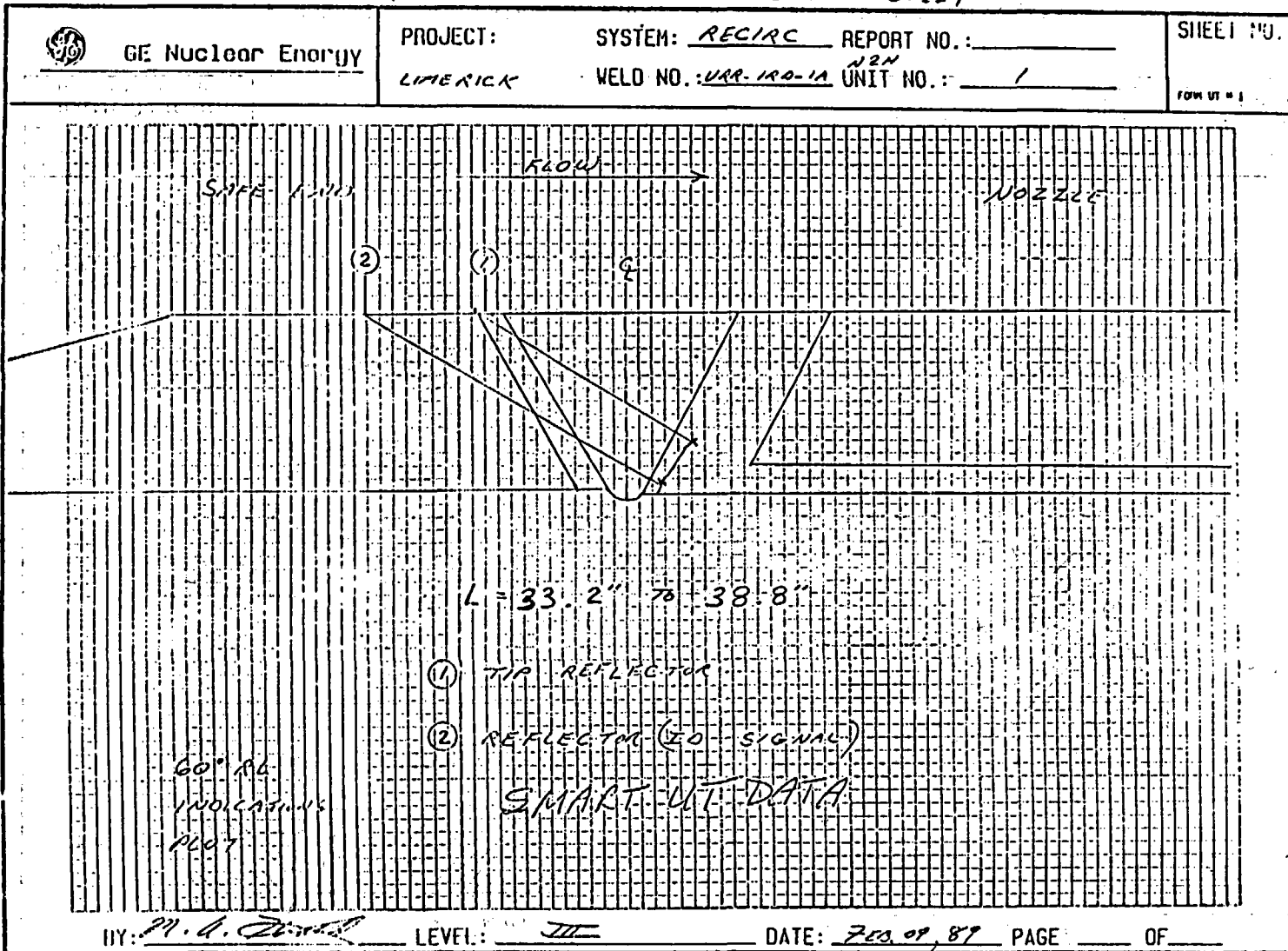
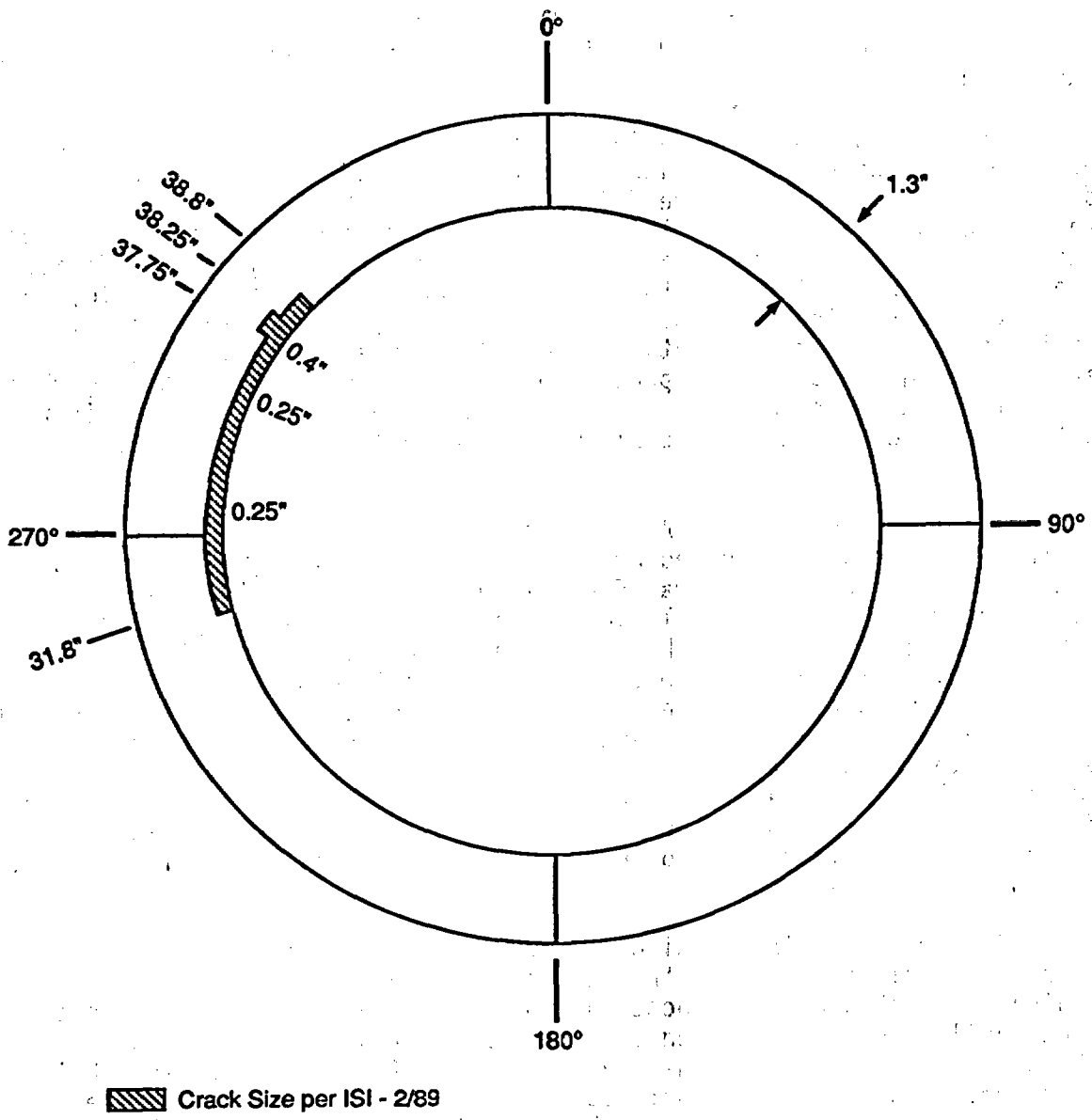


FIGURE 2. Location of Flaw Indication in N2H Weld - Limerick Unit 1 Reactor



R9110073.2

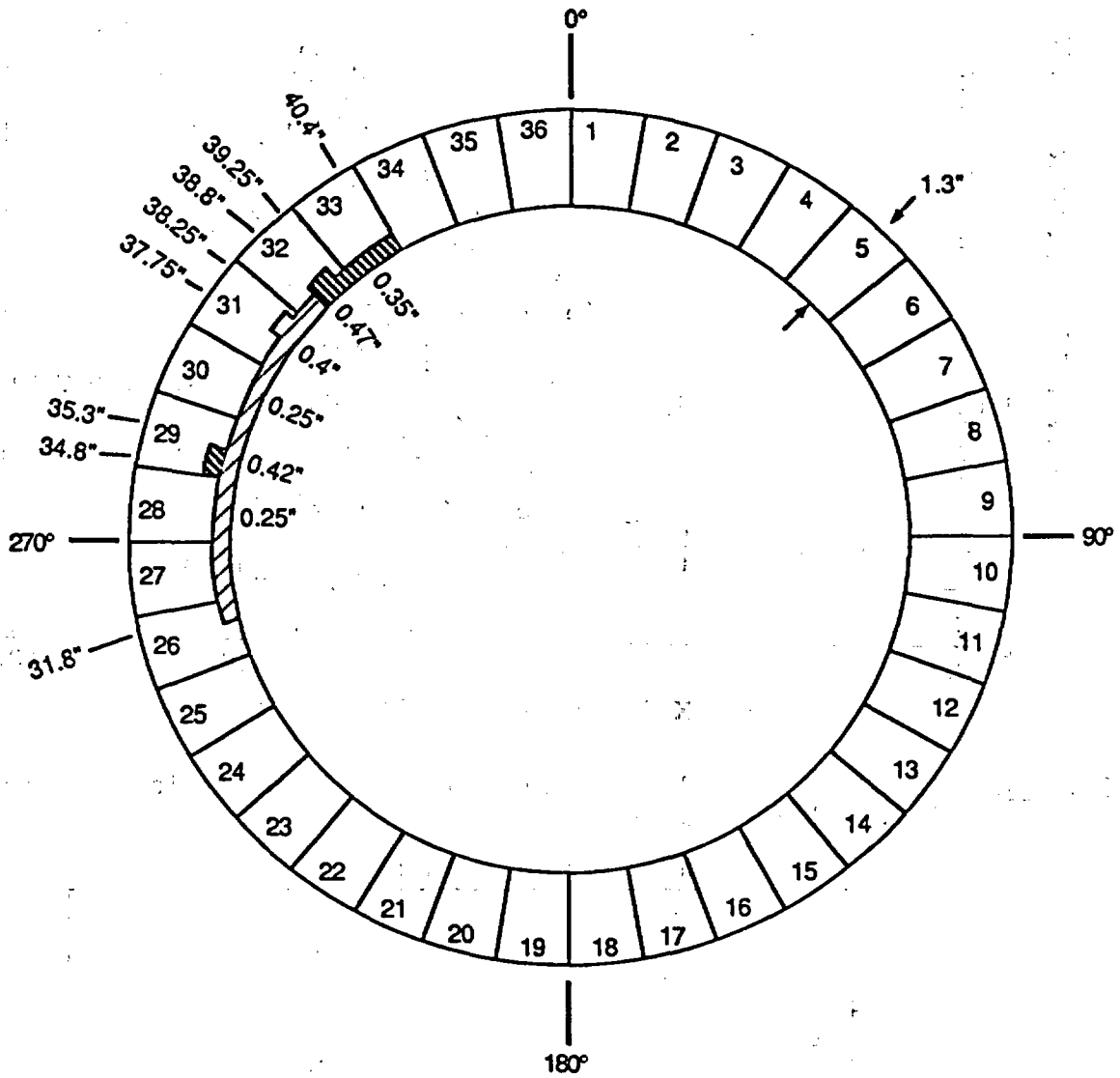
**FIGURE 3.** Pipe Cross Section Showing Profile of flaw Indicated by UT in February 1989 - N2H Weld at Limerick Unit 1 Reactor

the difficulty of precisely defining the position in time of the AE signal wave front.

Unshielded signal leads in the containment penetration presented a problem of transient noise signal pickup which had to be dealt with during AE data analysis. A restrictive filter was applied to the data played back from the field data cartridges. This filter limited accepted data to that which showed delta-time values rational for the geometry being monitored; i.e., it used the prior knowledge of the specific area of interest (the weld) to screen out extraneous noise signals. This is a totally acceptable method for this application or other applications under ASME Code Case N-471 where a specific area is being monitored as opposed to general volumetric monitoring where the site of cracking is unknown at the outset. General volumetric monitoring for detection of cracking is feasible with a normally quiet AE monitoring instrument.

The filtered AE data (AE count per source location element) was related to the crack growth indicated by ultrasonic inspection (UT) performed at the end of the fuel cycle (General Electric Nuclear Energy, 1990) shown in Figure 4. There was a direct correlation between AE and UT showing crack growth in source location element 29 which was used to calibrate an interpretive relationship. The AE/fatigue crack growth relationship shown in Figure 5, which was developed from experimental fatigue crack growth data, was tested using the location 29 AE data and the corresponding crack growth indicated by UT. The less conservative of the two curves [i.e.,  $dN/dt = 1.6 \times 10^{-4} (da/dt)^{1.9}$ ] fit the data quite well. Applying this relationship to the filtered AE data produced the crack growth estimate shown in Figure 6. Figure 7 presents the same crack growth estimate in pictorial form along with the original flaw indication.

Comparing the information in Figures 4 and 7, it is evident that there is some correlation between the AE and UT measurements but that the AE also indicates crack growth in locations not indicated by UT. This is not necessarily inconsistent when examined in light of the nominal detection threshold of about 20% of wall thickness for UT inspection. The AE indicated crack growth was small in most locations and the UT must detect the cracking by a far-side insonification which means that substantial crack size is needed before reliable UT detection can be assured. This is illustrated in Figure 8 where the nominal UT detection threshold is superimposed on the AE indicated cracking. At the same time, AE indications of crack growth less than 0.1 inches can be questioned on the basis of the small number of AE counts (3 to 5) from which they are derived. Of course, the only positive verification of the true crack growth will come if and when the weld is removed and can be examined destructively.



1.  Crack Size per ISI - 2/89
2.  Crack Growth per ISI - 10/90
3. Numbered Sectors Identify AE Source Location Elements - Each 10° Wide

R9103152.4

**FIGURE 4.** Profile of Original Flaw Indication and Flaw Growth from 2/89 to 10/90 Based on ISI - N2H Weld at Limerick Unit 1 Reactor

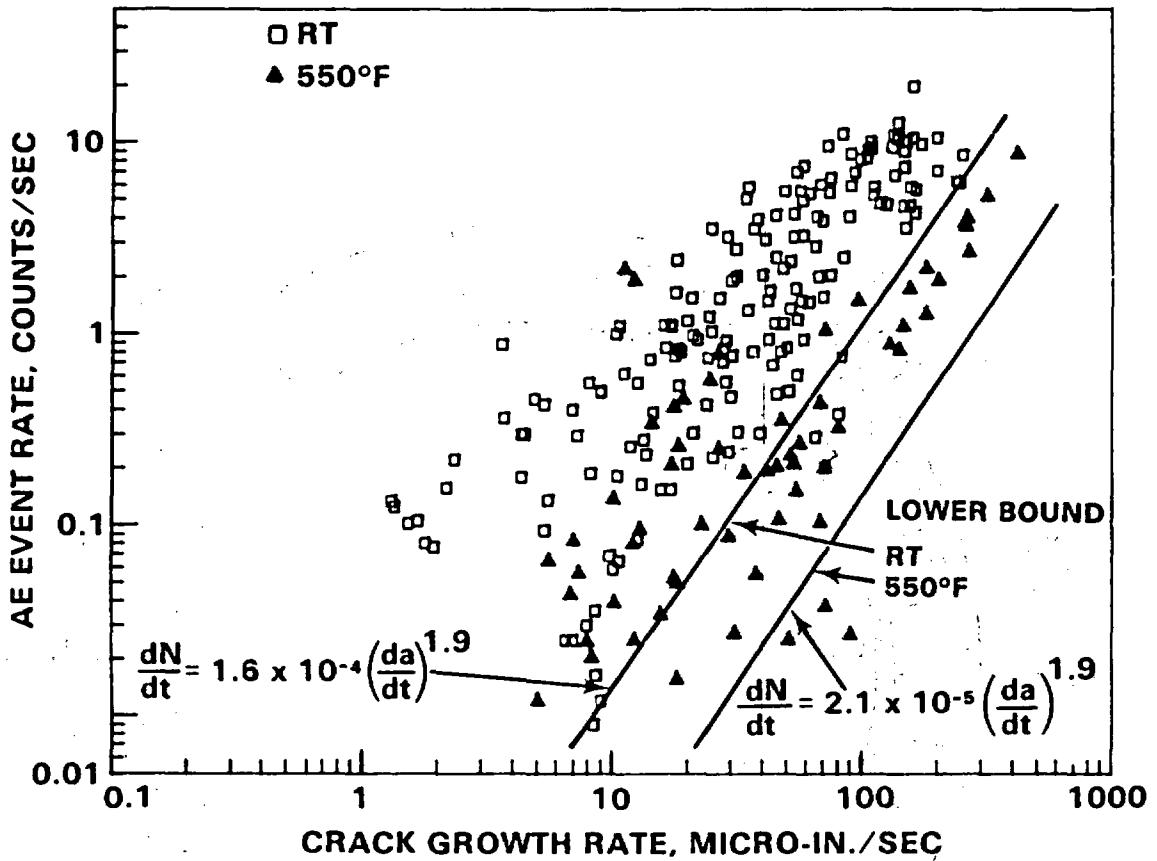


**FIGURE 5.** AE Rate - Crack Growth Rate Relationship for Cyclic Fatigue Crack Growth (Hutton 1985)

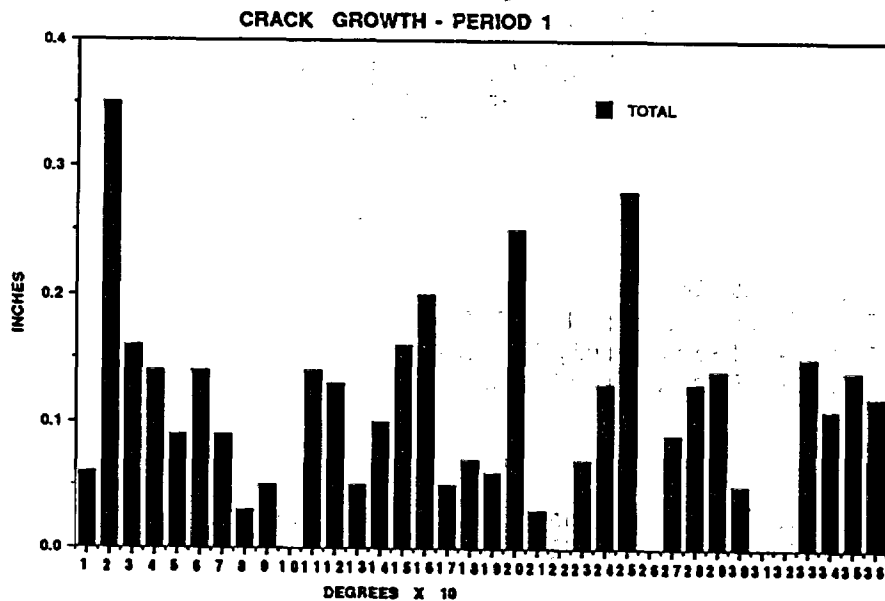
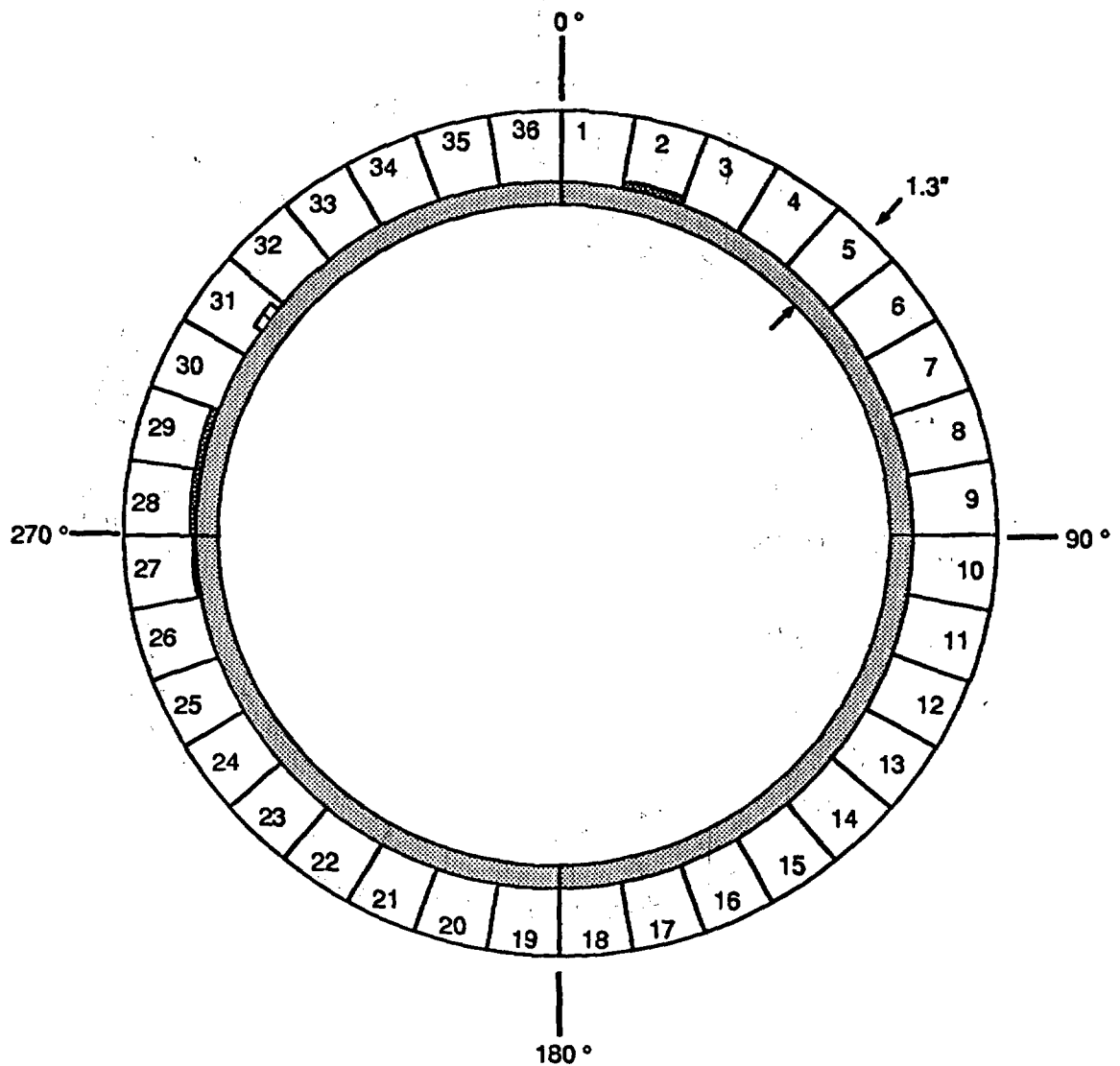


**FIGURE 6.** Crack Growth over the Period 5/89 to 9/90 as Indicated by AE - N2H Weld at Limerick Unit 1 Reactor





1.  Crack Size per ISI - 2/89
2.  Crack Growth during 5/12/89 - 9/11/90 period per AE
3. Numbered Sectors Identify AE Source Location Elements - Each 10° Wide.
4.  UT Detection Threshold @ 20% of Wall = 0.26"

R9110073.3.

**FIGURE 8.** UT Detection Threshold (20% of Wall) Superimposed on Crack Growth Prediction from AE Data - N2H Weld at Limerick Unit 1 Reactor

A crack-arrest-verification-specimen (CAVS) assembly previously used at Peach Bottom 2 reactor was installed at Limerick Unit 1 to provide the official basis for estimating growth of the flaw indication in Weld N2H during reactor operation. Basically, the CAVS system exposes a fracture mechanics specimen of appropriate material to the reactor coolant water. The specimen is loaded externally with the intent of simulating the stress present around the flaw indication and a potential drop method is used to measure resulting crack growth. Results from the CAVS system surveillance indicated a crack growth rate of 0.026 inches/year (Ranganath and Hale 1990).

Comparing the three surveillance methods on a common basis of maximum crack rate per year indicated: UT shows 0.38", AE shows 0.28", and CAVS shows 0.026". It is evident that the UT and AE indications are in reasonably good agreement, while the CAVS prediction is about an order-of-magnitude lower.

The first AE monitoring period at Limerick Unit 1 has been very valuable to the AE development effort - it has permitted demonstration that an AE system can be installed on an operating reactor, that noise problems can be overcome and coolant flow noise is not a problem, and that meaningful data can be obtained. PECO deserves high marks for their progressive attitude in making this opportunity available, and it goes without saying that the continued support of NRC-RES is invaluable.

## REPORTS

The final report for the AE/Flaw Characterization Program was published in October 1991. The report is titled:

NUREG/CR-5645  
Final Report  
ACOUSTIC EMISSION/FLAW RELATIONSHIPS  
FOR INSERVICE MONITORING OF LWRs

## SAFT-UT

### INTRODUCTION

A major multi-year program has been conducted to provide the engineering necessary to make the synthetic aperture focusing technique (SAFT) a real-time system, engineer a field prototypic system, provide field validation of the technology, and move the technology into the field for the purpose of inspecting light water reactor components. This phase of the work has been performed at PNL under support from the U.S. Nuclear Regulatory Commission, office of Nuclear Regulatory Research. The benefits to the NRC from this program are:

- improved reliability of flaw detection and

- more accurate characterization (sizing) of flaws in structural components

The program goals are nearing completion. A field-portable system has been developed and undergone extensive validation testing. The final field validation testing was conducted this year through participation in the PISC III Full Scale Vessel Test. The SAFT technology was successfully transferred to another commercial inspection vendor. The SAFT technology is being incorporated into the ASME Section V Code through a new appendix for computer-based UT systems. The details of these activities are described in the remainder of this paper.

### PISC-III FSV

The decision was made to evaluate the SAFT-UT technology in a series of blind tests. One of the tests selected was the PISC-III Full-Scale Vessel (FSV) Test located in Stuttgart, Germany at the Materialpruefungsanstalt (MPA) Laboratory that involved the characterization of 12 indications in a full-scale reactor pressure vessel.

During December 1990, three PNL staff traveled to Stuttgart and spent 11 days performing inspections on the FSV. Eight of the inspection zones were examined from both the inside and the outside surfaces of the reactor vessel. In these examinations, there were over 650 Mbytes of data collected. The inspections included 0°, ±45°, ±60°, ±70°, and tandem SAFT. The data was not analyzed in Germany, but was shipped back to PNL for this evaluation.

Field trip notes were developed during the course of the testing at the MPA site. These notes were recorded on a PC to document the activities that occurred during the testing. This turned out to be very useful because there were a number of confusing points that these detailed notes clarified.

There were a number of things that were learned in this exercise. The SAFT system, in general, performed very well; but there were several areas that were found where improvements were needed. The most important of which was that the header for the files needed to be changed to accommodate the sizes of numbers to cover the dimensions of a full-sized reactor pressure vessel.

During January the SAFT equipment was returned to the United States. Upon arrival the equipment was set up and checked out to determine its condition. Several minor problems were encountered and some maintenance was performed on the scanner.

All 650 Mbytes of data were methodically analyzed. The analysis was performed by first evaluating the data from the clad surface, followed by the data from the unclad surface, and then evaluating the data combined. This approach allowed us to learn more from the data evaluation and gave us the opportunity to determine optimum inspection combinations.

During the analysis, it became apparent that the amount of data to be analyzed was substantially more than had been analyzed previously for any other inspection. In other examinations, most of the scanned material were blank; but in this case every area scanned had substantial numbers of indications. One conclusion from this exercise is that improvements to the system are needed to facilitate handling of large data sets.

Another result from the data analysis was that the UT responses obtained from the various directions and inspection conditions lead to different conclusions about how to interpret the indication. Consequently, a decision was needed as to which signals and interpretation to believe. Every attempt was made to follow the rules that had been established from previous work, but there were many instances of ambiguity associated with the interpretation. In these cases, a decision was reached by looking at the strength of the signals (top tip signal amplitude versus bottom tip amplitude), or recognizing that volumetric indications should be detected during a normal beam scan, etc. The tandem scans were very useful in determining if an indication was surface connected or if two signal tips were from a single indication or two different indications.

At the completion of the analysis, the results were reviewed by several knowledgeable PNL staff to ensure that nothing was overlooked in the evaluation and to confirm the flaw size estimates. The SAFT inspection results were provided to the JRC at Ispra, Italy. Overall the results were felt to be good, but there were difficulties in interpreting the data. This was due, in part, to the number of indications in each of the zones examined, and the fact that defects have a large range of scattering properties. Some indications were easy to interpret, but others were quite complex and did not fit simple models.

Validation of the first analysis must await the destructive examination of each inspection zone. The destructive examination results are not expected to be available for correlation with the SAFT data until the later part of 1992.

#### TECHNOLOGY TRANSFER

This has been a driving force of the program at PNL from the start. A number of decisions were made to ensure that the program would be successful in moving the technology from PNL to the commercial nuclear industry. To date, PNL has transferred the SAFT technology to Combustion Engineering and Sandia National Laboratory. During this year, the SAFT technology was successfully transferred to the General Electric Co. (GE). GE is evaluating the SAFT technology for inclusion in the next generation of reactor pressure vessel inspection systems that they intend to build.

PNL has also had discussions with Dynacon to transfer the SAFT technology to them to become another processing option of the UDRPS system. This will be one of the activities to be pursued during the next fiscal year.

## SECTION V

Proactive participation in ASME Section V Subcommittee activities continued toward achieving ASME Code adoption of NRC-funded research results to improve the reliability of nondestructive examination (NDE) and inservice inspection (ISI). The objective of this task is to develop and promulgate upgraded criteria and requirements within the Section V Code book.

Proposed new Code requirements are being drafted to encourage broader utilization of the SAFT technology developed under NRC-sponsored research programs at PNL and the University of Michigan. These requirements were submitted to the ASME Section V Subgroup on Ultrasonic Testing (SGUT) to fulfill the need for Code rules to cover the computerized UT imaging systems that are being utilized by the NDE/ISI industry to examine critical nuclear power plant components. These proposed new requirements are organized to specify general requirements for computerized imaging systems, plus specific requirements covering calibration, SAFT-UT, L-SAFT, broadband holography, and UT-phased arrays.

The major attribute of computerized imaging techniques (CITs) is their effectiveness when used to characterize and evaluate indications; however, CITs may also be used to perform the basic scanning functions required for flaw detection. Computer-processed data analysis and display techniques are used in conjunction with automated scanning mechanisms to produce two- and three-dimensional images of flaws which provides an enhanced capability for examining important components and structures. Computer-graphics processes can then be used to quantitatively evaluate the type, size, shape, location, and orientation of flaws detected by ultrasonic testing or other NDE methods. Computerized imaging techniques should be qualified in accordance with the requirements for flaw detection and/or sizing (as applicable) that are specified in Appendix VIII of Section XI.

The written procedures for CIT applications should identify the specific test frequency and bandwidth to be utilized. In addition, such procedures should identify the signal processing algorithms, should include explicit guidelines for image interpretation, and should identify the software code/program version that is used. This information should be documented for availability when these functions must be accurately repeated at a later time if, and when, necessary. Calibration of CITs should be conducted in such a manner that the gain levels are optimized for imaging purposes. The traditional DAC-based calibration processes may also be required to establish specific scanning and/or flaw detection sensitivity levels.

In conjunction with the development of this text, two special ultrasonic test blocks were designed, fabricated, and evaluated. The purpose of these mild steel blocks is to evaluate the lateral and depth resolution of SAFT-type systems. The key design features of these blocks were then incorporated into the proposed T-435 writeup to describe calibration requirements for SAFT-type, computerized UT imaging systems. These proposed new requirements for Article 4 of ASME Section V were formally approved by the SGUT in mid-1991, and were then submitted for Subcommittee V consideration. Formal Subcommittee approval

was deferred to provide adequate time for review of additional SGUT revisions and detailed descriptions of newly developed lateral and depth resolution blocks. This proposed T-435 package received favorable consideration during the November 1991 Code meetings and is expected to receive formal Subcommittee approval during the Section V meetings scheduled for November 1991 and February 1992.

Extensive discussions have occurred regarding performance demonstration and the division of responsibilities between ASME Code Sections V and XI. This has not been resolved, and a number of proposals are being discussed.

#### REFERENCES

General Electric Nuclear Energy. 1989. Limerick Generating Station Unit 1 Inservice Inspection Report No. 89-003.

General Electric Nuclear Energy. 1990. Limerick Generating Station Unit 1 Inservice Inspection Report No. D-3001-4.

Hutton, P. H., R. J. Kurtz, M. A. Friesel, J. R. Skorpik, and J. F. Dawson. 1991. Final Report - Acoustic Emission/Flaw Relationships for Inservice Monitoring of LWRs, NUREG/CR-5645. Prepared for the U.S. Nuclear Regulatory Commission. Pacific Northwest Laboratory, Richland, Washington.

Hutton, P. H. and J. F. Dawson. 1989. Limerick Unit 1 Generating Station Mod. No. 043-002, Inservice Pipe Weld Monitoring Using the Acoustic Emission Method - Acoustic Emission System Installation. Battelle Northwest, Richland, Washington.

Hutton, P. H., R. J. Kurtz, R. A. Pappas, J. F. Dawson, L. S. Dake, and J. R. Skorpik. 1985. Acoustic Emission Results Obtained from Testing the ZB-1 Intermediate Scale Pressure Vessel. NUREG/CR-3915. Prepared for the U.S. Nuclear Regulatory Commission. Pacific Northwest Laboratory, Richland, Washington.

Ranganath, S. and D. A. Hale. 1990. Structural Evaluation of the Indication in the Limerick 1 Recirc. Inlet Nozzle N2H Safe End Weld. General Electric Nuclear Energy.

**AGING STUDIES OF 1E POWER AND REACTOR PROTECTION SYSTEMS,  
AND TRANSFORMERS<sup>a</sup>**

**J. L. Edson, V. Sharma, and E. W. Roberts**

**Idaho National Engineering Laboratory  
EG&G Idaho, Inc.  
Idaho Falls, ID 83415-2406**

**ABSTRACT**

Previous 1E power and Reactor Protection System Phase I aging studies have shown that a significant percentage of failures are not being detected by planned inspection, surveillance and monitoring methods (IS&MM). This paper presents a Phase II study that was performed to determine the effectiveness of current IS&MM, identify the risk significant 1E power system components, and identify additional IS&MM that may effectively supplement current practices. In addition, a Phase I aging study of 1E power system transformers was performed to identify stressors and failure mechanisms, investigate whether transformers are showing signs of increased failure rates as they grow older, and to determine if current surveillance methods are effective in mitigating aging effects.

---

a. Work performed by the U.S. Nuclear Regulatory Commission, Office of Research, under DOE Contract No. DE-AC07-76ID01570.

## INTRODUCTION

The Phase II aging study of the 1E Power and Reactor Protection System (RPS) has focused on determining the effectiveness of current IS&MM; identifying the risk significant 1E power system components; and the identification of additional IS&MM that may effectively supplement current practices. In addition, a Phase I aging study of power transformers was performed to identify stressors and failure mechanisms, investigate whether transformers are showing signs of increased failure rates as they grow older, and to determine if current surveillance methods are effective in mitigating aging effects.

Phase I aging studies have previously been performed for the 1E power system and the RPS as documented in NUREG/CR-5181 and NUREG/CR-4740, respectively. These studies showed that a significant percentage of failures in both systems are not being detected by planned (routine) IS&MM but rather by incidental (nonroutine) activities. This finding led to the conclusion that additional studies should be performed to further investigate the effectiveness of current IS&MM and identified methods that may improve the early detection of these failures.

The following sections of this paper discuss the studies that were performed for the 1E power system, the RPS, and transformers. Each section includes a brief description of the system or component, the methodology followed, and the results specific to the component or system. A discussion of an in-plant study of IS&MM that may supplement current IS&MM is then presented.

## 1E POWER SYSTEM AND TRANSFORMERS

### 1E POWER SYSTEM

A typical nuclear power station electrical diagram is shown in Figure 1. Each individual plant will have its own detailed 1E system configuration designed to meet particular needs, though the general setup shown here is typical.

The 1E power system covered by this aging study is shown within the dashed line area and includes the power distribution to all the safety systems. The following subsystems are included in this study:

- Plant alternating current (ac) power systems (PAC)
- Vital instrument ac power systems (IAC)
- Direct current (dc) power systems (DCP)
- Emergency power systems (EMP).

This study does not include the unit generators and their buses, generator breaker, startup transformers, connections to the station

switchyard, switchyard, transmission lines, or the offsite transmission network because they are outside the 1E power system boundary.

In general, actuated components are considered to be part of another system and are not within the boundaries of this study. For example, the high-pressure injection (HPI) pump motor, powered by the vital bus "1A," would be a part of the HPI system, not the 1E system.

As shown in Figure 1, the breaker feeding vital bus "1A" is considered the dividing point between the nonsafety power supply and the safety-related power supply (Class 1E). Each vital bus can range in voltage from 4,160 to 13,800 Vac, depending upon the nuclear steam supply system (NSSS) vendor and the specific plant design. The number of buses ranges from at least two to four, with one bus or a set of buses grouped in a separate train or channel. Each of these buses will have an emergency diesel generator (EDG) attached in case of bus failure. The EDG and its support components are classified as the emergency power (EMP) subsystem in this report.

This main vital bus (vital bus "1A"), feeds at least two secondary vital buses, vital bus "1A1," and "1A2." Each of these secondary vital buses feeds a vital load center such as the motor control center (MCC). Both the secondary vital buses and the MCC buses are rated from 208 to 600 Vac. The main and secondary vital buses, along with the vital load center buses (the latter which runs the battery chargers) are classified as part of the PAC subsystem.

Battery chargers and battery banks (with ratings of 125 to 250 Vdc) combine with dc control buses to comprise the dc power subsystem. The number of banks varies widely according to plant specific design; there are at least two banks per train/channel, though many designs call for three or four banks.

Inverters and vital instrument buses comprise the IAC subsystem, which is usually rated at 125 Vac. The buses normally receive power from the vital load center buses and use batteries as an emergency backup. One function of the IAC subsystem is to provide power for the Reactor Protection System channels.

An important aspect of the Class 1E system design is its redundancy in regard to operation. Multiple trains/channels can allow component failures while retaining system functionality. The many possible cross-ties and interconnections also protect against total loss of system function.

A flowchart detailing the methodology followed to perform this study is shown in Figure 2. Identified risk significant components were added to an existing component list (compiled from an evaluation of database records) to provide a final list of components and failure causes. This list contains components that have a significant portion of failures not detected with current, routine IS&MM and is composed of components failing most frequently as well as those considered risk significant. The failure causes not detected by current IS&MM are then identified for both the components that are failing

most often and those that are risk significant. These results are used to identify IS&MM that may improve the routine detection of failures.

Failure records were analyzed to determine the effectiveness of current IS&MM practices in detecting failures with routine methods (e.g., preventative maintenance, surveillance testing, and routine observation) and to identify specific components and failure causes where IS&MM practices could be improved. After considering three databases [the Nuclear Plant Reliability Data System (NPRDS), Licensee Event Reports (LERs), and the S. M. Stoller, Corporation Nuclear Plant Experience (NPE) database], NPRDS was selected for the following reasons: (a) NPRDS possesses the most accurate data on how events are detected, and provides a thorough representation of all events, (b) NPE records do not indicate how the failure was found, and (c) LER records, although they do indicate how the failure is found or detected, they only address events that affect the safety functions of the plant and not those that occur within a defined envelope of conditions; suggesting that they may not provide a realistic view of the routinely detected failures.

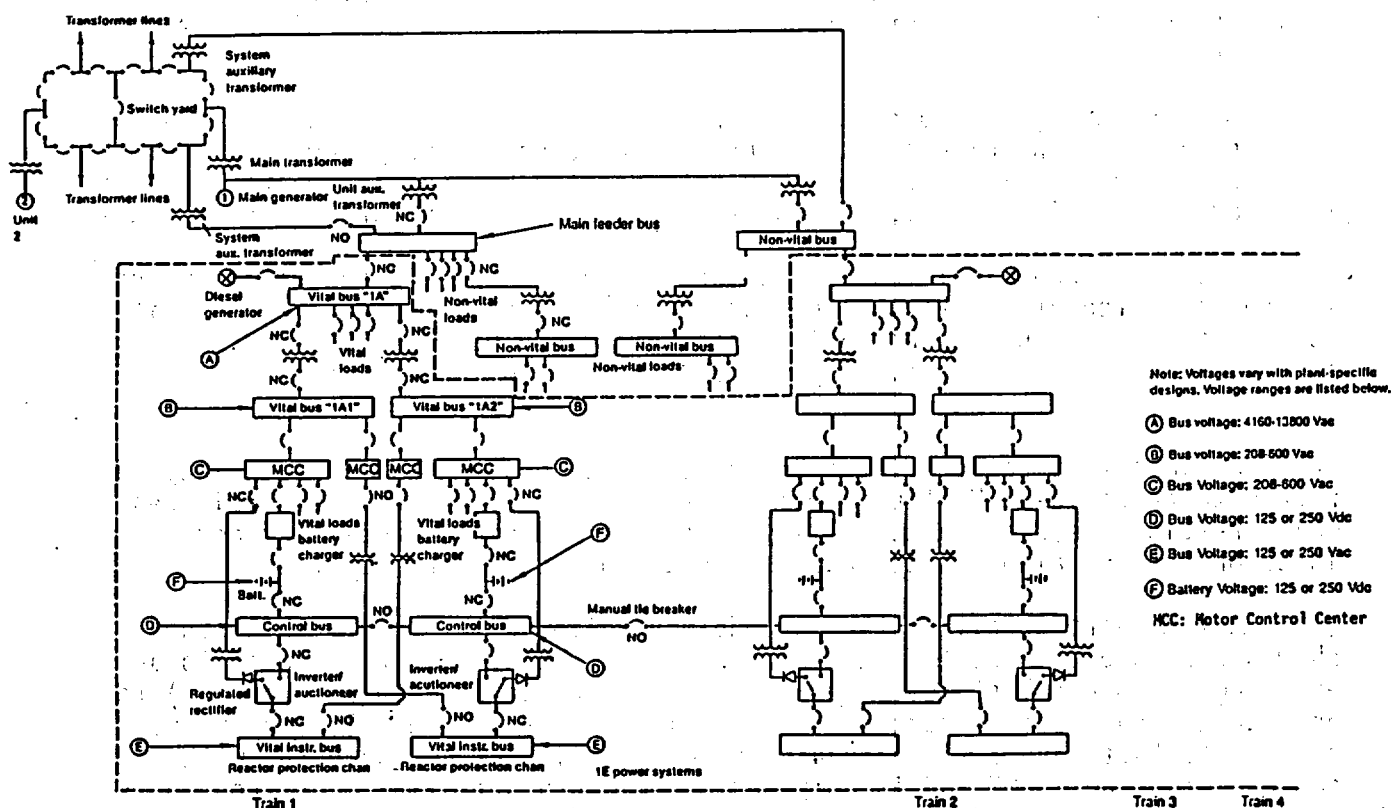


Figure 1. Typical Nuclear Power Station Electrical Diagram

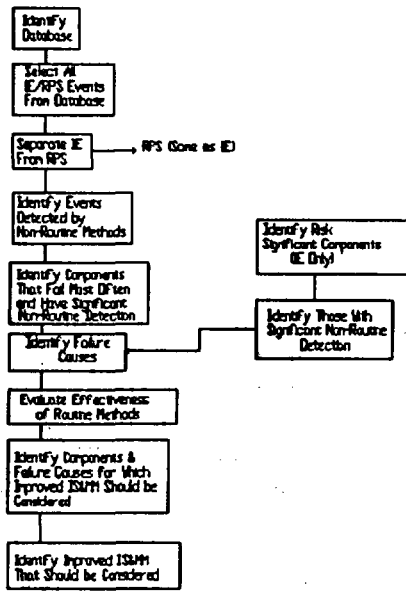


Figure 2. Program Methodology

When using any failure data from operational history databases, the limitations of that particular database must be considered. Reporting procedures can allow that an event listed on one database might not appear in another, and because each database requires different information in varying degrees of detail, a particular piece of data might be misconstrued. Another problem is that there are no strict guidelines on reporting failures, which can induce the reporting of the same failure at two separate plants with variations within the characteristics of the official failure report. For these reasons, the data or the findings in this report should not be used for any other purpose other than that expressed herein.

Over 8,000 failure records (NPRDS data through January 1990) were used for this analysis. The data comprised all failures of Class 1E electrical components and RPS components for both Pressurized Water Reactor (PWR) and Boiling Water Reactor (BWR) plants. These data were limited to records from those plants designed by the four major NSSS vendors: Babcox & Wilcox, General Electric, Westinghouse, and Combustion Engineering. Because the majority of U.S. plants use these companies, this limitation represented no appreciable data loss.

The NPRDS data were first separated into two groups: (a) Reactor Protection System Records and (b) Class 1E System Records. These groups were then sorted by detection method into failure detection method groups classified as either routine or nonroutine methods. The routine methods were chosen to include those that would normally be performed on a periodic basis or included in routine observations. The nonroutine methods were those that were unplanned. The following list shows all the detections methods utilized by NPRDS, those classified as routine, and those classified as nonroutine.

NPRDS Failure		
Detection Method	Routine	Non-Routine
In-Service Inspection	X	
Surveillance Testing	X	
Preventive Maintenance	X	
Routine Observation	X	
Operational Abnormality		X
Special Inspection		X
Audiovisual Alarm		X
Incidental Observation		X
Corrective Maintenance		X

For the Class 1E system, the two groups of records were then broken down into their respective subsystems: (a) plant ac power subsystem (PAC), (b) instrument ac power subsystem (IAC), (c) dc power subsystem (DCP), and (d) emergency power subsystem (EMP). The failure data have also been sorted by failure cause for all 1E components, 1E components in each subsystem, and RPS components. This nomenclature is consistent with that used in the NPRDS user's manual.

Review of the operational data shows that more 1E power system failures are being detected by nonroutine methods--approximately 52%--than are being detected by routine methods. Data taken from an examination of the failure causes suggest that routine detection methods are effectively detecting cyclic fatigue, set-point-drift, out of calibration, wear, and foreign materials but are ineffective for detecting open circuits, defective connections, burned components, short/ground circuits, and circuits that are out of adjustment. Because the failures not detected by routine detection methods represent about 52% of the 1E power system failures, it is evident that improving the effectiveness of routine detection methods for the 1E power system is needed.

The analysis then determined if nonroutine detection of failures is significant; also, NPRDS data were further reviewed to identify those components that failed most often. The analysis determined failure causes for each component: Batteries, breakers, inverters, and relays account for approximately 85% of all failures and have significant nonroutine detection rates, ranging from 30 to 77%. In addition, these components dominate the failures for each of the four subsystems. Breakers account for 72% of PAC failures, inverters account for 89% of IAC failures, batteries account for 84% of DCP failures, and breakers and relays combine to cause 56% of EMP failures. These data indicate that the performance of a subsystem can be significantly improved by concentrating on the detection methods of just one or two types of components that are significant for that respective subsystem. In addition, the components are different for the various subsystems.

Failure causes were examined to identify those for each component that are not being well detected with routine methods. Table 1 lists the failure causes for breakers, relays, inverters, batteries, transformers, and conductors in the corresponding subsystems (as discussed previously). Note that transformers and conductors have been included to this table even though they have a low number of failures (approximately 0.2%). They are included in the table because a risk assessment of 1E power system components (discussed

subsequently) has identified them as making significant contributions to the overall plant risk. Table 1 shows that the set of failure causes for each component differ from one another. This is anticipated because the components are dissimilar and perform significantly different functions. However, open circuit appears for each component and shorted/grounded and burned/burned out appear for more than one component. The most common circuit breaker, nonroutinely detected, failure causes were open circuit, weld related, and out-of-adjustment. Nonroutinely detected failures of inverters were primarily open circuits and shorted/grounded, while the largest battery nonroutine failures were shorted/grounded, open circuit, burned/burned out, normal/abnormal wear, and aging/cyclic fatigue. The most common nonroutinely detected failures of relays were caused by open circuit, normal/abnormal wear, burned/burned out, and out-of-adjustment. Defective connections, out-of-adjustment, and abnormal stress were the major nonroutine failure causes for transformers. The dominant failure causes for conductors were insulation breakdown and short/ground.

The components and nonroutinely detected failure causes identified in Table 1 either account for a significant number of IE power system failures or the components are significant contributors to overall plant risk. The table also provides the basis for identifying inspection, surveillance, and monitoring methods that have potential to significantly reduce the number of nonroutinely detected IE power system failures.

A partial aging risk analysis of the IE Power System was performed to determine if the aging of a single component or group of components has a significant impact on overall risk. The partial aging risk analysis was performed by using time-dependent failure rates for selected components of interest and constant failure rates for the balance. The nuclear plant PRA was chosen for prescreening because it is well documented in NRC supported literature and is familiar to many in the PRA community. Additionally, it had been previously loaded and verified on the Integrated Reliability and Risk Assessment System (IRRAS) software. Expected changes in failure rates as a function of time as developed by expert opinion were also used for screening. The Parametric HAZard function Estimation (PHAZE) computer code was used to estimate the time-dependent failure rate of a IE component. Finally, the aging risk, expressed in terms of core damage frequency, was quantified using the PHAZE estimate.

The fault trees for the nuclear plant PRA included breakers, transformers, buses, inverters, rectifiers, and batteries. The IE components discussed previously can be related to the nuclear plant PRA components as shown in Table 2.

Relays and isolation devices were the only major IE Power System components not included explicitly in the PRA.

Quantification of a PRA generally involves truncation of those cut sets that do not contribute significantly to the final core damage frequency--this was the case for the nuclear plant PRA. All cut sets with a probability of

**Table 1. NPRDS 1E Subsystem and Component major nonroutine failure causes.**

<u>System</u>	<u>Component</u>	<u>Nonroutine Cause</u>	<u>(%)</u>
PAC	BREAKER	open circuit	13
		weld fault	12
		out of adjustment	10
IAC	INVERTER	open circuit	16
		short/ground	14
DCP	BATTERY	short/ground	8
		open circuit	7
		burned circuit	6
		wear	5
		cyclic fatigue	5
EMP	RELAY	open circuit	20
		wear	13
		burned circuit	10
		out-of-adjustment	5
PAC	TRANSFORMER	defective connection	14
		out-of-adjustment	10
		abnormal stress	10
PAC	CONDUCTORS	insulation breakdown	50
		short/ground	50

**Table 2. Comparison of major class 1E components to the nuclear plant PRA 1E components.**

<u>Major Class 1E Components</u>	<u>Surry PRA 1E Components</u>
Battery	Battery
Breaker	Breaker
Conductor	Bus
Inverter	Inverter
Isolation Device	----
Charger	Rectifier
Relay	----
Transformer	Transformer

less than  $1.0E-09$  before recovery were truncated. The truncation resulted in the complete removal of the battery, inverter, and rectifier components from the final set of cut sets. This left only the breakers, transformers, and buses as potentially risk significant components.

It is possible to further screen components (based on the increase in risk caused) by assuming that the failure probability of a particular component is unity. If such an assumption does not result in a significant increase in risk, then the aging of the component is not risk significant. Assuming a failure probability of one for a key 1E breaker results in a risk increase of  $3.5E-04$ . Unity failure probability for a key 1E transformer

yields a risk increase of  $1.0E-04$ , and for a key bus yields a risk increase of  $1.3E-04$ . Comparing these increases to the total core damage frequency of  $3.30E-05$  indicates that significant increase in failure probability of breakers, transformers, and buses could contribute significantly to plant risk.

The major conclusion drawn from the analysis of the nuclear plant PRA is that aging of breakers, transformers, and buses has the potential to significantly increase core damage frequency. The effect of aging of inverters, rectifiers, and batteries on core damage frequency is assumed to be insignificant because these components are not initially risk significant. This assumption cannot be completely checked without a requantification of the PRA in which these components are not truncated. The requantification would be time intensive and was not performed.

The three components found to be risk significant prior to aging are breakers, transformers, and buses. It was also found that unity failure rates for these components resulted in significant changes in core damage frequency. However, unity failure rates are not expected, therefore, further screening of these three components was performed to determine the likely affect of reasonable aging. The screening was performed by simply applying the aging rates determined by expert opinion, as reported in the TIRGALEX Database to the initial failure rates used in the PRA to determine if significant changes occurred as a function of time. The aging rates in TIRGALEX are linear and are reported as failures per hour per year.

The initial failure rates, aging rates, and failure rates at time equal to 40 years are shown in Table 3. The failure rate at 40 years compared to the initial failure rate has increased by 20% for breakers, 6% for transformers, and by less than 1% for buses. Requantification of the nuclear plant PRA using the failure rates calculated at 40 years resulted in an increase in core damage frequency of less than 1%, therefore, none of these increases causes a significant change in overall plant risk. To confirm this conclusion on at least one component, an aging analysis (using operational data taken from NPRDS), was performed on the component expected to show the greatest increase, (i.e., the breakers).

Data were collected from the NPRDS database to allow estimation of the failure rate of breakers as a function of time. The estimate is made using a computer coded statistical approach as described by Atwood (1990). The needed inputs for the estimation are the in-service date for each breaker, the period of time over which failures were looked for, and the specific failure times. The data recorded in the NPRDS database are generally more reliable after 1984; therefore the period over which the failures were looked for was the beginning of 1984 to the end of 1989. If the in-service date was after the beginning of 1984, then the start of the observation period is adjusted accordingly.

The NPRDS records for the 63, 4 kV breakers representing 22 units were reviewed to determine which records reflected aging failures. The 22 units

Table 3. Failure rate as a function of time.

<u>Component</u>	<u>Initial Failure Rate (failures/hr)</u>	<u>Aging Rate (failures/hr/yr)</u>	<u>Failure Rate at 40 Years (failures/hr)</u>	<u>% Change in Failure Rate</u>
Breaker	4.1E-06 <sup>a</sup>	2.0E-08	4.9E-06	20
Transformer	1.7E-06 <sup>b</sup>	2.0E-09	1.8E-06	6
Bus	3.8E-06	1.0E-09	3.8E-06	<1

a. The failure rate for breakers is calculated from the failure probability of 3.0E-03 per demand and the demand rate of 1.4E-03 per hour. The demand frequency reflects a monthly test of the breaker.

b. The failure rate for transformers and buses is calculated from the failure probability per demand and a 24-hour mission time demand.

were specifically chosen because their associated databases have been subjected to more careful review by the maintainers of the NPRDS system and therefore are expected to be more reliable. The data were separated into two sets; if a record stated that the breaker failed but gave no root cause, it was classified as a broadly defined aging failure. The second input set is for only those records that were clearly classified as aging failures. This second set is referred to as narrowly defined aging failures and is a subset of the first set. It is necessary to develop these two sets in an attempt to make up for the deficiencies in the information supplied in failure reports. There are 20 potential/actual failures and 4 actual failures.

The failure rate estimates are 1.4E-06 and 6.9E-06 for the narrow and broad definitions of failure, respectively. Note that these estimated values of failure rate are in good agreement with the 3.4E-06 rate used in the nuclear plant PRA. The conclusion drawn from this statistical analysis of aging is the same as that based on the TIRGALEX results combined with the PRA (i.e., that the risk increase due to aging of 4 kV breakers is low).

We can conclude that breakers, transformers, and buses are the Class 1E components that have a significant contribution to the overall plant risk; even though this plant risk is not greatly affected by their aging.

#### POWER TRANSFORMERS

A Phase I study performed on the aging of Class 1E transformers is used as a basis for this discussion. Other critical 1E component studies have been conducted by corresponding researchers.

A nuclear plant usually has less than 10 Class 1E power transformers supplying the many safety-related systems and equipment. Figure 1 shows a typical nuclear plant electrical distribution system with the associated power transformers. Individual nuclear plants classify different power transformers as Class 1E, depending on their safety analysis. Normally, all nuclear plants acknowledge the power transformers included in the section surrounded by the dashed line (see Figure 1). Some plants take credit for high voltage equipment (located outside the dashed line) in their safety analysis and as a result have high voltage (15 kV or greater) Class 1E power transformers. The voltages on the high voltage winding (primary) of transformers--located outside the dashed line--varies between 15 and 500 kV; depending on the individual plants and the connected commercial power system.

Transformers currently installed in Class 1E applications consist of three general types: (a) dry-type, (b) gas-filled, and (c) liquid-filled. The dry-type transformers have air surrounding the winding insulation and the enclosure is usually vented to the surrounding atmosphere. Dry-type transformers account for about 77%, while 17% are liquid-filled, and 7% are gas filled. All of the transformers with a rating over 15 kV (7% of transformers) are oil-filled, using mineral oil as the insulator and cooling medium. Dry-type transformers, which are of lower voltage, are used in clean dry areas; gas and nonflammable fluid filled transformers are generally used in areas where a contaminated or moisture atmosphere is present.

Figure 3 shows the basic components of all power transformers. The figure shows that basic transformer components include a ferro-magnetic core, copper or aluminum windings (two or more with connections to the bushings), solid insulation, the insulator/coolant medium, electrical bushings (two per winding), external connections, and a tank (enclosure).

A transformer is a device with no moving parts. Power transformers are made by completing two separate copper windings on a silicon-steel core. Upon applying an ac voltage and current to one (primary) winding, a corresponding magnetic flux is created in the core. The magnetic flux in the core induces a voltage and current on the secondary winding. Some transformers have multiple secondary windings allowing power to be transferred at different voltages. The input to output voltages are in direct ratio to the number of turns on each winding. The use of power transformers allows power to be transmitted at high voltages (reducing line losses) and then lowered to usable voltages.

Each turn in a transformer has a certain potential (voltage) across it and must be insulated from the other turns to prevent electrical shorts. In addition, the separate windings (primary and secondaries) must be insulated from each other and from grounds for the same reason. Higher voltages result in higher potentials between turns, between separate windings, between energized and nonenergized conducting parts.

The degrading or failure of a transformer is caused by the opening of a winding or the electrical shorting between winding turns, windings, or windings to ground. Bushing failures or the open/high impedance external connections to the transformer windings also result in power system

transformer failures. As a result, the windings (wire), the solid insulation, bushings, and external connections are the critical parts of the transformer.

The delamination of the core itself would result in increasing core losses and heat that would seriously impact the solid insulation life. However, the delamination would not result in the immediate failure of the transformer. All other components of the transformer including the tank, insulator/coolant medium, and support systems to be discussed are considered noncritical because their failure would not cause immediate transformer failure. However, over a period of time, the failure of these support systems may result in degradation or even failure in a critical transformer component.

Table 4 shows the principal materials of construction for the components of power transformers. Previously it was pointed out that solid insulation and transformer bushings are two of most critical components in a power transformer. Both the higher voltage bushings and solid insulation use materials that are very susceptible to accelerated aging caused by heat. These components are also susceptible to failures caused by the entrance of contaminants or moisture. The other components (steel, copper, aluminum, gases, fluids, etc.) are constructed of materials that are not as susceptible to environmental aging effects. In addition, the fluids and gases may easily be tested, removed, and replaced with little or no effect on the operation of the transformer.

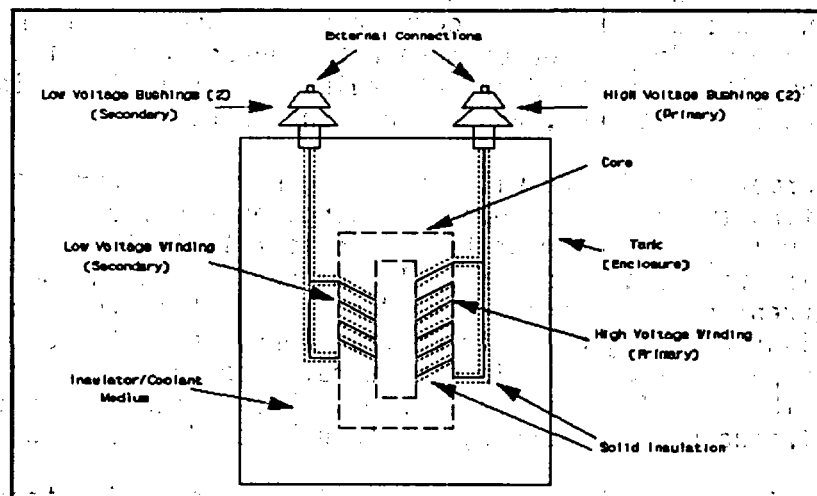


Figure 3. Basic Components of Power Transformers

Table 5 shows the aging stressor and the resultant effect for the components that are critical to the transformer operation. The table shows that the solid insulation, which is made of fibrous materials, can be seriously affected by heat, moisture, and contaminants. It is generally accepted that, if air (moisture) is present, the rate of aging for solid

Table 4. Components of Power Transformers and Materials of Construction.

Component	Materials	Comments
Core	Silicon-Steel	Laminated sheets
Windings	Copper/aluminum	Each turn may be made up of groups of strands.
Solid Insulation	Cellulose, Kraft paper, Phenolics, fiberglass, and Varnishes - shellac, enamel, or various resins	Used to bond and protect (mechanical and moisture) fibrous insulating material.
	Fibrous resin-paper laminates, pressboard and various kinds of paper (nylon or wood based)	Used to provide wire, turn, and layer insulation for the windings. Paper wrapping is also used on the leads coming from the windings.
Fluid - (Insulating/cooling Medium)	<u>High-flammability</u> Mineral oil	High dielectric strength and excellent heat transfer capability. No high voltage (> 15 kV) restrictions.
	<u>Low-flammability</u> Askarel, silicones, high-flash-point hydrocarbons, chlorinated benzenes, or chlorofluorocarbons	Good dielectric strength and heat transfer capabilities. High voltage limit is < 15 kV. Askarel is being phased out. Silicones are used on all modern low-flammability fluid transformers.
Gas - (Insulating/cooling Medium)	Air	Relative low dielectric strength and heat transfer capabilities.
	Nitrogen/fluorogas	Relative low dielectric strength and heat transfer capabilities. Requires pressure regulation system to maintain pressure in sealed tank.
Bushings	Porcelain, kraft paper, metal foil, mineral oil and copper/aluminum conductor	High voltage bushing use kraft paper, metal foil, and oil inside a porcelain outer surface. Lower voltage bushing use kraft paper and/or a copper conductor inside with a porcelain outer surface.
Tank	Steel	Heavy gauge steel, painted to prevent corrosion.
Connections	Copper and Aluminum	

**Table 5.--Component Stressors and Failure Mechanisms.**

<u>Component</u>	<u>Stressor</u>	<u>Failure Mechanism</u>	<u>Result</u>	<u>Comments</u>
Windings	High amperage	Solid insulation hot spot temperatures.	Increased aging of solid insulation.	Long term damage to the insulation is the most likely occurrence. (See "Solid insulation")
Core	Vibration	Delamination	Increase in core heat/hot spots.	See "Solid insulation."
Solid Insulation	Heat above design limits.	(1) Loss of mechanical strength - increases brittleness. (2) Eventual reduction in dielectric strength.	Breaking up of insulation by natural vibration. Heat speeds up the chemical action that eventually destroys the insulation.	Hot spot or average winding temperatures above the rated temperature increases the aging rate of the solid insulation. The effects of the overheating is accumulative.
	Moisture	Reduced dielectric strength of solid insulation.	Electrical shorts between turns, winding, and/or ground. Disable trans.	Moisture held in combined form releases under increasing temperatures producing same consequences as free moisture.
	Contaminants	See "moisture."	See "moisture."	Contaminants usually have inferior dielectric strength.
Bushings	Heat and moisture on inside of bushings	See "Solid insulation" for failure mechanisms, results & comments.		
	Contamination on outside of bushing	Reduced electrical distance though air to ground.	Short to tank (ground)	
Connections	Oxidation & vibration	High electrical resistance, arcing, and high heat.	Open circuits and protective relay tripping.	Visual and infrared inspection used to detect.
<u>Insulating/cooling mediums</u>				
Mineral oil	Air/moisture	Sludge & acid formed	Absorbs increasing amounts of moisture in solution.	See "Solid insulation - moisture"

insulation doubles for each 8°C above a 65°C average winding temperature. Even if the solid insulation is surrounded by protective fluids or gases, the presence of air/moisture in the fluid or gas accelerates the aging.

The materials used for the solid insulation are essentially the same for all transformer types and voltages. Fibrous materials under design conditions provide the necessary dielectric strength (insulate) to withstand the voltages within the transformer. However, as the voltages on the transformers increase it becomes more critical that the dielectric strength of fibrous materials is not degraded. As shown in Table 5, moisture and heat are two stressors that will cause the dielectric strength of the solid insulation to deteriorate. *It should be noted that solid insulations have over double the dielectric strength of any liquid or gas insulation material.* To prevent the entry of contaminating materials (including water) that would impair or destroy the transformer solid insulation, the windings, core, and other internal electric parts are surrounded by either a gas or liquid insulating medium. The materials also provide the method to remove the heat generated by core and winding losses.

Dry-type (air) transformers are designed to operate at lower voltages. The most important materials are resins/varnishes that are used to seal moisture/contaminants out of the solid insulation. However, the insulation ages in the same manner as the other types of transformers.

The transformer tank provides a personal protection barrier and barrier to the entry of contaminating materials. Sealed tanks are used for transformers using liquids and gases (excluding air) as an insulator/coolant medium. To allow for normal expansion and contraction of fluids in sealed tanks, various methods are used including: leaving an air space above the fluid in the seal tank blanketing the fluid with a pressurized nitrogen atmosphere (requires gas cylinders and pressure controls); using a sealed flexible diaphragm on top of the oil (with an air space above the diaphragm); and maintaining a low-pressure gas atmosphere in the sealed tank. The gas-filled transformer pressure is maintained using gas-filled cylinders, pressure gauges, and pressure regulators.

Mineral oil also ages at a rate depending on time, temperature, and the exposure to air and moisture. Oil aging results in the formation of sludge and acids, and while that is not considered critical, mineral oil with the presence of acids takes into solution an increasing amount of water. This in turn causes the solid insulation to age and deteriorate. Other fluids used in transformers have no normal stressors that change the composition of the fluids, however, they do carry any contamination that enters the tank to the solid insulation.

The aging stressors shown for the core are not normally expected during transformer operation. If they do occur, the effects will be detected if manufacturer's and industry recommended maintenance tests are completed by the licensees during their maintenance programs.

Although not part of the transformer proper there are certain support systems that are used on some of the transformers. The failure of the support systems can effect the life of the transformer and in some cases disable the transformer. The support systems include the following:

Load tap changer (LTC) - Some of the Class 1E high voltage (> 15 kV) transformers used in the nuclear plants have Load Tap Changing (LTC) equipment. This equipment maintains a constant plant system voltage by increasing or decreasing the active turns in the high voltage winding. The tap changer contacts, which arc during

changes, are located in a sealed oil-filled compartment that is isolated from the transformer core and windings. Voltage measuring and tap changer motor controls allow both a variable time delay and voltage operational band to prevent unnecessary wear of the system parts. transformer failures. As a result, the windings (wire), the solid insulation, bushings, and external connections are the critical parts of a transformer. The delamination of the core itself would result in increasing core losses and heat that would seriously impact the solid insulation life. However, the delamination would not result in the immediate failure of the transformer. All other components of the transformer including the tank, insulator/coolant medium, and support systems to be discussed are considered noncritical because their failure would not cause immediate transformer failure. However, over a period of time, the failure of these support systems may result in degradation or even failure of a critical transformer component.

Gas regulation system - Each gas insulated/cooled transformer requires a gas source (cylinders) and a tank pressure regulator to maintain the internal tank gas pressure within preset limits.

Gas Blanket - Liquid-filled transformers using a low-pressure nitrogen blanket require a gas source (cylinders) and a tank pressure regulator to maintain the internal tank gas pressure within preset limits.

Forced cooling - An important part in the operation of the transformer is the prevention of high core/winding temperatures that would shorten the life of the electrical insulation. All power transformers are designed to maintain the transformer temperatures below acceptable limits when the transformer load is operated below the kVA rating for each type of cooling. The following cooling methods are used to remove the winding/core heat:

*Natural convection (self-cooled)*--May or may not have radiators.

*Forced-air*--Requires radiators, temperature transducer, controls, and fans/motors.

*Forced-oil*--Uses forced-air radiators. Requires temperature transducer, controls and oil pump(s).

## OPERATING EXPERIENCE

Information from the NRC Licensee Event Reports (LERs), the Nuclear Plant Reliability Data System (NPRDS), the Nuclear Power Experience (NPE) databases, as well as from cooperating utilities, was used in the study of the nuclear plant transformer operating experience between 1983 and 1991. During this study, it was determined that the NPRDS was the only information source with nameplate data on the Class 1E power transformers used at the nuclear plants. Because this study was on the effects of power transformer aging, a decision was made to not use the transformer data on plants licensed since January 1, 1989. The subsequent review of NPRDS data showed that only 88 other plants had Class 1E transformer nameplate data included in the database.

During the study of 88 plants it was determined that there were 723 Class 1E transformers in the plants consisting of 77% dry-type (air), 17% liquid-filled, and 7% gas-filled. The high voltage transformers (> 15 kV), which are filled with mineral oil, made up 7% of the 1E total. It was also determined that 95% of the 1E transformers are under 20 years old and 75% are under 15 years old.

Table 6 shows the recorded Class 1E and aging related problems from January 1, 1983 through January 1, 1991. During this period, 33 problems were reported in Class 1E transformers. Five of these problems resulted in reportable events (LERs). Even though oil (liquid-filled) transformers only comprise 17% of the 88 plants studied, they incurred 64% of the reported problems. However, four of these problems occurred on the cooling system and seven were oil and nitrogen leaks. These types of problems would not normally result in the immediate failure of the transformer and would only be significant if not detected and/or no action taken. The bushing and tap changer problems all occurred on high voltage (> 15 kV) transformers. This is to be expected because the higher the voltages, the more critical the insulation becomes. The high voltage bushings are located outside and if not inspected, cleaned, and tested periodically can be shorted by airborne contaminants. In addition, because of the importance of the insulation and support systems, the transformers are provided with increased monitoring equipment, and the surveillance, inspection, testing, and maintenance programs are more rigorous than for transformers below 15 kV.

Although few problems were reported on the dry-type transformers, this does not mean that significant aging is not taking place. Because of the low voltages impressed on the transformers, the solid insulation can deteriorate for a long time until the dielectric strength of the insulation is low enough to allow voltage breakthrough. In addition, they have less monitoring devices and the surveillance/inspection of the solid insulation requires the removal of the case. Thus making online inspections difficult. Because dry-type transformers are exposed to the surrounding atmosphere, and even though the solid insulation is varnish coated to prevent the entry of moisture, the solid insulation will deteriorate more rapidly than that of liquid and gas-filled transformers. To prevent a more rapid deterioration of the insulation the transformer should be operated within the nameplate rating and located in area that is clean, dry, free from any contaminants that would remove the varnishes. To detect aging problems and prevent operational failures requires a rigorous periodic inspection, cleaning, testing and replacement program. We were unable to determine if this has been performed during this period.

To determine if there is an increasing trend of transformer problems, the yearly transformer problems were determined from January 1, 1983 through January 1, 1991. Table 7 shows the problems occurring each year during this period. There is no increasing trend in reported problems. However this is not totally unexpected, because the study found that over 95% of the transformers are less than 20 years old and 75% are less than 15 years old. Transformers are normally considered a long-life item; with proper operation and maintenance, transformers (with the exception of the dry-type) should provide reliable operation for more than 40 years.

To determine what was required to prevent, retard, and detect the aging of transformers (solid insulation) a review was made of the recommended procedures of all major transformer manufacturers, the IEEE/NEMA standards, and available technical literature. Discussions were also held with personnel responsible for the maintenance of transformers at the INEL and area utilities.

An idealized inspection, surveillance, testing, and maintenance program was developed to see how a nuclear plant would compare. The program from cooperating utilities was compared with the developed program. The utility program was found to compare favorably with only minor differences.

It is our opinion that by rigorously following the manufacturer's procedures and using the applicable industry standards the aging effects on transformer insulation can be retarded and significant deterioration can be detected in time to prevent most operational failures.

### REACTOR PROTECTION SYSTEM

The basic philosophy of the Reactor Protection System is to define an operating envelope for the plant, and to shut down the plant when the limits of this envelope are reached. The process of monitoring plant conditions and then acting upon them is accomplished through the use of various sensing devices, processing circuits, logic circuits and control and actuation circuits (see Figures 4 and 5).

The figures and explanations presented are general in nature. Specific designs vary greatly from plant-to-plant and between types of reactors.

The sensing devices--nuclear or process instrumentation--are only the first step in a complicated chain. The basic measured parameters are listed in Figure 4. The raw measurements from the sensing devices are then sent through various computation, amplification, and conditioning circuits.

The next set of circuits is used to decide if the operating envelope has been reached. These logic circuits take the processed signals and compare them to preset set-points. If the input signal does exceed the set-point then the actuation and control circuits are brought into play. These circuits control the various alarms and also the reactor trip breaker. If the trip breakers are actuated then the reactor is shutdown.

Table 6. Reported Class 1E Power Transformer Problems (1983-1991).

Problems and Failures	Type Transformers		Total	LERs
	Oil	Air		
Winding Failure	2	4	6	1
Bushing	2	1	3	1
Cooling System	4	3	7	0
Connections	1	4	5	1
Load Tap Changers	5	0	5	2
Oil or Gas Leakage	7	0	7	0
TOTAL	21(64%)	12(36%)	33	5

**Table 7. Class 1E Transformer Problems by Year.**

Problems Reported	Year							
	1983	1984	1985	1986	1987	1988	1989	1990
	2	5	7	2	8	3	1	5

As with the 1E power system, the high degree of redundancy of the RPS prevents total system failure while allowing for individual component failures. There are usually four reactor protection channels with a trip sensor string in each channel. Each of the trip strings also has dual isolated components to provide for component redundancy. Only one of these many trip sensors has to actuate to trip the entire channel. Two channels have to trip to cause the entire Reactor Protection system to trip. This system is called two-of-four logic; this logic prevents the accidental tripping of the RP system by a spurious signal in only one channel.

Non-routinely detected failures accounted for about 39% of all Reactor Protection System events. Transmitters, integrators, bistables, and power supplies had the most failures; they accounted for approximately 80% of all RPS events. Power supplies, generators, conductors, motors, transformers, and annunciators had the highest percentage of nonroutinely detected failures, but many of these components do not have a significant number of total failures. Power supplies, with 57% of its failures detected by nonroutine methods, ranked fourth in total failures; generators, conductors, motors, transformers and annunciators totaled only less than 1% of all the RPS failures (see Table 8).

For transmitters, routine methods were able to detect failures caused by out-of-calibration and set-point drift, while they missed events caused by wear and cyclic fatigue. Set-point drift and out-of-calibration failures were the two major routinely detected events for integrators. Cyclic fatigue and defective connections caused most of the failures not detected by routine methods for the integrators. Set-point drift, out-of-calibration, and wear were causes of failures detected by

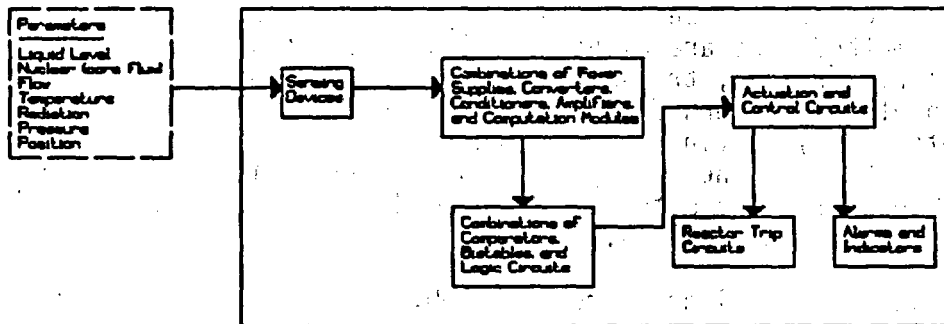


**Figure 4. Simplified Reactor Protection System Block Diagram.**

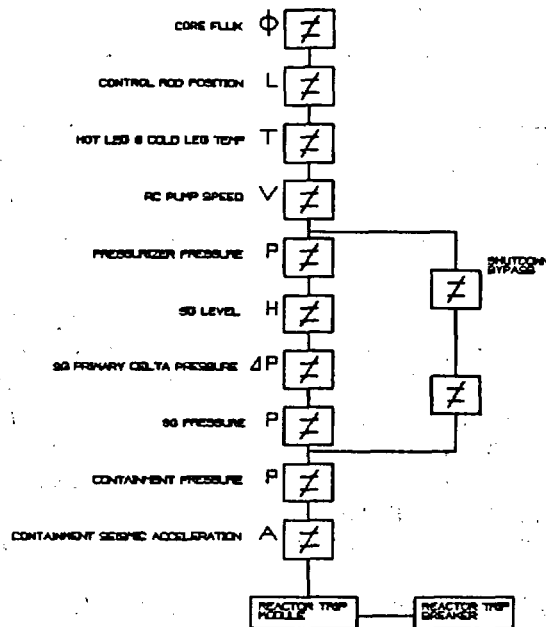


Figure 5. Typical Sensors on One Channel of the RP System

routine IS&MM for bistables. Open circuit and foreign material failures were not detected by routine methods for the bistables. Out-of-calibration, burned circuit, and wear were power supply failure causes that were detected by routine methods. For power supplies, routine methods were not able to detect failures caused by cyclic fatigue and short/ground circuits. Out-of-calibration, wear, and burned circuit were power supply failure causes that were detected by routine methods. For the power supplies, routine methods were not able to detect failures caused by cyclic fatigue and short/ground circuits (see Table 9).

#### IN-PLANT EVALUATION OF IMPROVED IS&MM FOR 1E POWER AND RPS

The previous sections have shown that routine detection methods for the 1E power system and the RPS are not detecting a large portion of the component failures. For the 1E power system breakers, batteries, inverters, transformers, and busses are components of concern because they have a high percentage of failures not detected by routine methods and are either failing most often or are risk significant. Similarly, relays, transmitters, integrators, bistables, and power supplies are components of concern for the RPS because they have a high percentage of failures not detected by routine methods and represent a significant percentage of the RPS failures. Because these components have a significant percentage of failures not detected by routine methods, improved detection methods have the potential to improve their reliability.

Current practices, as well as improved IS&MM, were evaluated at a nuclear facility that is utilizing improved IS&MM to supplement current practices. The in-plant evaluation involved collecting and evaluating procedures for current IS&MM practices, collecting and evaluating data previously obtained with improved IS&MM,

**Table 8. NPRDS RPS Component failure distribution.**

Component	Percent all failures	Percent routine	Percent nonroutine
TRANSMITTER	28.10	55.92	44.08
INTEGRATOR	23.47	61.64	38.36
BISTABLE	18.94	75.13	24.87
POWER SUPPLY	8.65	43.02	56.98
RELAY	6.65	64.58	35.42
INDICATOR	5.09	65.76	34.24
ISOLATION DEVICE	2.79	63.83	36.17
BREAKER	2.73	50.00	50.00
CONTROLS	2.71	56.20	43.80
GENERATOR	0.42	28.57	71.43
CONDUCTOR	0.28	28.57	71.43
MOTOR	0.14	14.29	85.71
ANNUNCIATOR	0.02	0.00	100.00
TRANSFORMER	0.02	0.00	100.00

**Table 9. NPRDS RPS Component major failure causes.**

Component	Routine Cause	Percent	Nonroutine Cause	Percent
TRANSMITTER	out-of-calibration	34.13	wear	6.55
	set point drift	13.85	cyclic fatigue	5.75
INTEGRATOR	out-of-calibration	17.24	defective connection	6.15
	set point drift	15.18	cyclic fatigue	5.05
BISTABLE	out-of-calibration	39.36	open circuit	6.30
	wear	17.55	foreign material	5.46
	set point drift	11.06		
POWER SUPPLY	out-of-calibration	3.06	cyclic failure	6.02
	wear	1.67	short/ground	5.62
	burned circuit	1.25		

and evaluating whether improved methods were able to provide detection capabilities not provided by current practices.

The results of evaluating current practices indicate that applicable data is acquired on some components in the RPS and 1E power system but methodologies are not in place which allow trending of the data. Surveillance tests are typically based on functionality and pass/fail tolerance measurements of voltage and current. "AS FOUND" and "AS LEFT" measurements are manually acquired and recorded on the data sheet, but long term comparisons are not performed. It is believed that this is standard throughout the industry mainly due to the costs associated with trending programs.

Following evaluation of current IS&MM, three advanced techniques, in use at the nuclear facility, were investigated for trending component degradation in the RPS and 1E power system. These included a state-of-the-art infrared thermography data acquisition and analysis system, the Redundant Instrumentation Monitoring System (RIMS™), and the Electronic Characterization and Diagnostic (ECAD™) System.

Though infrared has been used in industry for a long time, recent enhancements using microcomputers have allowed the technology to progress from pass/fail testing to condition monitoring. This has been achieved by going from black and white thermograms to color which allows greater visual resolution in detecting temperature changes. In addition, the ability to digitally store and recall temperature profiles of components has enhanced detection of incipient failures. Evaluation of the nuclear plant's infrared program has shown that infrared testing is applicable for detecting degradation in the RPS and 1E power systems where overheating would occur as a result of component degradation. For example, Figure 6 shows a thermogram of the bushings on a main output transformer. The three bushings are operating at different temperatures with the left bushing having a maximum temperature of about 143°F, the center bushing having a hot spot of about 189°F, and the right bushing having a maximum temperature of about 116°F. The center bushing is operating at a significantly higher temperature, indicating that degradation of the connection at the top of the bushing has occurred.

Evaluation of the RIMS showed that use of this system could have practical advantages for verifying instrumentation calibration and reducing failures caused by routine testing and calibration of RPS components. The RIMS uses a personal computer which reads instrument output data from plant computers. The system allows comparison of redundant channel outputs over time or trending of one channel. It has been demonstrated that RIMS can detect channel drift that has been identified as a significant aging related effect in the RPS. Figure 7 shows a RIMS monthly plot for three Safety Injection Tank level transmitters. Two transmitters have nearly identical output while the third has a noticeable deviation from the other two. In addition, the calibration of the third transmitter appears to be drifting toward increasing deviation.

The ECAD system has been used at the nuclear facility for condition monitoring and troubleshooting of de-energized circuits. The system uses a computer and digital test instrumentation to acquire basic electrical parameters of capacitance, dissipation factor, impedance, and insulation resistance. Test data shows that the system provides information that indicates degradation in components such as

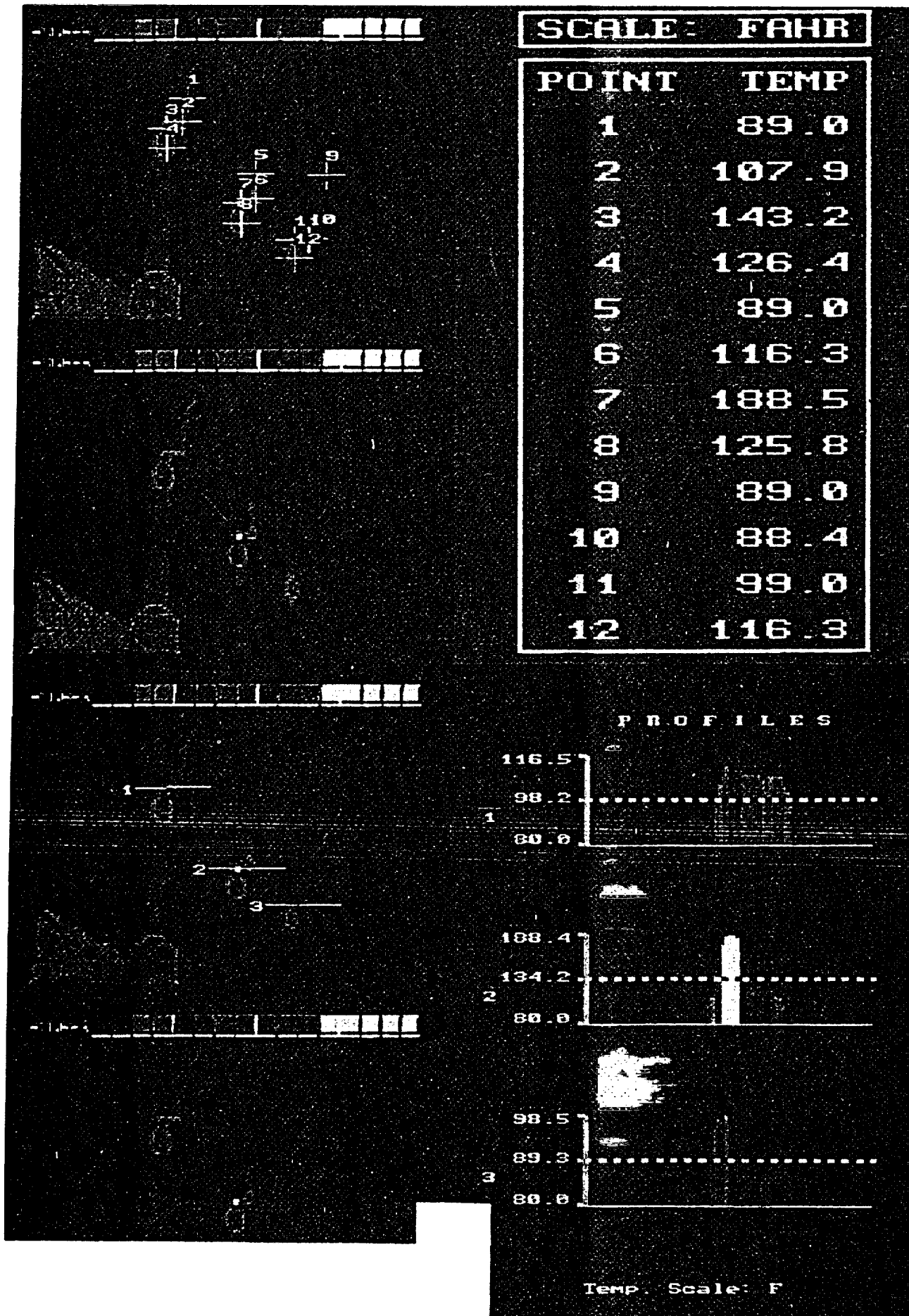


Figure 6. Main Output Transformer Bushing Thermogram

insulation degradation caused by harsh environments and corroded connections. Figure 8 shows a database sort of a flow transmitter that was tested on three different occasions. The first set of tests was performed on August 4, 1989 before abnormal conditions were noted and the transmitter was functioning properly. The second set of tests was conducted on May 1, 1990 following a failure of the transmitter circuit. The data show that the insulation resistance decreased and dissipation factor increased. TDR data showed that the change in insulations occurred at the transmitter. The transmitter was replaced and as a result the insulation resistance and dissipation factor improved as indicated by the third set of data in Figure 8. In fact, the insulation resistance and dissipation were improved from the original test data (the first set of data) indicating the circuit was already in some stage of degradation when first tested.

Improved IS&MM is recommended for RPS and IE power system components. The recommendations are made considering the RPS and IE components that could benefit from improved IS&MM and also the results of an in-plant evaluation of three improved IS&MM practices. In general, infrared thermography is suggested for IE power system components, online comparison of redundant channels is suggested for the RPS, and a computer controlled electronic circuit diagnostic system that measures and records basic circuit parameters is suggested for electrical circuit related diagnostics and trending. Table 10 shows a listing of components that could benefit from improved IS&MM, the applicable system, the dominant failure cause, and the suggested or likely effective IS&MM.

## CONCLUSIONS

The following conclusions can be made based on the research that has been performed:

A significant portion of failures in the IE power system and the RPS are not being detected by routine detection methods. Approximately 52% of the IE power system failures and 39% of RPS failures are being detected by nonroutine methods such as operational abnormality, special inspection, audiovisual alarm, incidental observation, and corrective maintenance.

Breakers, transformers, and busses are the components that are either failing most often or have risk significant concerns for the IE power system. A large portion of the failures for these components are not being detected by routine methods. Transmitters, integrators, bistables, and power supplies are RPS components that are failing most often and have a significant percentage of their failures being detected by nonroutine methods.

In-plant evaluation of improved IS&MM has shown that thermal imagery is effective for detecting many IE power system failures at the incipient stage. Online comparison of redundant channels is suggested for the RPS, and a computer controlled electronic circuit diagnostic system that measures and records basic circuit parameters is suggested for electrical circuit related diagnostics and trending.

# Unit 2

Average Daily SIT 7 Level

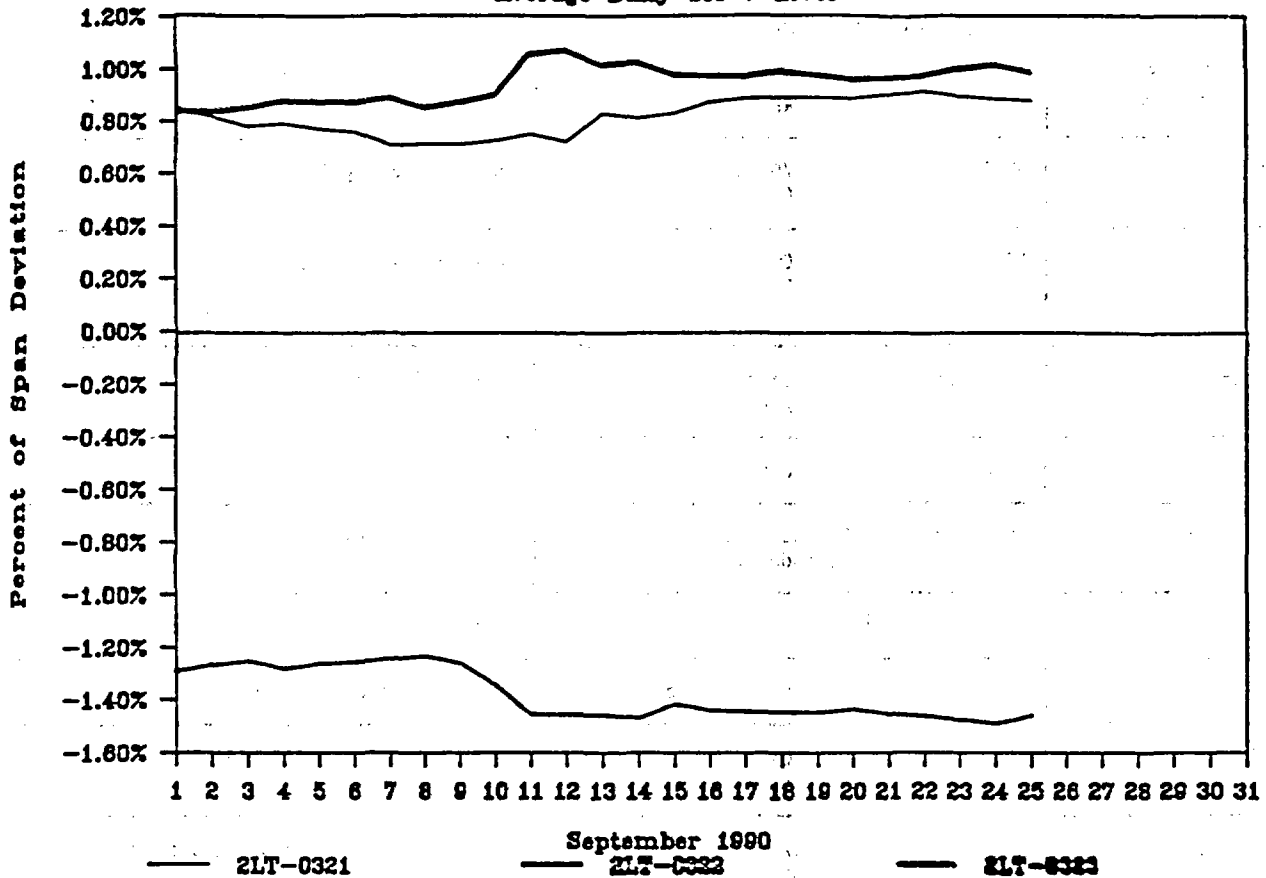


Figure 7. RIMS Data Plot

E C A D S Y S T E M 2 0 0 0

Page: 1  
Date: 08/22/90

Code	Cfg	Date	DC Res	Freq	L/C	Q/D
S1-RCS-FT-410	A	08/04/89	854.50 K	1.00 K	18.77 nF	63.43 mD
S1-RCS-FT-410	A	05/01/90	35.94 K	1.00 K	14.77 nF	405.37 mD
S1-RCS-FT-410	A	05/03/90	270.40 M	1.00 K	18.64 nF	59.13 mD
S1-RCS-FT-410	B	08/04/89	955.10 M	1.00 K	18.54 nF	10.73 mD
S1-RCS-FT-410	B	05/01/90	36.03 K	1.00 K	19.59 nF	244.57 mD
S1-RCS-FT-410	B	05/03/90	1.87 G	1.00 K	18.40 nF	0.87 mD
S1-RCS-FT-410	C	08/04/89	1.03 G	1.00 K	18.82 nF	9.72 mD
S1-RCS-FT-410	C	05/01/90	144.31 K	1.00 K	18.78 nF	29.68 mD
S1-RCS-FT-410	C	05/03/90	4.89 G	1.00 K	18.76 nF	0.85 mD

Figure 8. ECAD Data Sheet

**Table 10. IS&MM Evaluation Results.**

COMPONENT	SYSTEM	FAILURE CAUSE	LIKELY EFFECTIVE IMPROVED IS&MM
Battery	1E Power	Short/Ground Open Circuit	Thermal Imagery System
Circuit Breaker	1E Power	Open Circuit Weld Fault	Thermal Imagery System
Inverter	1E Power	Open circuit Short/Ground	Thermal Imagery System
Relay	1E Power	Open Circuit	Thermal Imagery System
Transformer	1E Power	Defective Connection Degraded Insulation	Thermal Imagery System
Transmitter	RPS	Wear	Instrumentation Monitoring System
Integrator	RPS	Defective Connection	Instrumentation Monitoring System
Bistable	RPS	Open Circuit Foreign Material	Instrumentation Monitoring System
Power Supply	RPS	Short/Ground Out-of-Calibration	Instrumentation Monitoring System
Conductors	1E Power and RPS	Short/Ground Insulation Breakdown Defective Connections	Circuit Diagnostic System

# METHOD FOR DETECTING DEGRADATION IN INSTALLED CABLES IN NUCLEAR POWER PLANTS

Yasuo KUSAMA, Toshiaki YAGI, Yosuke MORITA  
Seiji KAMIMURA\* and Hideki YAGYU\*

Japan Atomic Energy Research Institute (Takasaki)  
\*Hitachi Cable

## Abstract

The object of the investigation is to develop non-destructive detecting method for degradation of cables installed in nuclear power plants from the viewpoint of the safety operation and the life extension of the plants. Two kinds of detecting method a) torque-strain response and b) Thermogravimetry were studied in order to apply to the low voltage cables, for which effective detecting methods have not been completed. Applicability of the methods to the low voltage CV cables (cross-linked polyethylene insulation, polyvinylchloride jacket) were discussed by using elongation at break as a primary standard.

## 1. Introduction

Huge amounts of cables are used in nuclear power plants in wide varieties as power supply, instrumentation and control. These cables, especially used in safety systems, are considered to be one of the essential components as a pressure vessel and concrete structures, on which plant life inevitably depends.

Generally, cable life is dominated by the degradation of its organic insulation materials, because their thermal and/or radiation resistances are inferior to those of metal conductor. The degradation of cable insulators and jacket by thermal and/or radiation aging has been examined by visual observation and by tensile tests, and the degree of degradation has been evaluated from the ultimate strength and elongation.

Simple and precise methods for detecting degradation of the installed cables in the facility, therefore, are expected to develop from the view point of the safety operation and the maintenance of the plants which bring the plant life extension.

Cables used in the power plants can be divided roughly into two categories as high voltage use and low voltage use. For the high voltage power cables, monitoring method of their conditions has been studied about the leakage current for D.C. and comes into practical use. But for most of the low voltage cables, various detecting methods, for example indenter test[1], residual voltage[2], electronic characterization and diagnostic system:ECAD[3], and time domain spectrometry:TDS[4] have been investigated and the practical application of these methods are in progress.

In this report, we study two non-destructive methods for estimating the degradation of the installed cables. These methods are a torque-strain response and a thermogravimetry, which detect the degradation of PVC jacket material on the cables. We compare the data obtained by the two methods with

those obtained by tensile elongation which is standard indicator of the degradation of polymeric materials. These results have a linear relations each other from which we can estimate life time of PVC jacket materials.

## 2. Experimental

### Sample:

Low voltage (600V) CV cables (normal type, flame and/or heat resistant types) were used to study torque-strain response. Sheet samples(1.0 mm thick) of their jacket materials and sheet samples(0.5 mm thick) of PVC were prepared to study thermogravimetry.

### Irradiation and Thermal Aging:

The cable samples and the sheet samples of their jacket materials were irradiated by  $^{60}\text{Co}$  gamma rays at room temperature under pressurized oxygen at a dose rate of 5 kGy/h and in air at 0.03-1.09 kGy/h at room temperature. The sheet samples were irradiated at room temperature in air at 0.5 and 10 kGy/h and under pressurized oxygen at 5 kGy/h.

Thermal aging was carried out in an air circulated type oven in a temperature range of 100-158°C.

### Torque-Strain Response:

Fig.1 shows the scheme of a prototype apparatus for torque-strain response measurement. A fixed length of the cable was held with two chucks and small angle torsions(usually from +5 to +10 degrees)of variable frequency were added with one of the chuck. Stress(Torque) yielded by torsion was detected at the other side of the chuck.

### Thermogravimetry:

Small amounts of the sample (usually 4-5 mg) were scratched out from the surface of cable jacket and sheet samples. Their thermal decomposition temperatures were measured by thermogravimetric analyzer(TGA) in an inert gas atmosphere at a temperature rise of 10-20°C/min.

### Tensile Test:

After the measurement of torque-strain response, the dumbbell shaped specimens for tensile test were cut from the cable jacket in order to use elongation at break( $E_b$ ) as an indicator of degradation. Tensile properties of the cable and the sheet samples were measured by tensile tester at a chuck speed of 200 mm/min.

### Molecular Weight Measurement:

Molecular weight and molecular weight distribution were measured by gel permeation chromatograph in order to assure degradation mechanism.

## 3. Result and Discussion

Fig.2 shows basic idea for examining the degradation of the low voltage CV cables. In the low voltage CV cables, degradation of mechanical property is larger than that of

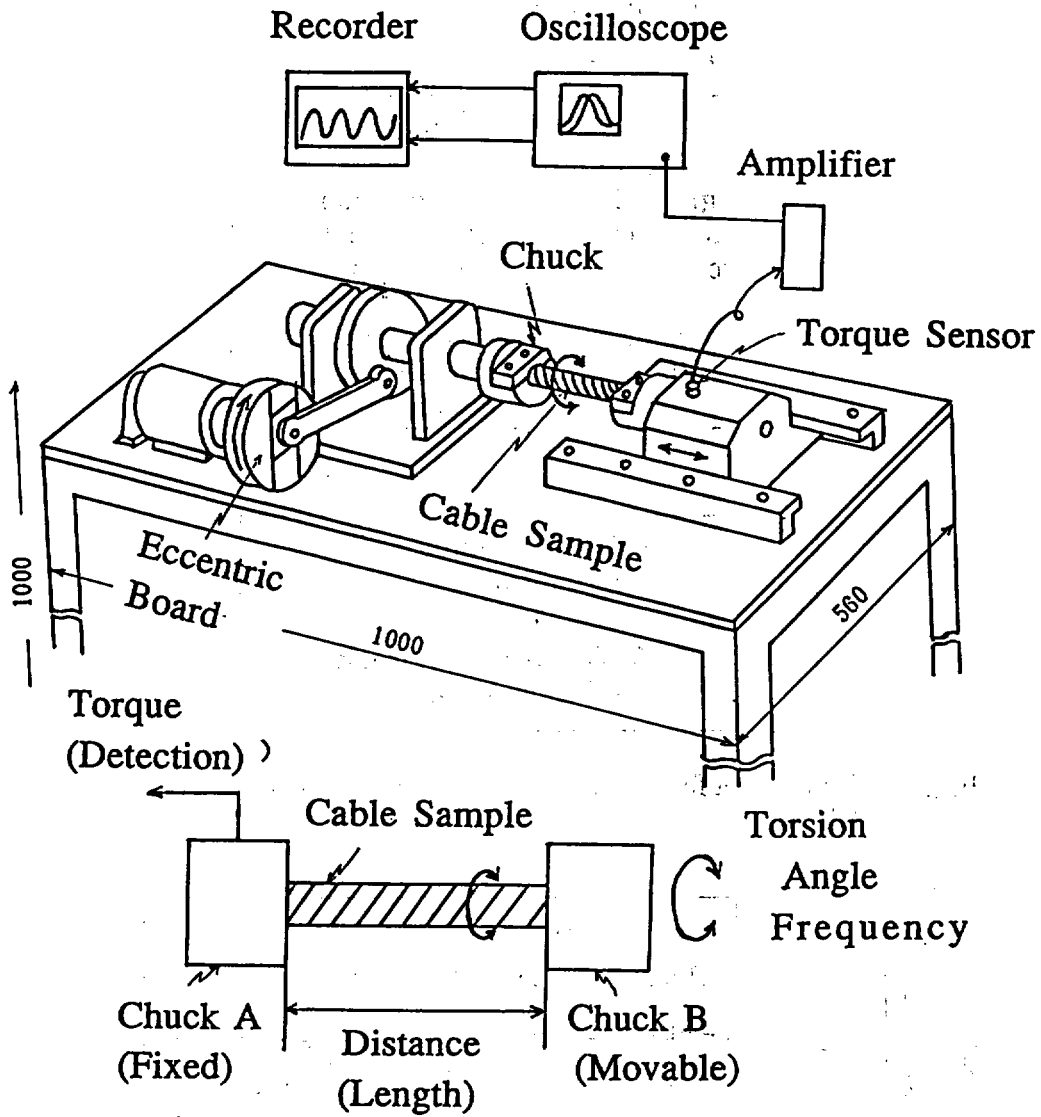


Fig.1 Scheme of a prototype apparatus for torque-strain response measurement.

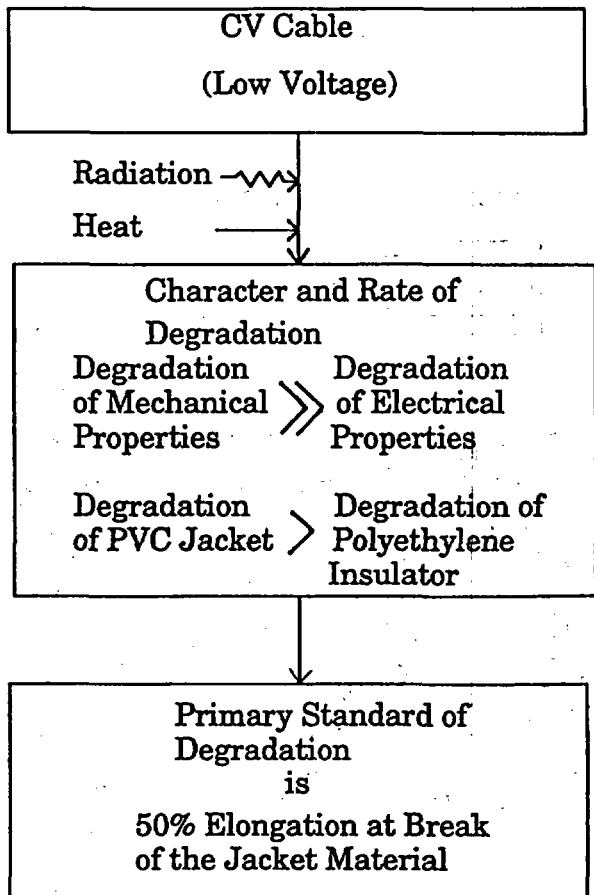


Fig.2 Basic idea for examining degradation of the CV cable.

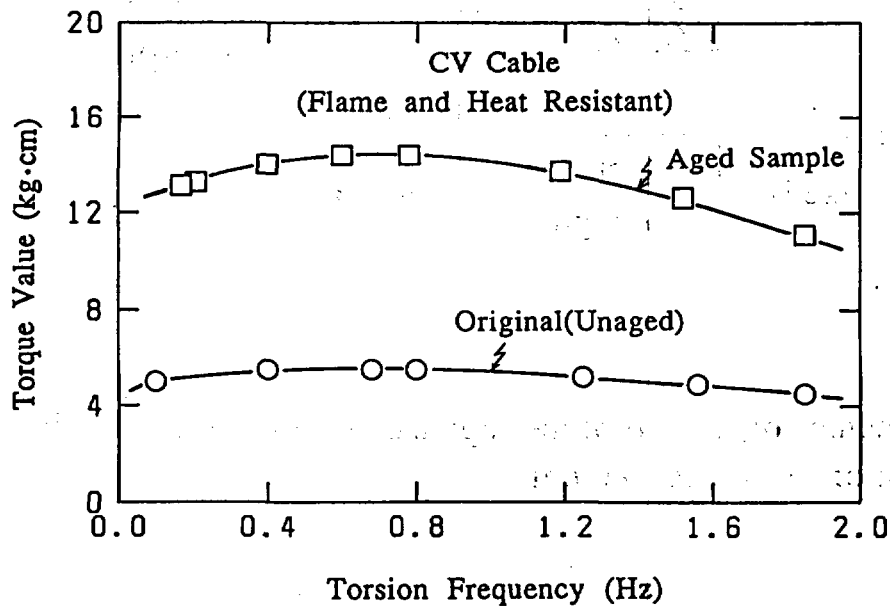


Fig.3 Effect of torsion frequency on torque value of the original and the aged CV cables.

electrical property, and thermal and/or radiation resistances of polyethylene insulator are superior to those of polyvinylchloride(PVC) jacket. Therefore, it is reasonable and careful consideration to estimate the degradation of the cables from the changes of mechanical properties of PVC jacket materials. The study is focused firstly on the degradation of PVC jacket materials.

#### a) Torque-Strain Response

To measure a torque-strain response on the sample cable, we made the prototype apparatus(see Fig. 1). The degradation of the jacket is mainly detected with the apparatus. In order to find out appropriate conditions for the measurement, factors considered to affect on torque-strain response were examined.

Fig.3 shows the effect of torsion frequency on torque value of the original and the aged CV cables. Torque value is nearly constant for the original in a range 0 - 2.0 Hz. The optimum value, which supposed to be related to the relaxation of the PVC, was found at approximately 0.8Hz for the aged cable. Appropriate frequency of torsion was found to be in a range of 0.4 - 1 Hz.

Fig.4 shows the effect of torsion angle on torque values. Torque value increases with increasing the degradation and also increases linearly with increasing torsion angle up to 10 degrees and levels off. At larger torsion angle, the effect of constituents rather than jacket on the torque-strain response becomes larger. These results show that smaller angle (below 10 degrees) will be preferable to the non-destructive measurement. Five degrees will be enough to detect change of the torque values of the aged cables. Effects of constituents such as conductor, insulation and inclusive on torque-strain response become larger with decreasing of the distance between the chucks. On the contrary, sensitivity of the torque-strain response decreases with increasing chuck distance. The distance of 50mm is most suitable to eliminate some kinds of effects from the constituents except the jacket.

Following conditions are found to be suitable for the torque-strain response measurement:

- Appropriate torsion frequency is in a range of 0.4 - 1 Hz.
- Small torsion angles(below 10 degrees) will be preferable to the non-destructive measurement
- The distance of 50 mm between two chucks is most suitable to eliminate effects from the constituents except jacket.

Fig. 5 shows correlations between elongation at break and torque value of the flame and heat resistant type PVC exposed to thermal aging. The dumbbell sheets for tensile test were cut from the cable jacket. Linear relations between Eb's and torque values were obtained in an Eb range of 300-40%.

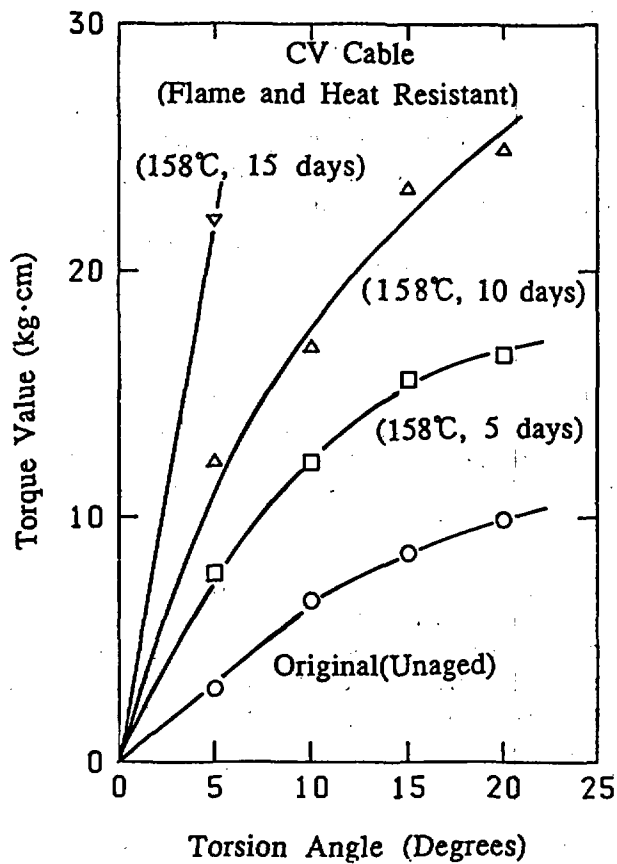


Fig.4 Effect of torsion angle on torque value of the original and the thermally aged CV cables.

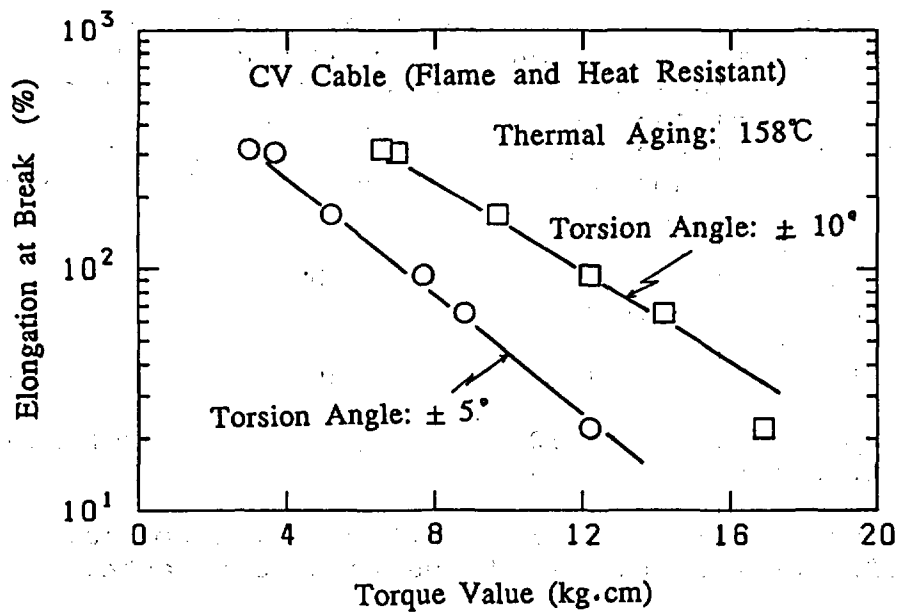


Fig.5 Elongation at break ( $E_b$ ) versus torque value of the flame and heat resistant type CV cables exposed to the thermal aging.

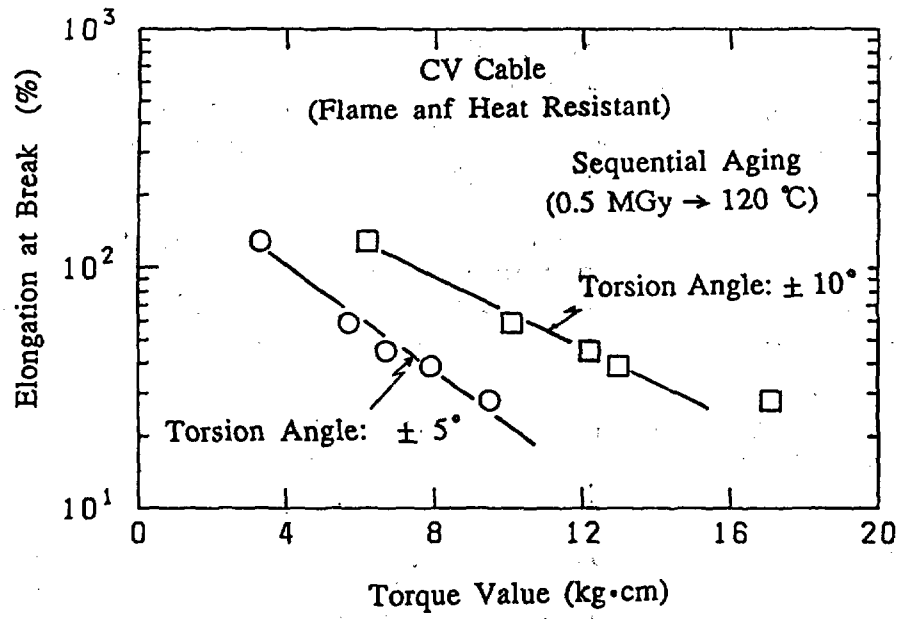


Fig.6 Eb versus torque value of the flame and heat resistant type CV cables exposed to the sequential aging of radiation followed by heat.

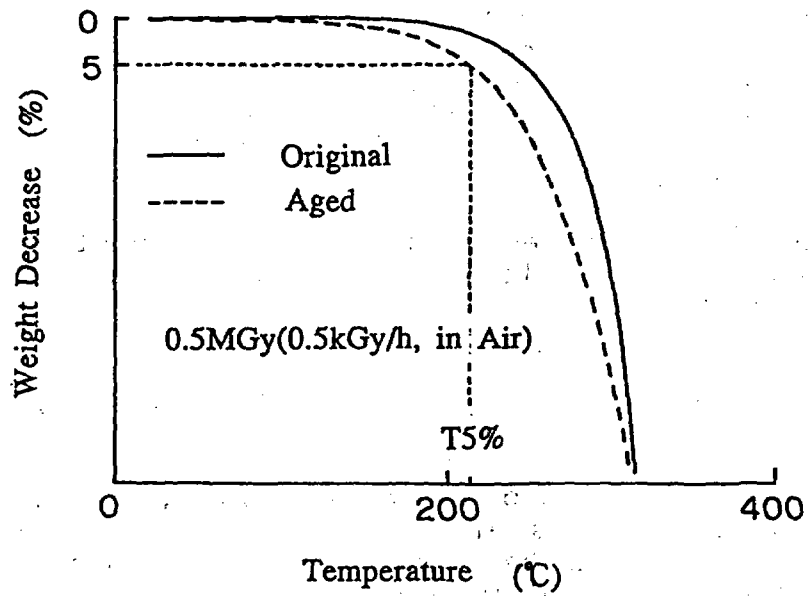


Fig.7 Thermal decomposition behaviors of the PVC sheet samples.

Fig.6 shows the result for flame and heat resistant type PVC exposed to the sequential aging of radiation followed by heat. Linear relations were also obtained in an Eb range of 150-30%.

These results show that torque-strain response is effective to detect the degradation of the jacket material in the installed cables.

These results show that degree of degradation in installed cables can be estimated non-destructively by using relations between the torque value and the elongation at break those obtained for the CV cables exposed to artificial aging.

#### b) Thermogravimetry

In order to examine the applicability to detect degradation of the installed cables, thermogravimetric analysis was examined by using PVC sheet samples.

Fig. 7 shows typical TG curves for the unirradiated and the irradiated PVC sheet samples. The solid line represents thermal decomposition behavior of the unirradiated sample and the broken line represents that of the irradiated one. Significant change in TG curve was observed in a temperature range of 200-300 °C, and the start point of thermal decomposition shifts to the lower temperature by irradiation. Temperature at which sample weight decreases by 5% (expressed as T5%) significantly changes with irradiation.

Fig.8 shows relation between elongation at break (Eb) and T5% of the PVC sheet sample irradiated with gamma-rays at various conditions. Linear relation was found between Eb and T5%. This result suggests that radiation degradation of the PVC is mainly due to the chemical structure change of the polymer. It is known that thermal degradation of insulating materials are caused by chemical change of their molecular structure and that property of the material unequivocally changes with their molecular structure[5].

It has been reported that rate of thermal decomposition of the PVC has a relation to the molecular weight of the polymer by following equation[6].

$$V = a + k \frac{1}{M} \quad (1)$$

where, V shows the rate of dehydrochloride, M is molecular weight of the polymer, a and k are constant. This equation suggests that good correlation between thermal decomposition temperature and the molecular weight will be obtained.

To clarify the degradation mechanism which contributes to Eb decrease, molecular weight of the polymer fraction was examined by using gel permeation chromatograph.

Fig.9 shows correlation between Eb and temperature at which the sample weight decreases by 5% (T5%) of the irradiated PVC sheet sample. Completely linear relation was found between

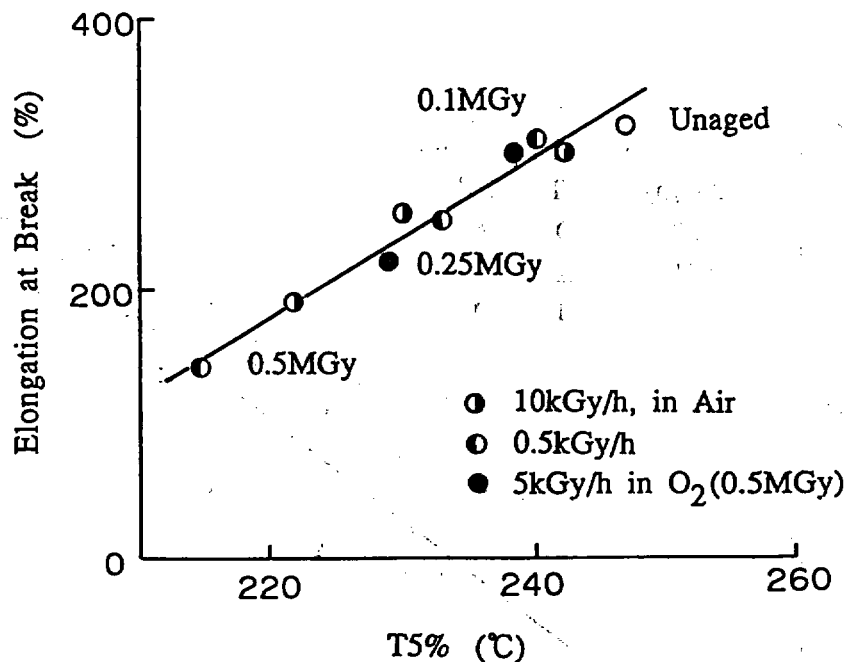


Fig.8 Relation between Eb and thermal decomposition temperature at which the sample weight decreases by 5%(T5%) of the PVC sheet samples irradiated with  $\gamma$ -rays at various conditions.

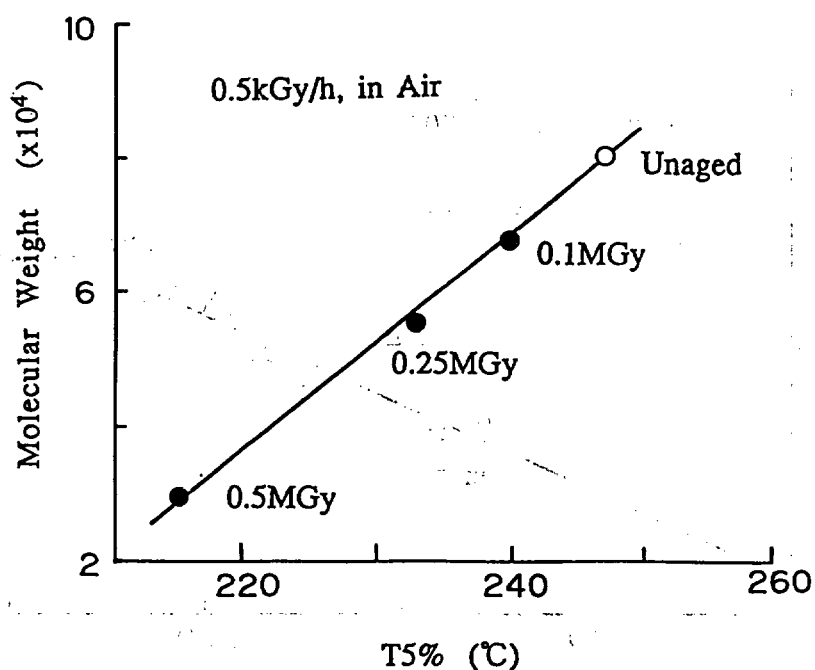


Fig.9 Correlation between molecular weight and thermal decomposition temperature at which the sample weight decreases by 5%(T5%).

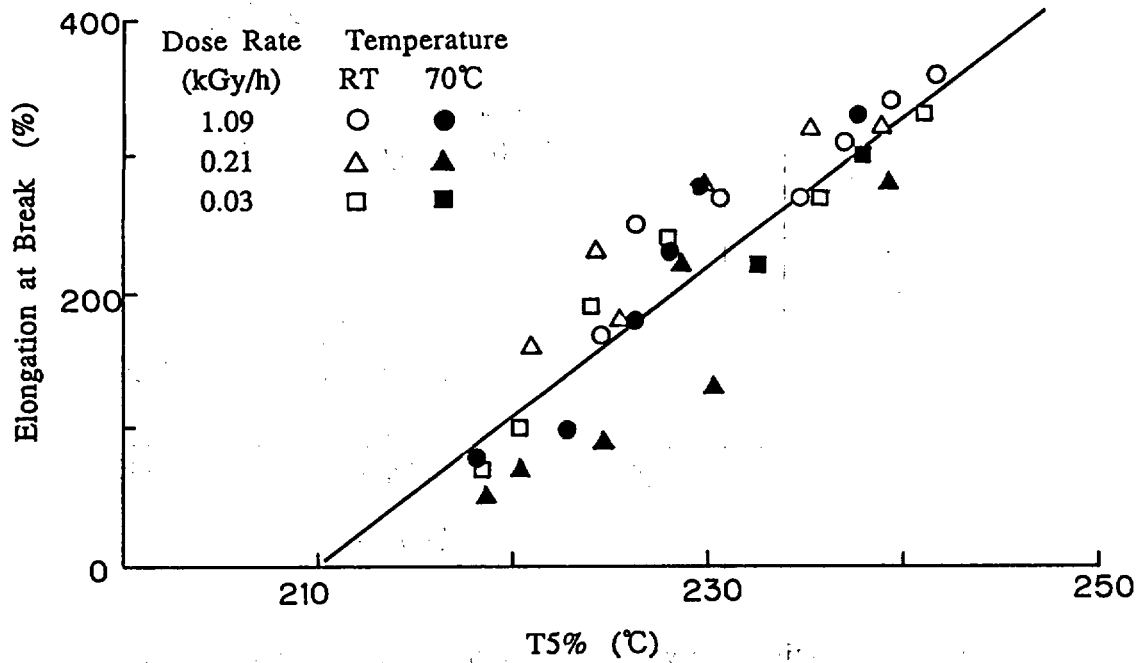


Fig.10 Eb versus T5% of the normal type CV cable jacket material irradiated at various conditions.

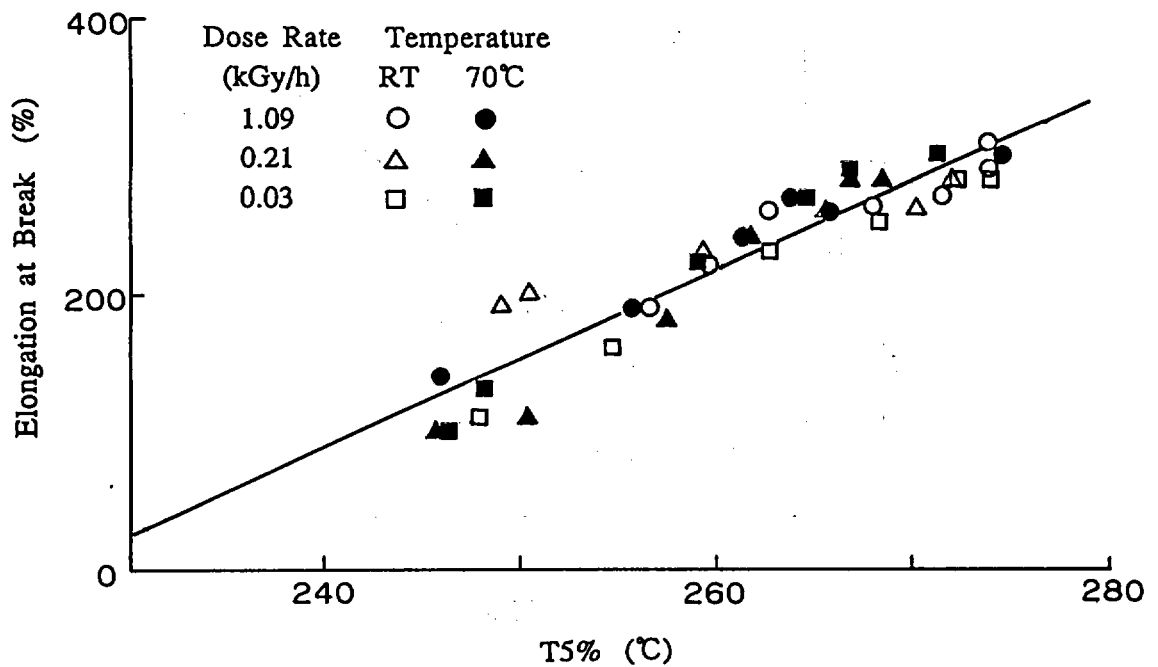


Fig.11 Eb versus T5% of the heat resistant type CV cable jacket materials irradiated at various conditions.

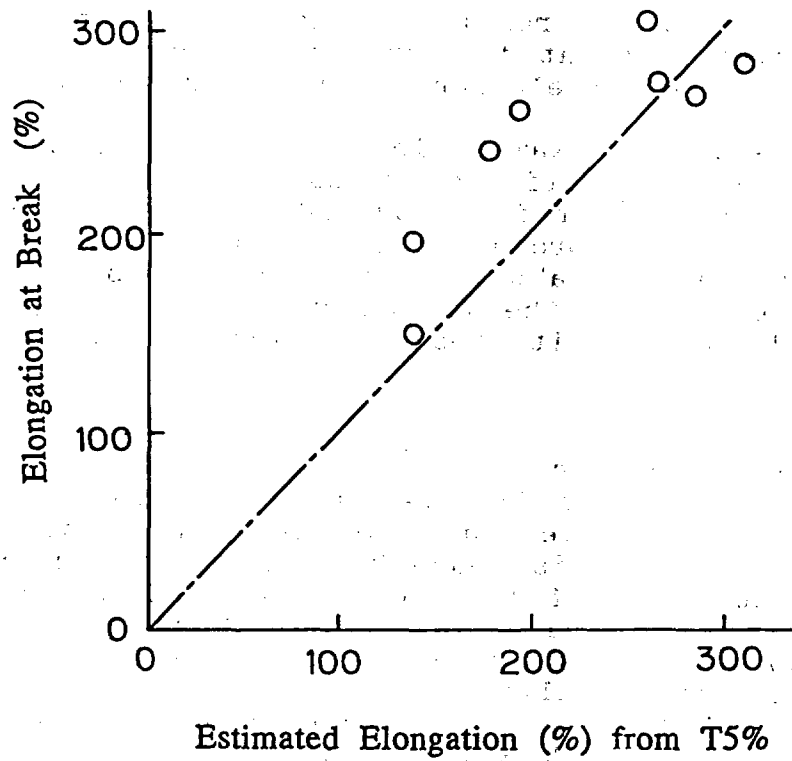


Fig.12 Estimated Eb value from T5% and Eb value obtained by tensile test of the cables which have been used for 20 years and removed from the power plant.

molecular weight and  $E_b$ . This result shows that degradation of PVC with gamma ray irradiation is attributed to the main chain scission of the polymer.

Fig.10 shows the results obtained for the normal type CV cable jacket material irradiated at various temperature and dose rate conditions. Good correlation between  $E_b$  and T5% was found in a wide  $E_b$  range.

Fig.11 shows the result for heat resistant type CV cable jacket material irradiated at various temperature and dose rate conditions. Good correlation was also found between  $E_b$  and T5%.

Fig.12 shows an example in application of thermogravimetry to estimate the degradation of CV cables which have been used in the nuclear power plant for about 20 years and removed from it. In this figure, the ordinates represents  $E_b$  value obtained by tensile test and the abscissa represents  $E_b$  value which was estimated from T5% of the TGA measurement.  $E_b$  value obtained from T5% well agrees with real  $E_b$  value obtained by destructive measurement.

#### 4. Conclusion

In the torque-strain response measurement, factors which affect on torque-strain response are found to be torsion frequency, torsion angle and distance between the chucks.

Good correlation is found between the torque value and the elongation at break of the cables exposed to the artificial aging. Experimental results show that the torque-strain response can be used as a non-destructive method to detect degree of degradation in installed cables.

In thermogravimetry, good correlation is also found between the elongation at break and the T5% of the CV cable exposed to artificial and natural aging. It can be concluded that these results will provide a possibility to practical application of these methods to detect degradation of installed cables in power plant.

## 5. References

- [1] S.P. Carfagno et al, "Development of a cable indenter to monitor cable aging in situ," International Conference on Operability of Nuclear Systems in Normal and Adverse Environments, Proceedings, Vol. 1, pp195-202, 1989
- [2] S. Yamanaka et al, "A method for obtaining the dielectric characteristics by analyzing the residual voltage," Trans. IEE of Japan, Vol. 110-A, No. 3, pp181-189, 1990
- [3] R.D. Meininger, "Electronic characterization and Diagnosis," Proceedings of Work Shop on Power Cable Condition Monitoring 19-1 EPRI EL/NP/CS-5914-SR, 1988
- [4] F.I. Mospik and F.D. Martzroff, "Time domain spectroscopy to monitor the condition of cable insulation," Proceedings of 16th Water Reactor Safety Information Meeting NUREG/CP-0097 Vol.3, pp 21-40, 1989
- [5] S. Okada et al, "Deterioration test of insulating materials of cables for nuclear power generating stations," J. of At. Energy Soc. JPN. Vol.21, No.10, pp808-814, 1979 (Japanese)
- [6] M.B. Neiman, "Aging and Stabilization of Polymers", 1964

## DETECTING AND MITIGATING AGING IN COMPONENT COOLING WATER SYSTEMS\*

Robert J. Lofaro  
Brookhaven National Laboratory  
Upton, New York 11973

### ABSTRACT

The time-dependent effects of aging on component cooling water (CCW) systems in nuclear power plants has been studied and documented as part of a research program sponsored by the U.S. Nuclear Regulatory Commission. It was found that age related degradation leads to failures in the CCW system which can result in an increase in system unavailability, if not properly detected and mitigated. To identify effective methods of managing this degradation, information on inspection, monitoring, and maintenance practices currently available was obtained from various operating plants and reviewed. The findings were correlated with the most common aging mechanisms and failure modes, and a compilation of aging detection and mitigation practices was formulated. This paper discusses the results of this work.

### INTRODUCTION

The component cooling water (CCW) system is one of many systems that is important for safe operation of nuclear power plants. In a research program sponsored by the U.S. Nuclear Regulatory Commission (NRC), the CCW system has been studied to determine how aging affects its performance and reliability. The study was performed in two phases and included extensive analyses of data obtained from national data bases, as well as data obtained from actual plant visits. This paper discusses how the results of those analyses can be used to help detect and mitigate the affects of aging in CCW systems.

The function of the CCW system is to remove heat from various loads throughout the plant and discard it to an open loop cooling system, such as the service water system. The loads serviced by the CCW system can be safety-related or non-safety-related, and include the reactor coolant pump seals, the shutdown heat exchangers, the residual heat removal heat exchangers, and the safety injection pumps. Due to the diversity of the loads dependent on it, the CCW system is continuously operating, and is required during normal, as well as off-normal plant operation. Therefore, the affects of aging must be properly managed to ensure safe plant operation in later years.

### PHASE I RESULTS

In phase I of the CCW system aging study<sup>1</sup> an analysis of past operating experience showed that the CCW components are susceptible to aging degradation,

\* Work performed under the auspices of the U.S. Nuclear Regulatory Commission

and that this degradation can lead to an increase in failure rate as the components age. Of the failures reviewed, over 70% were related to aging (Figure 1). The dominant cause of failure was found to be "normal service" (Figure 2), which includes exposure to all operating and environmental stresses the component is normally expected to see. As shown, the percentage of failures caused by normal service increases as the plants age. This can be partially attributed to aging and partially to a learning curve effect, which reduces the percentage of human error failures.

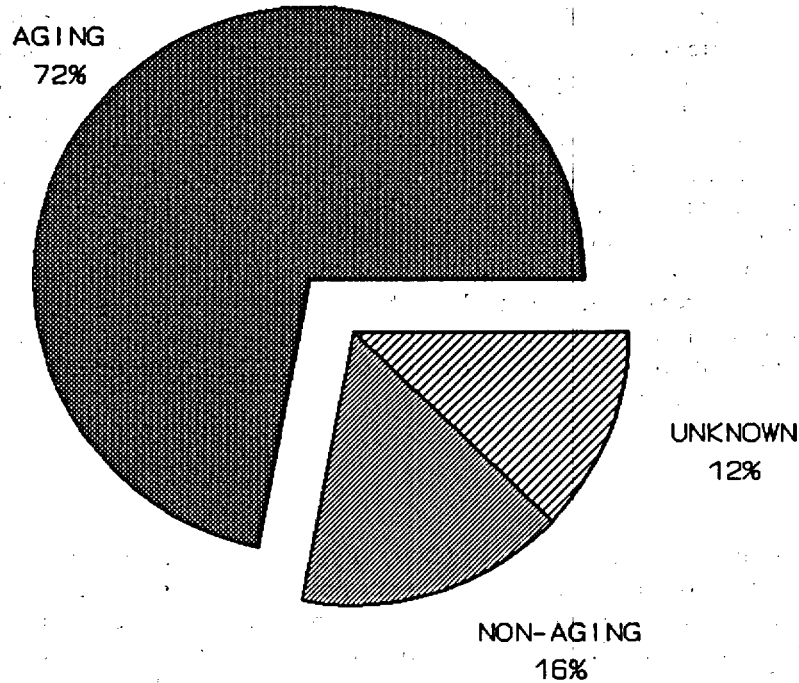


Figure 1 Fraction of failures related to aging

The dominant failure mechanism was "wear" (Figure 3), which is consistent with the high percentage of failures attributed to aging. Wear is an aging mechanism characterized by the physical wearing away of the component due to the relative motion between it and another component, such as valve packing being worn by the rotation of the valve shaft. Although wear accounted for over one-third of the failures, a number of other mechanisms were also found which can be related to aging. Each of these mechanisms can lead to component failures, if it is not properly monitored and controlled. In light of this, the need to have diverse monitoring methods to be able to detect all forms of aging mechanisms and mitigate degradation becomes apparent.

The data were also examined to identify the components having the largest number of failures. It was found that valves were the most commonly failed component, followed by pumps, instrumentation, and heat exchangers (Figure 4). It should be noted that the data were not normalized to account for population effects, therefore, valves are the dominant components failing due to their large population. However, these findings show which components require the most resources in terms of monitoring and maintenance.

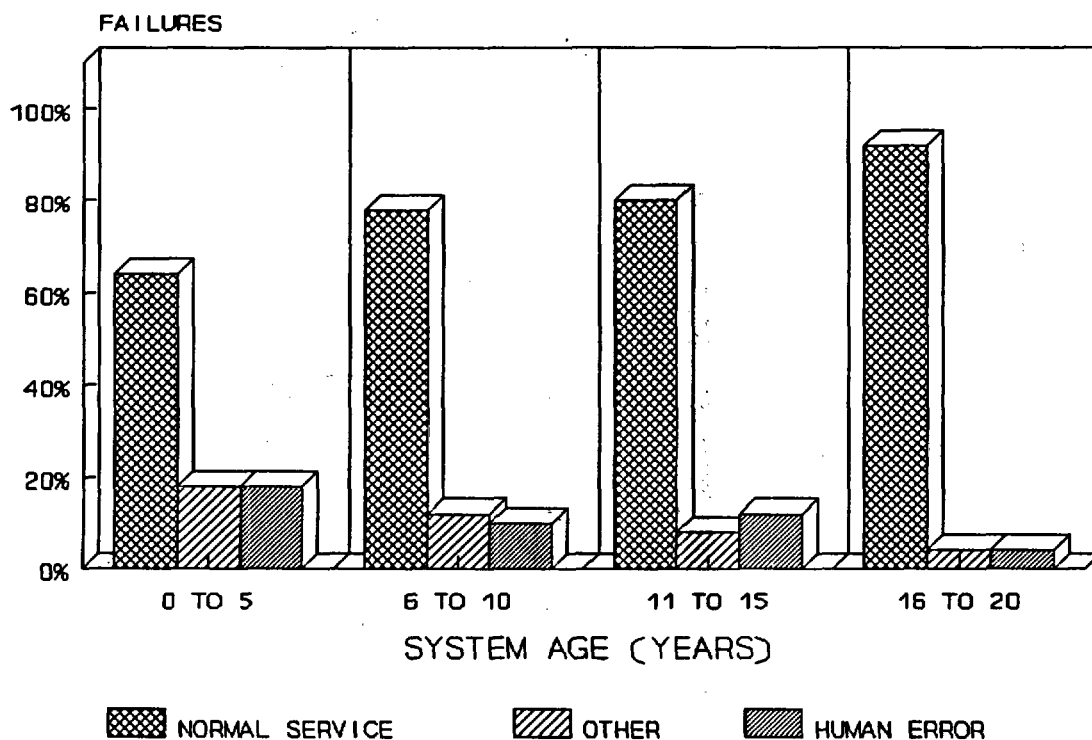


Figure 2 Causes of failures versus plant age

Using time-dependent failure rates calculated from the data, a simplified probabilistic risk assessment (PRA) analysis was done for a common CCW system design. For this analysis, the CCW valves, pumps and heat exchangers were given a failure rate that increases with time to simulate the effects of aging. The results showed that for component failure rates that increase by factors ranging from one (check valves) to nine (pumps) over a 40 year period, the unavailability of the system can increase by a factor of 40 (Figure 5). This is partially due to the combined aging of all components, and partially due to the degradation of multiple redundant components. Since the CCW system is important to safety, this could lead to an increase in plant risk. These findings clearly show that proper detection and mitigation of aging degradation should be an important part of daily plant operation.

#### PHASE II RESULTS

As indicated by the phase I results, aging degradation is present in CCW systems and must be controlled. This requires a two-step process involving detection and mitigation. It is important to be able to detect aging degradation before it results in failure, and it is equally important to mitigate the effects of degradation once it is detected. In the second phase of this study<sup>2</sup> these two areas were addressed.

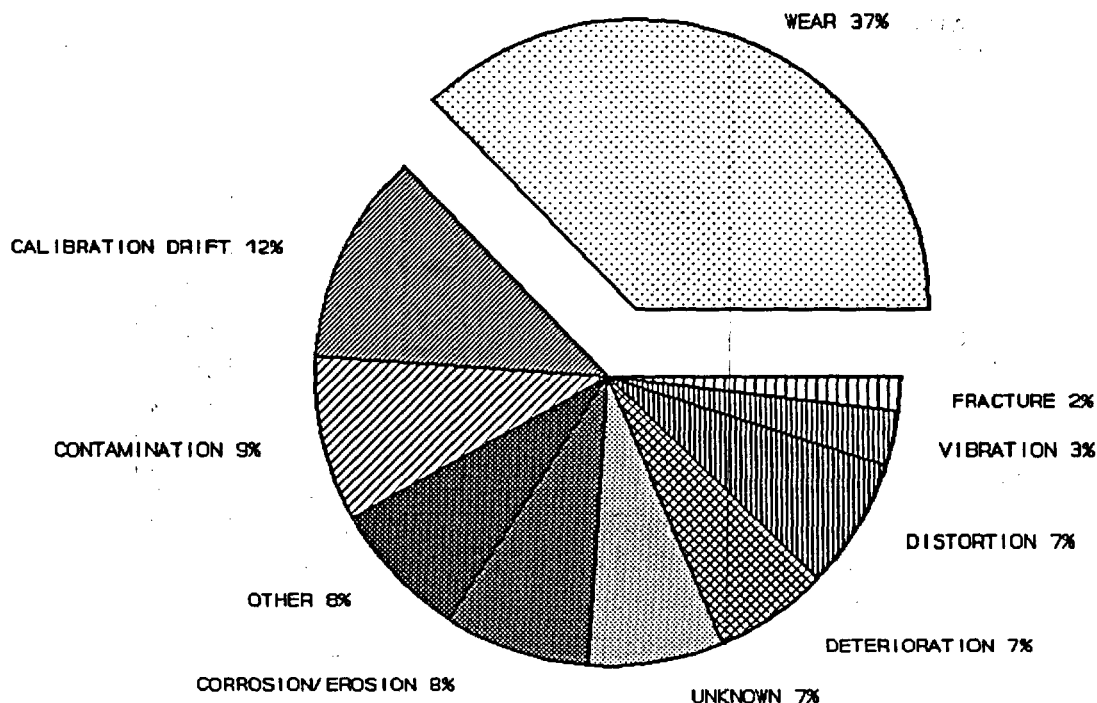


Figure 3 Mechanisms of failure

To determine the most effective methods of managing aging, inspection, surveillance, monitoring, and maintenance (ISM&M) practices were investigated. Information on ISM&M practices currently used at plants was obtained from a survey, along with actual plant visits and personnel interviews. In addition, various advanced practices were identified through literature searches and discussions with component manufacturers. The findings provided an excellent overview of what methods are available to properly control aging degradation.

The detection of aging degradation can be accomplished through the use of proper testing programs and monitoring practices. The objective in selecting the tests performed and the monitoring practices used should be to ensure that at least one measure is in place to detect each of the aging mechanisms most commonly encountered. Using the aging mechanisms identified previously, the objective of this phase II work was to identify what practices are available, and which aging mechanisms they can effectively detect.

Tables 1 and 2 are samples of the survey results, which address CCW pump and valve tests. As expected, these results reflect the ASME Section XI code requirements for in-service testing. It should be noted that not all units reported performing the Section XI requirements at the required frequency. This could be due to relief being granted by the NRC, misinterpretation of the survey question, or an error in responding. The results also show that, in addition to the code requirements, there are other actions which are performed by some of the units. Some examples include measuring pump motor voltage and current, and performing MOV signature analysis. These are typically performed based on past problems, or special plant operating or environmental conditions.

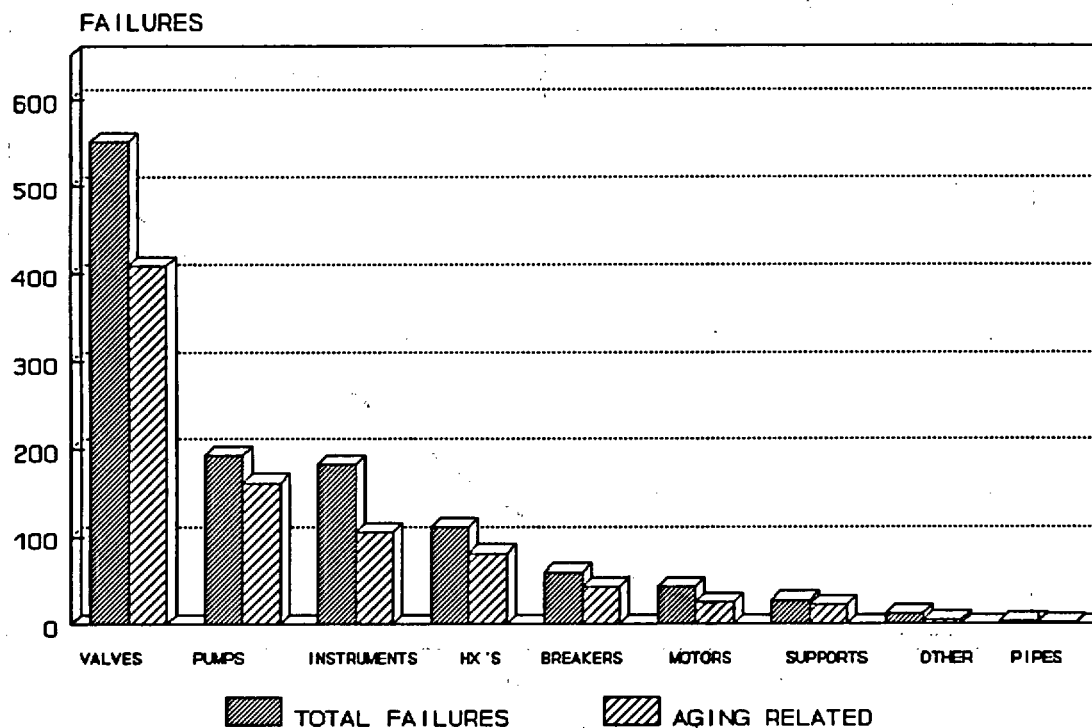


Figure 4 Components most frequently failed

The tests performed provide an indication of how the component is functioning and can help identify aging related problems. Each parameter tested can be used to detect an aging mechanism. For example, if the measured pump developed head is lower than expected, this could be an indication that the wear rings have worn excessively and need to be replaced. If a valve stroke time is slower than expected, this could be an indication that the valve internals are corroded and need to be refurbished, among other things. By understanding what aging mechanisms a component is susceptible to and what the test results indicate, in-service testing can be used to detect aging degradation.

In addition to testing, parameter monitoring can be used to evaluate system performance and help detect aging degradation. As part of the survey each unit was asked which common parameters are monitored on a routine basis. The results show that pump discharge pressure, pump motor amperage, and heat exchanger flow are the most commonly monitored; however, only five units out of the 12 units responding reported that they monitor these parameters routinely (Figure 6). Surge tank level is an excellent indicator of system leakage, however, only three units reported monitoring this parameter routinely. None of the units reported monitoring heat exchanger pressure drop routinely, although several said they would if a problem were suspected. Each of these monitoring practices can be helpful in detecting aging degradation and should be considered as part of a monitoring program.

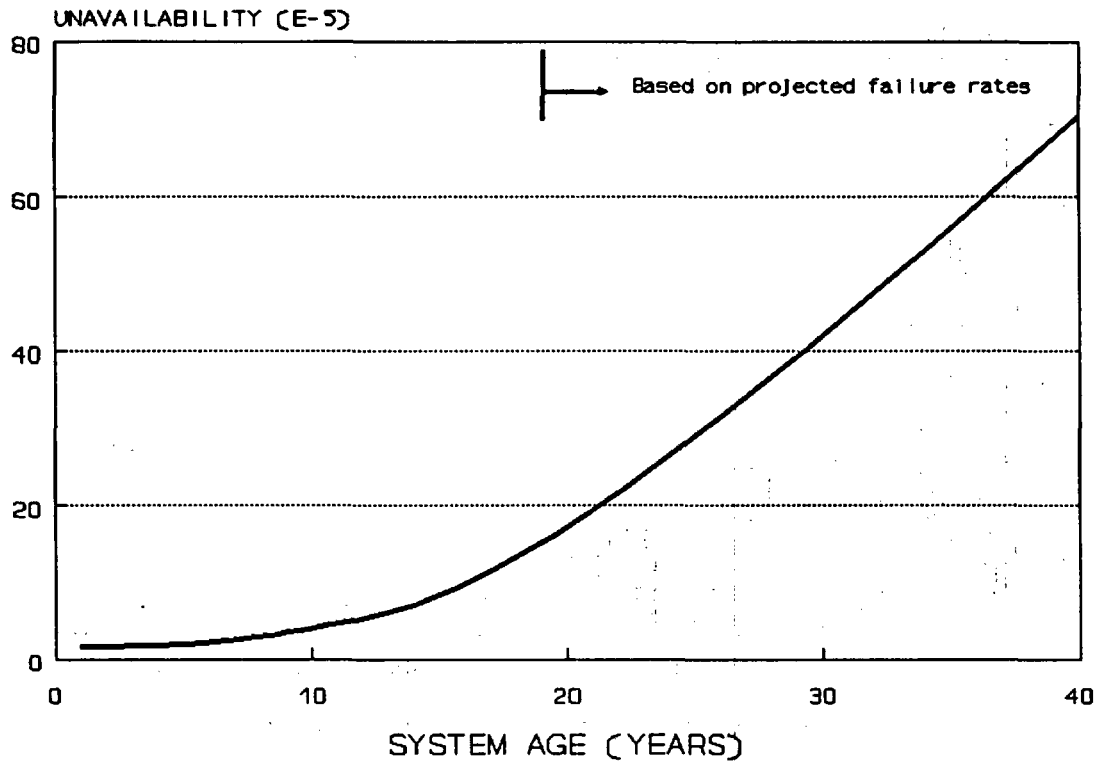


Figure 5 CCW system unavailability versus age

Table 1 CCW Pump Tests

Test Performed	Frequency (Months)		
	1	3	12
1. Measure Vibration Amplitude*	1 unit	10 units	3 units
2. Measure Pump Head*	3 units	10 units	
3. Measure Suction Pressure*	3 units	8 units	
4. Measure Flow Rate*	2 units	4 units	
5. Measure Bearing Temperature*		5 units	
6. Measure Lubricant Temperature*		2 units	2 units
7. Check Lubricant Level*		4 units	
8. Measure Motor Voltage/Current	1 unit	1 unit	

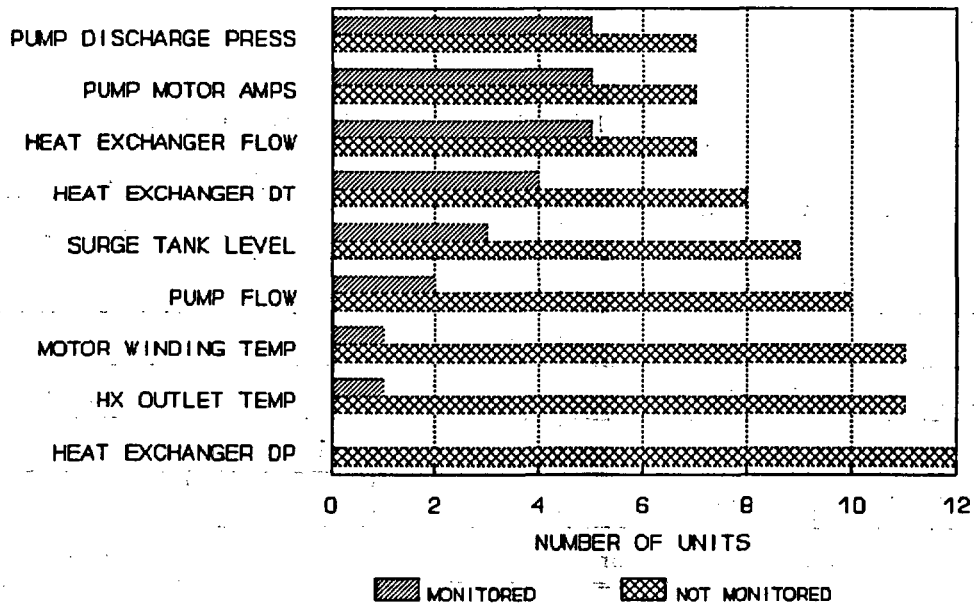
\* Test required by ASME Section XI

Table 2 CCW Valve Tests

Test Performed	Frequency (Months)			
	3	12	18	24
1. Measure MOV Stroke Time*	10 units			
2. Check Valve Leakage*	5 units		4 units	
3. Check Valve Flow*	5 units			
4. Remote Position Indicator*			1 unit	2 units
5. Valve Seat Leakage*	1 unit			
6. MOV Insulation Resistance		1 unit		
7. MOV Current Measurement		1 unit		
8. MOV Signature Analysis			1 unit	

\* Test required by ASME Section XI

PARAMETER



NOTE: BASED ON RESPONSES FROM 12 UNITS

Figure 6. Routine parameters monitored

The second part of an effective aging management program involves the mitigation of degradation. This typically is done through the use of preventive maintenance (PM) measures. As part of this study information on PM practices was obtained for the most commonly failed CCW components. Tables 3 and 4 are sample survey results which include the PM practices typically performed on CCW pumps and valves. As for the testing and monitoring practices discussed previously, each PM action can help mitigate one or more aging mechanisms. For example, lubrication of moving parts will help prevent wear and corrosion from occurring. Alignment of components will help prevent vibration, which can lead to weakening of materials. To ensure an effective PM program, all the aging mechanisms each component is susceptible to should be identified and a PM practice should be instituted to mitigate it.

As an aid in evaluating a plant's ISM&M programs, the various practices identified in this study were correlated with the aging mechanisms they can detect and/or mitigate, and the results were tabulated for the major components. Table 5 lists the basic practices which all units should perform along with the related aging mechanisms they can detect or mitigate. These include ASME Section XI requirements, as well as other commonly used practices already performed by some units. The frequency ranges are based on the ASME Section XI code requirements, which are recommended as a minimum, and the survey results. Tables 6 through 8 list the supplemental practices for pumps, valves, and heat exchangers which can be selected based on particular plant requirements. In using these tables the ISM&M programs should first be reviewed to identify any aging mechanisms that are not being addressed. Once this information is available, the tables can be used to identify an appropriate measure to be added to the maintenance or monitoring program.

Table 3 CCW pump preventive maintenance practices

PM Performed	Frequency (Months)			
	6 to 12	18 to 36	48 to 60	84 to 90
1. Lube oil system PM	4 units	2 units		
2. Bearing oil change	2 units			
3. Coupling lubrication	1 unit		1 unit	
4. Coupling alignment		1 unit		
5. Replace gaskets (EQ)				1 unit
6. Disassembly inspection			2 units	1 unit

#### CONCLUSIONS

The results of this study have shown that aging degradation leads to failures in the CCW system, which can result in an increase in system unavailability. In order to properly manage the effects of this degradation effective detection and mitigation methods are required. This study has identified various ISM&M practices which are currently used in the industry and

each practice has been reviewed to identify aging mechanisms it can potentially help to detect or mitigate.

From the study results it is seen that the currently used ISM&M practices fall into two categories; basic practices, which are typically required by codes or plant technical specifications, and supplemental practices, which are selected based on particular plant operating characteristics and environment. The basic practices alone are not comprehensive enough to control all types of aging degradation. An effective ISM&M program requires a combination of basic and supplemental practices to ensure that at least one method is in place to detect and mitigate each of the common aging mechanisms that may lead to component failure.

Table 4 CCW valve preventive maintenance practices

Preventive Maintenance	Frequency (Months)			
	3 to 12	18 to 36	40 to 43	48 to 60
1. MOV: Circuit breaker maint.	3 units			
2. MOV: Operator maintenance	2 units	3 units		
3. MOV: Operator EQ maintenance		2 units	2 units	
4. MOV: Packing replacement		1 unit		
5. MOV: Motor replacement				1 unit
6. MOV: Parts replacement			1 unit	
7. AOV: Lubrication	1 unit			
8. AOV: Packing replacement				1 unit
9. AOV: Diaphragm replacement				1 unit
10. AOV: Parts replacement			3 units	
11. MAN: Clean/lube stem	3 units			

REFERENCES

1. Higgins, J., et al., "Operating Experience and Aging Assessment of Component Cooling Water Systems in Pressurized Water Reactors," NUREG/CR-5052, July 1988.
2. Lofaro, R., et al., "Aging Assessment of Component Cooling Water Systems in Pressurized Water Reactors- Phase II," NUREG/CR-5693, To Be Published 1991.

Table 5 Recommended Basic ISM&M Practices For The CCW System and Components

Component	ISM&M Practice	Frequency	Aging Mechanism Detected/Mitigated
Pumps	Monitor Vibration	1 to 3 Months	- Wear/degradation of bearings
	Measure Developed Head	1 to 3 Months	- Wear of impeller, wear rings
	Check Lube Oil Level	Daily to Weekly	- Deterioration of oil seals
	Check for Unusual Noise	Daily to Weekly	- Distortion of internals
	Check for Excessive Leakage	Daily to Weekly	- Degradation of shaft seals - Deterioration of gaskets
	Lubricate Grease Bearings/Couplings	6 to 18 Months	- Wear of bearings/couplings
	Perform Lube Oil Analysis	1 to 6 Months	- Wear of bearings - Deterioration of oil seals
	Inspect Casing/Shaft/Internals for Cracks, Warping, Erosion, Corrosion	12 to 60 Months	- Corrosion/erosion of parts - Distortion of internals
	Check for Casing Wall Thinning	5 to 10 Years	- Wear of casing wall material
Valves	Stroke the Valve	3 to 18 Months	- Corrosion of internals - Distortion of components
	Check for Excessive Leakage/Corrosion	Daily to Weekly	- Deterioration of gaskets - Wear of packing
	Adjust Torque/Limit Switches	12 to 24 Months	- Calibration drift
	Lubricate Moving Parts	6 to 18 Months	- Wear of components
	Check for Body Wall Thinning	5 to 10 Years	- Wear of valve body wall
Heat Exchanger	Monitor Flow	Daily to Weekly	- Corrosion/fouling of internals
	Monitor Outlet Temperature	Daily to Weekly	- Fouling of tubes
	Check for Excessive Leakage/Corrosion	Daily to Weekly	- Deterioration of gaskets - Cracking/corrosion of shell
	Clean Tubes	As Needed	- Fouling of tubes
	Check for Shell/Tube Thinning	5 to 10 Years	- Wear of shell/tube wall
System	Monitor Surge Tank Level/Makeup Flow	4 to 24 Hours	- Corrosion/cracking of welds/walls - Deterioration of seals/gaskets
	Monitor Temperature at Loads	4 to 24 Hours	- Fouling of heat exchangers
	Monitor Flow to Loads	4 to 24 Hours	- Degradation of pump performance
	Check for Pipe Wall Thinning	5 to 10 Years	- Wear of pipe wall material
	Hydrostatic Test	5 to 10 Years	- Degradation of welds/walls - Deterioration of seals/gaskets

Table 6 Pump ISM&M practices versus aging mechanisms

PUMP AGING MECHANISMS													
1. WEAR OF BEARINGS/BUSHINGS	8. BINDING OF IMPELLER/SHAFT												
2. WEAR OF INTERNAL CONTACT SURFACES	9. CAVITATION DAMAGE TO IMPELLER/CASING												
3. EROSION/CORROSION OF INTERNALS													
4. VIBRATION INDUCED LOOSENING/MOVEMENT													
5. DISTORTION OF INTERNALS													
6. DETERIORATION OF PACKING/SEALS/GASKETS													
7. FATIGUE/THINNING OF CASING													
ISM&M PRACTICE	AGING MECHANISM DETECTED/MITIGATED												
	1	2	3	4	5	6	7	8	9				
BEARING TEMPERATURE MEASUREMENT	X							X					
FLOW RATE MEASUREMENT	X		X		X				X				
LUBE OIL LEVEL/PRESSURE CHECK						X							
MOTOR AMP/WINDING TEMP CHECK	X	X				X		X					
TRACK TIME AT MINIMUM FLOW		X			X								
PACKING/SEAL LEAKAGE MEASUREMENT						X							
NDE FOR CASING SHAFT CRACKS/FLAWS							X						
DISASSEMBLY INSPECTION/OVERHAUL	X	X	X		X	X	X		X				
BOLT TORQUE MEASUREMENT				X									
ROTOR TORQUE MEASUREMENT		X						X					
THERMOGRAPHY EXAMINATION	X	X						X					
CHANGE LUBE OIL	X												
REALIGN PUMP/DRIVER		X			X								
REPLACE BEARINGS	X												
RETORQUE BOLTS				X									
REWORK IMPELLER			X						X				
REPLACE GASKETS/SEALS						X							
REPLACE WEAR RINGS		X											
REPLACE SHAFT SLEEVES		X											
LUBRICATION SYSTEM PM	X												

Table 7 Valve ISM&M practices versus aging mechanisms

VALVE AGING MECHANISMS													
1. WEAR OF BEARINGS/BUSHINGS	8. DETERIORATION OF MOTOR WINDINGS (MOV)												
2. WEAR OF STEM CONTACT SURFACES	9. FATIGUE/THINNING OF CASING												
3. EROSION/CORROSION OF SEAT/DISK/INTERNALS	10. BINDING OF STEM/DISK												
4. VIBRATION INDUCED LOOSENING/MOVEMENT	11. SETPOINT DRIFT												
5. DISTORTION OF INTERNALS	12. DETERIORATION OF AIR DIAPHRAGM (AOV)												
6. DETERIORATION OF PACKING/SEALS/GASKETS	13. DEGRADATION OF ELECTRICAL CONTACTS/WIRES												
7. CALIBRATION DRIFT OF TORQUE/LIMIT SWITCHES													
ISM&M PRACTICE	AGING MECHANISM DETECTED/MITIGATED												
	1	2	3	4	5	6	7	8	9	10	11	12	13
INSPECT/CLEAN CONTACTS/WIRES													X
SEAT LEAKAGE TEST			X		X								
PRESSURE DIFFERENTIAL TEST			X							X			
STEM TORQUE MEASUREMENT					X					X			
BOLT TORQUE MEASUREMENT				X									
PACKING/SEAL LEAKAGE MEASUREMENT						X							
NDE FOR CASING CRACKS/FLAWS									X				
STEM PLAY MEASUREMENT		X											
VALVE OPERATOR ALIGNMENT CHECK				X	X								
MOTOR SIGNATURE ANALYSIS (MOV <sub>s</sub> )	X				X			X		X			
MOTOR AMP/VOLTAGE MEASUREMENT	X				X			X		X			
MOTOR MEGER/SURGE/CAPACITANCE								X					
DISASSEMBLY INSPECTION	X	X	X	X	X	X			X	X		X	X
BENCH TEST (RELIEF)											X		
REPLACE PACKING						X							
REALIGN OPERATOR				X									
COMPLETE OVERHAUL	X	X	X	X	X	X	X			X		X	X
REPLACE/REWORK SEATS		X											
REPLACE SEALS/GASKETS/PACKING						X							
RETORQUE BOLTS				X									
REPLACE DISK			X										
REPLACE TORQUE/LIMIT SWITCHES							X						
REPLACE MOTOR	X	X											
REPLACE AIR DIAPHRAGM			X										

**Table 8 Heat Exchanger ISM&M practices versus aging mechanisms**

HEAT EXCHANGER AGING MECHANISMS												
1. EROSION/CORROSION OF TUBES						8. FOULING OF TUBES						
2. DETERIORATION OF GASKETS												
3. PLUGGING OF TUBES												
4. CRACKING OF TUBES												
5. CRACKING/THINNING OF SHELL												
6. LOOSENING OF BOLTS OR INTERNALS												
7. EROSION/CORROSION OF INTERNALS												
ISM&M PRACTICE	AGING MECHANISM DETECTED/MITIGATED											
	1	2	3	4	5	6	7	8				
DISASSEMBLY INSPECTION/OVERHAUL	X	X	X	X	X	X	X	X				
EDDY CURRENT TEST				X	X							
ULTRASONIC TEST				X	X							
ACOUSTIC MEASUREMENT						X						
DYE PENETRANT TEST				X	X							
MONITOR FOR CCW CHEMICALS IN SW	X			X								
PRESSURE DROP MEASUREMENT	X		X									
HEAT BALANCE	X		X					X				
APPLY PROTECTIVE COATINGS							X					
REPLACE GASKETS/SEALS		X										
REPLACE/MONITOR SACRIFICIAL ANODES	X						X					
RETORQUE BOLTS						X						

# **The Effects of Aging on Friction of MOVs<sup>a</sup>**

**Thomas H. Hunt  
Upendra P. Sinha**

**Idaho National Engineering Laboratory  
EG&G Idaho, Inc.  
Idaho Falls, Idaho 83415**

## **ABSTRACT**

As part of the Nuclear Regulatory Commission's Nuclear Plant Aging Research Program, the Idaho National Engineering Laboratory studied aging mechanisms affecting the friction coefficients of motor-operated valves (MOV). The study reviewed current corrosion theory and MOV operating history data, observed in-service MOV conditions, and discussed valve operability failures with engineering and maintenance personnel to determine the effects of corrosion, erosion, and oxide deposition on valve sliding surface friction coefficients. This paper reports an overview of the study's methodology and results.

## **INTRODUCTION**

The ability of safety-related motor-operated valves (MOV) to operate under design basis conditions has been questioned because MOV failures have occurred at several operating facilities in recent years. As a result, the U.S. Nuclear Regulatory Commission (NRC) issued several information notices and a generic letter to address these concerns.

While working on Generic Issue 87 (GI 87) concerns for the NRC, engineers at the Idaho National Engineering Laboratory (INEL) developed a fault tree of factors that could cause high energy line MOVs at boiling water reactors (BWRs) to fail to isolate in the event of a line break. A portion of that fault tree is reproduced in Figure 1. In the shaded block, the aging mechanisms, corrosion, erosion, and deposition are identified as factors that could

---

a. Research sponsored by the Office of Nuclear Regulatory Research, U.S. Nuclear Regulatory Commission under contract DE-AC07-761D01570 with EG&G Idaho, Inc.

affect the surface condition of the valve's sliding surfaces. These changes may cause the valve's friction coefficients to increase above the value used to predict the valve's closing load. If this occurs, the predicted load will be less than the actual force required to close the valve. If the operator is undersized, the valve will not close. If the operator is adequately sized, the torque switch that limits the motor's output torque will be set too low, and the motor will trip before it enough force is generated to operate the valve to the desired position.

The force required to operate the valve under design conditions is found using an equation similar to Equation (1). This equation is typical of the equations that have been used in the past. The equation has three terms: stem packing drag, stem rejection, and disk load. The largest term is normally the disk load. This term contains the friction coefficient of concern to this study and identified in the fault tree as a potential problem.

$$F_t = F_p + A_s P + \mu_d A_d \Delta P \quad (1)$$

where

$F_t$  = total stem force required

$F_p$  = packing drag load

$A_s$  = cross-sectional area of the stem

$P$  = system pressure

$\mu_d$  = disk friction factor

$A_d$  = cross-sectional area of the disk

$\Delta P$  = differential pressure across the disk.

A typical value used for the disk friction coefficient is about 0.3, which may not be conservative enough to bound the operating force requirements at design conditions. Full-scale testing on MOVs typical of GI 87 valves done by the INEL indicates that this value is too low and may result in underpredicting the operating force requirements for the MOVs. Any increase in the actual friction coefficients will further jeopardize MOV operability in an accident scenario.

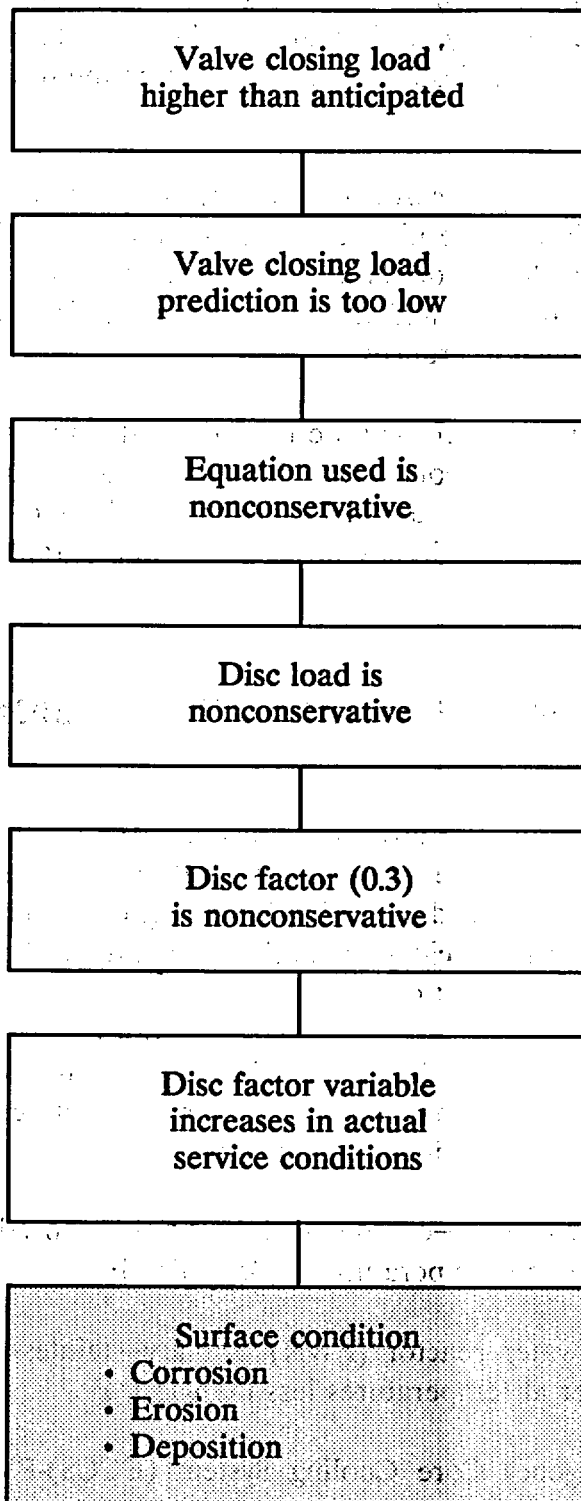


**Figure 1.** Events leading to motor-operated valve failure.  
(Source: DeWall 1987)

To evaluate aging and friction, we used a two-phased approach. First, we studied the aging mechanisms theoretically, to determine if they were likely to affect friction. Second, we reviewed MOV operating history data to determine the frequency of the failures caused by these aging mechanisms.

The theoretical review focused on the mechanisms that cause corrosion, erosion-corrosion, and deposition. We identified the rates at which these aging mechanisms are expected to occur and the factors affecting these rates. We also examined the effects of these mechanisms on friction, and the possibility of their products binding the valve by obstructing its mechanical tolerances.

For the operating history review, we used three databases as sources of MOV failure information. Interviews were conducted with MOV manufacturers and end users to obtain their experience with failures caused by the mechanisms of this study. Two operating facilities were also visited to directly observe and photograph the in-service condition of MOVs.

## **CORROSION, DEPOSITION, AND EROSION-CORROSION**

Corrosion, deposition, and erosion-corrosion can alter the surface finish of a valve's sliding surfaces. These changes may adversely affect the coefficients of friction of these surfaces and result in increased operating force requirements for the MOVs. This would be most pronounced during accident conditions when the disk is exposed to its highest flow and differential pressure conditions.

In this study, we sorted the MOV materials and the environmental conditions to which they are exposed into the following three groups, accounting for nearly all of the MOVs required to operate during accident conditions:

- BWR reactor coolant—carbon steel materials exposed to pure water or saturated steam at elevated temperatures of 450–550 °F
- Pressurized water reactor (PWR) primary—stainless steel materials exposed to borated water at temperatures less than 150 °F
- BWR Emergency Core Cooling System (ECCS)-PWR secondary—carbon steel materials exposed to pure water at temperatures of less than 150 °F.

## Corrosion

Corrosion can affect the operation of the MOVs in one of two ways. First, it attacks the metal surfaces and can roughen these surfaces. Second, the corrosion process produces an oxide film, and the oxide film's properties may affect the friction coefficient. Also, if the oxide film grows at a rapid rate, it may block the mechanical tolerances of the valve and bind the valve.

### Corrosion Rates

A variety of factors affects the rate of corrosion, including temperature, dissolved oxygen content, and coolant pH. In the three groups of conditions we evaluated (BWR reactor coolant, PWR primary, BWR ECCS-PWR secondary), the corrosion rates ranged from a low value of 0.01 mil/year to a high value of 16 mil/year. Table 1 lists these values.

The corrosion rates presented in Table 1 represent rates calculated from the mass of the oxide formed and do not represent the thickness of the oxide film produced. To determine the oxide thickness or its growth rate, another factor, the Pilling/Bedworth (P/B) ratio, is required. The P/B ratio is defined as the volume of the oxidized form of a metal divided by the volume of its unoxidized form. For the oxides produced by corrosion in commercial reactors, the P/B ratios range from about 1.5 to 2.4. These values were used to bound the oxide film growth rates, and are presented in the oxide growth rate column of Table 1. The growth rates are useful for determining whether the oxide film is likely to block the mechanical tolerances of the valve.

For most of the valves used in commercial reactor systems, the mechanical tolerances range from about 20 to 250 mils. The only condition where the annual growth rate exceeds the minimum tolerances is during BWR startup and shutdown. However, BWRs spend only a small fraction (less than 5%) of their operating time in these conditions, so it should not have a great impact on their MOVs. Also, these MOVs are cycled once per quarter in most cases, and at least once per operating cycle, to meet American Society of Mechanical Engineers (ASME) requirements. This cycling should limit the buildup on the sliding surfaces because valve operation tends to "wipe" the oxide film from these surfaces. The combination of periodic operation and the annual oxide growth rates being less than typical tolerances should ensure that oxide binding of the valves is not a significant concern.

**Table 1.** Corrosion rates of valve materials under simulated boiling water reactor and pressurized water reactor conditions.

<u>Reactor Conditions</u>	<u>Corrosion Rate (mil/yr)</u>	<u>Oxide Film Growth Rate (mil/yr)<sup>a</sup></u>
<b>BWR reactor coolant</b>		
Operating <sup>b</sup>	0.06–2.2	0.09–5.5
Startup/shutdown <sup>c</sup>	4.4–16	6.6–40
<b>PWR primary</b>		
All conditions <sup>d</sup>	0.01–0.03	0.02–0.08
<b>BWR ECCS and PWR secondary</b>		
All conditions <sup>e</sup>	0.18	0.27–0.45

- a. Oxide film growth rate is determined by using the P-B ratio in conjunction with the material's corrosion rate.
- b. Sources: Macdonald et al. 1983, Hornsveld 1968, Videm et al. 1971, Vreeland et al. 1961, Breden 1962.
- c. Source: Macdonald et al. 1983.
- d. Sources: Warzee and Sonnen 1967, Larrick and Kratzer 1972, Bloom and Demmitt 1967.
- e. Source: Westinghouse Electric Corporation 1967.

### **Types of Corrosion Products**

Several types of iron oxide compounds may form on the valve surfaces. The type that is formed is normally a function of the oxygen content of the water in the valve. When oxygen content is elevated, hematite and maghemite tend to predominate. At low oxygen contents, magnetite and iron hydroxides tend to predominate. These oxides generally form as hard and relatively adherent crystals on the surfaces, giving the surface a shiny black or brown appearance depending on the oxide that is formed. These oxides will roughen the surface. This roughening, coupled with their adherence, may contribute to increased frictional loads on the motor operator.

## **Corrosion Mechanisms**

The corrosion mechanism that is expected to occur in all reactor chemistry conditions produces a two-layer oxide film. The significance of the two-layer film is that as it forms, it creates a protective barrier against further corrosion, causing corrosion rates to decrease with respect to time.

Another time-dependent mechanism occurs that tends to moderate the growth of the oxide layer. The oxide layer can dissolve in the aqueous solution surrounding it. One study showed that after 1,000 hours of exposure to 550°F pure water, 12% of the oxides on stainless steel and 1% of those on carbon steel dissolved. (Honda et al. 1987) The combination of corrosion rates decreasing with time and oxides dissolving should tend to mitigate the effects of corrosion induced oxide film growth.

The effects of corrosion are expected to have a detrimental effect on the friction coefficients of MOVs. It will roughen the surface by creating hard and adherent oxides, and attack the base metal, degrading its surface finish. Corrosion is not expected to create enough oxides to pose a significant threat to MOV operability by binding the valve. Its oxide growth rate is less than the typical mechanical tolerances of the valves used in the industry. Also, the oxide layer growth should be mitigated by the protective two-layer oxide film and the dissolution of the oxides.

## **Corrosion Product Deposition**

Deposition on valve surfaces typically occurs where changes in fluid hydrodynamics, fluid temperature, or the redox potential occur. These deposits can adversely affect valve performance by fouling the sliding surfaces causing increased friction and possibly obstructing operation of sliding surfaces. Deposition could be a greater problem than corrosion induced oxide film growth for three reasons: (a) large amounts of oxides can be deposited in short time periods, (b) the oxides can be very adherent and crystalline in nature, and (c) localized thick oxide deposits can be produced.

### **Deposition Rates**

Existing information is incomplete about the nature and rate of deposition on valve materials for the environmental conditions of PWRs and BWRs. Most of this information addresses deposition on fuel elements or activation product transfer, and neglects iron oxide deposition on materials used in valves. For these types of conditions, the highest reported

rate of deposition was about 0.1 mil/year. This value is an order of magnitude less than the expected rates for corrosion in BWR conditions reported in the previous section of this paper. However, since deposition occurs in more localized areas than corrosion, lower rates may produce thicker localized deposits than corrosion. Because of this, the effect of these deposits on the binding of valves is not clear.

### **Deposition Mechanisms and Deposit Characteristics**

There are two ways deposition occurs on valve surfaces. The first involves the crystallization of materials in solution on the surfaces. Depending on the oxide that is crystallized, these deposits can be hard and highly adherent to the surface, which would roughen the surfaces where the deposits form.

The second way involves the adhesion of suspended particles on the valve's surfaces. These deposits tend to be porous and weakly adherent. Although this mechanism results in a weakly bound deposit, if it is left undisturbed, it can be converted to a harder, more adherent deposit by recrystallization and Ostwald ripening.

In BWR conditions, magnetite and maghemite would be expected to deposit. These are hard, crystalline, and highly adherent deposits. In the PWR primary and BWR ECCS-PWR secondary conditions, a softer deposit of iron hydroxide and iron hydroxyl-oxide should predominate. The harder deposits are expected to increase the friction coefficients of the valve. The effect of the softer deposits on friction is uncertain.

### **Erosion-Corrosion**

Erosion-corrosion is an accelerated corrosion process induced by fluid flow breaking down the protective oxide layer on the metal's surface. As the oxide layer erodes, new metal is exposed and subsequently corrodes. The highest erosion-corrosion rates occur in wet steam environments (40 to 80% quality) and at temperatures around 300°F. The only safety-related valves exposed to these conditions are the steam line valves for BWR high-pressure injection systems and steam line valves for PWR auxiliary feedwater systems. None of the valves in these systems are normally exposed to these conditions for extended periods of time, however. Also, the only sliding surfaces exposed to these conditions are the valve seats. These are usually hard-faced with Stellite, which is not very susceptible to erosion-corrosion. Because of these factors, erosion-corrosion is not expected to significantly affect the friction coefficients of MOVs.

## **Corrosion Review Summary**

Corrosion of and deposition on valve sliding surfaces should degrade their surface finish and produce an oxide layer on them. Since the friction coefficient is dependent on surface finish, the extent of the surface finish change will determine the change in friction. The influence of the oxide layer on the friction coefficient may also increase friction depending on the type of oxide formed. These two effects are expected to cause increases in friction, and consequently increased operating force requirements for the valve.

## **OPERATING EXPERIENCE REVIEW**

We reviewed the operating history of MOVs to identify the extent of problems being experienced as a result of the three aging mechanisms of this study. This information was obtained from three sources:

- Operating history databases
- Interviews with industry personnel with MOV operations and maintenance experience
- Direct observation of the in-service condition of MOVs.

### **Operating History Databases**

To identify MOV failures that have occurred in recent years, we surveyed three databases: NRC's Licensee Event Reports (LERs), the Institute of Nuclear Power Operations' Nuclear Plant Reliability Data System (NPRDS), and Stoller Engineering's Nuclear Plant Experience (NPE). The failure records were reviewed and filtered to eliminate those not caused by problems associated with valve internals. Of the failure records eliminated in this process, the largest group (more than 50%) were external leakage events that were caused mostly by stem packing seal failures. Other failures that were eliminated included events such as electrical or mechanical failures of the motor operators and human-related failures. The resulting data sets represented failures of MOVs that were the result of some malfunction of a component internal to the valve. This set contains those failures that result from aging of the sliding surfaces of this study.

The data review showed that only corrosion was specifically identified in each of the databases. Deposition failures were contained in related causes such as particulate

contamination and foreign material. Erosion-corrosion failures were in causes such as normal/abnormal wear and seat damage. To standardize the data between the sources, we evaluated and grouped the failures into five categories: erosion-related, corrosion-related, deposition-related, increased operating force-related, and other failures. The cause categories identified in each of these groupings are presented in Table 2.

**Table 2.** Failure causes identified for each of the databases reviewed.

<u>Failure Cause</u>	<u>Failure to Close</u>	<u>Failure to Open</u>	<u>Failure to Operate</u>
<b>Erosion categories</b>			
Normal/abnormal wear	X	X	X
Seat damage	X		
<b>Deposition categories</b>			
Dirty	X	X	X
Particulate contamination	X	X	X
Foreign material	X		
<b>Corrosion category</b>			
Corrosion	X	X	
<b>Increased operating force categories</b>			
Binding	X	X	X
Torque switch	X		
Lubrication	X	X	X
<b>Other categories</b>			
Excessive stress		X	X
Mechanical adjustment	X	X	X
Mechanical damage	X	X	X
Aging/cyclic fatigue	X	X	X
Wrong part		X	X
Prior repair			X
Unidentified	X	X	X

After the grouping was done, we then narrowed the data sets to evaluate those failures that would be indicative of events where the motor operator did not develop sufficient force to operate the valve. These were the failure to function mode events consisting of failure to open, failure to close, or failure to operate events. The failure to operate category included instances such as a failure of a Generic Letter 89-10 diagnostic or a stroke time

test. While these latter failures are not gross failures, we do feel they indicate an incipient failure if the MOV experiences the increased stress of accident conditions and is thus included in this data set.

### Licensee Event Report Failure Data

The INEL had an existing database of LERs for MOV failures that contained about 1,100 valve failures reported between January 1980 and June 1989. The initial filtering reduced the number of failure events to 423 valve failures. Internal leakage accounted for 377 of these failures. Failure to function mode failures were identified in 36 of the events. Pressure boundary corrosion or unidentified failure modes accounted for the remaining records.

Table 3 presents the failure cause distribution of the failure to function mode failures showing the raw number of events classified in these failure modes. These records were then reviewed to identify the events caused by this study's aging mechanisms. Table 4 presents the results of this review.

**Table 3. LER failure cause distribution for failure to function mode failures.**

<u>Failure Cause</u>	<u>Failure to Close</u>	<u>Failure to Open</u>	<u>Failure to Operate</u>	<u>Total</u>
<b>Deposition group</b>				
Foreign material	1			1
<b>Corrosion group</b>				
Corrosion	1			1
<b>Increased operating force group</b>				
Torque switch	5			5
Binding	21	2	2	25
<b>Other failures</b>				
Unidentified		2	2	4

**Table 4.** LER MOV failure events directly caused by corrosion, deposition, and erosion-corrosion for the failure to function mode failures.

<u>Failure Group</u>	<u>Number of Failures</u>
Deposition group	1
Corrosion group	1
Increased operating force group	19
Other failures	0

Nineteen failure records in the increased operating force group were related to one of the mechanisms of this study. Corrosion and deposition were specifically identified in one event each. In all, 21 failures (about 5% of the failures caused by an internal component problem) were related to one or more of the aging mechanisms of this study.

#### **Nuclear Plant Reliability Data System Failure Data**

Of the three data sources, NPRDS provided the greatest detail regarding the root causes of the failures. Not only does it allow the member utilities to report the primary cause of the failure, but there is provision to include an additional two contributing causes. This feature helped us identify events where the aging mechanisms contributed to events such as binding of the valve. About 760 failure records, reported between January 1988 and January 1990, were initially retrieved. The initial review and culling reduced this number to 309 records. Internal leakage was the predominant failure mode with 177 of these records. Failure to function accounted for 131 records. There was also a single event caused by flow blockage in this set.

Table 5 presents the failure cause distribution of the failure to function mode failures. It shows the raw number of failure events that were coded as failure to function mode failures. We reviewed each failure to function mode record to determine the number of failures that were directly attributable to the three aging mechanisms of this study. Table 6 presents the results of this review, detailing the failures attributable to each of the five groups of failure causes.

No records conclusively identified corrosion as the primary cause of a failure from some form of frictional increase. Two records were coded with corrosion as the primary cause of the valve failing to close. However, their event narratives made it unclear whether the event was caused by corrosion of the valve, or if some corrosion-related debris had

**Table 5. NPRDS failure to function modes failure cause distribution.**

<u>Failure Cause</u>	<u>Failure to Close</u>	<u>Failure to Open</u>	<u>Failure to Operate</u>	<u>Total</u>
<b>Erosion group</b>				
Normal or abnormal wear	5	1	13	19
<b>Deposition group</b>				
Dirty	1	5	1	7
Particulate contamination	7	1	2	10
<b>Corrosion group</b>				
Corrosion	2	0	0	2
<b>Increased operating force group</b>				
Binding <sup>a</sup>	10	25	16	51
Lubrication	2	7	6	15
<b>Other failures</b>				
Abnormal stress	0	3	0	3
Aging/cyclic fatigue	1	0	1	2
Out of mechanical adjustment	2	3	1	6
Mechanical damage <sup>a</sup>	1	1	6	8
Previous repair/installation status	2	0	0	2
Incorrect part	0	1	3	4

a. We reviewed the NPRDS category of mechanical damage/binding to identify the binding events.

obstructed the seating area preventing full valve closure. Corrosion was indicated as a contributing factor in six of the increased operating force category events.

Deposition caused six of the failures. In each of these failure narratives, specific mention was made that deposits on one or more sliding surfaces contributed to the failure.

**Table 6.** NPRDS failure events directly caused by corrosion, deposition, or erosion-corrosion for failure to function mode failures.

<u>Failure Group</u>	<u>Number of Failures</u>
Corrosion Group	0 <sup>a</sup>
Deposition group	6
Erosion group	0 <sup>b</sup>
Increased operating force group	19
Other failures	0

a. Corrosion was identified as a contributing factor in 6 of the increased operating force events.

b. Four events identified disk-guide binding without identifying the cause of the binding.

Erosion-corrosion did not cause any failure to function events. There were four events that identified the cause of their failures as binding between the disk and the valve body's guides. However, the narrative did not provide enough information to determine if these events were caused by normal wear or erosion-corrosion.

The increased operating force group contained the most failures. This grouping included the causes of binding and lubrication. In most cases, the records were either inconclusive regarding the relation to these aging mechanisms or specified a non-related cause. However, nineteen events coded corrosion or deposition as contributing secondary or tertiary causes or inferred their contribution to the event in the narrative.

In all, NPRDS revealed 25 events (8.1% of all failures caused by an internal component problem) that were likely to be caused by the aging mechanisms of this study.

### **Nuclear Plant Experience Failure Data**

The NPE database provided 228 records identifying MOV failures reported between January 1988 and January 1990. Frequently, the NPE records contained multiple failures in each record, so after the initial elimination of unrelated failure records, 62 records remained identifying 206 valve failures. There were 167 internal leakage events, 37 failure to function events, and two flow blockage events.

Table 7 presents the failure cause distribution for the failure to function mode events. It shows the raw number of failures for these failure modes. This data set was then

reviewed to identify the failures caused by corrosion, deposition, and erosion-corrosion. Table 8 presents the results of that review.

**Table 7. NPE failure cause distribution for failure to function mode failures.**

<u>Failure Cause</u>	<u>Failure to Close</u>	<u>Failure to Open</u>	<u>Failure to Operate</u>	<u>Total</u>
Erosion group				
Normal or abnormal wear			1	1
Seat damage	1			1
Corrosion group				
Corrosion		1	1	2
Increased operating force group				
Binding	1	10		11
Torque switch	3			3
Other failure causes				
Aging/cyclic fatigue		3		3
Mechanical damage	1			1
Unidentifiable	2	5		7

**Table 8. NPE MOV failure events directly caused by corrosion, deposition, or erosion-corrosion for failure to function mode failures.**

<u>Failure Group</u>	<u>Number of Failures</u>
Erosion group	0
Deposition group	0
Corrosion group	1
Increased operating force group	7
Other failures	0

Like the NPRDS and LER data, the increased operating force group contained the greatest number of related failures. Seven of the events in this group were caused by one of the three mechanisms. The corrosion group contained the only other failure related to

this study. Neither the erosion-corrosion or deposition groups contained any related failures in this instance. In all, the NPE data had eight related failures accounting for about 4% of the 206 failures associated with an internal component problem.

## **Operating Experience Summary**

From 4% to 8% of valve failures caused by problems with internal components of the valve were caused by corrosion, deposition, or erosion-corrosion. Although these percentages are low, they may be significantly higher if the valves were tested or operated more frequently at or near design conditions because increases in friction at low loads are not expected to challenge the motor-operator's capability.

## **In-Plant Observations**

We visited two operating facilities, one PWR and one BWR, to obtain first-hand information about the in-service condition of MOVs. We either directly observed and photographed, or obtained copies of existing photographs from 16 MOVs (12 of carbon steel and four of stainless steel construction).

The observations and photographs agreed with the appearance of the oxide layer for the carbon steel valves as predicted by the corrosion study. The carbon steel valves exposed to relatively high oxygen concentrations and low temperatures tended to have brown to rusty colored deposits typical of the hematite oxides and iron hydroxides the study predicted should be present. Those exposed to higher temperatures and lower oxygen concentrations had a darker brown to black oxide layer typical of the magnetite and maghemite also predicted. The stainless steel valves showed little evidence of oxide buildup, which agreed with the low rates of corrosion predicted for these valves.

Although the observations could not characterize the surface conditions of the valves in detail, certain conditions were obvious from the observations. The three stainless steel valves observed at the PWR showed no obvious indications of surface oxidation or roughening although they had been in service for more than ten years and had not been serviced for more than 18 months. In fact, one of the valve disks still showed the traces of the bluing dye used in the leak check performed 18 months earlier. All of the carbon steel valves had obvious oxidation and an apparent rough surface from the oxide layer. Another feature that appeared in several of the carbon steel valves was an apparent "wiping" of the oxide layer from the surfaces that contact each other during valve operation. This included the valve guides in the valve body and the seating surface on one of the valve disks. This supports the ASME surveillance requirement to periodically stroke test those valves with

safety functions, as it appears to reduce the likelihood of obstructing mechanical tolerances by oxide layer growth. Although this "wiping" removed some of the oxide layer, its effect on the surface finish was indeterminate from the photographs.

## CONCLUSIONS

The review of existing corrosion theory and operating experience led us to the following conclusions:

- Obstruction of the mechanical tolerances of the valve is not expected to be a significant problem as a result of corrosion and deposition fouling of valve surfaces. The expected annual rates of oxide formation on the surfaces are much smaller than the typical mechanical tolerances of the valves. Also, the normal surveillance practice of periodically operating valves with safety significance should limit the gross accumulation of oxide material on their sliding surfaces.
- It is likely that the corrosion and deposition mechanisms will result in increases in the coefficients of friction of the valve's sliding surfaces. Both of these mechanisms can produce degraded, roughened surface finishes, which would increase friction. Also, the hard, crystalline deposits and corrosion products on the surfaces may increase the friction coefficients.
- Further study to quantify the effects of deposits and corrosion products on the friction coefficients of MOV materials is needed. Studies currently are in progress at the INEL to provide the initial answers to this question.
- Increases in the failure rates of MOVs at design conditions as a result of corrosion, deposition, and erosion-corrosion induced frictional increases cannot be ruled out. The occurrence of these types of failures during operation under low-stress conditions supports the premise that increases may occur since the total load increase on the motor operator will be much higher under high-stress accident conditions.

## REFERENCES

- Bloom, G. R., and T. F. Demmitt, 1967, *Corrosion and Boron Deposition in Boric Acid Solutions*, USAEC Report BNWL-520, December.
- Breden, C. R., 1962, *Boiling Water Reactor Technology Status of the Art Report, Volume II Water Chemistry and Corrosion*, USAEC Report BNWL-520, December.
- DeWall, K.G., 1987, *Generic Issue 87 Research Plan*, EGG-REQ-7676, July.
- Honda, T., et al., 1987, "Corrosion of Ferrous Materials and Deposition of Trace Metal Ions at High Temperature and in Ultra-pure Water," *Corrosion Engineering*, 36, 5, p. 257.
- Hornsveld, E. M., 1968, *Corrosion of Carbon Steel*, Institute for Atomenergi Kjeller Research Establishment, KR-127, May.
- Larrick, A. P., and W. K. Kratzer, 1972, *Corrosion Monitoring in N-Reactor*, USAEC Report DUN-5A-194.
- MacDonald, D. D., et al., 1983, *The General and Localized Corrosion of Carbon and Low-Alloy Steels in Oxygenated High-Temperature Water*, EPRI NP-2853, February.
- Videm, K. L., Lunde S. Ans, and K. Fjellestad, 1971, *Mild Steel in the Primary Circuit of Water Cooled Reactors*, Institute for Atomenergi, HPR-143, September.
- Vreeland, D. C., G. G. Gaul, and W. L. Pearl, 1961, "Corrosion of Carbon and Low-Alloy Steels in Out-of-Pile Boiling Water Reactor Environment," *Corrosion*, 17, 6, June, pp. 269t-276t.
- Warzee, M., and C. Sonnen, 1967, *Corrosion of Carbon Steels and Stainless Steels in Pressurized Water at High-Temperature*, EURAEC Report-1896, July.
- Westinghouse Electric Corporation, 1967, *Absorption of Corrosion Hydrogen by A302B Steel at 70 to 500° F*, USAEC Report WCAP-7099, December 1.

**NRC TEST RESULTS AND OPERATIONS EXPERIENCE  
PROVIDE INSIGHTS FOR A  
NEW GATE VALVE STEM FORCE CORRELATION\***

J. C. Watkins, R. Steele, K. G. DeWall

Idaho National Engineering Laboratory  
EG&G Idaho, Inc.  
Idaho Falls, Idaho 83415

**ABSTRACT**

The Idaho National Engineering Laboratory (INEL) is performing motor-operated valve (MOV) research in support of the U.S. Nuclear Regulatory Commission's (NRC's) efforts regarding Generic Issue 87, "Failure of HPCI [High-Pressure Coolant Injection] Steam Line Without Isolation," and Generic Letter 89-10 (GL-89-10), "Safety-Related Motor-Operated Valve Testing and Surveillance." This paper presents the results of testing to assess valve and motor operator performance under varying pressure and fluid conditions. This effort included an examination of the methods used by the industry to predict the required stem force of a valve, and research to provide guidelines for the extrapolation of in situ test results to design basis conditions.

This research has identified several inconsistencies with the existing industry gate valve stem force equation and has challenged the overly simplistic assumptions inherent in its use. This paper discusses the development of the INEL correlation to bound the stem force necessary to close flexwedge gate valves whose operational characteristics have been shown to be predictable. The authors also present a method whereby the results of testing such valves at low differential pressure can be used to bound valve response at conditions up to their design basis.

---

a. Work supported by the U.S. Nuclear Regulatory Commission, Office of Nuclear Regulatory Research, Division of Engineering and Division of Safety Issues Resolution, under DOE Contract No. DE-AC07-76ID01570; G. H. Weidenhamer and O. O. Rothberg, Technical Monitors.

## INTRODUCTION

Flexwedge gate valves were tested in two U.S. Nuclear Regulatory Commission (NRC) test programs and reported in NUREG/CR-5406 (DeWall and Steele, 1989) and NUREG/CR-5558 (Steele et al., 1990). Both reports were published in support of Generic Issue 87. After the latter report was published, we developed a technique to (a) bound the stem force of a five-degree flexwedge gate valve closing against medium to high flow conditions and (b) validate a low differential pressure closure test and then bound the stem force of a flexwedge gate valve closing against design basis conditions.

In the two test programs mentioned above, six valves with a total of seven different internal designs were tested. The valves were subjected to a broad range of fluid conditions and flow rates, from normal system flows to design basis line break flows. Two of the valves, including the valve that was tested with two discs, performed in a manner we have called predictable. A predictable valve is one that does not exhibit evidence of internal damage during testing. In such valves, the highest stem forces occur when the disc is riding on the valve body seats just before wedging. Conversely, an unpredictable valve exhibits evidence of internal valve damage during testing, characterized by an erratic, sawtooth shaped stem force response. In these valves, the highest stem force requirements typically occur while the disc is riding on the guides rather than just before wedging.

The test results were initially evaluated with the standard industry gate valve stem force equation. Although some of the manufacturers modify the variables in this equation slightly, the application of the equation is basically the same.

$$F_t = \mu_d A_d \Delta P \pm A_s P + F_p \quad (1)$$

where

- $F_t$  = stem force
- $\mu_d$  = disc factor
- $A_d$  = disc area
- $\Delta P$  = differential pressure across the valve
- $A_s$  = area of the stem
- $P$  = pressure upstream of the valve
- $F_p$  = packing drag force.

For wedge-type gate valves, the industry has normally used a disc factor of 0.3, although they sometimes specify a more conservative disc factor of 0.5. The disc factor acts in conjunction with the disc area and the differential pressure, and the three multiplied together represents the largest component in the stem force equation. However, the disc area term is not used uniformly throughout the industry. This term is based on the orifice diameter by some manufacturers, on the mean seat diameter by others, or even on the orifice diameter times one or

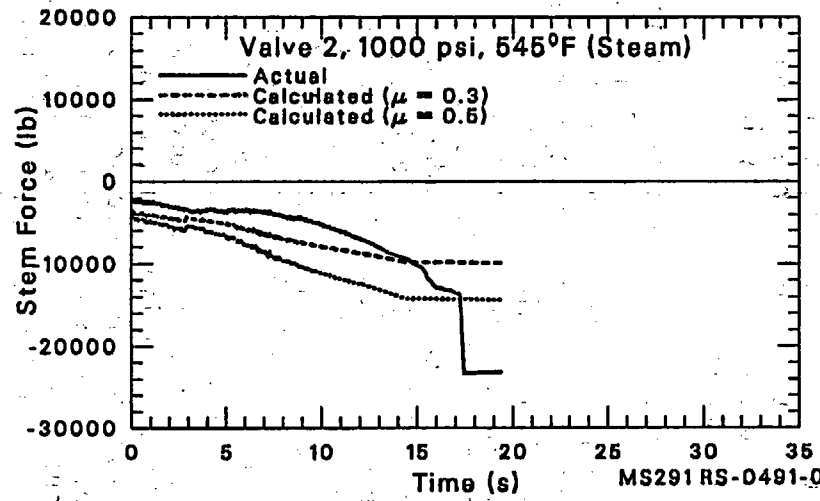
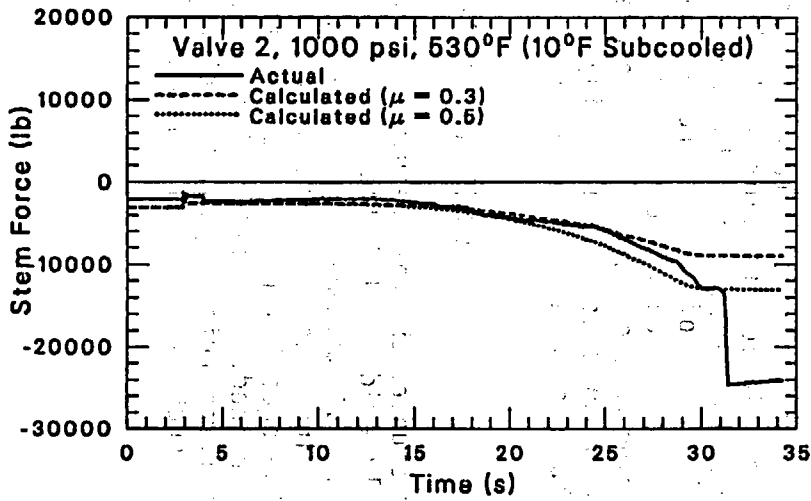
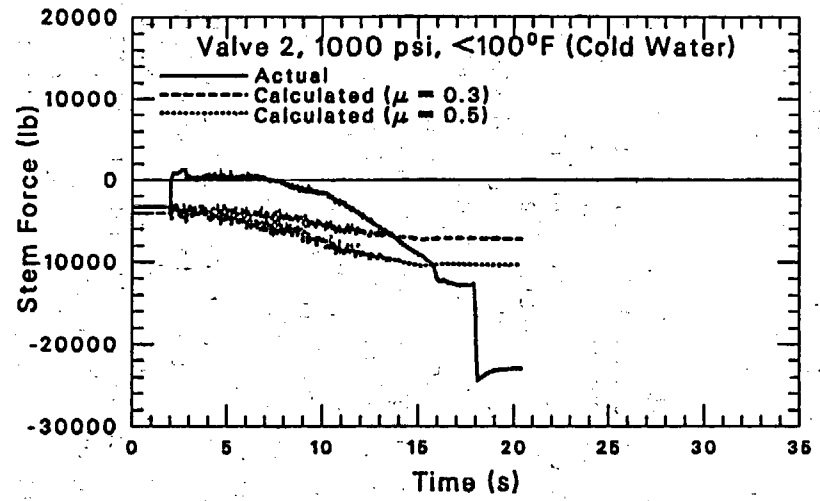
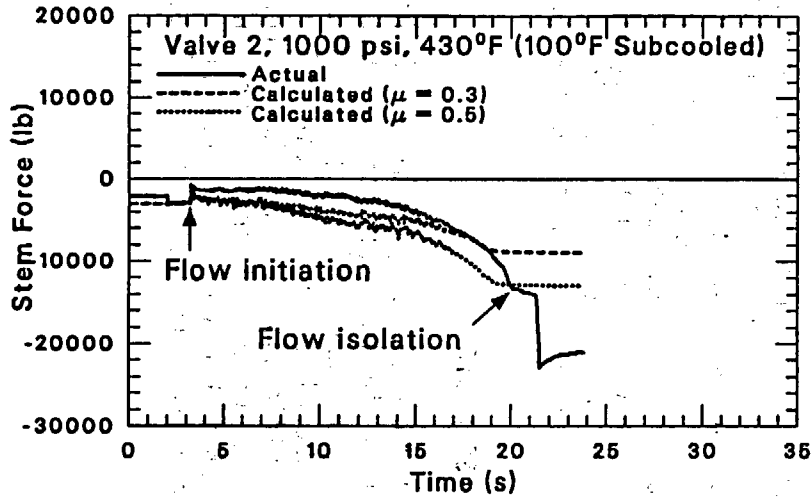
more factors to artificially enlarge the area on which the differential pressure acts. We used a disc area based on the orifice diameter when we evaluated the standard industry stem force equation because it represents the least conservative use of the term by industry. This results in a lower estimate of required stem force.

Comparisons of the industry equation, Equation (1), with selected test results are shown in Figure 1. This figure presents the results of the same valve isolating a break at a common upstream pressure of approximately 1000 psig, but with the fluid at various degrees of subcooling. The subcooling ranges from none (steam) to approximately 400°F (cold water) with intermediate values of 10°F and 100°F. The recorded stem force is shown as a solid line; the dashed lines show two calculations of the stem force history using the industry equation and real time test data with standard industry disc factors of 0.3 and 0.5. This figure shows that at flow isolation, each test required more force to close the valve than would be estimated using the standard industry disc factor of 0.3. In fact, for the tests shown on this figure, the more conservative industry disc factor of 0.5 ranges from acceptable (the steam test) to marginally acceptable (the 10°F subcooled fluid test) to unacceptable (the 100°F and the 400°F subcooled fluid tests). Note that although the results of the industry equation are presented over the entire closure cycle, the equation represents a bounding estimate of the maximum stem force. As such, only the estimated stem force at the final horizontal line, just before wedging, is applicable. The results are presented for the entire closure to aid in identifying trends in the recorded stem force, not to assess the equation throughout the closure cycle. Note also that although the same valve and operator were used for each test, the closure durations are different. Due to facility limitations, some of the tests were initiated with the valve partially closed.

It is also interesting to note that the shape of the recorded stem force from flow initiation to flow isolation varies depending on the degree of subcooling of the fluid. In tests with greater subcooling, the stem force during the initial portion of the closure is lower. In fact, during the test with cold water, the stem force trace was initially positive (i.e., the valve was self closing during this portion of the closure). However, just prior to wedging, the required stem force is generally higher in tests with greater subcooling of the fluid so that closure against cold water requires more force than closure against steam.

#### ASSESSMENT OF THE DISC FACTOR

As we studied the test results and analyzed the industry equation, it became increasingly evident that the disc factor used in the equation was not well understood. It appeared that the disc factor depended on parameters not currently being accounted for, such as the subcooling of the fluid. Thus, we examined the equation in more detail, and specifically the disc factor term as currently defined. To perform this evaluation, we used both the baseline and applicable parametric testing to determine what influence pressure and fluid properties, such as subcooling, had on the required stem force of a valve.



MS291 RS-0491-04

Figure 1. Comparison of the standard industry gate valve stem force equation with selected test results.

If all of the parametric studies could have resulted in just one parameter being varied, then the tests could have been compared to each other to determine the effect of that one parameter (e.g., fluid properties). That was not the case, however. It was impossible to provide such precise temperature and pressure control at the valve. This, along with other facility limitations, such as the total system supply volume, resulted in tests that cannot be compared to one another without some type of normalization.

We normalized the test results using Equation (1) by solving for the disc factor. This was possible because the stem force, the system pressure, and the valve differential pressure throughout the closure cycle were known. The results of a typical comparison are shown in Figure 2. The plot is read from right to left as the valve closes. As time increases, the disc factor increases in the negative convention (indicating valve closure) and is plotted against stem position. The zero stem position represents that point in the valve closure where the horizontal visual area is blocked so that you could not see down the pipe. Remember, however, that although the visual area is blocked, fluid can still flow under the disc and through the valve. At this point, the disc area term in Equation (1) becomes constant. The differential pressure term is also near its maximum during this portion of the valve closure. From the zero stem position to the minus 10% stem position, the stem travel involves seating and finally wedging. There are no terms in the industry equation to represent the increased resistance before wedging. The figure also indicates that the disc factor is influenced by fluid properties, steam being the best performer with the lowest disc factor and cold water the worst with the highest disc factor. This fluid properties effect is evident not only at the zero stem position, but from the minus 5% to the minus 10% stem position, when the disc is riding on the seats just before wedging. This effect is contrary to what was expected; one would expect water to be a better lubricant than steam.

Our next effort was to determine if the disc factor was dependent on pressure. Figure 3 shows a comparison for using three parametric tests where the fluid properties remained constant but the pressure was varied. Although the disc factor did not exhibit a significant pressure dependency at the zero stem position, it did from the minus 5% to the minus 10% stem position when the disc was riding on the seats just before wedging. The figure also indicates that the disc factor was lowest during the 1400 psig test and highest during the 600 psig test. This, too, is contrary to what was expected; one would expect a lightly loaded disc to have a thicker lubrication film and thus a lower coefficient of friction than a heavily loaded disc.

Figure 4 depicts the effect of pressure in the opening direction, further highlighting inconsistencies with Equation (1). This plot is read from left to right as the valve opens. Although the disc factor (a positive value because the valve is opening) did not exhibit a pressure dependency at the zero stem position, it did from the minus 5% to the minus 10% stem position. This trend is similar to what was observed in the closing direction. The figure also reaffirms our previous observations that the disc factor is lower during a high-pressure test and higher during a low-pressure test. The opening disc factor is also observed to be higher than the closing disc factor at its peak, non-wedging value.

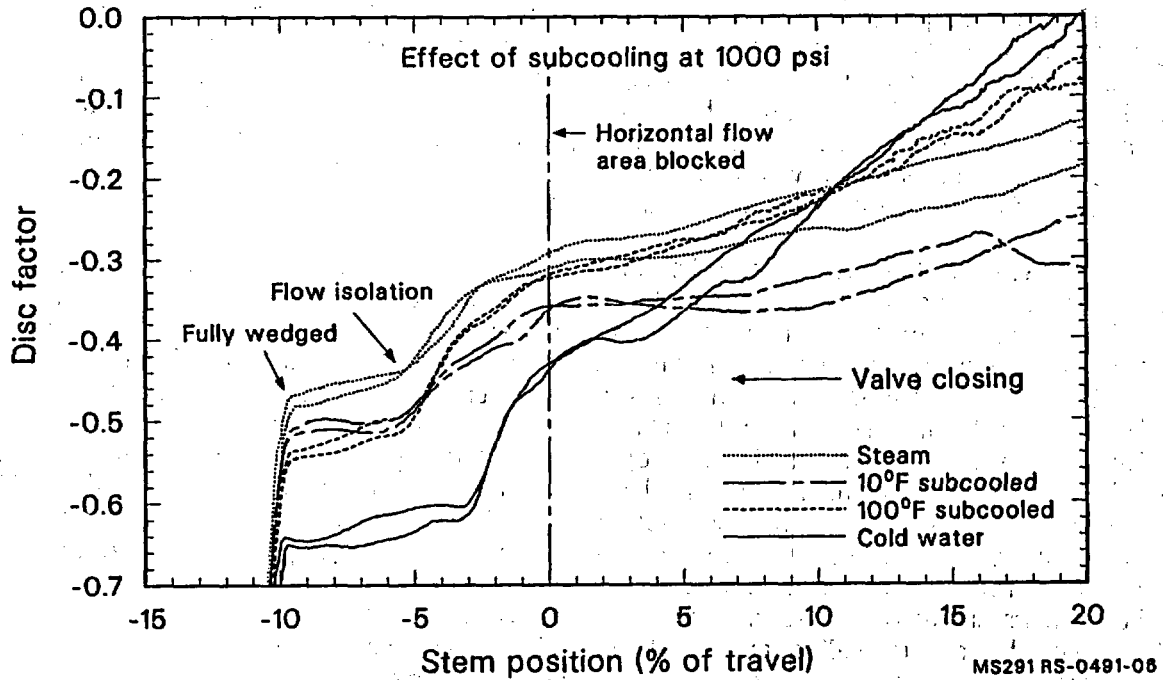


Figure 2. Disc factor for Gate Valve 2 closing on line break flow, effect of subcooling at 1000 psig.

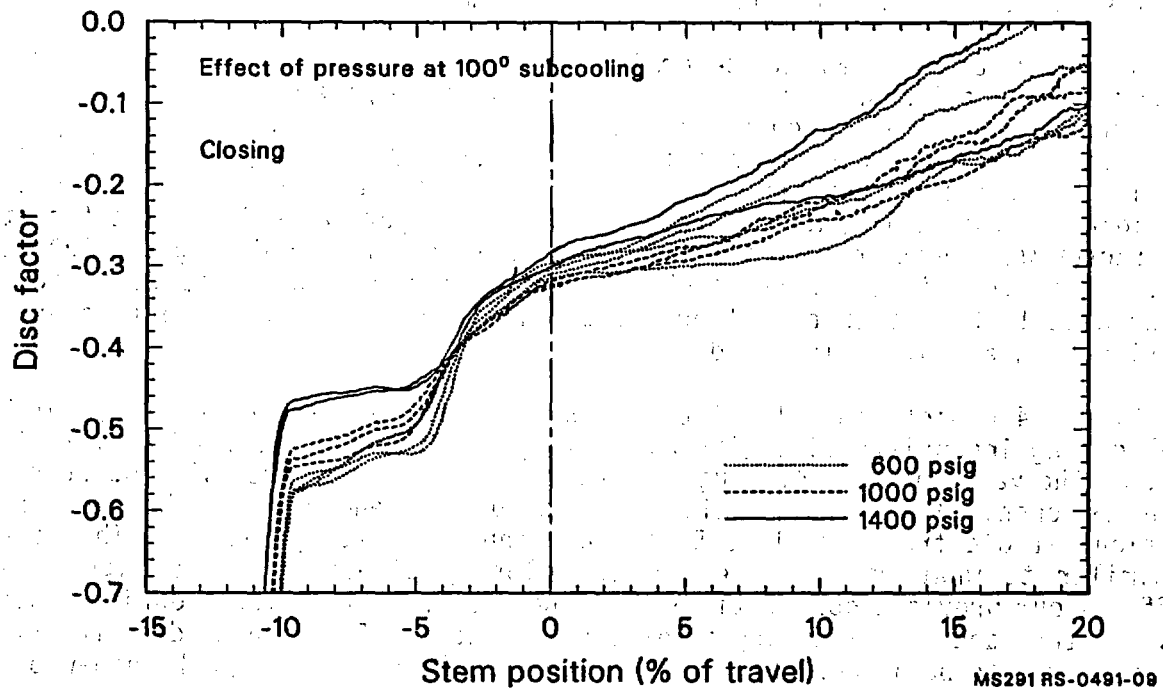
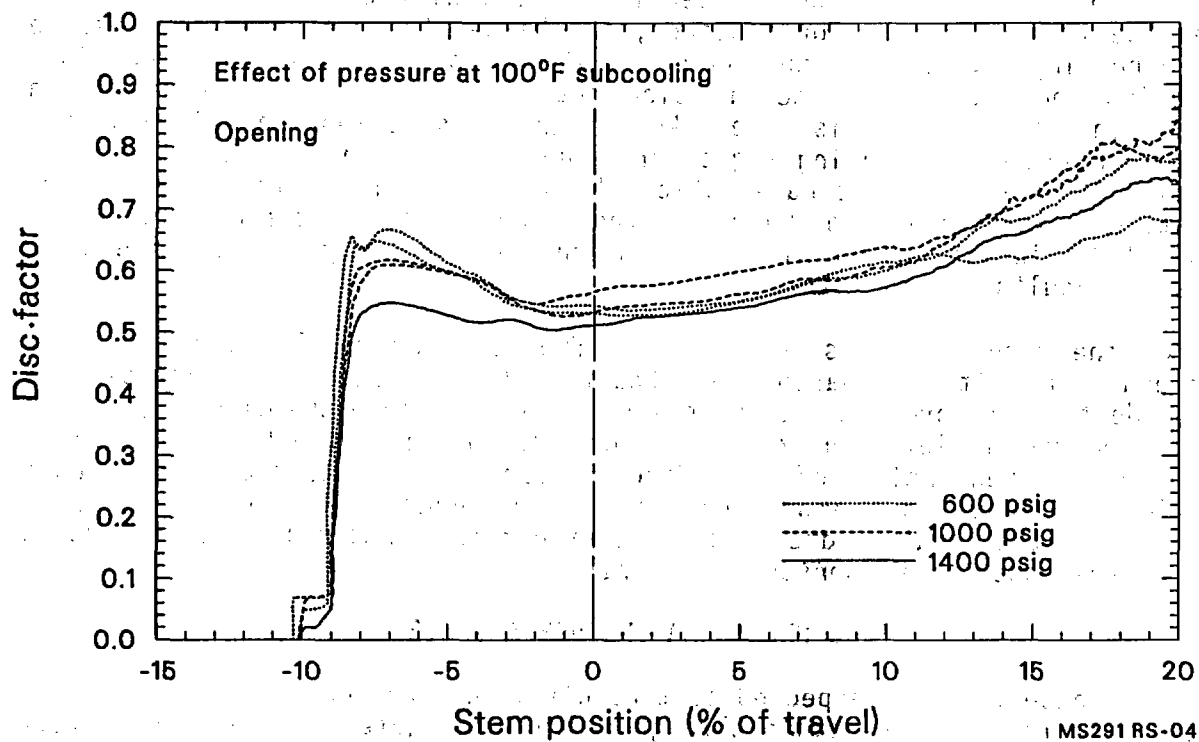


Figure 3. Disc factor for Gate Valve 2 closing on line break flow, effect of pressure at 100°F subcooling.



MS291 RS-0491-10

Figure 4. Disc factor for Gate Valve 2 opening on line break flow, effect of pressure at 100°F subcooling.

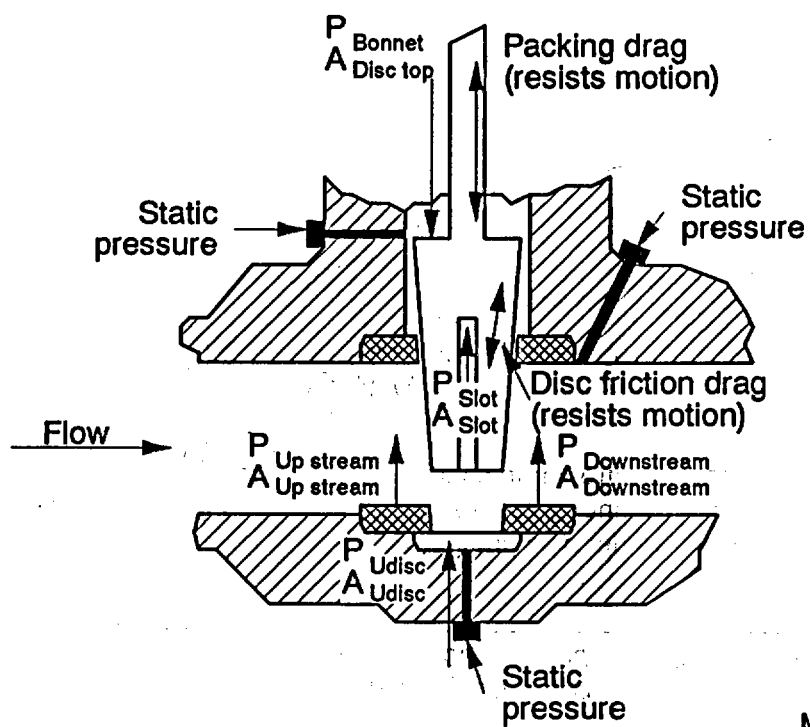
The previously unaccounted influence of fluid subcooling and pressure on the disc factor is very evident. This influence is also contrary to what one might expect in terms of the effectiveness of a lubricant. However, what was expected is based on a lubrication that separates the load bearing surfaces with a relatively thick film of lubricant to minimize metal-to-metal contact. This type of lubrication is known as thick film lubrication. In the event the load bearing surfaces are not separated by a film of lubrication, metal-to-metal contact can occur. This condition is known as thin film lubrication. The deficiencies of this type of lubrication are aggravated by surface areas that are too small to carry the maximum load, a load that exceeds the maximum expected or design basis load, or a decrease in the velocity between the moving surfaces.

When metal-to-metal contact exists, any condition that increases the ability of the lubricant to penetrate the bearing region will decrease the friction between the two surfaces. For instance, the higher the differential pressure across a bearing region, the more likely a given lubricant will be forced into this region and thus lower the friction between the surfaces. Likewise, a lubricant in a vapor state is more likely than the same lubricant in a liquid state to penetrate the bearing region and thus lower the friction between the surfaces. Other researchers have noticed these same phenomenon; however, they attribute this sensitivity to changes in the temperature of the fluid and metal. We are still investigating this phenomenon, and we hope to provide more conclusive results in the future.

From the results discussed above and from similar results for the other valves evaluated, it is apparent that Equation (1) is incomplete and does not totally identify and predict the increasing stem force once the disc is past the horizontal visual isolation or zero position. In addition, the fluid subcooling and pressure dependencies of the disc factor are inconsistent with past assumptions inherent in the application of the industry equation. Thus, we concluded that the equation does not consider parameters that have an important effect on the observed responses of the valves.

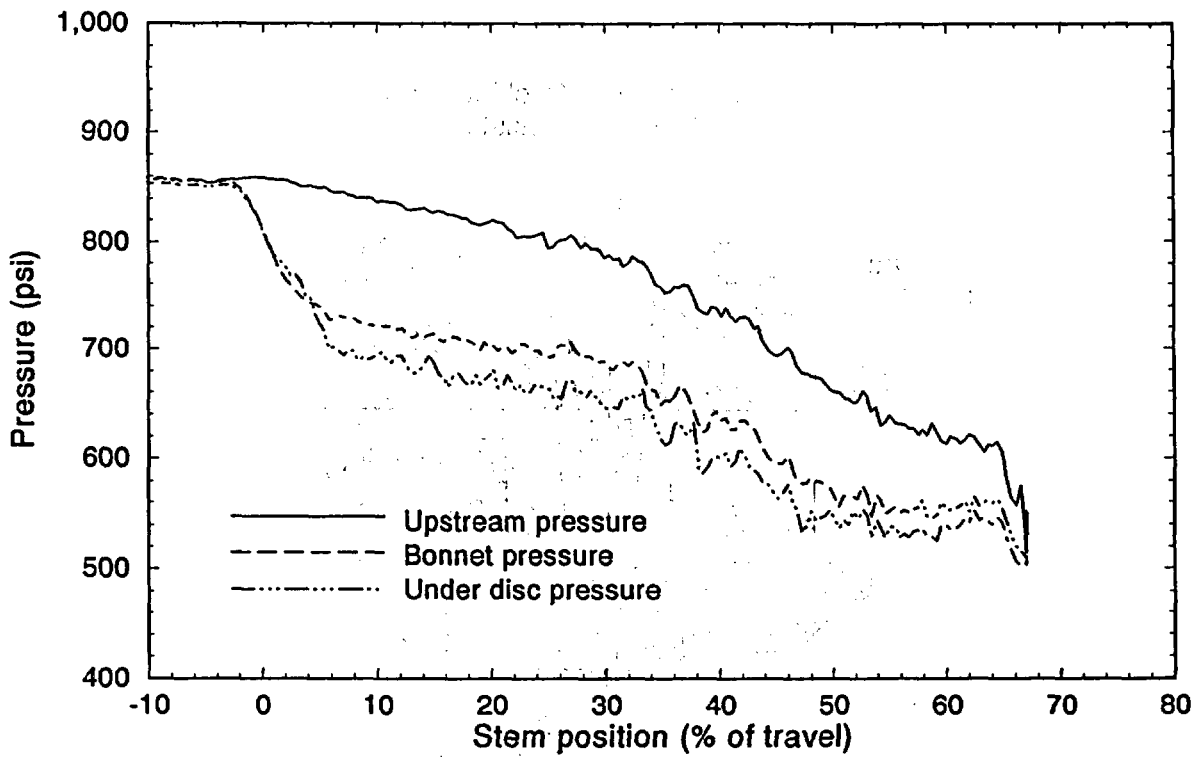
#### FLOW PHENOMENA THROUGH A VALVE

In response to the unexpected test results, we directed our efforts toward investigating the flow phenomena through a flexwedge gate valve and the effect that pressures throughout the valve had on the resultant stem force. Figure 5 shows a cross section of a typical flexwedge gate valve and identifies those areas on the disc and stem where the various pressure forces can act. This figure also indicates where we drilled three pressure measurement ports into each of the valve bodies prior to the Phase II testing to assist in this internal pressure distribution study. Figure 6 shows a typical pressure distribution observed during our testing. The pressure in both the bonnet region of the valve and under the disc are lower than the upstream pressure during most of the valve closure cycle. This reduction in pressure is due to the Bernoulli effect, the result of fluid accelerating through a valve in response to a reduction in the flow area. This phenomenon is dependent on the pressure and subcooling of the fluid and on the magnitude of the reduction in flow area through the valve. Thus, the Bernoulli effect will be system and fluid dependent. The bonnet area also shows a lower pressure because of the split in the disc and because of the



M291 rs-0491-07

Figure 5. Gate valve disc cross section showing pressure forces.



M291 re-0491-11

Figure 6. Gate valve internal pressure distribution.

gap between the disc and the valve body seats; these structural features provide a path such that the pressure in the bonnet region can more closely follow the pressure in the region under the disc.

However, from the minus 3% to the minus 10% stem position during this test, the pressures converge. During this portion of the valve stroke, flow has been isolated and the disc is riding on the valve body seats; however, wedging of the disc has not yet begun. It is also during this portion of the valve stroke that predictable valves exhibit the largest stem force. Thus, we concentrated our efforts on this segment of the valve closure cycle. Wedging forces were not considered because these forces are not the result of fluid dynamic and frictional effects, but instead depend on the force capabilities of a given operator and on the structural stiffness characteristics of a specific disc and valve body.

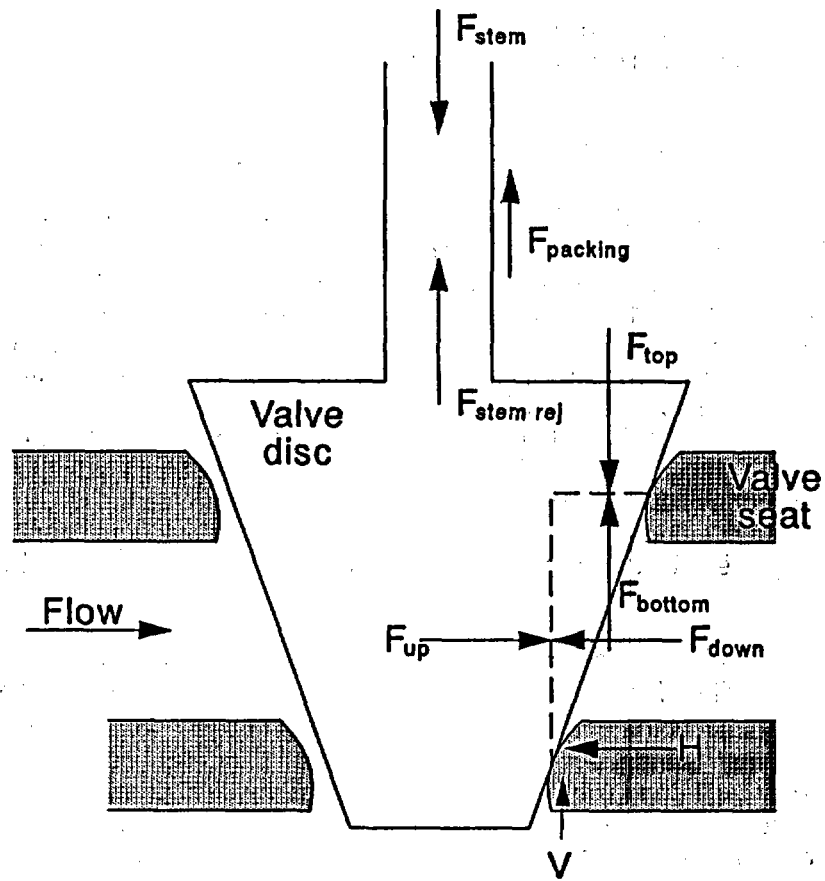
### DEVELOPMENT OF THE INEL CORRELATION

Our first effort was to develop a relatively detailed free body diagram of the disc while it is moving in the closing direction, after the flow has been isolated but before wedging. This was done with the hope of better understanding the pressure and area terms that effect the stem force. Figure 7 presents the results of this effort and identifies all the nonsymmetrical forces acting on the disc. Note that according to the free body diagram, the forces acting on the disc ultimately react through the valve body seats, which are at a slight angle (for a flexwedge gate valve) relative to the horizontal and vertical valve coordinate system. To account for this slight seat angle so that the forces are expressed in values consistent with the definition of a traditional friction factor, we found it necessary to transform the horizontal and vertical forces into a coordinate system that is normal and tangent to the valve body seating surfaces.

Following this logic, we theorized the existence of two horizontal forces acting on the disc. The first horizontal force ( $F_{up}$ ) is due to the upstream pressure ( $P_{up}$ ) acting on that area of the disc defined by the mean diameter of the downstream seating surface. The downstream seating surface presents a circular profile in the horizontal plane. The mean seat diameter was selected because it best approximates that area of the disc in contact with the crown of the downstream seating surface over which the various pressure forces act.  $F_{up}$  is defined as

$$F_{up} = P_{up} \left( \frac{\pi D_{mean}^2}{4} \right) \quad (2)$$

Resisting this force ( $F_{up}$ ) is a horizontal force ( $F_{down}$ ) due to the downstream pressure ( $P_{down}$ ) also acting on that area of the disc defined by the mean diameter of the downstream seating surface.  $F_{down}$  is defined as



M291 rs-0491-12

Figure 7. Gate valve disc cross section showing unbalanced forces just before wedging.

$$F_{down} = P_{down} \left[ \frac{\pi D_{mean}^2}{4} \right] \quad (3)$$

These two forces represent the only horizontal forces acting on the disc and provide a far more realistic estimate of the horizontal force component than the orifice area term which is often used in the industry equation. The net horizontal force component (H) can be expressed as

$$H = F_{up} - F_{down} \quad (4)$$

Likewise, the free body diagram indicates that there are actually five vertical forces acting on the disc. The first vertical force is due to the operator and represents the net stem force delivered to the valve.

$$F_{stem} = \text{stem load} \quad (5)$$

The second is due to the resistance of the packing while the valve is closing. The effect of the disc and stem weights is also included in this term.

$$F_{packing} = \text{packing drag - disc and stem weight} \quad (6)$$

The third represents the stem rejection force, the result of the pressure under the disc ( $P_{up}$  once the flow has been isolated) trying to expel the stem.

$$F_{stem\ rej} = P_{up} \left[ \frac{\pi D_{stem}^2}{4} \right] \quad (7)$$

The fourth force is due to the pressure in the bonnet region of the valve ( $P_{up}$  once the flow has been isolated) acting on the area of the disc defined by the mean diameter of the seat cast in the vertical direction. This area term is the result of the slight angle of the seat in a flexwedge type gate valve (nominally a five-degree angle) and results in an elliptical area over which the pressure acts. The major diameter is equal to the mean diameter of the seat; the minor diameter is equal to the mean diameter of the seat times the tangent of the angle the seat makes with the vertical axis of the valve.

$$F_{top} = P_{up} \left[ \frac{\pi D_{mean}^2}{4} \right] \tan \alpha \quad (8)$$

Resisting  $F_{top}$  is a fifth force due to the downstream pressure ( $P_{down}$ ) acting on the area of the disc defined by the mean diameter of the seat cast in the vertical direction. This force is also the result of the slight angle of the seat.

$$F_{bottom} = P_{down} \left[ \frac{\pi D_{mean}^2}{4} \right] \tan \alpha \quad (9)$$

The net vertical force component ( $V$ ) during valve closure can thus be expressed as

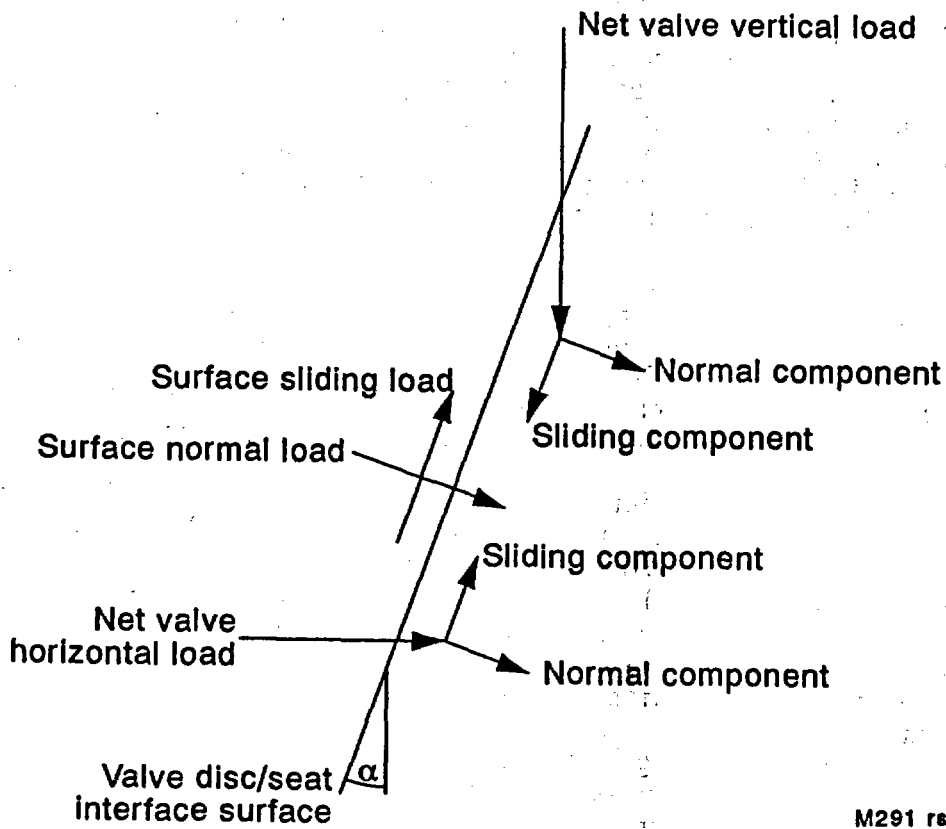
$$V = F_{stem} - F_{packing} - F_{stem\ rej} + F_{top} - F_{bottom} \quad (10)$$

The net horizontal and vertical forces can now be recast into the plane defined by the valve body seat and normalized to remove the effect of valve size. Figure 8 shows these two forces and their resolution into forces normal and tangent to the seats. Note that the two normal forces resulting from this transformation act in the same direction, whereas the two tangent or sliding forces oppose each other. These can be expressed as follows for the normalized normal force ( $F_n$ ) and the normalized sliding force ( $F_s$ ), respectively

$$F_n = \frac{H \cos \alpha + V \sin \alpha}{\left[ \frac{\pi D_{mean}^2}{4} \right]} \quad (11)$$

$$F_s = \frac{H \sin \alpha - V \cos \alpha}{\left[ \frac{\pi D_{mean}^2}{4} \right]} \quad (12)$$

The analysis described above allows us to better characterize the normal and sliding forces acting on a flexwedge gate valve disc just before wedging. Our next effort was to determine if the Phase I and Phase II flexwedge gate valve test data supported a relationship between these forces. We extracted from our data base the test results of all predictable valves during the closure cycle when the disc was riding on the seats. We did not include the results of any



M291 rs-0491-08

Figure 8. Resolution of horizontal and vertical gate valve disc forces into surface normal and sliding forces.

testing if severe internal damage was evident. However, if the valve exhibited evidence of internal damage while the disc was riding on the guides but showed no evidence of such behavior while the disc was riding on the valve body seats, we included the results.

The Phase II data extraction included testing with three valves representing two valve sizes (6-in. and 10-in.). Design basis flow isolation tests and normal operating flow isolation tests were used; upstream pressures ranged from 600 psig to 1400 psig, and fluid conditions ranged from steam to 400°F subcooled water. However, the results of tests when the differential pressure was less than 20% of the upstream pressure or when both the differential pressure and the stem force were increasing very rapidly while the disc was riding on the valve seat were not included. This is because the magnitude and trends of the resulting forces are obscured by relatively low loadings on the valve disc (which affect the transition from thick film lubrication to thin film lubrication), and by rapid changes in both the stem force and the differential pressure. This extraction yielded data from 30 tests.

The Phase I data extraction included testing with two valves representing a single valve size (6-in.). By way of comparison, these valves were nearly the same as Valves 1 and 2 in the Phase II testing. Only design basis flow isolation tests were used from the Phase I testing. Upstream pressures ranged from 400 psig to 1400 psig, and fluid conditions ranged from 10°F subcooled to 140°F subcooled water. This extraction yielded data from 12 tests.

The results of both data extractions were used in the force balance developed as described above and presented in Figures 9 and 10. The results reveal two linear relationships between the normal force on a seat ( $F_n$ ) and the tangent or sliding force ( $F_s$ ) necessary to induce motion. One is representative of a fluid subcooling of less than 70°F, while the other is representative of a fluid subcooling of 70°F or greater. The two dashed lines on either side of the solid line represent the limits of the observed data scatter. The tight grouping of the data scatter lends confidence that not only can we bound the force requirements of a flexwedge gate valve, but we can also devise a method where the results of low differential pressure flexwedge gate valve testing can be verified and then the design basis conditions used to bound the maximum stem force. Note also that the dashed lines do not extend below a normalized normal force of 400  $lb_f/in^2$ . Due to the limited low pressure and low differential pressure data available and the postulated friction mechanism, the applicability of the INEL correlation is currently limited to normalized normal forces of 400  $lb_f/in^2$  and above. We are continuing to extend the applicability of the INEL correlation.

#### THE INEL CORRELATION

We can now rearrange the previously developed force balance and solve for the stem force based on a linear relationship between the normalized normal and sliding forces. Using Figures 9 and 10, the slope of the solid line (the friction factor between the disc and the seat) can be used to relate the normalized normal force ( $F_n$ ) to the normalized sliding force ( $F_s$ ) as

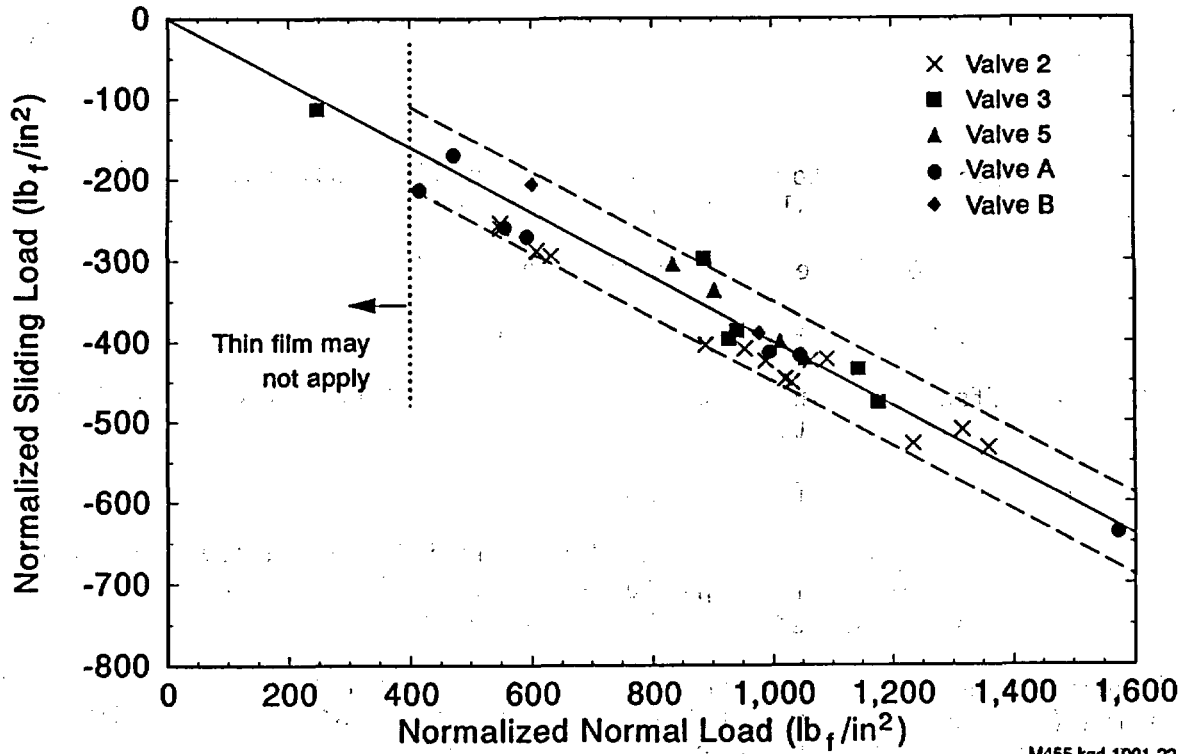


Figure 9. Normalized surface sliding force versus normalized surface normal force for gate valves closing against less than 70°F subcooled fluid.

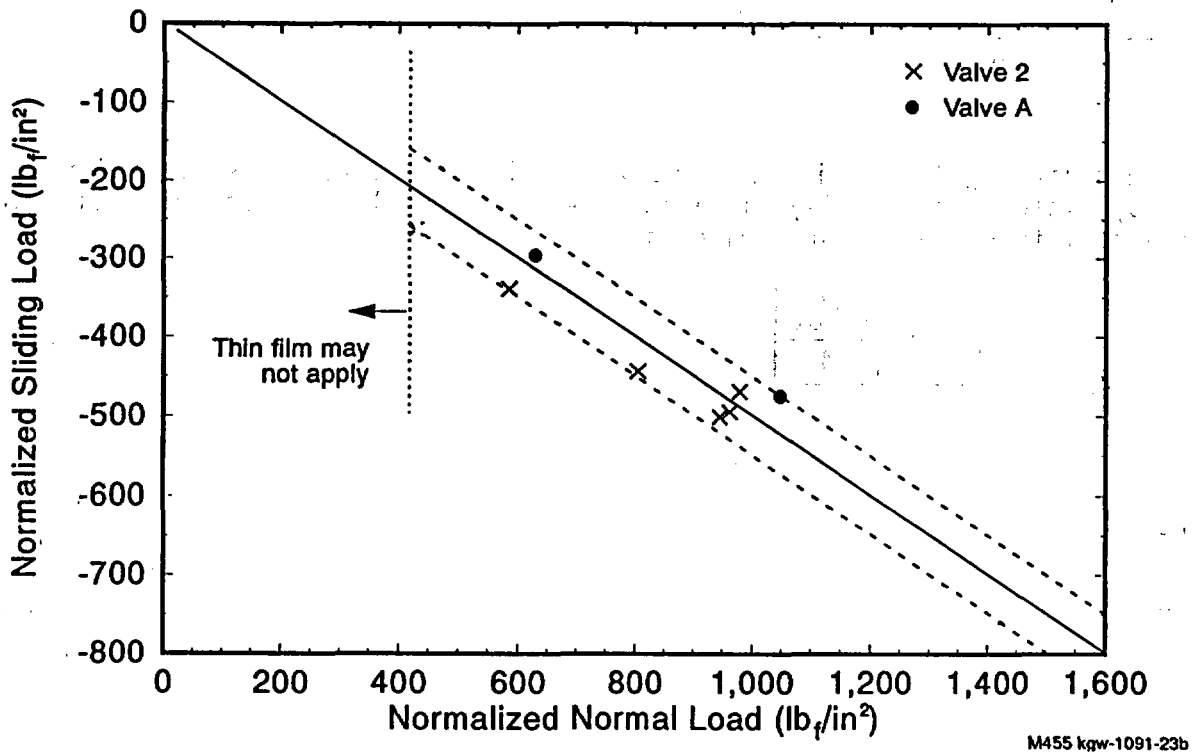


Figure 10. Normalized surface sliding force versus normalized surface normal force for gate valves closing against 70°F or greater subcooled fluid.

$$F_s = -f F_n \pm C \quad (13)$$

where

$f$  = friction factor, the slope of the line that relates the normal force to the sliding force and is equal to

0.400 if the fluid is less than 70°F subcooled

0.500 if the fluid is 70°F or greater subcooled

$C$  = offset bounding term reflecting the scatter in the observed data and is equal to

0 for no offset bounding

50 lb<sub>f</sub>/in<sup>2</sup> to bound the data provided a normalized normal force of 400 lb<sub>f</sub>/in<sup>2</sup> or greater exists according to Equation (11) (shown as the dashed lines in Figures 9 and 10).

Substituting the horizontal and vertical components of the normal force [Equation (11)] and the horizontal and vertical components of the sliding force [Equation (12)] into the above relationship yields

$$V = \frac{H (f \cos \alpha + \sin \alpha) \pm C \left[ \frac{\pi D_{mean}^2}{4} \right]}{(\cos \alpha - f \sin \alpha)} \quad (14)$$

Now, substituting the horizontal and vertical force components [Equations (4) and (10)] into Equation (14), limiting the final result to a bounding estimate of the stem force, and rearranging yields

$$F_{stem} = F_v + \frac{\theta_1 F_h + 50 \left[ \frac{\pi D_{mean}^2}{4} \right]}{\theta_2} \quad (15)$$

where

$$F_h = F_{up} - F_{down} \quad (16)$$

$$F_v = F_{packing} + F_{stem\ rej} - F_{top} + F_{bottom} \quad (17)$$

$$\theta_1 = f \cos \alpha + \sin \alpha \quad (18)$$

$$\theta_2 = \cos \alpha - f \sin \alpha \quad (19)$$

f = friction factor and is equal to

0.400 if the fluid is less than 70°F subcooled

0.500 if the fluid is 70°F or greater subcooled.

Thus, Equation (15) can be used to bound the maximum stem force requirements of a flexwedge gate valve closing against medium to high flows whose operational characteristics have been demonstrated to be predictable at design basis pressures and temperatures. This method will also provide the basis by which the results of in situ tests conducted on predictable valves at less than design basis conditions can be verified. Then the design basis conditions can be used to bound the maximum stem force. Note that the correlation applies only to flexwedge gate valve closure against medium to high flows, flows that will result in a normalized normal force of 400 lb<sub>f</sub>/in<sup>2</sup> or greater according to Equation (11).

#### USE OF THE INEL CORRELATION

To use the INEL correlation to bound the closing stem force requirements of a flexwedge gate valve, the analyst must first determine if operational characteristics of the valve are considered to be predictable. If the valve is predictable, the following information can be used to bound the stem force:

- The mean diameter of the valve body seat (the average of the inside diameter and the outside diameter of the valve body seats measured in the plane perpendicular to the stem)
- The angle the valve body seat makes with the vertical or stem axis
- The outside diameter of the stem
- An estimate of the maximum packing drag expected less the effects of the weight of the disc and stem
- The maximum upstream pressure that would exist after flow isolation but prior to wedging, typically the design basis pressure

- The maximum differential pressure that would exist after flow isolation but prior to wedging, typically the design basis differential pressure
- The subcooling of the fluid at design basis conditions, either less than 70°F subcooled or 70°F or greater subcooled.

With this information, the net horizontal force ( $F_h$ ) can be estimated with Equation (16) and Equations (2) and (3). The net vertical force ( $F_v$ ) can then be estimated with Equation (17) and Equations (6) through (9). The angle between the seat and the vertical or stem axis can then be used with Equations (18) and (19) to estimate terms associated with transforming the horizontal forces into forces on the disc and seat, and finally into a vertical force. Thus, all the terms in Equation (15) can be determined, and the maximum stem force necessary to isolate flow at the specified pressure and differential pressure can be estimated.

By way of example, the actual upstream pressure and differential pressure recorded after flow isolation but prior to wedging during one of the tests will be used, and the maximum stem force requirements of the valve using the INEL correlation will be estimated. The result will then be compared with the actual stem force recorded during the test.

The results from Valve 2, Test 3, Step 25 will be used for this comparison. Since this was a cold water test (400°F subcooled fluid), the 70°F or greater subcooled friction factor will be used in the INEL correlation. Pertinent valve information and the pressure and differential pressure recorded just before wedging are

Stem diameter	1.750 inches
Orifice diameter	5.187 inches
Seat inside diameter	5.192 inches
Seat outside diameter	5.945 inches
Packing drag	200 lb <sub>f</sub>
Upstream pressure just before wedging	746 psig
Differential pressure just before wedging	753 psid

This information can be used with the INEL correlation as follows:

$$D_{mean} = \frac{(seat\ ID + seat\ OD)}{2} = \frac{(5.192 + 5.945)}{2} = 5.569$$

$$A_{mean} = \frac{\pi D_{mean}^2}{4} = \frac{\pi(5.569)^2}{4} = 24.354$$

$$A_{stem} = \frac{\pi D_{stem}^2}{4} = \frac{\pi(1.750)^2}{4} = 2.405$$

$$F_{up} = P_{up} A_{mean} = (746)(24.354) = 18,168$$

$$F_{down} = P_{down} A_{mean} = (746 - 753)(24.354) = -170$$

$$F_{top} = P_{up} A_{mean} \tan \alpha = (746)(24.354) \tan 5 = 1590$$

$$F_{bottom} = P_{down} A_{mean} \tan \alpha = (746 - 753)(24.354) \tan 5 = -15$$

$$F_{stem\ rej} = P_{up} A_{stem} = (746)(2.405) = 1794$$

$$F_h = F_{up} - F_{down} = 18,168 - (-170) = 18,338$$

$$F_v = P_{pecking} + F_{stem\ rej} - F_{top} + F_{bottom} = 200 + 1794 - 1590 + (-15) = 389$$

$$\theta_1 = f \cos \alpha + \sin \alpha = 0.500 \cos 5 + \sin 5 = 0.585$$

$$\theta_2 = \cos \alpha - f \sin \alpha = \cos 5 - 0.500 \sin 5 = 0.953$$

$$F_{stem} = F_v + \frac{\theta_1 F_h + 50 A_{mean}}{\theta_2} = 389 + \frac{(0.585)(18,338) + (50)(24.354)}{0.953} = 12,924$$

During this test, the peak stem force recorded just before wedging was 12,787 lb<sub>f</sub>. Thus, the INEL correlation bounds the actual recorded stem force. Similar comparisons using the industry equation do not consistently bound the observed stem force with either a 0.3 or a 0.5 disc factor and using either the orifice area or the mean seat area.

#### LOW DIFFERENTIAL PRESSURE TEST VERIFICATION

Utilities have numerous flexwedge gate valves in systems throughout a nuclear power plant; many of these valves must function in various design basis events. The capability of these valves to operate at design basis conditions usually cannot be verified with in situ testing, especially for valves where design basis conditions include high pressures and medium to high flows. Usually, only low flow and low differential pressure conditions can be developed near valve closure. Where the utility can demonstrate that their medium to high flow valve designs exhibit predictable behavior at design basis conditions, through type testing or other means, in situ testing at low flows and differential pressures can be used in conjunction with the INEL correlation to verify that the valve being tested is representative of the valves tested by the INEL. If so, the INEL correlation can then be used to bound the stem force requirements of the candidate flexwedge gate valve at design basis conditions. This is accomplished as follows:

- Step 1: A differential pressure test is performed. The results of the testing are then used to estimate the normalized normal and sliding forces for the valve according to Equations (11) and (12). If the upstream pressure and differential pressure while the disc is riding on the seats results in a normalized normal force of not less than 400 lb/in<sup>2</sup> and if the resulting forces fall within the upper and lower bounds expected for valves of this design (see Figures 9 and 10), the valve is considered to be representative of the valves tested by the INEL. If the resulting forces do not fall within the expected band, the results of our testing are not representative of the valve being tested and the INEL correlation may not be applicable.
- Step 2: If the results of Step 1 fall within the expected band, actual design basis conditions can be used in the INEL correlation to bound the stem force requirement of the valve being tested. This maximum stem force estimate is then used, along with the other necessary motor operator sizing calculations, to verify the size of the operator and the setting of the torque switch to ensure that sufficient stem force is available to operate the valve at design basis conditions.

#### CONCLUSIONS

The industry's traditional gate valve sizing equation is incomplete regardless of the disc area term or the disc factor used. This is because more terms are included in the disc factor than the sliding friction term.

A new correlation was developed based on the results of two full-scale flexwedge gate valve qualification and flow interruption test programs. This correlation has been shown to consistently bound the stem force requirements of a flexwedge gate valve whose operational characteristics have been shown to be predictable. This correlation also allows a flexwedge gate valve to be verified based on the results of a low differential pressure test. If so verified, the results of the INEL correlation are shown to be applicable at design basis conditions.

#### REFERENCES

- DeWall, K. G., and R. Steele, Jr., 1989, BWR Reactor Water Cleanup System Flexible Wedge Gate Isolation Valve Qualification and High Energy Flow Interruption Test, NUREG/CR-5406, EGG-2569.
- Steele, R., Jr., K. G. DeWall, and J. C. Watkins, 1990, Generic Issue 87 Flexible Wedge Gate Valve Test Program, Phase II Results and Analysis, NUREG/CR-5558, EGG-2600.

## NOTICE

This report was prepared as an account of work sponsored by an agency of the United States Government. Neither the United States Government nor any agency thereof, or any of their employees, makes any warranty, expressed or implied, or assumes any legal liability or responsibility for any third party's use, or the results of such use, of any information, apparatus, product, or process disclosed in this report, or represents that its use by such third party would not infringe privately owned rights. The views expressed in this report are not necessarily those of the U.S. Nuclear Regulatory Commission.

# APPLICATIONS AND EXTENSIONS OF DEGRADATION MODELING\*

F. Hsu, W.E. Vesely†, M. Subudhi, and P.K. Samanta

Department of Nuclear Energy  
Brookhaven National Laboratory  
Upton, New York 11973, USA

†Science Applications International Corporation, Ohio, USA

## ABSTRACT

Component degradation modeling being developed to understand the aging process can have many applications with potential advantages. Previous work has focussed on developing the basic concepts and mathematical development of a simple degradation model. Using this simple model, times of degradations and failures occurrences were analyzed for standby components to detect indications of aging and to infer the effectiveness of maintenance in preventing age-related degradations from transforming to failures. Degradation modeling approaches can have broader applications in aging studies and in this paper, we discuss some of the extensions and applications of degradation modeling.

The application and extension of degradation modeling approaches, presented in this paper, cover two aspects: (a) application to a continuously operating component, and (b) extension of the approach to analyze degradation-failure rate relationship.

The application of the modeling approach to a continuously operating component (namely, air compressors) shows the usefulness of this approach in studying aging effects and the role of maintenance in this type component. In this case, aging effects in air compressors are demonstrated by the increase in both the degradation and failure rate and the faster increase in the failure rate compared to the degradation rate shows the ineffectiveness of the existing maintenance practices. Degradation-failure rate relationship was analyzed using data from residual heat removal system pumps. A simple linear model with a time-lag between these two parameters was studied. The application in this case showed a time-lag of 2 years for degradations to affect failure occurrences.

## 1. INTRODUCTION

Component degradation modeling includes modeling of occurrences of component degradations and analyses of these occurrences to understand the aging-degradation process and its implications. In this modeling approach, dividing the operational performance of a component into three states - normal operating state, degraded state, and failure state, we established relations among these states using rates of degradation and failure occurrences. The relations are used to define estimates of the effectiveness of maintenance in preventing degradation from becoming failures. In an earlier paper<sup>1</sup> we have focussed on basic concepts and mathematical development of simple degradation modeling as applicable to aging and maintenance effectiveness applications.

---

\*This work was performed under the auspices of the U.S. Nuclear Regulatory Commission.

In this paper, we study further application and extensions of degradation modeling approaches focusing on two aspects:

- a) applications of degradation modeling approaches to a continuously operating component, and
- b) extension of degradation modeling approaches to analyze degradation-failure rate relationship.

Previously, we studied standby "active" components.<sup>1</sup> Here, we analyze degradation and failure data for air compressors to study the applicability of this modeling approach to a continuously operative component. Thus, the degradation modeling analysis of air compressors shows the applicability of the approach for an active component under different operating conditions. Also, because they are continuously operating component, air compressors are expected to suffer degradations which are detected and corrected; thus, making them ideal candidates for degradation modeling analysis.

Understanding the relationship between degradations and failures is important in aging studies and can result in significant benefits in defining maintenance strategies for controlling aging and in conducting aging reliability and risk studies particularly when aging failure data are sparse. In terms of maintenance strategies, if degradation-failure relationship is known, then effective maintenance/repair/refurbishment can be performed through monitoring of degradations, thus avoiding component failures. For aging reliability studies, relationship between degradations and failure is important since it can be used to estimate failure rates from degradation rates when failure data are sparse. In this paper, this important correlation between degradations and failures is statistically studied and the concept of a delayed effect of degradation on failures is explored.

## **2. DEGRADATION ANALYSIS USING AIR COMPRESSOR AGING DATA**

Here, our objective is to explore the applicability of degradation modeling approaches for a continuously operating component, different from standby components studied previously. We selected an air compressor for this analysis. The analysis approach is similar to that followed for the components studied in our earlier work.<sup>1</sup>

### **Definitions of Degradations**

To analyze degradations, the degraded state of the component must first be defined so it can be identified and analyzed. Definitions of the degraded state can be at a gross level or at a detailed level. At a gross level, a component is described as degraded whenever any deterioration occurs which does not cause loss of function. The operational performance of the component is divided into three states: the normal operating state, the degraded state, and the failure state. An example of a gross definition of degradation is that a component degradation occurs whenever corrective maintenance is required, but the component has not failed.

More detailed modeling of degradations involves dividing the degradation space into multiple degraded states. A given degraded state is then associated with a given range of characteristics of the component or performances of the component. For example, detailed degraded states for circuit breakers can be defined based on defined ranges for the pick-up/drop-out voltage, inrush/holding current, and other measurable degradation characteristics.

The advantage of defining more detailed degradation states is that we can accurately predict impacts on the failure rate of the component. When aging occurs, the component generally progresses

through a series of degradation states before failure occurs. By analyzing and modeling this progression, we can more accurately predict when failure will occur. For initial work, the gross definition of degradation can be used, which basically equates the degradation state occurring whenever corrective maintenance is required.

Table 1 presents an example of data analyses for an air compressor identifying degraded states, along with failure states of the component. In this example, failure states and degraded states of air compressors are distinguished based on engineers' judgement using the information on failure effect and the identified effected subcomponent. In some situations, judgements were used to determine whether the degradation was of the magnitude to be defined as a failure. For example, in general, an oil leak at the piston rod seal can be a degraded state for an air compressor, but in the example in Table 1, the leak was of sufficient magnitude to be called a failure of the air compressor.

**Table 1. Typical Examples of Compressor Degradation Levels and Failure Mode and Effect**

Compressor Subcomponent	Failure Classification	Failure Effect	Failure Mode	Degradation Level
Bearings	D	Monthly preventive maintenance - bearings greased		Low D
Filter	D	Monthly P.M. - filter cleaned		Low D
Gasket	D	Oil leak by gasket	Gasket deterioration	Intermediate D
Jacket Heat Exchanger	D	Corrosion deposits built up by aftercooler	Mechanical debris; poor water chemistry	Intermediate D
Bolts and Fasteners	D	Fractured stud on spacer	Mechanical vibration	High D
Pistons	D	Brass filings in high and low pressure regions found during P.M.	Mechanical wear	High D
Piston	F	Oil leak at piston rod seal	Mechanical wear	F
Lube Oil System	F	Pump seized and became inoperable	High temperature, mechanical wear	F

**Analysis Approach**

The main objective of the analysis was to obtain the aging failure rate and degradation rate based on component age-related failure and degradation data, respectively. These two parameters are used to obtain the effectiveness of maintenance in preventing age-related failure.

For the analysis of air compressors, aging data from only one of two BWRs were used. Based on the statistical test, the aging data in the two available units were not compatible with each other. Therefore, the aging data from unit one was used to provide a data base from four similar compressors. Similarly, statistical tests were also conducted to justify the data pooling across the four components. Details of the analysis are presented in Reference 2.

The process of data collection provides specific degradation and failure times of four similar compressors from one BWR. The data for each of the compressors individually were insufficient to determine the parameters (degradation rate and aging failure rate). Therefore, we analyzed data from the group of components (i.e., four compressors). Similar to the analysis on RHR pumps<sup>1</sup>, statistical tests were conducted to justify the use of data across components.

(1) Mann-Whitney U Test

The Mann-Whitney U test was used in the analysis to identify components belonging to the same population. The four components in unit studied showed statistically identical distributions of times between degradations (and failures). Thus, the aging data from across the four components in unit one is combined for the analysis.

(2) Trend Testing and Identification of Age-Group with Degradation and Failure Times

The data obtained by the "data combining" method<sup>1</sup> were tested for time trends before developing age-related degradation and failure rates. Statistical tests were used to define component age groups showing similar aging behavior. We observed that the first three years of the compressors life showed a decreasing trend, and the last five years showed a increasing trend on both degradation rate and failure rate.

Aging Effects on Degradation

We analyzed the degradation data for the compressors with the following objectives:

- (a) To identify age-groups where statistically significant time trends exist, and
- (b) To determine time trends and degradation rates, using regression analysis.

The results and the characteristics of estimated degradation rate are summarized in Figure 1, which shows both the degradation rate ( $\lambda_d$ ) and the logarithm of the degradation rate ( $\ln\lambda_d$ ) that characterized the air compressors over ten years (presented as 40 quarters). Statistical tests showed that the degradation behavior across these components are similar, and accordingly, a generic degradation characteristic was studied. The age-dependent degradation rate is based on approximately 240 degradation occurrences observed for four compressors over the ten years of operation.

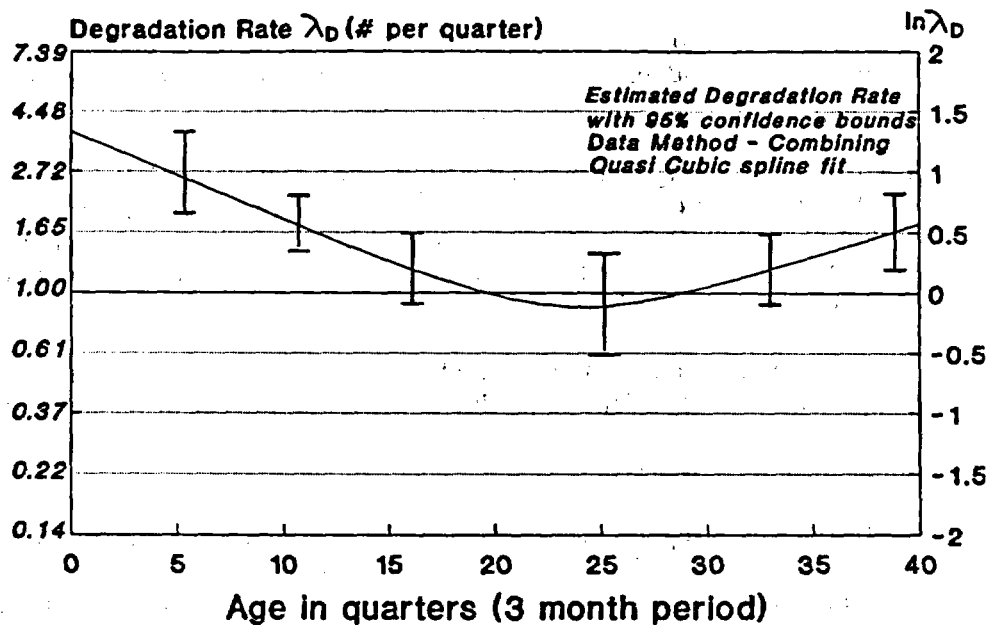


Figure 1. Age-dependent degradation rate (data on 4 air compressors)

The following observations can be made from the age-dependent degradation rate for the underlying air compressors.

- (a) The degradation rate shows significant age-dependence; the early life of the compressors (the first five years) shows a statistically significant decreasing trend, and the later life (last five years) shows a statistically significant increasing trend with the age of the compressors.
- (b) The increase in degradation rate, which is of interest in aging studies, is significant.
- (c) The 95% confidence bounds for the degradation rate show that the uncertainty in the estimation is reasonably small. The large number of degradations observed in the component contributed to this lower uncertainty.

#### Aging Effects on Failures

The aging-failure data for the compressors were also analyzed with the following objectives:

- (a) To identify age-groups where statistically significant time trends exist, and
- (b) To determine aging-failure rates in the age-groups where time trends exist.

Figure 2 shows both the failure rate ( $\lambda_f$ ) and the logarithm of the failure rate ( $\ln \lambda_f$ ) for the air compressors over ten years. The age-dependent failure rate presented is based on 25 failures observed for four compressors over ten years of operation.

The following observations can be made from the aging-failure rate obtained for the air compressors:

- (a) The aging-failure rate shows significant decreasing trend in the first two and a half years (in 10 quarters), and an increasing trend for the last five years of the component's ten-year life.
- (b) The behavior of aging-failure rate is similar to the degradation rate in the early two and one-half years, but differs after that. The aging-failure rate was generally lower (factor of 2 to 8) than the degradation rate and the difference decreased with increasing age. The aging failure rate reached about the same level as the degradation rate at the end of the component's ten years of operation.
- (c) The 95% confidence bounds associated with aging-failure rate show higher uncertainty compared to the degradation rate due to the lower number of failures observed.

### Evaluation of Maintenance Effectiveness

As discussed in our earlier report<sup>1</sup>, the degradation modeling approach estimates the effectiveness of maintenance in preventing age-related failures. The transition probability from a maintenance state to a failure state signifies the ineffectiveness of maintenance in the simplified model studied. The complement of maintenance ineffectiveness is maintenance effectiveness.

The maintenance effectiveness for the air compressors is obtained for each ten quarters of age. The maintenance effectiveness (1 = excellent maintenance, 0 = poor or no maintenance), as plotted in Figure 3, varies between 0.3 and 0.9 for the first 30 quarters, but is significantly lower (about 0.1) in the last 10 quarters, which signifies the small difference maintenances made in preventing degradations of components from transferring to failures.

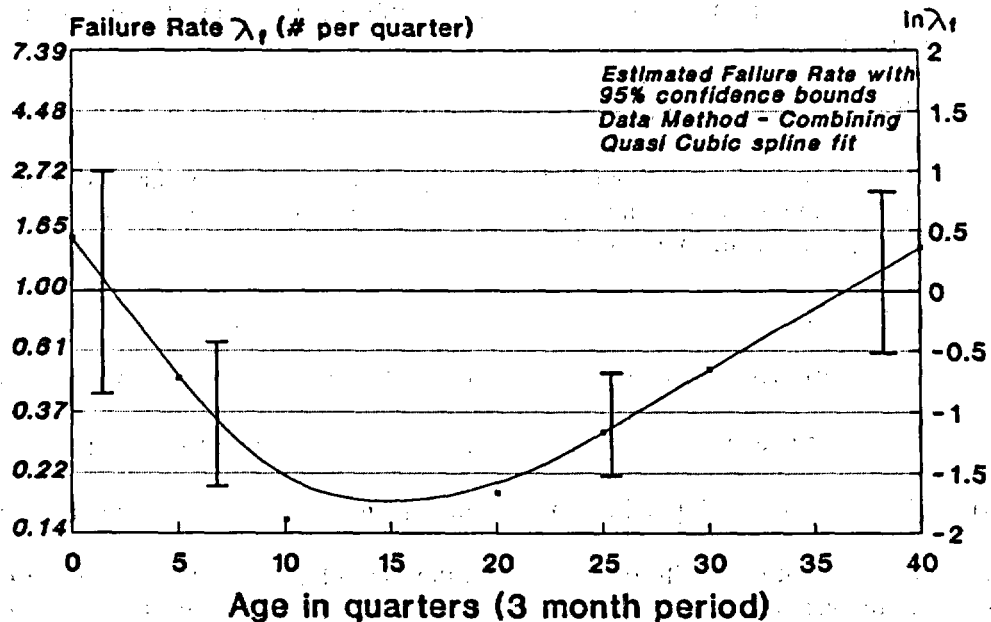


Figure 2. Age-dependent failure rate (component: 4 air compressors)

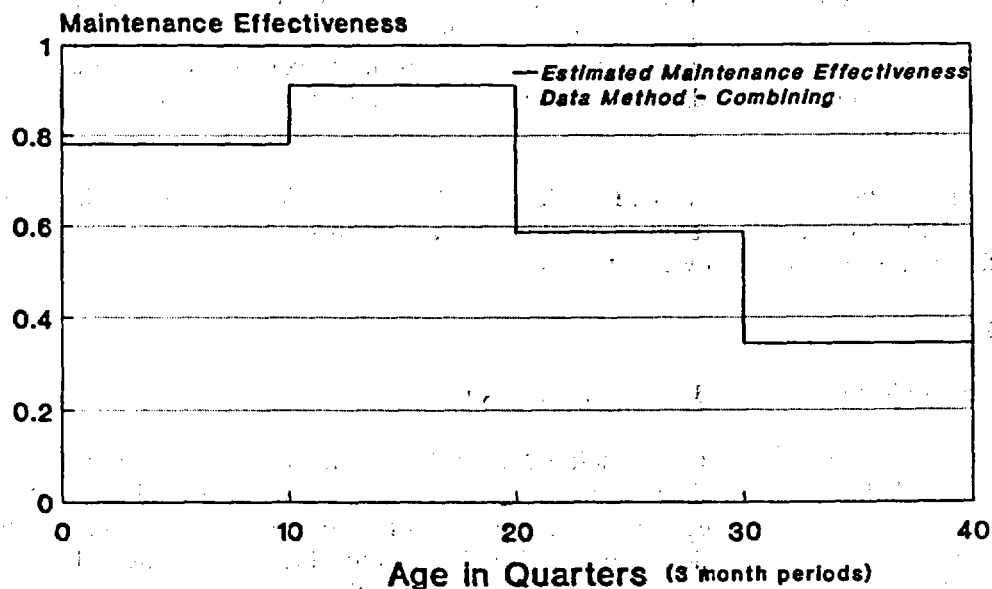


Figure 3. Estimated maintenance effectiveness (component: air compressors)

### 3. ANALYSIS OF DEGRADATION-FAILURE RELATIONSHIP

In this chapter, we present an event-count based approach for data analysis to study the relationship between degradations and failures. This approach uses non-parametric statistical methods to estimate and seek relations between degradation and failure rates based solely on the number of observed degradations and failures in each unit time or age interval.

This approach provides a simple framework for exploring the relationship between degradation and failure rate. Since aging-related failures, in general, pass through a degraded state first, the degradation rate serves as a precursor to the failure rate. Increasing aging trend in the degradation rate can signal future increasing aging trends in the failure rate. We study simple linear relationship between these two parameters considering any delayed effect that degradations may have on failure occurrences.

In general, disciplines that can be used to develop relationships between the degradation rate and the failure rate include engineering, reliability, and statistical disciplines. Engineering and reliability disciplines are required to develop the theoretical models between the degradation rate and failure rate. Statistical disciplines are required to estimate unknown parameters and to validate the theoretical models. The relationships between the degradation rate and failure rate, which are studied here, are among the simplest models to develop; they are consistent with reliability and engineering considerations. In the relationships which are developed, the degradation rate is related to the failure rate by appropriate transition probabilities. These transition probabilities are obtained by studying the correlations between occurrences of degradation and failures. They also include the effectiveness of maintenance in controlling the degradations before becoming failures.

### Analysis of Correlation Between Degradation and Failure Frequencies - Time-Lag Considerations

As we stated, the objective of degradation modeling is to develop relationships between the component degradation rate and the component failure rate. These relationships involve predicting how the component failure rate will change based on observations of the component degradation rate. Of most interest is predicting aging trends in the failure rates based on observed aging trends and patterns in the degradation rate.

If  $\lambda_f$  denotes the failure rate, and  $\lambda_d$  denotes the degradation rate, then the objective of degradation modeling can be interpreted as developing relationships between  $\lambda_d$  and  $\lambda_f$ . If the symbol "R" denotes these relationships then we may write:

$$\lambda_f = R(\lambda_d) \quad (1)$$

Thus, the objective of degradation modeling is to find the relationship R.

This equation expresses the relationship between degradation and failure rate increasing aging trends in the degradation rate can signal future increasing aging trends in the failure rate. Also, by recording the characteristics of the degradations, the severity of the degradation rate can be determined. Increasing severities of the degradation rate can also signal future increases in the failure rate. We, however, focused on relating occurrence rates and did not study the impact of increased severity of the degradation to failure rate at this time. Effect of increased degradation severity can be studied by expanding the Markov modeling approach to multiple degraded states supported by engineering criteria and data to obtain the necessary information from tests on component, maintenance, and operability records.

For our study, the relationship (1) is expressed as:

$$\lambda_f(t+l) = C_{df} \lambda_d(t) \quad (2)$$

where,

$\lambda_d(t)$  is the degradation rate at time (t)

$\lambda_f(t+l)$  is the failure rate at time (t+l)

l is the time-lag at which degradations impact failure occurrences

$C_{df}$  is the correlation coefficient between degradation occurrences and failure occurrences

The above expression assumes a linear relationship where  $C_{df}$  to be estimated from data analyses, is similar to the parameter of maintenance ineffectiveness. The parameter l represents the delayed effect because the component generally passes through a degraded state before experiencing failures, and is also estimated from data.

We used the event-count based data analysis to determine the correlation coefficient as well as the lagged time between degradation and failure frequencies. Using the data, the Kendall's Rank Correlation analysis method was employed to estimate the correlation coefficient for each individual plant data, as well as the combined data of the 3 plants. A statistical software package (STATGRAPH) was used to calculate the correlation coefficient for a large number of possible time-lag values. Among all

the calculated time-lag correlation coefficients, the correlation coefficient using a time-lag of 2 years reached the maximum value at a significance level of  $\alpha=0.029$ . The statistical results of Kendall's Rank Correlation coefficients are summarized in Table 2 and Table 3.

**Table 2. Kendall's Rank Correlation Analysis Results for RHR Pumps at 3 Units**

Correlation Analyses Between  $N_f$  and  $N_d$ .

Plant 1:	Correlation Coefficient:	0.3570
	Significance Level:	0.0139
Plant 2:	Correlation Coefficient:	0.5429
	Significance Level:	0.0005
Plant 3:	Correlation Coefficient:	-0.2067
	Significance Level:	0.5134
3 Plant Combined:		
$N_f$ vs. $N_d$ :	Correlation Coefficient:	0.3721
	Significance Level:	0.0692

$N_f$  = number of failures

$N_d$  = number of degradations

**Table 3. Kendall's Rank Correlation Analysis Using Time-Lag Considerations (Data on RHR Pumps from 3 Units)**

**No Time-Lag**

Correlation Coefficient:	0.3721
Significance Level:	0.0692

**One-Year Time-Lag**

Correlation Coefficient:	0.1826
Significance Level:	0.3966

**Two-year Time-Lag**

Correlation Coefficient:	0.505
Significance Level:	0.0294

### Estimation of Failure Rate from Degradation Data - Time-Lag Regression

One of the applications of degradation modeling is to estimate the failure rate from the degradation rate of a component. Here, using the time-lag correlation coefficients obtained in the previous section, the failure counts are estimated from degradations counts. The lagged regression technique was used to estimate the failure frequency based on the correlation coefficient and estimated time-lag. A linear regression model was used, although time-lag regression methods can use exponential or other non-linear models depending on the data distribution properties.

Analysis of data on RHR pumps is presented as an example of this application. Figure 4 presents the estimated failure frequency from the degradation frequency.

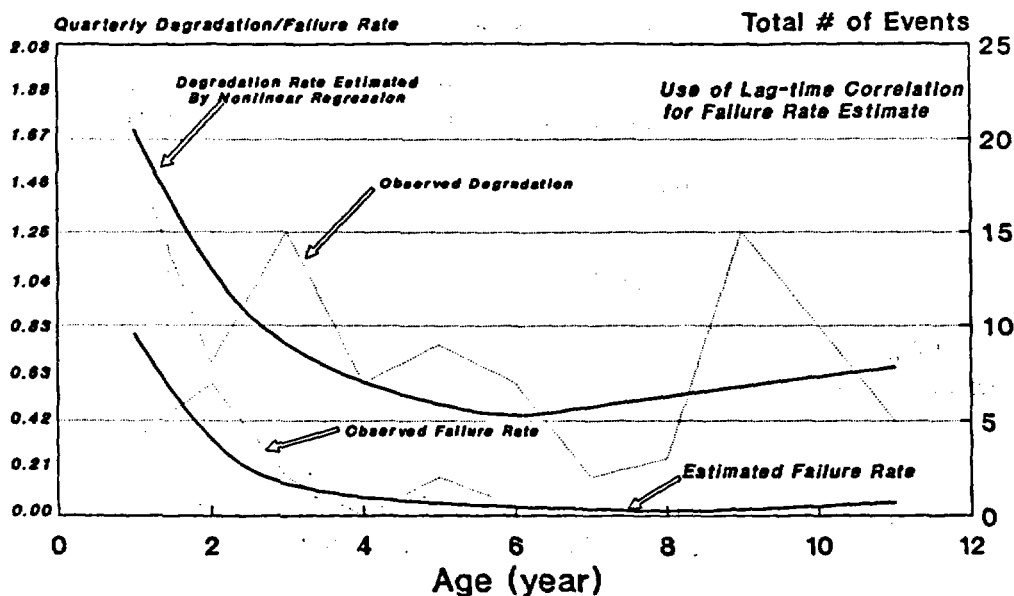


Figure 4. Degradation & failure rate estimation  
(event-counts based approach - data on RHR pumps from 3 units)

In this figure, the estimated failure rate in the last two years (age 9 to 11) is obtained from the degradation rate. This estimated failure rate is obtained by using equation 2, where both the correlation between degradation and failures and the delayed effects are incorporated. The correlation coefficient and the 2-year time-lag were estimated using the first 9 years of data. The estimated failure rate shows the increasing trend similar to the degradation rate, but lagged by 2 years. This estimated failure rate is comparable to the failure rate obtained by assuming no failures during this period (age 9 to 11). However, because of the increasing trend, the estimated rate starts becoming larger than that obtained otherwise. As we discussed previously, estimating failure rate from degradation data can significantly help risk-evaluation of aging, but the results need to be validated further.

### Applications of the Degradation Rate-Failure Rate Relationship

Once the relationship between the degradation rate and the failure rate is determined, it can be applied in several important ways. We studied one application (estimation of component failure rate from degradation rate), but other important applications can be studied with potential advantages. Some are summarized below.

1. The component failure rate can be estimated from degradation data. This estimation greatly increases the accuracy of the failure rate estimation for reliability and risk evaluations, and allows the failure rate to be estimated even if there is no failure data. If failure data exists, the estimate of the failure rate from the failure data can be optimally combined with the estimate from the degradation data.
2. Aging trends in the component failure rate can be estimated from aging trends in the degradation rate. This estimation is one of the most powerful applications of the degradation rate-failure rate relationship. Aging trends, which are identified in degradation data, can be input into the relationship to predict the aging trend in the failure rate. The determined aging-dependent failure rate in turn, can, be input to reliability and risk models to predict the resulting, impact on the reliability and risk.
3. Degradations can be monitored for their reliability and risk impacts. Alert levels and warning levels can be designed to monitor degradation to indicate when the failure rate is too high or is significantly increasing.
4. Maintenance can be monitored for its reliability and risk effectiveness. This again immediately follows from the degradation rate-failure rate relationship. The degradation rate-failure rate relationship which is determined through degradation modeling, is a function of the maintenance program. If the degradation rate as determined from the data on corrective maintenance and preventative maintenance implies that the failure rate is too high or is significantly increasing, then the maintenance is ineffective. If the failure rate is maintained at an acceptable level, then the maintenance is effective from a reliability and risk standpoint.

The accuracy and extent to which degradation rate-failure rate relationship can be determined are critical in demonstrating these applications. These applications can provide important inputs in maintenance decisions and aging evaluations, because in the past, degradations and maintenances have not been explicitly related to the failure rate, except in special cases.

#### 4. SUMMARY

In this paper, we presented application of degradation modeling approaches to a continuously operating component, different from a standby component. In addition, the relationship between degradation and failure frequency was studied to predict failure rates based on degradations. The major findings are summarized below.

#### Application of Degradation Modeling to a Continuously Operating Component

The application of degradation modeling approaches to a continuously operating component (air compressors) shows the usefulness of this modeling approach in studying aging effects and the role of maintenance in this type of component. Analyses of degradation and failure data of air compressors using degradation modeling approaches show that aging effects are evident in both degradation and

failure occurrences. In this case, both rates show aging effects; however, the faster increase in the failure rate compared to the degradation rate indicates the ineffectiveness of maintenance, which is reflected in the evaluation of maintenance effectiveness. The decline in maintenance effectiveness with age signifies that maintenance is ineffective in preventing age-related degradations from failures.

### **Relation between Degradation and Failure Frequency**

Understanding the relationship between degradations and failures is an important aspect in the degradation modeling approaches. Knowledge of relationships between degradations and failures will help define the maintenance activities necessary for preventing degradation-caused failures and can be used in risk-evaluations of aging. In this report, an event-count based approach to data analysis is presented to study correlations between degradation and failure frequencies. We used this approach to discover if there were delayed effects of degradations on failures. For the specific component studies (RHR pumps), a lag-time of 2 years was observed between degradation and failure occurrences. Existence of such lag-times, which are expected to be component specific, can be beneficial for deciding the maintenance activities that are necessary to mitigate the effects of aging. Additional applications will be needed to demonstrate the validity of the existence of time-lag between degradations and failures.

### **REFERENCES**

1. P.K. Samanta, W.E. Vesely, F. Hsu, and M. Subudhi, "Degradation Modeling with Application to Aging and Maintenance Effectiveness Evaluations," NUREG/CR-5612, BNL-NUREG-52252, March 1991.
2. F. Hsu, W.E. Vesely, E. Grove, M. Subudhi, and P.K. Samanta, "Degradation Modeling: Extensions and Applications," BNL Technical Report A-3270 6-21-91, June 1991.

# AGING ASSESSMENT OF BWR CONTROL ROD DRIVE SYSTEMS\*

Rebecca H. Greene

Oak Ridge National Laboratory  
Operated by Martin Marietta Energy Systems, Inc.  
P. O. Box 2009  
Oak Ridge, TN 37831-8038

"The submitted manuscript has been authored by a contractor of the U.S. Government under contract No. DE-AC05-84OR21400. Accordingly, the U.S. Government retains a nonexclusive, royalty-free license to publish or reproduce the published form of this contribution, or allow others to do so, for U.S. Government purposes."

## ABSTRACT

This Phase I NPAR study examines the aging phenomena associated with boiling water reactor (BWR) control rod drive mechanisms (CRDMs) and assesses the merits of various methods of managing this aging. Information for this study was acquired from (1) the results of a special CRDM aging questionnaire distributed to each U.S. BWR utility, (2) a first-of-its-kind workshop held to discuss CRDM aging and maintenance concerns, (3) an analysis of Nuclear Plant Reliability Data System (NPRDS) failure cases attributed to the CRD system, and (4) personal information exchange with industry experts.

An eight-page questionnaire was prepared by the Oak Ridge National Laboratory (ORNL) and distributed to all domestic BWR plants. The survey solicited site-specific data on CRDM degradation and failure experience, maintenance and aging interactions, and current testing procedures. To obtain firsthand information on CRDM aging histories, a workshop was sponsored by ORNL to discuss CRDM performance and the overall questionnaire results with utility participants. The three-day meeting on CRDM aging and maintenance was attended by 26 utility personnel from 21 BWR plants and 14 vendor and commercial representatives. These attendees provided invaluable information needed for understanding degradation mechanisms and maintenance constraints associated with BWR CRDMs.

As part of this study, nearly 3500 NPRDS failure reports have been analyzed to examine the prevailing failure trends for CRD system components. An investigation was conducted to summarize the occurrence frequency of these component failures, discovery methods, reported failure causes, their respective symptoms, and actions taken by utilities to restore component and system service.

The results of this research have identified the predominant CRDM failure modes and causes. In addition, recommendations are presented that identify specific actions utilities can implement to mitigate CRDM aging. An evaluation has also been made of certain maintenance practices and tooling which have enabled some utilities to reduce ALARA exposures received from routine CRDM replacement and rebuilding activities.

---

\* Research sponsored by the Office of Nuclear Regulatory Research, U. S. Nuclear Regulatory Commission under Interagency Agreement DOE 1886-8082-8B with the U. S. Department of Energy under contract No. DE-AC05-84OR21400 with the Martin Marietta Energy Systems, Inc.

## INTRODUCTION

Control rod drive mechanisms (CRDMs) are located at the bottom of boiling water reactor (BWR) pressure vessels, and they position the neutron absorbing control rod assemblies (CRAs) within the reactor core to provide reactivity control during startup and shutdown of the reactor, flux shaping at power, and emergency shutdown (scram). The CRD system consists of the CRDMs, the hydraulic control units (HCUs), and various valves, pumps, and headers that supply, move, and retain the system's operating fluid.

The CRDM is a double-acting, mechanically latched, hydraulic cylinder that uses reactor quality water as its operating medium. Each CRDM has a companion HCU that contains numerous valves which regulate the operating flows and pressures delivered to the device. A CRA is attached to each CRDM at the spud, and movement is accomplished by admitting pressurized water into the appropriate part of the CRDM (Fig. 1). The drive mechanism is capable of inserting or withdrawing a CRA at a slow, controlled rate in order to vary reactor power, or can provide scram insertion to accomplish rapid shutdown of the reactor within a few seconds.

General Electric has manufactured six different models of CRDMs and four basic models of HCUs which are in service at BWRs throughout the United States. Improved scram times and enhanced operational performance have been the basis for many of the design differences occurring among the various models of both the CRDM and the HCU. Some aging-related degradation reported in the BWR-2, -3, -4, and -5 design CRDMs has been substantially reduced by material improvements and design features inherent to the BWR-6 models. Other types of reported component degradation are subject to plant operational parameters, such as water chemistry, and vary in frequency of occurrence with each different BWR unit.

Normal CRDM maintenance involves the overall cleaning and replacement of a relatively standard set of components with new or spare parts. If necessary, any part of the the CRDM can be replaced during rebuilding activities. Several utilities have established maintenance goals that require the refurbishment of all the CRDMs in a BWR unit every 10 years. However, historical data suggest that the maintenance interval varies for CRDMs with respect to their location in the core: centrally located drives are rebuilt more often than drives located along the periphery. The cause for dissimilar maintenance intervals is uncertain but could be attributed to the fact that peripheral drives (which have a limited power shaping contribution) do not experience the higher core fluxes or undergo as many "feet of travel" as centrally located CRDMs.

Selection criteria for CRDM changeout does vary between plants. To monitor service wear and degradation, most utilities routinely trend individual CRDM withdrawal stall flows and operating temperatures. In addition, plant technical specifications require scheduled scram time testing and weekly-to-monthly CRDM "exercise" tests to ensure operability. In general, CRDM components degrade slowly as they age, and most operational problems do not occur suddenly but over a time interval of at least several months.

When a CRDM's performance does not meet plant requirements, it is scheduled for maintenance, usually during the next plant refueling outage. In recent years, advancements in maintenance tooling, changeout and rebuilding training, CRDM handling devices, and improvements in worker comfort have significantly decreased the human error contribution to CRDM aging as well as reducing ALARA exposures. The following sections highlight the predominant modes of CRD system degradation and specific steps taken by utilities to mitigate component aging and curtail maintenance related doses. Final research results are to be published in NUREG/CR-5699, Vol. 1, entitled "Aging and Service Wear of Control Rod Drive Mechanisms for BWR Nuclear Plants."

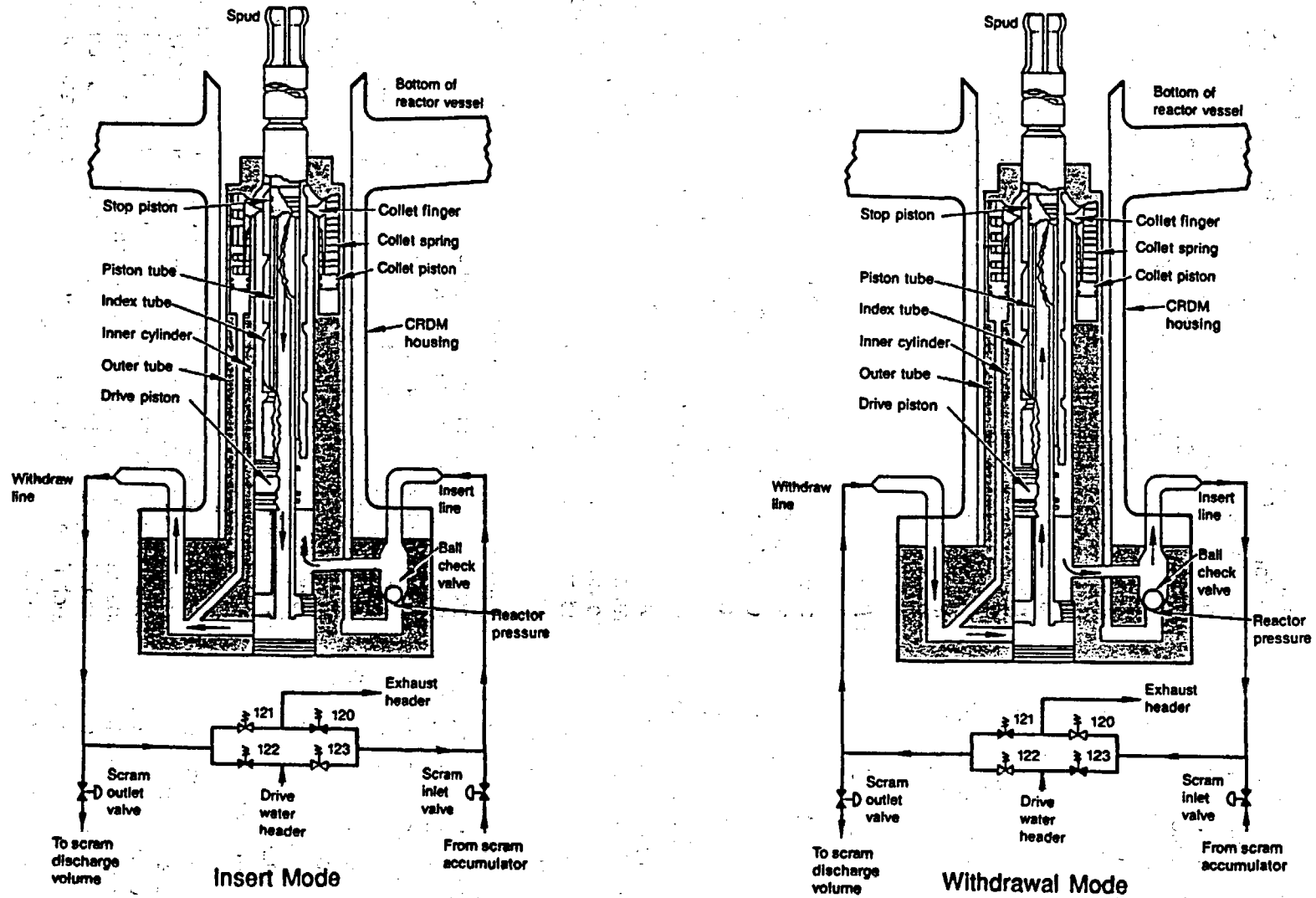


Figure 1. CRDM operation: insert and withdrawal modes.<sup>1</sup>

## **CRDM Degradation: Causes and Corrective Actions**

As a whole, the 21 nuclear plants that responded to the CRDM aging workshop questionnaire reported a good performance history for the BWR control rod drive mechanisms. NPRDS data analysis confirms this observation, with 72% of the failure reports being discovered by scheduled testing or routine observation, 24% by control room personnel, and only 2% as a result of a failed service demand (the remaining 2% of the NPRDS reports did not identify a discovery method in the failure narrative). The term "failure" applied in these NPRDS case histories refers to a component that did not perform its design function and does not necessarily imply the occurrence of an operational event.

Workshop participants were also asked to share their observations regarding the primary causes of CRDM aging. In addition to normal service wear, the reported causes of CRDM degradation are Graphitar seal embrittlement, fatigue fracture, and thermal degradation, collet housing cracking, nitrided surface corrosion, human errors made during drive changeout and rebuilding activities, and, to a lesser extent, plastic deformation due to improper storage methods.

### *Water Chemistry, Corrosion, and IGSCC*

Poor plant water chemistry has been a primary contributor to corrosion and "crud" formation (dirt particles, debris, and foreign materials that are found in varying amounts in the coolant). Corrosion usually occurs first on CRDM components having nitrided surfaces: the index tube, piston tube, guide cap, and collet assembly. Debris becomes entrapped in the CRDM during normal operations, and its presence scars metal surfaces and defaces the Graphitar seals. As crud accumulates in the CRDM, the device's coolant flow rate may decrease and cause drive temperatures to increase, thus contributing to the thermal degradation of the seals. After a scram, coolant flow rates may increase and CRDM temperatures decrease because some of the crud has been "shaken out" of the drive. In addition, entrapped crud in the Graphitar seal seating surfaces (on the drive and stop pistons) creates uneven force distributions that can cause seal breakage during scrams.

To reduce the amount of crud that can become entrapped in the CRDM, some utilities are vacuuming the bottom of the reactor vessel in and around the guide tubes during refueling operations. In addition, the pre-BWR-6 design CRDMs had problems with the cooling water orifices becoming plugged with crud, which caused increased operating temperatures. Many utilities have retrofitted the older CRDMs with upgrade kits that modified the design of the cooling water orifice to mitigate this potential problem. Water chemistry has also been modified by the addition of hydrogen in at least nine BWR facilities to reduce the potential for corrosion in the primary coolant system. However, one workshop attendee reported that their plant management was considering discontinuing this practice because an increase in system radioactivity levels had been observed since its incorporation.

Nitrided surface corrosion has also been aggravated by poor storage methods. Occasionally, CRDMs are stored wet in air for more than 30 days before they can be rebuilt, usually due to strained outage schedules. The nitrided surfaces of the CRDMs begin to corrode, and the drive becomes excessively hard to disassemble for rebuilding. CRDM components can be inadvertently damaged during a difficult disassembly process from mishandling. One utility is currently employing a long-term storage technique which places its "dirty" CRDMs in an aqueous solution of triethanolamine, a corrosion inhibitor, so that they can be rebuilt during the next outage,

just prior to installation. Since there will be radioactive decay during the twelve to eighteen months of storage, it is hoped that the doses obtained from rebuilding these CRDMs will be lower than if they had been rebuilt soon after they were pulled from the vessel. According to attendees at the workshop, this method of storage has been used several times before without any noticeable component deterioration.

Significant numbers of CRDMs have been retired from service due to collet housing cracking. This intergranular stress corrosion cracking (IGSCC) phenomenon has been found in the model A, B, and C drives that were originally installed in BWR-2, -3, -4, and -5 plants. One utility reported in the questionnaire that 46% of the cylinder, tube, and flange assemblies in its CRDMs had to be replaced because of this type of degradation. Later CRDM designs (models D, E, and F) that were supplied in BWR-6 plants changed this component's material from a 304 to a 304L stainless steel. These improved models have not experienced this problem. Utilities observing collet housing cracking in their drives have either replaced affected CRDMs with the later model drives or improved the earlier models with upgrade kits from the vendor.

#### *Radiation-induced Effects*

Radiation-induced degradation is suspected to be the cause of certain effects observed in the spud, the CRDM component that engages the control rod assembly blade via the uncoupling rod. There have been reports of the "fingers" of this Inconel X-750 component being easily bent after a prolonged service history (> 15 years) in the reactor vessel. CRDM rebuilding technicians have described the effect as "the fingers losing their memory." The strength and resilience, which normally typifies parts made of this alloy, no longer remains. Although no professional metallurgical examinations have been performed on these components, the cause of this phenomena is speculated to be neutron annealing, because the observed effects are similar to those recorded by researchers who irradiated different reactor materials to low dose ( $<10^{20}$  neutron  $\text{cm}^{-2}$ ), thermalized neutrons <sup>2</sup>. With this type of material degradation, spud fingers can become deformed in-service and lose their concentricity, as shown in Figure 2. This type of spud damage can present a myriad of coupling and uncoupling difficulties with the CRA. The spud, like all CRDM components, can be exchanged with a new spare part during rebuilding activities.

#### *Nitrided Surface Degradation*

In some CRDMs having a continuous service history greater than 15 years, degradation of the nitriding has been observed to the extent that, in one particular example, the unusually rough surface of an index tube could be easily scored with a piece of wood.<sup>3</sup> Although no formal metallurgical investigations have been conducted to determine the nature of this effect, it could be the result of a combination of causes: prolonged radiation exposure, poor water chemistry, and variations in the case hardening from the nitriding process. No operational problems were reported for the CRDM whose "striped" index tube is shown in Figure 3, but the component was not reused in the rebuilt device because its continued serviceability was considered questionable.

#### *Graphitar Seal Wear and Breakage*

Replacement of the Graphitar seals is a standard requirement during CRDM rebuilding activities. An intact and correctly seated seal allows differential hydraulic pressures (upon withdrawal, insert, and scram signals) to position the drive. As these seals degrade and become less effective, i.e., become broken, scarred, or chipped due to numerous scram impacts, undergo

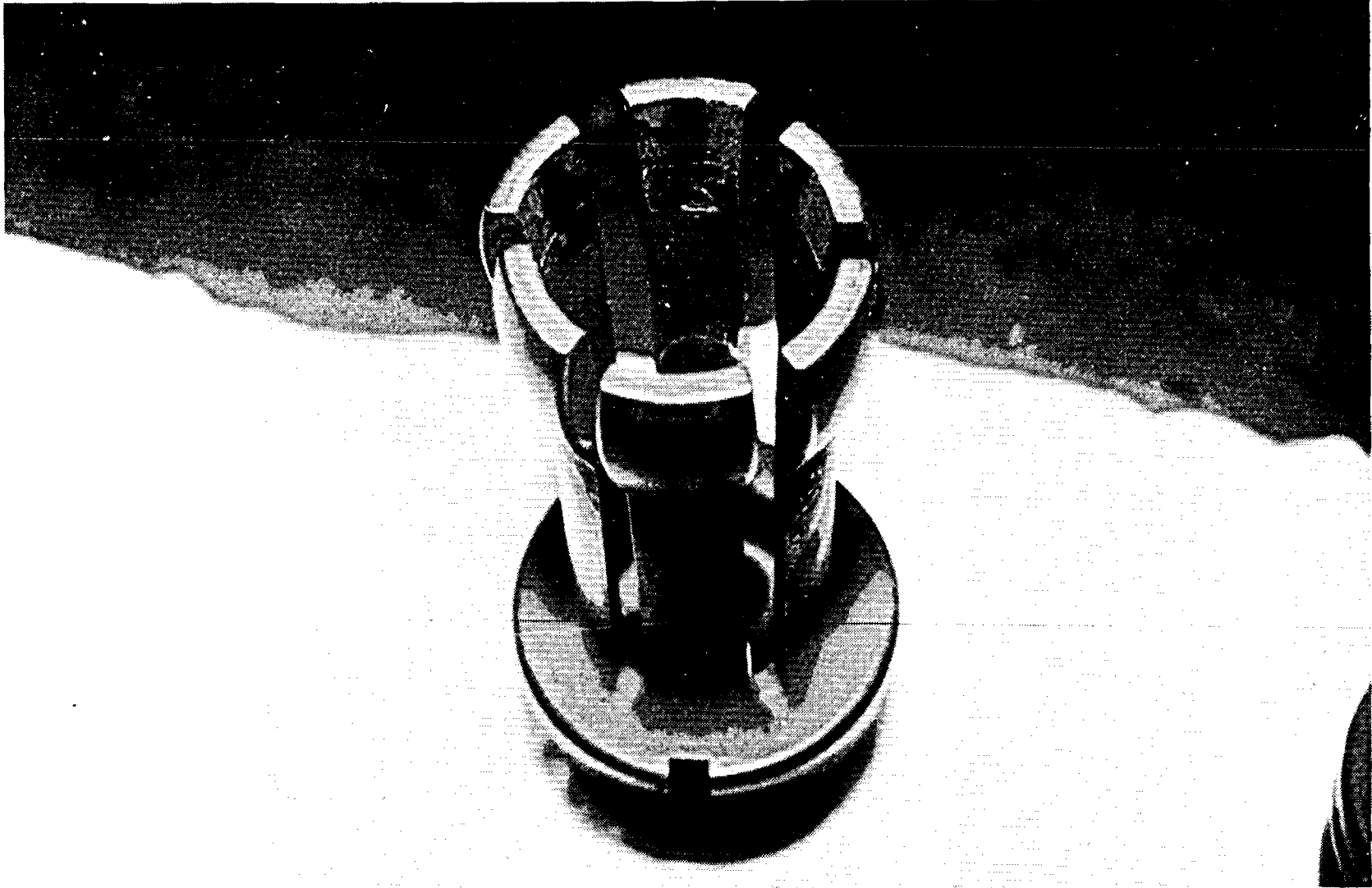


Figure 2. Bent CRDM spud fingers (notice lack of concentricity).



Figure 3. CRDM index tube surface degradation (notice striping left by collet fingers).

normal surface wear, or experience thermal degradation (caused by drive temperatures greater than 350° F), the CRDM's stall flows increase and greater hydraulic pressures are required to maneuver the drive. There were 275 NPRDS failure reports that cited Graphitar seal wear as the cause of deteriorating CRDM performance. The predominant location of the seal failures was on the stop piston. CRDM withdrawal stall flows over 5.0 gpm (not attributable to the valving configuration on the HCU) are considered indicative of deteriorated seals that need to be replaced. Both General Electric and the Toshiba Corporation have developed improved Graphitar seals designed to be more durable and have a longer service life than those currently used in domestic BWR CRDMs. General Electric's new CRDMs are equipped with these improved seals, but an improved replacement seal kit for earlier models is currently not available to utilities.

#### *Inner Filter Disengagement*

Each CRDM has an inner and outer filter which serves to collect debris from the cooling water and reactor water that might otherwise damage the CRDM. The inner filter has been attributed with 90 failure reports in the NPRDS. Installation and maintenance errors were cited in 35 cases. Inner filters that are incorrectly installed during CRDM rebuilding can become loose during drive operation and cause the CRA to uncouple itself from the CRDM's spud. Uncoupling is a symptom observed in 27 of these reports.

The inner filter is mechanically attached to the stop piston by means of a spring clip (Fig. 4). When assembled, the inner filter engages the piston connector knob and is retained by locking flats that capture its spring clip after the filter is pushed onto the piston knob and rotated about 90° (Fig. 5). To test the proper installation of the inner filter, General Electric recommends using a filter assembly tool to pull the inner filter away from the stop piston with a force of about 20 to 30 pounds. After engagement has been verified, the tool is removed from the CRDM, sometimes with an unintentional jiggling or twisting motion. When this is done, the filter becomes improperly oriented and can easily be disengaged. Even if the filter is not fully rotated 90°, the filter may be inadvertently rotated more during CRDM rebuilding and handling activities.

After this CRDM has been placed into service, a long, continuous withdrawal signal can cause the disengaged inner filter to become buoyed. Hydraulic pressures push the filter against the uncoupling rod, lifting it upwards and pushing the locking plug above the spud fingers. At this point uncoupling may occur. Even if operations personnel succeed in recoupling the drive with the CRA, repeated uncoupling and recoupling caused by a disengaged inner filter can result in a bent uncoupling rod.

The Toshiba Corporation has instituted a modification in its inner filter's base configuration in order to provide an improved design that would prevent uncoupling trouble due to misassembly. To date, there have been no design enhancements made in the attachment configuration of inner filters used in CRDMs operating in US BWRs that would circumvent this type of disengagement.

#### *Improper CRDM Storage Methods*

The 15-foot-long, 450-pound CRDM can be a challenge to store. Inadequate storage support has been blamed for a few observed cases of CRDM "sagging", which were confirmed by performing runout measurements along the length of the drive. Utilities store CRDMs in shielded vaults, on specially built racks, and sometimes in their original shipping crates. CRDM components can be damaged by laying drives on the floor with only the collet housing and the flange end supporting the weight as shown in Figure 6. CRDMs should not be stacked on top of each other,

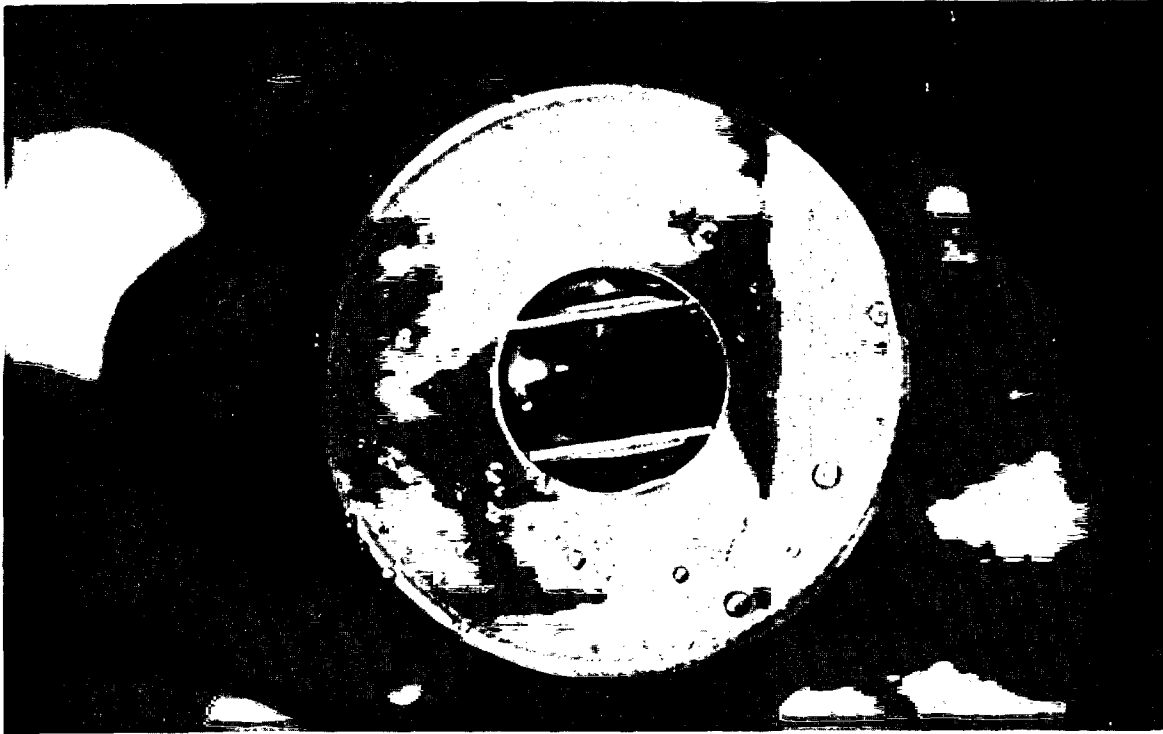


**Figure 4. CRDM inner filter spring clip.**

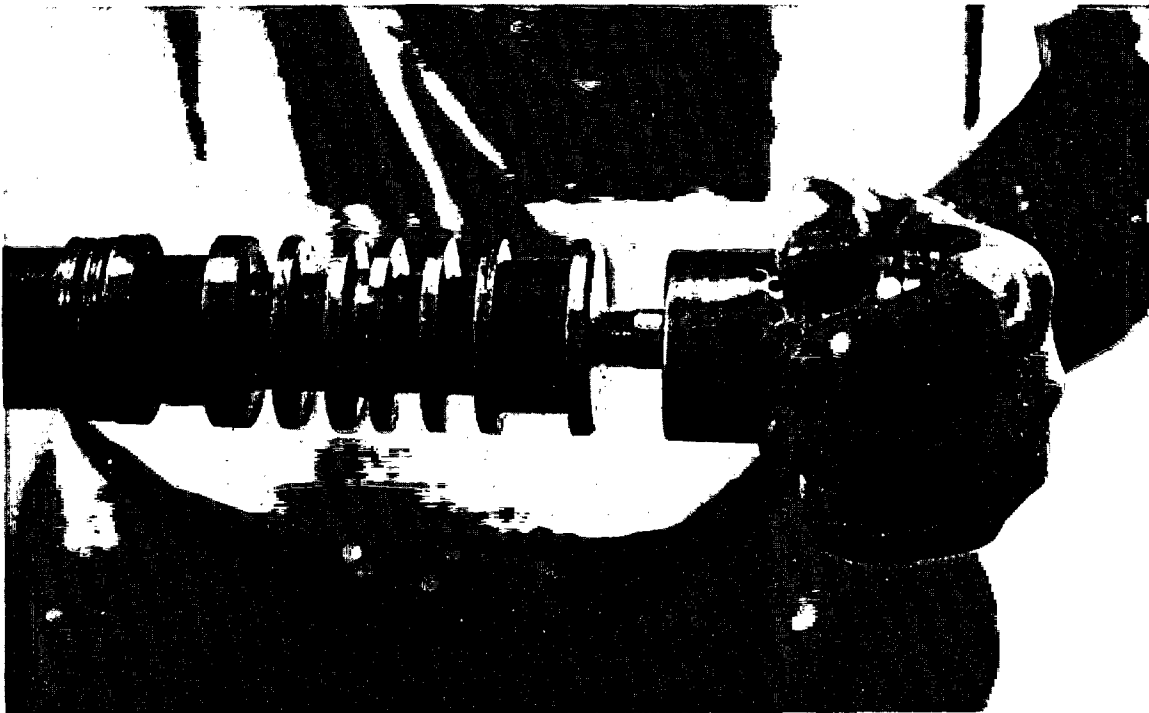


**Figure 5. Attachment of inner filter to stop piston.**

separated by wooden blocks, which, in essence, transmits the weight of the stack to the lowest drive. Heavy, lead shielding "pigs" are sometimes left hanging on the spud end of "hot" drives for long periods of time, which places a moment on the collet housing. As shown in Figure 7, CRDMs should be stored in racks or vaults with a minimum of 2 points of support located 24 inches from the flange end and 54 inches from the spud end.

### **HCU Degradation: Causes and Corrective Actions**

The NPRDS analysis yielded specific information on HCU degradation. Over 59% of the CRD system failures are attributable to the HCU. The HCU components requiring the most maintenance and replacement (as reported in the NPRDS) are identified in Figure 8. The following information discusses the HCU components requiring the most maintenance and the causes of their aging.

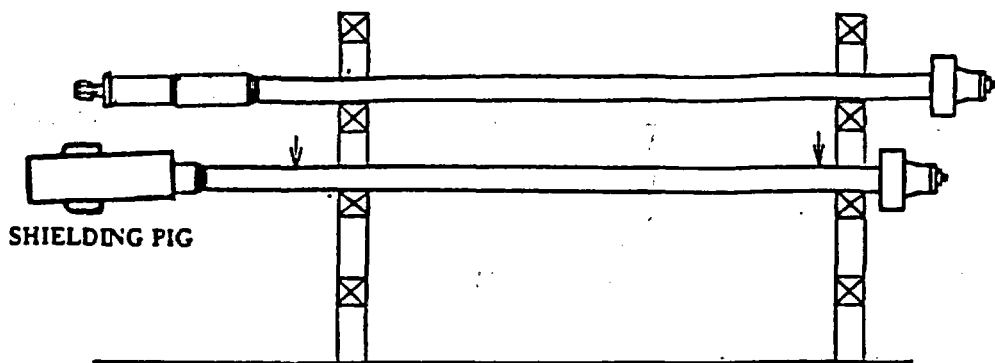
#### ***Accumulator Nitrogen Charging Cartridge Valve (HCU part no. 111)***

There were 526 NPRDS failure reports on this particular valve. The leading reported cause of failure was attributed to worn valve packing (189 cases -- 36%). Normal valve wear or aging was "runner-up" in the cause category (164 cases -- 31%), and a worn valve stem ranked third among failure causes (71 cases -- 14%). Additional reported failure causes were multiple-cause valve aging (cites the failures of several valve parts), valve seat aging, and worn valve seals.

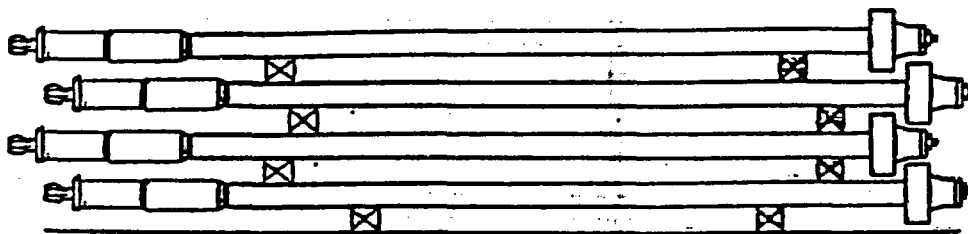
The cartridge valve is located at the bottom of the HCU on the instrumentation block. This component is frequently referred to as the "star valve" because of the shape of the hand crank on the stem. Many of the failures of the "U-cup" packing may be attributed to incorrect installation. General Electric manufactures a four-part packing installation tool that was specifically designed to replace the U-cup packing in this valve. If the packing tool is not used when repacking the valve, it is easy to damage the packing on the valve stem threads during installation and create a new leak. It has also been reported that utility maintenance personnel occasionally adjust the star valve with their foot, rather than bending over and using their hand. This practice could easily bend the narrow valve stem in addition to damaging the packing.

#### ***Scram Water Accumulator (HCU part no. 125)***

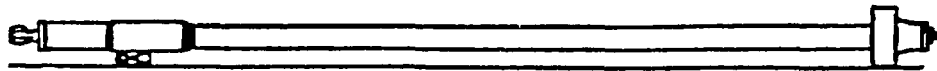
The NPRDS has recorded 189 failure reports of this component with 119 of them requiring replacement units. In the pre-BWR-6 models, the chromium plating liner of this carbon steel tank is porous enough to allow water to seep in and cause corrosion of the carbon steel. General Electric issued a service information letter regarding the interior surfaces of these accumulators and determined that high-chloride, low pH water conditions would produce blistering and pitting of the plating throughout the cylinder. It was further reported that loose flakes of this plating may leave the accumulator and collect on the Teflon seat of the inlet scram valve and cause some leakage. If this occurs, it can result in control rod insertion. In addition, the tank's corrosion flakes can etch Teflon from the scram valve seat and subsequently become entrapped in the cooling water orifice of the companion CRDM. General Electric and the Toshiba Corporation have developed stainless steel replacement units for this component. The predominant symptom of accumulator degradation reported in the NPRDS is a high water level alarm for the accumulator.



**IMPROPERLY SUPPORTED CRDMs  
WITH ADDITIONAL WEIGHT FACTOR**



**IMPROPERLY SUPPORTED CRDMs  
WITH STACKING BLOCKS**



**IMPROPERLY SUPPORTED CRDMs**

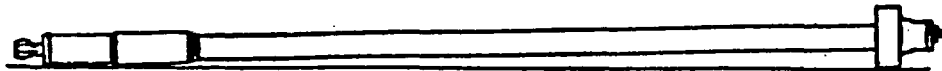


**Figure 6. Improper CRDM storage scenarios.<sup>3</sup>**

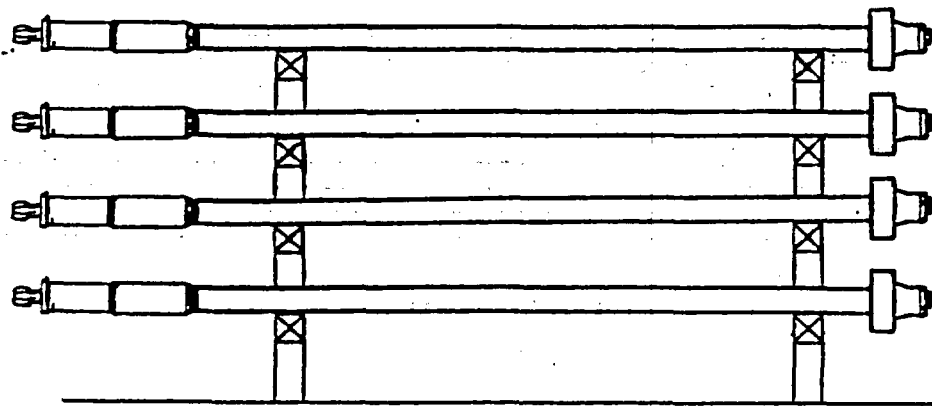
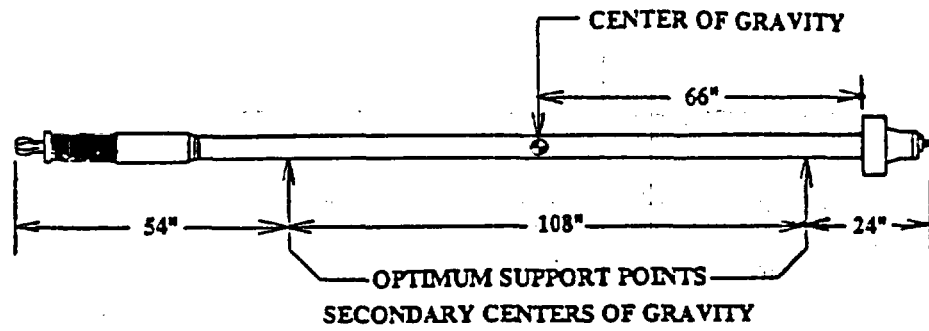


Figure 7. Acceptable CRDM storage arrangement.<sup>3</sup>

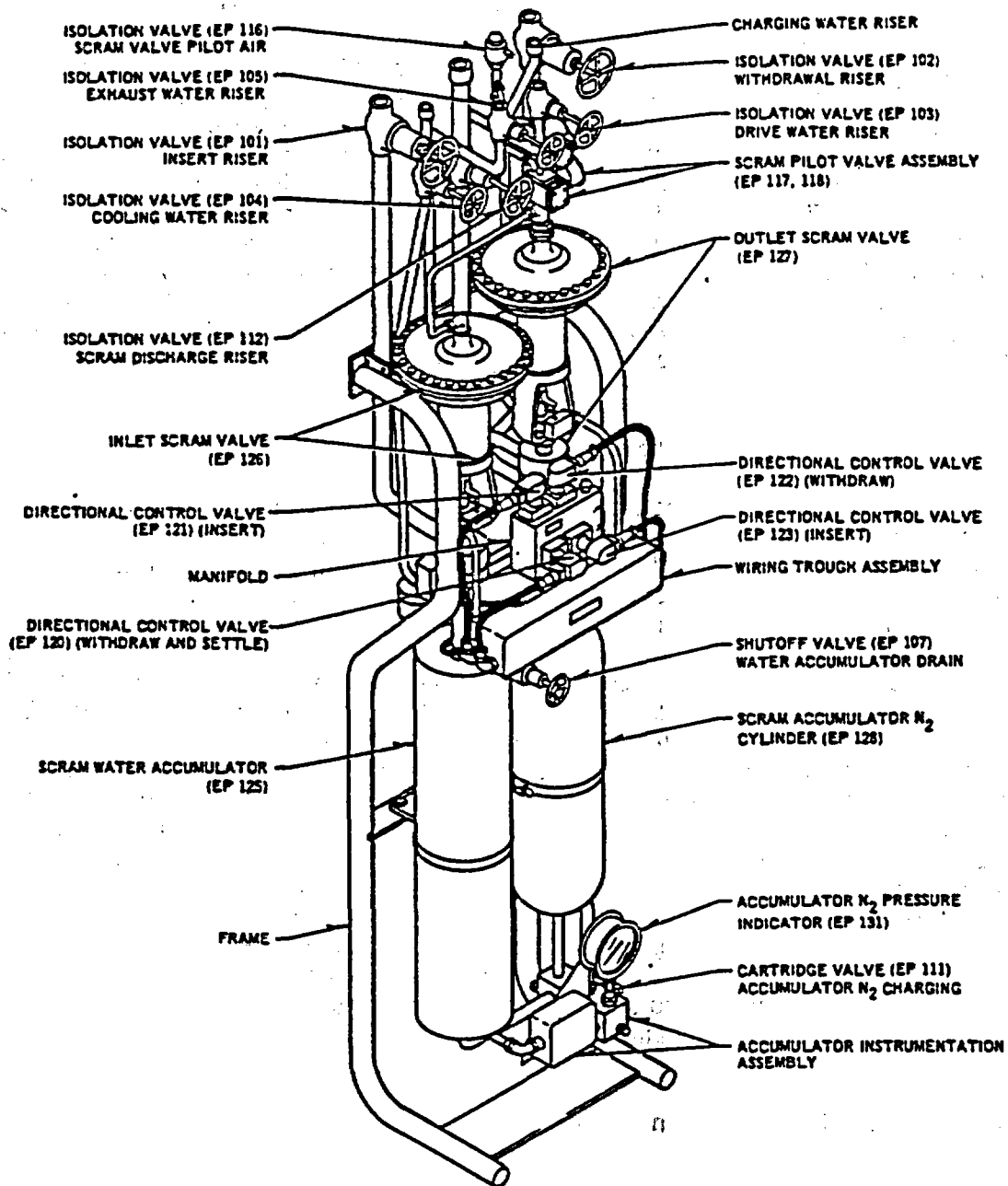


Figure 8. A BWR hydraulic control unit (HCU) and its components.<sup>5</sup>

### *Inlet and Outlet Scram Valves (HCU part nos. 126 and 127)*

There were 129 failure reports on the inlet scram valve (No. 126). The primary causes of degradation identified in the NPRDS were aging of the valve seat, multiple valve parts aging, worn valve packing, and worn valve diaphragms. Almost 65% of these reported failures have required valve rebuilding or replacement. As previously discussed, flakes of plating from a corroded accumulator can collect and erode the Teflon seat of this valve. In addition, the diaphragms of this valve are made from Buna-N reinforced with nylon. In a service information letter issued on this valve, General Electric recommends the lifetime (elapsed time between diaphragm cure and installation plus time in service) of this component to be 15 years for BWR/2s through BWR/5s and 12 years for BWR/6s. A supplemental service information letter from General Electric also stated that the nylon fibers around the diaphragm center hole on the Hammel-Dahl scram valve diaphragms could be damaged by the valve stem thread during diaphragm installation if the stem nut is tightened with the spring force applied under the diaphragm button. The outlet scram valve (No. 127) had 77 failure reports that cited incorrect operation, worn seats, worn diaphragms, and worn stems and packing. More than 85% of the outlet scram valve failures reported in the NPRDS have required rebuilding or replacement to restore service.

### *Scram Pilot Valve Assemblies and Solenoids (HCU part nos. 117 and 118)*

There were 71 and 69 failure reports on the Nos. 117 and 118 valves, respectively. The causes of failure observed most frequently for this valve were a worn diaphragm, aged solenoid components (such as a coil "short" or a "blown" fuse), and normal valve wear or aging. The scram pilot valve solenoids had 241 reports of failure (185 by one plant) that cited the primary causes of failure as a worn seat (or disc). General Electric issued a service information letter indicating that cracking of the Buna-N rubber discs had been observed at a BWR plant causing delays in CRDM scram times. The cracking and deterioration of the Buna-N disc material was accelerated by long-term exposure to the heat of the normally energized solenoid coil. Since there is a continuous heat source from these normally energized solenoids, utilities could periodically monitor and trend surface temperatures to detect coil degradation, which was cited as the secondary cause of failure for these valves (increasing temperatures can indicate imminent coil failure)<sup>4</sup>. Industrial pyrometers could be used to obtain these data. General Electric also recommended in a service information letter that all BWR utilities establish a preventive maintenance program to replace all core assemblies, diaphragms, and associated parts in all CRD scram pilot valves, backup scram valves, and scram discharge volume test valves at periodic intervals since the Buna-N parts in these valves have a combined 7-year shelf and in-service life that elapses from the packaging date on the rebuilt kit. The symptoms of scram pilot valve and solenoid degradation include slow scram times, leaking air, and abnormal solenoid noise (chattering rattling, or ac hum).

### **Balance-of-CRD-System Component Failures**

If failure report cited in the NPRDS was not attributed to a component associated with either the HCU or the CRDM, this analysis effort classified it as a balance-of-CRD system (BOCRDS) component failure. Only 18% of the failures reported in the NPRDS were attributed to components comprising this category. The following paragraphs discuss those component categories which had the higher numbers of failure reports.

### ***CRD System Pumps and Pump Components***

The CRD system pumps and pump components had 117 failure reports in the NPRDS. Worn bearings, seals, piping and parts erosion, looseness, and normal wear or aging are the most prevalent problems identified in this data base. Over 98% of the pump failures were discovered by testing or routine maintenance. Several U.S. utilities (both BWR and PWR) have instituted monthly-to-quarterly vibration signature analysis programs on various types of rotating machinery in their stations as part of their overall maintenance and ALARA reduction efforts. Bearing anomalies, misalignment, unbalance, looseness, and soft foundations are readily analyzed and diagnosed using fast Fourier transform (FFT) analysis. Other programs augment their diagnostics by utilizing oil analysis to examine metallic parts degradation. Although there have been a few CRD pumps completely changed out, pump components have normally been replaced on an "as-needed basis" to restore service, and occasionally, entirely rebuilt.

### ***Miscellaneous Scram Discharge Volume Valves***

There were 44 failure reports on valves associated with the scram discharge volume. In 25% of these cases, the valve actuator or operator was simply out of adjustment. Over 27% of the reports cited entrapped debris causing component failure. One station reported corrosion and entrapped debris on the scram discharge volume vent valve due to a failure in procedures to regularly cycle the valve. To mitigate buildup of debris, procedures were enhanced to require quarterly timing and results trending of valve actuation. Another station reported a failure of the scram discharge volume drain valve caused by an accumulation of dirt and corrosion on the seat surface. The failure narrative reported that the maintenance staff felt this may have been caused by a prolonged shutdown. The majority of these valve failures (80%) required valve rebuilding or replacement.

### ***HCU and BOCRDS Electrical Components***

This section groups the results of the electrical component failures for the HCU and CRD system, including any electrical components associated with the CRD pumps. The group includes the reported failures of electrical relays, switches, controllers, transmitters, power supplies, circuit breakers, and fuses. There were 207 failures altogether comprising 65 reports attributed to the HCU and 142 associated with the BOCRDS. There were no electrical component reports on the CRDM. The predominant causes of failure in these areas were cited as electrical component aging and the device being out of calibration (includes setpoint drift). As might be expected, the component was restored to service either via adjustment or complete replacement.

### ***CRD System Instrumentation***

There were 79 reports of failed gauges and instrumentation in the entire CRD system. As in the case of electrical components, the predominant causes of failure identified in the NPRDS were electronic component aging and out-of-calibration. Over 91% of these failures were corrected by an adjustment and the remainder required a like-for-like replacement.

### ***Selection Criteria for CRDM Changeout and Rebuilding***

There is much debate regarding the criteria applied by utilities to select CRDMs for changeout and rebuilding. Although there are many contributing factors that may vary the rate and effects

of CRDM aging, the historical recommended maintenance interval of a CRDM has been ten years. With this figure in mind, many utilities have designed CRDM changeout schedules to reflect a 100 percent rebuild of all CRDMs in the reactor every ten years. Other utilities, that are rigorously and routinely monitoring and trending stall flow rates, operating temperatures, and acquiring friction traces of their CRDMs, feel they can confidently assess the operability of their CRDMs without scheduling drives for maintenance based solely on elapsed service time. The workshop reviewed the CRDM changeout history for 20 BWR units. The data suggests that centrally located drives undergo more maintenance than peripheral drives. Attendees at the workshop stated that not all the CRDMs that had been changed out exhibited operational problems, and that, frequently, operational problems had been erroneously attributed to CRDMs that should have really been directed at components on the companion HCU.

The selection of CRDMs to be rebuilt can be initiated by classifying drives into two groups: *Priority 1 CRDMs*, those drives which must be exchanged or rebuilt, and *Priority 2 CRDMs*, those drives which should be exchanged or rebuilt, and incorporated into the outage schedule if at all possible. Attendees at the workshop agreed on the following operational characteristics that would place suspect CRDMs into these two categories:

Table 1 - Characteristics of Priority 1 CRDMs -- Must be Exchanged or Rebuilt

1. Excessive scram times - violation of plant technical specifications.
2. CRDM does not fully insert during a scram.
3. CRDM has a history of uncoupling.
4. CRDM will not go into position 48 (fully withdrawn).
5. CRDM consistently has a withdrawal stall flow greater than 5.0 gpm.

Table 2 - Characteristics of Priority 2 CRDMs -- Should be Exchanged or Rebuilt

1. Consistently high temperatures throughout length of travel (>350° F).
2. Unacceptable withdrawal or insertion times that are unrelated to the HCU.
3. Repeated episodes of "double-notching" when moving, or CRDMs that continually require increased drive pressures to move (unrelated to the HCU).
4. CRDMs with high or abnormal friction traces not attributable to misalignment with fuel assemblies.

Attendees at the workshop also stated that when CRDMs began to display operational problems, several of the anomalies listed in Tables 1 and 2 would usually be manifested concurrently. For that reason, many utilities choose to rebuild CRDMs if they display *any* of the operational characteristics mentioned in these categories, and might also include those drives that have a continuous service time of ten years. Most CRDM operational problems, however, do have a long lead time and do not suddenly occur without exhibiting characteristic warning signals.

### **ALARA Reduction During CRDM Changeout and Rebuilding**

Workshop attendees commented that CRDM changeout and rebuilding is one of the highest dose, most physically demanding, and complicated maintenance activities routinely accomplished by BWR utilities. In the 30 years since the BWR design concept for commercial nuclear power production was first successfully demonstrated, there have been many enhancements in the maintenance techniques used to pull and refurbish CRDMs. However, some utilities have not taken advantage of new tooling and continue to use outdated maintenance equipment, which still adequately performs the task, yet inevitably results in higher doses delivered to the nuclear worker. According to questionnaire responses and nuclear commercial services input, substantial ALARA reduction can be realized by focusing improvements in three key areas associated with CRDM maintenance work: CRDM handling and exchange tools, worker comfort and environment, and worker training.

#### *CRDM Handling and Exchange Tools*

There are currently five different companies offering pneumatically or hydraulically operated devices which can be placed in existing BWR undervessel work platforms to assist CRDM personnel with changeout activities. They replace conventional, electrically driven winch systems supplied with the plants and require only two technicians for equipment operation. More than half of the sites responding to the questionnaire stated that they had either purchased or contracted the use of this type of device in their CRDM changeout work, and also verified that it had significantly improved the performance of CRDM maintenance. Most further stated that this type of device had reduced job-related exposures, with two plants reporting overall exposure reductions of 38 and 56 percent.

#### *CRDM Worker Comfort and Environment*

The CRDM Aging Questionnaire asked utilities to indicate which conditions during CRDM changeout had the most influence toward improper CRDM maintenance. High temperatures were recognized by 65 percent of those participants as having the biggest negative impact on worker performance. In addition, high radiation levels (creating, in some cases, a false sense of urgency in workers not accustomed to this type of work), extremely cramped working conditions (a person works "hunched over" for long periods of time during changeout operations), poor vision (obstructed from instrumentation cabling and hampered by insufficient lighting), and inadequate communication were prevalent conditions that further complicate an already complex task. Other job location factors contributing to mishandling errors were disorientation, remoteness, cumbersome protection clothing, and visual impairment during CRDM "rainshowers" (the normal 2 to 3 gpm leak of reactor water when drives are removed from the vessel).

There are several utilities which have invested much time and money into developing improved maintenance conditions for CRDM changeout work. Some plants have revised and streamlined procedures, while others are testing new designs of radiation protection clothing, portable air conditioning apparatus, installing temporary lighting, and developing specialized tools for these tasks. The overall consensus of the workshop attendees was that any utility which sought ways to improve worker comfort during these activities would realize benefits not only in ALARA reduction but also in fewer maintenance errors.

### *CRDM Worker Training*

CRDM worker training, particularly with undervessel mockups, improves crew performance and helps expedite tight outage schedules. "Full-rad dress" rehearsals are particularly valuable in acquainting technicians with working under restrained conditions. Both the CRDM changeout and rebuild crews should receive specialized training to correctly perform these tasks. More than half of the participants responding to the questionnaire either trained their own crews on mockup assemblies or employed contractors that had completed similar training. Many of the utilities provide three to five days of training to crews involved in changeout and rebuilding activities. In some cases, shortened "refresher" courses are provided to those personnel with previous experience. Several utilities stated that the training also involved individual testing. All of those utilities providing training or using specialized crews verified that these activities yielded improvements in job performance. Other benefits mentioned were reductions in radiation doses, increased worker safety, improved worker attitude, and fewer rebuild errors.

Other modifications made by utilities to reduce radiation exposures acquired during CRDM changeout and rebuilding activities include:

- Inner and outer filters were discarded as waste rather than cleaned.
- Shielded inner and outer filter removal tools were used.
- Flush tanks were used during CRDM rebuilding activities.
- Installed ALARA shielding achieved reductions at several sites that historically have "hot" drives.
- Shielded storage racks and/or customized concrete vaults have been built into CRDM rebuilding rooms.
- Remote cameras installed under the vessel and in the rebuild room have helped to better coordinate activities, save time, and reduce exposures.

## Conclusions

As a whole, BWR control rod drive mechanisms have a good service record at U. S. nuclear plants. The BWR-6 design CRDMs have incorporated modifications that have eliminated problems experienced by the earlier models. The primary causes of CRDM aging are embrittlement, fatigue fracture and thermal degradation of the Graphitar seals, nitrated surface corrosion, mishandling and rebuilding errors occurring during CRDM maintenance and, to a lesser extent, improper storage support. According to NRPDS failure reports, the majority of maintenance for the CRD system occurs on the HCU. The HCU components reporting the most failures are the scram water accumulator, the accumulator nitrogen charging cartridge valve, the inlet and outlet scram valves, and their scram pilot valve assemblies and solenoids.

CRDM changeout and rebuilding activities occur at all BWR nuclear plants, but with varying amounts of worker exposures and time expended on the removal and refurbishment of drives. Many utilities are seeking ways to improve their overall CRDM maintenance processes. Some plants are aggressively pursuing ways to reduce radiation exposures acquired during CRDM maintenance by installing state-of-the-art tooling, improving worker comfort, and increasing maintenance training.

## References

1. *Residual Life Assessment of Major Light Water Reactor Components -- Overview*, V. N. Shah and P. E. MacDonald, Editors, NUREG/CR-4731, November 1 1989. Available for purchase from the National Technical Information Service, Springfield, Virginia 22161.
2. *Effect of Prior History on the Response of Some Commercial Aluminum Alloys to Low Dose Neutron Irradiation*, Z. H. Ismail and H. G. Mohammed, Nuclear Research Center, Atomic Energy Commission, Cairo, Egypt. *Scripta Metallurgica*, 1989, Vol 23, pp 2067-2072. Available for purchase from Pergamon Press, New York.
3. *Control Rod Maintenance Strategies*, presented by Lee Penney at the ORNL Workshop on Control Rod Drive Aging, January 30, 1991. Available from Nuclear Energy Services, Inc., Danbury, CT.
4. *Aging and Service Wear of Solenoid-Operated Valves Used in Safety Systems of Nuclear Power Plants*, Vol. 2: Monitoring Methods Evaluation," R. C. Kryter, NUREG/CR-4819, Vol.2, September 1991. Available for purchase from the National Technical Information Service, Springfield, Virginia 22161.
5. *Operation and Maintenance Instructions for Hydraulic Control Unit Part Nos. 729E950G1 through G6*, GEK-9582A, General Electric Company, San Jose, CA.

# THE EFFECT OF AGING UPON CE AND B&W CONTROL ROD DRIVES

Edward Grove and William Gunther  
Brookhaven National Laboratory  
Upton, New York 11973

## ABSTRACT

The effect of aging upon the Babcock & Wilcox (B&W) and Combustion Engineering (CE) Control Rod Drive (CRD) systems has been evaluated as part of the USNRC Nuclear Plant Aging Research (NPAR) program. Operating experience data for the 1980-1990 time period was reviewed to identify predominant failure modes, causes, and effects. These results, in conjunction with an assessment of component materials and operating environment, conclude that both systems are susceptible to age degradation. System failures have resulted in significant plant effects, including power reductions, plant shutdowns, scrams, and Engineered Safety Feature (ESF) actuation. Current industry inspection and maintenance practices were assessed. Some of these practices effectively address aging, while others do not.

## Introduction

The Babcock & Wilcox (B&W) and Combustion Engineering (CE) control rod drive (CRD) systems consist of the mechanical and electrical components necessary to position the control rod assemblies in the core in response to automatic or manual reactivity control signals. Both systems are designed to provide a rapid insertion of the control rods upon loss of AC power. As part of the USNRC Nuclear Plant Aging Research (NPAR) program, the design, materials, maintenance, and operation of both designs were evaluated to determine the potential for age degradation.

The system boundaries used for this aging study included the control rod drive mechanisms (CRDMs), CRDM power and control systems, rod position indication systems, CRDM cooling systems, and the control rod assemblies. The fuel assembly and upper internal guide tubes were also included, since failure of these components could preclude control rod insertion.

## System Design

Reactivity control in B&W reactors is supplied by a combination of control rod assemblies (CRAs) and axial power shaping rod assemblies (APSRAs). Each B&W control rod assembly consists of sixteen individual poison rods connected to a spider assembly which geometrically arranges the rods for insertion into the fuel assembly guide tubes. The spider assembly also provides for attachment between the CRA and the CRDM leadscrew. APSRAs mechanically resemble the CRAs, and are used to control the axial power shape across the core during the fuel cycle. The APSRA drive mechanisms are modified to prevent them from inserting rapidly during a reactor scram.

All eight of the B&W plants use the roller nut type CRDM. These consist of an electrically driven, rotating nut assembly within the primary coolant pressure boundary; a four pole six phase,

water cooled, stator; and a translating leadscrew which converts the rotary motion of the nut assembly to linear travel of the leadscrew and CRA. The CRDMs are flange mounted on top of the reactor vessel head, allowing for removal and maintenance without compromising system integrity. A vent valve located on top of the CRDM allows for remote coupling/decoupling of the CRA and bleeding all non-condensable gases from the top of the vessel following reactor head removal.

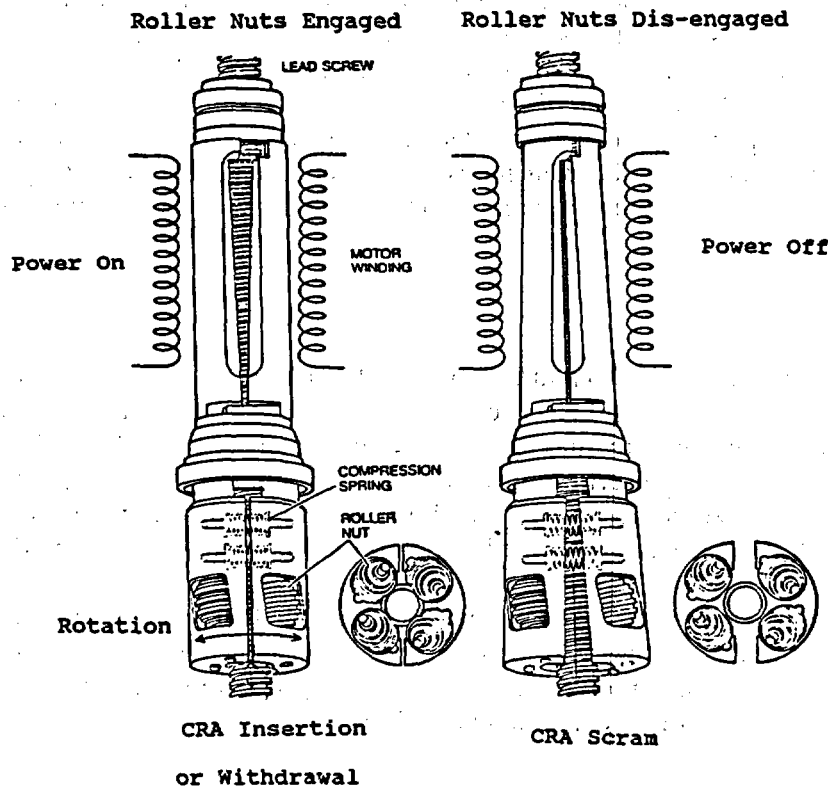


Figure 1. B&W Control Rod Drive Mechanism

When sequentially energized by the power and control system, the stator coils produce a rotating magnetic field which causes the roller nut assembly to engage and rotate about the leadscrew as illustrated in Figure 1. CRA motion results either into or out of the core, depending upon roller nut rotational direction. Magnetically actuated reed switches, located in a housing adjacent to the CRDM pressure housing, provide actual rod position indication. Demanded rod position is provided by monitoring the pulses supplied to the CRDM.

When compared to the B&W CRA design, each CE control element assembly (CEA) consists of fewer, but larger diameter, absorber rods. The CEAs consist of four, five, or twelve full and part length absorber rods attached to a spider. Each CEA is attached to a control element drive mechanism (CEDM) which is threaded and welded to the top of the reactor vessel head. All but two CE plants use the magnetic jack CEDM (Figure 2), consisting of four or five electrical coils which, when energized, actuate a series of grippers. The grippers engage a notched drive shaft to insert or withdraw the CEA. The gripper coils are cooled by a forced air cooling system. Similar to B&W, actual rod position is provided by a series of magnetically actuated reed switches, while the plant computer monitors the command pulses supplied to the coils to provide the demanded position.

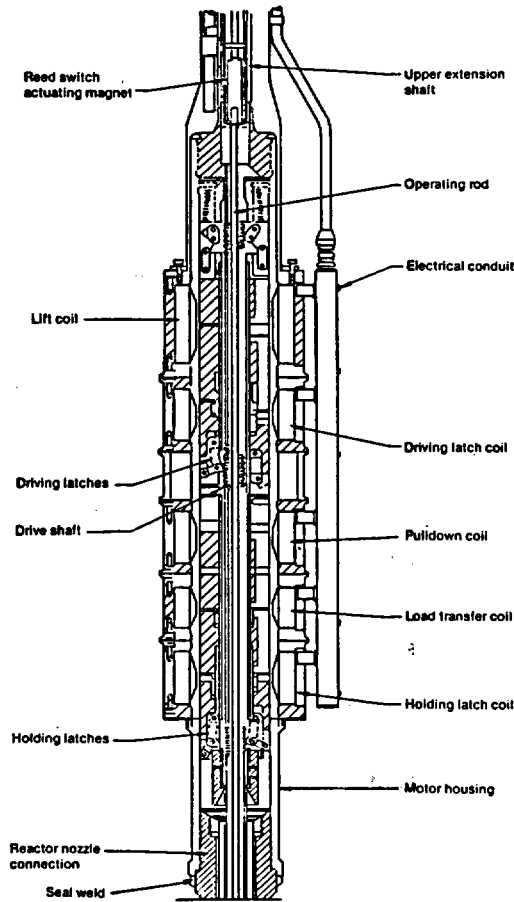


Figure 2. CE Magnetic Jack CEDM

Depending upon the vintage of the plant, CE has two power and control system designs. The older plants use the Control Element Drive System (CEDS), which supplies electrical signals to coil power programmers (CPP) which actuate the coils. The newer plants use the Control Element Drive Mechanism Control System (CEDMCS), which combines the CEDS and the CPP into one integrated system. Digital techniques are used in the CEDMCS to increase the accuracy and flexibility of the coil timing functions. CEDMCS also incorporates an on-line monitor to check and modify the voltage supplied to the coils to ensure proper functioning.

Palisades and Fort Calhoun are the two CE plants which use the rack and pinion type CEDM. This CEDM is an electric motor driven mechanism which has a drive shaft running parallel to the rack. The electric motor, operating through a gear reducer and magnetic clutch, drives the attached CEA. When the magnetic clutch is de-energized, the CEA inserts freely into the core.

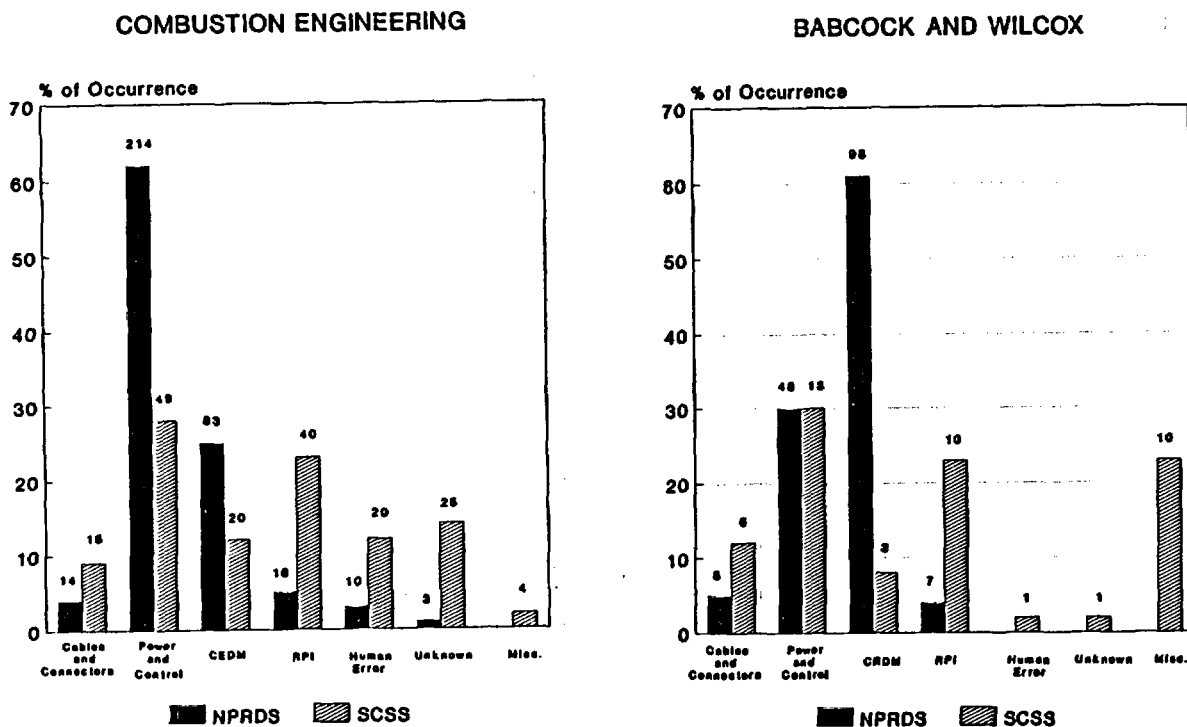


Figure 3. CRD System Failure Causes

### Operating Experience

A detailed operating experience review of three commercially available databases (Licensee Event Report or SCSS Database, Nuclear Plant Reliability Data System, and Nuclear Power Experience), plus applicable NRC and industry research was conducted to determine the affect of aging on the control rod drive systems for the 1980-1990 time period. As illustrated on Figure 3, degradation and failures of the power and control system accounted for the majority of CE CEDM failures. Failures of the CRDM accounted for the majority of B&W control rod drive system failures. The differences between the databases is due to the type of failures reported to each. Failures which occurred during plant operation, and directly affected the functioning of the system, were normally reported on an LER. Failures and degradation which were discovered at other times (outages, shutdowns, etc.), and did not affect plant operation, were normally reported to the NPRDS database.

As shown in Figure 4, aging was the direct failure cause for 40% of the CE power and control system failures, and 55% of the B&W CRDM failures as reported to the NPRDS database. Also a significant percentage of the reported failures were classified as "potentially due to aging." This reflects the reported failures with no defined cause. When compared to similar failures at other plants, which were identified as being the result of aging, engineering judgement dictates that a majority of these unknown failure cause events were also due to aging. However, no such assumptions were made in this study, and these events were classified as potentially aging. Failures of electrical cables and connectors and the RPI sub-system commonly did not have failure causes reported, due primarily to the replaceability of these components.

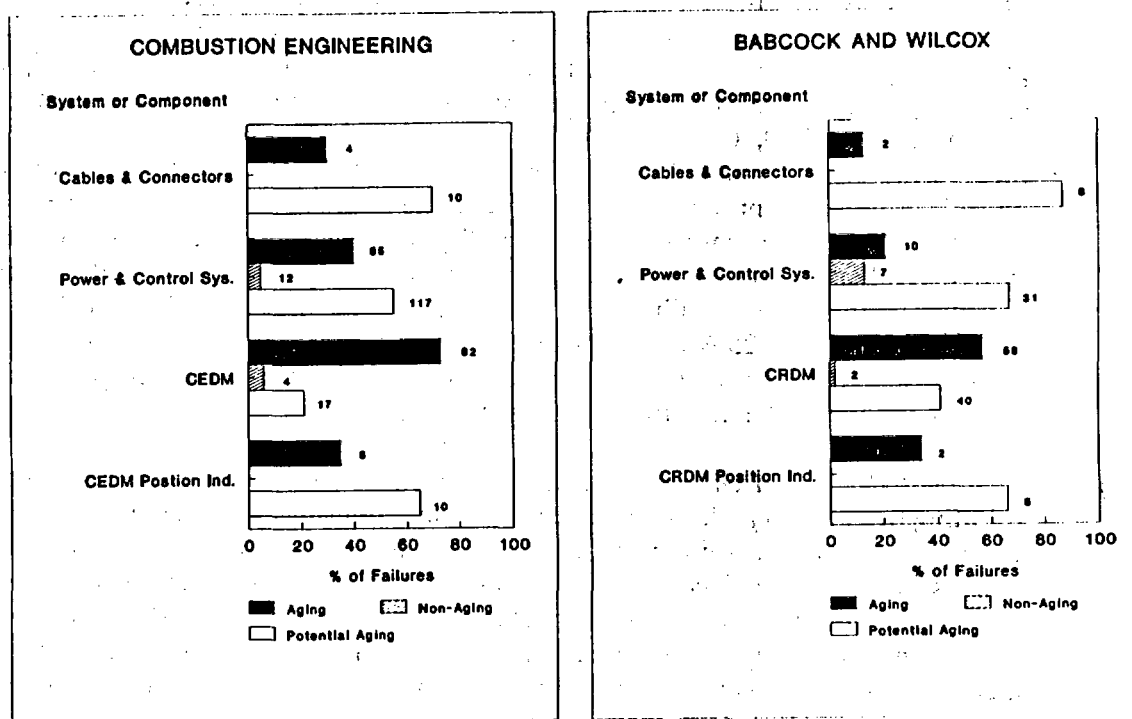


Figure 4. CRD System Failures Due to Aging

It is important to note that the operating experience review for CE and B&W indicated that neither control rod drive system ever failed to perform its primary safety function. This is due to the fail safe design of the CRD system. Any loss of power to the system results in the rapid insertion of the control rods. However, component degradation and failure resulted in increased component stresses, and unnecessary thermal and pressure cycles which challenged the operation of other safety systems. These occurrences may represent a significant increase in plant risk.

The majority of significant plant effects resulted from slipped rods, resulting in power reductions while efforts to recover and re-align the slipped rods were performed. Multiple dropped rods resulted in plant scrams and ESF actuations on some occasions.

An example of the most significant failures for the major sub-systems are described below:

- a) *Cables and Connectors* - Cables and connectors are used extensively throughout the system. The power and control cables located on the top of the reactor head are located in a much more severe environment (radiation, temperature, humidity) than those used in the power and control cabinets located outside of the containment. Brittle and cracked CEDM electrical cabling has been found and replaced at several plants. Loose and broken electrical connections were also frequently noted.
- b) *Power and Control System Failures* - This system consists primarily of modularized electrical components centrally located in control cabinets outside of the primary containment. Numerous instances of failed system power supplies were reported resulting in dropped rods. No actual cause of failure was provided. As a corrective action, many utilities are modifying their system design to incorporate redundant power supplies. Another common reported failure early in the 1980's was slipped or dropped rods due to the improper or sluggish actuation of the grippers. As previously described, CE has modified the power and control system design to incorporate the Automatic CEDM Timer Module (ACTM). The ACTM monitors and adjusts the current waveshape supplied to the grippers to ensure proper gripper actuation. This has improved the reliability of the gripper actuation. Control system breaker failures were not common, however one plant experienced a manual trip due to this type of failure. Subsequent testing indicated that the breaker opened at 30 amps, 25% less than the designed 40 amps. All of the sub-system molded case circuit breakers were subsequently added to the plants PM program to insure continued reliability for the 40 year design life.
- c) *Control Rod Drive Mechanisms* - Numerous instances of primary coolant leakage resulting from failed gaskets and cracked pressure housings were reported. Gasket embrittlement due to aging was the primary failure cause for the B&W flexitallic gaskets. B&W has replaced the original asbestos impregnated spiral wound design with a graphite impregnated stainless steel spiral wound design. Primary coolant leakage in a high temperature area, will cause the boric acid to boil and concentrate, increasing its corrosiveness and acidity. Uncorrected, the boric acid crystals may accumulate and block cooling passages.

Though only two plants use the rack and pinion CEDM, failures of the rotating seals used in the mechanism accounted for 60% of the CE primary coolant leakage occurrences. Cracked pressure housings resulting from stress corrosion cracking has also been identified on the rack and pinion CEDMs. The design of this CEDM is conducive to this type of failure if the drives are not adequately vented.

Immovable control rod assemblies caused by fractured internal CRDM components were also reported. These fragments became lodged between the roller nuts and the leadscrew, preventing movement. Plant operational procedures were modified to include visual verification of proper CRDM component alignment each time a CRA was coupled to a CRDM.

- d) *Rod Position Indication* - Due to the redundancy provided by the two position indication systems, RPI failure primarily resulted in a redundancy loss, and operational procedure changes designed to verify the proper positioning of the rods while the RPI system is inoperable. The location of the reed switches in the same

severe environment as the CRDM has been the primary failure cause. Moisture intrusion has caused reed switch corrosion. Failures of the CE Control Element Assembly Calculator (CEAC) has resulted in reactor power reductions and subsequent scrams. The CEAC monitors CEA position in the core and provides this information to the Core Protection Calculator (CPC). The CPC, based upon this information, provides overly conservative penalty factors to the automatic protection and control systems resulting in the power reductions and scrams.

- e) *Control Rod Assembly* - Failures of the control rod assemblies and the fuel assembly and upper internal guide tubes may be significant since they can interfere with or prevent the insertion of the CRAs. A CE plant recently reported the failure of a control rod due to the radiation induced swelling of the B4C poison. This resulted in an increase in the clad stress which eventually led to the propagation of a crack around the rod. The lower portion of the rod and the poison pellets fell out of the rod into the guide tube, preventing the insertion of the CRA. Subsequent inspections revealed other similarly cracked rods. Other instances of immovable CRAs due to loose parts in the reactor core being wedged between the rod and the guide tubes, were noted.

CE fuel assembly guide tubes have also experienced through wall wear caused by the control element rods. When fully withdrawn, the tips of the rods remain engaged with the upper portion of the fuel assembly guide tube. Flow induced vibration caused by the coolant was the root cause of the failure. To prevent this wear, a stainless steel sleeve is inserted in the upper portion of the guide tubes. Though CE has subsequently modified the fuel flow characteristics of the fuel assembly to preclude this type of wear, the sleeves are still being used.

Since 1980, B&W plants have reported 64 instances of cracked fuel assembly hold down springs. Though none of these cases has interfered with control rod insertion, they remain a cause of concern. Due to the close proximity of the hold down spring with the control rods, failures resulting in the displacement of spring material may interfere with the movement of the control rods.

In addition to the sub-system failures, the operational experience review also demonstrated that the CRD system was susceptible to failures and degradation due to human error and inadequate maintenance. Examples of these were errors during the performance of normal system maintenance and refueling operations. System maintenance errors typically resulted in dropped or slipped rods, while errors during refueling resulted in damaged CEDM extension shafts. Numerous instances of Technical Specification violations, primarily due to missed surveillance intervals, were also noted.

A significant number of failures were also reported which either gave no failure report or listed the cause as unknown. These occurrences resulted in significant plant effects, and on several occasions, similar failures were reported before the root failure cause was determined. As noted, this may be indicative of an inadequate root failure cause program. Though the modularized design of many electrical components allows easy replacement, efforts to identify and correct the failure causes are still needed.

## **Current Utility Inspection, Maintenance, and Surveillance Practices**

An operating survey was conducted to obtain information on current utility system maintenance and inspection practices. Responses were received from two B&W plants, and four CE plants (representing eight units). Meetings were also held with cognizant vendor system design personnel.

Combustion Engineering and Babcock & Wilcox recommended annual system inspections are listed in Table 1. The majority of the recommended inspections are electrical. The actual inspections performed on the control rod drive system, as determined by the survey, are provided in Table 2. A comparison between these tables indicate that not all of the vendor recommended system maintenance is actually performed.

Most utilities commonly use meggering to check electrical integrity of the system components. Meggering is a go/no-go test which is not capable of providing data which can be trended to detect age degradation. Also, failure of meggering is not conclusive of component failure, since moisture intrusion will result in low megohm readings. CE plants obtain gripper coil traces each cycle. These traces document the current and actuation time of each of the gripper coils. The results are visually compared to those obtained from the previous cycle. CE recommends that traces which represent a 10% difference be dispositioned by them. Again, aging degradation may not be clearly discernable from this type of test.

Visual inspections for primary coolant leakage are conducted following each cycle. If the leakage is judged unacceptable (>1 gpm.) the mechanism is removed, and the gasket replaced or weld repaired. The lack of space between mechanisms on the top of the reactor head makes this inspection very difficult to perform, and therefore should not be relied upon to solely detect leakage. Other methods, such as viewing ports around the circumference of the CRDM cooling shroud have been useful in enhancing the visual inspections.

Visual inspections are also performed on the vent valve for any leakage indication. If the leak cannot be readily corrected, some utilities have seal welded the valve shut. CE recommends that the internal ball and o-ring be replaced each time the valve is used.

All respondents reported as being in compliance with the ten year ISI inspections applicable to CRDMs. The current requirement is that only 10% of the peripheral housings be inspected every 10 years. Given the continued instances of housing defects and failures, modification of this requirement should be considered to include interior mechanisms as well.

The majority of the respondents reported that they do not have a reliability program. Such a program should be established, and include accessing one (or more) of the operating data bases. This would result in a more efficient predictive maintenance program capable of alerting utility personnel to failures at other plants, and allowing for corrective maintenance before component failure. Relying solely on vendor supplied information may not be timely enough.

**Table 1. Recommended CRD System Annual Preventive Maintenance**

<b>Combustion Engineering</b>	
I. Gripper Coils	<ul style="list-style-type: none"> <li>a) Coil Operating Traces</li> <li>b) Coil Resistance</li> <li>c) Visual Inspection (in the event of CEDM Cooling System degradation)</li> </ul>
II. Vent Valve	<ul style="list-style-type: none"> <li>a) Replace O-Rings</li> <li>b) Replace Stainless Steel Sealing Ball</li> </ul>
III. Drive Shafts	<ul style="list-style-type: none"> <li>a) Visual Inspection (when upper reactor internals are removed)</li> </ul>
<b>Babcock &amp; Wilcox</b>	
I. Stator	<ul style="list-style-type: none"> <li>A. Electrical Tests                             <ul style="list-style-type: none"> <li>1. DC Resistance</li> <li>2. Insulation Resistance</li> <li>3. Thermocouple Resistance</li> </ul> </li> <li>B. Functional Tests                             <ul style="list-style-type: none"> <li>1. Minimum Run Current</li> <li>2. Latching and Unlatching Current</li> </ul> </li> </ul>

The use of commercially available, advanced system monitoring and inspection techniques should be evaluated for use with the CRD system. These methods are non-invasive, and capable of detecting and trending age degradation. These methods include infrared thermography for electronic components, motor current signature analysis to verify proper CRDM mechanical operation, and alternatives to meggering, [such as Electronic Characterization and Diagnostics (ECAD)] for assessing electrical integrity.

**Table 2. CRD System Preventive Maintenance Performed  
by Survey Respondents**

CRD Inspection	B&W Plants		CE Plants			
	A	B	C	D	E	F
Control Rod Drive Visual Inspection			X	X		
CRD Pressure Housing 10 Year ISI	X	X	X	X	X	X
CRD Flange Inspection	X	X	X	X	X	X
CRDM Vent Valve Inspection			X	X		
<b>Stator Coil</b>						
- Visual Inspection					X	
- Electrical (Meggering)	X	X	X	X	X	
<b>Electrical Cables</b>						
- Insulation Integrity	X	X	X	X	X	
- Electrical Connectors	X	X	X		X	
- Moisture Seal Integrity	X		X			
Power Supply Inspection	X	X	X	X	X	X
Electronic Cabinet Inspection	X				X	X
<b>RPI</b>						
- Visual Inspection	X					
- Electrical Test	X				X	X
CRDM Cooling System			X	X	X	X
Control Rod Assy, Fuel Assy. Guide Tube			X		X	
<b>System Tests</b>						
- Position Verification	X	X	X	X	X	X
- Rod Drop Time	X	X	X	X	X	X
- CRA Exercising	X	X	X	X		X

## **Conclusions**

The results of this NPAR study show that aging degradation and failures have occurred in both the B&W and CE Control Rod Drive Systems. Though these occurrences have not prevented the system from performing its primary safety function, they do present unnecessary challenges to the operation of other plant safety systems when they result in unplanned reactor scrams. As the results of the utility survey indicate, CRD aging has been recognized and is being addressed, to varying degrees, by the utilities' inspection and maintenance programs. However, aging degradation and failures are still occurring. The results of this study highlight these areas, and recommendations are provided regarding preventive and predictive maintenance which may further reduce aging failures.

## **References**

1. NUREG-1144, Rev. 2, "Nuclear Plant Aging Research (NPAR) Program Plan," June 1991.
2. Grove, E. and Gunther, W., "An Operational Assessment of the Babcock & Wilcox and Combustion Engineering Control Rod Drives," BNL Technical Report TR-3270-9-90, September 1990.
3. Grove, E. and Gunther, W., "An Aging Assessment of the Combustion Engineering and Babcock & Wilcox Control Rod Drives," Draft NUREG/CR-5783, September 1991.
4. Gunther, W. and Sullivan, K., "Aging Assessment of the Westinghouse PWR Control Rod Drive System," NUREG/CR-5555, March 1991.

**Aging Related Degradation in Turbine Drives  
and Governors for Safety Related Pumps\***

Daryl F. Cox  
Oak Ridge National Laboratory  
Oak Ridge, Tennessee

**ABSTRACT**

This study is being performed to examine the relationship between time dependent degradation, and current industry practices in the areas of maintenance, surveillance, and operation of steam turbine drives for safety related pumps. These pumps are located in the Auxiliary Feedwater (AFW) system for pressurized water reactor (PWR) plants, and the Reactor Core Isolation Cooling (RCIC) and High Pressure Coolant Injection (HPCI) systems for Boiling Water Reactor (BWR) facilities. This research has been conducted by examining current information in the Nuclear Plant Reliability Data System (NPRDS), reviewing Licensee Event Reports, thoroughly investigating contacts with operating plant personnel, and by personal observation. This information was reviewed to determine the cause of each reported event and the method of discovery. From this data attempts have been made at determining the predictability of events and possible preventive measures that may be implemented.

Findings from a recent study on the Auxiliary Feedwater System<sup>1</sup> indicate that the turbine drive is the single largest contributor to AFW system degradation. This is evidenced in the loss of feedwater event at the Davis Besse Nuclear Plant in 1985. However, examination of the data show that the turbine itself is a reliable piece of equipment with a good service record. Most of the documented failures are the result of problems with the turbine controls and the mechanical overspeed trip mechanism, which apparently stem from three major causes:

1. Originally designed as a continuous drive mechanism, with a slow start-up sequence, the turbines are now used in stand-by service with normal start-up in approximately 30 seconds. The turbines are normally run once a month during pump in-service testing. The data indicate that this lack of continuous operation can actually be a major contributor to turbine degradation. Moisture trapped inside the steam supply piping and controls can cause damaging corrosion to the governor and the governor valve.
2. Maintenance enhancements have, in some cases, been poorly implemented, resulting in corrective maintenance instead of preventive/predictive maintenance.
3. Design changes by the manufacturer have been implemented with varying degrees of success because of the change in service from the original design.

Recent improvements in maintenance practices and procedures, combined with a stabilization of the design seem to indicate that this equipment can be a reliable component in safety systems.

\*Research sponsored by the Office of Nuclear Regulatory Research, U. S. Nuclear Regulatory Commission under Interagency Agreement DOE 1886-8082-8B with the U. S. Department of Energy under contract No. DE-AC05-84OR21400 with the Martin Marietta Energy Systems, Inc.

## 1.0 Introduction

Steam turbine drives for safety-related pumps are used at most of the commercial nuclear power plants in the United States. Turbine driven pumps are used in Pressurized Water Reactors (PWRs) in the Auxiliary Feedwater (AFW) system to supplement the motor driven pumps. Turbine driven pumps are also used at Boiling Water Reactor (BWR) sites. For BWRs they are located in the Reactor Core Isolation Cooling (RCIC) system, and the High Pressure Coolant Injection system. When off-site power is lost these pumps may provide the only means for pumping emergency cooling water to the Emergency Core Cooling systems.

The turbine drives were originally designed as commercial equipment, driving equipment at petroleum, chemical, and fossil power plants. In commercial applications the turbines were started slowly, and run continuously. When run in this manner the turbines have operated reliably. For nuclear service, however, the turbines are used in a standby capacity, and are operated most often during surveillance testing. Rapid starting of the turbine, combined with the rapid acceleration capability of the turbine can cause the turbine to trip on overspeed during startup. Long idle periods may contribute to increased turbine degradation.

The information for this paper has been gathered from failure database searches [the Nuclear Plant Reliability Database System (NPRDS) & Licensee Event Reports (LERs)], visits to operating facilities, visits to manufacturer facilities, and numerous discussions with vendors and industry contacts.

For this report the turbine system will be discussed as six component areas (ref fig 1):

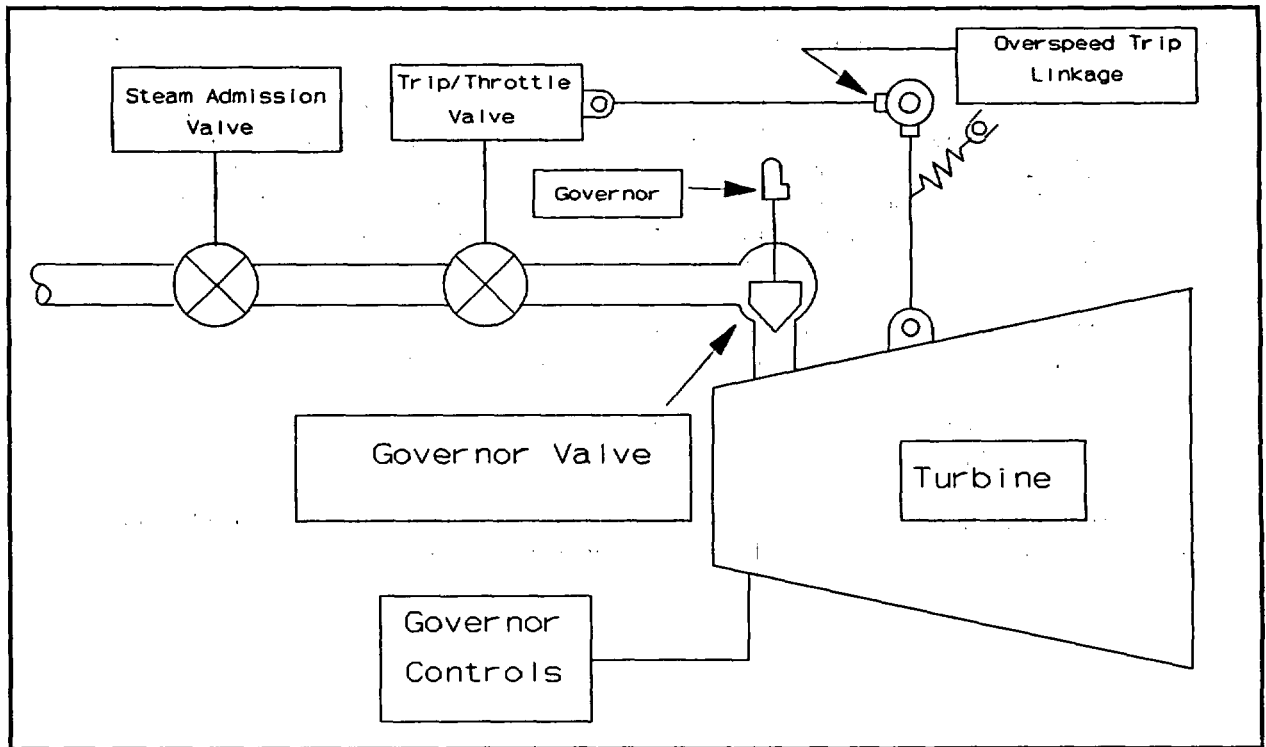


Figure 1 - Basic Turbine Configuration

- Steam Admission Valve
- Governor/Governor Controls
- Turbine
- Trip/Throttle Valve
- Governor Valve
- Overspeed Trip Mechanism

## 2.0 Configuration of the turbine

**Steam Admission Valve:** The Steam Admission Valve isolates the turbine system from the steam supply. This valve opens on a turbine start signal, if the trip/throttle valve is normally closed, to start the turbine.

**Trip Throttle Valve:** "The primary function of the trip and throttle valve is to rapidly shut off the flow of inlet steam to the turbine upon actuation of the overspeed trip."<sup>2</sup> The trip and throttle valve also may be used to start the turbine if the steam admission valve is normally open.

**Governor:** The governor maintains the turbine speed such that the pump flow remains constant. It provides a positioning signal to the servo mechanism that manipulates the governor valve linkage. The governor may be either a mechanical/hydraulic unit with its own control oil, or an analog electric/hydraulic unit that draws control oil from the turbine lubricating oil sump.

**Governor Valve:** The governor valve regulates the amount of steam entering the turbine, which controls turbine speed.

**Turbine:** The turbine is the actual driver for the safety-related pump. It is a solid wheel design, capable of rapid starts and operation with a wide range of steam quality.

**Overspeed Trip Mechanism:** The mechanical overspeed trip mechanism actuates when the turbine exceeds a predetermined speed to close the trip and throttle valve, and thus stop steam flow to the turbine.

## 3.0 Review of Failure Data

The failure databases noted above were reviewed and the following parameters were extracted.

**Method of discovery:** This field determines how the failure was discovered from a list of six possible options.

- **Demand Failures:** These are failures that occur when the system is called upon to function in a non-test situation.
- **Testing:** Testing failures occurred during surveillance, post maintenance testing, or periodic operability testing. Also included are instances where the turbine may not have failed to operate, but has been declared inoperable due to unacceptable oil samples.
- **Inspection:** This category includes both In-Service Inspection and any special inspection performed on the turbine.
- **Maintenance:** Any item discovered during preventive or corrective maintenance.
- **Routine/Incidental Observation:** Those items that are observed as part of an individual's normal job. This includes operators, system engineers, or any other person who periodically examines the turbine for visible

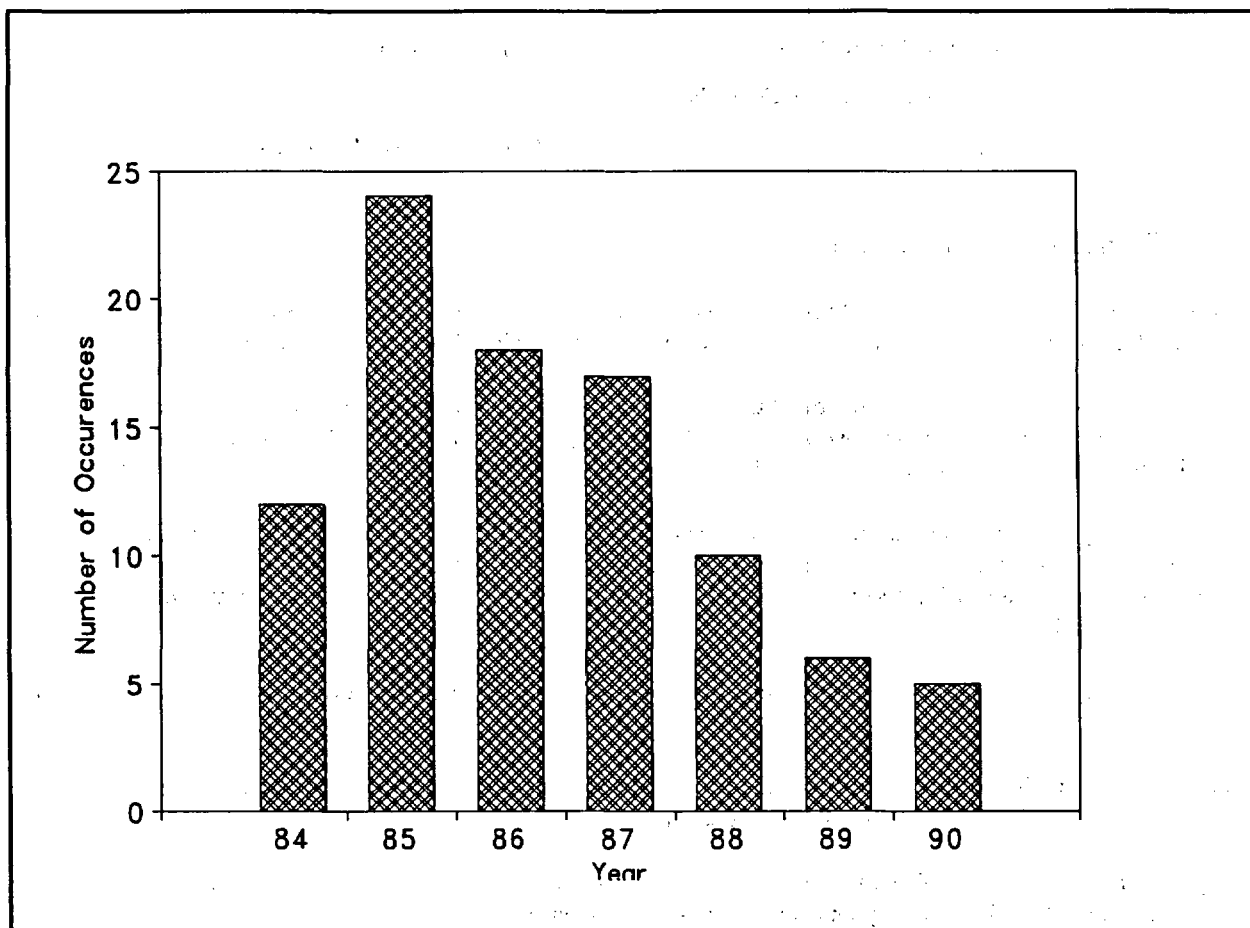


**Figure 2 - Reported demand failures per year**

degradation or breakage.

- **Audiovisual Alarm:** Failures that were discovered by an alarm in the control room. For these items the alarm initiated before any other method of detection.

Examination of the databases actually shows that of the 447 failures reported between 1984 and 1990, most have been found as a result of testing (52.8%), followed by demand failures (21.5%), Routine/Incidental Observation (11.6%), Inspection (7.4%), Maintenance (3.8%), and Audiovisual Alarms (2.9%).

The amount of failures discovered during operational demand are significant because of the small amount of time the turbines are actually operated on demand. The number of demand failures at first seems unreasonably high. However, an examination of these failures by the year in which they occurred indicates a dramatic decrease in the number of demand failures per year in the time period between 1985 and 1990 (see Fig. 2). This decrease in demand failures also indicates an increase in turbine reliability.

The data also indicates that a majority of the problems (72%) found can be traced to the components responsible for speed control. These components include the governor, governor valve, and the mechanical overspeed trip mechanism. Therefore, the balance of this document will concentrate on the failures associated with these

component groups.

**Mechanical Overspeed Trip Mechanism:** The mechanical overspeed trip mechanism is comprised of the actual trip assembly and a linkage which connects it to the trip and throttle valve. The linkage is spring loaded, actuating when the trip assembly is triggered. The three main modes of failure for this assembly are:

- (a) maladjustment of the trip pin
- (b) breakage/binding of the trip tappet
- (c) improper tension adjustment of the linkage spring

The trip pin is normally mounted on the turbine shaft. It moves radially outward, striking the trip tappet when the turbine shaft speed exceeds a preset value. Maladjustment of the trip pin will either prevent it from striking the tappet head, prevent it from striking the tappet head hard enough to trip the mechanism, or cause the trip pin to strike the tappet head too hard and bend the tappet stem.

The head of the trip tappet (which is the part actually struck by the trip pin) is normally made of urethane. Several design changes have taken place over the years to create a head that will absorb the impact of being struck at high speed without shattering. Once damage occurs to the head of the trip tappet, sufficient force cannot be transmitted to the rest of the mechanism to close the trip and throttle valve. Binding will happen if the urethane head swells from a chemical reaction with turbine oil (older tappets). Binding may also occur if the tappet stem is bent from excess impact, caused by a maladjusted trip pin. Swelling of the trip tappet head, or a bent stem may prevent resetting the mechanical overspeed trip mechanism.

The vendor recommends adjusting the overspeed trip linkage spring to 28 -32 lbs tension when measured in the direction of linkage travel. If the spring tension is weak, a trip may not occur. Too much spring tension may accelerate wear of the trip mechanism, and cause premature turbine trips.

**Governor Valve:** The fundamental problem associated with the governor valve is degraded response times, which allow overspeed trips. This is primarily caused by a degraded valve stem or a degraded linkage between the governor and the governor valve. Either situation can cause the turbine to overspeed. The linkage, for this report, shall be considered part of the governor valve.

Binding of the governor valve causes a loss of the ability to maintain speed control of the turbine. Corroded or bent valve stems can drag against the governor valve packing. The research indicates that stem corrosion has two primary sources: leakage of the steam supply isolation valve, and scale build-up from periodic testing. Since the turbines are infrequently operated, the presence of steam during the time between monthly pump tests can corrode the valve stem. This condition can result from leaking isolation valves, which place the valve stem in a consistently hot, wet environment. The scale build-up then tends to drag on the valve packing, increasing wear on the packing and degrading governor valve response. In extreme cases binding can result in buckling of the valve stem. In addition, valve stem scale can also cause erratic behavior of the governor valve. Design basis conditions for the steam supply can cause pressures as low as 105 psig. The capability of operating at such low pressures leads to the tendency for very rapid accelerations at normal steam supply pressures. Normal inlet steam pressure (1000 psig) is capable of accelerating the turbine at approximately 2000 rpm/sec. Therefore, any binding of the governor valve may result in an overspeed trip.

**Governor:** Degraded governor response may be caused primarily by worn or improperly adjusted control oil valves inside the governor, drift in the settings of electronic controller boards, or contaminated control oil. Improperly adjusted valves can result in sluggish, erratic, or unstable governor responses. Too much restriction in the valve ports prevents the governor from responding to load changes in an acceptable manner.

The electronic governors currently in use are analog devices. As such these devices are subject to set point drift

(approx. 15% of the reported governor problems). In general, it can be seen that calibration of the governor is not a requirement of the plant technical specifications. Therefore, calibrations are not always done with regularity or on a timely schedule.

Additionally, problems can result from the accumulation of contaminants in the governor oil. These contaminants can be water, particulate, degraded oil additives, and/or dirt. Oil contamination can come from several sources; worn bearings, contaminants introduced at the time the oil was put in the turbine, poor house keeping during maintenance, left over machine filings from manufacturing, turbine wear (electric governor systems), buildup from infrequent changes, clogged filters, etc. Recent problems at several utilities also indicate that contaminated control oil may cause the governor response to be too slow to control turbine starts. The electric governors (EG series) are particularly susceptible to this phenomena. This is because the governor control oil is supplied from the turbine lubricating oil sump. Therefore contamination of one system leads to contamination of both systems. These contaminants may accumulate on any surface that is normally in contact with the oil.

The quality of the oil used in the governor is critical to proper governor function. Supplement 2 to NRC Information Notice 86-14 clearly demonstrates performance degradation due to dirty oil. For purposes of this report dirty oil will be called contaminated oil.

Water contamination has two primary sources: Leaking oil coolers, and leaking steam seals. Once steam has leaked past the shaft seals it can condense and contaminate the control oil. For EG systems the shaft seals most affected are the turbine shaft seals. For mechanical (PG) type governors leakage past the governor drive shaft is the most probable path of steam leakage.

Water in the control oil of the governor can create rust inside the governor. Rust clogs orifices, causing the governor to respond poorly. Water in the control oil also tends to change the viscosity of the control oil, and thus changing the operating characteristics of the governor.

Many times the root cause of a problem is not determined. Since this is a safety system, its failure may put the plant in a Limiting Condition of Operation (LCO). The system must be returned to operation within a certain period (typically 72 hours), or the plant must be shut down. Therefore, the entire governor assembly may be replaced, and the root cause never determined.

#### **4.0 Conclusions**

The aging study of turbine pump drives is ongoing. The data evaluated to date indicate an increase in turbine reliability in recent years. Demand failures are decreasing and more problems are being found during inspection/testing. Experience and education appear to have a major part in these positive trends. With proper maintenance the turbine can be a reliable part of nuclear plant safety systems.

#### **5.0 Recommendations**

Three areas are particularly important to enhancing turbine system reliability:

- Periodically perform complete chemical analysis of turbine and governor oil. This will reveal the presence of contaminants and/or oil degradation. The experience of each utility should be used to determine a time period that will increase reliability (for example, annual or semi-annual analysis).
- Calibrate governors on a regular basis. Currently, this is not a requirement in the plant technical operating specifications.

- Periodically verify overspeed trip operation by manually taking the turbine to overspeed to verify the function of the mechanical overspeed trip mechanism. This is a vendor recommendation, and will give a positive indication that the entire mechanical overspeed trip mechanism is properly functioning.
- 

#### References

1. D.A. Casada, Oak Ridge National Laboratory, Auxiliary Feedwater System Aging Study - NUREG/CR-5404
2. Terry Turbine Controls Guide, EPRI NP-6909s

SAND91-1397C

**Aging, Condition Monitoring, and Loss-of-Coolant Accident (LOCA) Tests  
of Class 1E Electrical Cables: Summary of Results**

Mark J. Jacobus

Sandia National Laboratories  
Albuquerque, NM 87185

**Abstract**

This paper summarizes the results of aging, condition monitoring, and accident testing of Class 1E cables used in nuclear power generating stations. Three sets of cables were aged for up to 9 months under simultaneous thermal ( $\sim 100^\circ\text{C}$ ) and radiation ( $\sim 0.10\text{ kGy/hr}$ ) conditions. After the aging, the cables were exposed to a simulated accident consisting of high dose rate irradiation ( $\sim 6\text{ kGy/hr}$ ) followed by a high temperature steam exposure. A fourth set of cables, which were unaged, were also exposed to the accident conditions. The cables that were aged for 3 months and then accident tested were subsequently exposed to a high temperature steam fragility test (up to  $400^\circ\text{C}$ ), while the cables that were aged for 6 months and then accident tested were subsequently exposed to a 1000-hour submergence test in a chemical solution. The results of the tests indicate that the feasibility of life extension of many popular nuclear power plant cable products is promising and that mechanical measurements (primarily elongation, modulus, and density) were more effective than electrical measurements for monitoring age-related degradation. In the high temperature steam test, ethylene propylene rubber (EPR) cable materials generally survived to higher temperatures than crosslinked polyolefin (XLPO) cable materials. In dielectric testing after the submergence testing, the XLPO materials performed better than the EPR materials. This paper presents some recent experimental data that are not yet available elsewhere and a summary of findings from the entire experimental program.

**1.0 INTRODUCTION**

Cables are used throughout nuclear power plants in a wide variety of applications. Cable qualification typically includes thermal and radiation aging intended to put the cable in its end-of-life condition. The radiation dose is normally applied at high dose rates (1-10 kGy/hr) with Arrhenius methods used to establish accelerated aging times and temperatures. Generally, the radiation and thermal aging are applied to the specimens sequentially. Because of the high dose rates and temperatures that are typically employed, cable materials can experience oxygen diffusion effects that result in non-uniform aging. Consequently, it is of interest to determine the extent to which these factors might have affected previous testing. Typical qualification programs also provide very little information that is useful for establishing effective condition monitoring programs to assess remaining cable life. The current experimental program goes beyond previous efforts by employing considerably less accelerated, simultaneous thermal and radiation aging conditions; by employing many more condition monitoring measurements during aging; and by performing similar accident tests on cables aged to three different nominal lifetimes.

The broad objectives of this experimental program were to determine the life extension potential of popular cable products used in nuclear power plants and to determine the potential of condition monitoring (CM) for residual life assessment.

\* The Aging Degradation of Cables Program is supported by the United States Nuclear Regulatory Commission and performed at Sandia National Laboratories, which is operated for the U.S. Department of Energy under contract number DE-AC04-76DP00789.

A number of previous publications describe different aspects of this experimental program. Reference [1] describes the overall test program, some details of the electrical condition monitoring measurements, and a small amount of the electrical condition monitoring data. Reference [2] gives an overview of some of the mechanical property measurements for many different cable types, while References [3] and [4] provide more detailed mechanical property data for XLPO and EPR cable products, respectively. None of the density or modulus profile data is available in References [2-4]; therefore some of that data will be included in this paper. Reference [5] gives an overview of the LOCA test data from the cables that were aged to a nominal lifetime of 60 years. Reference [6] gives more LOCA test data with some comparisons of the accident behavior of cables aged to the three different nominal lifetimes. Reference [7] gives detailed results of the high temperature steam test and the submergence test. Finally, a series of three reports [8-10] that describe the complete testing program (except the information already included in Reference [7]) is in preparation.

## 2.0 EXPERIMENTAL ARRANGEMENT

The experimental program consisted of two phases. Phase I was a simultaneous thermal ( $\approx 100^\circ\text{C}$ ) and radiation aging ( $\approx 0.10\text{ kGy/hr}$ ) exposure, and Phase II was an accident exposure consisting of high dose rate irradiation ( $\approx 6\text{ kGy/hr}$ ) followed by a simulated loss-of-coolant accident (LOCA) steam exposure. Our test program generally followed the guidance of IEEE 323-1974 [11] and IEEE 383-1974 [12].

In Phase I, we included up to 12 different cable products (see Table 1) in three different test chambers, with the cables in each chamber aged to a different extent prior to accident testing. Cables were aged for 3 months in the first chamber, 6 months in the second chamber, and 9 months in the third chamber. (A fourth chamber, containing unaged cables, was only used for the accident exposure of Phase II.) The accelerated aging temperature was determined by equating the 6-month exposure to a 40-year life and assuming an activation energy of  $1.15\text{ eV}$  and a plant ambient temperature of  $55^\circ\text{C}$ . The accelerated radiation aging dose rate was determined by assuming a 40-year radiation dose of  $400\text{ kGy}$ . The 3-month chamber was therefore nominally equivalent to 20 years of aging and the 9-month chamber was nominally equivalent to 60 years of aging. The aging was performed in Sandia's Low Intensity Cobalt Array (LICA) facility. During the aging exposure, cable lead wires and penetrations were shielded to reduce their radiation and thermal exposures and reduce artificial failures that might occur at these locations.

For each cable type, 23-m (76-ft) lengths of cable were wrapped around a mandrel. The effective cable length inside the test chamber was typically 4.6-6.1 m (15-20 ft), with the remainder of the cable used for external connections. Where both single and multiconductors samples of the same cable were tested, the single conductors were obtained by stripping the jacket from the multiconductor and removing all filler materials.

Dose rates in the chambers were determined using thermoluminescent dosimeters (TLDs). The estimated uncertainty in the radiation aging exposure data is  $\pm 20\%$ . The test chamber temperature was maintained using electric wall heaters and electric inlet air heaters. Temperature uniformity was controlled to the extent possible by insulating the chamber and providing air circulation. About  $4.7\text{ l/s}$  ( $10\text{ ft}^3/\text{min}$ ) of outside air (about 40 air changes per hour) was introduced into the chamber to maintain circulation and ambient oxygen concentration. The pressure in each chamber was maintained slightly above ambient to prevent water leakage into the chamber. The pressure was not continuously recorded nor controlled. With Albuquerque's altitude reducing ambient

**Table 1 Cable Products Included in the Test Program**

<u>Supplier</u>	<u>Description</u>
1. Brand Rex	XLPE Insulation, CSPE Jacket, 12 AWG, 3/C, 600 V
2. Rockbestos	Firewall 3, Irradiation XLPE, Neoprene Jacket, 12 AWG, 3/C, 600 V
3. Raychem	Flamtrol, XLPE Insulation, 12 AWG, 1/C, 600 V
4. Samuel Moore	Dekoron Polyset, XLPO Insulation, CSPE Jacket, 12 AWG, 3/C and Drain
5. Anaconda	Anaconda Y Flame-Guard FR-EP, EPR Insulation, CPE Jacket, 12 AWG, 3/C, 600 V
5a. Anaconda *	Anaconda Flame-Guard EP, EPR Insulation, Individual CSPE Jacket, CSPE Jacket, 12 AWG, 3/C, 1000 V
6. Okonite	Okonite Okolon, EPR Insulation, CSPE Jacket, 12 AWG, 1/C, 600 V
7. Samuel Moore	Dekoron Dekorad Type 1952, EPDM Insulation, Individual CSPE Jackets, Overall CSPE Jacket, 16 AWG, 2/C TSP, 600 V
8. Kerite	Kerite 1977, FR Insulation, FR Jacket, 12 AWG, 1/C, 600 V
9. Rockbestos	RSS-6-104/LE Coaxial Cable, 22 AWG, 1/C Shielded
10. Rockbestos	Firewall Silicone Rubber Insulation, Fiberglass Braided Jacket, 16 AWG, 1/C, 600 V
11. Champlain	Polyimide (Kapton) Insulation, Unjacketed, 12 AWG, 1/C
12. BIW	Bostrad 7E, EPR Insulation, Individual CSPE Jackets, Overall CSPE Jacket, 16 AWG, 2/C TSP, 600 V

\* This cable was only used for the multiconductor samples in the 3-month chamber.

Abbreviations used in table:

- XLPO - Cross-linked polyolefin
- XLPE - Cross-linked polyethylene, a subset of XLPO
- CSPE - Chlorosulfonated polyethylene
- AWG - American Wire Gauge
- /C - number of conductors
- FR-EP - Flame retardant ethylene propylene
- CPE - Chlorinated polyethylene
- EPR - Ethylene propylene rubber
- EPDM - Ethylene propylene diene monomer
- TSP - Twisted shielded pair
- FR - Flame retardant
- BIW - Boston Insulated Wire

pressure of about 20% from sea level conditions, the positive gauge pressure in the test chamber resulted in an absolute pressure close to ambient pressure at sea level.

In addition to the 23-m lengths of cable, 15-cm (6-in) insulation and jacket specimens and 36-cm (14-in) single and multiconductor cable samples were also included in the test chambers during aging. The 15-cm insulation and jacket samples were used for tensile strength and elongation testing. The copper conductors were removed from these cable samples prior to the beginning of aging. The 36-cm completed cable samples, which were simply cut from a reel of cable, were used for hardness and modulus testing.

During the aging exposure, various electrical and mechanical condition monitoring measurements were performed on the cables. Some of the measurements were performed on completed cable samples and others were performed on the small samples removed from the test chambers during aging. The parameters measured included insulation resistance and polarization index at three different voltages, capacitance and dissipation factor over a wide range of frequencies, elongation and tensile strength at failure, modulus profiles, cable indenter modulus tests (using a cable indenter developed at Franklin Research Center under Electric Power Research Institute funding [13,14]), hardness, and bulk density.

Phase II consisted of exposing each set of aged cables, as well as the set of unaged cables, to a simulated LOCA environment in Sandia's Area I facility. The cables were first exposed to a nominal accident radiation dose of 1100 kGy at a dose rate of 6 kGy/hr. The estimated uncertainty in the actual accident radiation exposure data is  $\pm 10\%$ . The samples were then exposed to a high temperature and pressure steam environment. The test profile generally followed that given in IEEE 323-1974 [11] for a combined BWR/PWR generic test except that the final portion of our tests was at a higher temperature and for a shorter duration than IEEE 323 suggests. Four separate LOCA tests were performed, one for each test chamber. The cables were energized at 110 Vdc during the accident simulations. Insulation resistance measurements (IRs) were measured on-line throughout the test. IRs were also measured periodically with an independent measurement technique that is more accurate than the on-line measurement system at IRs above  $10^8 \Omega$ . No chemical spray was used during the steam exposure, but a 1000-hr post-LOCA submergence test was performed on the cables that had been aged for 6 months and accident tested. The submergence test used a chemical spray solution similar to the spray solution recommended by IEEE 323-1974 [11]. The nominal conditions during the submergence test were  $95 \pm 5^\circ\text{C}$  with a slightly positive pressure. The cables that had been aged for 3 months and then accident test were subsequently exposed to a high temperature steam fragility test that included a peak temperature of  $400^\circ\text{C}$  ( $750^\circ\text{F}$ ). The test profile for the high temperature steam test is shown in Figure 1. The purpose of the high temperature steam test was to study the ultimate fragility level of typical cable; the test conditions are well beyond the design basis for nuclear power plants. Details of the submergence and high temperature steam tests may be found in Reference [7].

Details of the mechanical measurement techniques, except for density and modulus profiling, are available in Reference [4] and will not be repeated here. Details of the electrical measurement techniques are given in Reference [1] and will not be repeated here. Descriptions of the modulus profiling and density measurement techniques are given below:

- a. Modulus profiles were determined using an apparatus developed at Sandia [15,16]. The modulus is a measure of the slope of the stress versus strain curve in the initial linear portion of the curve. The modulus profile gives information on the modulus of the sample across its cross section. It also gives an indication of the uniformity of the aging process [15,16]. The primary purpose for using modulus profiling in

this test program was to establish the uniformity of the aging process, and therefore, this technique was used only on a few selected samples.

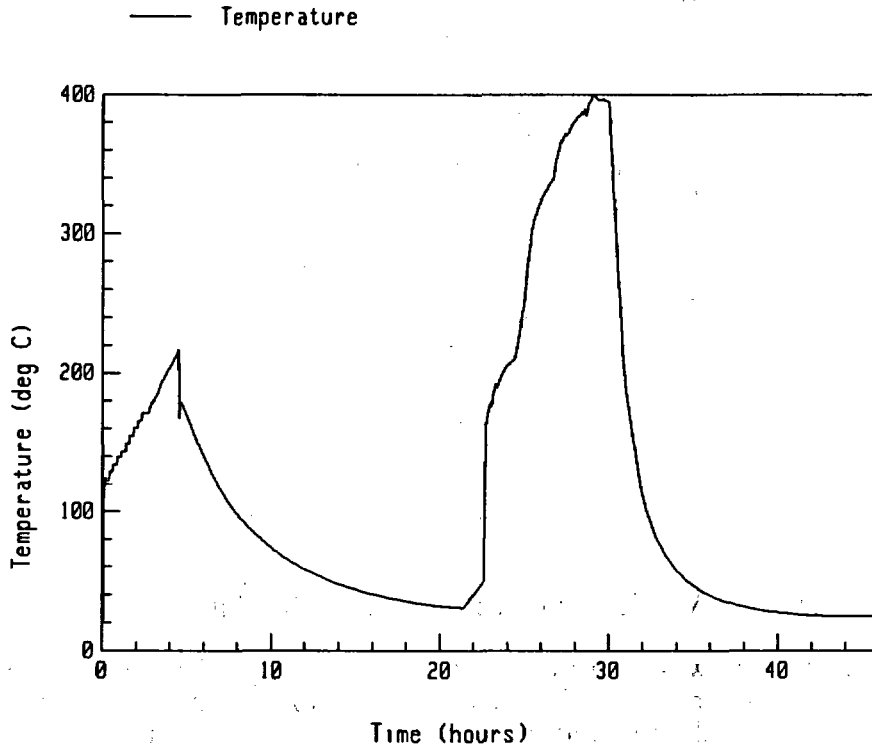


Figure 1 Temperature Profile During High Temperature Steam Test

To perform the modulus profiles, 1.25-cm samples were cut from the 36-cm cable specimens. For cable products that were tested in both single and multiconductor configurations, samples were only removed from the multiconductor 36-cm specimens because oxygen diffusion effects will be most severe in the multiconductors. In some cases, the 1.25-cm samples were surrounded with heat shrinkable tubing to hold them in place. The samples were then encapsulated in epoxy, allowed to cure and polished prior to the modulus measurements. Figure 2 shows a diagram of a typical multiconductor cable prepared for testing. For cable products supplied as single conductors, modulus profile samples were prepared in a similar fashion, but four single conductor samples were typically grouped in a diamond pattern for potting in epoxy. For the multiconductors, modulus testing would typically proceed across the centerline of two specimens from the point labelled "start measurement" to the point labelled "end measurement." The measurements would be performed on the first cable's insulation, wrap (if used), and jacket, and then measurements would be performed on the second cable's jacket, wrap (if used), and insulation. For single conductors, a similar path through two cable samples was followed.

- b. Bulk density measurement of small samples was performed in density gradient columns covering a range from 1.20 to 1.55 g/cm<sup>3</sup>. The samples were on the order of 5 mm<sup>3</sup> and most were removed from 15-cm insulation and jacket specimens that were not used for tensile testing. For insulation materials that had composite insulations, only the primary insulation was used for the density measurements. Density profiling has demonstrated that density tends to increase with aging [16], but similar to modulus, density may be subject to gradients resulting from oxygen diffusion effects.

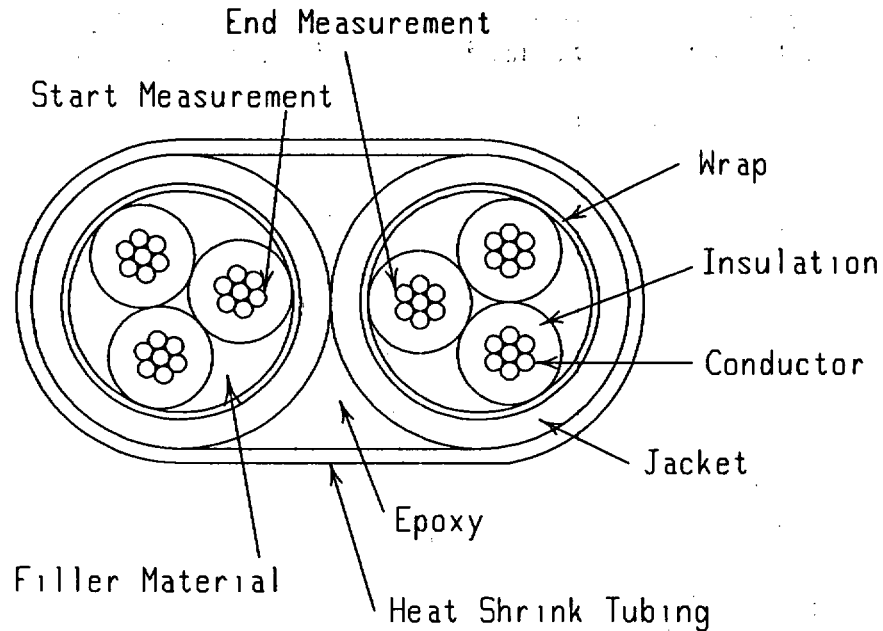


Figure 2 Diagram of Multiconductor Prepared for Modulus Profiling

In this program, bulk density was measured and the modulus profiling was used to give an indication of the gradients resulting from oxygen diffusion. Density profiling was not performed because it is considerably more tedious than modulus profiling and tends to yield complementary information.

Appendix A contains some recent density and modulus profiling data that is not yet available in other publications. Also, some recent post-accident elongation data from XLPO cable materials is included in Appendix A.

### 3.0 SUMMARY OF RESULTS

Although some final testing and analysis remains to be completed, the preliminary conclusions from the overall test program will be presented in this section. This section will be divided into four categories: general conclusions regarding aging and condition monitoring, general conclusions regarding the accident performance of aged cables, specific conclusions from the accident testing of XLPO cable products, and general conclusions from the submergence and high temperature steam testing. The specific conclusions section for XLPO cable products discusses testing and analysis that have been completed on these cables, but not on the remaining cables.

#### 3.1 Aging and Condition Monitoring

- a. Of the condition monitoring parameters tested, elongation at break tends to show the most correlation with amount of aging for the most cable types. For all cable materials tested except one, a consistent decrease in elongation occurs with aging. The one exception was Rockbestos Firewall III XLPO insulation, which had an initial increase in elongation of about 10%, followed by a consistent decrease in elongation.
- b. For the jacket materials and a few of the insulation materials, both hardness and indenter modulus increased with aging. For these cases, indenter modulus was clearly the more sensitive of the two techniques. For other insulation materials,

particularly EPR materials that did not have a bonded jacket and XLPO materials, hardness and indenter modulus did not change consistently.

- c. Over the 9-month aging period, density increased by 1-6% for many of the insulation and jacket materials. However, a few materials had no change or inconsistent changes in density.
- d. Although there were some exceptions, neither tensile strength nor any of the electrical measurements had any significant, consistent trend with aging.
- e. The modulus profiles indicated that oxygen diffusion effects were minimal in most cases. Some materials did experience diffusion effects, but evidence indicated that these effects were not overly severe.

### **3.2 Accident Performance of Aged Cables**

- a. In most cases, the maximum differences between the accident insulation resistance of unaged cables and cables aged to the three different lifetimes was about two orders of magnitude. The range of the accident insulation resistances of the cables aged to the three different lifetimes was normally less than one order of magnitude. In most cases, insulation resistance during the accident was lower for cables that had greater amounts of aging.
- b. The accident insulation resistance of individual conductors removed from multiconductor cables was typically higher than the insulation resistance of the multiconductor cable, indicating that testing of only single conductor cables (as permitted by IEEE 383-1974 [12]) may not adequately represent the insulation resistance behavior of multiconductor cables.
- c. Over the range from 50-250 V, insulation resistance was largely independent of test voltage during both aging and accident testing for all materials.
- d. As expected, during accident testing, the insulation resistance of most cables tested behaved in a reasonably consistent inverse temperature fashion, i.e., as the temperature was reduced, the insulation resistance increased.
- e. During the initial steam transients, some cables had insulation resistances that fell well below the steady state value and then recovered. Except for this overshoot phenomenon, periodic measurements of IR would have been sufficient to indicate cable performance throughout the accident tests.

### **3.3 Accident Performance of Aged XLPO Cables**

- a. The three XLPO multiconductor cable products tested had accident IRs that were within an order of magnitude of each other. The single conductor cable product tested had IRs that were 2-3 orders of magnitude higher than the multiconductors.
- b. Only one XLPO conductor failed during the accident tests. This was one of three conductors of one of two Rockbestos multiconductor cables that had been aged for 9 months (nominal equivalent of 60 years). Thus, the generic life extension potential of the XLPO cable products is very promising.
- c. A statistically significant conclusion regarding the number of failures versus the amount of aging for XLPO cable products is difficult. However, the only XLPO

conductor that failed during an accident test was one that had been aged for the maximum amount of time.

- d. The accident IR performance of our XLPO cables aged to three different lifetimes was comparable to the accident performance of aged XLPO cables in industry tests at somewhat different aging conditions. This observation reinforces the notion that gross electrical failures during accident conditions are necessarily preceded by mechanical degradation, which may be either global or local (e.g., material flaw).
- e. With the exception of the one conductor that failed during the LOCA test, all XLPO conductors successfully passed high voltage tests at an applied voltage of 80 V/mil following the accident tests. Three conductors (all Dekoron Polyset XLPO) failed a similar high voltage test after an IEEE 383-1974 [12] post-accident mandrel bend test. However, the location of the failures may have received more thermal aging than the rest of the cable. All three conductors failed within 5 cm (2 in) of each other, near where the cables began wrapping on the aging/accident test mandrel.
- f. Following the accident exposure, dielectric withstand voltages of XLPO cables were very high. Mechanical damage (cracking) was generally necessary to cause breakdown voltages to occur at voltages below 80 V/mil of insulation.
- g. When cracking was observed after mandrel bends, it was usually through to the conductor and very obvious.
- h. For three of the four XLPO materials that had been aged for 9 months, the elongation was greater after the accident test than before the accident test. This may be a result of moisture being absorbed into the cable and acting as a plasticizer or a result of the crystalline structure of the XLPO materials being melted and reformed.
- i. Although the IEEE 383-1974 [12] mandrel bend requirement is quite severe, most of the XLPO materials tested to our conditions survived mandrel bends significantly more severe than the IEEE 383 requirement. This result is consistent with the elongations of the cables following exposure to the accident conditions. Based on the elongation prior to the steam exposure, the cables would not have done as well in bend tests if they had been tested prior to the steam exposure.

#### 3.4 Submergence Testing and High Temperature Steam Testing

- a. EPR cables generally survived to higher temperatures than XLPO cables in the high temperature steam fragility test. The XLPO-insulated conductors had no insulation remaining at the end of the test (after a 400°C peak exposure)
- b. A number of cables that performed well during the submergence test failed post-submergence dielectric withstand testing (either before or after the mandrel bend). This demonstrates that the IEEE 383 dielectric withstand tests and mandrel bends can induce failure of otherwise functional cables. Note that this conclusion does not imply a criticism of the IEEE 383 requirements, which are intended to provide a level of conservatism in the testing.
- c. The IEEE 383 dielectric withstand tests are very severe even if a mandrel bend is not performed. This is evidenced by the failure of nine conductors and the near failure of three more conductors in the post-submergence dielectric withstand test

(with no prior mandrel bend). Near failure in this case was leakage currents still slightly below the acceptance criterion, but an order of magnitude higher than those prior to the submergence test. Only two of the conductors that failed this dielectric test indicated strong degradation during the submergence test.

- d. XLPO cables generally performed better than EPR cables in the submergence test and in the post-submergence dielectric testing. By the end of the final dielectric test (after a 40xD mandrel bend), only 1 of 11 XLPO-insulated conductors had failed, while 17 of 20 EPR-insulated conductors had failed.

#### 4.0 REFERENCES

1. M. J. Jacobus, "Condition Monitoring Methods Applied to Class 1E Cables," *International Journal of Nuclear Engineering and Design*, 118 (1990) pp. 497-503.
2. M. J. Jacobus and G. F. Fuehrer, "Mechanical Properties of Cables Exposed to Simultaneous Thermal and Radiation Aging," SAND90-1690C, Appears in *Proceedings of the U.S. Nuclear Regulatory Commission Eighteenth Water Reactor Safety Information Meeting*, NUREG/CP-0114, Vol.3, April, 1991.
3. M. J. Jacobus, "Mechanical Property Condition Monitoring of Cables Exposed to Long-Term Thermal and Radiation Aging--XLPO Results," SAND91-0187C, ANS Topical Meeting on Nuclear Power Plant & Facility Maintenance, Salt Lake City, UT, April, 1991.
4. M. J. Jacobus, "Mechanical Property Condition Monitoring of Cables Exposed to Long-Term Thermal and Radiation Aging--EPR Results," SAND91-0186C, 15th Biennial Reactor Operations Topical Meeting, Bellevue, WA, August, 1991.
5. M. J. Jacobus, "Loss-of-Coolant Accident (LOCA) Testing of Aged Cables for Nuclear Plant Life Extension", Appears in *Proceedings of the U.S. Nuclear Regulatory Commission Seventeenth Water Reactor Safety Information Meeting*, NUREG/CP-0105, Vol.3, March, 1990.
6. M. J. Jacobus, "Loss-of-Coolant Accident (LOCA) Testing of Aged Cables with Application to Nuclear Plant Life Extension," SAND90-0811J, submitted to the *International Journal of Nuclear Engineering and Design*.
7. M. J. Jacobus and G. F. Fuehrer, *Submergence and High Temperature Steam Testing of Class 1E Electrical Cables*, NUREG/CR-5655, SAND90-2629, April, 1991.
8. M. J. Jacobus, *Aging, Condition Monitoring, and Loss-of-Coolant Accident (LOCA) Tests of Class 1E Electrical Cables, Volume 1: Crosslinked Polyolefin Cables*, NUREG/CR-5772, SAND91-1766/1, In preparation.
9. M. J. Jacobus, *Aging, Condition Monitoring, and Loss-of-Coolant Accident (LOCA) Tests of Class 1E Electrical Cables, Volume 2: Ethylene Propylene Rubber Cables*, NUREG/CR-5772, SAND91-1766/2, In preparation.
10. M. J. Jacobus, *Aging, Condition Monitoring, and Loss-of-Coolant Accident (LOCA) Tests of Class 1E Electrical Cables, Volume 3: Miscellaneous Cable Types*, EG/CR-5772, SAND91-1766/3, In preparation.
11. IEEE Standard for Qualifying Class 1E Equipment for Nuclear Power Generating Stations, IEEE Standard 323-1974, New York, NY.

12. IEEE Standard for Type Test of Class 1E Electric Cables, Field Splices, and Connections for Nuclear Power Generating Stations, ANSI/IEEE Standard 383-1974 (ANSI N41.1C-1975), New York, NY.
13. Toman, G. J. and G. Sliter, "Development of a Nondestructive Mechanical Condition Evaluation Test for Cable Insulation," *Proceedings: Operability of Nuclear Power Systems in Normal and Adverse Environments*, Albuquerque, New Mexico, September 29-October 3, 1986.
14. Gardner, J. B. and T. A. Shook, "Status and Prospective Application of Methodologies from an EPRI Sponsored Indenter Test Project," Appears in *Proceedings: Workshop on Power Plant Cable Condition Monitoring*, EPRI EL/NP/CS-5914-SR, July 1988.
15. Gillen, K. T., R. L. Clough, and C. A. Quintana, "Modulus Profiling of Polymers," *Polymer Degradation and Stability*, Vol. 17, p. 31, 1987.
16. Clough, R. L., K. T. Gillen, and C. A. Quintana, *Heterogeneous Oxidative Degradation in Irradiated Polymers*, NUREG/CR-3643, SAND83-2493, Sandia National Laboratories, Albuquerque, New Mexico, April 1984.

## APPENDIX A Recent Experimental Data

This appendix presents some recent experimental data that has not yet been published elsewhere. Some results from density and modulus profile measurements are given along with some data from elongation testing of XLPO materials after accident testing.

### A.1 Bulk Density

Plots of density relative to the initial value ( $D/D_0$ ) are presented in this section as a function of total radiation dose. For reference, the baseline density,  $D_0$ , is shown on the plots. Note that small changes in density are readily detectable, so that a change of only 1-2% can be very significant.

The density data is plotted against total radiation dose. Because of radiation gradients in the test chambers, equal total dose on the plots does not necessarily imply an equal amount of thermal aging. Data from the aging portion of the exposure is coupled with data for the aging plus accident radiation exposures. The data below 600 kGy is from the aging exposures. The data above 600 kGy (as many as four data points) is from the aging (0, 3, 6, or 9 months) plus accident radiation exposures. Unaged samples that were exposed to accident radiation only were included in the 6-month chamber for the accident dose and give a data point at about 800-1000 kGy. This total dose range is below the nominal accident dose because of the locations of the samples in the test chamber.

The density of Brand Rex XLPE insulation (Figure A-3) had a consistent increase to 1.5% above the initial value during the aging exposure. The accident radiation generally increased the density slightly, but after the 9-month aging exposure, the density decreased slightly as a result of the accident radiation exposure. The density of Brand Rex CSPE jacket (Figure A-4) first increased until the total dose reached 100 kGy, then decreased during the remainder of the aging exposure. The accident radiation exposure did not produce any notable effects on the density.

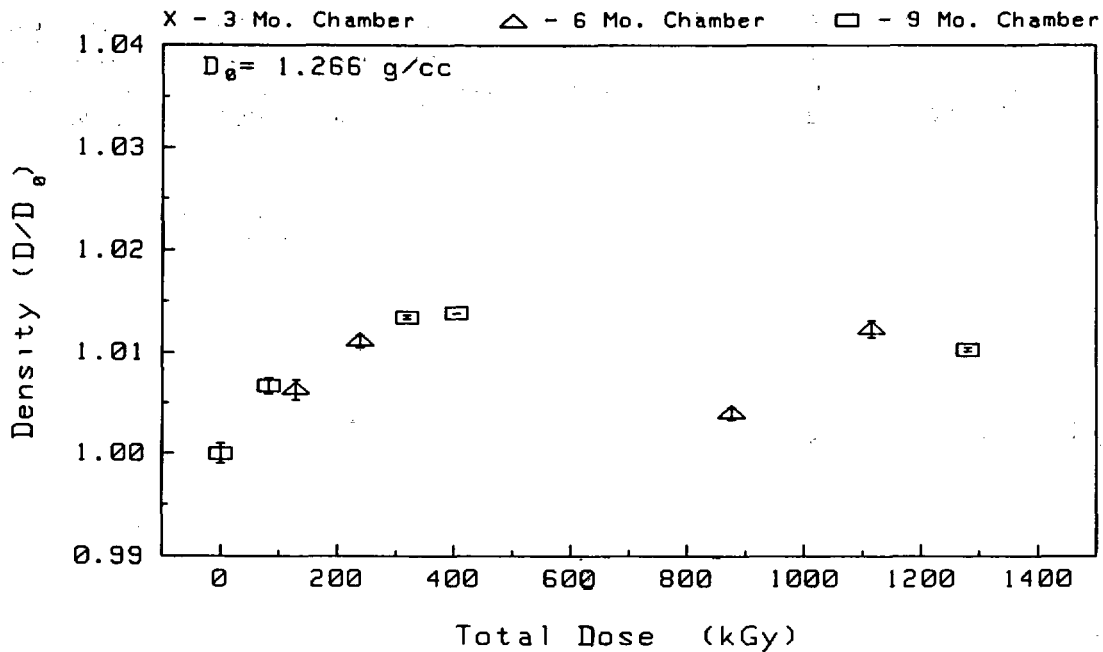


Figure A-3 Density of Brand Rex XLPE Insulation

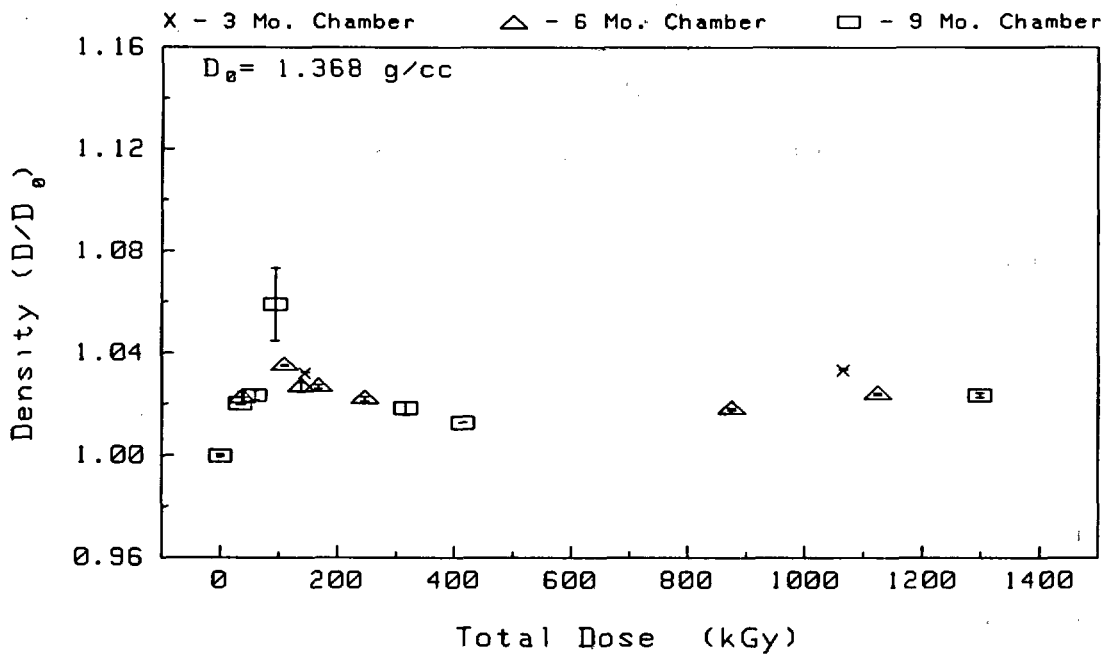


Figure A-4 Density of Brand Rex CSPE Jacket

The density of Rockbestos XLPE insulation (Figure A-5) changed significantly during aging, increasing to 3.5% above the baseline value. For the conditions tested, accident radiation also caused increases in density. Density of the Rockbestos neoprene jacket could not be measured with our density gradient columns because the density was too high.

The density of the BIW CSPE jacket (Figure A-6) had a consistent increase in density, which reached about 4% after the first 250 kGy of aging exposure. Measurements at the highest aging exposures exceeded the range of our density gradient column, indicating that over the entire aging exposure, the density increase was at least 6%. For all the samples tested, the accident radiation exposure caused little or no change in density.

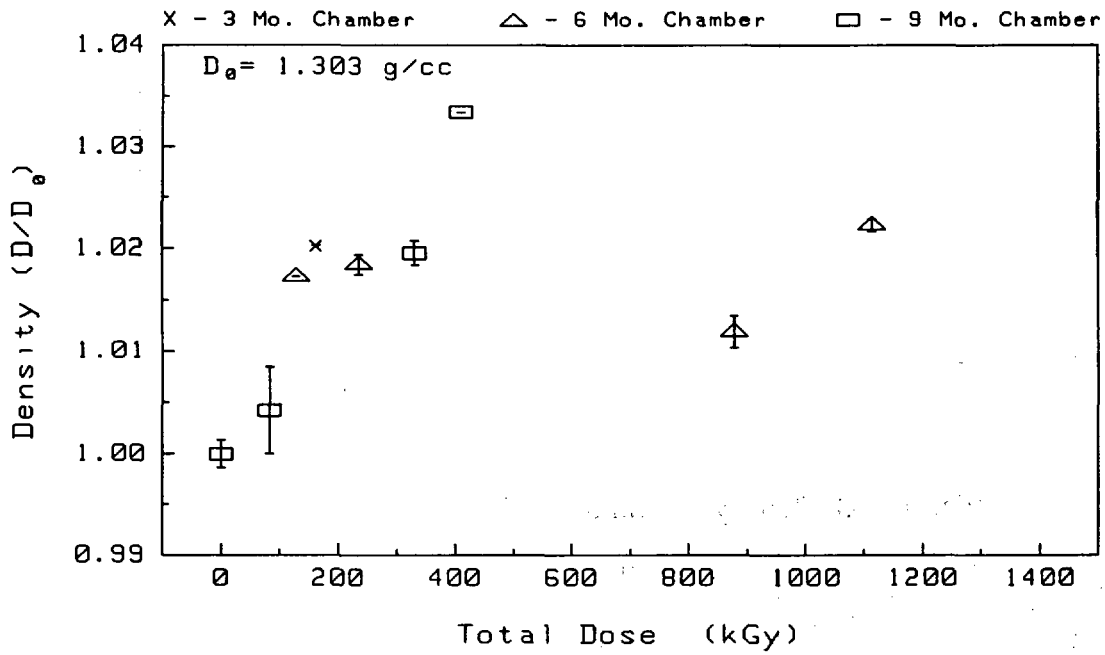


Figure A-5 Density of Rockbestos XLPE Insulation

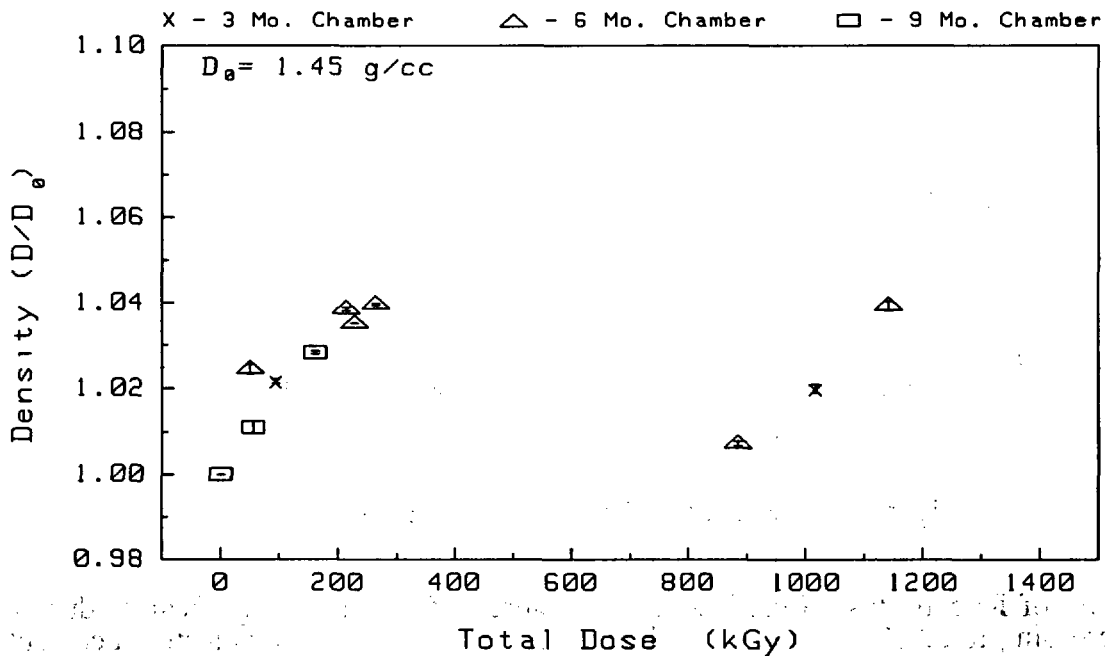


Figure A-6 Density of BIW CSPE Jacket

The density of Dekoron EPDM insulation (Figure A-7) had a consistent and significant increase of about 6% during the 400 kGy aging exposure. The accident radiation exposure caused slight further increases in density for all conditions tested.

## A.2 Modulus Profiling

Modulus profiles are presented in Figures A-8, A-9, A-10, and A-11 for Brand Rex cables. The figures indicate which data is for the insulations and which data is for the jackets (see Figure 2). Each of the figures has data for one pair of cable samples removed from the same 36-cm cable specimen. The air exposed surface during aging was between the two cables in each case. A flat profile through a material is generally expected for unaged samples. A flat profile after aging (assuming a reasonable change in modulus from baseline conditions) generally indicates the absence of significant oxygen diffusion effects. Oxygen diffusion effects occur when aging reactions use oxygen in the material more rapidly than it can be replenished through diffusion. In such cases, material farther from the oxygen supply (i.e., the ambient air) participates less fully in reactions involving oxygen, leading to non-uniform aging. Because aging generally increases the modulus of the materials used in this study, diffusion effects normally result in higher modulus increases at edges that have been exposed to oxygen. Oxygen diffusion effects generally increase with higher temperatures and with higher radiation dose rates. The more that oxygen diffusion effects can be eliminated in a test, the closer the test simulates natural aging conditions. Thus, a major reason for performing the profiles is to evaluate the shape of the profiles, although changes in the absolute value of modulus can also be significant. It should be noted that oxygen diffusion effects may not be the only dose rate effect that a material exhibits. Thus, absence of diffusion effects does not necessarily imply the absence of all dose rate effects.

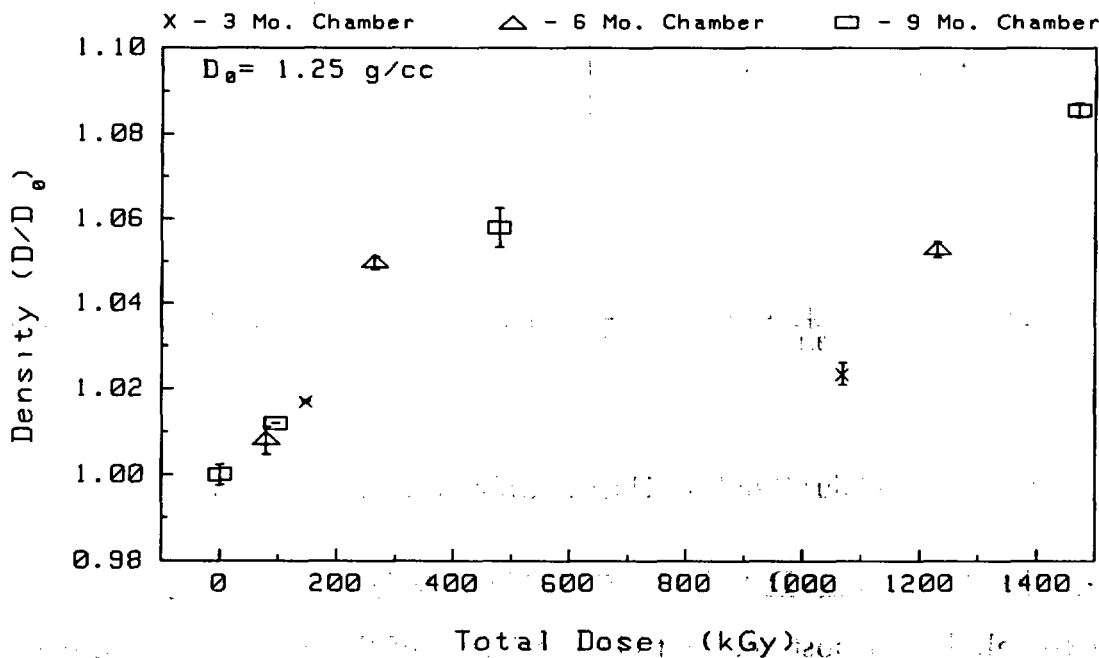


Figure A-7 Density of Dekoron Dekorad EPDM Insulation

The baseline modulus profile of the Brand Rex cable (Figure A-8) is essentially flat for both the insulation and jacket materials. Because the change in modulus of the

insulation was small throughout aging, the following discussion focuses on the jacket modulus. After 3 months of aging (Figure A-9), jacket profile is still flat and the jacket modulus has doubled. After 6 months of aging (Figure A-10), an oxygen diffusion profile has begun to appear in the jacket and after 9 months of aging (Figure A-11), the profile has become more pronounced. Thus, oxygen diffusion effects have apparently not been completely eliminated for this cable. By the end of aging, the average modulus in the jacket increased by a factor of about 100, with a factor of 2-5 gradient in the modulus across the jacket. The jacket surface exposed to the ambient conditions had greater modulus increases than the jacket material that was next to the insulation, as is generally expected when oxygen diffusion effects are present. The lack of diffusion effects until after 3 months of aging indicates that the decrease in oxygen permeation rate as the jacket hardens is probably a significant factor contributing to the diffusion effects later in aging. Because the total aging doses used in this study are significantly higher than those currently postulated for most nuclear power plant locations, diffusion effects that only occur later in aging are less significant than if they had occurred earlier in aging. The small changes in modulus of the insulation make conclusions about possible diffusion effects in the insulation difficult.

Modulus profile data indicted oxygen diffusion effects for some, but not all, of the other cables. Where diffusion effects did occur, evidence indicated the the effects were not severe. Complete analysis of the modulus profile data has not yet been completed.

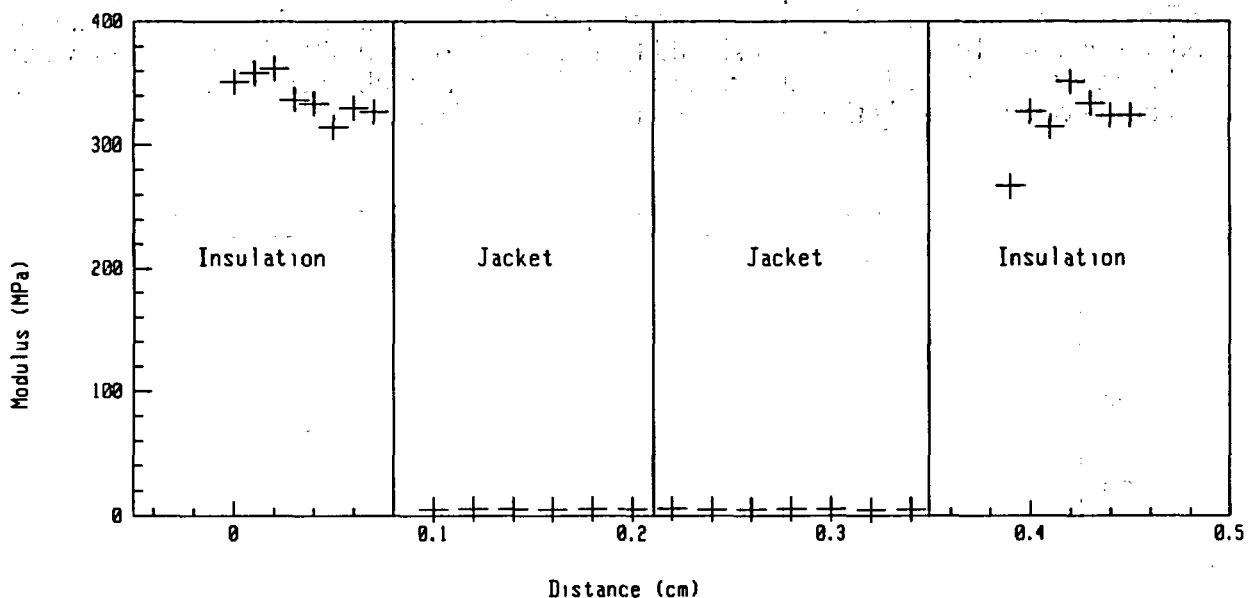


Figure A-8 Modulus Profile of Unaged Brand Rex XLPO Cables

### A.3 Post-Accident Elongation Data for XLPO Cable Materials Aged for 9 Months

Following completion of post-accident electrical tests of the cables that had been exposed to 9 months of aging and then accident tested, the insulation of each XLPO cable product was subjected to elongation testing. Test samples were cut from near the middle of the cables and the copper conductors were removed. The samples were then tested using an Instron Model 1000 tester. The following compares the elongation of each XLPO insulation material at the end of the accident radiation exposure (before the steam exposure) with the elongation after the accident steam exposure:

Cable Type	Before Steam	After Steam
Brand Rex	10%	40%
Rockbestos	<10%	20%
Dekoron Polysat	40%	30%
Raychem	<10%	50%

The above data indicates that elongations of three of the XLPO materials improved with the exposure to the accident environment. (It should be noted that the "After Steam" elongation measurements were performed a long time after completion of the accident steam exposure.) Since the accident environment had apparently improved the properties of some of the XLPO materials, we decided to boil several samples in water for 30 minutes to see if that affected the elongations of the materials. We boiled three samples, one Brand Rex, one Raychem, one Rockbestos. After boiling, the Raychem conductor's elongation was 10%, the Brand Rex conductor's elongation was 40%, and the Rockbestos conductor's elongation was 50%. Note that these values are each higher than comparable samples that were not boiled, indicating that the boiling had a positive effect on the elongation properties of these XLPO materials, consistent with the observed effects of the accident simulation. The increase in flexibility as a result of accident testing or boiling is probably because of plasticizer effects of the moisture and/or the melting and reforming the crystalline structure of the XLPO materials.

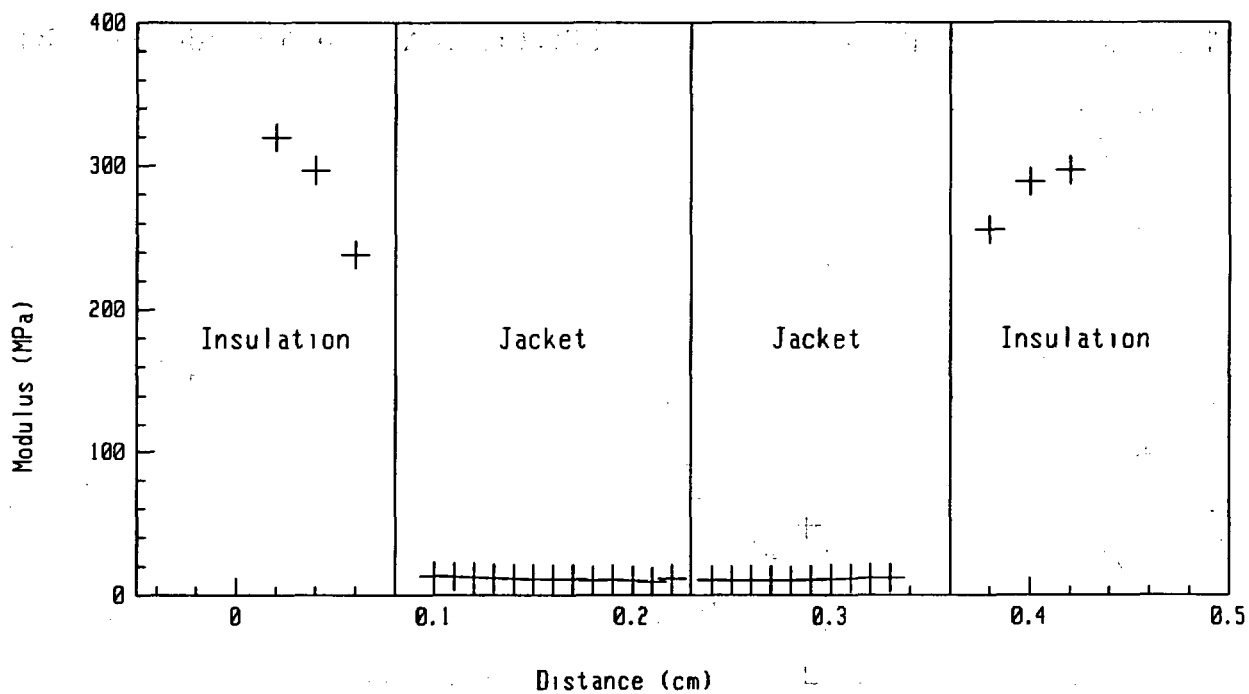


Figure A-9 Modulus Profile of Brand Rex XLPO Cables Aged for 3 Months (89.7 kGy)

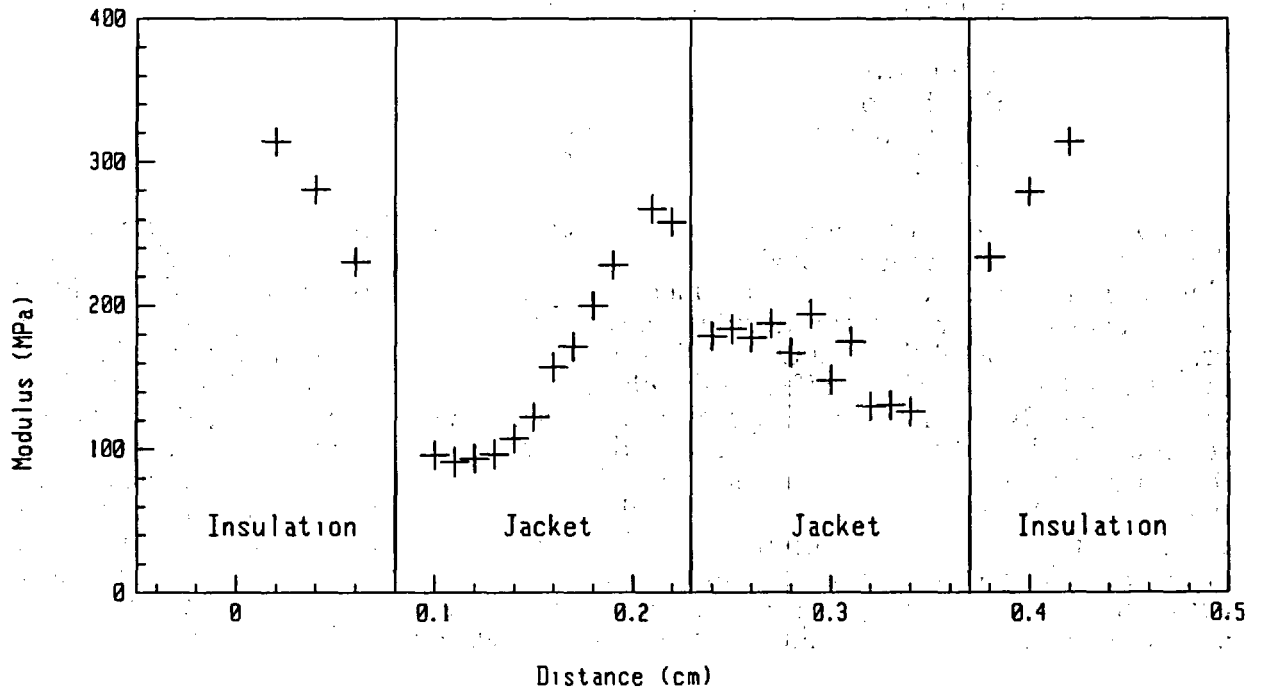


Figure A-10 Modulus Profile of Brand Rex XLPO Cables Aged for 6 Months (359 kGy)

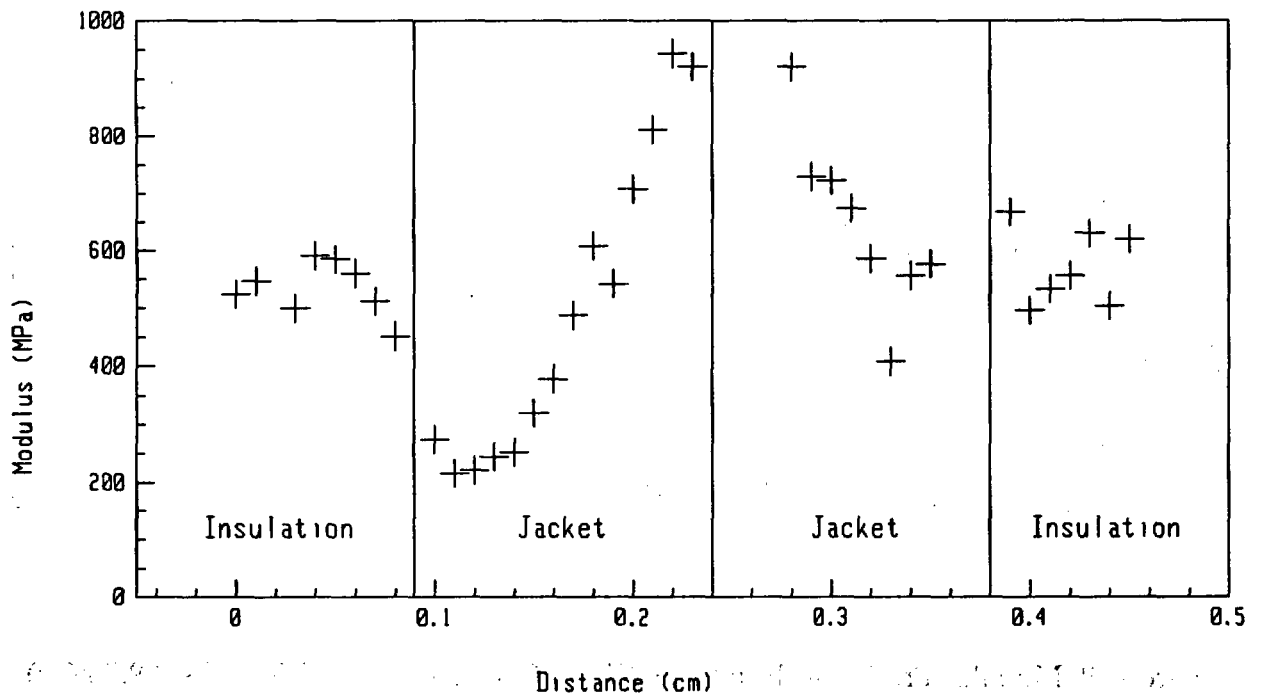


Figure A-11 Modulus Profile of Brand Rex XLPO Cables Aged for 9 Months (484 kGy)

EFFECTS OF AGING ON CALIBRATION AND  
RESPONSE TIME OF NUCLEAR PLANT  
PRESSURE TRANSMITTERS

H. M. Hashemian

Analysis and Measurement Services Corporation  
AMS 9111 Cross Park Drive  
Knoxville, Tennessee 37923

(615) 691-1756

---

ABSTRACT

This paper reports on a comprehensive research project being conducted for the Nuclear Regulatory Commission (NRC) to quantify the effects of normal aging on calibration and response time of nuclear plant pressure, level, and flow transmitters (hereafter referred to as pressure transmitters). The project involved laboratory testing and analysis of typical pressure transmitters of the types used for safety-related pressure measurements in nuclear power plants. The transmitters were aged in simulated reactor conditions and their response time and calibration were tested periodically to determine their long term performance characteristics. Normal aging was emphasized as opposed to accelerated aging.

The project involved research in six areas as follows:

- Aging tests of complete transmitter assembly
- Aging of critical components of transmitters
- Clogging of pressure sensing lines
- Oil loss phenomenon in Rosemount and other transmitters
- Evaluation of methods for on-line testing of pressure transmitters
- Analysis of Licensee Event Report (LER) and Nuclear Plant Reliability Data System (NPRDS) databases for failures of pressure sensing systems in nuclear power plants.

The above research areas are individually discussed in the paper and their key results are presented.

The majority of the transmitters tested in this study were from four U.S. manufacturers: Barton, Foxboro, Rosemount, and Tobar (Tobar was formerly known as Westinghouse Veritrak). These manufacturers supply the majority of the transmitters that are currently used for safety-related pressure measurements in U.S. nuclear power plants.

## 1. INTRODUCTION

A pressure sensing channel in a nuclear power plant consists of three components: the pressure transmitter, sensing lines, and the signal conditioning equipment including the reactor trip circuitry. The first two systems are generally located in the plant and the third one is located in the control room area. Aging can cause degradation in the mechanical or electronic systems within the transmitter, produce clogging in sensing lines, or cause drift in the signal conditioning equipment. To account for these problems, the three components of the system should be tested periodically to ensure that the performance of the sensing channel is maintained within an acceptable limit while the plant is operating. The three components may be tested separately or combined. The testing frequency should be based on an assessment of the degradation rate of the system.

Currently, pressure transmitters are generally calibrated once every fuel cycle and response time tested once every four fuel cycles. The sensing lines are rarely tested for clogging, and the signal conditioning equipment and trip circuitry are tested as often as every month. These testing frequencies are based on the accessibility and availability of the components for testing, rather than their degradation rates. Ironically, pressure transmitters and sensing lines that are mostly located in the harsh environments in the field are tested much less often than the signal conditioning equipment that is located in the control room area in a mild environment.

The aging study that is reported here was the first systematic attempt to estimate the degradation of pressure transmitters and sensing lines. The degradation of the signal conditioning equipment in a pressure sensing channel was not studied since this equipment is in mild environments of the plant and is adequately tested already.

## 2. PROJECT OBJECTIVES

The current nuclear industry practice is to calibrate all and response time test one-fourth of the safety-related pressure transmitters once every fuel cycle. The goal of the research project reported herein was to evaluate the adequacy of this testing practice for management of aging of nuclear plant pressure transmitters.

The results of the research conducted here have indicated that calibrating the transmitters once every fuel cycle is adequate, but response time testing should not be limited to one-fourth of the redundant transmitters. As in the case of calibration, response time testing should be performed on all pressure transmitters once every fuel cycle. This is particularly important for those transmitters such as Barton transmitters, whose response time can degrade due to both the aging of the transmitter itself, and clogging of its sensing lines.

Testing the response time of one of each four redundant pressure transmitters once every fuel cycle can leave up to ten years in between the response time tests of these transmitters. This period is too long considering the research results reported herein, the statistics in the LER and NPRDS databases, and the experience with response time testing of pressure transmitters in nuclear power plants.

### 3. AGING TEST OF COMPLETE TRANSMITTER ASSEMBLIES

The project began by aging a group of pressure transmitters for the effect of heat and humidity. The transmitters were first calibrated and response time tested, and then installed in an environmental chamber and activated. The normal steady state output of the transmitters were monitored throughout the aging period to characterize their drift. The tests were performed for approximately twelve months at 110°F and 65 percent relative humidity. The transmitters were removed from the environmental chamber at the end of the aging period and calibrated and response time tested to determine their total shift for the twelve months of aging.

Twenty-three pressure transmitters (not including a few reference transmitters) representing Barton, Foxboro, Rosemount, and Tobar (Veritrak) were included in the aging tests in the environmental chamber. Various behavior was exhibited by these transmitters. This included monotonic upward or downward drift, sudden shifts in output, erratic output, and normal output with no detectable drift or unusual behavior. Figure 1 shows the four predominant behaviors exhibited by the transmitters. Overall, the aging test results showed that a unique drift rate cannot be identified for the transmitters and we therefore characterized the transmitters' drift in terms of a drift band as opposed to a drift rate. The average drift band of the transmitters tested in the environmental chamber was approximately  $\pm 2$  percent of calibrated span for one year at 110°F and 65 percent relative humidity. Figure 2 shows some of the aging test results.

In addition to the steady state performance, the effects of heat and humidity on the dynamic response of the transmitters were evaluated. Response time measurements were performed before and after the transmitters were installed in the environmental chamber and the results were compared to identify any changes beyond 20%. The 20% threshold was selected as a reasonable value for the repeatability of response time measurements and any background degradation. Three of the twenty-three transmitters (13%) showed a shift in response time beyond the 20% threshold (Table 1).

In the aging tests described above, a few transmitters were installed outside of the environmental chamber as reference transmitters to account for the repeatability of the tests and any background degradation associated with shelf-life drift.

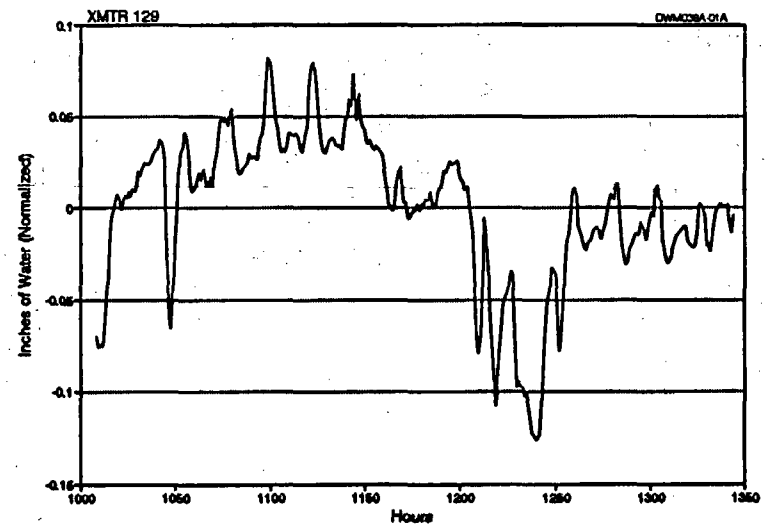
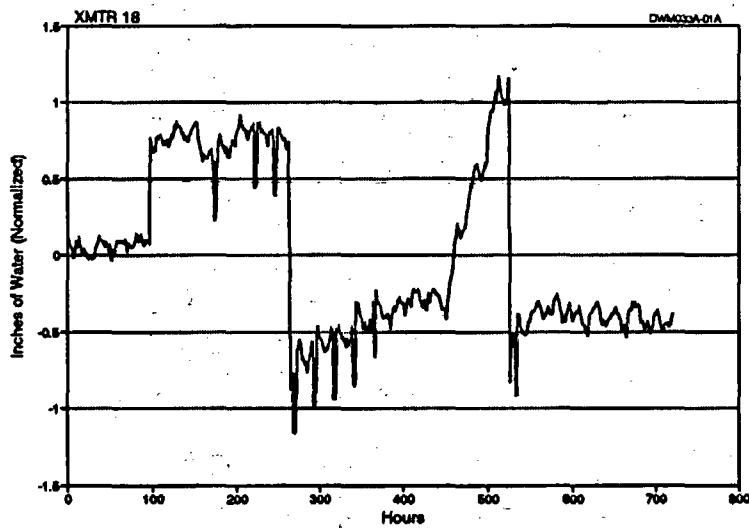
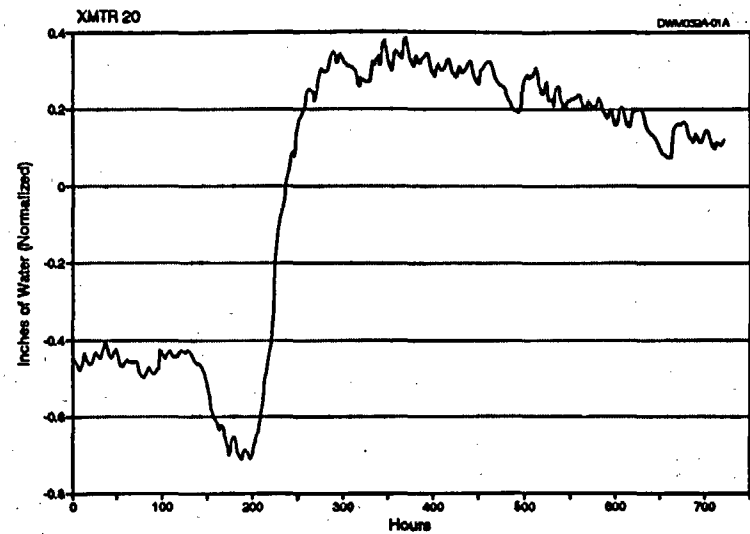
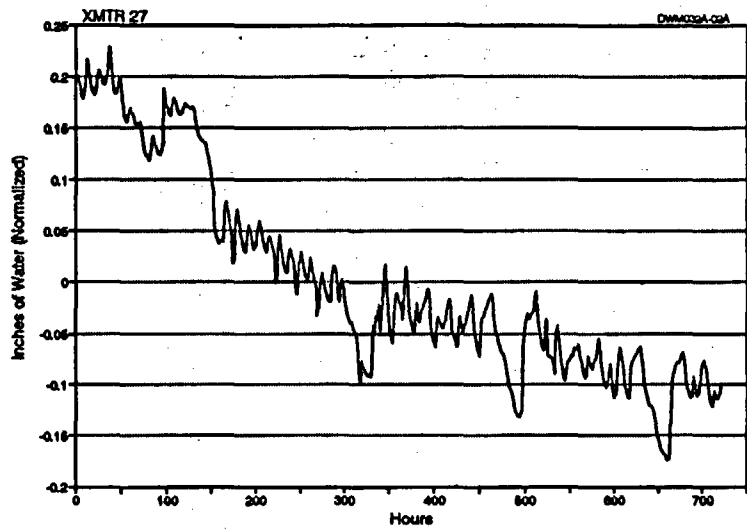


Figure 1. Behavior of Pressure Transmitters Under Heat and Humidity Aging.

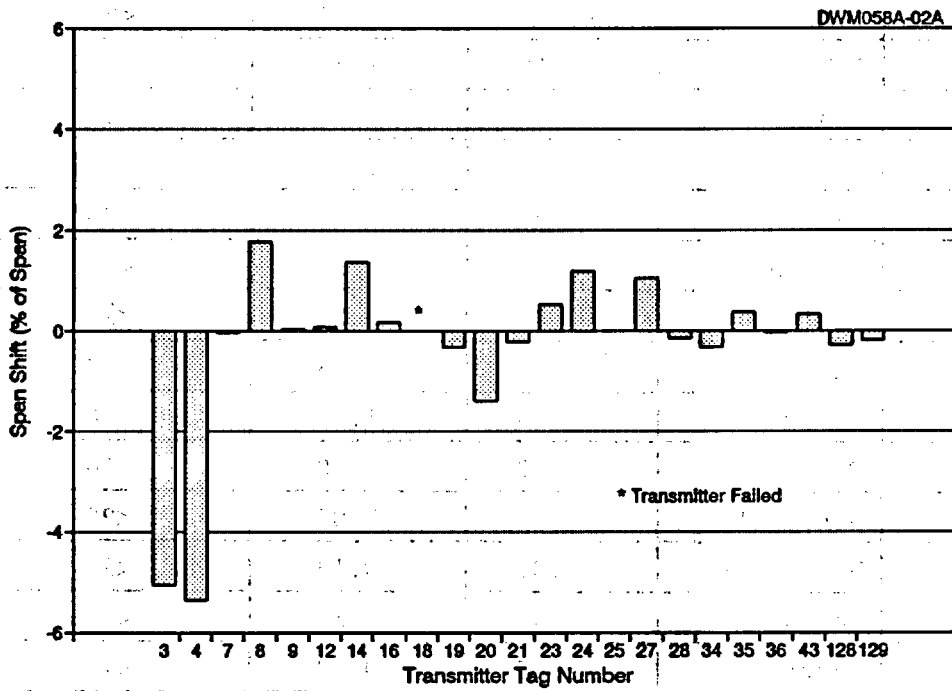
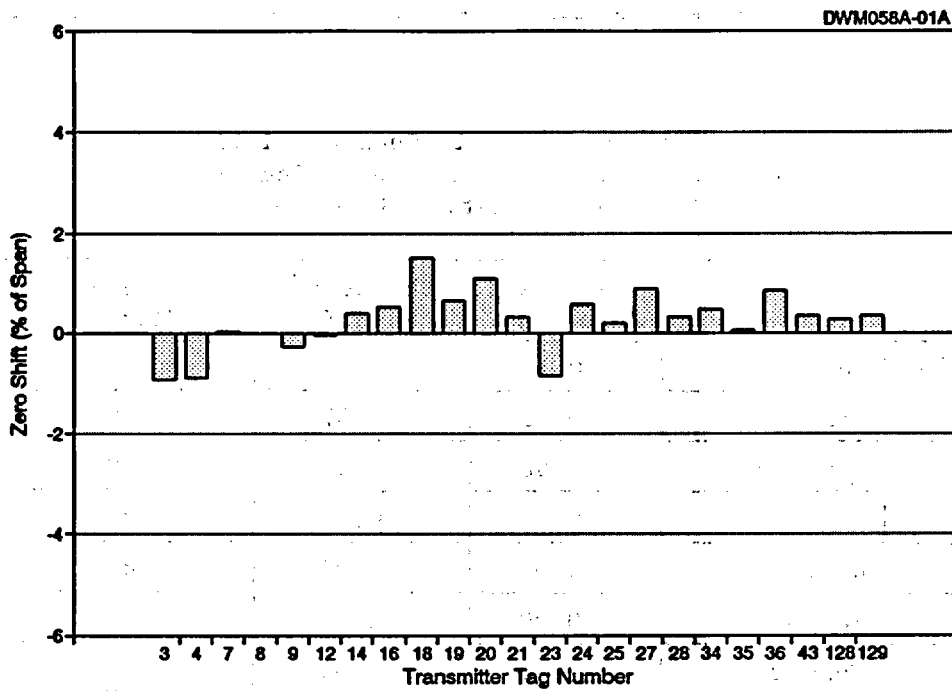


Figure 2. Sample Results of Aging Tests for the Effect of Heat and Humidity.

**TABLE 1**

**Changes in Static and Dynamic Characteristics of Transmitters for 12 Months of Aging at 110°F and 65% Relative Humidity**

Tag #	Make	Calibration Shifts <sup>(1)</sup>		Response Time <sup>(2)</sup> Changes (%)
		Zero (%)	Span (%)	
1 <sup>(3)</sup>	Foxboro	0.53	-3.35	<20
3	Foxboro	-0.93	-5.07	23%
4	Foxboro	-0.88	-5.37	<20
6 <sup>(3)</sup>	Foxboro	0.00	0.55	<20
7	RSMT	0.03	-0.03	<20
8	Foxboro	0.00	1.75	<20
9	Foxboro	-0.28	0.03	<20
11 <sup>(3)</sup>	Foxboro	0.08	1.92	<20
12	RSMT	-0.03	0.08	<20
14	RSMT	0.40	1.35	>100%
16	Tobar	0.53	0.18	<20
18	Barton	1.50	20.00	>100%
19	Barton	0.65	-0.30	<20
20	Barton	1.11	-1.39	<20
21	RSMT	0.32	-0.22	<20
23	Barton	-0.85	0.53	<20
24	Tobar	0.58	1.17	<20
25	Tobar	0.20	0.00	<20
27	Honeywell	0.88	1.05	<20
28	Honeywell	0.33	-0.13	<20
34	Barton	0.48	-0.30	<20
35	Barton	-0.05	0.37	<20
36	Barton	0.85	-0.03	<20
43	RSMT	0.35	0.32	<20
128	Bailey	0.28	-0.28	<20
129	Bailey	0.35	-0.18	<20

- (1) All calibration shifts are presented as percentage of total calibration span.  
 (2) Response times were measured using the ramp test method.  
 (3) Reference transmitter.

#### 4. COMPONENT AGING

Component aging was performed by two methods. The first method employed a commercial software package called "P Spice" which is used for the study of steady state and transient response of electrical and electronic circuits. The electronics of typical pressure transmitters were simulated in P Spice and their response to changes in the values of electronic components were determined. Typical results are shown in Table 2 for a Barton model 764 pressure transmitter.

The second method involved thermal aging of the individual components for a few hours at approximately 150°F. The transmitters were tested before, during and after the aging. Sample results are shown in Figure 3 for a few circuit components of a Rosemount Transmitter. Similar results are shown in Table 3. It is apparent that the application of the heat did not cause any permanent change in the value of the components as evident in the results of tests after the aging.

#### 5. DEGRADATION OF PRESSURE SENSING LINES

Sensing lines are used to bring the pressure signal from the process to pressure transmitters located about 20 to 200 feet away from the process, depending on the plant and the pressures being measured. There are pneumatic, oil-filled, and water-filled sensing lines in nuclear power plants. Water-filled sensing lines are the most prevalent type and were therefore the type selected to be studied in this project.

Water-filled sensing lines can become partially or totally blocked over a period of time as sludge is built up in the system, boron solidification, and other effects. The blockage will not have a significant effect on the steady state performance of transmitters, but can cause a large increase in the response time of transmitters.

The study of sensing lines in this project involved simulating blockages using snubbers placed in the sensing lines in a laboratory test loop. Figure 4 shows laboratory response time results as a function of induced blockages in the sensing lines. It is apparent that the effect of blockages is different in different transmitters. More specifically, the effects of sensing line blockages on the response time of a pressure sensing system depends predominantly on the volumetric displacement of the sensing element in the transmitter. If the transmitter operates based on a measurable volumetric displacement of sensing element when a pressure is applied, then its response time will depend very much on any blockage in the sensing line that can restrict the flow to the transmitter. On the other hand, if the sensing element does not have to move much to indicate the pressure, sensing line blockages will not be as important unless they are advanced to over 90 percent of the original diameter of the sensing line.

**TABLE 2**

**PSpice Simulation of Barton 764 Transmitter**

**Transmitter Output Sensitivity**

<b>Component</b>	<b>mV Change/ 1% Change in Component Value</b>	<b>% of Span Change/ 1% Change in Component Value</b>
R <sub>1</sub>	44.5	1.1
R <sub>3</sub>	- 73.4	1.8
R <sub>9</sub>	83.5	2.1
R <sub>15</sub>	- 48.6	1.2
R <sub>14</sub>	35.1	0.9
R <sub>10</sub>	- 32.7	0.8
R <sub>17</sub>	29.8	0.7
R <sub>18</sub>	- 29.6	0.7

R<sub>x</sub>s are resistors used in the electronics of the Barton transmitter.

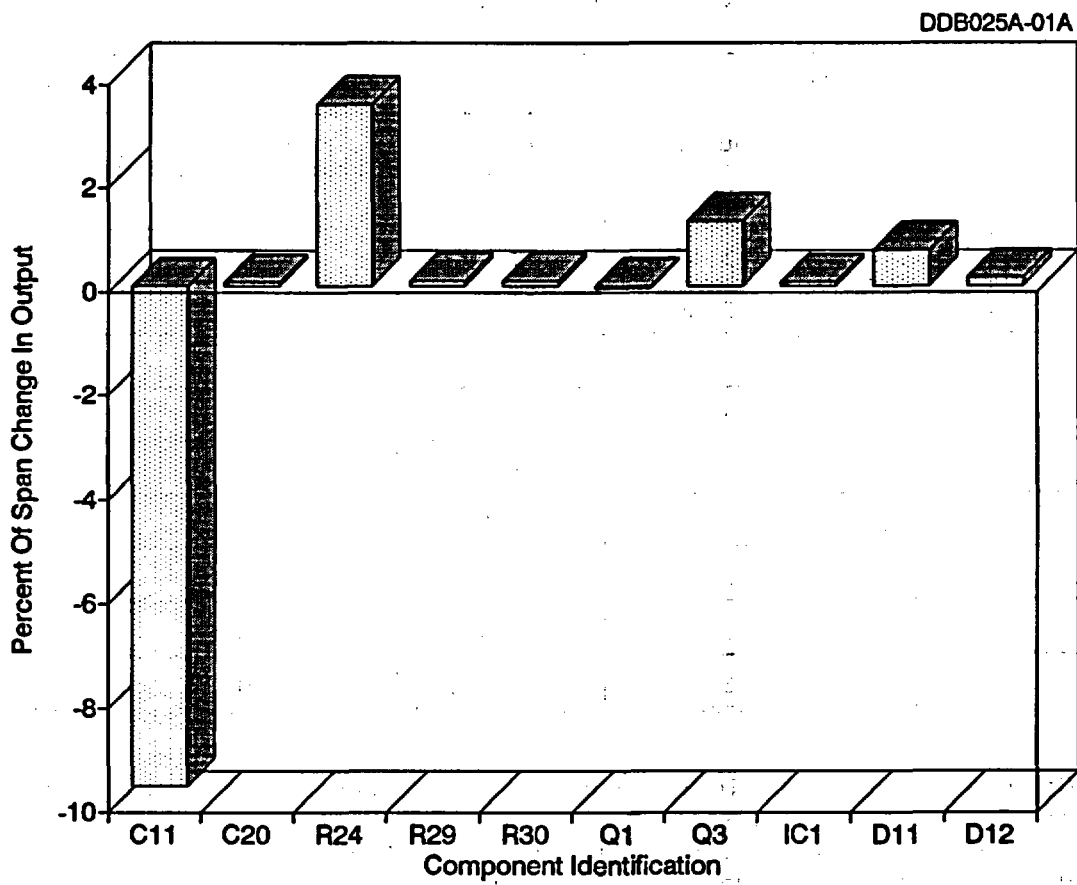


Figure 3. Sample Results of Component Aging Tests.

**TABLE 3**

**Component Aging Test Results for Selected Components of the  
Amplifier Circuit Board in a Rosemount 1151 Transmitter**

Component Identification	Transmitter Output			Change in Output Percent of Span	
	Before	During	After	During	After
C11	3.483	3.148	3.483	-9.62	0
C20	3.483	3.485	3.483	0.06	0
R24	3.483	3.605	3.483	3.50	0
R29	3.483	3.486	3.483	0.09	0
R30	3.483	3.486	3.483	0.09	0
Q1	3.483	3.481	3.483	-0.06	0
Q3	3.483	3.526	3.483	1.23	0
IC1	3.483	3.485	3.483	0.06	0
D11	3.483	3.507	3.483	0.69	0
D12	3.483	3.489	3.483	0.17	0

- C: Designates a critical capacitor in the transmitter electronics.
- R: Designates a resistor in the transmitter electronics.
- Q: Designates a transistor in the transmitter electronics.
- D: Designates a diode in the transmitter electronics.

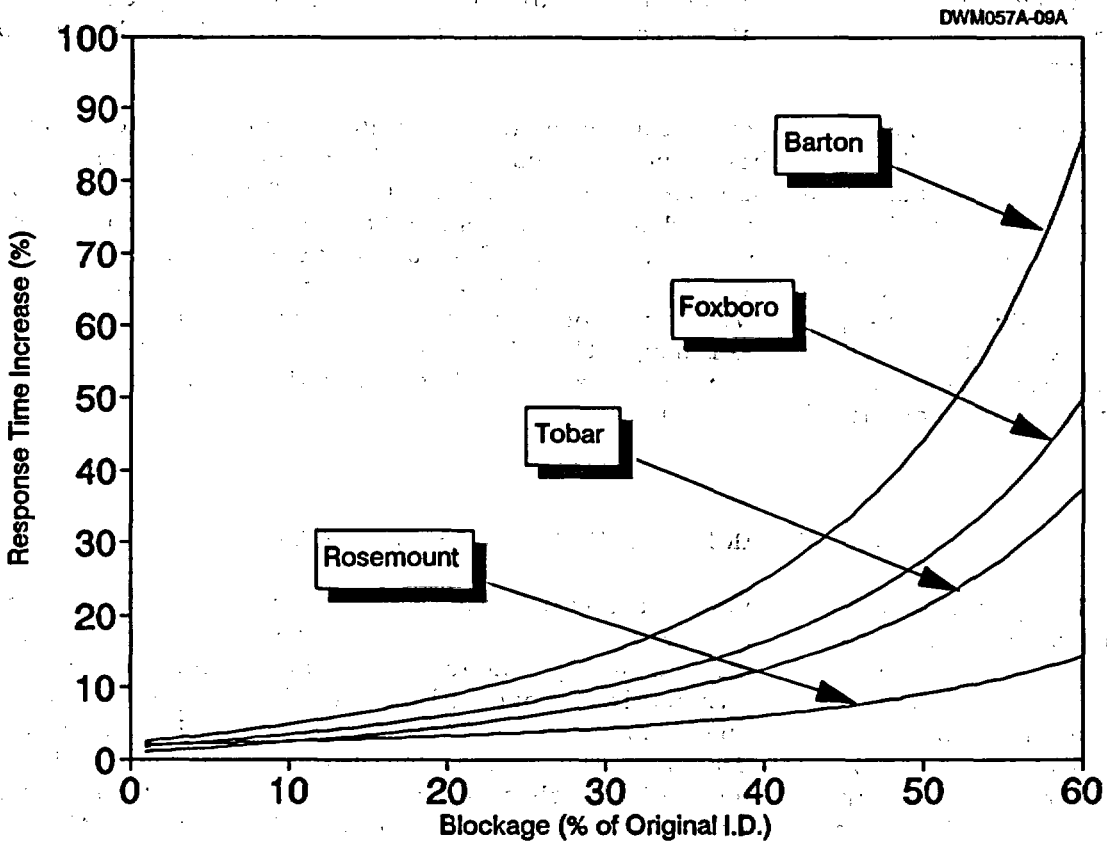


**Figure 4. Effect of Sensing Line Blockage on Response Time of Pressure Transmitters.**

## 6. OIL LOSS PHENOMENON

Oil loss is a well-known problem in certain models of pressure transmitters made by Rosemount. In these Rosemount transmitters, silicon oil is used to transfer the pressure signal from the isolation diaphragm that is in contact with the process fluid to the sensing diaphragm inside the transmitter. If the oil leaks out of the transmitter, the dynamic response of the transmitter can become sluggish in addition to a change in calibration (Zero and Span) that occurs slowly as oil leaks from the transmitter. Table 4 shows oil loss results from experiments with a normal and a failed Rosemount model 1153 transmitter. Note that the transmitter that has suffered oil loss is not only sluggish compared to the normal transmitter, but also it has become nonlinear as evident in the large differences between the response time results from tests with increasing and decreasing ramp input signals. The nonlinearity problem makes it more difficult to identify the oil loss with on-line or off-line test methods especially if the transmitter does not operate close to its pressure setpoint during plant operation.

The performance of transmitters other than Rosemount are not adversely affected by the oil loss phenomenon because the oil is used as a damping fluid in these transmitters, as opposed to a transfer fluid. Table 5 shows response time test results for a Tobar and a Barton transmitter with and without induced oil loss. Figure 5 shows the response time of a Barton transmitter as a function of oil removed. It is apparent that the Tobar and Barton transmitters become faster in dynamic response with oil loss due to less damping of the mechanical system of the transmitters. Although the oil loss is not immediately detrimental to the performance of these transmitters, it has a significant effect on their longevity and mechanical integrity.

## 7. ON-LINE TEST OF PRESSURE TRANSMITTERS

The performance of pressure transmitters is verified by period calibration and response time testing. Presently, calibration testing cannot be done on-line, but new methods are currently under development and validation and should be available for use in nuclear power plants in 2 to 4 years. Response time testing, however, can be performed on-line using the noise analysis and Power Interrupt (PI) techniques. The noise analysis technique is based on monitoring the natural fluctuations that exist at the output of pressure transmitters while the process is operating. It has been shown that these fluctuations can be analyzed to give the response time of pressure transmitters including the sensing lines.<sup>(1)</sup>

The PI method is applicable only to force balance pressure transmitters. It is based on turning the transmitter's power off, and then on. It has been shown that the transmitter's output after the power is turned on is a transient that can be analyzed to give the response time of the complete electromechanical system of the transmitter.<sup>(2)</sup>

**TABLE 4**

**Results of Laboratory Response Time Tests  
of Rosemount 1153 Transmitters**

Transmitter Setting	Response Time (sec)	
	Increasing Ramp	Decreasing Ramp
<u>Normal 1153</u>		
Low	0.12	0.13
Medium	0.12	0.13
High	0.15	0.13
<u>Failed 1153</u>		
Low	0.23	171.0
Medium	0.25	19.0
High	0.25	1.1

**TABLE 5**

**TOBAR TRANSMITTER**

**Response Time Results  
Before and After Induced Oil Loss**

<b>Test Signal</b>	<b>Response Time (sec)</b>	
	<b>Before</b>	<b>After</b>
<b>Increasing Ramp</b>	<b>0.17</b>	<b>0.11</b>
<b>Decreasing Ramp</b>	<b>0.18</b>	<b>0.12</b>

**BARTON TRANSMITTER**

**Response Time Results Versus Percentage of Oil  
Removed From the Transmitter**

<b>Amount of Oil Removed</b>	<b>Response Time (sec)</b>	
	<b>Increasing Ramp</b>	<b>Decreasing Ramp</b>
<b>FULL</b>	<b>0.19</b>	<b>0.19</b>
<b>50%</b>	<b>0.16</b>	<b>0.16</b>
<b>75%</b>	<b>0.12</b>	<b>0.12</b>
<b>100%</b>	<b>0.10</b>	<b>0.11</b>

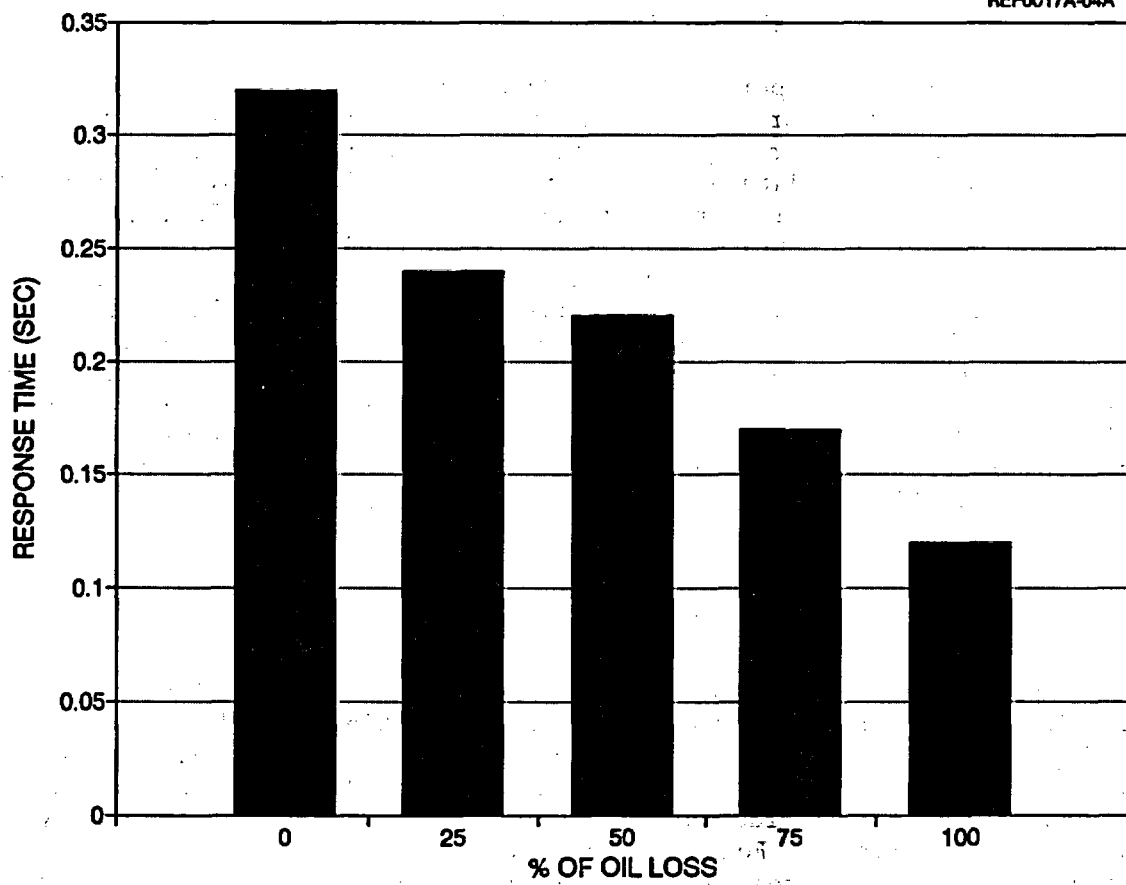


Figure 5. Response Time of a Barton Transmitter for Various Amounts of Oil in the Transmitter.

The validity of the noise analysis and Power Interrupt methods has been established by laboratory testing of representative transmitters from Barton, Foxboro, Rosemount, Tobar, and Veritrak. Based on the results of the laboratory validation tests, it has been determined that the accuracy of the noise analysis and PI methods for typical transmitters is better than 0.10 seconds, provided that the dynamic characteristics of the transmitters are predominantly linear, and in the case of noise analysis, the transmitters are driven by wideband process noise with suitable spectral characteristics.

The noise analysis and PI methods are currently used in many nuclear power plants for quantitative response time measurements on pressure, level and flow transmitters.

### 8. SEARCH OF LER AND NPRDS DATABASES

The Licensee Event Report (LER) and Nuclear Plant Reliability Data System (NPRDS) databases were searched for failures of pressure sensing systems in nuclear power plants. The analysis of these databases has shown that there is not enough data in the databases to draw a reliable conclusion about the degradation trend of pressure transmitters in nuclear power plants. Figure 6 shows how the number of failure reports in NPRDS database has increased after 1983. The increase is most likely due to changes in reporting requirements and reporting commitments rather than increased frequency of failure of pressure transmitters. Figure 7 shows a decrease in the number of LERs after 1983. This is because of a change in the LER reporting requirement that became effective in the 1983 time period. It is apparent that it will take several more years before LER and NPRDS databases are full and stable enough to serve as a reliable source for trending information about performance of pressure transmitters. Note in Figure 6 that the 1988 data is not for the whole year.

### 9. CONCLUSIONS

A comprehensive research project has been underway for the last three years to determine the effects of normal aging on calibration stability and response times of pressure, level and flow transmitters in nuclear power plants. The project involved experimental aging of representative transmitters in simulated reactor conditions in a laboratory. The work was performed on typical transmitters from Barton, Foxboro, Rosemount, Tobar, and Veritrak. These manufacturers represent almost all the pressure transmitters that are currently used for safety-related pressure measurements in U.S. nuclear power plants.

The main goal of the project was to determine if the nuclear industry's practice of testing the transmitters once every fuel cycle is adequate for management of aging of the transmitters. In addition, other outstanding issues such as the oil loss phenomenon in Rosemount and other pressure transmitters were addressed, the effects of sensing line blockages on response time of pressure

NPRDS for Transmitters

JJG014A-01A

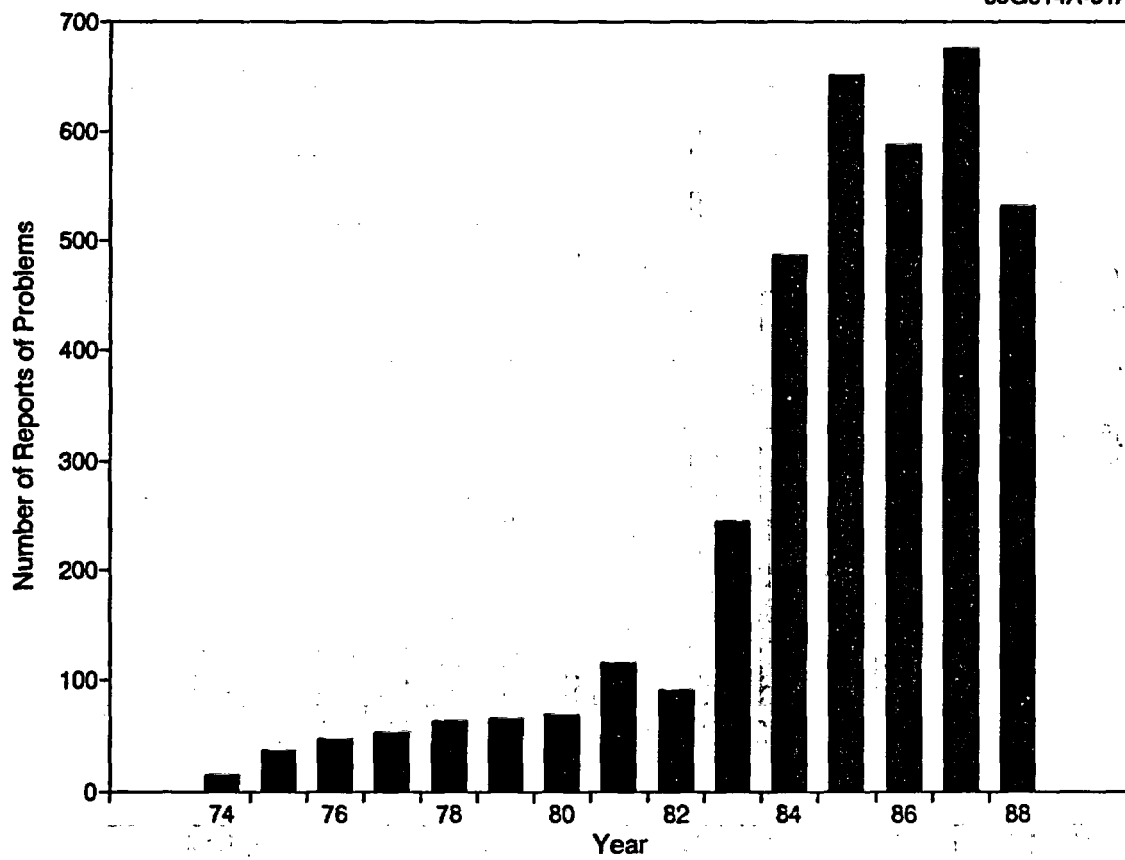


Figure 6. NPRDS Reports of Failures of Pressure Sensing Systems in Nuclear Power Plants.

### Instrumentation Failures In All Systems

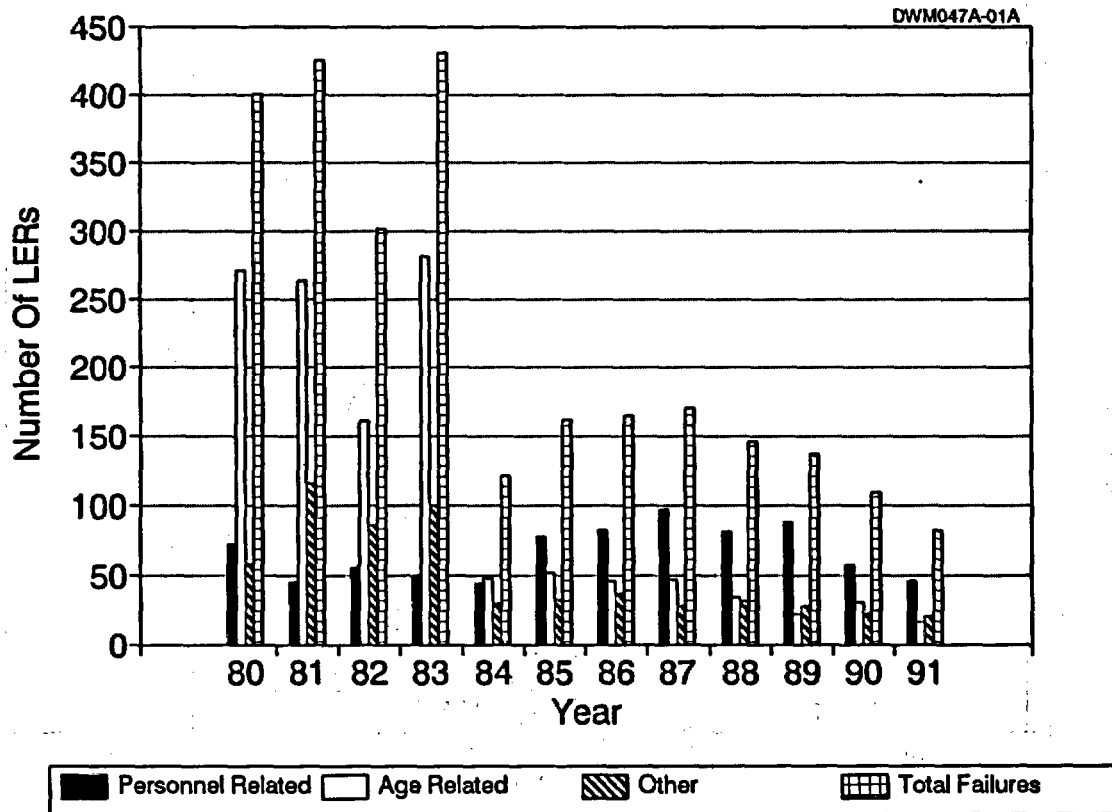


Figure 7. LER Reports of Failures of Pressure Sensing System in Nuclear Power Plants.

transmitters were quantified, and the on-line methods for response time testing and calibration of pressure transmitters were evaluated. The LER and NPRDS databases were searched as a part of the project and analyzed for failures of pressure sensing systems in nuclear power plants.

The project has concluded that in light of a moderate number of degradations that were observed in the project and found in databases, testing the response time and calibration of pressure transmitters once every fuel cycle or every 18 to 24 months should be adequate for management of normal aging of pressure transmitters, provided that all safety-related pressure transmitters are tested as opposed to testing only one out of four redundant transmitters.

The oil loss phenomenon was found to be an important safety issue only in Rosemount pressure transmitters in which silicon oil is used to transfer the pressure signal from the process to the sensing element in the center of the transmitter. In other pressure transmitters (i.e., Barton, Foxboro, Tobar, and Veritrak) the oil is used as a damping fluid and it does not play a major role in the normal performance of the transmitters. The significance of oil loss in Rosemount transmitters is that it can lead to calibration shift and response time degradation, both of which can go undetected unless an on-line monitoring system is implemented or periodic tests are performed to account for the problem.

The search and analysis of the LER and NPRDS databases did not reveal any unusual or systematic problem in the pressure sensing systems of nuclear power plants except to confirm our laboratory findings that pressure transmitters suffer calibration shifts and response time degradation in a moderate rate, and the current testing practices in the nuclear industry is therefore justified for aging management of the transmitters from the manufacturers we tested in this study.

## 10. REFERENCES

1. Hashemian, H.M., et.al, "Effect of Aging on Response Time of Nuclear Plant Pressure Sensors", U.S. Nuclear Regulatory Commission, NUREG/CR-5383, (June 1989).
2. Hashemian, H.M., Petersen, K.M., "Response Time Testing of Pressure Transmitters in Nuclear Power Plants", Instrument Society of America, First Annual Joint ISA/EPRI Power Instrumentation Symposium, St. Petersburg, FL, (June 1991).

# SNUBBER AGING ASSESSMENT: RESULTS OF NPAR PHASE II IN-PLANT RESEARCH<sup>(a)</sup>

D. E. Blahnik and E. V. Werry  
D. P. Brown<sup>(b)</sup>

Pacific Northwest Laboratory<sup>(c)</sup>  
Richland, Washington 99352

## ABSTRACT

Snubbers are safety-related devices used to restrain undesirable dynamic loads at various piping and large equipment locations in nuclear power plants (NPPs). Snubbers are designed to accommodate normal thermal movements of a plant's operating systems or equipment and to be capable of restraining the maximum off-normal dynamic loads postulated for its specific location. Snubbers are subject to the effects of aging, and the factors that degrade their safety performance need to be better understood. This paper describes the U.S. Nuclear Regulatory Commission (NRC) Phase II Nuclear Plant Aging Research (NPAR) in-plant aging study conducted to enhance the understanding of snubber aging, providing a basis to mitigate its consequences. The research methodology, results, recommendations, and conclusions are described in this paper. Recommendations for monitoring the service life of snubbers is a principal result of the research, and will provide input to the American Society of Mechanical Engineers (ASME) Operations and Maintenance (OM) Code, Sub-section ISTD.

## DISCUSSION

### SNUBBER USAGE

Snubbers are dynamic restraining devices used in commercial nuclear power plants (NPPs). Snubbers are available in two basic types: hydraulic and mechanical. Hydraulic snubbers, which have been in service for many years, are used to restrain safety-related equipment and piping systems. The majority of mechanical snubbers, which have been used predominantly within the last decade, are used solely to restrain piping systems.

- 
- (a) Work supported by the U.S. Nuclear Regulatory Commission, Office of Nuclear Regulatory Research.
- (b) Lake Engineering Company, Greenville, Rhode Island 02828.
- (c) Operated for the U.S. Department of Energy by Battelle Memorial Institute under Contract DE-AC06-76RLO 1830.

Snubber procurement and usage falls within the purview of Title 10, Part 50 of the Code of Federal Regulations (CFR), Appendix A (General Design Criteria for Nuclear Power Plants) and Appendix B (Quality Assurance Criteria for Nuclear Power Plants). These regulations stipulate that systems, structures, and components, (e.g., snubbers) shall be designed to withstand the effects of normal and off-normal dynamic reactions. The principal normal dynamic reactions are those associated with thermal expansions and contractions during plant start-ups and shutdowns; off-normal dynamic reactions are primarily those associated with postulated seismic loads. To comply with the CFR, each snubber must therefore allow for expansion or contraction under normal plant operations, while maintaining the capability to restrain the maximum off-normal dynamic load by locking up and restraining dynamic motion.

### SNUBBER RESEARCH AND OBJECTIVES

The NPP industry and the codes and standard groups, i.e., ASME and the NRC, have recognized the need to enhance the performance of snubbers. Snubbers are subject to age-related degradation, and their effective operation is important to a plant's continued safe operation. The NRC's NPAR Program Plan,<sup>(1)</sup> originally introduced in 1985, provided a logical avenue for sponsorship of snubber aging research and the identification of improved service-life monitoring techniques for snubbers. The NPAR strategy involves a two-phase approach for conducting research. Phase I<sup>(2)</sup> provided a preliminary assessment of snubber aging. A Phase II interim study<sup>(3)</sup> provided an aging assessment and recommendations for snubber research. Specific information on snubber performance, obtained through in-plant research, involved sending research staff to various NPPs.<sup>(4)</sup> The following research objectives for evaluating the effects of aging on mechanical and hydraulic snubbers were developed during Phase II:

- enhance the understanding of how snubbers age and degrade
- enhance the understanding of snubber failure characteristics
- determine the technical information needed to improve the level of snubber performance.

This paper describes the in-plant research to meet these objectives and the results of the research. Cooperation from various utilities significantly enhanced this effort.

### SUMMARY OF IN-PLANT RESEARCH

The in-plant research involved 1) selecting potential sites for research, 2) conducting interviews and determining which sites were to be visited, and 3) site visits to obtain and analyze snubber service data. The first two tasks were vitally important in determining the quality and quantity of snubber data available. The study was structured to select plants with comprehensive inspection and testing programs and plants that maintained records on snubber failures.

The third task, the information gathering and analysis process, was conducted in two parts. Part one involved interviews with the site engineering and maintenance staff and review of snubber tracking databases, snubber failure reports, functional test data, and maintenance practices. Part two involved analysis of the special data collected at each site, e.g., the maintenance records and the inservice inspection (ISI) and test records.

Eight sites (13 plants) were visited. The principal goal of the plant visits was to gain an updated perspective of recent performance history for both mechanical and hydraulic snubbers. Because there was little information on mechanical snubbers, special emphasis was placed on gathering information on the performance, testing, and maintenance of these devices. Five of the sites were key sites for evaluating mechanical snubbers, two sites were key sites for evaluating hydraulic snubbers, and one site was selected for snubber service-life monitoring techniques.

Approximately 95% of all mechanical snubbers in NPP service are the acceleration-limiting type; most of the remaining 5% incorporate a velocity-limiting feature. Approximately 99% of all hydraulic snubbers in NPP service utilize a dual-mode, lock-up/bleed type control valve; the remaining 1% utilize a single-mode, velocity-limiting design. The aging research primarily focused on the aging characteristics of acceleration-limiting mechanical snubbers and lock-up/bleed type hydraulic snubbers. It should be noted, however, that much of the information obtained in the research would also be expected to be characteristic of the remaining snubber types because of similarities of design features, e.g., ball nut and screw for mechanicals, seals for hydraulics, etc., and common environmental stressors.

In addition to the site visits, the research results are based upon over 70 telephone interviews conducted with knowledgeable plant staff. (This includes a review of records of prior telephone conversations between Lake Engineering and utility personnel.) Selected snubbers were also disassembled and examined at the Lake Engineering Rhode Island facility. Some of the research insight was acquired from snubber experience and in-house information at Lake Engineering and Wyle Laboratories.

#### REVIEW OF INDUSTRY INFORMATION

The information obtained during the in-plant research included the number and type of snubber failures. Special attention was given to failure category analysis, with particular emphasis on distinction between age-related and nonage-related failures. This distinction has not been emphasized in previous studies. The majority of failures, for both mechanical and hydraulic snubbers, were detected during functional testing; the number of failures found by visual examination, on the other hand, was minimal.

The following five failure categories were selected:

1. Mishandling (i.e., installation, handling, and maintenance-related deficiencies)

2. Environmental influences, e.g., heat or moisture (aging related)
3. Vibration and transients (aging related)
4. Manufacturing/design defects
5. Unknown.

Figures 1 and 2 illustrate that age-related failures are occurring. As shown in Figure 1 for mechanical snubbers, 59 failures were attributed to the *environment* category and 94 were attributed to the *vibration and transients* category. Thus, approximately 43% of the failures were associated with actual plant service conditions that may be classified as age-related (see Figure 3).

As shown in Figure 2 for hydraulic snubbers, 26 failures were attributed to the *environment* category and 18 were attributed to the *vibration and transients* category. Thus, approximately 51% of the failures were associated with service-related conditions that may be classified as age-related (see Figure 4).

#### EVALUATION OF SNUBBER AGING-RELATED FAILURES

The review of the in-plant research information suggests that aging-related failures are predominantly associated with environmental influences. Results of the research suggest that temperature, vibration, transients, and moisture are the principal aging stressors for both mechanical and hydraulic snubbers. Radiation appears to be a less significant stressor than was originally anticipated.

#### Mechanical Snubber Aging Failures Resulting from Service Stressors

Mechanical snubbers were designed to provide a service life of 40 years, with no planned maintenance. However, the results of the research indicate that environmental influences such as heat, moisture, vibration, and load transients can adversely influence the performance of mechanical snubbers, resulting in two basic failure modes described below.

- High drag force or high breakaway force; drag force is defined as the force required to maintain snubber movement at a low velocity; drag force limits for most plants vary from 2% to 5% of the snubber's rated load.
- High acceleration threshold; acceleration-limiting mechanical snubbers are designed to activate<sup>(a)</sup> at a given level (threshold) of acceleration; acceptance limits for acceleration range from 0.2 to 0.04 g (maximum).

---

(a) Activation is defined as the change of condition from passive to active, in which the snubber resists the rapid displacement of the attached pipe or component/equipment.

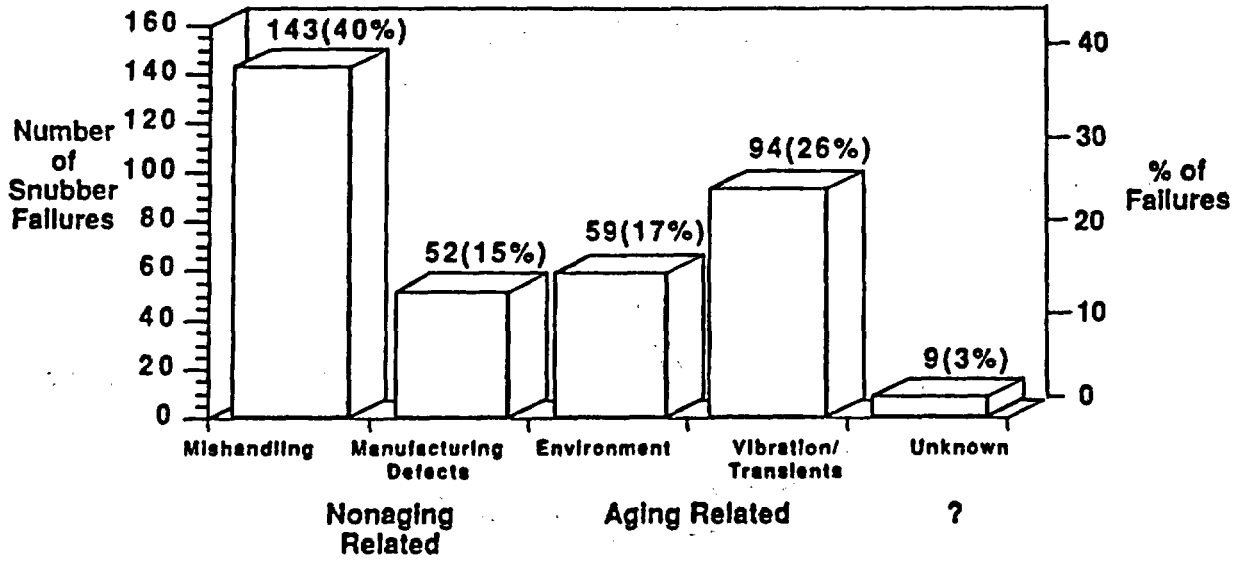


FIGURE 1. Mechanical Snubber Failures by Category

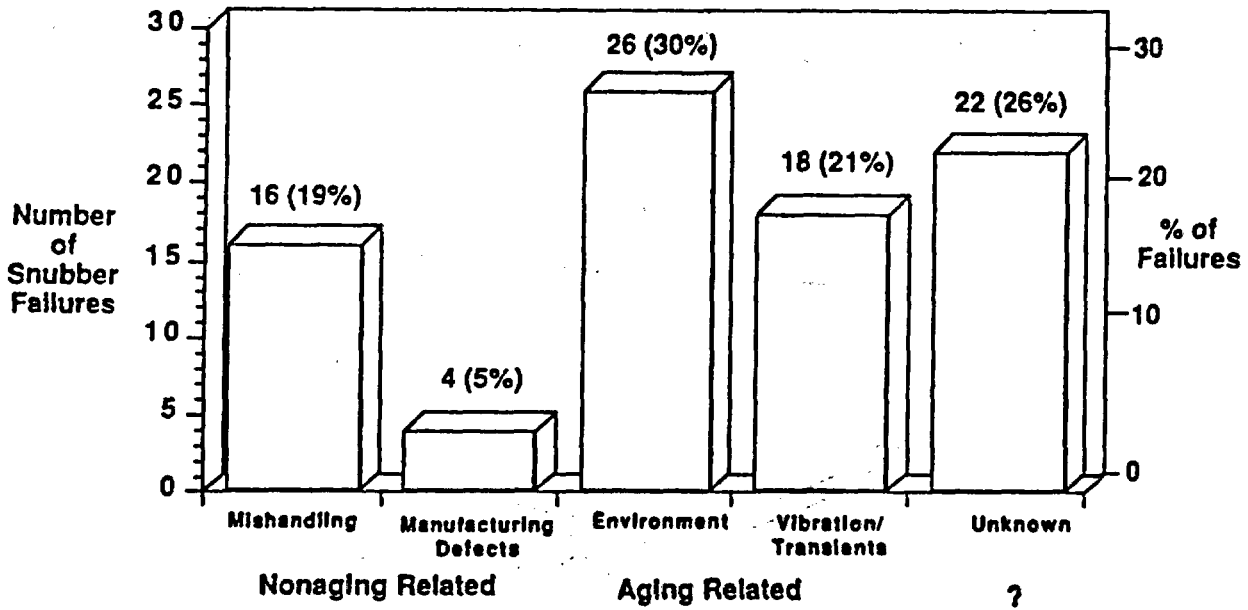
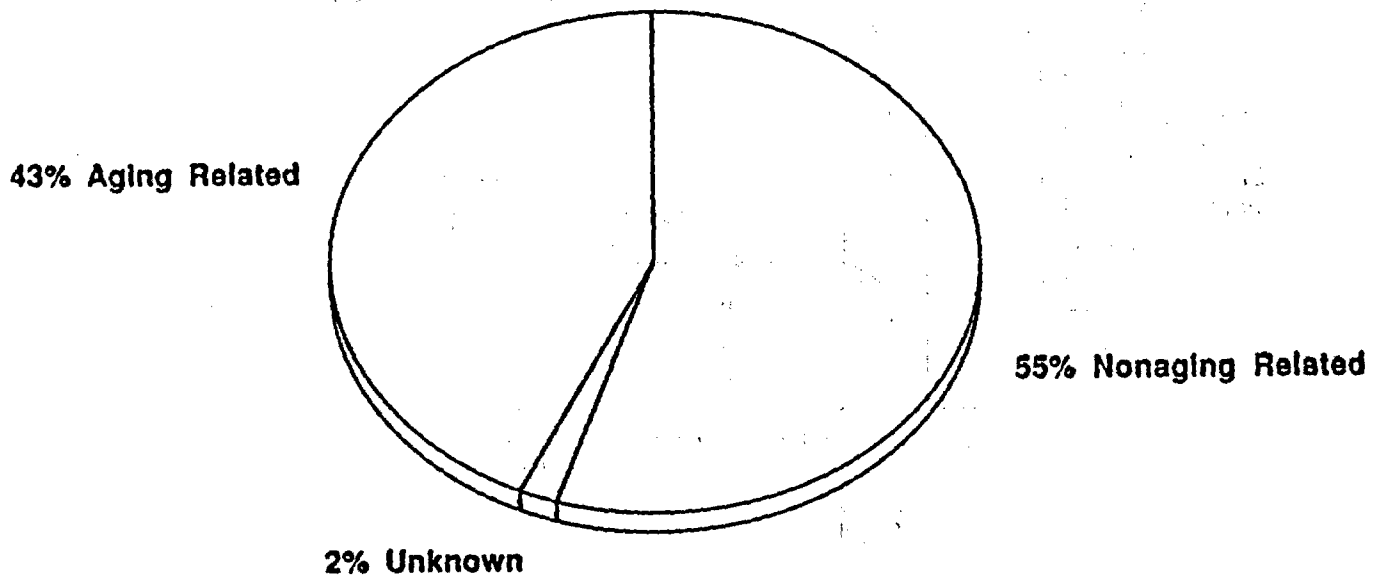
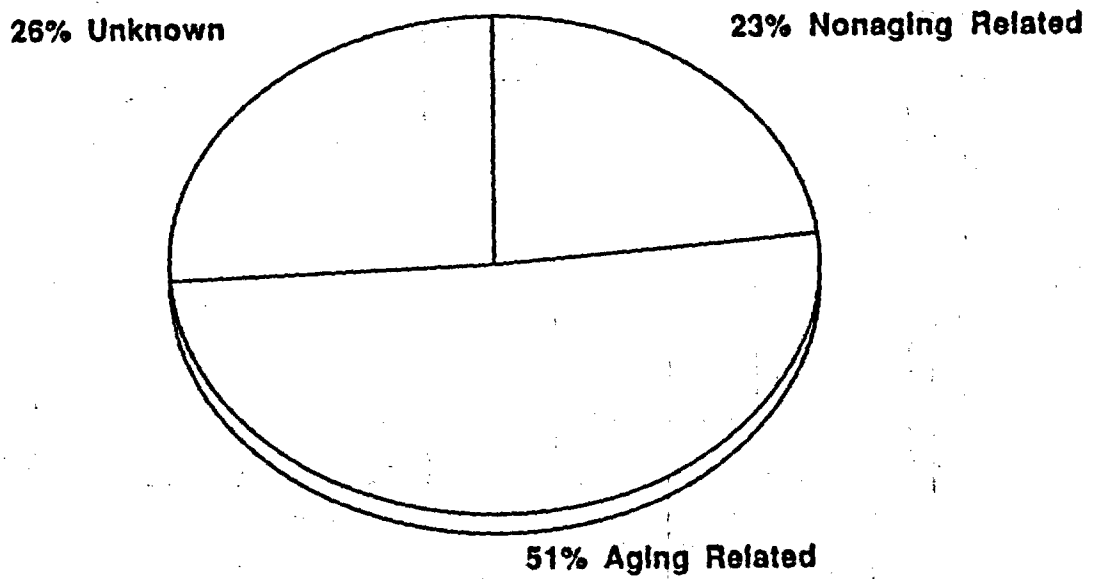


FIGURE 2. Hydraulic Snubber Failures by Category



**FIGURE 3.** Aging-Related Failures Versus Nonaging-Related Failures in Mechanical Snubbers



**FIGURE 4.** Aging-Related Failures Versus Nonaging-Related Failures in Hydraulic Snubbers

Common service stressors and typical mechanical snubber failure mechanisms are discussed below:

- Prolonged high temperature can result in the solidification of lubricants, which can increase drag force.
- High amplitude vibration can result in localized fretting and wear of mating parts, such as lead screws, thrust bearings, pins, capstan springs and attachment lugs. Such degradation can lead to an increase in drag force, an increase in mechanical clearances, jamming, and/or an increase in acceleration threshold. (High amplitude vibration is defined as vibration that has an amplitude that exceeds the mechanical clearances between the clevis and pin in the snubber.)
- Low amplitude vibration primarily can result in loosening of fasteners and wear of attachment pins and clevises. (Low amplitude vibration is defined as vibration that has an amplitude that is less than the mechanical clearances between the clevis and pin in the snubber.)
- Dynamic transient loads, such as those resulting from water hammer, turbine trip, etc., are significant degradation stressors for mechanical snubbers, causing damage to structural members and snubber internal parts, e.g., thrust bearing, ball screw, etc.
- Moisture can lead to internal corrosion, resulting in an increase in drag force, jamming, or a decrease in the activation acceleration due to a rust buildup between the capstan and capstan spring. (Snubbers installed in a vertical position are more vulnerable due to their propensity to trap water.)

#### Hydraulic Snubber Aging Failures Resulting from Service Stressors

The design service life for metallic components used in most hydraulic snubbers is 40 years. The service life for nonmetallic elements such as seals and fluid ranges from 5 to 16 years, depending on the level of conservatism preferred by the vendor or user. Some snubber models utilize thermoplastic and metallic seals with a design life of 40 years.

The results of the research indicate that environmental influences such as heat, vibration, and moisture can degrade the performance of hydraulic snubbers, resulting in a service life that is shorter than that initially assumed. The primary concern, in this regard, is the effects of such environments on the seals and fluid, that might result in snubber failure. The most common hydraulic snubber failure modes are high and low locking velocity and high and low bleed (release) rate.

Significant service stressors and typical hydraulic snubber failure mechanisms are discussed below:

- Excessive heat can have several adverse effects, including hardening, permanent deformation and surface cracking of seals, and deformation of

plastic reservoirs. These effects can lead to loss of hydraulic fluid that may result in snubber failure. Seal degradation resulting from severe high temperature applications, a limited number of which are common to most plants, can result in leakage in one or two operating intervals. This supports the assumption that seal degradation can be accelerated by elevated temperature.

- Vibration can cause extensive wear of hydraulic snubber metallic parts, e.g., piston, cylinder, clevis pins, attachment hardware, etc. and loosening of threaded fasteners. Gelated hydraulic fluid has been identified in several hydraulic snubbers that were exposed to significant high amplitude vibration; such gelation has occasionally affected the snubber control valve performance. Although the exact cause of this gelation has not been determined, it is generally thought to be the result of localized internal vibration effects caused by the high amplitude vibration.
- Dynamic transient loads resulting from water hammer, turbine trip, etc., can cause significant structural damage to a hydraulic snubber, e.g., deformed piston rod, deformed structural attachments, sheared piston threads, etc.
- Moisture contributes to the corrosion of metallic parts. Parts used in hydraulic snubbers are not always corrosion resistant. The silicone hydraulic fluid used in most hydraulic snubbers readily absorbs moisture, particularly for snubbers with vented reservoirs; in some cases, this has resulted in internal corrosion. Corrosion products can cause particulate contamination of the hydraulic fluid, potentially degrading the control valve performance.

#### RESULTS AND CONCLUSIONS OF THE IN-PLANT RESEARCH

The results of the in-plant research confirm that aging can degrade the performance of mechanical and hydraulic snubbers. Analysis of service data shows that heat, high and low amplitude vibration, transients, and moisture contribute to approximately half of all failures. The remaining failures are primarily caused by design/manufacturing deficiencies, and installation/mishandling errors.

Snubbers subject to rapid degradation as a result of abnormally severe operating environments should be managed on a case-by-case basis and may require augmented surveillance or maintenance. Representative snubbers from the remaining plant population should be monitored for progressive degradation using trendable degradation parameters.

The nuclear power industry has progressed in the areas of snubber inspection, testing, maintenance, and snubber reduction, demonstrating an improved understanding of safety implications and performance. Some plants have identified severe environments and have modified the environment or replaced snubbers with more durable models. The NPAR snubber aging research<sup>(2,3)</sup> has contributed in this regard by providing useful information pertaining to snubber aging

mechanisms and aging management. Additionally, more effective and realistic functional test acceptance limits have been developed to significantly reduce failure rates. Most plants have yet to implement a formal service-life monitoring program. The recommended service-life monitoring guidelines resulting from the NPAR research should be useful to establish such programs.

#### RECOMMENDED SERVICE-LIFE MONITORING GUIDELINES FOR SNUBBERS

NRC standard technical specifications<sup>(5)</sup> (STS) require that plants maintain a service-life monitoring program. The ASME Subsection ISTD Working Group on mechanical equipment restraints is developing mandatory service-life monitoring requirements that will likely be included in Subsection ISTD of the OM Code. A non-mandatory appendix that will provide some guidelines for service-life monitoring is also being developed by the Working Group. Although a number of plants have conducted specific seal-life evaluations, most have yet to implement a formal service-life monitoring program. Based on the results of the research, the following guidelines are recommended for implementation in the snubber service-life monitoring program.

- It is important to distinguish between service-related and nonservice-related failures. For this reason the root causes of snubber failures and degradation should be determined. Diagnostic testing is useful for this purpose as well as visual evaluation, particularly during snubber disassembly. Personnel training in failure evaluation techniques is also important.
- Because plant operating environments may differ from design specifications, general area snubber environmental conditions, e.g., temperature, should be monitored. Depending on the range of environmental stressors in the plant, it may be practical to establish more than one service-life population.
- Specific snubber applications (locations) involving severe environmental influences that could cause short-term degradation, e.g., high temperatures, high amplitude vibration, etc., should be identified and dealt with on a case-by-case basis. Such applications may require specific in situ monitoring equipment, frequent surveillance, maintenance, or snubber replacement.
- Service-life for the general snubber population (snubbers in a moderate environment that are not subject to short-term degradation) should be established by trending relevant degradation parameters in representative snubbers. For example, because the primary failure mode of concern for seals is gradual loss of fluid, snubber seal life should be based on predicted low pressure seal performance. Baseline data are essential for trending.
- "Hands-on" evaluation methods, such as hand stroking, can be used to identify potential snubber degradation, particularly that caused by dynamic load transients.

- Evaluation of test parameter time traces obtained during routine functional tests is useful to identify performance anomalies that may be indicators of snubber degradation.
- Test machines used for trending and for diagnostic tests should be capable of providing a time trace of load and velocity. Accuracy and repeatability are important features of test machines used for trending. A feature that is important for diagnostic testing is the ability to vary the level of test parameters, such as velocity and load.
- Service-life projections based on data from snubbers exposed to actual plant operating environments are generally preferable to laboratory developed service-life projections.

#### REFERENCES

1. U.S. Nuclear Regulatory Commission. 1991. Nuclear Plant Aging Research (NPAR) Program Plan. NUREG-1144, Rev. 2, U.S. Nuclear Regulatory Commission, Washington, D.C.
2. Bush, S. H., P. G. Heasler, and R. E. Dodge. 1986. Aging and Service Wear of Hydraulic and Mechanical Snubbers Used on Safety-Related Piping and Components of Nuclear Power Plants. NUREG/CR-4279, PNL-5479, Vol. 1, U.S. Nuclear Regulatory Commission, Washington, D.C.
3. Brown, D. P., G. R. Palmer, E. V. Werry, and D. E. Blahnik. 1990. Basis for Snubber Aging Research: Nuclear Plant Aging Research Program. NUREG/CR-5386, PNL-6911, U.S. Nuclear Regulatory Commission, Washington, D.C.
4. Wyle Laboratories and Lake Engineering Company. 1990. NPAR Snubber Aging Research. Wyle Report No. 17131-01, Letter Report Prepared by Wyle Laboratories and Lake Engineering Company for Pacific Northwest Laboratory, Richland, Washington.
5. U.S. Nuclear Regulatory Commission. 1984. Technical Specifications for Snubbers. Generic Letter 84-13, U.S. Nuclear Regulatory Commission, Washington, D.C.

**PRELIMINARY RESULTS OF THE PWR LOW POWER AND SHUTDOWN  
ACCIDENT FREQUENCIES PROGRAM - COARSE SCREENING  
ANALYSIS FOR SURRY\***

T-L. Chu, Z. Musicki, W. Luckas, S.M. Wong, L. Neymotin,  
D.J. Diamond, C-J. Hsu, G. Bozoki, P. Kohut, R. Fitzpatrick, N. Siu\*\*

Department of Nuclear Energy  
Brookhaven National Laboratory  
Upton, New York 11973 U.S.A.

**ABSTRACT**

This document presents the preliminary internal events Level 1 results (including fire and flood) obtained as a result of a coarse screening analysis on the low power and shutdown accident frequencies of the Surry Nuclear Power Plant. The work was performed by Brookhaven National Laboratory (BNL) for the Nuclear Regulatory Commission Office of Nuclear Regulatory Research (RES). This coarse screening analysis was performed in support of the NRC staff's follow-up actions subsequent to the March 20, 1990 Vogtle incident with the objective of providing high-level qualitative insights within a relatively short time frame. It is the first phase of a major study that will ultimately produce estimates on the core damage frequency of a pressurized water reactor (PWR) during low power and shutdown conditions. Phase 2 of the study will be guided by the Phase 1 results in order to concentrate the effort on the various plant operational states, the dominant accident sequences, and pertinent data items according to their importance to core damage frequency and risk.

---

\* This work was performed under the auspices of the U.S. Nuclear Regulatory Commission.  
\*\*Massachusetts Institute of Technology

## 1. BACKGROUND

This paper presents the preliminary internal events Level 1 results (including fire and flood) obtained as a result of a coarse screening analysis on the low power and shutdown accident frequencies of the Surry Nuclear Power Plant. The work was performed by Brookhaven National Laboratory (BNL) for the Nuclear Regulatory Commission Office of Nuclear Regulatory Research (RES). This coarse screening analysis was performed in order to meet the RES commitment to the Office of Nuclear Reactor Regulation (NRR), in support of the NRC staff's follow-up actions subsequent to the March 20, 1990 Vogtle incident. It is the first phase of a study that will produce final estimates on the core damage frequency of a pressurized water reactor (PWR) during low power and shutdown conditions. Phase 2 of the study is to produce a final Level 1 PRA analysis. It will be guided by the Phase 1 results. In Phase 2, effort will concentrate on the various plant operational states, the dominant accident sequences, and pertinent data items according to their importance to core damage frequency and risk.

Surry Unit 1 was chosen as the PWR to be analyzed, in part because the Surry plant was previously analyzed in the Reactor Safety Study and NUREG-1150 and in part because Virginia Power offered their cooperation. This will facilitate comparison of the core damage frequency or risk during shutdown operations with that of power operations. The Surry Plant contains two units each rated at 788 megawatts (electrical) capacity and is located near Surry in Virginia. Grand Gulf, a boiling water reactor, was selected as the plant to be analyzed in a parallel study<sup>2</sup> performed by Sandia National Laboratories (SNL).

This study is concerned with 'traditional' internal events as well as internal fires and floods. External events are beyond the scope of the BNL effort. A separate NRC-sponsored project entitled "Scoping Analysis of LWR Shutdown Accidents Initiated by Earthquakes," performed by Future Resources Associates Inc. and PRD Consulting, addresses seismic induced accidents. In that study, seismic induced loss-of-offsite-power transients were analyzed with the plant-specific fragilities generated in the NUREG-1150 seismic PRA for Surry, and the loss-of-offsite-power event tree developed in this study.

## 2. RESULTS AND INSIGHTS

Due to the necessarily conservative nature of the coarse screening analysis, it was decided that qualitative results will be stressed in this document. Qualitative discussions highlighting the results follow. It is believed that these highlights are generally applicable to all PWRs.

### 2.1 Potentially Vulnerable Configurations

In the coarse screening analysis, some plant configurations in an outage were found to be more vulnerable than others. These configurations are based on the operational practices at the Surry plant and are routinely entered during shutdown operations. Their descriptions follow:

Mid-loop Operations Approximately twice a year, the plant has gone into mid-loop operation with the vessel level maintained at 9 inches above the reactor coolant loop hot leg mid-plane. This mode can occur within one day after shutdown with decay heat still as high as 12.4 Mw. Under these conditions, core

uncovery can occur as early as 1.5 hours after a loss of cooling event. In past refueling outages, one or more reactor coolant loops have been isolated for extended periods of time, including a large fraction (if not total) of the mid-loop operation period. This leaves the associated steam generator(s) ineffective as a heat sink.

Use of Temporary Seals at the Seal Table In-core flux thimbles (and core-exit thermocouples) are normally inserted up into the core region through the guide tubes that penetrate the bottom head of the reactor vessel. The space between the moveable thimble tubes and fixed guide tubes forms part of the reactor coolant pressure boundary. This space is sealed against full system pressure at the seal table during normal operation. In a refueling outage, the in-core flux thimbles are retracted out of the core, and temporary seals are used at the seal table. These temporary seals can only withstand approximately 15-25 psig. A slight increase in system pressure could cause failure of the temporary seals inducing a loss of coolant accident. Further pressurization can quickly lead to core uncovery. It was estimated that approximately 10 days during a refueling outage such seals are in place with the reactor coolant system (RCS) closed and vessel head in place. It is during this period that such a scenario can potentially occur.

Isolation of the Steam Generators During an outage, the secondary sides of the steam generators are often filled to approximately 98-100 percent wide range level (called "wet layup"), and represent a good heat sink if connected to the RCS. As discussed above, in a refueling outage, reactor coolant loops can be isolated for extended periods of time. This removes the one or more steam generators as a potential heat sink.

During a RCS cooldown prior to initiating the RHR system, the motor operated valves (MOV) in the individual steam generator feed lines from the auxiliary feedwater (AFW) system are closed. After the RCS temperature decreases to 228-250° F, the main steam trip valves (and non-return valves) are closed. Therefore, the secondary side of the steam generators are isolated from the main steam system. This configuration makes it difficult for the plant to cope with station blackout (SBO) events during shutdown. Basically, the AFW lines to each individual steam generators are isolated with the MOVs located inside the containment. The steam generator relief valves (atmospheric dumps) fail closed on loss of air and cannot be opened manually (quite unique at the Surry plant).

The loss-of-all-AC-power emergency procedure instructs the operators to manually open the bypass valves (locally at the valves) around the main steam trip valves, close the condenser vacuum breaker, "evacuate [the] turbine deck", and dump steam to the main condenser (and ultimately to the turbine building above the turbine deck). The timely success in manually dumping steam into the turbine building is essential to the mitigation of an SBO at Surry. This is especially true because the operating RHR removal system is a weakness in the RCS pressure boundary, and the RCS side relief valves are not capable of relieving the large volume of steam that could be generated in the vessel.

It was estimated that an overpressurization of the RHR system can occur as early as 0.7 hours after a SBO occurs. The RHR system has a design pressure of 600 psig. It is connected to the RCS prior to the SBO. The relief valves that may be available are the pressurizer PORVs, the RHR relief valve and possibly the

relief valve in the CVCS letdown line. During a SBO, these valves are expected to relieve either liquid or two phase flow. It was estimated that the combined capacity of the valves is 2550 gpm at 600 psig, equivalent to the volumetric vapor generation rate of 5.8 Mw of decay heat. This corresponds to the decay heat approximately 17 days after shutdown. After 17 days, the relief valves should be able to relieve. However, they may still be inoperable or fail to open upon demand.

## 2.2 Maintenance Unavailability and Simultaneous Maintenance of Redundant Equipment

Preliminary analysis of the data collected indicates that maintenance unavailabilities at shutdown are much higher than that during power operation. With the plant at cold shutdown, few Surry Technical Specification requirements are applicable. In terms of inventory makeup to the RCS, one high head injection train and one low head injection train are required to be operable while the RCS level is below 15.3' (i.e., reduced inventory), which is less than 3 feet above the 12.5' mid-loop level. This requirement is not in the Surry Technical Specifications, but is written in the operating procedure as a result of Surry's response to Generic Letter 88-17.

One concern regarding maintenance unavailability is simultaneous maintenance of redundant equipment. Preliminary review of the Surry data indicates that simultaneous maintenance of the two motor driven AFW pumps has taken place. In principle, simultaneous maintenance may take place if not otherwise prohibited. In this coarse screening analysis, the assumption that simultaneous maintenance can occur was applied and simultaneous maintenance turned out to be the dominant cause for core damage in many sequences. A more realistic maintenance model based upon actual plant practice will be developed in Phase 2 of this study. For example, discussions with plant personnel indicated that, in practice, no two emergency diesel generators (EDGs) could be maintained at the same time. (Note: there are a total of three EDGs at the Surry site, that are available for both units).

## 2.3 Reactivity Accident Scenarios Identified in the French PRA

Two reactivity accident scenarios identified in the French PRA were analyzed taking into consideration the Surry-specific design and operation. The first scenario involves startup of a reactor coolant pump after improper dilution during a loss of offsite power transient. The second scenario involves a dilution event while the plant is in the mid-loop condition. Conservative assumptions were made in the coarse screening analysis, and the results indicate that the scenarios have high frequency. It is believed that some of the assumptions are very conservative. For example, in the first scenario, it was assumed that the decay heat is so low that natural circulation does not cause mixing of the unborated water with the reactor coolant. It is expected that more deterministic analysis is needed to resolve the issue in support of the Phase 2 effort.

## 2.4 Findings of Fire and Flood Analysis

The results of the analysis show that fire and flood risk at shutdown could be potentially significant. More detailed analysis is planned in Phase 2 for the following areas.

	<u>Fire</u>	<u>Flood</u>
Cable vault and tunnels	Yes	No
Emergency switchgear and relay room	Yes	Yes
Control room	Yes	No
Containment	Yes	Yes
Aux. Building	Yes	Yes
Safeguard area	Yes	Yes
Turbine building	Yes	Yes

In the process of performing this portion of the Phase 1 study, some issues that only apply to shutdown conditions were identified:

1. Surry's compliance with Appendix R requirements emphasizes power operations not shutdown conditions. For example, Appendix R states that

"Both trains of equipment necessary to achieve cold shutdown may be damaged by a single fire ... but damage must be limited so that at least one train can be repaired or made operable within 72 hours using onsite capability."

Based on this statement, the Surry implementation of Appendix R relies on repair or replacement of the residual heat removal (RHR) pump cables rather than cable separation. According to the associated analysis, cable replacement will take 35 hours. Therefore, if the fire starts while the plant is operating, there is enough time to achieve cold shutdown within the allowed 72 hours. However, in this study, it is assumed that the plant is already in cold shutdown when the fire occurs. In this case, the 35 hour replacement time appears to be too long for the scenarios analyzed. The basic difference here is that, from power, the steam generators can be utilized to delay the need for RHR. At shutdown, this delay capability is not available.

Arguing in a similar manner, the credit taken by the Appendix R submittal for repair or replacement of the component cooling water (CCW) pump motors and cables, while acceptable for fires starting when the plant is at power, appears to be inappropriate for fires starting when the plant is shut down.

Two other situations which appear to have been overlooked due to the emphasis on fires during operation involve the steam generator pilot-operated relief valves (SG PORVs) and Main Control Room fires. In the case of a fire that causes the loss of the SG PORVs, the alternative shutdown method prescribed by the Appendix R submittal employs the SG code safety valves. Although this is a viable approach at power, the setpoints of the valves are too high to be useful for decay heat removal while at cold shutdown. In the case of Main Control Room fires, the operators may have to use the Auxiliary Shutdown Panel (in the Emergency Switchgear Room) to control the plant. However, as seen from Tables 5-2a and 5-2b of the Appendix R submittal, this panel does not have control circuits for the RHR pumps. (At Surry, the RHR system is located within containment and is separate from the low pressure injection system.)

It should be pointed out that the above finding regarding Appendix R's coverage of shutdown fires is generic; plants that rely on alternative shutdown

methods rather than separation may need to develop means to maintain a plant at cold shutdown, given that a fire occurs when the plant is shut down (or in the process of shutting down).

2. Fire or flood barriers that are available during power operations may be removed during shutdown. They include cable and pipe penetrations, fire doors, flood dikes, floor plugs, and backflow preventers in the floor drain system. Surry did have some reported incidents in which one flood dike and two backflow preventers were removed.

### 3. Future Work

The Findings presented in this paper are based on the preliminary results<sup>1</sup> of the Phase 1 Study of the PWR Low Power and Shutdown Accident Frequencies Program. The program is the Level 1 part of an over-all program that addresses the risks of a PWR during low power and shutdown conditions. The Level 2 and 3 part of the program is being initiated. In phase 2 of the level 1 study, detailed analysis will be performed, particularly in the areas of system analysis, human reliability analysis, and accident scenario development. Interfaces with levels 2 and 3 will be established, and the resulting risk measures for low power and shutdown conditions will be compared with those of power operations.

#### REFERENCES:

1. Chu, T-L., et al., "PWR Low Power and Shutdown Accident Frequencies Program, Phase 1A - Coarse Screening Analysis," Rough Draft Letter Report, November 13, 1991.
2. Whitehead, D.W., et al., "BWR Low Power and Shutdown Accident Sequence Frequencies Project," Phase 1 - Coarse Screening Analysis, Vol. 1-3, Rough Draft Letter Report, Sandia National Laboratories, September 21, 1991.

SAND91-1610C  
STATUS OF THE LOW POWER AND SHUTDOWN ACCIDENT SEQUENCE  
ANALYSIS PROJECT FOR THE GRAND GULF NUCLEAR POWER STATION

Donnie W. Whitehead<sup>1</sup>  
John Darby<sup>2</sup>  
Bevan D. Staple<sup>1</sup>  
Bob Walsh<sup>2</sup>  
Thomas D. Brown<sup>3</sup>

<sup>1</sup>Reactor Systems Safety Analysis Division  
Sandia National Laboratories  
Albuquerque, New Mexico 87185

<sup>2</sup>Science & Engineering Associates, Inc.  
Albuquerque, New Mexico 87110

<sup>3</sup>Reactor Modeling & Regulatory Applications Division  
Sandia National Laboratories  
Albuquerque, New Mexico 87185

#### ABSTRACT

This paper describes the current status of Phases 1 and 1A of the BWR Low Power and Shutdown Accident Frequencies Program being conducted at Sandia National Laboratories for the U.S. Nuclear Regulatory Commission. The major focus of the project to date has been the identification and coarse screening quantification of accident sequences initiated in modes of operation other than full power. The coarse screening provides a filtering mechanism whereby the potentially important accident sequences are identified. The information obtained during these two phases will be used to prioritize the more detailed analyses which will occur during Phase 2 of the project. A summarization of the project including results and insights from Phases 1 and 1A is presented.

#### INTRODUCTION

The purpose of this paper is to provide a brief overview of the work being conducted at Sandia National Laboratories (SNL) with regard to the identification and quantification of accident sequences initiated in modes of operation other than full power for the Grand Gulf Nuclear Power Plant.

As discussed in a previous paper on this subject [1], probabilistic risk assessments (PRAs) for nuclear power plants traditionally have characterized the

---

This work is supported by the United States Nuclear Regulatory Commission and is performed at Sandia National Laboratories, which is operated for the U.S. Department of Energy under Contract Number DE-AC04-76DP00789.

risk associated with accidents initiated while the plant is in full-power operation. This concentration of effort on full-power events was based on the judgment that the level of risk associated with accidents that could occur during full-power operation is greater than that associated with accidents that could occur during the other modes of operation, such as low power and shutdown. As was stated in Reference 1, the primary justification for such a claim appeared to be that lower decay heat levels are generally associated with these other modes of operation, so more time is available to recover from adverse situations arising in these modes. However, as a result of the Chernobyl accident and other precursor events, the U.S. Nuclear Regulatory Commission's Office of Nuclear Regulatory Research has undertaken a two-phase project to analyze the frequencies, consequences, and risk of accidents occurring during modes of operation other than full power.

This paper summarizes the activities that have occurred during the first phase of the project (i.e., Phase 1 and Phase 1A) for a boiling water reactor (BWR) and presents preliminary results based on the objectives for the first phase. A companion project for a pressurized water reactor (PWR) was conducted by Brookhaven National Laboratory and results of that analysis will be described in a separate paper.

#### **OBJECTIVES AND SCOPE**

The overall project objectives are to:

- (1) assess the frequencies of severe accidents initiated during plant operational modes other than full power for a U.S. BWR;
- (2) compare the estimated core damage frequencies, important accident sequences, and other qualitative and quantitative results of this study with those of accidents initiated during full-power operation; and
- (3) demonstrate methodologies for accident sequence analysis for plants in non full-power modes of operation.

However, the Phase 1 and 1A objectives are more narrow in scope and include the following:

- (1) Perform a coarse screening analysis to provide some estimation of the potential for accidents during low power and shutdown conditions by:
  - determining which, if any, plant configuration (i.e., plant operational state) is more susceptible to core damage accident sequences,
  - identifying the set of accident initiating events applicable to each plant operational state, and

- grouping the core damage sequences into either a high, medium, or low category based on the potential core damage frequency of each sequence.
- (2) Characterize the potential risk associated with each of the core damage sequences surviving truncation based upon the following:
- Is the containment open or closed,
  - Is the reactor vessel open, closed, or vented, and
  - Does core damage occur in a fast or intermediate time frame?
- (3) Use the results of the accident sequence analysis to prioritize the work to be performed during Phase 2 (i.e., the detailed analysis phase) of the project.

The scope of this project includes the analysis of the potential accidents that could occur at the Grand Gulf Nuclear Power Plant as the plant operates in modes other than full power. This includes operation of the plant at:

1. Low power (i.e., a subset of the Power mode of operation as defined by the plant's Technical Specifications), where the power level is less than or equal to 15 percent of rated power.
2. Startup as defined by the Technical Specifications.
3. Hot Shutdown as defined by the Technical Specifications.
4. Cold Shutdown as defined by the Technical Specifications.
5. Refueling as defined by the Technical Specifications.

The analysis for the Refueling mode of operation was limited to those events that could affect the fuel inside the reactor vessel, thereby excluding events such as fuel transfer accidents once the fuel bundle passed through an imaginary right circular cylinder defined by the reactor vessel.

Included in the program scope was a coarse screening analysis of potential accidents initiated by internal floods and internal fires for one plant operational state. (NOTE: The effects of seismically induced accidents are being examined in another study.)

The program scope for this study excluded examination of the long term issues following a reactor accident from full power, except for the special case defined by the uppermost success path in the full power event trees. The exclusion of the "other" paths in the full power event trees from this study is not meant to imply that they are unimportant. The exclusion simply reflects the resources available at this time. Also excluded from this study is an analysis of the potential accidents that could occur during the first time startup of the plant,

the final shutdown of the plant, and all external initiating events other than seismic.

**METHODOLOGY**

The approach used is a modification of the standard Level I probabilistic risk assessment (PRA) approach used in many full power PRAs. The information contained in the NUREG/CR-4550 analysis of the Grand Gulf plant [2] was used as the starting point for this analysis. Event trees were constructed, top events were modeled using fault trees of various sizes, and the top events quantified using point estimates to produce the sequence frequencies.

The Phase 1 analysis included all the normal tasks associated with a Level I analysis, with the exception that no cut set dependent recovery analysis task was performed. In addition to the normal set of tasks, two additional tasks were performed. The first task was necessary in order to understand how the plant changes its operational status. The second task identified the reasons why a plant changes its operational status and also identified equipment unavailabilities that resulted from such a change. While all the normal tasks, with the noted exception, were performed, some tasks made use of screening information only. The use of screening information and the lack of a significant recovery analysis task resulted in conservative estimates for the accident sequences. However, this reduced the possibility that, in this first comprehensive look at a BWR in these other modes of operation, potentially significant accidents would be eliminated before any detailed analysis of the accidents took place. A complete list of the steps performed during the coarse screening phase of this project is given in Table 1.

Step	Description of Step
1	Develop Plant Operational States (POSS)
2	Identify POS Initiating Events (IEs)
3	Identify Accident IEs
4	Determine System/Success Criteria
5	Develop Accident Sequence Event Trees
6	Construct System (Top Events) Models
7	Data Analysis
8	Human Reliability Analysis
9	Accident Sequence Quantification

**Table 1**  
**Analysis Steps in the BWR Low Power and Shutdown Project**

## RESULTS

### Develop Plant Operational States (POSSs)

The approach, as described above, was applied to the Grand Gulf Nuclear Power Station as it operates in modes other than full power. As originally envisioned, the study would have identified and quantified potential accidents for the five modes of operation as defined by the plant's Technical Specifications (Tech Specs). However, as the review of the plant's operating procedures progressed, it became apparent that another means of classifying the status of the plant would be necessary if the objectives of this project were to be met.

This new classification scheme needed to account for the various system configurations, decay heat loads, pressure and temperature parameters, and water levels that occur during transition from power operation to refueling and back to power operation or some subset of the above transitions. As a result of this need, a new classification scheme was developed. This new scheme is composed of plant operational states (POSSs). These POSSs, defined in terms of a set of systems that are normally expected to provide the functions for maintaining the plant within a particular power, pressure, and temperature regime, provided a means of analyzing the plant as it transitions from low power operation to refueling.

From an examination of the plant's operating procedures and a look at the various decay heat loads the plant might experience during low power and/or shutdown conditions, thirteen (13) POSSs were identified. For the Coarse Screening Phase (i.e. Phase 1 and 1A) of this project, these thirteen POSSs were combined into seven POSSs. This simplification was accomplished by combining the time spent in a high decay heat POS with the time spent in the low decay heat POS counterpart. Table 2 provides a description of the seven POSSs used during the Coarse Screening Phase of this project.

### Identify POS Initiating Events (IEs)

After an understanding of how the plant operates and/or transitions among the identified POSSs was obtained, it became necessary to identify the reasons why the plant would be required to change its POS and the implications of such a change (i.e., known pre-existing system and/or component unavailabilities). Since the major concern of this study was with accidents occurring in non full power POSSs, its focus was on controlled shutdown initiating events. Also included, are reactor trip events which allow orderly transition (the sequence of events as defined in the top success path of a full power accident event tree) among POSSs, hereafter called 'nuisance trips'. Thus, for this study, a new term was developed and defined to represent the need for a change from one POS to another. This term, called a POS Initiator, can be defined as follows: an event which initiates controlled shutdown of the plant from full power, a nuisance trip from full power, an event which requires the plant to transition to some state considered to be "safer" than its current state, or the transition back to its "normal" state after having corrected the problem requiring the transition in the first place.

POS <sup>2</sup>	Description
1	Consists of OC <sup>1</sup> 1 and OC 2 with pressure at rated conditions (about 1000 psig) and thermal power no greater than 15 percent.
2	Consists of OC 3 from rated pressure to 500 psig.
3	Consists of OC 3 from 500 psig to where RHR/SDC is initiated (about 100 psig).
4	Consists of OC 3 with the unit on RHR/SDC.
5	Consists of OC 4 and OC 5 until the vessel head is off and level is raised to the steam lines.
6	Consists of OC 5 with the head off, level raised to the steam lines, and until the upper pool is filled.
7	Consists of OC 5 with the head off, the upper pool filled, and the refueling transfer tube open.
<sup>1</sup> Operational Condition (i.e., Mode of Operation)	
<sup>2</sup> Control rods are fully inserted in POS 2, 3, 4, 5, 6, and 7.	

Table 2  
Description of POSs

Currently, this study does not address the long term issues following a reactor trip from full power (i.e., a POS change initiator) which proceeds along any full power event tree path (sequence) other than the top success path. The fact that this study does address the above defined nuisance trips and not the more stressful, but less likely, trips which progress along an event tree path other than the top success path, should not be taken to imply that a transition to a POS following a nuisance trips is believed to be of higher risk than long term considerations following the more stressful trips. Rather, it is a reflection of two facts: (1) nuisance trips occur relatively frequently (on the order of one to ten times a year depending on the particular plant), and (2) the methodology developed for quantifying accidents occurring following transitions among POSs can easily handle the nuisance trips as defined above.

Table 3 provides a brief description of the seven categories or classes of POS Initiators identified during by this study.

After these seven classes of POS Initiators were developed, they were examined to determine if a change in the plant's POS necessitated by one of these events would impact known pre-existing unavailabilities. For Class 1 the following assumption was made. The plant would not enter refueling (i.e., POSs 6 and 7) knowing that a system required during the refueling outage was unavailable. Class 2 events can impose pre-existing unavailabilities. If the system is required during shutdown, then entry into an action statement will impose a known pre-existing unavailability. If not, then no known pre-existing unavailability exists. Events in Class 3 do not impose known pre-existing unavailabilities. Class 4 events may impose pre-existing unavailabilities. If the equipment is taken credit for in a PRA (i.e., used to mitigate an accident initiating event),

then it does impose a pre-existing unavailability. If not, then no pre-existing unavailability exists. Class 5 events do not impose pre-existing unavailabilities. If the equipment were non-functional, then it would be in Class 2 or 4. Class 6 events could very well impose pre-existing unavailabilities. However, this study is limited to only those events that progress along the top success path of the full power accident event trees, and further, the assumption was made that whatever caused the nuisance trip is corrected before the plant transitions out of the POS it entered while responding to the trip. No exact determination of Class 7 events was made, as these events are outside the scope of this project.

Class	Description
1	Refueling. The plant is scheduled for its next refueling outage.
2	Controlled shutdown required by Tech Specs due to violation of a Safety Limit (SL) or Limiting Condition of Operation (LCO).
3	Controlled shutdown required by Tech Specs due to missed Surveillance Requirement (SR).
4	Controlled shutdown due to failures in non-Tech Spec equipment.
5	Preventive maintenance.
6	Change necessitated by a reactor trip from full power (nuisance trip only).
7	First time startup or final shutdown.

Table 3  
Description of Seven POS Initiator Classes

#### Identify Accident Initiating Events

The accident initiating event analysis task for this project was performed in much the same manner as for any full power PRA. First, a definition of what is meant by an initiating event was developed, and then a search for events which fit the definition was made. Finally, information was analyzed to produce estimates of the frequency for each initiating event.

In this study there are two definitions used for an initiating event depending upon the initial POS of the plant. For power operation, an initiating event is defined as an event which requires a rapid shutdown or trip of the plant, so as to challenge the safety systems to remove the decay heat still being generated in the reactor core. For non-power operations, an initiating event is defined as an event which would require an automatic or manual response to prevent core damage in the vessel. Table 4 provides a list of the initiating events

identified during this study. The table also includes the applicability of each initiating event to each POS and the screening value used for the frequency of the event.

#### Determine System/Success Criteria

After the initiating events were identified, the next step was to determine the applicable systems and success criteria for each initiating event or group of initiating events with respect to each POS. The success criteria used for the initiating events applicable in POSs 1, 2, and 3 are those used in the full power study [2]. For POSs 4, 5, 6, and 7 new success criteria were developed. The new success criteria are based on two basic methods of cooling the core:

- (1) Injecting a small quantity of subcooled or saturated water so that the fluid exiting the vessel after being heated by decay heat is subcooled or is a two phase mixture of low quality.
- (2) Injecting subcooled or saturated water in small quantities and steaming out the vessel.

These two cooling methods, in conjunction with the systems available at Grand Gulf and the decay heat loads experienced during POSs 4, 5, 6, and 7, result in a number of possible specific combinations of systems which can prevent core damage.

#### Develop Accident Sequence Event Trees

The construction of event trees for the seven POSs was a major task. Approximately 160 initiating event specific event trees were developed. Most of these event specific event trees transfer to several additional trees, bringing the total number of "event trees" developed to more than 500. In an attempt to make the event trees as realistic as possible, several cooling options were included. Some of these options are not specifically included in Grand Gulf's Emergency Procedures, but were nevertheless included in the trees for completeness. Due to the large number of trees developed no specific trees are included in this paper.

#### Construct System (Top Events) Models

Most of the system models used during this study were based upon those created in Reference 2 with appropriate modifications as necessary for the low power and shutdown conditions being examined in this study. In addition to using and modifying the Reference 2 models, two new systems were modeled. These new systems included the Alternate Decay Heat Removal System and the Fuel Pool Cooling and Cleanup System. Both systems can be used during low power and shutdown to provide cooling to the reactor vessel. These systems were modeled to approximately the same level of detail as was the systems obtained from Reference 2.

Initiating Event Nomenclature	Description	Mean Frequency (per year) for Each POS						
		1	2	3	4	5	6	7
T1	Loss of Offsite Power (LOSP) transient	0.07	0.13	0.13	0.13	0.13	0.13	0.13
T2	Transient with loss of the Power Conversion System (PCS)	1.62	1.62	1.62	-	-	-	-
T3A	Transient with PCS initially available	4.54	4.54	4.54	-	-	-	-
T3B	Transients involving loss of Feedwater	0.88	0.88	0.88	-	-	-	-
T3C	Transient caused by Inadvertent Open Relief Valve	0.14	0.14	0.14	-	-	-	-
A	Large LOCA	1E-4	1E-4	1E-4	1E-4	1E-5	1E-5	1E-5
S1	Intermediate LOCA	3E-4	3E-4	3E-4	3E-4	3E-5	3E-5	3E-5
S2	Small LOCA	3E-3	3E-3	3E-3	3E-3	3E-4	3E-4	3E-4
S3	Small-Small LOCA	3E-2	3E-2	3E-2	3E-2	3E-3	3E-3	3E-3
V	Interfacing System LOCA	-	-	-	-	-	-	-
R	Vessel Rupture	-	-	-	-	-	-	-
H1	Diversion to Suppression Pool via RHR	-	-	-	8E-2	8E-2	8E-2	8E-2
H2	Diversion to Condenser via RWCU	-	-	-	-	-	-	-
J1	LOCA in Connected System (RCIC)	8E-4	8E-4	8E-4	-	-	-	-
J2	LOCA in Connected System (RHR)	-	-	-	5E-2	5E-2	5E-2	5E-2
K	Test/Maintenance-Induced LOCA	-	-	-	-	-	-	-
E1B	Isolation of SDC Loop B only	-	-	-	0.1	0.1	0.1	0.1
E1C	Isolation of RWCU as DHR	-	-	-	-	-	-	0.1
E1D	Isolation of ADERS only	-	-	-	-	0.1	0.1	0.1
E1T	Isolation of SDC Common Suction Line	-	-	-	0.1	0.1	0.1	0.1

Table 4  
Initiating Events for Grand Gulf

Initiating Event Nomenclature	Description	Mean Frequency (per year) for Each FCS						
E1V	Isolation of Common Suction Line for ADHRS	-	-	-	-	0.1	0.1	0.1
E2B	Loss of SDC Loop B only	-	-	-	0.37	0.37	0.37	0.37
E2C	Loss of RWCU as DHR	-	-	-	-	-	-	0.1
E2D	Loss of ADHRS only	-	-	-	-	0.37	0.37	0.37
E2T	Loss of SDC Common Suction Line	-	-	-	0.37	0.37	0.37	0.37
E2V	Loss of Common Suction Line for ADHRS	-	-	-	-	0.37	0.37	0.37
T4A	Rod Withdrawal Error	-	-	-	-	-	-	-
T4B	Refueling Accident (Rod or Fuel Misposition)	-	-	-	-	-	-	-
T4C	Instability Event	-	-	-	-	-	-	-
T5A	Loss of all SSW	-	-	-	1.8E-2	1.8E-2	1.8E-2	1.8E-2
T5B	Loss of all TBCW	1.8E-2	1.8E-2	1.8E-2	1.8E-2	1.8E-2	1.8E-2	-
T5C	Loss of all PSW (includes Radial Well)	1.8E-2	1.8E-2	1.8E-2	1.8E-2	1.8E-2	1.8E-2	-
T5D	Loss of all CCW	-	-	-	1.8E-2	1.8E-2	1.8E-2	-
TAB	Loss of 1E 4160 V AC Bus B	-	-	-	9E-4	9E-4	9E-4	9E-4
TDB	Loss of 1E 125 V DC Bus B	-	-	-	6E-3	6E-3	6E-3	6E-3
TIA	Loss of Instrument Air	0.5	0.5	0.5	0.5	0.5	0.5	-
TORV	Inadvertent Open Relief Valve at Shutdown	-	-	-	0.1	-	-	-
TIOP	Inadvertent Overpressurization (makeup greater than letdown)	-	-	-	0.16	0.16	-	-
TIHP	Inadvertent Overpressurization via Spurious HPCS Actuation	-	-	-	1E-2	1E-2	-	-
TIOF	Inadvertent Overfill via LPCS or LPCI	-	-	-	4E-2	4E-2	-	-
TLM	Loss of Makeup	-	-	-	0.49	0.49	0.49	-

Table 4 (Concluded)  
Initiating Events for Grand Gulf

### Data Analysis

Beyond the usual data analysis task of providing estimates for the basic events in the system fault trees, it was necessary to produce estimates for the fraction of time the plant spends in each of the POSs. This was accomplished by examining plant specific information. The approach used was to perform a step-wise decomposition of total plant time, choosing, at each step, an appropriate method for estimating the plant life fractions. As a result of this work, estimates for the fraction of time spent in each of the seven POSs were obtained. See Table 5 for the final results of decomposition.

POS	Fraction of Time Spent in Each POS
1	0.03
2	0.01
3	0.01
4	0.005
5	0.07
6	0.03
7	0.05

Table 5  
Fraction of Time Spent in Each POS

### Human Reliability Analysis

For the Coarse Screening Phase of this project, the values used for the pre-accident human errors (e.g., failure to restore a component after test and/or maintenance) were the same values as was used in Reference 2. Most of the work associated with post-accident human errors concentrated on identifying the human actions to be included in either the event trees or the system fault trees, and no cut set specific human actions were incorporated into the analysis due to the large number of sequences that were analyzed.

To date all of the estimates for post-accident human errors incorporated into the analysis have been conservative screening values. The use of screening values served two purposes. First, it minimized the possibility of eliminating an important accident sequence before it could be analyzed in the detailed phase. Second, it significantly reduced the number of sequences that had to be analyzed. While it is recognized that this may limit the usefulness of this specific analysis, the project overall was able to meet its objectives of identifying those areas which should be examined in more detail.

## Accident Sequence Quantification

First, the sequence logic was generated using the event trees developed for this project. Second, the sequence logic generated was checked for any error. This step was used as a sanity check by the project members to make sure that the sequences resulting from the combination of the event trees were in actuality valid sequences. This was deemed necessary due to the large number of event trees constructed during this project. Third, any accident specific data changes were made. Finally, the sequences were quantified.

As a means of accomplishing the major objective of this study, to identify those POSs and/or initiating events requiring more detailed analysis, 4188 accident non-fire/flood sequences were analyzed for the seven POSs. The results of this coarse screening analysis indicated that 1163 survived the screening truncation level of  $1E-8$ . Of the 1163 sequences that did survive, 303 sequences were categorized as having potentially high core damage frequencies. Of the 303 sequences, approximately 22 percent would have about 14 hours for any recovery actions to be completed. Many of the remaining sequences have as a minimum, 2 to 2.5 hours for recovery.

There were 351 sequences that were classified as having potentially medium core damage frequencies. Of these, approximately 16 percent have about 14 hours for any recovery actions to be completed. Many of the remaining sequences have as a minimum, 2 to 2.5 hours for recovery.

The remaining sequences, 509, were classified as having low core damage frequencies. Of these, approximately 3 percent have about 14 hours for any recovery actions to be completed. Many of the remaining sequences have as a minimum, 2 to 2.5 hours for recovery.

Screening analyses were performed on fire and flood initiated accidents for a single POS (i.e., POS 4). For accident sequences initiated by a fire, 692 sequences were quantified. Of these 692 sequences 319 sequences were truncated, leaving 373 sequences surviving truncation. Of the 373 sequences surviving truncation, 106 sequences were classified as having potentially medium core damage frequencies while 267 were classified as having low core damage frequencies. None of the surviving fire sequences were classified as having potentially high core damage frequencies. For accident sequences initiated by a flood, 792 sequences were quantified. Of the flood sequences quantified, 243 survived truncation while 549 sequences were truncated. Of those flood sequences surviving truncation, 59 were classified as having potentially medium core damage frequencies while 184 sequences were classified as having low core damage frequencies. Again, no flood sequences were classified as having potentially high core damage frequencies.

---

The sequences are classified as "potentially" high (or medium) since recovery actions have not been applied. After including recovery actions, it is possible that sequences would no longer be classified in the high (or medium) category.

## INSIGHTS

Since this was a screening analysis to identify events requiring more detailed study, only results that correspond to the objectives of this phase of the study will be presented.

Not surprisingly, one significant insight of the study is the importance of human actions. While the analysis used screening estimates for many of the human recovery actions included in the accident sequences, it is expected that human actions will continue to be important even when a more detailed human reliability analysis takes place during the detailed analysis phase. This outcome is expected due to the number of human actions incorporated into the models and used in the solution of the accident sequences. The importance associated with the human actions should not be construed to be all negative. It is very likely that human recovery actions will positively affect (i.e., significantly reduce) the quantitative results of the detailed analysis.

Another insight from the study is the importance of ensuring that adequate means of removing decay heat from the reactor vessel as the plant transitions from low power operation to refueling and back are preserved. One means of removing decay heat deals with the availability of the safety relief valves (SRVs) as the plant transitions to refueling. During POS 5 (which corresponds to Cold Shutdown), Grand Gulf requires that one SRV be operable at all times. This Grand Gulf requirement exceeds the Technical Specifications requirements for SRVs in this POS. While the availability of one SRV is important since it provides the option of removing decay heat via steaming, Grand Gulf's procedure for dealing with loss of decay heat removal capability indicates that two SRVs should be opened when establishing a water solid loop to the suppression pool. For this analysis, the water solid means of removing decay heat was assumed to be unavailable, thereby increasing the importance of the SRVs.

A third insight from the analysis is the identification of two potentially important accident initiating events or classes of events. The initiating events identified as potentially important include loss of instrument air as a unique initiating event (the result of which is the loss of several potential mitigation systems) and the loss of the operating decay heat removal system (train) as a class of events. For the loss of instrument air, this is not particularly surprising, given an understanding of the relationship of this support system to the front-line systems that could be used to provide the functions necessary for maintaining the plant in the POS. The importance of the loss of the operating decay heat removal system is even less surprising. Removing decay heat is the main function necessary for preventing core damage.

A final insight from the study is the identification of two POSs as potentially important operational states. These two POSs include POS 5 (Cold Shutdown to Refueling when the water level is raised to the steam lines) and POS 6 (Refueling with the water level raised to the steam lines). Many of the sequences classified in the potentially high or medium categories occurred in these two POSs.

Having made the above statements, the reader is cautioned that these insights are

based on coarse screening results. As has been stated before, the major objective of the coarse screening phase was to provide information that could be used to prioritize the detailed work of Phase 2. The authors believe that this has been accomplished. Nevertheless, we wish to emphasize that the specific insights identified above are subject to change once the detailed phase of this project has been completed.

#### REFERENCES

- [1] D. W. Whitehead and T. M. Hake, "Accident Sequence Analysis for a BWR During Low Power and Shutdown Operations," Eighteenth Water Reactor Safety Information Meeting, NUREG/CP-0114, Vol. 2, page 449, 1990.
- [2] M. T. Drouin, et. al., Analysis of Core Damage Frequency: Grand Gulf Unit 1 Internal Events, NUREG/CR-4550, Vol. 6, Rev. 1, SAND86-2084, Sandia National Laboratories, September 1989.

SAND91-1668C  
Integrated Level III Risk Assessment for the  
LaSalle Unit 2 Nuclear Power Plant\*

Arthur C. Payne Jr.  
Thomas D. Brown  
LeAnn A. Miller

Sandia National Laboratories  
Albuquerque, New Mexico 87185

**Abstract**

In this paper we discuss the methodology and results of the integrated Level III Probabilistic Risk Assessment (PRA) of the LaSalle County Station Unit 2 Nuclear Power Plant. Methods were developed for integrating internal and external events into one analysis based on a common model of the plant and a common method for representing the output. Additional methods were developed for representing and propagating uncertainties in the basic inputs to the models to determine their effects on the final (or intermediate) results. The integrated core damage frequency for the LaSalle plant is  $1.01E-4/R\text{-yr.}$ , with a 5th percentile of  $5.34E-6/R\text{-yr.}$ , a median value of  $2.92E-5/R\text{-yr.}$ , and a 95th percentile of  $2.93E-4/R\text{-yr.}$  The dominant sequence is short-term station blackout. The risk from the LaSalle plant is low, especially with respect to the NRC safety goals. The mean individual early fatality risk within one mile and the mean individual latent cancer risk are  $1.1E-10/R\text{-yr.}$  and  $8.5E-9/R\text{-yr.}$ , respectively; both of which are several orders of magnitude less than the safety goals.

1. Introduction

An integrated Level III Probabilistic Risk Assessment (PRA) was performed on the LaSalle County Station Unit 2 Nuclear Power Plant by Sandia National Laboratories (SNL) for the Nuclear Regulatory Commission (NRC)[1,2]. This study had three primary objectives:

1. To perform a Level III PRA analysis on a BWR-5 nuclear power plant with a Mark II containment,
2. To develop, implement, and demonstrate methods for integrating internal and external events into one consistent analysis, and

---

\* This work was supported by the U. S. Nuclear Regulatory Commission and performed at Sandia National Laboratories which is operated for the U. S. Department of Energy under Contract No. DE-AC04-76DP00789.

3. To develop, implement, and demonstrate methods for representing and propagating uncertainties in the various PRA inputs through the analysis to determine their effects on the final risk results.

The LaSalle County Station is a two-unit nuclear power plant located 55 miles southwest of Chicago, Illinois. LaSalle County Station is operated by Commonwealth Edison Company and began commercial operation in 1984. Each unit utilizes a Mark II containment to house a General Electric 3323 MWT BWR-5 reactor. This PRA, which was performed on Unit 2, included both internal and external events. External events that survived the screening process and were propagated through the analysis included: earthquakes, internal fires, and internal floods. The internal events included: transients, transient-induced LOCAs (inadvertent stuck open relief valves), anticipated transients without scram (ATWS), and loss of coolant accidents (LOCAs). Uncertainties were included in the accident sequence analysis, the accident progression analysis, and the source term analysis. For the consequence analysis, in addition to the weather uncertainties, uncertainty in the warning time was included; however, no other parameter uncertainties were included.

In this paper selected results from the accident sequence, accident progression, source term, consequence, and integrated risk analysis are discussed and the methods used to perform a fully integrated Level III PRA are examined.

## 2. Integrated Level I Analysis

### 2.1. Methods Used in the Integrated Level I Analysis

As mentioned in the introduction, one of the primary purposes of the LaSalle PRA was to develop methods for integrating internal and external event analyses into a common framework using the same basic plant model to evaluate all initiating events. This resulted in a common representation of the accident sequence analysis output. Because of this common representation, in terms of cut sets similar to the standard internal event analysis, the results of the individual analyses could be combined into one integrated result.

The basic plant model consists of one set of accident sequence event trees used for all analyses and a set of very detailed fault trees that were extended from the usual level of detail used in PRA modeling to include:

1. All components both active and passive that might be affected by any of the initiators,
2. A tracing and mapping of the locations of all components and associated cabling for location based analysis,
3. Modeling of spurious failures that could be important in some external event analyses, and
4. Non-safety systems that could be used for accident mitigation or support functions were modeled to the same level of detail as the safety systems.

The model was then solved for the accident sequences for each class of initiators (internal, seismic, fire, and flood). Information on the impact of the initiators on the systems or information unique to that analysis (e.g., cable routing for the internal fire propagation analysis) was mapped into the model so that the final sequence results from each analysis consisted of collections of cut sets of the same general form. For each analysis, the individual events in the cut sets could represent either the occurrence of component failure or success, the occurrence of some physical phenomena, or the susceptibility of a component to some phenomena depending on the analysis characteristics. Data analyses and supporting thermal/hydraulic and other deterministic calculations were performed as required to quantify the events in the cut sets. Expert judgment or data was used to define probability distributions for the events. A new code, TEMAC[3], was developed to perform the integrated importance and uncertainty analysis.

## 2.2. Results of the Integrated Level I Analysis

The total core damage frequency from all events included in the analysis has a mean value of  $1.01E-4/R\text{-yr}$ . This result is considered to be low given that all initiators (both internal and external) are included in this result and that this is the first time a PRA has been performed on this plant. Usually the first time a PRA is performed certain design faults are found that lead to significantly higher accident sequence frequencies than would have occurred without the design faults. At LaSalle, while some design deficiencies were found, none compromised redundancy to the point where they created accident sequences which were significantly higher in frequency than those from the general level of the design.

The overall integrated core damage cumulative distribution function (CDF) is shown in Figure 1. A density plot showing the fraction of the Latin Hypercube observations with final core damage frequencies within each frequency interval is overlaid on the integrated core damage CDF plot. Figure 2 is a comparison of the CDFs for the seismic, flood, fire, internal events, and integrated analyses. Figure 3 has pie charts showing the relative contributions to the mean integrated core damage frequency. The categories are: seismic, fire, flood, and internal events. The internal events is broken into LOCAs, ATWS, transients, and transient-induced LOCAs. Figure 4 has a pie chart showing the relative contribution of various initiators to the internal events mean core damage frequency.

By examining the above plots and figures, one can see that seismic sequences do not contribute significantly to the integrated core damage frequency. Flood sequences are moderate contributors at all quantiles of the distribution. Since the integrated core damage frequency distribution is very similar to the internal events core damage frequency in all but the 90 to 100th quantile range, the integrated core damage frequency comes mostly from internal events. However, at the very top of the distribution, one can see that the fire sequences contribution actually becomes greater than that for internal initiators. This occurs at about the 95th percentile. The dominant fire sequence is initiated by a control room fire. The sparse fire data for calculating control room fire initiating event frequencies results in a

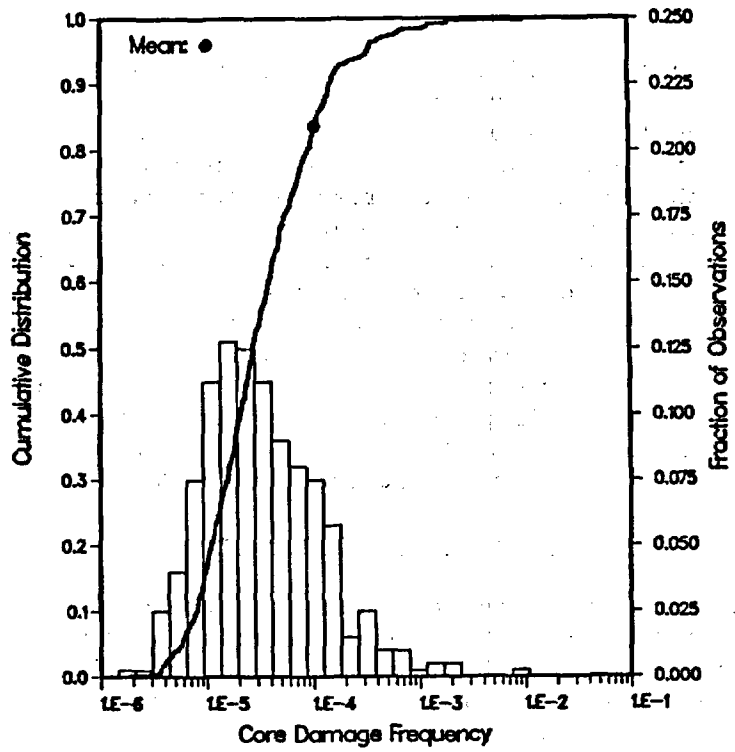


Figure 1 Integrated Core Damage Frequency Distribution

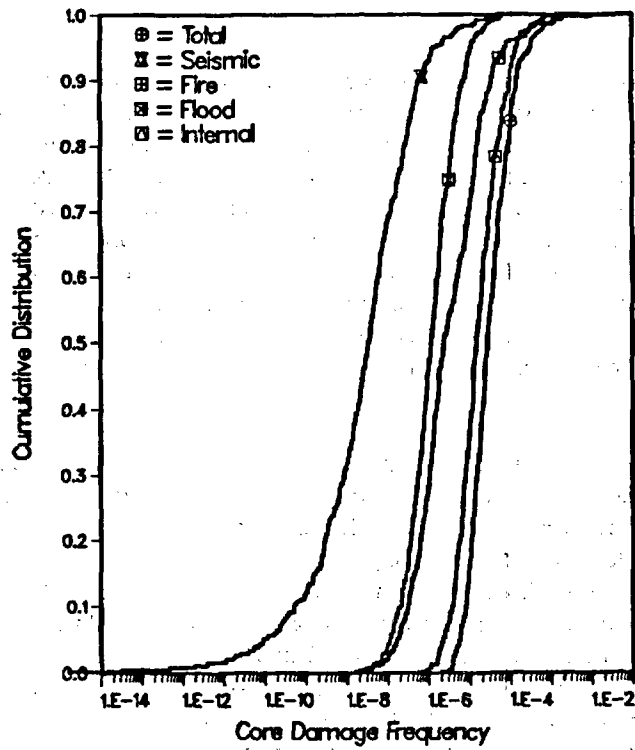


Figure 2 Seismic, Flood, Fire, Internal, and Integrated CDFs

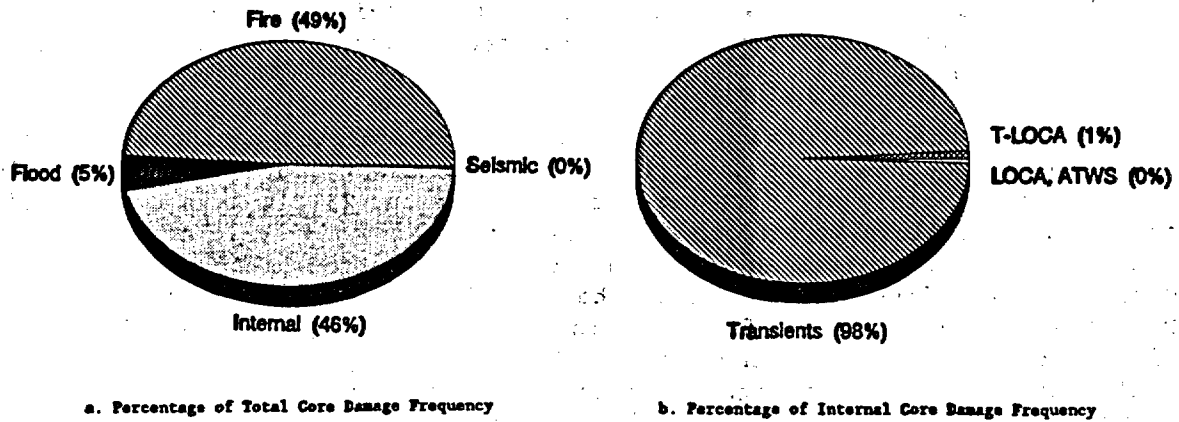


Figure 3 Contribution to Integrated Core Damage Frequency

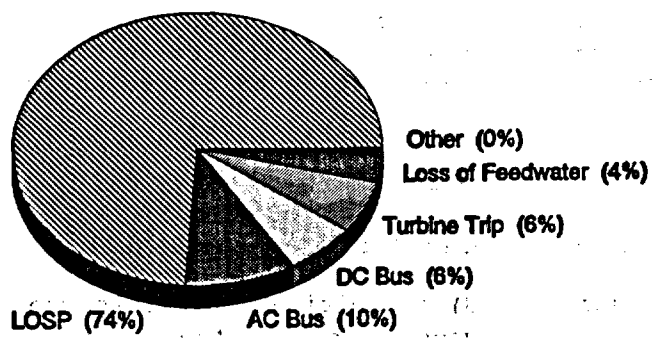


Figure 4 Contribution to Internal Core Damage Frequency

distribution with very wide uncertainty bounds. Thus the mean value of the fire core damage frequency is dominated by a few observations from the latin Hypercube sample at the upper end of the distribution. In these cases, the fire contribution can be substantial. Table 1 contains a comparison of the individual analysis final core damage frequency distribution statistics to the integrated result.

Table 2 shows the core damage statistics of the dominant accident sequences. The dominant sequence is T100 which is a transient with loss of all injection. It is composed mainly of short-term station blackout (90%), loss of DC train A with a random failure of component cooling by common mode failure which results in the loss of all injection (6%), and long-term station blackout with partial AC until the DG fails to run (4%). The second most dominant sequence is FIRE-CR. This is a control room fire with failure to manually suppress the fire and failure to use the remote shutdown panel successfully. Loss of all injection results in a short-term high pressure core damage sequence. The third most dominant sequence is FIRE-W2. This is the result of a fire in the Div. 2 essential switchgear room which fails train B of containment heat removal (CHR). Random failures fail train A CHR resulting in a long-term TW type sequence.

The events most important to risk reduction are: the frequency of loss of offsite power, the frequency of control room fires, the percentage of control room fires that are not extinguished before smoke forces abandonment of the control room, the probability that the operators will not successfully recover the plant from the remote shutdown panel, the non-recovery of offsite power within one hour, the diesel cooling water pump common mode failure, and the non-recoverable isolation of RCIC during station blackouts. The events most important to risk increase are: the internal flood pipe failure frequency, the failure of various AC power circuit breakers resulting in partial loss of onsite AC power, the failure to scram, and the diesel generator cooling water pump random failure rate (which determines the magnitude of the common mode contribution). The dominant contributors to uncertainty are: the uncertainty in control circuit failure rates, the uncertainty in relay coil failure to energize, the uncertainty in energized relay coils failing deenergized, and the uncertainty in the response of systems to severe environments in the reactor building.

### 3. Plant Damage State Definition

#### 3.1. Methodology for Plant Damage State Definition

The plant damage state (PDS) definition represents the interface between the Level I and Level II analyses. Because the goals of the two analyses are different (i.e., Level I - analyze the sequences with respect to those characteristics which are important to the determination of core damage vs. Level II - analyze the sequences with respect to those characteristics which are important to the determination of the source term), it is important to structure this process to ensure the completeness and accuracy of the transformation.

Table 1  
LaSalle Final Core Damage Statistics By Event Type

	5%	MEDIAN	MEAN	95%
INTERNAL GLOBAL	2.0500E-06	1.6400E-05	4.4100E-05	1.3900E-04
FIRE GLOBAL	1.3200E-07	1.9900E-06	3.2100E-05	5.9400E-05
FLOOD GLOBAL	9.6200E-08	1.1300E-06	3.3900E-06	1.0900E-05
SEISMIC GLOBAL	4.0700E-11	1.7400E-08	7.5800E-07	1.2100E-06
INTEGRATED	5.3400E-06	2.9200E-05	1.0100E-04	2.9300E-04

Table 2  
LaSalle Final Core Damage Statistics By Sequence

	5%	MEDIAN	MEAN	95%	FRAC OF TOT
1. T100	1.1000E-06	9.0700E-06	2.8700E-05	9.7400E-05	3.5413E-01
2. FIRE-CR	6.1800E-14	1.2500E-12	1.3900E-05	3.6700E-06	1.7151E-01
3. FIRE-W2	0.0000E+00	0.0000E+00	6.7100E-06	1.3500E-05	8.2796E-02
4. T62	3.1800E-07	2.3900E-06	6.5300E-06	2.4100E-05	8.0575E-02
5. T18	0.0000E+00	0.0000E+00	4.9900E-06	2.0900E-05	6.1572E-02
6. FIRE-Y2	0.0000E+00	0.0000E+00	3.3900E-06	7.9000E-06	4.1830E-02
7. FS2	9.5100E-08	1.0900E-06	3.1800E-06	1.0500E-05	3.9238E-02
8. FIRE-T	4.4800E-08	6.7700E-07	2.2700E-06	7.7800E-06	2.8010E-02
9. FIRE-W1	0.0000E+00	0.0000E+00	1.8000E-06	1.8700E-06	2.2210E-02
10. FIRE-Y1	0.0000E+00	0.0000E+00	1.7600E-06	1.9100E-06	2.1717E-02
11. T20	0.0000E+00	0.0000E+00	1.2800E-06	8.0300E-06	1.5794E-02
12. T22	0.0000E+00	0.0000E+00	1.1400E-06	3.9900E-06	1.4067E-02
INTEGRATED	5.3400E-06	2.9200E-05	1.0100E-04	2.9300E-04	

For the LaSalle PRA, the following method was used to perform this analysis:

1. A set of plant characteristics were defined that presented a set of unique initial and boundary conditions for the accident progression analysis,
2. Each cut set in the final sequences was examined and the possible set of values for the characteristics was determined,
3. The unique sets of values were determined and defined the PDSs, and
4. The cut sets were rearranged into PDS groups and the frequencies of the groups were recalculated.

### 3.2 Results of Plant Damage State Definition

There were 50 sequences in the integrated analysis with frequencies above  $1.0E-8$ /R-yr. These sequences, which accounted for 99.9% of the core damage frequency, were used to define the PDSs. A total of 30 PDSs were defined with 16 additional sub-PDSs included in the analysis. Table 3 is a list of all the PDSs and their relative contributions to core damage frequency.

The dominant plant damage states were IT2, FI5, and FL1, with 0.368, 0.107, and 0.105 mean fractional contributions to the total core damage frequency, respectively. IT2 is a transient-induced short-term station blackout PDS with core damage beginning at about 80 minutes after the accident initiation. Containment failure has not yet occurred and venting is recoverable if AC power is restored. There are three sub-PDSs: (1) ADS and almost all injection systems are recoverable if AC power is restored, (2) ADS is available during the core damage process and almost all injection is recoverable if AC power is restored, and (3) ADS is available during the core damage process but only MFW, CDS, and RCIC are recoverable if AC power is restored.

FI5 is a fire initiated accident sequence resulting in a partial loss of containment heat removal. Random failures complete the loss of CHR and a long-term loss of CHR sequence results (TW type). Primary injection into the RPV is available using the HPCS system although other systems may be used for some part of the time. Containment pressurizes, RCIC isolates at 30 psig, the ADS valves reclose at 100 psig, and low pressure injection fails on repressurization of the vessel. High pressure injection continues and the containment pressurizes until structural failure of the containment, resulting in blowdown to the reactor building, occurs anywhere from 150 to 275 psig (mean value 191 psig). The severe environment created in the reactor building by the blowdown results in failure of any remaining injection systems and core damage occurs with a failed containment.

FL1 is an internal flood initiated by a service water pipe or valve rupture on the ground floor of the reactor building. The flood fails all injection systems except diesel-driven fire water which is not used in time to prevent core damage. ADS and containment heat venting are available. This sequence is a short-term loss of all injection (TQUV type) sequence.

Table 3  
LaSalle Conditional Plant Damage State Frequency Distributions

PDS NO.	PDS	5TH PCT	MEDIAN	95TH PCT	MEAN
1	EQ1	0.391E-07	0.111E-04	0.216E-02	0.798E-03
2	EQ2	0.254E-05	0.114E-02	0.836E-01	0.143E-01
3	FI1	0.200E-08	0.568E-07	0.222E+00	0.398E-01
4	FI2	0.411E-04	0.969E-03	0.170E-01	0.410E-02
5	FI3	0.684E-03	0.242E-01	0.276E+00	0.671E-01
6	FI4	0.106E-03	0.376E-02	0.838E-01	0.204E-01
7	FI5	0.000E+00	0.000E+00	0.613E+00	0.107E+00
8	FI6	0.000E+00	0.000E+00	0.201E-03	0.446E-04
9	FL1	0.900E-06	0.114E-03	0.241E-01	0.503E-02
10	FL2	0.140E-02	0.375E-01	0.470E+00	0.105E+00
11	IA1	0.000E+00	0.000E+00	0.120E-02	0.356E-03
12	IA2	0.256E-04	0.102E-02	0.191E-01	0.430E-02
13	IL1	0.000E+00	0.000E+00	0.110E-02	0.182E-03
14	IT1	0.764E-03	0.156E-01	0.951E-01	0.297E-01
15	IT2	0.171E-01	0.338E+00	0.763E+00	0.368E+00
16	IT3	0.568E-02	0.669E-01	0.183E+00	0.784E-01
17	IT4	0.467E-03	0.106E-01	0.215E+00	0.489E-01
18	IT5	0.294E-03	0.462E-02	0.823E-01	0.191E-01
19	IT6	0.112E-04	0.231E-03	0.589E-02	0.152E-02
20	IT7	0.244E-05	0.858E-04	0.211E-02	0.497E-03
21	IT8	0.000E+00	0.000E+00	0.406E+00	0.688E-01
22	IT9	0.000E+00	0.000E+00	0.170E-01	0.254E-02
23	IT10	0.000E+00	0.000E+00	0.115E-01	0.247E-02
24	IT11	0.000E+00	0.000E+00	0.178E-01	0.359E-02
25	ITL1	0.316E-05	0.117E-03	0.194E-02	0.478E-03
26	ITL2	0.545E-04	0.126E-02	0.691E-02	0.223E-02
27	ITL3	0.837E-06	0.329E-04	0.307E-03	0.853E-04
28	ITL4	0.172E-05	0.682E-04	0.702E-03	0.213E-03
29	ITL5	0.968E-05	0.164E-03	0.247E-02	0.613E-03
30	ITL6	0.555E-04	0.148E-02	0.177E-01	0.456E-02

#### 4. Integrated Level II Analysis

##### 4.1 Methodology Used in the Integrated Level II Analysis

In the Level II analysis the possible evolutionary paths that the PDSs can take are delineated and the associated source terms are estimated. We do this by constructing a decision tree called the accident progression event tree (APET). This event tree consists of a series of questions about the probability of occurrence of events (i.e., phenomena, hardware, human actions) which can impact the accident progression. This event tree is analyzed using the EVNTRE [4] code developed originally for the Severe Accident and Risk Reduction Program (SARRP) program and completely rewritten for this analysis. This code was used in the final NUREG-1150 [5] analysis but additional changes were made to the code and event tree structure to satisfy the need to perform an integrated analysis. First, the code change was made to allow direct sampling of multiple branches. Second, all of the PDS definition logic was built into the initial questions in the APET so that all PDSs could be evaluated in one run (i.e., conditional probabilities of each PDS were calculated from the total core damage frequency on a sample by sample basis and all PDSs were calculated simultaneously). The output of the event tree analysis is grouped into accident progression bins which are determined based on those accident progression characteristics important to the determination of the source term. The source terms are evaluated using a parametric code called LASSOR [2]. The LASSOR code is one of the XSOR [6] codes and calculates the source term for each accident progression bin. The LASSOR code used for the LaSalle analysis has more detail than the XSOR codes used in NUREG-1150. Three release times were used to describe the plume segments and a more detailed release pathway model was developed which also allowed the release pathway to change for different release segments.

##### 4.2 Results of the Integrated Level II Analysis

The accident progression results showed that the majority of the accidents analyzed will proceed to vessel failure. Although notable, the mean conditional probability of core damage arrest is still fairly small, approximately 0.15. Figure 5 shows the distribution on core damage arrest for the summary PDSs. The probability of core damage arrest is driven the likelihood of in-vessel steam explosions, by the recovery of AC power for the short-term station blackouts, and the lack of available or recoverable injection systems for the other accidents.

Given that core damage occurs, it is likely that the containment's integrity will be compromised during the course of the accident by either containment failure or containment venting. The mean probability that the containment will remain intact throughout the accident is only 0.12. Figure 6 shows the mean conditional probability of containment failure modes at all times. Furthermore, it is fairly likely that the containment will fail early in the accident; the mean probability of early containment failure is 0.33. It is also likely that the operators will vent the containment during the accident; the mean probability of accidents in which the containment is vented is 0.46. Figure 7 shows the distribution on early containment failure for the summary PDSs.

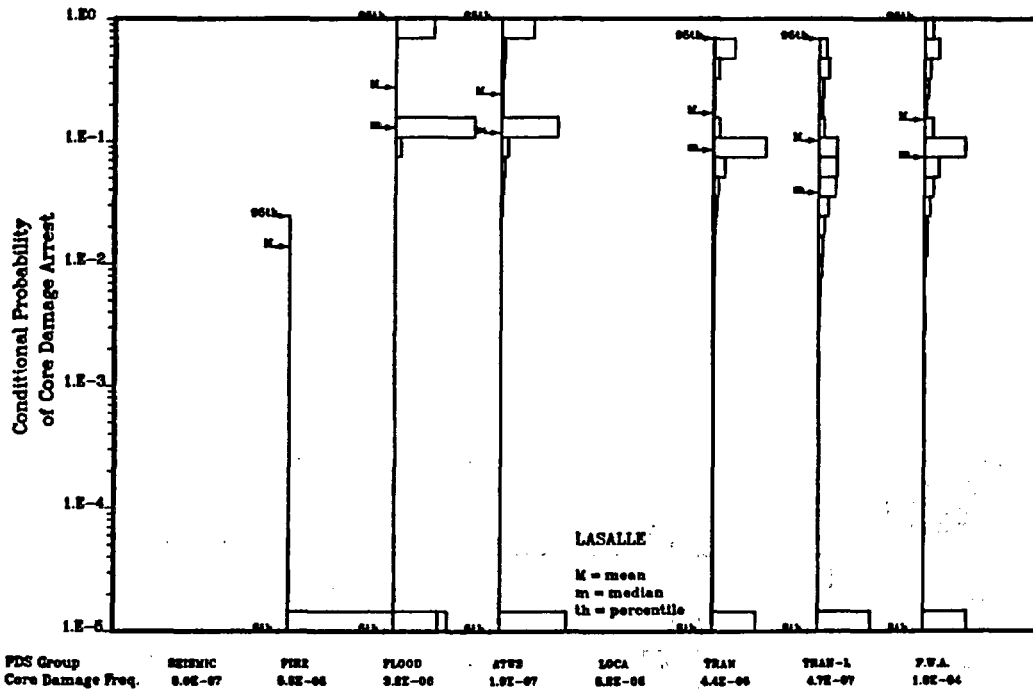


Figure 5 Conditional probability of Core Damage Arrest

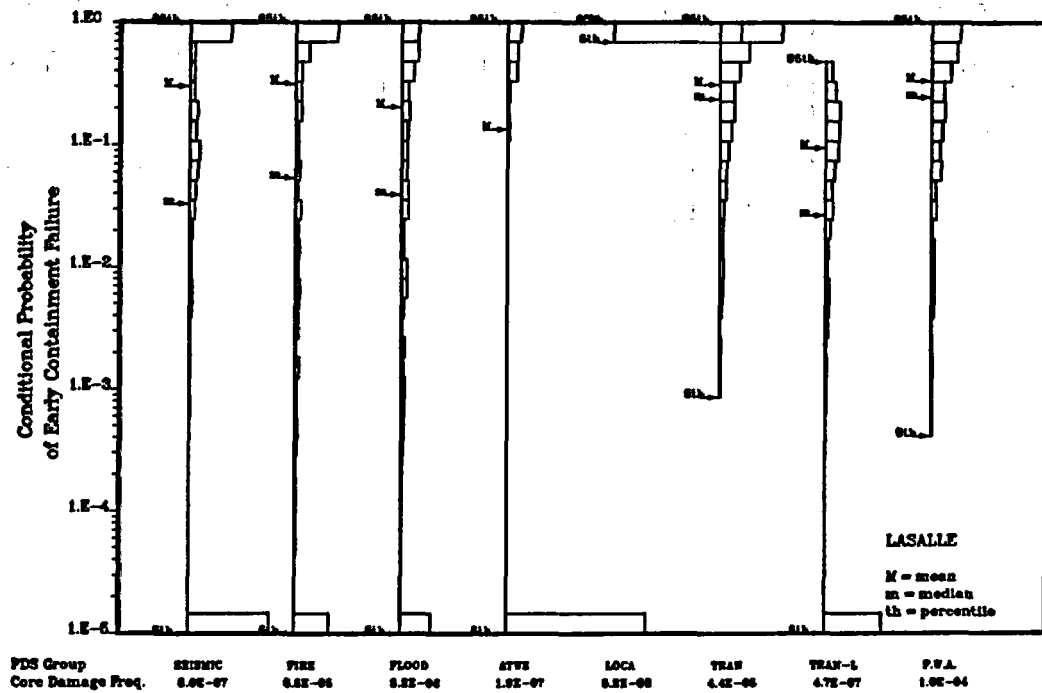
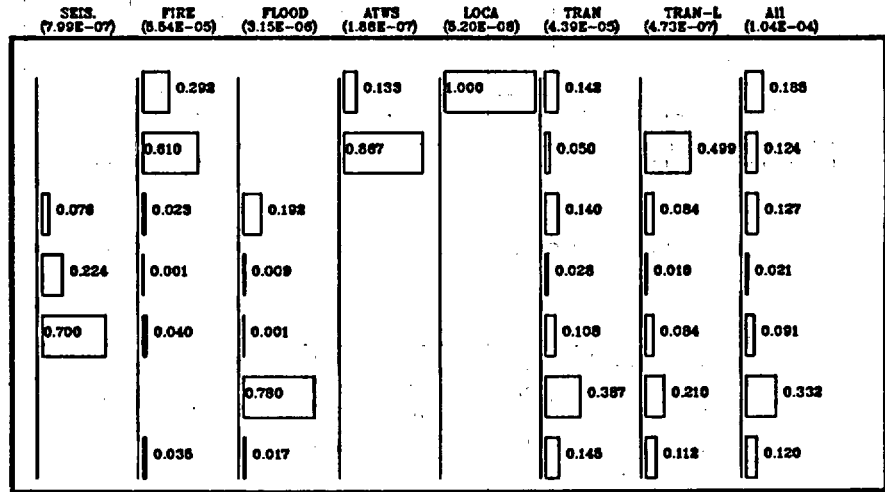


Figure 6 Conditional Probability of Early Containment Failure

**SUMMARY  
ACCIDENT  
PROGRESSION  
BIN GROUP**

**PLANT DAMAGE STATES  
(Mean Core Damage Frequency)**



VB = Vessel Breach  
CF = Containment Failure

LASALLE

Figure 7 Mean Conditional Probability of Early Containment Failure

Given that core damage occurs, it is likely that the core debris released from the vessel will participate in core-concrete interactions (CCI). The mean probability of CCI, conditional on core damage, is 0.77. Thus, the potential exists for a large release late in the accident. Figure 8 shows the mean conditional probability of various categories of CCI.

The events that result in containment failure before core damage are slow pressurization events that result from the accumulation of steam and noncondensibles during accidents in which CHR is lost or inadequate (i.e., long-term loss of CHR accidents, long-term station blackout accidents, and ATWS accidents). Events that result in containment failure around the time of vessel breach include fast pressurization of the containment from loads accompanying vessel breach (i.e., DCH, ex-vessel steam explosions, RPV blowdown), alpha mode events, drywell failure induced by reactor pedestal failure, and cavity drain line isolation failure). Late in the accident, events that result in containment failure include the slow pressurization of the containment from the steam and noncondensibles generated during CCI and failure of the reactor pedestal caused by concrete erosion during CCI. Figure 9 shows the mean conditional probability of summary accident progression bins for various summary PDSs.

The source term results showed that the pressure of the RPV does not significantly affect the total source term for a particular accident progression if vessel breach occurs. This is due to the differences in the fraction of a species released from the fuel before vessel breach being negated when the vessel breaches and the radionuclides in the vessel revolatilize (i.e., low release before vessel breach results in high release after vessel breach and vice versa).

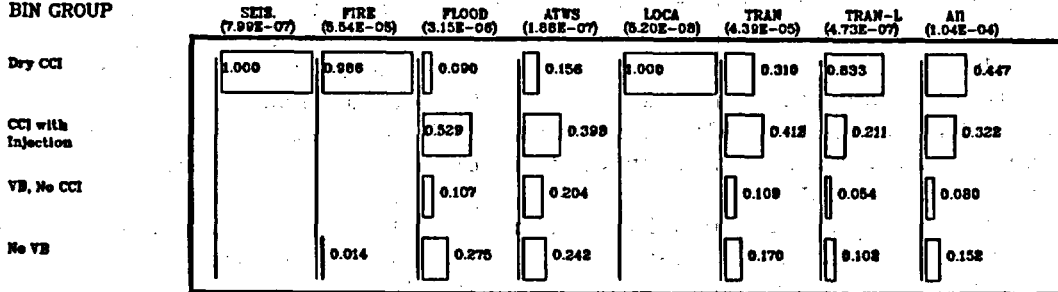
The release path through which the radionuclides pass was determined to be important. The path that resulted in the highest release to the environment is through the wetwell above the water line. If the cavity floor failed, radionuclides may leave the containment without being scrubbed by sprays or the suppression pool. The venting pathway is also through the wetwell above the water line. In most cases, containment failures in the drywell or drywell head were accompanied by successful operation of containment sprays which significantly reduced the amount of radionuclides being released. Also, for many of the cases for which containment failure in the drywell head occurred, core damage did not occur because severe environments were not created in the reactor building and injection systems did not subsequently fail.

The analysis showed that late iodine revolatilization results in significant releases due to much of the iodine being scrubbed by the suppression pool initially and being revolatilized later when the removal mechanisms are not as effective. For this reason, the modeling of late iodine revolatilization may need to be investigated further.

The regression analysis shows that much of the uncertainty in the final results is due to uncertainty in the source term parameters. Much of the uncertainty may be due to the fact the distributions being used were elicited for cases with large uncertainties in the initial and boundary conditions. Some of this

SUMMARY  
ACCIDENT  
PROGRESSION  
BIN GROUP

PLANT DAMAGE STATES  
(Mean Core Damage Frequency)



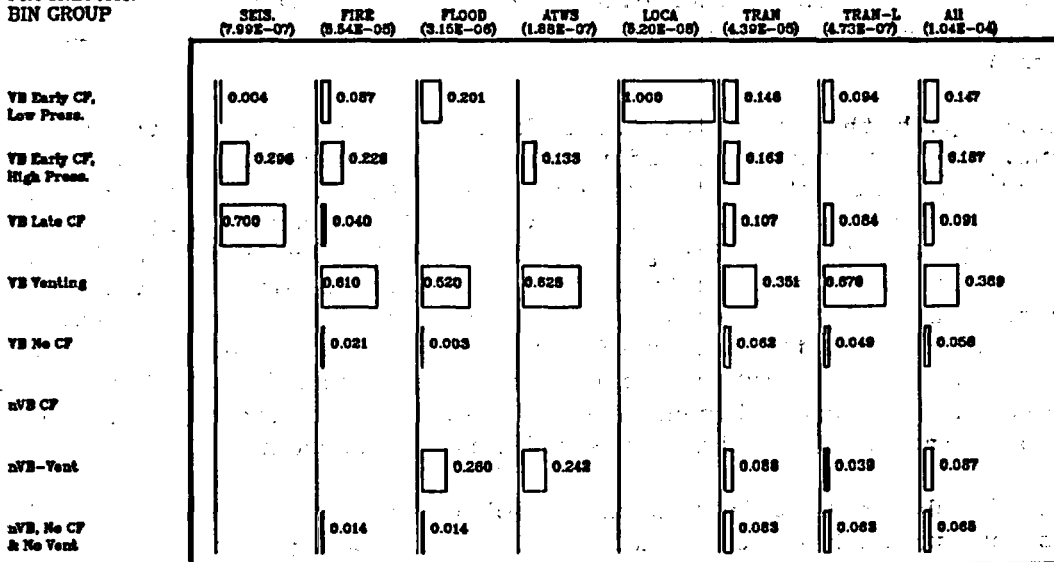
VB = Vessel Breach  
CF = Containment Failure

LASALLE

Figure 8 Mean Conditional Probability of Various Categories of CCI

SUMMARY  
ACCIDENT  
PROGRESSION  
BIN GROUP

PLANT DAMAGE STATES  
(Mean Core Damage Frequency)



VB = Vessel Breach  
CF = Containment Failure

LASALLE

Figure 9 Mean Conditional Probability of Summary Accident Progression Bins

uncertainty might be eliminated by a more detailed case structure in the APET and LASSOR codes with new distributions for these more specific cases. Figure 10 shows the CCDFs for release fractions for several classes for the integrated results.

## 5. Integrated Level III Analysis

### 5.1 Methodology Used For the Integrated Level III Analysis

Just as we had to transform accident sequences defined with respect to core damage characteristics into plant damage states defined with respect to accident progression and source term characteristics, we have to transform accident progressions bins and their associated source terms into source term groups which present unique initial and boundary conditions to the consequence analysis. The PARTITION [7] code (also used in the final NUREG-1150 analysis) was developed to perform this grouping. The code was modified further for the final analysis from the version used in NUREG-1150 so that partitioning could be done not only on early and latent health effect weights but also upon frequency, evacuation parameters, and release parameters. Also, a discrete parameter was introduced to allow specific subanalysis source terms to be grouped only within themselves (this was primarily for seismic high g and low g accidents which had unique evacuation characteristics).

Each source term group was then relatively homogeneous in those parameters thought to be important to the consequence calculation. These source term groups were input into the MACCS [8] code along with appropriate site specific data and consequence calculations were performed. The MACCS input was modified to (1) run all source term partitions at the same time and allow for different evacuation assumptions, (2) evaluate three release segments, and (3) account for more realistic shielding factors for the low-g seismic case than those used in NUREG-1150.

The PRAMIS [9] code was developed to combine the plant damage state frequencies, the accident progression bin conditional probabilities, and the consequence values and calculate the risk. Output from the PRAMIS code can be used by the SAS [10] code to perform regression analyses.

### 5.2 Results of the Integrated Level III Analysis

Figure 10 shows the basic results of the integrated risk analysis for internal and external initiators at LaSalle. This figure shows the complementary cumulative distribution functions (CCDFs) for early fatalities and latent cancer fatalities. The CCDFs display the relationship between the frequency and the magnitude of the consequence. Figure 11 shows the distribution of annual risk and a comparison to the NRC safety goals. The safety goals are expressed in terms of individual fatality risk, which is really an individual's probability of becoming a casualty of a reactor accident in a given year. The plots for individual risk in Figure 11 show that both risk distributions for LaSalle fall well below the safety goal. Table 4 contains summary statistics for the total core damage frequency and six measures of annual risk.

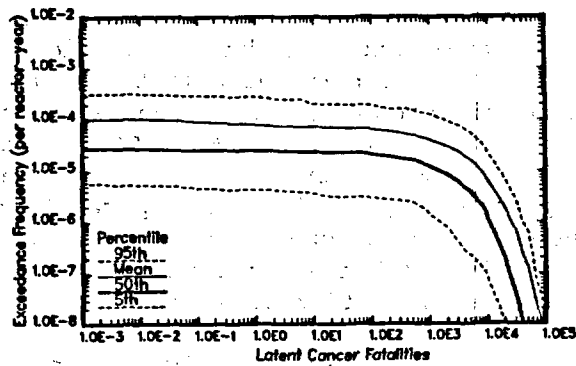
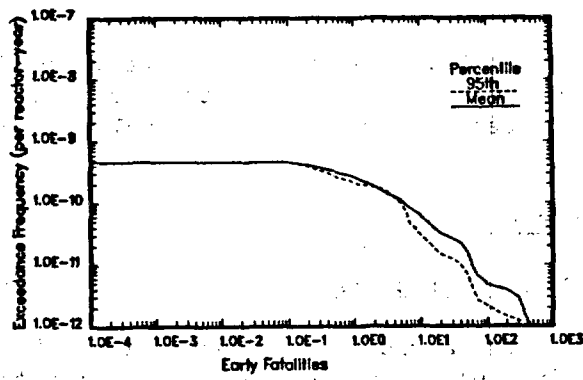


Figure 10 Integrated CCDFs For Early and Latent Cancer Fatalities

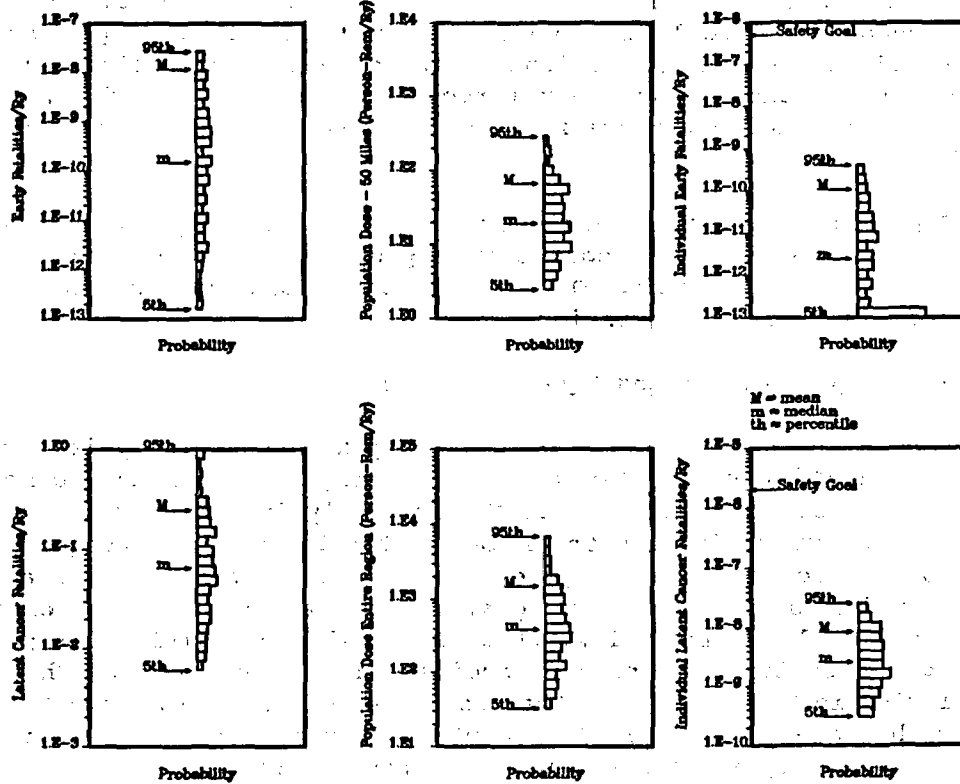


Figure 11 Distributions of Annual Risk

Table 4  
 Distributions for Annual Risk at LaSalle for  
 Internal and External Initiators  
 (All values per reactor-year)  
 (Population doses in person-rem)

<u>Risk Measure</u>	<u>5<sup>th</sup>tile</u>	<u>Median</u>	<u>Mean</u>	<u>95<sup>th</sup>tile</u>
Core Damage	5.7E-6	2.7E-5	1.0E-4	3.2E-4
Early Fatalities	1.9E-13	1.5E-10	1.2E-8	2.5E-8
Latent Cancer Fat.	7.3E-3	6.5E-2	2.5E-1	8.4E-1
Population Dose 50 mi.	2.7E+0	1.9E+1	6.6E+1	2.3E+2
Population Dose Entire Region	4.3E+1	3.9E+2	1.5E+3	5.2E+3
Ind. Early Fat. Risk 0 to 1 mile	3.6E-15	2.5E-12	1.1E-10	3.0E-10
Ind. L. C. Fatalities Risk--0 to 10 miles	3.8E-10	2.6E-09	8.5E-09	2.6E-08

Table 5 shows the contribution of seven summary PDS groups to the various risk measures. For all of the consequence measures, the risk is dominated by the fire PDS group and the transient PDS group. These groups are also the dominant contributors to the core damage frequency. The LOCA and the transient-induced LOCA PDS groups, on the other hand, are very minor contributors to the risk. The seismic, ATWS, and flood groups are intermediate contributors. The seismic and ATWS PDS groups involve potentially high consequence accidents, however, their frequency of occurrence is sufficiently low that the resulting risk does not dominate the risk profile.

Table 6 shows the contribution of eight summary accident progression bins to the various risk measures. The risk is dominated by accidents that progress to vessel breach and involve loss of containment integrity. Vessel breach is important because it affects the magnitude of the source term. If the core damage process is arrested, there are only in-vessel releases which are likely to be scrubbed by the suppression pool. If, on the other hand, vessel breach occurs, there are both in-vessel releases and ex-vessel releases. Releases from core-concrete interactions, which is an ex-vessel release, can be a significant contributor to the total release. Loss of containment integrity is important, because if the containment remains intact the release to the environment through normal leakage is extremely small and is a negligible contributor to risk. For this analysis the timing of the release did not significantly influence the risk.

There are several factors that lead to these low values for risk. First, while the mean core damage frequency for LaSalle,  $1.0E-04/R\text{-yr.}$ , appears high when compared to the NUREG-1150 plants, it must be remembered that this is an integrated value and represents not only accidents from internal initiators but also accidents from fire, flood, and seismic initiators. In fact, if one adds up the mean core damage frequencies for the internal, fire, and seismic analyses at the Peach Bottom plant analyzed in NUREG-1150, the mean core damage frequency is  $1.4E-04/R\text{-yr.}$  with LLNL seismic hazard curve and  $6.6E-05/R\text{-yr.}$  with the EPRI curve. This is in the same range as the LaSalle core damage frequency and the Peach Bottom analysis did not include internal flooding which was included in the LaSalle analysis. Second, two features of the LaSalle plant that reduce the magnitude of the source term are the suppression pool and the reactor building. In the majority of the accidents analyzed, the in-vessel releases (i.e., early releases) are scrubbed by the suppression pool. In addition to the suppression pool, the reactor building surrounding the LaSalle containment also traps a portion of the radionuclides that escape the containment. Third, for all of the non-seismic source term groups that were generated during the partitioning process, the population in the emergency planning zone, EPZ, began evacuation before the start of the release. Thus, the dose received by the evacuating population was generally small and no early fatalities resulted from this fraction of the population. Because of the rapid evacuation, the timing of containment failure was not important in the LaSalle analysis. Changes in the evacuation assumptions could change this conclusion.

The latent cancer fatalities are generally associated with the population that is beyond the emergency evacuation zone. Thus, this risk measure is not particularly sensitive to the timing of containment failure, but rather to

Table 5  
Fractional PDS Contributions (in percent) to Annual  
Risk at LaSalle Due to All Initiators

Summary PDS Group	Method	Core Dose	Early Fatalities	Latent Cancer Fatalities	Population Dose 50 miles	Population Dose Region	Ind. E. F. Risk-1 mile	Ind. L.C.F. Risk-10 mile
Seismic	FCMR	0.7	5.2	1.3	1.1	1.2	2.9	1.0
	MFCR	1.5	4.6	2.3	2.1	2.3	4.4	2.2
Fire	FCMR	53.3	46.2	63.1	60.6	62.7	71.6	61.8
	MFCR	23.8	22.0	37.8	35.9	37.5	23.7	37.5
Flood	FCMR	3.0	0.6	1.7	2.0	1.7	0.6	1.7
	MFCR	11.0	8.1	6.5	7.4	6.6	8.3	6.6
ATWS	FCMR	0.2	<0.1	0.2	0.1	0.2	<0.1	0.1
	MFCR	0.5	10.0	0.7	0.6	0.7	9.8	0.5
LOCA	FCMR	0.0	<0.1	<0.1	<0.1	<0.1	<0.1	<0.1
	MFCR	0.0	<0.1	<0.1	<0.1	<0.1	<0.1	<0.1
Transients	FCMR	42.3	46.2	32.1	31.7	32.5	23.4	33.3
	MFCR	62.4	52.4	50.2	34.4	50.4	51.2	50.7
Trans-LOCA	FCMR	0.5	0.8	0.7	0.7	0.7	1.0	0.7
	MFCR	0.8	1.4	1.5	1.3	1.5	1.5	1.4

Table 6  
Fractional APB Contribution (in percent) to Annual  
Rsk at LaSalle Due to All Initiators

Summary Accident Progression	Method	Prob. Cond. CD	Early Fatalities	Latent Cancer Fatalities	Population Dose 50 miles	Population Dose Region	Ind. E. F. Risk-1 mile	Ind. L.C.F. Risk-10 mile
VB, Early CF, RPV at Low Press.	FCMR	-	16.2	28.7	23.2	27.9	20.4	20.1
	MFCR	0.15	26.8	19.2	18.2	19.3	26.5	17.1
VB, Early CF, RPV at High Press.	FCMR	-	17.8	42.7	43.7	42.8	34.3	31.2
	MFCR	0.19	13.6	25.5	24.5	25.3	13.3	25.8
VB, Late CF	FCMR	-	30.0	6.6	8.6	7.1	6.5	6.4
	MFCR	0.09	10.3	10.5	10.4	10.4	8.6	10.5
VB, Early or Late Venting	FCMR	-	34.7	20.6	22.4	20.9	36.2	20.3
	MFCR	0.37	44.3	41.9	42.9	42.1	46.9	42.8
VB, no CF	FCMR	-	<0.1	<0.1	<0.1	<0.1	<0.1	<0.1
	MFCR	0.06	<0.1	<0.1	<0.1	<0.1	<0.1	<0.1
No VB, CF	FCMR	-	<0.1	<0.1	<0.1	<0.1	<0.1	<0.1
	MFCR	0.0	<0.1	<0.1	<0.1	<0.1	<0.1	<0.1
No VB, Vent	FCMR	-	0.2	0.5	0.9	0.5	0.4	0.8
	MFCR	0.09	4.3	1.9	2.8	2.0	4.5	2.7
No VB, No CF, and No Vent	FCMR	-	<0.1	<0.1	<0.1	<0.1	<0.1	<0.1
	MFCR	0.06	<0.1	<0.1	<0.1	<0.1	<0.1	<0.1

whether the containment fails or not. Therefore, the latent cancer fatality risk is primarily dependent on the frequency of containment failure and the magnitude of the radionuclide release. Because of the plant features that reduce the magnitude of the source term, the latent cancer fatality risk remains low even though there is a high likelihood that the containment will fail in most of the core damage accidents that were analyzed.

### 5.3 Regression Analysis

Sensitivity analysis results for the six consequence measures used to express risk are presented in Table 7. This table contains the results of performing a stepwise linear regression on the risk. The statistical package SAS [10] was used to perform the regression.

For each consequence measure, Table 7 lists the variables in the order that they entered the regression analysis, gives the sign of the regression coefficients for that variable, and shows the  $R^2$  values that result with the entry of successive variables into the model. The order that the variables enter the model is based on the fraction of the uncertainty that is explained by each variable. First, the fraction of the uncertainty that is explained by each variable individually is determined. The variable with the largest fraction is the first variable that is entered into the model. Second, the variability that is explained by this variable is removed and the process is repeated with the remaining variables. The tendency of a dependent variable to increase and decrease with an independent variable is indicated by a positive or negative regression coefficient, respectively.

The regression analyses for early fatalities and the individual risk of an early fatality within 1 mile only account for about 49% of the observed variability. The top four variables (the release from CCI, the retention in the containment, reactor building decontamination factor, and the late release of iodine) determine the magnitude of the source term. The regression analyses for the other four consequence measures are somewhat more successful as they are able to account for about 60% of the variability. Twelve of the eighteen variables are from the Level I analysis and are used to determine the frequency of core damage. Five variables are from the source term analysis and one from the accident progression analysis. For latent cancer fatalities the dominant variables are: control circuit failure, severe environment failure of injection systems in the reactor building, and ex-vessel release to the reactor building.

The early fatality measures are critically dependent on the magnitude of the release and whether or not people are caught in the plume. Since most people evacuate ahead of the plume, the fraction remaining is fairly constant in most scenarios and the magnitude of the source term is of primary importance. Latent cancer fatalities and the other measures depend on the total exposure over long periods of time and are therefore driven mostly by uncertainties in the frequency of occurrence of the accidents. Because this is a highly non-linear problem, the results of this regression should be taken as preliminary. Much of the uncertainty is unexplained and other variables could show up with more detailed analysis. The methods used in this analysis and in NUREG-1150 need further development before definitive statements can be made as to the relative

Table 7  
 Summary of Regression Analyses for  
 Annual Risk at LaSalle (All Initiators)

Step	Early Fatalities			Latent Cancer Fatalities			Population Dose--50 miles		
	VAR <sup>a</sup>	RC <sup>b</sup>	R <sup>2c</sup>	VAR	RC	R <sup>2</sup>	VAR	RC	R <sup>2</sup>
1	FCCI	Pos	0.12	CFM-114	Pos	0.13	CFM-114	Pos	0.16
2	FCONG	Pos	0.22	SUR-006-L	Pos	0.23	SUR-06-L	Pos	0.29
3	RBDF	Neg	0.31	SUR-022-R	Pos	0.32	SUR-22-R	Pos	0.39
4	FLTI	Pos	0.37	FCONG	Pos	0.37	IE-LOSP	Pos	0.41
5	CFM-114	Pos	0.41	RBDF	Neg	0.41	CFM-37	Pos	0.43
6	FCOR	Neg	0.44	FCOR	Neg	0.44	RBDF	Neg	0.45
7	ALPHA	Pos	0.46	SUR-27-R	Pos	0.46	SUR-27-R	Pos	0.47
8	DFCAV	Pos	0.48	FCCI	Pos	0.48	FCONG	Pos	0.49
9	MODE VB	Pos	0.49	IE-LOSP	Pos	0.50	AC RECOV	Pos	0.50
10				CFM-37	Pos	0.51	LPCI-BET	Pos	0.52
11				AC RECOV	Pos	0.53	N-ISTmEx	Neg	0.53
12				LPCI-BETA	Pos	0.54	ExStmEx	Pos	0.54
13				LAM-CR	Pos	0.55	LAM-CR	Pos	0.55
14				No-ISTmEx	Neg	0.56	LAM-SVGR	Pos	0.56
15				IE-VAL-R	Pos	0.57	IE-VAL-R	Pos	0.57
16				LAM-SVGR	Pos	0.58	FCOR	Neg	0.58
17				LAM-AUX	Pos	0.59	SUR-3-R	Neg	0.58
18				DFCPA	Neg	0.60	FCCI	Pos	0.59
19							No VB	Neg	0.60

Table 7 (continued)

Step	Population Dose Entire Region			Individual Early Fat. Risk 0-1 mile			Individual Latent Can. Fat. Risk 0-10 mi.		
	VAR <sup>a</sup>	RC <sup>b</sup>	R <sup>2c</sup>	VAR	RC	R <sup>2</sup>	VAR	RC	R <sup>2</sup>
1	CFM-114	Pos	0.14	FCCI	Pos	0.11	LEAKTRB	Pos	0.21
2	SUR-6-L	Pos	0.23	RBDF	Neg	0.21	CFM-114	Pos	0.34
3	SUR-22-R	Pos	0.32	FCONC	Pos	0.30	SUR-22-R	Pos	0.46
4	FCONC	Pos	0.36	FLTI	Pos	0.37	SUR-27-R	Pos	0.47
5	RBDF	Neg	0.41	CFM-114	Pos	0.41	IE-LOSP	Pos	0.49
6	FCOR	Neg	0.44	FCOR	Neg	0.44	CFM-37	Pos	0.51
7	SUR-27-R	Pos	0.46	ALPHA	Pos	0.46	AC RECOV	Pos	0.52
8	FCCI	Pos	0.48	DFCAV	Pos	0.48	LPCI-BET	Pos	0.54
9	IE-LOSP	Pos	0.50	SUR-25-R	Pos	0.49	NoIStmEx	Neg	0.55
10	CFM-37	Pos	0.51				LAM-SVGR	Pos	0.56
11	AC RECOV	Pos	0.53				SUR-3-R	Neg	0.57
12	LPCI-BET	Pos	0.54				IE-VAL-R	Pos	0.58
13	LAM-CR	Pos	0.55				LAM-CR	Pos	0.59
14	N-IStmEx	Neg	0.56						
15	IE-VAL-R	Pos	0.57						
16	LAM-SVGR	Pos	0.58						
17	LAM-AUX	Pos	0.59						
18	NO VB	Neg	0.60						

<sup>a</sup> Variables listed in the order that they entered the regression analysis.

<sup>b</sup> Sign on the regression coefficients (RCs) in final regression model.

Pos: Increase in independent variable increases dependent variable

Neg: Increase in independent variable decreases dependent variable

<sup>c</sup> R<sup>2</sup> values with the entry of successive variables into the regression model.

importance of various variables. Also, consequence parameter uncertainty and evacuation parameter uncertainty need to be explicitly included before any final statement can be made about the relative importance of various parameters to risk.

## 6. References

- [1] A. C. Payne Jr., et. al., "Analysis of the LaSalle Unit 2 Nuclear Power Plant: Risk Methods Integration and Evaluation Program (RMIEP)," Vol. 1-10, NUREG/CR-4832, SAND87-7157, Sandia National Laboratories, Albuquerque, NM, (in preparation).
- [2] T. D. Brown., A. C. Payne Jr., et. al., "Integrated Risk Assessment for the LaSalle Unit 2 Nuclear Power Plant: Phenomenology and Risk Uncertainty Evaluation Program (PRUEP)," Vol. 1-3, NUREG/CR-5305, SAND90-2765, Sandia National Laboratories, Albuquerque, NM, (in preparation).
- [3] R. L. Iman, M. J. Shortencarier, "A User's Guide for the Top Event Matrix Analysis Code (TEMAC)," NUREG/CR-4598, SAND86-0960, Sandia National Laboratories, Albuquerque, NM, August 1986.
- [4] J. M. Griesmeyer, and L. N. Smith, "A Reference Manual for the Event Progression Analysis Code (EVNTRE)," NUREG/CR-5174, SAND88-1607, Sandia National Laboratories, Albuquerque, NM, September 1989.
- [5] "Severe Accident Risks: An Assessment for Five U.S. Nuclear Power Plants," NUREG-1150 Vols. 1 and 2, Final Summary Report, U.S. Nuclear Regulatory Commission, December 1990.
- [6] H-N Jow, W. B. Murffin, and J. D. Johnson, "XSOR Codes User's Manual," NUREG/CR-5360, SAND89-0943, Sandia National Laboratories, Albuquerque, NM, (in preparation).
- [7] R. L. Iman, J. C. Helton, and J. D. Johnson, "PARTITION: A Program for Defining the Source Term/Consequence Analysis Interface in the NUREG-1150 Probabilistic Risk Assessments User's Guide," NUREG/CR-5253, SAND88-2940, Sandia National Laboratories, Albuquerque, NM, May 1990.
- [8] D.I. Chanin, et.al., "MELCOR Accident Consequence Code System (MACCS)," Vol. 1-3, NUREG/CR-4691, SAND86-1562, Sandia National Laboratories, Albuquerque, NM, February 1990.
- [9] R. L. Iman, J. D. Johnson, and J. C. Helton, "PRAMIS: Probabilistic Risk Assessment Model Integration System User's Guide," NUREG/CR-5262, SAND88-3093, Sandia National Laboratories, Albuquerque, NM, May 1990.
- [10] SAS Institute Inc., "SAS User's Guide: Basics, Version 5 Edition," SAS Institute Inc., Cary, NC, 1985.

## RISK-BASED PERFORMANCE INDICATORS\*

M.A. Azarm and W.E. Vesely\*\*  
Engineering Technology Division  
Department of Nuclear Energy  
Brookhaven National Laboratory  
Upton, New York 11973

\*\*Science Applications International Corporation

This research was sponsored by the U.S. Nuclear Regulatory Commission (NRC) to develop methods for monitoring an aspect of safety performance of licensed nuclear power plants; i.e., unavailability of safety systems.

Various options were evaluated<sup>1</sup> for constructing system unavailability indicators using basic reliability principles and consistent with the content of data collected. The capabilities of each indicator option, in terms of detection probabilities and false alarm rates within a fixed response period for various types of anomalies, were evaluated through detailed simulation studies<sup>2-4</sup>. As an example, the option of using system vs train downtimes to construct safety system unavailability indicators was evaluated. Comparison of response times indicated that the latter option has significantly shorter response periods (by factors of 10 - 30), i.e., more timely results.

Brookhaven National Laboratory performed two studies<sup>5,6</sup> to evaluate the capability of NPRDS (Nuclear Plant Reliability Data System) as a data source for construction of system unavailability indicators. Specific indicators were developed consistent with the limited scope of NPRDS data. In order to generate system unavailability indicators in an efficient manner, the processes for NPRDS data acquisition, indicator construction, and analyses were automated using PC software<sup>7</sup>. Limited pilot applications and verification were also performed.

An important aspect of risk-based indicators deals with the concept of dependent failures. The conventional dependent failure definition which consists of simultaneous failures of similar redundant components will generate a long response time for proper detection of anomalies, and it is not suitable for construction of an indicator. A recent study<sup>8</sup> attempted to relax the definition of dependent failures by defining a time window within which the failure of similar redundant components can be accounted for. In this study, we have developed a model using basic reliability principles to treat the time between the failures of similar redundant components as a continuum rather than a truncated window. Using detailed reliability models we have developed a formulation for evaluating the risk implication of various failure patterns realized when the observation time is treated as a continuum<sup>9</sup>. This methodology not only provides

---

\*Work performed under the auspices of the U.S. Nuclear Regulatory Commission

the framework within which present PRA (Probabilistic Risk Assessment) methodologies can be enhanced but also provides the basic model upon which dependent failure indicators can be constructed. Specific indicators of dependent failures are presently being developed and evaluated.

Finally, limited pilot application of the indicator technology has revealed a large amount of information on short- and long-term trends in component failure rates, clustering of failures in similar components in and across systems, systematic effects and correlated trends, etc. Currently, there is no integrated methodology within existing PRA formulations that can incorporate such information and evaluate its risk implications and prediction.

The effort taken in this project can be grossly categorized in five steps. These are:

1. indicator objective,
2. availability of data and models,
3. formulation of the candidate indicators,
4. characteristics of the candidate indicators, and
5. pilot application of candidate indicators.

The following briefly discusses the effort taken by this study for each of the above steps.

#### Indicator Objective

From an operational standpoint, unavailability is the fraction of time a component or system is down in a given time period. More specifically, the unavailability in a given time period is the downtime divided by the total time period;

$$\text{Unavailability} = \frac{\text{Downtime Period}}{\text{Time Period}} \quad (1)$$

This is the basic formula for unavailability.\*

The downtime period includes the sum of the following contributions:

1. the time period the failure exists before it is detected (the undetected failure downtime),
2. the time period to repair the failure (the repair downtime),
3. the time period the component is unavailable due to maintenance (the maintenance downtime), and

---

\*In reliability literature, this formula is termed the formula for interval unavailability since an interval of time is involved.

4. the time period the component is unavailable due to testing (the testing downtime).

For unavailability during plant operation, the time period refers to an observed plant operating time period and the downtime refers to the downtime occurring in the operating time period. Unavailability during operation was the focus of the unavailability indicators developed. All unavailability indicators which were developed in the work are applications of the general formula given by Eq. (1).

Unavailability of safety systems during operation was the focus of the work since it is a critical performance parameter which determines the risk level of the plant during operation. Probabilistic risk assessment (PRAs) show that public risk during plant operation is basically a product of three factors, the initiating event frequency, the unavailability of safety systems required to respond, and the accident consequences which result if the safety systems fail:

$$\text{Public Risk} = \text{Initiating Event Frequency} \times \text{Safety System Unavailability} \times \text{Accident Consequences} \quad (2)$$

Thus, by developing indicators of safety system unavailability one can monitor a critical factor of public risk. Trends in safety system unavailability will be a significant indicator of trends in public risk. It is a proven concept that constructing system unavailability indicators based on the observed downtime of its components provide significantly faster response times than direct system unavailability indicators.

To construct the system unavailability indicators, it is also important to identify the potential uses of the indicators. Some of the main uses identified for the system unavailability indicators are to detect:

1. a short-term trend,
2. a long-term trend,
3. an outlier performance compared to its past, and
4. an outlier performance compared to the performance of similar designs.

The indicators shall be designed such that the above inferences can be easily made through visual inspection of the indicator graph. As an example, to identify an outlier performance, calibration lines are to be superimposed on the indicator graphs.

#### Availability of Data and Models

Another set of considerations for developing industry-wide system unavailability indicators is imposed by the state of the risk and reliability models available for all nuclear power plants. System reliability models (e.g., fault tree generated minimal cutsets) are required to construct system unavailability indicators from the train unavailability indicators. Detailed system reliability models are not presently available for all nuclear power plants. Therefore, it

was decided to construct unavailability indicators which required only basic models which could be developed for all nuclear power plants for a limited number of systems. These systems were selected based on their risk significance. The basic system models developed are based on defining the number of independent active trains in the system and the system operation criteria (success criteria for the system). The system success criteria are defined considering the most demanding system requirements. In such basic system modeling, cross-connections, common supply and discharge lines, and support system interactions are not included.

The other constraint on the application of the unavailability indicators stems from the lack of plant operational event data. Utilities do not routinely report to NRC detailed data on the unavailability of components or trains of safety systems. Therefore, a viable option is to use the NPRDS. The smaller scope reported in NPRDS requires additional considerations in the indicator formulation. As such, they are: the indicator aggregation across systems to reduce the effect of missing data, construction of quarterly (every three (3) months) indicators to reduce the effect of reporting delay, etc.

Considering these limitations in the system models and considering the data constraints, the indicators which can be constructed will not monitor the precise unavailability or be a precise dynamic predictor of unavailability. Rather, the indicators will satisfy the preceding objectives and identify gross trends and gross changes in performance. Gross unavailability trends and anomalies can be detected with indicators that are correlated to the underlying unavailability but do not necessarily indicate the precise unavailability value.

#### Formulation of Candidate Indicators

Four different types of indicators were considered:

1. SSFT: Safety System Function Trend Indicators
2. TASI: Train Average System Indicators
3. TDSI: Simplified Three Downtime System Indicators
4. FDSI: Simplified Four Downtime System Indicators

The SSFT, TDSI, and FDSI are developed under the assumption that the utility reported quarterly downtime data is for each specific train within the system. The TASI indicator is developed for application where the reported downtime data is the sum of the downtimes for all trains within the system.

Detailed formulations of these indicators and their bases are detailed in Reference 3.

#### Characteristics of the Candidate Indicators

The extent to which a candidate system unavailability indicator is responsive to the earlier identified objectives was evaluated through computer simulations. This is a widely used method in statistical process control. The capability of an indicator to respond to a given objective (e.g., detection of a time trend in unavailability), is measured by two characteristics. These are the:

- 1) detection probability: The probability of detecting an anomaly when the anomaly exist, and
- 2) false alarm probability: The probability of erroneously indicating an anomaly when it does not exist.

In addition to the false alarm and detection probabilities, the third important characteristics of an indicator is the indicator response time which is an indication of how fast after the initiation of an anomaly the indicator detects it. The indicator response time is usually measured as the average time it takes to detect an anomaly and is called the Average Run Length (ARL). A detection is credited if the anomaly is indicated in a fixed period of time (about 1.5 years after the anomaly occurs). Anomalies indicated beyond this period are not credited in calculating the detection probabilities.

To determine the detection probability, a large number of similar anomalies are modeled to generate computer simulated data for the component failures and downtimes. This detection probability was then determined by taking the fraction of anomalies detected over the total number of anomalies simulated. The means for detection of an anomaly can be either based on statistical tests or by visual identification. The first phase validation concentrated on the latter i.e., the anomalies were detected consistent with visual examination of the indicator graph. A computer code GSCI was developed to perform these simulations. The false alarm probabilities were determined in the similar manner as the detection probabilities.

Figures 1 and 2 present some of the results of the simulation studies in regard to the detection and false alarm probability of the indicators. An indicator is considered superior if it posses higher detection probability and lower false alarm rate.

#### Pilot Application and Field Validation

Two types of pilot applications were performed. In one case, a total of 10 plants and over 38 years of plant historical data were collected for the purpose of constructing system unavailability indicators. These case studies, referred to as the retrospective case studies, were performed to verify if the indicators can confirm instances that were suspected of high, low, or changing unavailability of safety systems. Figure 3 depicts a typical unavailability graph generated from this analyses which shows the instances of high unavailability of the auxiliary feedwater system in Plant 2.

In the other case study, the indicators generated for all PWR plants using automated retrieval of NPRDS data and computerized calculations and analyses of the indicators. The program generates indicator graphs with applicable calibration lines. The pilot application covered five years of data for all PWRs for three systems; auxiliary feedwater system, high-pressure injection system, and low-pressure injection system. The anomalies detected by the indicators were then correlated with precursor events. The correlation results supported the usefulness of the indicators.

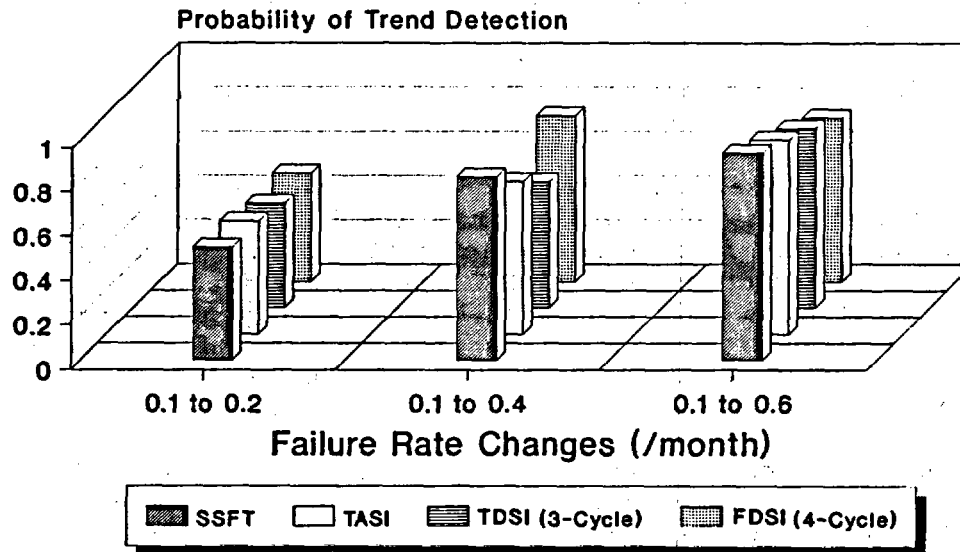


Figure 1. Sensitivity analysis of trend detection probability vs different change ratios of  $\lambda_f$

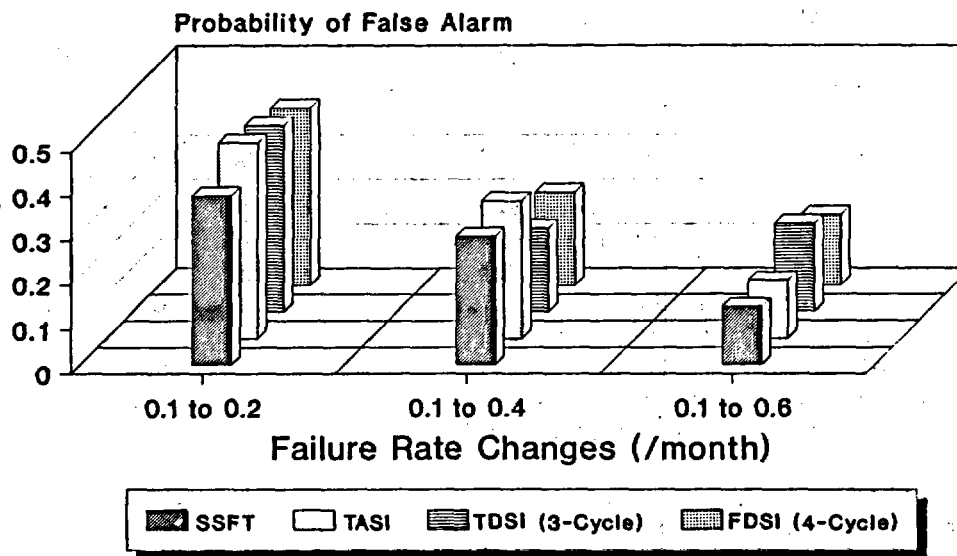
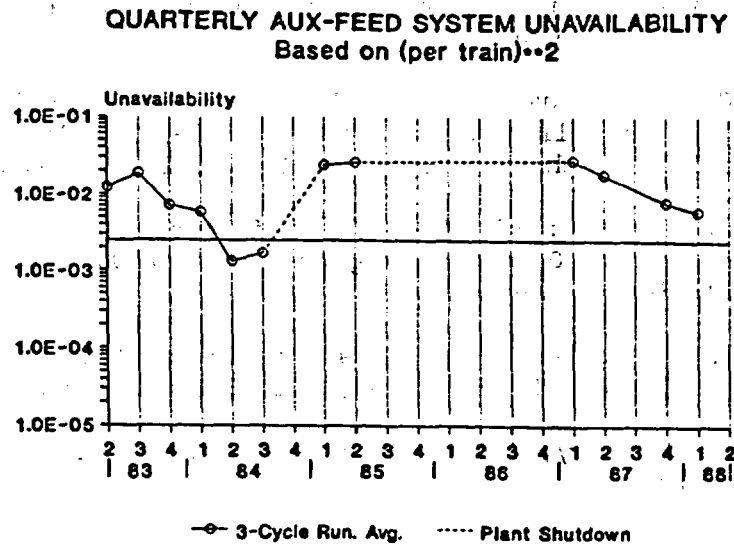


Figure 2. Sensitivity analysis of trend detection - false alarm probability vs different change ratios of  $\lambda_f$



PLANT 2

Figure 3. Plant 2, aux feed system unavailability indicator

Conclusion

Feasibility and potential benefit of the system unavailability indicators were studied. Automated construction and analyses of the indicator given the available data and models for all nuclear power plants were developed. Work is ongoing to develop indicators of dependency to complement the existing system unavailability indicators. The findings of this study can also streamline the potential extension of the PRA methodologies needed for achieving living PRAs in the future.

REFERENCES

1. Vesely, W.E. and Azarm, M.A., "System Unavailability Indicators," BNL Technical Report A-3295 9-30-87, September 1987.
2. Azarm, M.A. and Vesely, W.E., "Short-Term Indicators of Unavailability and Unreliability," BNL Technical Report A-3295 4-29-88, April 1988.
3. Hsu, F., Azarm, M.A., and Vesely, W.E., "Basis and Framework for Evaluating Display Indicators: Application to System Unavailability Indicators," BNL Technical Report A-3295 4-4-90, April 1990.
4. Boccio, J.L. et al., "Validation of Risk-Based Performance Indicators: Safety System Function Trends," NUREG/CR-5323, BNL-NUREG-52186, October 1989.

5. Azarm, M.A. et al., "Automated Use of NPRDS for Construction of Indicators of System Unavailabilities and Aggregate Component Failures," Draft, BNL Technical Report, November 1990.
6. Economos, C., Carbonaro, J.F., and Azarm, M.A., "Applicability of the Nuclear Plant Reliability Data System for Risk-Based Performance Indicator Development," BNL Technical Report A-3295 10-2-89, October 1989.
7. Carbonaro, J.F. and Azarm, M.A., "Quantification of SSFT Indicators: A Comparison of Plant Operating Log Data and NPRDS Data," BNL Technical Report A-3295 8-1-90, August 1990.
8. Zikria, A.F. and Mosleh, A., "A Parametric Model for Time Delay Common-Cause Failures," ANS Transactions, Vol. 61, pp. 210-211, June 1990.
9. Azarm, M.A. and Vesely, W.E., "Dependent Failure Indicators," Draft Letter Report, July 1991.

## INTERSYSTEM LOCA RISK ASSESSMENT: METHODOLOGY AND RESULTS

W. J. GALYEAN, D. L. KELLY, J. A. SCHROEDER  
J. L. AUFLICK, H. S. BLACKMAN, D. I. GERTMAN, L. N. HANEY  
INEL/EG&G Idaho, Inc., P.O. Box 1626, Idaho Falls, Idaho 83415

### ABSTRACT

The United States Nuclear Regulatory Commission (NRC) is sponsoring a research program to develop an improved understanding of the human factors, hardware, and accident consequence issues that dominate the risk from an Intersystem Loss-of-Coolant Accident (ISLOCA) at a nuclear power plant. To accomplish the goals of this program, a methodology has been developed for estimating ISLOCA core damage frequency and risk. The steps in this methodology are briefly described, along with the results obtained from an application of the methodology at three pressurized water reactors (PWRs).

### INTRODUCTION

ISLOCAs have been included in probabilistic risk assessments (PRAs) since WASH-1400 [1]. While they have not been significant contributors to core damage frequency, ISLOCAs have been identified as major contributors to offsite risk, because they have the potential to cause core damage and containment bypass, leading to an early release of large quantities of fission products offsite. Recent events at several operating reactors in the U. S. and abroad have been labeled as ISLOCA precursors. These events have raised concerns that the frequency of ISLOCA sequences might be underestimated in PRAs performed to date.

### ANALYSIS OBJECTIVES AND SCOPE

In order to support the resolution of Generic Issue 105, the NRC is sponsoring an ISLOCA research program, conducted by EG&G Idaho, Inc. at the Idaho National Engineering Laboratory. The objective of this program is to obtain information, both qualitative and quantitative, on the hardware, human factors, and accident consequence issues that dominate ISLOCA risks. To meet this objective, the approach being taken includes analysis of all interfaces between the reactor coolant system and other, lower pressure systems. The historical record (primarily Licensee Event Reports) has provided the basis for setting the scope of the analysis with respect to potential pressure isolation boundary failure mechanisms. It is important to note that, in the vast majority of these historical events, the primary failure of concern was a human error. Because of their significance in this regard, human errors are given particular attention in the present analysis.

## ANALYSIS METHODOLOGY

A methodology has been developed for estimating the core damage frequency and risk associated with an ISLOCA, and this methodology has been applied to three individual U. S. nuclear power plants [2-4].

### Initiating Event and Scenario Identification

This methodology consists of a series of detailed, integrated steps. In the first step, piping and instrumentation diagrams (P&IDs), system descriptions, and operating procedures are reviewed to screen the plant's reactor coolant system (RCS) interfaces. These interfaces are the pressure isolation boundaries between the RCS and an interfacing system that is designed for pressures and temperatures lower than the normal operating pressure and temperature of the RCS. This screening identifies those interfaces which, if breached, would allow significant reactor coolant flow rates into the interfacing systems. A lower limit on line diameter of 1 inch was used to screen out the many small instrumentation and drain lines. This size cutoff is based on the approximate leak rate (about 200 gpm) produced by failure of a 1-inch line connected to the RCS, as well as the normal makeup capacity to the RCS (about 150 gpm) and the volume of water available for makeup (e.g. RWST - about 400,000 gal.).

In the second step, plant operations are examined in more detail to identify scenarios that could possibly breach an RCS pressure isolation boundary. This operations review relied upon historical experience (i.e., applicable Licensee Event Reports on ISLOCA "precursors"), plant procedures and practices, and discussions with plant personnel. The relatively high likelihood of human errors initiating or contributing to the occurrence of potential ISLOCA sequences is particularly well-supported in the historical data (see Appendix A of Reference 2). Therefore, in this portion of the analysis, extra attention was focused on identifying possible human errors of commission that could lead to an ISLOCA.

An extended visit to each plant allowed the analysts to gather the information needed to complete these reviews and to develop and analyze the candidate ISLOCA scenarios. Members of the team that developed the candidate scenarios obtained information by interviewing plant personnel and walking down the systems of interest. This task was performed in conjunction with a special ISLOCA team inspection conducted by the Office of Nuclear Reactor Regulation of the U. S. NRC. Information obtained during this visit included:

- a. Detailed information on the hardware that would be involved in an ISLOCA, for example, data on control valves, relief valves, piping, flanges, pumps, and heat exchangers,
- b. Detailed information on the procedures, guidelines, and practices followed by plant personnel during startup, normal power operation, and shutdown of the plant, as well as detailed information on maintenance and in-service testing, and

- c. Detailed information on factors that could influence performance of plant personnel as related to initiation, detection, diagnosis, prevention, or mitigation of an ISLOCA.

After the plant-specific information was collected, a final list of low pressure interfaces and candidate scenarios was compiled and the detailed accident sequence analysis begun. This analysis was a joint effort of PRA and human factors specialists. The scenarios were modeled using (primarily) component level event trees combining the hardware faults and human errors that constitute each sequence in the scenario. In general, each event tree comprised three phases:

1. The initiating events, which are those combinations of failures, both hardware and human-related, that breach the RCS pressure isolation boundary and expose the low pressure interfacing system to the RCS,
2. The rupture events, which model a break in the interfacing system, its size, and location, and
3. The post-rupture events, which model the performance of the control room and auxiliary operators in recovering from or mitigating the consequences of the ISLOCA. The list of possible ISLOCA sequences contains both hardware-based sequences (as found in typical PRAs) and sequences initiated by human error. The potential human errors in both types of sequence comprised errors of omission, commission, and preexisting or latent errors.

#### Rupture Probability Estimation

After the possible ISLOCA sequences were developed in the event trees, simple RELAP5 [5] computer models of the interfacing system were constructed to estimate the pressure that would likely be generated in the interfacing system by a breach of the RCS pressure isolation boundary. Convoluting these local system pressures with estimates of the pressure capacities of system components gave the rupture probabilities of individual components. The combination of these probabilities then gave the rupture probability of the interfacing system as a whole.

The failure pressure distributions used in the rupture probability calculations were developed from an independent component and piping structural analysis performed by Impell Corporation [6]. Not only were failure pressures calculated for components and piping in the interfacing systems, but likely leak rates and leak areas, also. In this respect, bolted flanges were found to be somewhat unique in that there are actually two failure pressures of interest. First, there is the estimated gross leak pressure (GLP), at which a measurable leak area develops. At pressures below the GLP, seepage around the flange gasket is possible, but the leak rates are very small (of the order of mg/sec). Once pressure exceeds the GLP, the flange bolts begin to stretch (elastically deform) and the flange surfaces begin to separate. At some yet higher pressure ( $P_0$ ), the bolts begin to

deform plastically. At this point, large leak areas begin to develop with correspondingly large leak rates. These three regimes (below GLP, between GLP and  $P_o$ , and greater than  $P_o$ ) are associated with three leak sizes: spray leaks, small leaks, and large leaks, respectively.

Other components, specifically pipes and vessels (including heat exchangers) were estimated to fail catastrophically at their failure pressure. This is the case because the likely failure mode includes the formation of cracks that grow very rapidly, resulting in very large ruptures.

The net result of this analysis is that low-pressure-rated systems (for example, the decay heat removal (DHR) system at the Babcock and Wilcox (B&W) plant, which contains 150 and 300 psi-rated components) are able to withstand several times their design pressure. However, they cannot withstand normal RCS operating pressure. The B&W DHR system aggregate (i.e., total system) median failure pressure was calculated to be approximately 1150 psig. This is the failure pressure associated with a large rupture, that is, a rupture large enough to depressurize and protect the rest of the DHR system. The likely failure locations were the DHR heat exchanger and the DHR pump suction piping.

### Recovery and Mitigation

Given the very rapid pressure rise predicted by the RELAP calculations (approximately 30 seconds to equilibrium pressure for systems with flow, i.e., open-ended systems or systems with little relief valve capacity), there is not much potential for operator recovery before a rupture occurs in the interfacing system. However, using conservatively bounded thermal-hydraulic assumptions, core uncover was estimated to occur at between two and four hours after the break (for large and small ruptures, respectively). This time interval is used in estimating the probability of the operators isolating the rupture (and terminating the sequence) and initiating any mitigative actions that could reduce the severity of the offsite release. Isolating the rupture would entail re-establishing the pressure isolation boundary (if the hardware is still available and accessible), while an example of a mitigative action might be manual actuation of fire protection sprays in the area of the release.

### Human Reliability Analysis

The predominant human errors for each scenario in the ISLOCA PRA were modeled using the techniques of human reliability analysis (HRA). HRA is a methodological tool used for prediction, evaluation, and quantitative analysis of work-oriented human performance. As a diagnostic tool, HRA can estimate the error rate anticipated for individual tasks and can identify where errors are likely to be most frequent.

The general methodological framework for the ISLOCA HRA was based on guidelines (under development) from the NRC-sponsored Task Analysis-Linked Evaluation Technique (TALENT) Program [7], which recommends the use of task analyses, time line analyses, and interface analyses in a detailed HRA. NUREG/CR-1278, the Handbook of Human Reliability Analysis with Emphasis on

Nuclear Power Plant Applications (THERP) [8], recommends similar techniques and, in addition, provides a data base that can be used for estimating human error probabilities (HEPs). Finally, the ISLOCA HRA integrated the steps from the Systematic Human Action Reliability Procedure (SHARP) [9] and A Guide for General Principles of Human Action Reliability Analysis for Nuclear Power Generation Stations (the draft IEEE standard P1082/D7 [10]).

From this combination of approaches, the analysts identified 11 basic steps to be followed in performing the HRA:

1. Select the analysis team and train them on relevant plant functions and systems (IEEE P1082);
2. Familiarize the team with the plant through the use of system walkdowns, simulator observations, etc. (IEEE P1082);
3. Ensure that the full range of potential human actions and interactions is considered in the analysis (SHARP) (IEEE P1082);
4. Construct the initial model of the relevant systems and interactions (IEEE P1082);
5. Identify and screen specific human actions that are significant contributors to safe operation of the plant. This was accomplished through detailed task analyses, time line analyses, observations of operator performance in the plant and in the simulator, and evaluations of the human-machine interface (SHARP and IEEE P1082);
6. Develop a detailed description of the important human interactions and associated key factors necessary to complete the plant model. This description should include the key failure modes, an identification of errors of omission/commission, and a review of relevant performance shaping factors (SHARP) (IEEE P1082);
7. Select and apply the appropriate HRA techniques for modeling the important human actions (SHARP);
8. Evaluate the impact on ISLOCA of significant human actions identified in Step 6 (SHARP);
9. Estimate error probabilities for the various human actions and interactions, determine sensitivities, and establish uncertainty ranges (SHARP and IEEE P1082);
10. Review results for completeness and relevance (IEEE P1082);
11. Document all information necessary to provide an audit trail and to make the information understandable (SHARP).

Because most of the human actions in this HRA involved the use of written normal, abnormal, and emergency operating procedures, THERP-type HRA

event trees [8] were used to model most of the human actions in the detailed analysis. However, not all ISLOCA scenarios were best represented by THERP event trees alone. In those cases, HRA fault trees were used in conjunction with the THERP event trees. The fault trees and THERP event trees were used in a detailed analysis to estimate the probability of human error for each of the dominant human actions.

The basic, or unmodified, HEPs for branches in the HRA event trees were estimated using techniques from THERP and HCR (Human Cognitive Reliability, see [11]). These basic HEP estimates were then revised by using performance shaping factors (PSFs) to more realistically model the work process at the plant. Each PSF was either positive or negative and, accordingly, either decreased or increased the likelihood of a given human error. For example, an analog meter, like a pressure gauge, if it does not have easily seen limit marks, would be judged to be a negative PSF. Thus, there would be a higher-than-normal probability for error in reading the gauge. Individual PSFs were derived from task analyses, time line analyses, evaluation of the human-machine interface, and direct observations of operator performance.

Specific PSFs which were investigated include:

- 1 - the quality of the human-machine interface;
- 2 - written procedures (emergency, abnormal, maintenance, etc.);
- 3 - P&IDs;
- 4 - response times for systems and personnel;
- 5 - communication requirements;
- 6 - whether operator actions were skill, rule, or knowledge-based;
- 7 - crew experience;
- 8 - levels of operator stress (situation-specific);
- 9 - feedback from systems in the plant;
- 10 - task dependence and operator dependence;
- 11 - location of the task (control room, auxiliary building, etc.);
- 12 - training for individual operator actions, especially those required in ISLOCA situations.

Finally, the combination of all identified failure paths (i.e., sequences that included either single or multiple human errors leading to a failure of the action modeled by the HRA tree) gave the failure probability for the top-level action modeled in the HRA tree. The guidelines of THERP were followed in identifying the individual error paths. Probabilities for each unique error path were calculated by multiplying each HEP on a given error path by other HEPs on the same path.

#### Core Damage Frequency and Risk

After quantifying the recovery and mitigative actions, the frequency of core damage was calculated with the event tree models. Offsite consequences and risk were also calculated, using surrogate source terms and site data with the MACCS code [13,14]. The existing literature on containment bypass source

terms was reviewed to find an appropriate surrogate source term. The containment bypass (V sequence) source term from the Oconee PRA [15] was selected for the B&W plant, while the NUREG-1150 V sequence source term for Sequoyah was used for the Westinghouse and CE plants. Similarly, the site data were those used in the consequence calculations for the Surry analysis in NUREG-1150 [16]. Surry was chosen as the representative site based on a comparison (performed for the present work) among the 5 NUREG-1150 sites and the average of the 91 sites examined in the Sandia Siting Study [17]. This comparison of the wind rose-weighted site population factors indicated that Surry was a reasonably good representative of an "average" U. S. site.

### Auxiliary Building Environmental Analysis

One of the issues that has arisen during the course of the ISLOCA research program concerns the effects a break outside containment would have on equipment in the break compartment and in adjacent compartments. The possibility exists that multiple redundant trains of emergency core cooling systems (ECCS) could be disabled by high temperature, high humidity, and flooding. Thus, the assumption that only equipment in the break compartment is impaired by the break may not be accurate.

To help resolve this issue, mechanistic calculations have, to date, been performed for the B&W plant to estimate the environmental conditions in the auxiliary building during an ISLOCA accident sequence (prior to core damage). The parameters of interest are the pressure, temperature, relative humidity, and water level in affected ECCS equipment rooms. The results of these calculations will be used, in a subsequent analysis, to estimate the extent to which equipment in compartments adjacent to the break compartment fails because of high temperature or submergence, and to estimate the extent to which operator recovery actions would be limited by steam and water propagation through the auxiliary building.

Five break sequences were evaluated using a combination of RELAP5 and CONTAIN [18] thermal-hydraulic models. The five sequences involved breaks in the following locations within the B&W decay heat removal/low pressure injection (DHR/LPI) and high pressure injection (HPI) systems:

- 1) A 12-inch break with discharge into room 236 of the auxiliary building. This occurred as a result of premature entry into DHR cooldown, with the RCS at an elevated pressure.
- 2) A simultaneous rupture in both DHR heat exchangers, with discharge into room 113 of the auxiliary building. The limiting flow area (choke plane) for this break was in the 2.5-inch bypass lines around valves DH-1517 and DH-1518. This occurred as a result of premature entry into DHR cooldown, with the RCS at an elevated pressure.
- 3) A simultaneous rupture in the low-pressure DHR pump suction piping, discharging into both rooms 105 and 113 of the auxiliary building. As above, the limiting flow area was in the 2.5-inch

bypass lines around valves DH-1517 and DH-1518. This occurred as a result of premature entry into DHR cooldown, with the RCS at an elevated pressure.

- 4) Rupture of the 1-2 decay heat cooler with discharge into room 113 of the auxiliary building. The break occurred because pressure isolation check valves in the injection piping of the LPI system failed internally.
- 5) A rupture in the suction piping to HPI pump 1-2 with discharge into room 115 of the auxiliary building. The break occurred as a result of internal failure of the HPI discharge isolation check valves.

Figures 1-4 are simplified P&IDs of the systems in which the modeled breaks were located.

The auxiliary building pressures, temperatures, and water levels depend on the steam flow rate into the building, the steam energy, the volume of the auxiliary building, flow paths through the building, and the rate of heat removal by condensation of steam on structural materials, equipment, and removal by fire sprays. The steam energy and flow rate into the building were calculated with simple RELAP5 models of the RCS. The resulting steam source data were then used as boundary conditions for a CONTAIN calculation of the auxiliary building response to the ISLOCA.

The RELAP5 models of the RCS comprised five volumes: the cold leg, lower plenum, core, upper plenum, and hot leg. Decay heat was modeled with a best-estimate Oconee core model normalized to the B&W reference plant operating power level. ECCS injection was included in the model via pressure-dependent flow tables, while pressure losses between the RCS and the break location were estimated by including detailed models of the piping run. The purpose of this approach was to obtain a first order approximation of RCS behavior on the premise that the auxiliary building response to the ISLOCA is not strongly dependent on fine details of RCS behavior.

The CONTAIN computer code was used to calculate the time response of the auxiliary building parameters. CONTAIN is a containment modeling code that has adequate steam-condensing heat transfer models for the scenarios of interest, and engineered system models that allow modeling of fire sprays, compartment sumps, and drainage paths between compartments. The approach used in this calculation was to construct detailed cell models of compartments with ECCS equipment that might be affected by the ISLOCA. These were auxiliary building rooms 105, 113, 115, and 236. The remaining spaces in the plant were lumped into a single balance-of-plant volume. The nodalization diagram for the CONTAIN model is shown in Figure 5.

The CONTAIN model used in this analysis included a best-estimate representation of the gas volume of each compartment, the flow loss characteristics and area of flow paths between each compartment, and a description of heat transfer surfaces within each compartment, and a

description of drainage paths between compartments. The code tracked pool depths in each compartment that resulted from both condensation of steam, and drainage of fire sprays or condensate from adjacent compartments. This is an important aspect of the large-break sequences because the high break discharge flow rates quickly fill the compartment sumps, causing flooding of adjacent compartments and compartments at a lower elevation. Only one compartment in this analysis (room 236) has fire sprays. Since these can be expected to actuate early in the break sequence, resulting in an aggravated flooding problem, they are included in the model.

Compartment sump pumps, fan coolers, and pump heat were excluded from the model. The sump pumps were excluded because they do not have adequate capacity to remove the break discharge, condensate, and firewater. In the small-break sequences, where the combined accumulation of water from these sources was close to the sump pump capacity, the impact of sump pump operation was evaluated qualitatively. Pump heat was neglected because it would be removed by the fan coolers, and the fan coolers were not modeled because a large fraction of their capacity would be used to remove pump heat.

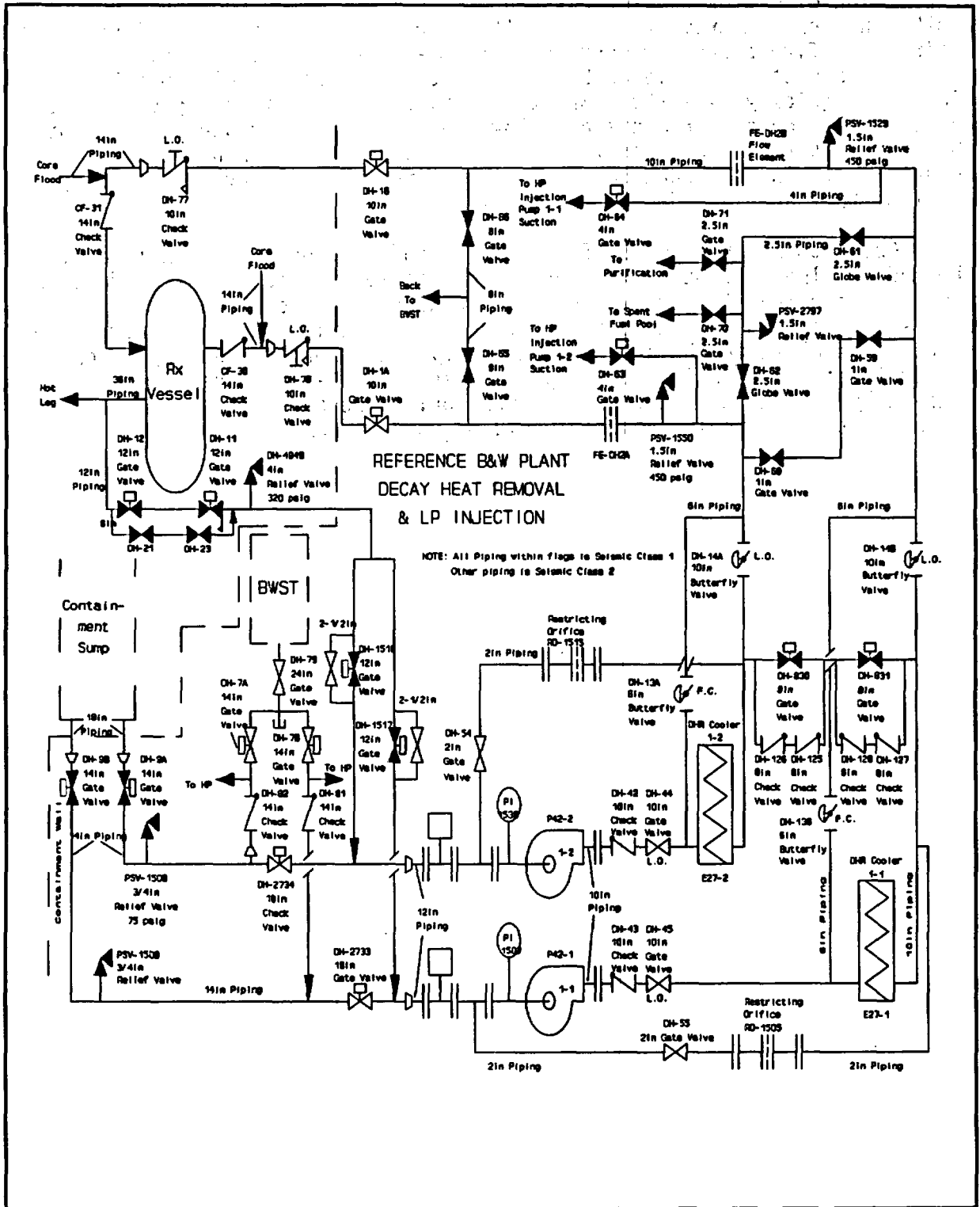


Figure 1. Simplified piping diagram showing the break location for sequence 1.

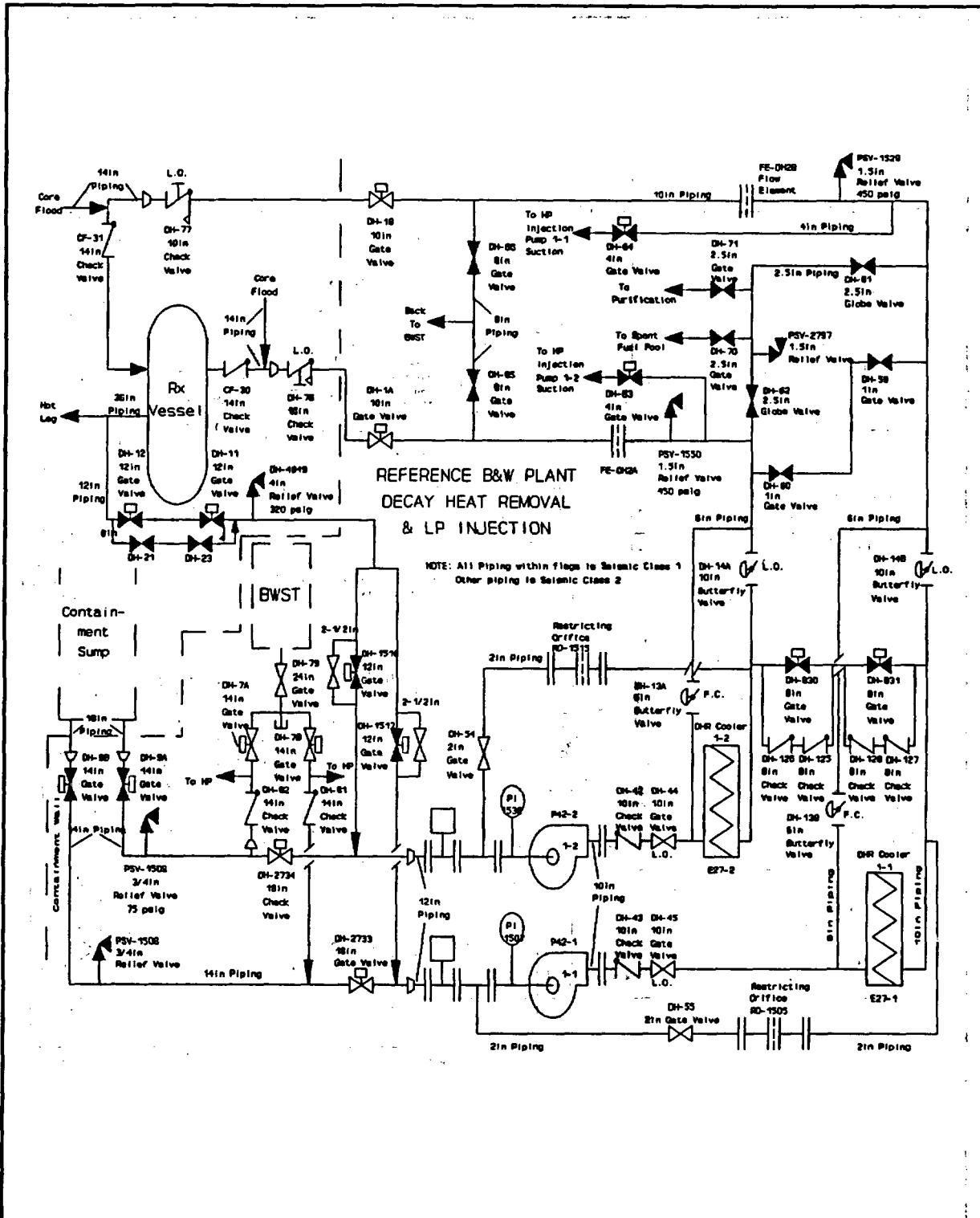
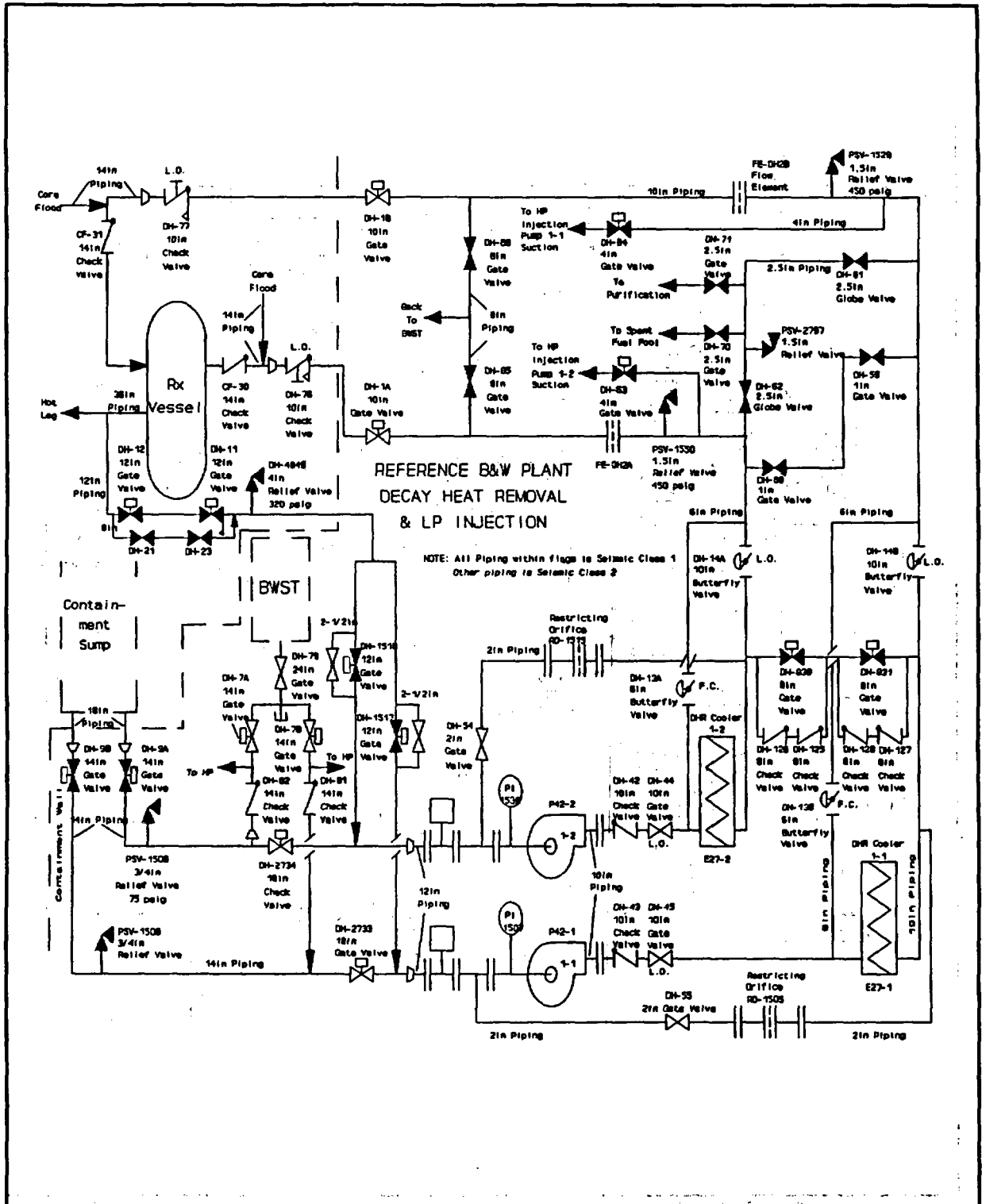


Figure 2. Simplified piping diagram showing the break locations for sequence 2.



**Figure 3. Simplified piping diagram showing break locations for sequences 3 and 4.**

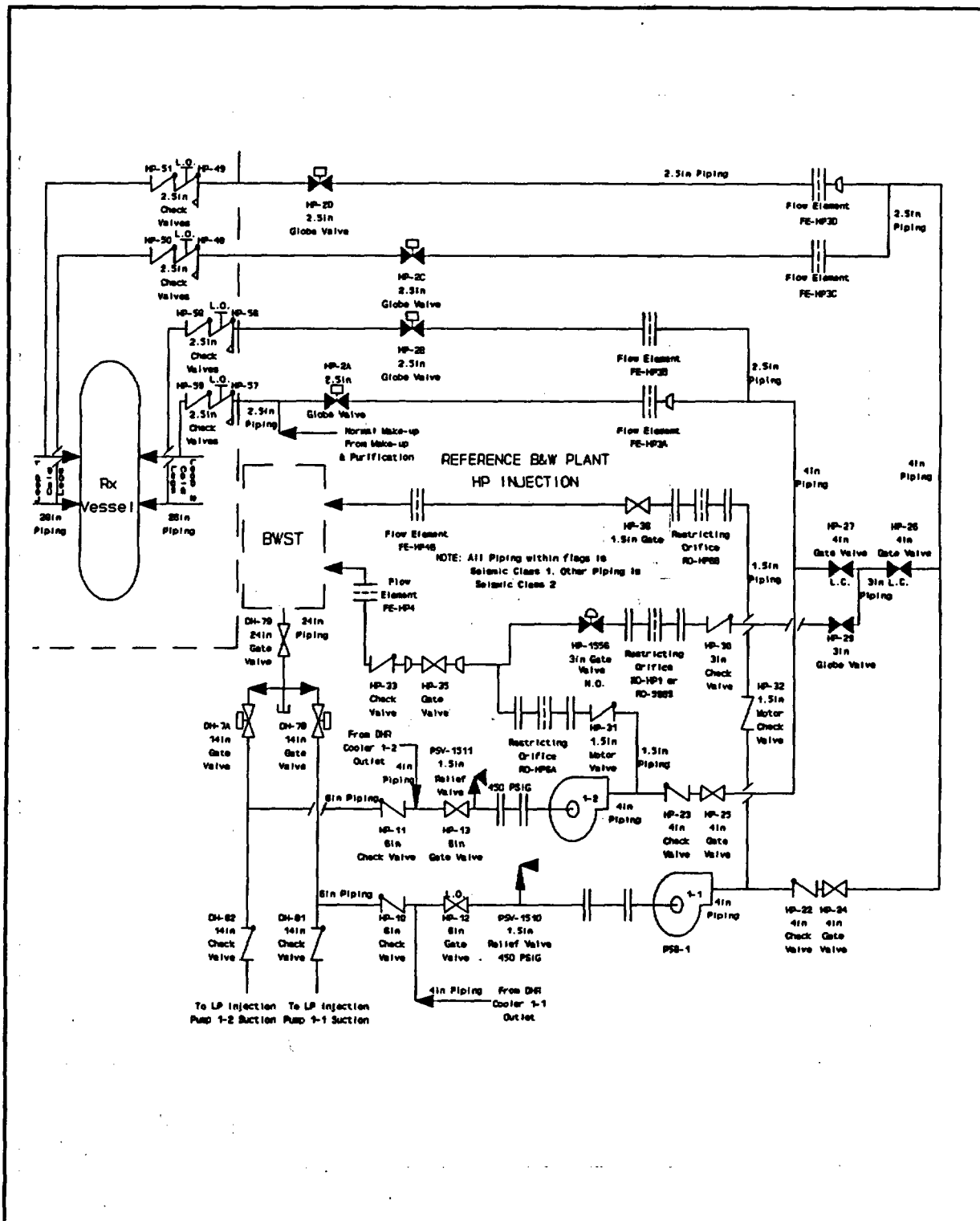


Figure 4. Simplified piping diagram showing the break location for sequence 5.

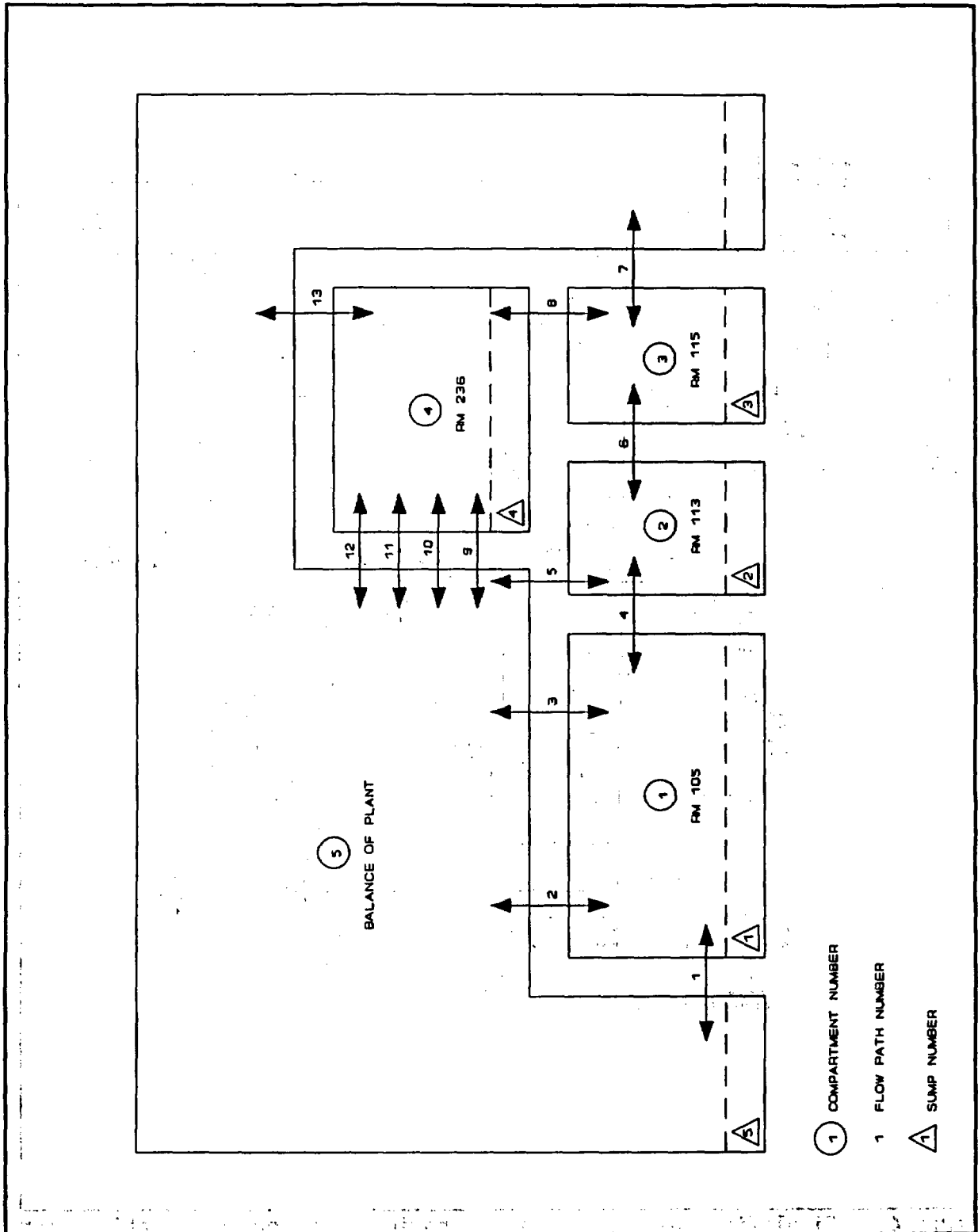


Figure 5. CONTAIN nodalization diagram for the B&W auxiliary building

## RESULTS FOR THE THREE PLANTS ANALYZED

The trial application of this state-of-the-art ISLOCA methodology to three U. S. nuclear power plants provided the following results. The reader is cautioned that extrapolating these results to other plants at this time without further analysis would be highly speculative.

### B&W Plant Findings

1. The total ISLOCA core damage frequency was estimated to be  $\sim 2 \times 10^{-6}$  per reactor-year.
2. Potential human errors during mode changes were found to be the dominant contributors to ISLOCA core damage frequency and risk. ISLOCA initiating events driven by human error were composed of errors of commission that could occur during execution of normal procedural tasks, such as entering shutdown cooling.
3. Scenarios initiated primarily by hardware failures of pressure isolation valves were relatively small contributors to ISLOCA core damage frequency and risk.
4. Break isolation would be required to prevent core damage, because the makeup capacity to the borated water storage tank (BWST) is insufficient to maintain an adequate reactor coolant inventory for breaks larger than two inches in diameter. Although the analysis indicates that hardware would probably be available to isolate these breaks, specific procedures and training were not in place at the time of the plant visit to ensure that this hardware is used.
5. Operational experience related to ISLOCA made credible the specific human errors of commission that were the dominant contributors to ISLOCA risk.

The large contribution to ISLOCA risk from human errors that could occur during shutdown highlights the importance of including a comprehensive assessment of the role of plant personnel in an ISLOCA risk evaluation. To be complete, this assessment should consider the potential for errors of commission and the effect that possible latent errors could have on the normal execution of procedures.

The CONTAIN calculations performed for this plant show that pressurization of the auxiliary building is limited to less than 1 psig, because the modeled auxiliary building compartments are very well connected to one another. The modeling parameters that affect the calculated pressure rise between compartments are flow area, discharge coefficient, and L/D. These parameters were all accurately modeled for the ECCS rooms, so any uncertainties in the flow model (and hence the pressure calculation) would stem from the number of flow junctions neglected in the balance-of-plant portion of the model. The largest pressure drop in the auxiliary building

model should occur as the fluid passes from the break compartment to the immediately adjacent compartments (assuming roughly equal flow areas connecting each compartment). At each successive flow junction, the mass flow will be reduced by the mass condensed in passing through each compartment, and the effective area associated with the flow will increase as more and more parallel flow paths become available to the fluid. Therefore, pressure drops at each succeeding junction will decrease as distance from the break increases. This effect leads to the conclusion that refinements to the CONTAIN model would not have a appreciable affect on the calculated pressures.

CONTAIN predicts that, for the range of break sizes analyzed, temperatures in the auxiliary building will not exceed 212° F. However, there is one modeling uncertainty that could change this result significantly: the quality of the water-steam mixture discharged from the break into the auxiliary building. For all of the break sequences analyzed, the break discharge is a two-phase mixture with steam quality no higher than approximately 0.90. Because CONTAIN models the RCS blow down as an isenthalpic expansion from RCS pressure to compartment pressure, the resulting compartment temperatures will always be at, or very near, the saturation temperature associated with the calculated compartment pressure, as long as the break quality does not exceed approximately 0.93. At break qualities higher than 0.93, the enthalpy of the discharged fluid will be high enough (greater than 1150 Btu/lbm) to produce superheated steam in the compartment. The maximum steam temperature obtainable by this process is approximately 320° F., and occurs when dry saturated steam at approximately 500 psia is discharged from the RCS through the break. It must be emphasized that none of the simplified model predictions indicate that dry steam will be present in the break discharge. However, recent best-estimate Oconee SBLOCA calculations do show prolonged periods during which the discharge is very nearly dry. Given the uncertainty inherent in any calculation of this type, one cannot rule out the possibility that high quality steam will be discharged for a long enough period of time to superheat the steam in the break compartment.

The relative humidity predictions were similar in each sequence. All of the auxiliary building rooms that were evaluated experienced periods of 100% relative humidity.

The rate of flooding varied considerably among the five sequences, as illustrated by Figures 6 and 7. Figure 6 shows compartment pool depths plotted against time after rupture for a large break in the DHR letdown line. In this sequence (sequence 1), the source of flooding is located in room 236. The flood propagated through a pipe chase in the floor of room 236 into room 115. From there water spilled over two flood walls to flood rooms 113 and 105, submerging all ECCS pump motors in a little over 30 minutes. This was primarily the result of propagation of the unflashed portion of the break discharge. In this sequence, sump pump operation would have been ineffective in mitigating the flooding, because of the low capacity of the sump pumps.

## BS-1 Auxiliary Building Pool Depths

12 Inch pipe break in room 236

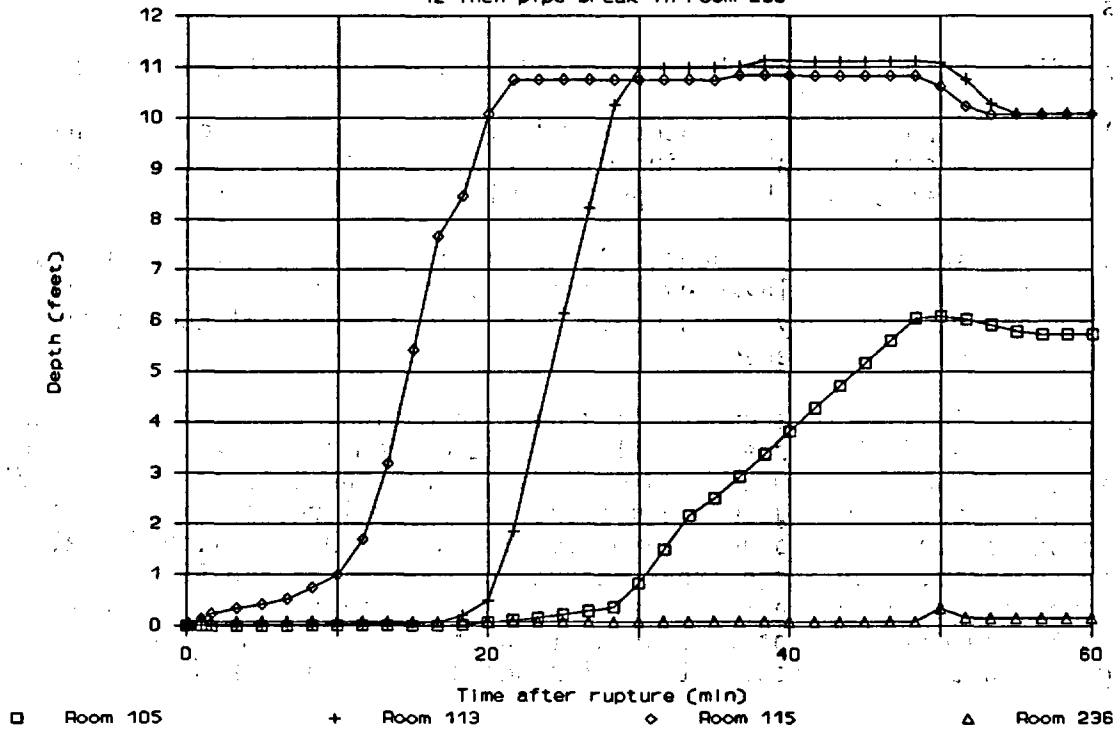


Figure 6. Auxiliary building pool depths resulting from a DHR system piping rupture in Room 236 (break sequence 1). The discharge-limiting flow area is 0.6012 ft<sup>2</sup>.

Figure 7 shows pool depths for a small-break sequence (sequence 5). The resulting flood was minimal because the mass discharged from the break was relatively small, and much of it flashed to steam. The steam was then carried through the building and released to the outside atmosphere through blowouts, or was condensed well away from the break location. Furthermore, sump pumps, had they been included in the model, could have slowed pool growth and delayed the submergence threat to the ECCS equipment. Flooding in this sequence occurs primarily because firewater discharged from the sprinkler system in room 236 drains into the ECCS compartment below (room 115). At the end of two hours the flood had not yet reached the top of the spill wall separating room 115 and room 113. Equipment in room 105 would not be threatened for a number of hours.

The flooding results can be summarized with two general statements:

- 1) For large-break sequences 1 and 4, flooding will occur in the break compartment and in adjacent compartments at a rate that will cover essential ECCS components within one hour.
- 2) For small-break sequences 2, 3, and 5, flooding will occur slowly and could be delayed by operation of the compartment sump pumps. A period of many hours would pass before essential ECCS components would be threatened.

Of the various factors controlling pool formation, two dominate. The first is the rate of discharge of unflashed fluid from the break. The second is the extent to which firewater and condensate from the balance-of-plant find their way into rooms housing ECCS equipment. For the large-break sequences, the principal contributor to pool formation is the discharged liquid that does not flash to steam. For large-break sequences 1 and 4, as the RCS cools down, this becomes essentially the runout flow of the surviving ECCS. In sequences 2, 3, and 5, the discharge of fire protection sprays provides a greater flooding hazard than the accumulation of condensate or unflashed break discharge.

The results from the steam propagation analysis show that operator entry into the auxiliary building would be prohibited by the live steam environment that forms within minutes of system rupture. The results also show that the most limiting environmental factor is water pool formation in the ECCS compartments. When the pools reach a depth of two feet, the ECCS pump motors will be submerged, failing the ECCS pumps. The time at which this failure becomes the limiting time available for operator recovery of the plant. The temperature and humidity effects were not important at the B&W study plant because the ECCS equipment was qualified for the postulated environment produced by a high energy line break, a more severe environment than predicted here.

# BS-5 Auxiliary Building Pool Depths

4 inch pipe rupture in Room 115

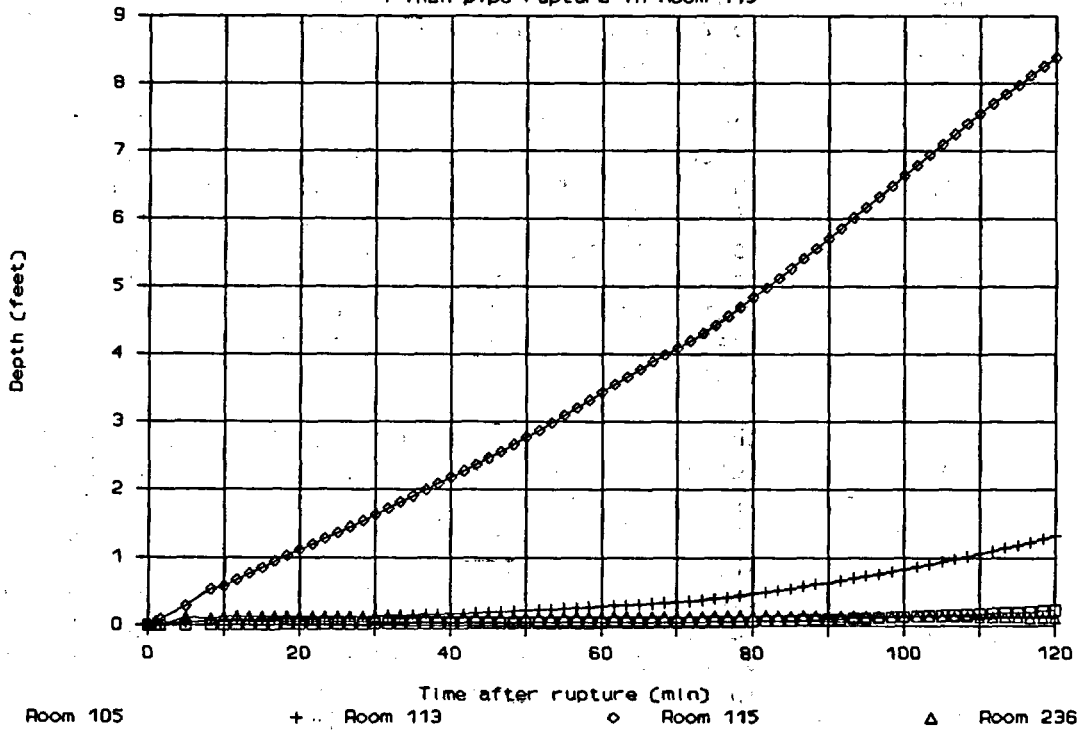


Figure 7. Auxiliary building pool depths resulting from an HPI pump suction line rupture (break sequence 5). The discharge-limiting flow area is 0.02463 ft<sup>2</sup>.

## Westinghouse plant results

1. The total ISLOCA core damage frequency was estimated to be  $-2 \times 10^{-6}$  per reactor-year.
2. Human errors that could occur during startup and shutdown of the plant were negligible contributors to ISLOCA core damage frequency and risk. This is in contrast to the finding for the B&W plant and is a direct result of the high quality of the administrative controls and safety culture found at the Westinghouse plant.
3. Sequences initiated by hardware failures of pressure isolation check valves were the only significant contributors to ISLOCA core damage frequency and risk.
4. As in the B&W plant, break isolation would be an important recovery action, because the makeup capacity from the refueling water storage tank (RWST) is insufficient to maintain an adequate reactor coolant inventory for breaks that are larger than approximately two inches in diameter. The analysis indicates that hardware would be available to isolate these ISLOCA breaks, and, in contrast with the finding for the B&W plant, adequate procedures and training are generally available to ensure that this hardware is used.
5. At the time of the plant visit, a general survey was made of the interfacing system flow paths to qualitatively estimate the impact on equipment of ruptures in various locations. This survey could not verify that the ECCS components are adequately separated such that any postulated rupture would not affect redundant ECCS trains. In particular, in the case of the residual heat removal (RHR) system, the pumps for units 1 and 2 (the analyzed plant is located at a two-unit site) are located in the basement of the auxiliary building and a common corridor runs outside of the individual pump rooms. If there were a pipe break and blowdown of steam and liquid from the RCS into one of the RHR pump rooms, this configuration may not ensure that at least one train of ECCS would still be available following the rupture. In other words, because of the common corridor, a rupture in the RHR pump room of one unit could conceivably disable the RHR pumps for the other unit, also.
6. A significant reduction in ISLOCA risk through relatively simple changes to procedures, training, and instrumentation does not appear achievable.

## Combustion Engineering Plant Results

1. The total ISLOCA core damage frequency was estimated to be  $\sim 2 \times 10^{-6}$  per reactor-year.
1. As at the Westinghouse plant, human errors that could occur during startup and shutdown of the plant were negligible contributors to ISLOCA core damage frequency and risk. Again, this is a direct result of the high quality of the administrative controls and safety culture found at the plant.
2. Sequences initiated by hardware failures of pressure isolation check valves were the dominant contributors to ISLOCA core damage frequency and risk. However, at the CE plant, exposure of the low-pressure interfacing system is precipitated by stroke-testing of a normally closed injection flow control valve.
3. As in the other two plants, break isolation would be an important recovery action, because makeup capacity to the refueling water storage pool (RWSP) is insufficient to maintain an adequate reactor coolant inventory for breaks that are larger than approximately two inches in diameter. The analysis indicates that hardware would be available to isolate these ISLOCA breaks; however, as for the B&W plant, procedures were not available at the time of the plant visit to ensure that this hardware is used in all sequences.
4. At the time of the plant visit, a general survey was made of the interfacing system flow paths to qualitatively estimate the impact on equipment of ruptures in various locations. As for the Westinghouse plant, this survey could not verify that the emergency core cooling systems (ECCS) are adequately separated such that any postulated rupture would not affect redundant ECCS trains.
5. It appears that relatively simple changes to procedures and training could reduce ISLOCA risk by reducing the initiator frequency and by increasing the likelihood of successfully isolating an intersystem break.

## **FUTURE RESEARCH AREAS**

Further research is planned in the following areas to achieve final resolution of GI-105:

- 1) Screening criteria will be developed to evaluate the threat to ECCS equipment from the post-break auxiliary building environment.
- 2) An evaluation will be made of the ISLOCA risk at BWRs.

- 3) Guidelines will be developed for use in evaluating ISLOCA risk at other plants.
- 4) An evaluation will be made of the ISLOCA risk for advanced light water reactor designs.

#### ACKNOWLEDGEMENT

This program is under the sponsorship of the U. S. Nuclear Regulatory Commission, Office of Nuclear Regulatory Research, Division of Safety Issue Resolution - Dr. Gary R. Burdick, NRC Project Manager.

#### REFERENCES

1. U. S. Nuclear Regulatory Commission, Reactor Safety Study-An Assessment of Accident Risks in U.S. Commercial Nuclear Power Plants, WASH-1400 (NUREG/75-014), October 1975.
2. W. J. Galyean et al., Assessment of ISLOCA Risk - Methodology and Application: Babcock and Wilcox Nuclear Power Station (Draft), EG&G Idaho, Inc., NUREG/CR-5604 (EGG-5604), February 1991.
3. D. L. Kelly et al., Assessment of ISLOCA Risks - Methodology and Application: Westinghouse Four-Loop Ice Condenser Plant, NUREG/CR-5744, to be published.
4. D. L. Kelly et al., Assessment of ISLOCA Risks - Methodology and Application: Combustion Engineering Plant, NUREG/CR-5745, to be published.
5. V. H. Ransom et al., RELAP5/MOD2 Code Manual, EG&G Idaho, Inc., EGG-2396, August 1985.
6. D. A. Wesley et al., Component Pressure Fragilities for Piping Components, ABB Impell Corporation, NUREG/CR-5603 (EGG-2607), October 1990.
7. T. G. Ryan, "A Task Analysis Linked Approach for Integrating the Human Factor in Reliability Assessment of NPP," Reliability Engineering and System Safety, vol. 22, 1988.
8. A. Swain and H. Gutman, Handbook of Human Reliability Analysis with Emphasis on Nuclear Power Plant Applications, NUREG/CR-1278, August 1983.
9. G. Hannaman and A. Spurgin, Systematic Human Action Reliability Procedure (SHARP), EPRI NP-3583, 1984.
10. R. Hall (ed.), A Guide for General Principles of Human Action Reliability Analysis for Nuclear Power Generation Stations, IEEE Draft Standard P1082/D7, August 1989.

11. G. W. Hannaman, A. Spurgin, and Y. Lukic, Human Cognitive Reliability Model for PRA Analysis, NUS-4531, Electric Power Research Institute, 1984.
12. U.S. Nuclear Regulatory Commission, Office of Nuclear Regulatory Research, Severe Accident Risks: An Assessment for Five U.S. Nuclear Power Plants, NUREG-1150, Volume 1, Second Draft for Peer Review, June 1989.
13. K. R. Jones, C. A. Dobbe, and D. L. Knudson, INEL Personal Computer Version of MACCS 1.5, NUREG/CR-5667, March 1991.
14. MELCOR Accident Consequence Code System, MACCS Version 1.5 User's Manual, NUREG/CR-4691, Vol. 1, February 1990.
15. Oconee PRA: A Probabilistic Risk Assessment of Oconee Unit 3, Nuclear Safety Analysis Center (Electric Power Research Institute) and Duke Power Company, NSAC-60, June 1984.
16. Evaluation of Severe Accident Risks and the Potential for Risk Reduction: Surry Power Station, Unit 1, NUREG/CR-4551 (SAND86-1309), Draft Report for Comment, February 1987.
17. D. C. Aldrich et al., Technical Guidance for Siting Criteria Development, Sandia National Laboratory, NUREG/CR-2239 (SAND81-1549), 1982.
18. K. K. Murata et al., User's Manual for CONTAIN 1.1: A Computer Code for Severe Nuclear Reactor Accident Analysis, NUREG/CR-5026, November 1989.

**BIBLIOGRAPHIC DATA SHEET**

*(See instructions on the reverse)*

1. REPORT NUMBER  
(Assigned by NRC. Add Vol., Supp., Rev.,  
and Addendum Numbers, if any.)

NUREG/CP-0119  
Vol. 1

2. TITLE AND SUBTITLE

Proceedings of the Nineteenth Water Reactor  
Safety Information Meeting

3. DATE REPORT PUBLISHED

MONTH YEAR  
April 1992

4. FIN OR GRANT NUMBER

A-3988

5. AUTHOR(S)

Compiled by Allen J. Weiss, BNL

6. TYPE OF REPORT  
Proceedings of confer-  
ence on safety research

7. PERIOD COVERED (Inclusive Dates)

October 28-30, 1991

8. PERFORMING ORGANIZATION - NAME AND ADDRESS (If NRC, provide Division, Office or Region, U.S. Nuclear Regulatory Commission, and mailing address; if contractor, provide name and mailing address.)

Office of Nuclear Regulatory Research  
U.S. Nuclear Regulatory Commission  
Washington, D.C. 20555

9. SPONSORING ORGANIZATION - NAME AND ADDRESS (If NRC, type "Same as above"; if contractor, provide NRC Division, Office or Region, U.S. Nuclear Regulatory Commission, and mailing address.)

Same as Item 8 above

10. SUPPLEMENTARY NOTES

Proceedings prepared by Brookhaven National Laboratory

11. ABSTRACT (200 words or less)

This three-volume report contains 83 papers out of the 108 that were presented at the Nineteenth Water Reactor Safety Information Meeting held at the Bethesda Marriott Hotel, Bethesda, Maryland, during the week of October 28-30, 1991. The papers are printed in the order of their presentation in each session and describe progress and results of programs in nuclear safety research conducted in this country and abroad. Foreign participation in the meeting included 14 different papers presented by researchers from Canada, Germany, France, Japan, Sweden, Taiwan, and USSR. The titles of the papers and names of the authors have been updated and may differ from those that appeared in the final program of the meeting.

12. KEY WORDS/DESCRIPTORS (List words or phrases that will assist researchers in locating the report.)

reactor safety - meetings, research programs - reviews, reactor accidents, reactor components, nuclear power plants - reliability, nuclear power plants - risk assessment, probabilistic estimation, loss of coolant, reactor accidents - management, human factors, systems analysis, leading abstract - proceedings, seismic effects, hydraulics - heat transfer, environmental engineering.

13. AVAILABILITY STATEMENT

Unlimited

14. SECURITY CLASSIFICATION

(This Page)

Unclassified

(This Report)

Unclassified

15. NUMBER OF PAGES

16. PRICE

**THIS DOCUMENT WAS PRINTED USING RECYCLED PAPER**

---

OFFICIAL BUSINESS  
PENALTY FOR PRIVATE USE, \$300